AN ELECTROPHYSIOLOGICAL INVESTIGATION OF AGE-RELATED MACULAR DEGENERATION

ALISON MARY BINNS

DOCTOR OF PHILOSOPHY

SCHOOL OF OPTOMETRY AND VISION SCIENCE

CARDIFF UNIVERSITY

APRIL 2005

UMI Number: U584699

UMI

Dissertation Publishing

ProQuest

<u>SUMMARY</u>

Age-related macular degeneration (AMD) affects 12.7 million people in Europe and North America (*Klein et al, 1995; Klein et al 1999*). As a combination of decreasing birth rate and increasing longevity alter the demographic of the population, the impact of this disease can only increase. This places an immense burden, not only on the individuals afflicted by the condition, but on the financial resources of society as a whole. Unfortunately, treatment for AMD is still very restricted, and even our understanding of the pathogenesis of the disease is far from complete.

One concern in tackling the growing problem of AMD is that methods used in the assessment of the condition are limited, usually based on fundus appearance and visual acuity. The aim of this study was to develop a battery of electrophysiological tests which would be sensitive to the most subtle changes in retinal function in AMD. Such tests may aid diagnosis, provide a more sensitive measure of disease progression, and allow an early identification of phenotypic subtypes.

Protocols were included for the recording of the focal rod ERG, the focal cone ERG, the S-cone ERG and the dynamic focal cone ERG, along with psychophysical tests of colour vision and dark adaptation. These tests were then applied to 31 subjects with ARM (12 with bilateral ARM, 11 with unilateral wet AMD and 8 with unilateral dry AMD), and 28 controls.

In the analysis of ERG amplitudes a ratio of focal to full-field amplitude was introduced as a novel means of reducing intersubject variability in response. This was found to increase the accuracy of all tests in distinguishing between subject groups. The greatest separation between ARM and control groups was provided by the dynamic tests of visual function i.e. rod-cone break time of the dark adaptation function, and time constant of recovery of the dynamic focal cone ERG. The time to rod-cone break also showed potential in identifying subjects at increased risk of exudative retinal changes.

Subjects were assigned to groups in this study on the basis of fundus appearance. However, individuals within each subject group showed a range of retinal function which belied the homogeneity of retinal signs. This raises the question of whether 'form' or 'function' should form the basis of classification and assessment of individuals with ARM and AMD.

To my parents, Richard and Jenny Binns

ACKNOWLEDGEMENTS

CONTENTS

CHAPTER 4: OCULAR ELECTROPHYSIOLOGY

LIST OF FIGURES

xiv

LIST OF TABLES

CHAPTER 1: GENERAL INTRODUCTION

Age-related macular degeneration (AMD) is a disease of the outer retina, retinal pigment epithelium, Bruch's membrane and choroid. It is the leading cause of blindness in the developed world, and currently affects about 12.7 million people in Europe and North America (*Klein et al, 1995, Klein et al, 1999*). People with AMD find reading, writing and recognising faces particularly difficult because AMD destroys the central retina (macula) which facilitates the resolution of fine detail. Age-related macular degeneration principally affects those over the age of 55, and the risk of developing the condition increases with advancing age. This means that the impact of AMD can only increase as general health and medicine improves, and life expectancy increases. The social implications of this disease are severe at an individual level, but also in terms of the costs incurred in treatment and palliative care.

Our understanding of the pathogenesis of AMD is limited. Laser photocoagulation and photodynamic therapy can slow disease progression in some people with the exudative form of the disease but unfortunately, for the majority of people with AMD, there is no treatment.

The early form of AMD, in which visual acuity remains relatively unimpaired but retinal changes are seen, is known as Age-Related Maculopathy (ARM). People with ARM may go on to develop one of two end-stages of the disease. Dry AMD is characterised by pigmentary disturbances, photoreceptor death and an insidious loss of vision, which may progress over a period of years. Wet or exudative AMD is caused by the growth of new blood vessels through breaks in Bruch's membrane. If not detected and treated at an early stage, the leakage and haemorrhage of these new vessels can result in a dramatic loss of central vision.

The International Classification System (*Bird et al, 1995*) provides guidelines for the classification and grading of the severity of ARM and AMD according to retinal appearance. Retinal signs of ARM such as soft drusen and focal pigmentary abnormalities signify an underlying disturbance of the outer retina and Bruch's membrane (*Sarks, 1976*). These anatomical changes also impact on the functional integrity of the retina. The question remains as to whether there are measurable functional changes, which precede the appearance of the retinal signs of ARM.

In the clinic the assessment of visual function is usually limited to the measurement of visual acuity. However, visual acuity is solely a measure of foveal cone function. Recent evidence

suggests that the functional deficit in AMD is more widespread, and abnormalities have been reported in dark adaptation (*Owsley et al, 2001*), colour vision (*Cheng & Vingrys, 1993*), contrast sensitivity (*Owsley et al, 1990*), and retinal sensitivity (*Owsley et al, 2001*) even in people with ARM whose visual acuity is near normal.

The literature on electrophysiological investigations of visual function in AMD is limited. Full-field responses are generally found to be comparable between AMD and control groups (*Sunness et al, 1985; Holopigian et al, 1997*). Investigation using focal stimuli has been limited to the assessment of cone responses from the central 10° of retina (*Biersdorf & Diller, 1969; Birch & Fish, 1988, Sandberg et al, 1993; Remulla et al, 1995, Falsini et al, 1999; 2000*).

The general aim of this study was to determine which aspects of visual function are particularly affected by early ARM, and to develop tests which would be sensitive to these changes. Electrophysiological techniques were used to obtain an objective assessment of static cone and rod functional integrity and to evaluate the dynamic capacity of the macula to regain normal function following exposure to a bright adapting light. The diagnostic potential of these tests was also evaluated.

Considerable research is being directed towards the advancement of treatment strategies for AMD. Tests that are particularly sensitive to early functional changes in the disease may be of value in the assessment of the efficacy of these interventions. There is also the potential to develop tests capable of discriminating between those individuals with ARM who will go on to develop neovascular changes and those who will not. This would be valuable in ensuring the prompt referral for treatment of those individuals appropriate for laser photocoagulation and photodynamic therapy. The prognosis of such treatment is greatly improved by early intervention.

Psychophysical studies of visual function have suggested that rod function may be affected early in the disease process (*Steinmetz et al, 1993; Jackson et al, 1998; Curcio et al, 2000; Owsley et al, 2000*). There is also some evidence to suggest that abnormalities in parameters of dark adaptation precede static sensitivity loss (*Owsley et al, 2001*). An assessment of the central retina using electrophysiological techniques targeting these specific areas of retinal function might clarify the mechanisms underlying the disease process and provide support for these findings.

This study describes the development of a battery of electrophysiological tests designed to be sensitive to the earliest changes which occur in ARM, and the application of these tests to a group of subjects with ARM, and a group of age-matched control subjects.

<u>**CHAPTER 2: THE RETINA**</u>

2.1   Introduction

Every sensory system has receptors which can detect external stimuli, and convert them into electrical signals. In the visual system this process occurs in the retina, the innermost layer of the eye. This is where the optics of the eye focuses images, and where the process of photochemical transduction converts light energy into nerve impulses.
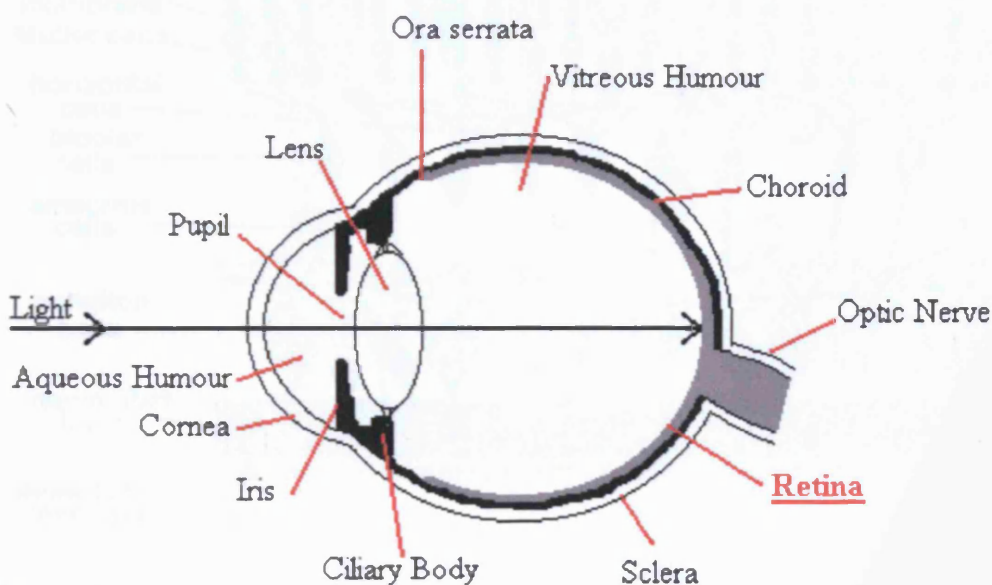
Figure 2.1. Diagram of a horizontal section through the human eye, illustrating the passage of light from the cornea to the retina.

The retina is located between the choroid and the vitreous humour. It extends from the optic nerve, and terminates at the ora serrata, just posterior to the ciliary body.

As well as being the site where nerve impulses are initiated, the retina also forms the first part of the visual pathway. The electrical impulses which are generated in the photoreceptors are relayed through the retina by bipolar cells and ganglion cells, whilst the signal is also modified and integrated by intermediate neurones, such as the horizontal cells, amacrine cells, and interplexiform cells.

2.2   General Structure

When a vertical section of the human retina is studied using a light microscope, it appears to consist of 10 different layers, although further examination reveals that not all of these are true layers. All vertebrate retinas consist of an outer pigmented layer, three layers of neuronal cell bodies, and two layers of synaptic connections.
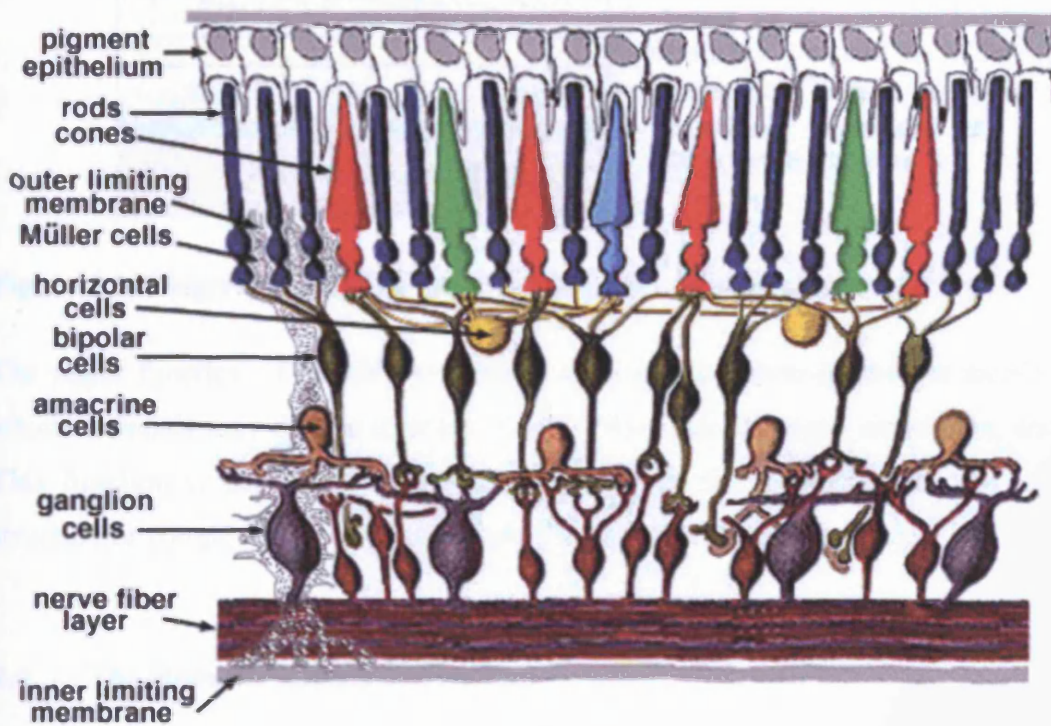
Figure 2.2. Diagram illustrating the basic structure of the retina (*after Kolb et al, 2003*).

2.3   Bruch's Membrane

Whilst not a part of the retina itself, Bruch's membrane is closely associated with the basement membrane of the retinal pigment epithelium, and forms a barrier between the retina and the choroidal circulation.

Bruch's membrane is generally accepted to consist of the five layers shown in Figure 2.3, although strictly speaking the basement membranes of the RPE and choriocapillaris might be considered as separate from the true structure of Bruch's.

The inner and outer collagenous layers are composed of interwoven collagen fibres, which are also continuous through the elastic layer. The interfibre matrix is composed largely of heparin

sulphate, adjacent to the RPE, and chondroitin, within the collagenous layers (*Guymer et al*, *1998*).
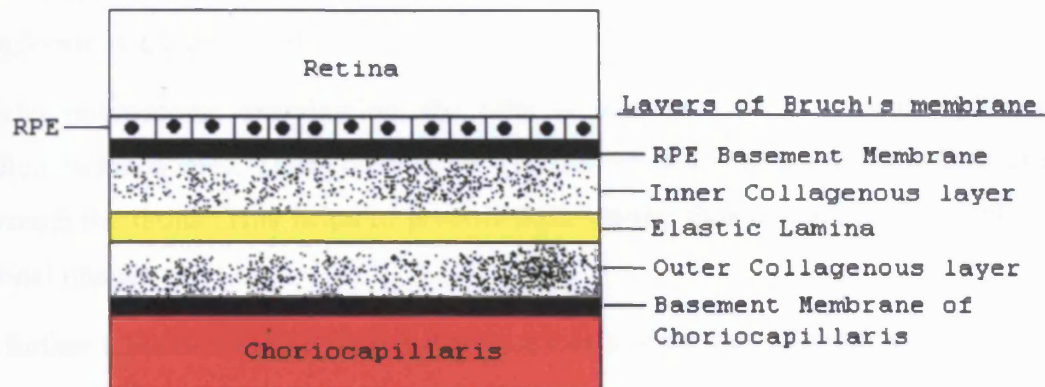
Figure 2.3. Diagram illustrating the structure of Bruch's membrane.

The major function of Bruch's membrane is to act as a semi-permeable membrane through which materials may diffuse to reach the RPE from the choroidal circulation, and vice versa. This function is dependent on the pH and charge of the membrane, and any change in structure or composition could impact on the diffusion properties

2.4   The Retinal Pigment Epithelium

The retinal pigment epithelium (RPE) is the outermost layer of the retina. It is a monolayer of hexagonal cells, which are columnar in the posterior polar region, and become larger with increasing retinal eccentricity. The basement membrane of the RPE forms part of Bruch's membrane. Invaginations of the basal aspect of the RPE cells interdigitate with the basement membrane and ensure a close association between the RPE and choroid.

The apical surface of the RPE faces the neural retina, and numerous microvilli in the apical cell membranes envelop the tips of the photoreceptor outer segments. There are no intercellular junctions physically connecting these two layers of the retina. A potential space therefore exists between the RPE and the neural retina. The close connection between these two layers is maintained by a number of elements, including passive forces such as intraocular and osmotic pressure (*Fatt & Shantinath, 1971; Kita & Marmor, 1991*), fluid transport (*Marmor et al, 1980; Kita & Marmor, 1992*), the presence of the vitreous, and adhesive forces from material which occupies extracellular space (*deGuillebon & Zauberman*, *1972; Hageman et al, 1995*). The extracellular material, which surrounds the outer segments

of the photoreceptors and the apical surface of the RPE, is known as the interphotoreceptor matrix. It has a robust honeycomb structure (*Hollyfield et al, 1990*), which helps to maintain adhesion between the RPE and neural retina, and facilitates the transport of metabolites (*Sigleman & Ozanics, 1982*).

Under microscopic examination, the RPE is seen to contain numerous pigment granules called melanosomes. These contain the pigment melanin, which absorbs light after it passes through the retina. This helps to prevent light scatter, thus maintaining the optical quality of retinal images.

A further function of the RPE is the phagocytosis of the tips of photoreceptor outer segments, as new membranous discs are formed adjacent to the inner segment. This gives rise to another pigment located in the RPE, lipofuscin. Lipofuscin accumulates with age and has its origins in the incomplete digestion of the photoreceptor outer segments by the RPE.

Adjacent RPE cells are strongly bound by zonular adherens and zonular occludens terminal bars (*Hogan & Alvarado, 1971*). This tight connection between cells enables another function of the RPE, which is to act as a blood-retinal barrier between the neural retina and the choroidal circulation (*Hudspeth & Yee, 1973*). Gap junctions between cells allow for the controlled passage of metabolites and ions, but the free exchange of materials between the blood supply and the retina is prevented.

The RPE also has an important role in the regeneration of visual pigment following photoisomerisation. In the absence of the RPE all-*trans* retinal cannot be converted back to its 11-*cis* configuration (*Kuhne et al, 1977*).

2.5   The Photoreceptor Layer and Outer Nuclear Layer

The photoreceptors are special cells adapted to perform the process of photochemical transduction – the absorption of photons of light to generate a nervous impulse. The human retina contains four types of photoreceptor. Rod photoreceptors are sensitive to low levels of illumination. Cone photoreceptors are active at higher levels of illumination. In the human retina there are three types of cone, each of which has a peak sensitivity to a different wavelength. The three different cone mechanisms present in the human retina, which are maximally sensitive to long (558nm), medium (531nm) and short (420nm) wavelength light, are the basis of trichromatic colour vision (*Gouras, 1984*).

The density of rods and cones varies across the retina. Cone density peaks at the fovea, and then declines rapidly with increasing eccentricity to reach a constant level in the peripheral retina (*Osterberg, 1935, Curcio et al, 1987*). Rods are completely absent from the fovea. Maximum rod density is at approximately 18 degrees eccentricity, and then slowly diminishes in the peripheral retina (*Osterberg 1935*). The total number of rods in the retina has been estimated as being about 110-125 million, whilst the total number of cones is believed to be between 6.3 and 6.8 million (*Snell & Lemp, 1998*).
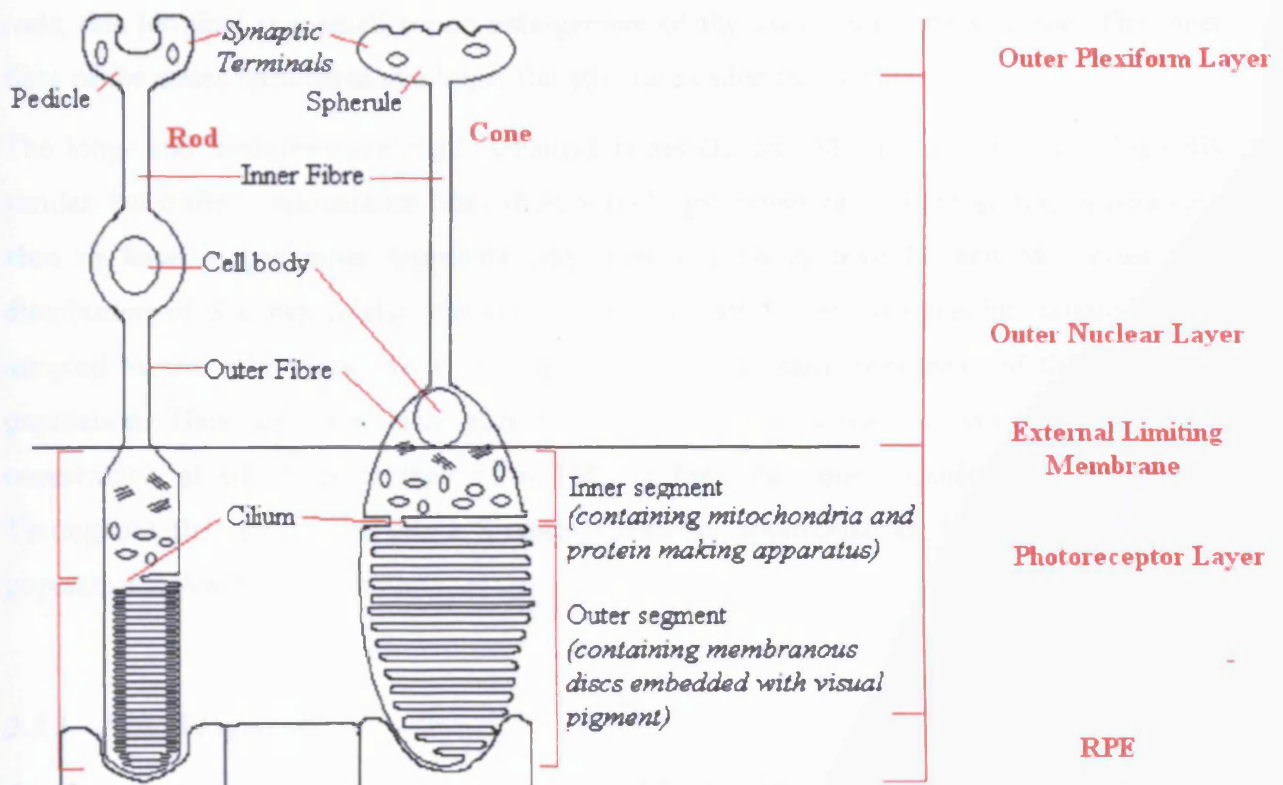
Figure 2.4. Diagram showing the structure of rod and cone photoreceptors, and their retinal location.

Figure 2.4 illustrates the structure of rod and cone photoreceptors. Both can be seen to be composed of the same basic elements. The most distal part of the photoreceptors is the outer segment. This is adjacent to the retinal pigment epithelium, and the tips of the photoreceptors are enveloped by RPE cells. The outer segments contain stacks of membranous discs, in which visual pigment molecules are embedded. In rods these discs are free floating, but in cones they remain attached to the outer segment membrane. These membranous discs have been shown in both rod and cones to be generated at the base of the outer segment (*Young, 1967; Anderson et al, 1978*). As new discs are formed the old ones are displaced towards the

tip of the outer segment, where they are shed and phagocytosed by the retinal pigment epithelium (*Young & Bok, 1969*).

The inner segment of the photoreceptors contains cellular structures such as the endoplasmic reticulum and golgi body, for the production of proteins, and numerous mitochondria to provide energy. The outer fibre connects the inner segment to the cell body, the portion of the photoreceptor containing the nucleus. The inner fibre contains microtubules, which extend from the cell body to the proximal tip of the photoreceptors and the synaptic terminals. In the rods, this terminal is a small round enlargement of the axon called the spherule. The inner fibre of the cones terminates in a large, flat structure called the pedicle.

The long- and medium-wavelength sensitive cones (L- and M- cones) are morphologically similar, but differ in appearance from short-wavelength sensitive cones (S-cones). S-cones are seen to have longer inner segments and smaller pedicles than L- and M- cones. The distribution of S-cones is also distinct, as they do not fit into the regular mosaic pattern adopted by the other cone types. S-cones form only a small percentage of the total cone population. They are completely absent from the central fovea, and reach a peak at 1° eccentricity, at which point they form 15% of the total cone population in the region. Throughout the rest of the retina S-cones constitute approximately 8% of the total cone population (*Ahnelt et al, 1987*).

2.5.1   Visual Pigments

As described above, the outer segments of both rods and cones contain numerous membranous discs, embedded with visual pigment molecules. In rods this visual pigment is called rhodopsin, whilst each cone contains one of three types of the pigment iodopsin. Each visual pigment molecule consists of a protein, opsin, bound to a chromophore, retinal (*Schertler, 1993*). Retinal is common to all human visual pigments, and differences in the absorption characteristics of the different pigments are conferred by variations in the structure of the opsin component.

2.5.2   Visual Transduction

In the dark a current flows between the inner and outer segments of the photoreceptors, the so-called 'dark current'. Light sensitive cation channels in the outer segment membrane,

which are open in the dark, allow the influx of Na^+ ions from the extracellular matrix into the photoreceptor, according to an electrochemical gradient (*Hagins et al, 1970; Baylor et al, 1979*). Sodium ions then move to the photoreceptor inner segment via the cytoplasm of the connecting cilium. An ATP dependent Na^+/K^+ pump in the inner segment maintains K^+ and Na^+ gradients inside and outside the cell (*Stirling & Lee, 1980*). Although the principal generator of the dark current is the flow of sodium ions, there is also an influx of Ca^{2+} through the cation channels, the cytoplasmic concentration of which is kept stable by means of a Na^+/Ca^{2+} exchanger in the outer segment (*Ohyama et al, 2000; Bauer, 2002*).

This dark current leads to partial depolarisation, which in turn results in a steady, high level release of neurotransmitter, glutamate, from the photoreceptor synaptic terminals in the dark.

When exposed to light, the cation channels in the photoreceptor outer segment close, resulting in hyperpolarisation. The extent of this hyperpolarisation is proportional to the intensity of retinal illumination, and leads to a graded reduction in the release of neurotransmitter from the photoreceptor synaptic terminal. Hyperpolarisation or depolarisation of synapsing second order neurones then ensues (*Copenhagen & Jahr, 1989*).

A single photon of light, when absorbed by a rhodopsin molecule, will result in the isomerisation of the retinal component of the visual pigment. This leads to a change in the retinal molecule from an 11-*cis* to an all-*trans* configuration. Since the visual pigment molecules are restricted to the membranous discs within the photoreceptor outer segments, it is clear that a secondary messenger must be involved in the process, which leads from isomerisation of retinal to closure of cation channels. For some time it was believed that Ca^{2+} might directly block the light sensitive channels (*Yoshikami, & Hagins, 1971*), but later patch-clamp experiments indicated that the cation channels were directly activated by cGMP (*Fesenko et al, 1985*).

The process by which the activation of rhodopsin leads to the deactivation of the light-sensitive channels may be summarised as follows. Upon the absorption of a photon of light, rhodopsin is converted to the form active metarhodopsin II, which then binds to a complex of transducin and GDP. This association leads to the exchange of bound GDP for GTP (*Dessauer et al, 1996*), which results in the activation of the transducin molecule (*Fung et al, 1990*). Activated transducin is responsible for the removal of the inhibitory subunit from molecules of phosphodiesterase (*Deterre et al, 1988*), which in turn catalyse the hydrolysis of

cGMP molecules. This reduction in the concentration of free cGMP molecules results in the closure of the cation channels, initiating photoreceptor hyperpolarisation (*Chabre, 1998*).

At light offset transducin deactivates (*Yee, 1978; Vuong & Chabre, 1991*), which in turn results in the inactivation of phosphodiesterase molecules. Metarhodopsin II is phosphorylated and then binds to, and is inactivated by, the protein arrestin (*Wilden, 1986*). The rhodopsin molecule is eventually split into its component opsin and retinal molecules, and separated from both arrestin and phosphate. The all-*trans* retinal must then be processed back to its 11-*cis* form for the regeneration of the visual pigment.

2.5.3   Regeneration of Visual pigment

Following its release from the rhodopsin molecule all-*trans* retinal does not accumulate in the photoreceptor outer segments but is reduced in a reaction catalysed by the enzyme all-*trans* retinal dehydrogenase into the form all-*trans*-retinol (*Wald & Brown, 1965*). All-*trans* retinol then diffuses into the retinal pigment epithelium (RPE), where it is esterified to form all-*trans* retinyl (*Krinsky, 1958*). This is then isomerised back to the pre-bleach 11-*cis* configuration in the form of *11-cis*-retinol (*Deigner et al, 1989*). The energy for this isomerisation is provided by the hydrolysis of the retinyl ester bond (*Rando, 1990*). The enzymes which catalyse this hydrolysis are solely found in the RPE, thus explaining the supreme importance of the RPE in the regeneration of visual pigment (*Kuhne et al, 1977*). 11-*cis* retinol may then either be esterified and stored, or oxidised to 11-*cis* retinal (*Lion et al, 1975*). The retinal, now back in its pre-bleach 11-*cis* configuration, then diffuses back to the photoreceptor outer segments, where it recombines with opsin to regenerate the visual pigment.

Most retinol is recycled in this manner, but must eventually become degraded and oxidised through the course of this process. New retinol (vitamin A) is provided by the choroidal circulation, via Bruch's membrane (*See Saari et al, 2000 for a review of photopigment regeneration*).

2.6   The Outer Limiting Membrane

This retinal layer lies internal to the photoreceptor layer, and is composed of intercellular adherens junctions between photoreceptor cell inner segments, and Müller cells. As such, it is

not a true membrane, but is able to act as a semi-permeable barrier limiting the flow of some large molecules (*Cohen, 1992*).

2.7   The Outer Plexiform Layer

This is the first synaptic layer of the retina, in which photoreceptors synapse with bipolar cells, and horizontal cells. There is also a certain amount of direct communication between adjacent cone pedicles, and from cone pedicles to rod spherules (*Nelson, 1977*). Feedback circuitry in the outer plexiform layer provides information to cones from the horizontal cells, and to bipolars from the inner plexiform layer.

Both rod and cone photoreceptors exhibit synaptic ribbons at their synaptic terminals, which form invaginating connections with second order neurones. Cone pedicles have approximately 30 synaptic ribbons, each associated with a 'triad' of invaginating processes - usually one bipolar cell, and two horizontal cells (*Missotten, 1965; Kolb, 1970; Ahnelt et al, 1990*). Rod spherules have only two synaptic ribbons, which form invaginating connections with two horizontal cells and two rod bipolar cells (*Missotten, 1965; Kolb, 1970*). Cone pedicles also have two other types of synaptic connections. Small projections called telodendria extend from the pedicles to form gap junctions with neighbouring rod spherules and cone pedicles (*Nelson, 1977*). At basal junctions, cone pedicles make non-invaginating synapses with flat varieties of bipolar cell (*Lasansky, 1969*).

2.7.1   Bipolar Cells

Bipolar cells convey signals from the photoreceptors in the outer plexiform layer to the amacrine and ganglion cells in the inner plexiform layer. Golgi staining reveals the presence of up to 11 types of bipolar cell in the human retina (*Boycott & Wassle, 1991, Kolb et al, 1992; Kolb et al, 2001*). Figure 2.5 illustrates the structure of these bipolar cell types.

One type of bipolar cell is specific to the rod pathway. The rod bipolar cell has a tuft of dendritic terminals in the outer plexiform layer, each of which terminates at the spherule of a rod photoreceptor. In the central retina each rod bipolar cell synapses with only 15-20 rods, but convergence increases in the periphery such that each rod bipolar is liable to connect to 40-50 rods (*Kolb, 1991*). The axons of the rod bipolars terminate in the innermost part of the inner plexiform layer (*Boycott & Kolb, 1973*).
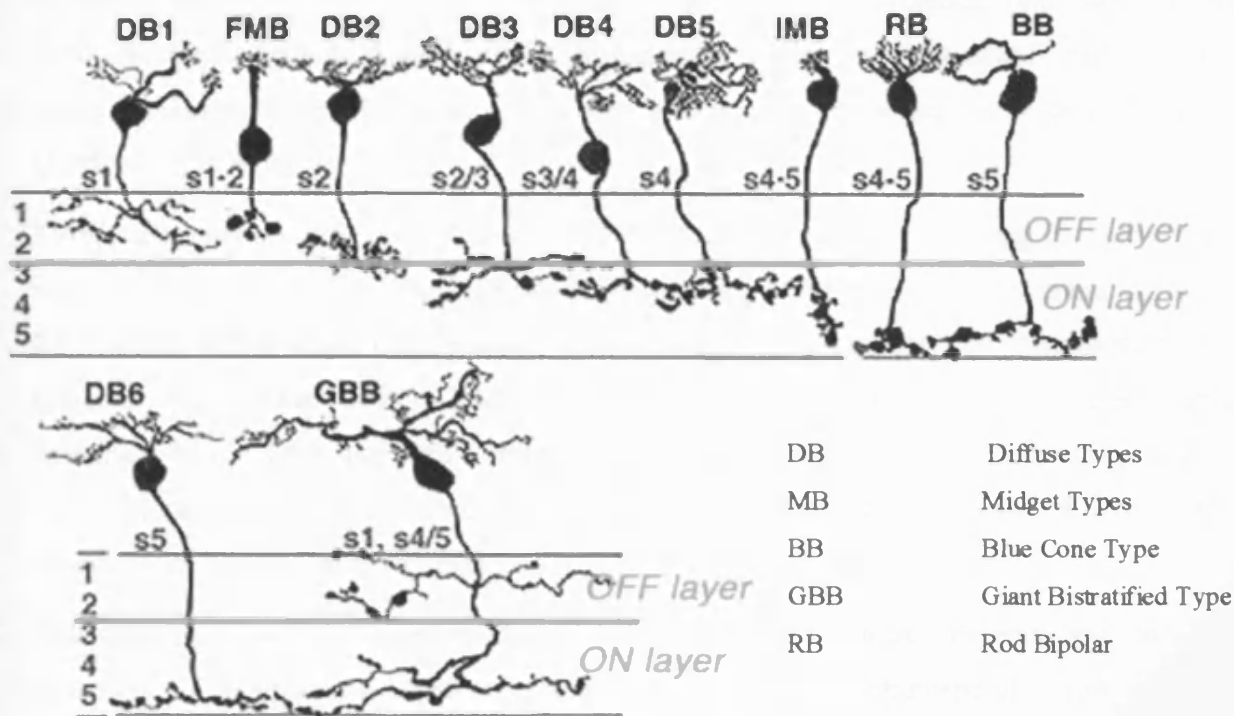
Figure 2.5. Bipolar cell types of the human retina, revealed by Golgi staining (*From Kolb et al, 2001*).

The remaining types of bipolar cell synapse with cone pedicles in the outer nuclear layer. They fall into two main categories, the diffuse bipolars, of which there are 6 types, and the midget bipolars, of which there are 2 types. Another bipolar has been suggested to be specific to the short wavelength sensitive pathway (*Boycott & Wassle, 1991*). The final type of bipolar identified, the giant bistratified cone bipolar cell, is also believed to be involved with the short-wavelength pathway (Kolb et al., 1997).

The diffuse cone bipolars are so named because of their wide dendritic fields, synapsing with 5-7 cones in the central retina, or as many as 12-14 cones in the peripheral retina. In contrast, the midget bipolars will only synapse with a single cone (*Kolb, 1991*). The diffuse bipolars are further subdivided according to the nature of their dendritic terminals in the outer plexiform layer. Diffuse bipolars 1-3 have wide cleft basal junctions at the synapse with cones, and form only superficial contacts with the cone pedicles; these are termed diffuse flat bipolars. Diffuse bipolars 4-6 are known as invaginating bipolars. They form a deeper contact with cone pedicles, forming part of the triad of synapses (*Boycott & Kolb, 1973*). As a general rule, the axons of the flat diffuse bipolars branch in the outer region of the inner plexiform

layer and are OFF- cells i.e. are hyperpolarised by a stimulus projected onto their receptive field centre (*Famiglietti & Kolb, 1976*). Invaginating diffuse bipolars stratify further into the inner plexiform layer. These are ON-cells, which are depolarised by a central stimulus (*Famiglietti & Kolb, 1976*).

Midget bipolars are also divided into flat and invaginating forms according to their dendritic endings (*Kolb et al, 1969*). An individual invaginating midget bipolar may make as many as 25 contacts with a single cone pedicle, whilst the flat midget bipolar can form as many as 50 (*Boycott & Hopkins, 1991*). The axons of these invaginating and flat midget bipolars terminate in the ON- and OFF- strata of the inner plexiform layer respectively, and it is therefore assumed that they conform to the general rule that flat bipolars are OFF-cells, whilst invaginating bipolars are ON-cells.

Pharmacologic studies suggest that ON-bipolar cells exhibit metabotropic glutamate receptors, i.e. G-protein-coupled receptors, at the synapse with photoreceptors (*Shiells, 1981*), whilst OFF-bipolar cells have conventional ionotropic glutamate receptors, i.e. ligand-gated ion channel receptors (*Atwell, 1987*).

The S-cone bipolar cell in the macaque retina was characterised by Mariani (*1984*). S-cone bipolars are ON- type cells and have invaginating synapses in the outer plexiform layer. Like the other ON-bipolar cells, their axons terminate close to the ganglion cell layer in the inner plexiform layer. In addition to the invaginating ribbon synapse of the S-cone bipolar, the S-cone also makes basal junction contact with a small number of fine bipolar dendrites, possibly belonging to the giant bistratified bipolar cell (*Mariani, 1984; Boycott & Wassle, 1991*).

2.7.2 Horizontal Cells

Horizontal cells are a type of interneurone, forming synapses with photoreceptors and bipolar cells at the level of the outer plexiform layer. They also make electrical connections with each other, via gap junctions. Horizontal cells are therefore able to communicate information laterally across the retina, enabling them to provide a negative feedback signal to photoreceptors and feedforward to bipolar cells (*Kamermans & Spekreijse, 1999*). Both of these functions are mediated by GABAergic synapses (*Chun & Wassle, 1989; Grunert & Wassle, 1990*). These feedback mechanisms form the basis of receptive field surrounds in bipolar and ganglion cells (*Dacey, 1999*).

Three types of horizontal cell have been identified in the human retina, termed HI (*Polyak,* *1941*), HII (*Kolb et al, 1980*), and HIII (*Kolb et al, 1994*). HI has a relatively small dendritic field. It has clusters of dendritic terminals, which synapse with approximately 7 cones at the fovea and up to 18 in the periphery. Dendrites of the HI cell primarily make connections with L- and M- cone pedicles, but will also contact a small number of S-cones within their receptive field (*Goodchild et al, 1996*). The axons of HI cells make numerous connections with rod spherules and also a smaller number of connections with L- and M- cone pedicles (*Kolb, 1970*). HIII cells are nearly identical in morphology to HI cells, apart from having dendritic fields which are about 1/3 larger (*Kolb, 1994*). They therefore form dendritic connections with a greater number of cones than HI cells, but in contrast to the HI cells none of these synapses are with S-cones (*Ahnelt & Kolb, 1994*). More recently it has been suggested that HI and HIII cells do not actually form two separate neural networks, but rather a single mosaic of cells, which makes numerous connections with rods and L- and M- cones but only a limited number with S-cones (*Dacey, 1999*).

HII cells have more spidery and intricate dendritic trees than the other two types (*Kolb et al, 1980*). Unlike the HI and HIII cells they direct major dendrites towards S-cones within their receptive fields, although they will also synapse with L- and M- cones (*Dacey, 1999*). The HII cell axon makes connections with S-cones only.

The HI/HIII cells are dominated indiscriminately by inputs from the L- and M- cones, whilst the HII pathway is dominated by S-cone activity. The input to both HI/HIII and HII horizontal cells is hyperpolarising. Therefore horizontal cells in humans do not show spectral opponency, and that they are unlikely to have a role in colour coding (*Dacey, 1999*).

2.8   The Inner Nuclear Layer

Proximal to the outer plexiform layer lies the inner nuclear layer. The inner nuclear layer contains the cell bodies of bipolar and horizontal cells. Amacrine cells, interplexiform cells, Müller glial cells, and some displaced ganglion cells also have cell bodies residing in this layer.

The nuclei of horizontal cells are located close to the outer plexiform layer, in which both their axons and dendrites terminate. Similarly, the nuclei of amacrine cells are located towards the inner plexiform layer, in which their synaptic processes terminate. Bipolar and

interplexiform cells have axons in the inner plexiform layer, and dendrites in the outer plexiform layer (*Linberg & Fisher, 1986*).

The inner nuclear layer also contains deep capillaries from the inner retinal vasculature.

2.9   The Inner Plexiform Layer

The inner plexiform layer is where synapses occur between bipolar cell axons and ganglion cell dendrites. Invaginating synapses of depolarising ON- bipolars are found in the inner part of the inner plexiform layer. Rod bipolars also synapse in this part of the inner plexiform layer. The flat synapses of hyperpolarising OFF- bipolars are found in the outer part of the layer. Amacrine cells also have their processes in the inner plexiform layer, forming contacts with bipolar cells, other amacrine cells, interplexiform cells and ganglion cells (*Dowling, 1966*).

Specialised ribbon synapses in the inner plexiform layer connect a bipolar axon, an amacrine cell process, and a ganglion dendrite (*Dowling, 1966*). A reciprocal synapse is also made between a second terminal of the amacrine cell, and the bipolar axon, providing a negative feedback loop (*Park, 1994*).

2.9.1   Amacrine Cells

The term 'amacrine' was used by Cajal (*1892*), to describe a group of interneurones which lack an axon, but which have a complex dendritic tree in the inner plexiform layer. Their role lies in the integration and modulation of the neural signal presented to the ganglion cells. The majority of amacrine cells have their cell bodies in the inner nuclear layer. A significant minority, however, which may comprise up to 20% of the total population, have cell bodies in the ganglion cell layer (*Wassle et al, 1987*). These are known as displaced amacrine cells.

At least 25 amacrine cell types have already been identified in the human retina (*Mariani, 1990; Kolb et al, 1992*). Diversity in appearance and physiology of these sub-types of amacrine cells appears to reflect a wide range of functions. One example of this is the group of somatostatin-immunoreactive amacrine cells (*Rickman & Brecha, 1989*). These have dendrites and cell bodies in the lower retina, whilst their axons extend into the upper retina. Somatostatin has been found to render ganglion cells more responsive to light (*Zalutsky & Miller, 1990*). The function of this group of amacrine cells is therefore believed to be the

modulation of retinal function to allow for differences in the ambient illumination of the upper and lower areas of the retina.

Amacrine cells are classified according to dendritic tree size and branching characteristics, according to neurotransmitters released at chemical synapses, and also according to the stratification of their dendrites in the inner plexiform layer (*Mariani, 1990; Kolb et al, 1992*). Cajal (*1892*) arbitrarily subdivided the inner plexiform layer into 5 strata in the classification of amacrine cells. Neurones terminating in different strata are unable to form synapses with each other, and therefore certain information regarding the function and circuitry of the amacrine cell types may be derived from the location of their end processes within the inner plexiform layer. Amacrine cells whose dendritic processes are solely confined to one stratum are said to be stratified, whilst those whose dendritic trees span all 5 strata are said to be diffuse types. Cajal's 5 strata have also been grouped into 2 sublamina, according to the nature of synapses made within those layers. Strata 1 and 2 comprise sublamina a, which contains bipolar cell axons, and ganglion cell dendrites which make connections with OFF-centre ganglion cells, whilst strata 3, 4 and 5 make up sublamina b, which is the ON- stratum of the inner plexiform layer (*Famiglietti & Kolb, 1976*).

The amacrine cells utilise a wide range of neurotransmitters in their chemical synapses. These may be excitatory, although the majority of amacrine cells in vertebrates form inhibitory synapses. Nearly half of amacrine cells use the inhibitory amino acid glycine. All glycinergic amacrine cells have diffuse dendritic fields. This means that they have dendritic terminals in multiple strata of the inner plexiform layer, and can thus communicate with all bipolar types.

One well-characterised small-field glycinergic amacrine cell, found in almost all mammals, is AII (*Boycott & Dowling, 1969*). AII has its major input from rod bipolar axons in sublamina b, although it also has a smaller input from OFF-centre bipolar cells in sublamina a (*Strettoi et al, 1992*). The major output of the AII amacrine cell is to OFF-centre ganglion cell dendrites in sublamina a (*Famiglietti & Kolb, 1975; Kolb & Nelson, 1993*), although they also synapse via gap junctions with cone bipolar cells which then make connections with ON-centre ganglion cells in sublamina b. Diffuse cells such as AII are therefore able to integrate information from ON-, OFF- and rod pathways.

In contrast, cholinergic amacrine cells have stratified dendritic trees. It appears that about half of cholinergic amacrine cells have cell bodies in the ganglion cell layer, and stratify in the inner layer of the inner plexiform layer, forming contacts with ON- cells. The other half of the

cells have cell bodies in the inner nuclear layer, and stratify in the outer region of the inner plexiform layer, synapsing with OFF- cells (*Hayden et al, 1980; Bloomfield & Miller, 1986*). These cholinergic cells have been found to release both acetyl choline and GABA at synapses (*O'Malley & Masland, 1989*), i.e. they release both excitatory and inhibitory neurotransmitters. It is thought that this characteristic may help to determine the directional sensitivity of the ganglion cells with which the cholinergic amacrines synapse (*Masland & Ames, 1976; Ariel & Daw, 1982*).

GABA-ergic amacrine cells constitute 30% of the total amacrine cell population, and the majority of the displaced amacrine cells. An example of a GABA-ergic type of amacrine cell is A17. This cell forms a key part of the rod circuitry, and is the second most common type of amacrine cell in the retina. It is reciprocal to the rod bipolar cell, providing a negative feedback loop.

In addition, smaller numbers of amacrine cells have been found to incorporate dopamine (*Pourcho, 1996*), seratonin (*Vaney, 1986*), and somatostatin (*Pourcho, 1996*) as their neurotransmitters.

2.9.2 Interplexiform Cells

The interplexiform cell is an interneurone, which has processes extending into both the inner and outer plexiform layers. It appears from electron microscopy studies that interplexiform cells form GABA-ergic synapses in the inner plexiform layer with a type of amacrine cell, as yet unclassified, as well as with rod and cone bipolar cells. In the inner nuclear layer and outer plexiform layer the cells make connections with rod and cone bipolar cell bodies and dendrites (*Kolb & West, 1977; Nakamura et al, 1980, Lindberg & Fisher, 1986*). There is also evidence that processes from the interplexiform cells contact cone pedicles via specialised gap junctions (*Lindberg & Fisher, 1986*).

The interplexiform cell appears to provide feedback to the photoreceptors from the inner retinal layers (*Kolb et al, 1992*).

2.10   The Ganglion Cell Layer

The cell bodies of ganglion cells and displaced amacrine cells are located within the innermost nuclear layer of the retina, the ganglion cell layer. It is generally a single cell thick,

except around the macula, where the cells displaced from the central fovea reside. Some displaced Müller cell bodies and astroglial cells may also be found in the ganglion cell layer (*Cohen, 1992*).

2.10.1 Ganglion Cells

Ganglion cells are the final mediator of the retinal part of the visual pathway. By the time the neural signal is passed to the ganglion cells, via synapses in the inner plexiform layer, it has already been modified by the processing which occurs in the vertical and lateral pathways within the outer layers of the retina.

Cajal (*1892*) first used a Golgi staining technique to identify various types of ganglion cell in the vertebrate retina. He classified them according to dendritic morphology, dendritic tree and cell body size, and stratification characteristics in the inner plexiform layer. In 1941 Polyak extended this classification to primate retinas, and identified 6 types of ganglion cells according to shape and size. He named them midget, parasol, shrub, small diffuse, garland and giant. Of these, midget and parasol are most prevalent in the human retina.

Ganglion cells in the cat retina have been described according to their physiological behaviour as X-, Y- and W- cells (*Enroth-Cugell et al, 1966; Cleland et al 1971; Fukada, 1971*). X- cells predominate in the central retina, and show strong, sustained responses to stationary stimuli, whilst being unresponsive to fast-moving stimuli. The X-cell axons have a slower conduction velocity than Y- and W- cells, and thus have longer response latency. Y- cells, by comparison, are more prevalent in the retinal periphery, show transient, weak responses to stationary stimuli, whilst responding strongly to fast-moving stimuli. W- cells have a conduction velocity faster than both X- and Y- ganglion cells (*Stone & Fukuda, 1974*).

Boycott & Wassle (*1974*) found the morphological correlates of the X- Y- and W- type cells. X- type cells were labelled as beta ganglion cells, and Y- type as alpha ganglion cells. They also found two more classes of ganglion cells, which they labelled gamma, and delta. Approximately 3% of cat ganglion cells are alpha cells, whilst 45-50% are beta cells (*Fukuda & Stone, 1974; Stone & Fukuda, 1974*). Both can be further subclassified according to their level of stratification in the inner plexiform layer (*Famiglietti & Kolb, 1976*). Cells which stratify in the outer sublamina, a, are cells with OFF- centre receptive fields, whilst those forming synapses in the inner sublamina, b, have ON- centre receptive fields. ON- and OFF- ganglion cells are always paired, and cover a similar receptive field area. Alpha and beta cells

are arranged in a closely packed pattern across the retina, but there is very little overlapping of dendritic trees of adjacent ganglion cells. This means that, towards the periphery, where the receptive field size is greater, the density of ganglion cells decreases.

In addition to the alpha and beta cells there are 21 other types of ganglion cell, which have been identified in the cat retina (*Kolb, 1981*). These cells constitute 50-60% of the cat ganglion cell population (*Fukuda & Stone, 1974*). These have been named G3-G23, according to cell body size and dendritic form. G3 is equivalent to the gamma cell of Boycott and Wassle, whilst G19 is equivalent to the delta ganglion cell.

At least 18 types of ganglion cell have been identified in the primate retina (*Kolb et al, 1992*). The tonic cells of the primate retina are equivalent in many ways to the cat X- type or beta ganglion cells, showing the same small, concentric receptive fields, predominating in the central retina. The main difference between these and the X-cells of cat, is the colour antagonistic receptive field in the tonic cells of the primate retina. The midget cells identified in the primate retina by Polyak (*1941*) are the morphological correlate of these tonic cells. They project to the parvocellular layers of the lateral geniculate nucleus, and are therefore labelled as P-type. The midget ganglion cell has only a single dendrite, and may be connected to only one midget bipolar, which in turn synapses with only one cone photoreceptor (*Kolb & Dekorvar, 1991*). This leads to a high definition channel, which is also capable of colour resolution. Studies have suggested that up to 80% of the monkey ganglion cell population is composed of midget cells (*Perry, 1984*).

The Y-type or alpha cells of the cat are similar to the phasic ganglion cells of the primate retina, which also respond maximally to transient, fast-moving stimuli. The parasol ganglion cell (*Polyak, 1941*) shows phasic type activity. Parasol cells project to the magnocellular layers of the lateral geniculate nucleus, and are thus described as M-type.

2.11   The Nerve Fibre Layer

The nerve fibre layer consists of the axons of ganglion cells as they run across the inner surface of the retina towards the optic nerve head. Here, ganglion cell fibres turn through 90 degrees to exit the retina through the lamina cribrosa. The ganglion cell axons are unmyelinated as they pass across the retina, which reduces the light scattering properties of this layer.

Figure 2.6 illustrates the path taken by ganglion cell axons as they run parallel to the retina to reach the optic nerve head.
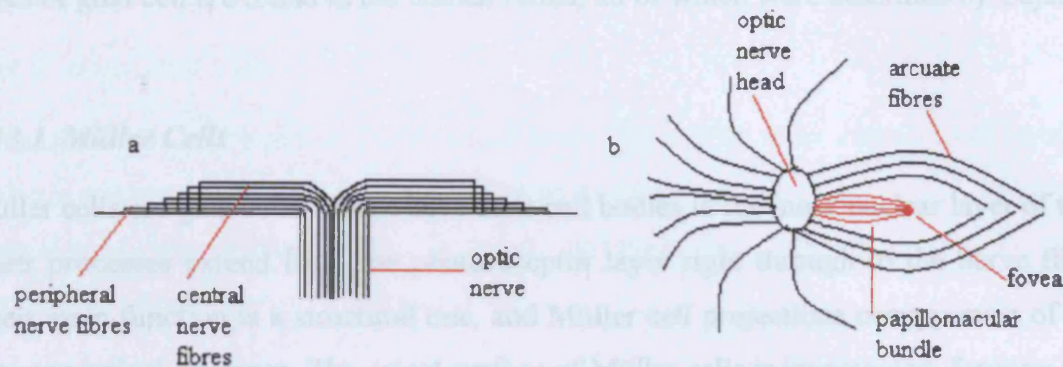
Figure 2.6. a) Cross-sectional illustration of the path taken by central and peripheral nerve fibres towards the optic nerve head. The peripheral fibres underlie the central nerve fibres. b) Illustration of the path taken by temporal, nasal and foveal ganglion cell fibres towards the optic nerve head. Axons from the macula form a spindle-shaped papillomacular bundle, entering the temporal optic nerve head. Temporal fibres take an arcuate course around this bundle, whilst axons from the nasal ganglion cells take a direct course to the optic nerve head (*Henson, 1993*).

Fibres from the macular region form a spindle-like configuration, called the papillomacular bundle, which enters the temporal sector of the optic nerve head. Temporal fibres describe an arcuate path to the optic nerve head as they circumnavigate the papillomacular bundle, whilst nasal fibres take a more direct route. Peripheral fibres are overlaid by more central fibres with decreasing distance from the disc, which results in an increase in the thickness of the nerve fibre layer. The nerve fibre layer is at its thickest at the optic disc margin.

In addition to ganglion cell fibres, the nerve fibre layer also contains vessels of the inner retinal circulation. These may also pass into the ganglion cell layer.

2.12   The Inner Limiting Membrane

The inner limiting membrane is the innermost layer of the retina. It is composed of the lateral connections between Müller cell end feet, and associated basement membrane material. The connection between inner limiting membrane and vitreous is not fully characterised, but in the periphery vitreal fibres are actually incorporated into the inner limiting membrane (*Park et al, 1994*).

2.13 Glial Cells

Glial cells have structural, supportive, buffering and healing roles within the retina. Three types of glial cell are found in the human retina, all of which were described by Cajal in 1892.

2.13.1 Müller Cells

Müller cells are glial cells, which have their cell bodies in the inner nuclear layer of the retina. Their processes extend from the photoreceptor layer right through to the nerve fibre layer. Their main function is a structural one, and Müller cell projections occupy most of the space between retinal neurones. The apical surface of Müller cells is invaginated, forming numerous microvilli, which support the inner segments of the photoreceptors (*Hogan & Alvarado, 1971*). Basal processes of Müller cells insinuate their way between the ganglion axons of the nerve fibre layer, and form sheaths around blood vessels (*Hogan & Alvarado, 1971*). At the inner surface of the retina, Müller cell endfeet, associated with basement membrane material, form the barrier which separates the retina from the vitreous. Embryologically, the Müller cells arise from the neuroepithelium, which is the progenitor of all retinal neurones (*Turner & Cepko, 1987*). It is believed that Müller cells guide developing neurones as they migrate to their final locations and differentiate.

In addition to this supportive role, Müller cells are also involved in retinal metabolism through the provision of glycogen, the mopping up and recycling of waste materials within the retina, and the release of neuroactive substances such as GABA, taurine and dopamine. Müller cells also fulfil a homeostatic role in the retina, through the uptake of extracellular K+ and its redistribution through the retina.

2.13.2 Astrocytes

Embryologically, astrocytes originate from the brain, travelling to the eye along the developing optic nerve (*Stone & Dreher, 1987*). These stellate glial cells are located mainly in the nerve fibre layer of the retina, with the greatest density over the optic nerve head. Astrocytes form a network around ganglion cell axons, and retinal vessels. They have a role in maintaining a blood-brain barrier between the neurones and the inner retinal circulation. Other potential roles include the provision of glucose to neurones from an intracellular

glycogen store, the homeostatic control of extracellular potassium levels, and the metabolism of neurotransmitters.

2.13.3 Microglial Cells

Microglial cells are found in every retinal layer. They arise from mesodermal layers, and as such are not neuroglial cells in the same sense as Müller cells and astrocytes. Microglial cells phagocytose degenerating retinal neurones, and thus their number is seen to increase in response to retinal trauma, or inflammation.

2.14   The Blood Supply to the Retina

The blood supply to the retina consists of two separate circulations, one nourishing the inner layers of the retina, and another providing for the outer retinal layers. All intraocular vessels originate with the ophthalmic artery, a branch of the internal carotid artery. The ophthalmic artery branches to form the central retinal artery, 2-3 posterior ciliary arteries, and several anterior ciliary arteries (*Hayreh, 1962*). The central retinal artery forms the inner retinal circulation, whilst the posterior ciliary arteries are responsible for the choroidal network of vessels which nourish the outer retina.

2.14.1 The Inner Retinal Circulation

The central retinal artery enters the eye through the optic nerve, usually slightly nasally, and immediately bifurcates upon leaving the optic nerve head, forming superior and inferior branches. These both divide once more into nasal and temporal divisions, and these vessels traverse the retina within the nerve fibre layer, just below the internal limiting membrane. These major vessels then continue to bifurcate, forming an intricate network of capillaries. The capillaries consist of a single layer of unfenestrated endothelium, surrounded by a basement membrane, and an irregular layer of pericytes (*Warwick, 1976; Fine & Yanoff, 1979*). The endothelial cells are joined by zonulae occludens (*Hogan & Alvarado, 1971*) and form a blood-retinal barrier limiting the flow of metabolites between retina and circulation.

The capillaries are localised in two layers throughout the majority of the retina. The superficial capillary network runs in the nerve fibre layer, or the ganglion cell layer, whilst the deep network lies in the inner nuclear layer, near the outer plexiform layer (*Toussaint et al,*

1961; Alm, 2003). The extreme retinal periphery is avascular, with vessels terminating in capillary arcades 1mm from the ora serrata. The macular area and areas immediately surrounding arterioles are also capillary-free (*Fine & Yanoff, 1979*).

The retinal circulation is does not anastomose with another system of blood vessels (*Warwick, 1976*). The significance of this is that any occlusion of the retinal vessels will result in irreparable damage to the inner retina. In 15-20% of the population, however, a separate cilioretinal artery enters the retina from the edge of the optic disc. This vessel is derived from the choroidal vasculature, and is able to maintain the viability of the central retina, even in the event of central retinal artery occlusion (*Hayreh, 1963; Alm, 2003*).

The retinal venous blood is drained from the capillary network by the central retinal vein, which usually has one branch in each quadrant of the retina. The central retinal vein leaves the eye via the optic nerve, and then drains into the cavernous sinus.

2.14.2 The Outer Retinal Circulation

The short posterior ciliary arteries, derived from the ophthalmic artery, form the basis of the choroidal circulation. They enter via the sclera at the posterior pole of the eye and bifurcate to form a single layer of anastomosing, fenestrated capillaries. Occasional pericytes are found around the capillary wall, but the fenestrations of the endothelium mean that the choriocapillaris does not form a blood-retinal barrier, and the tight junctions between retinal pigment epithelium cells must fulfil this purpose (*Hudspeth & Yee, 1973*).

The choriocapillaris provides metabolites to the outer retinal layers, and is the only blood supply to the avascular region of the macula, an area approximately 0.5mm in diameter (*Fine & Yanoff, 1979*). The choroidal blood supply is therefore at its densest in the macular area.

2.15   The Macula

The macula is the central region of the retina, which is specialised to provide high-resolution visual acuity. The macula can be defined clinically as an area of the posterior retina 5-6mm in diameter, which is centred on the fovea, and lies within the major vascular arcades. It is the region responsible for the central 15-20 degrees of visual angle (*Bernstein, 1999*). Anatomical definitions primarily demarcate the macular area as that in which that the ganglion cell layer is more than 1 cell thick.

The macular region is comprised of perifovea, parafovea, and fovea. The very centre of the fovea is known as the foveal pit (*Polyak, 1941*). This is the point at which the retina has maximum resolving power, and is packed with a high density mosaic of cone photoreceptors. Rods and S-cones are absent from the foveal pit, but it is the locus of greatest cone density within the retina (200,000 cells per mm^{-2}) (*Curcio et al, 1990*). Despite the high concentration of photoreceptor cell bodies in the outer nuclear layer, the thickness of the retina at this point is at its minimum. This is due to the lateral displacement of second order neurones and inner retinal layers, achieved by oblique elongation of cone cell axons. The absence of bipolar and ganglion cells from the foveal pit ensures that high-resolution central vision is not disturbed by the scattering of light prior to absorption by the photoreceptors. The foveal pit is only 200μm in diameter, but there is some radial displacement of inner retinal layers throughout the foveal region. The elongated cone axons form a pale-staining layer known as the Henle Fibre layer. As a result of the displacement of the second and third order neurones from the foveal pit, the area at the rim of the fovea has ganglion cells piled as deep as 6 layers, making this parafoveal region the thickest part of the retina (*Polyak, 1941*).

The high concentration of photoreceptors at the fovea leads to several structural consequences in the outer retina. Foveal cones tend to take on a more rod-like shape than peripheral cones due to a greater photoreceptor density. Also the ratio of cones to RPE cells at the fovea is 30:1, compared to a ratio of rods to RPE cells of 22:1 in the periphery of the retina, putting a greater load on each RPE cell (*Rapaport et al, 1995*).

Another adaptation in the macula is the presence of macular pigment, which is mainly located in the cone axons of the Henle fibre layer (*Rodieck, 1973*). This pigment consists of a mixture of lutein and zeaxanthin - two xanthophyll carotenoids (*Snodderly et al, 1984*). The macular pigment is believed to have an important role in helping to protect the macula by acting as an antioxidant, and by filtering out short wavelength light (*Snodderly, 1995*).

2.16   From Retina to Visual Cortex

Visual information is channelled into three distinct parallel pathways at the level of the retina. The parvocellular pathway (P-pathway) carries cone-specific information regarding colour and high-resolution vision. The magnocellular pathway (M-pathway), in contrast, receives inputs from both cone and rods, and is concerned with achromatic and low-resolution vision, as well as phasic responses. The konicocellular pathway (K-pathway) is thought to process

information from the S-cones (*Casagrande, 1994; Hendry & Reid, 2000*). Figure 2.7 illustrates the route of these pathways from retina to primary visual cortex.

eye

optic nerve

optic chiasm

optic tract

lateral geniculate
nucleus

optic radiation

primary
visual cortex
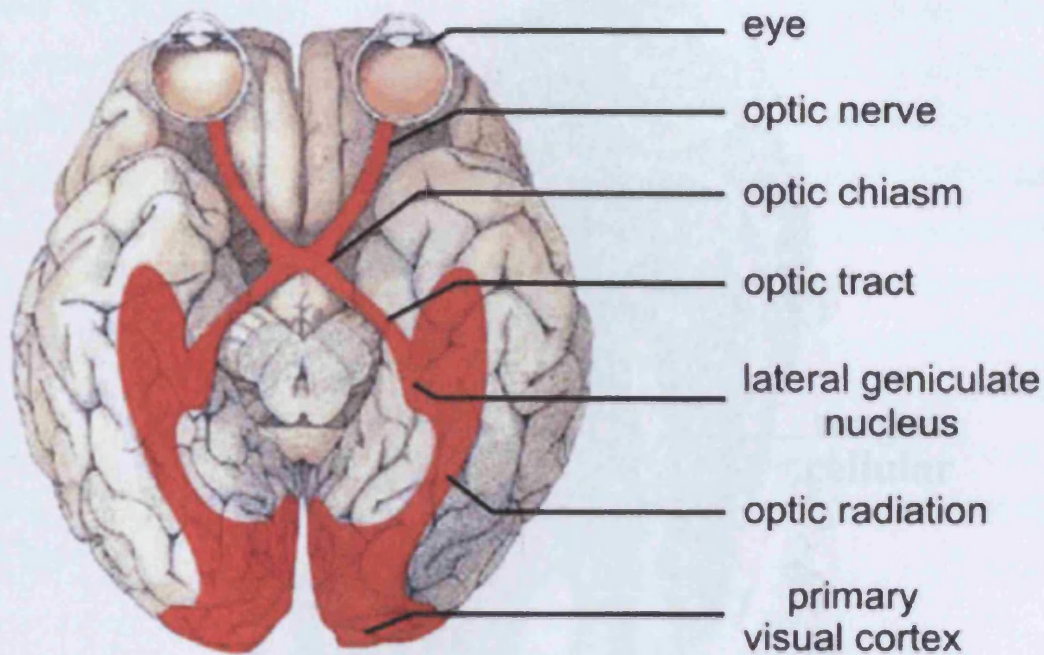
Figure 2.7 Schematic diagram of the visual pathway (*From Hubel, 1988*).

Upon leaving the retina, ganglion cell axons join to form the optic nerve – a bundle of between 1 and 2.2 million visual fibres (*Jonas et al, 1992*). The information from the right and left eyes is kept separate until the optic chiasm. Here the fibres from the nasal retina of both eyes decussate, switching into the optic tract on the opposite side of the brain. This crossing ensures that information from the left side of the visual field is carried to the right side of the brain, and vice versa.

The visual fibres continue without synapsing along the optic tracts to reach the lateral geniculate nucleus (LGN). The LGN is responsible for preparing visual information to be passed on to the visual cortex. It is composed of 6 layers, two of which contain large cells which process magnocellular information, with the remaining 4 layers being responsible for the parvocellular pathway. The tonic midget ganglion cells which predominate in the central retina project to the parvocellular layers of the LGN, whilst the phasic large parasol ganglion cells project to the magnocellular layers (*Rodieck, 1985*). Cells situated between these layers receive information from the K- pathway (*Casagrande, 1994*). The structure of the LGN may be seen in the histological section shown in Figure 2.8. The lateral geniculate nucleus not only relays the visual information on to higher cortical centres, but also receives input from

cortical and subcortical centres of the brain, and reciprocal information from the visual cortex, which allows a modification of the signal (*Lachica, 1993*).
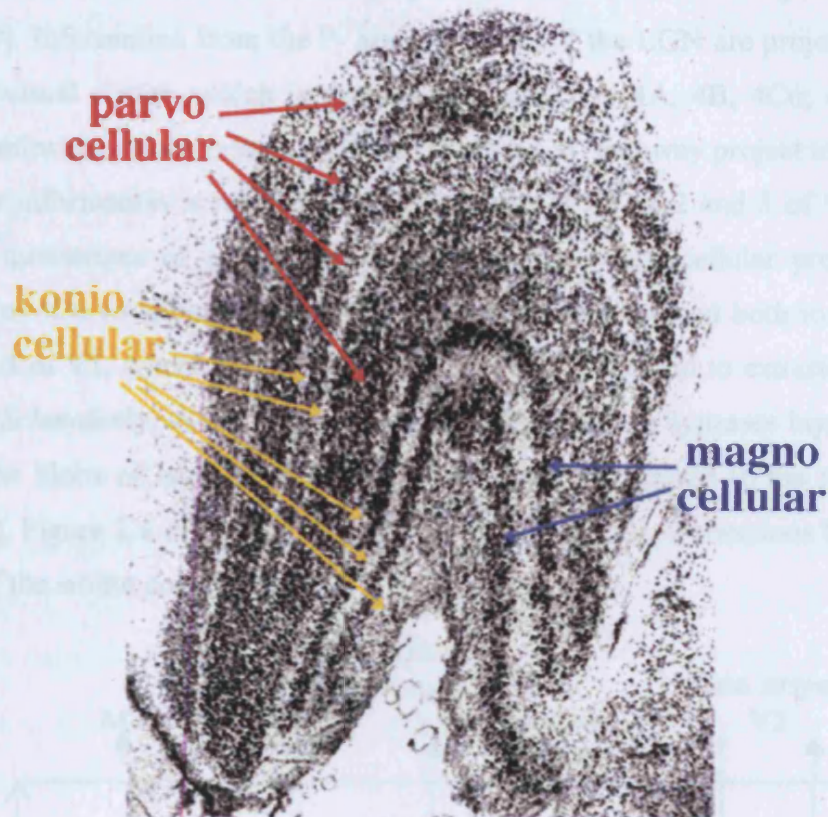
Figure 2.8. Histological section of the LGN showing the parvocellular, magnocellular, and konicocellular regions (*from Gouras, 2001*).

Following the first extra-retinal synapse in the LGN, information is conveyed via the optic radiations to the striate cortex. The optic radiations are a group of fibres, which spread out as they pass laterally and inferiorly through the white matter of the cerebral cortex. They pass through the temporal and parietal lobes of the brain before converging on the primary visual cortex in the occipital lobe (*Warwick, 1976*).

The primary visual cortex (also known as the striate cortex, or V1) is organised into a number of layers. Six layers were originally identified and labelled by Brodmann, but these have since been subdivided. The structure of V1 has also been categorised according to cytochrome oxidase (CO) staining, and has been found to consist of staining areas, known as 'blobs', and non-staining areas called 'interblobs'. Increased cytochrome oxidase staining is indicative of high cellular activity. Cells within the blobs appear in general to have strong colour sensitivity, but poor orientation selectivity (*Regan, 1989*). Blobs receive input from the

magno-, parvo- and konicocellular pathways. In the extrastriate region V2 of the visual cortex, cytochrome oxidase staining shows thin and thick stripes, and pale interstripes.

The 3 parallel pathways for vision each project to different areas and layers of V1 (*Hubel & Wiesel, 1972*). Information from the P- and M- layers of the LGN are projected to layer 4 of the primary visual cortex, which is divided into sublayers 4A, 4B, 4Cα, and 4Cβ. Signals from the P-pathway project to layer 4Cβ, and from the M- pathway project to 4Cα. From here, parvocellular information is relayed to the interblobs of layers 2 and 3 of V1, via layer 4A. then to the interstripes of extrastriate region V2. The magnocellular processing pathway proceeds from 4Cα to layer 4B, from where information is passed both to the interblobs of layers 2 and 3 of V1, where it converges with the P-pathway, and to extrastriate regions MT, V2 and V3 (*Schmolesky, 2000; Regan; 1989*). The K-pathway bypasses layer 4, and projects directly to the blobs of layer 3, from where information is passed to the thin stripes of V2 (*Ding, 1997*). Figure 2.9 illustrates a schematic diagram of the connections between the LGN and layers of the striate cortex.
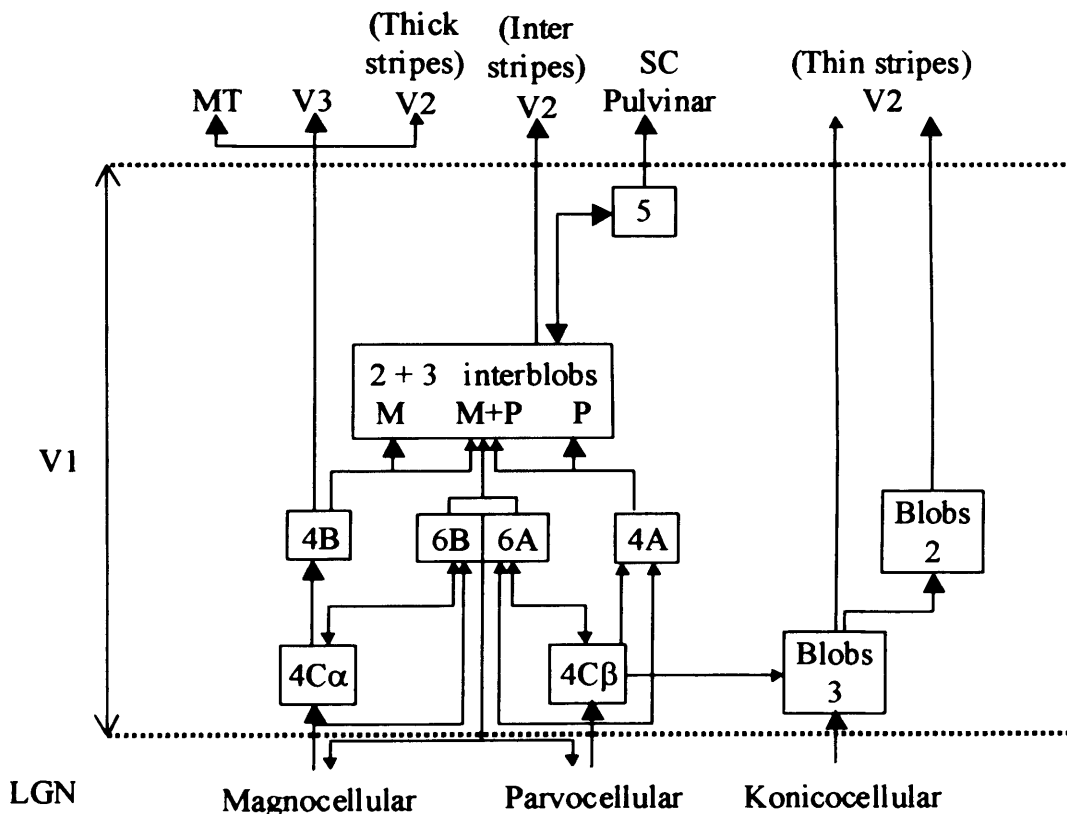
Figure 2.9. The hierarchical arrangement of cortical layers, showing the input from LGN to V1, and the feedback and feedforward pathways. Small arrows indicate minor pathways, large arrows indicate major pathways (*From Regan et al, 1989*).

Three major types of neurone have been identified in the primate V1 through golgi staining techniques (*Hubel, 1988*). Spiny pyrimidal and spiny stellate cells are both excitatory, and

have spiny dendrites. Pyramidal cells have been found in all layers except 1 and 4, whilst stellate cells are located throughout the layers of the striate cortex, and it is with these neurones that axons from the LGN synapse. The smooth or sparsly spinous interneurones mainly form inhibitory GABAergic synapses, and have few or no spikes on their dendrites.

Layers 2 and 3 of V1 have numerous projections to the extrastriate cortical regions (V2, V3, V4, MT) where further processing occurs, and feedback from these regions is processed in layers 1 and 2. V1 layers 5 and 6 are responsible for providing feedback to subcortical regions such as the thalamus, midbrain, and pons (*Schmolesky, 2000*). Feedback to the superior colliculus, for example, is important for visual orientation, foveation, and control of saccadic eye movements (*Horton, 1992*). The feedback from layer 6 to the LGN is important in providing a pathway for the striate cortex to modulate its own input (*Casagrande & Ichida, 1989*).

In addition to the input to the primary visual cortex from the LGN, and feedback from higher visual processing regions, further information is received by V1 from other areas including the brainstem, basal forebrain nuclei, thalamus, and pulvinar (*Casagrande & Ichida, 2003*).

The neurones of V1 exhibit a retinotopic organisation reflecting the location of their receptive fields within visual space. The area of the cortex devoted to each part of the retina is determined by the size of receptive fields in that area. The central retina therefore has a relatively high cortical representation as a result of the higher density of ganglion cells in this region (*Horton, 1991*).

The primary visual cortex also has a columnar organisation (*Hubel & Wiesel, 1972*) with neurones organised according to function and structure (*See Figure 2.10*). All neurones within an ocular dominance column, for example, will be innervated to the same extent by the right and left eyes (*Levay et al, 1980*). Similarly, cells within an orientation column will respond maximally to stimuli of the same orientation. There is an ordered progression in orientation preference as the columns are transversed (*Hubel et al, 1977*). The visual cortex may be construed as having an 'ice-cube' structure consisting of functional modules, within each are cells which have every possible combination of orientation, dominance and colour selectivity.

The ocular dominance columns of layer 4C are innervated completely by either the right or the left eye. These monocular outputs later converge such that other layers are binocular, and innervated to varying extents by each eye (*Horton, 1992*).
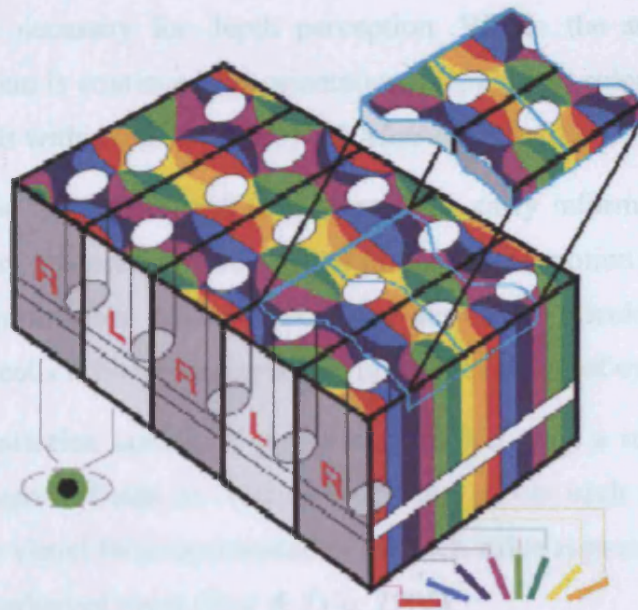
Figure 2.10. Schematic diagram of 'ice-cube' organisation of the primary visual cortex. The white ovals represent the 'blobs'. The coloured 'pinwheels' indicate orientation columns, with each colour representing sensitivity to a specific orientation. The light and dark grey columns separated by black lines represent the ocular dominance columns. The upper slice consists of two functional units, each containing neurones sensitive to all combinations of orientation, ocular dominance and colour coding (*From Van Gisbergen, 2004*).

The primary visual cortex is just the first site of analysis of the visual information. From here the processed neural signals are distributed to more than 30 other specialised visual association areas where further interpretation occurs (*Horton, 1992*). Visual areas and visual association areas in one hemisphere are connected to the corresponding regions of the opposite hemisphere via the posterior portion of the corpus callosum (*Regan, 1989*).

The extrastriate visual cortex receives nearly all visual information from V1 (except for a minor stream directly from the LGN and pulvinar, which may be responsible for blindsight) (*Cowey & Stoerig, 1991*). The main extrastriate projections of V1 are to V2, V3, V4, and V5/MT. The inputs to these different regions arise from different groups of neurones in V1 (*see Figure 2.9*). As described above, area V2 shows patterns of cytochrome oxidase staining, which are seen as thin stripes, thick stripes, and interstripes. The input to the thick stripes is dominated fairly directly by information from the magnocellular pathway, whilst the input to the thin stripes and interstripes appears to be dominated by parvocellular information, through a more indirect pathway. The majority of cells within the thin stripes lack orientation selectivity, and show colour opponent receptive fields, whilst those within the interstripes tend to be orientation selective, but lack colour coding. In comparison, the receptive fields of cells within the thick stripes predominantly show orientation selectivity, and sensitivity to

retinal disparity, a necessity for depth perception. Within the stripes and interstripes a columnar organisation is continued for orientation, disparity or colour opponency, depending on the nature of cells within the stripe (*Boyd & Matsurbara, 2003*).

Projections from the thin stripes and interstripes then carry information to the cortical area V4, involved in form processing. Thick stripes project to the motion processing centre MT, as well as sending information to the subcortical superior colliculus. The retinal disparity sensitivity of these cells is likely to play a role in the generation of eye movements.

A retinotopic organisation continues at the level of V2, with a regular progression in the location of the receptive fields of cells as you move across each stripe. However, there is actually a complete visual field representation for each stripe type such that the visual map of V2 consists of 3 interleaved maps (*Roe & Ts'o, 1995*).

Visual area V3 is divided into dorsal and ventral halves, which represent the lower and upper quadrants of the visual field respectively. These are termed dorsal V3 and the ventral posterior area (VP). Only dorsal V3 receives direct projections from V1, originating in the magnocellular dominated layer 4B. However, both VP and dorsal V3 form connections with V2, MT, and the parietal lobe (*Felleman et al, 1997*). In VP most cells are sensitive to colour and orientation, but not direction, whilst those cells in dorsal V3 tend to be less colour selective, and more direction selective (*Boyd & Matsubara, 2003*).

The other extrastriate region of the visual cortex to receive a primarily magnocellular input is MT. MT is a heavily myelinated area, which represents the complete contralateral visual field. It receives a strong magnocellular input from Layers 4B and 6 of V1, and the thick stripes of V2 (*Movshon & Newsome, 1996*). Area MT has a columnar organisation of cells according to direction and retinal disparity tuning. Cells in MT are also arranged in columns according to either wide-field or local motion contrast sensitivity (*Albright et al, 1984*). Local motion contrast is achieved by antagonistic receptive field surrounds, and allows detection of motion boundaries. Wide-field motion contrast provides information regarding global motion, allowing orientation of an individual within their environment. Information from V3 and MT is relayed to the temporal and parietal lobe areas (*Boyd & Matsubara, 2003*).

Area V4 is located between ventral V3 and MT. It receives projections from V1 and V2, and has inputs from both magno- and parvocellular pathways. Projections from V1 originate in layers 2 and 3, in blobs and interblobs. Both thin stripes and interstripes of V2 project to V4, but input from the two is kept segregated. Cells in V4 are sensitive to parameters which might

be involved in object recognition e.g. colour, orientation, size and binocular disparity. This information is then relayed to the inferotemporal areas of the temporal lobe, which also receive input directly from V2. The inferotemporal cortex contains areas which are sensitive to combinations of stimulus features. For example, some neurones will respond selectively to faces. There is a columnar organisation of cells, with cells within a column responding to similar features (*Wang et al, 1998*).

CHAPTER 3 : AGE-RELATED MACULAR DEGENERATION

3.1 Introduction

Age-related macular degeneration (AMD) is the leading cause of blindness in the Western World (*Leibowitz et al, 1980; Klein et al, 1995; 1999*). It is a condition which ravages the central retina and can have a devastating effect on an individual's lifestyle and independence. Age-related macular degeneration was first described by Haab in 1888, although according to Verhoeff and Grossman (*1935*), the clinical features may have been described as early as 1875 by Pagenstecher. Over the past century, our understanding of the condition has improved, but is still far from complete, and treatments remain limited in their efficacy.

Age-related maculopathy (ARM) is the early form of the disease, characterised by soft indistinct or distinct drusen and RPE abnormalities, but with limited visual function deficits (*Bird et al, 1995; Mitchell et al, 1995; Sarraf et al, 1999*). This may then develop into either nonexudative (dry) or exudative (wet or neovascular) AMD. Dry AMD is characterised by the presence of drusen and atrophy of the retinal pigment epithelium. It is associated with a slow decline in visual acuity. Exudative AMD starts with the growth of new, fragile vessels from the choroidal circulation, which penetrate through breaks in Bruch's membrane to proliferate beneath the retina. In exudative AMD vision may be lost more rapidly, over a larger area, and often at an earlier age than in dry AMD, due to serous or haemorrhagic exudates from the choroidal neovascular vessels. Although far less common than the nonexudative form of the disease, exudative AMD is responsible for eighty-nine percent of cases of legal blindness attributed to AMD (*Ferris, 1983; Ferris et al, 1984*).

3.2 Clinical Features of Age-Related Macular Degeneration

3.2.1 Drusen

First described by Donders in 1854, drusen are deposits of extracellular membranous debris. They may be located between the RPE and its basement membrane (basal laminar drusen) or sandwiched between the RPE basement membrane and the inner collagenous zone of Bruch's membrane (basal linear drusen).

Drusen constitute the first clinically detectable feature of AMD, but do not in themselves define the condition. Drusen, particularly of the small, hard variety, are commonly found even in healthy retinas. For example, in a cross-sectional study of 777 individuals, Bressler et al (*1989*) found more than 80% of individuals over the age of 30 had at least one druse within 1500 μm of the foveal centre. The prevalence of large, confluent or soft drusen is much lower, and is believed to be more indicative of the potential onset of AMD (*Bressler, 1989*).

Drusen may disappear over time. Atrophy of the RPE, choriocapillaris and outer retina may develop as this happens, also sub-RPE globular deposits, and an infolded and collapsed RPE basement membrane may ensue (*Sarks et al, 1999*). However, drusen can regress with no evidence of atrophy. Drusen vary greatly in size, colour, shape, elevation, and in the distinctness of their borders. Some of the main categories are discussed below.

3.2.1.1 Hard drusen

These are small (<63μm), round, discrete, yellowish-white deposits, associated with a local dysfunction of the RPE. They consist of hyaline material, located between the RPE basement membrane, and the inner collagenous layer of Bruch's membrane (*Sarks, 1976*). Microdrusen are focal densifications of Bruch's inner collagenous zone, which may precede the formation of overlying hard drusen (*Sarks et al, 1999*).

Hard drusen are generally regarded as being part of the normal ageing process (*Bird et al, 1995*), although recent epidemiological work has suggested that a high number of hard drusen may lead to an increased risk of development of soft drusen and AMD (*Klein et al, 2002*). The presence of an excessive number of hard drusen at a relatively young age may also increase the risk of RPE atrophy (*Sarks, 1982*).

3.2.1.2 Soft Drusen

Soft drusen are larger in size than hard drusen, and yellow or grey in colour. They are localised between the RPE basement membrane, and Bruch's membrane. They may arise from the enlargement of pre-existing hard drusen (*Sarks et al, 1994*), or can simply form as soft membranous drusen. Their borders may be distinct or indistinct, and several soft drusen may enlarge and coalesce to form confluent drusen. As the drusen each result in a minor

detachment of the RPE, the coalescence of a number of drusen can result in a significant area of detachment, known as a drusenoid pigment epithelial detachment (*Bressler et al, 1994*).

In persons over 55 years of age soft drusen are associated with the presence of a diffuse thickening of the inner aspect of Bruch's membrane (*Bressler et al, 1994*). Large soft drusen have been found to be a significant risk factor for the development of advanced AMD (*Holz et al, 1994*).

3.2.1.3 Basal Laminar Drusen

Basal laminar drusen are numerous small, white, discrete, round deposits located between the RPE and its basement membrane (*Spraul, 1997*). They are composed of hyalinised nodular thickening of the basement membrane of the RPE and are not associated with AMD (*Gass, 1985; Loeffler et al, 1986*).

3.2.1.4 Calcified Drusen

Calcified drusen result from the dystrophic calcification of any other type of drusen, leaving them with a glistening appearance. Calcification of soft drusen usually heralds drusen regression, and the development of RPE atrophy.

3.2.1.5 Reticular Drusen

Reticular drusen are yellowish ribbonlike or lobular areas seen in the outer regions of the macula. Recent studies have indicated that the locus of these drusen is in the inner Bruch's membrane, and that they are associated with geographic atrophy rather than exudative changes (*Jorzic et al, 2002*).

3.2.1.6 Diffuse Drusen

Unlike other drusen types, which are discrete and often visible by ophthalmoscopy, diffuse drusen can only be seen under the microscope, and are characterised by a diffuse thickening of Bruch's membrane. Although such deposits are not themselves clinically visible, they are often accompanied by secondary changes, such as the development of soft drusen, RPE pigmentary changes, and advanced AMD.

Basal laminar deposit is a term referring to the amorphous material, which accumulates between the plasma membrane, and the basement membrane of the RPE (*Sarks, 1976*). This is composed mainly of wide-spaced collagen, but also consists of laminin, membrane-bound vesicles, and fibronectin (*Loeffler et al, 1986; 1992*). It accumulates during the seventh decade of normal ageing. Sarks noted that this deposit tends to accumulate first over thickened segments of Bruch's membrane, and could be the response to altered filtration at these sites (*Sarks, 1976*). It possibly facilitates the passage of membranous debris into the inner collagenous zone by separating the RPE from its basement membrane, predisposing towards the development of soft drusen (*Curcio et al, 1999*).

In contrast, basal linear deposit accumulates external to the RPE basement membrane. It appears to be more specific to AMD than basal laminar deposit (*Curcio et al 1999*). Basal linear deposit consists of granular and vesicular, or membranous debris (*Feeney-Burns & Ellersieck, 1985*), resembling phospholipid bilayers in morphology. There is a tendency for a cleavage to occur between the RPE basement membrane and the inner collagenous layer of Bruch's membrane, which when localised will lead to the formation of soft drusen. Larger breaks can lead to the development of serous RPE detachments (*Green & Enger, 1993*).

3.2.1.7 Drusen Formation

The pathogenesis of drusen remains unclear. One theory is that this extracellular material is composed of basally secreted metabolic waste products from the RPE (*Ishibashi, 1986; Sarks, 1994*). This has been supported by an analysis of the components of the drusen, which have been found to be composed mainly of fatty acids and phospholipids (*Sheraidah et al, 1993*). If this were to be the case, it would indicate that an initial dysfunction of the RPE leads to the incomplete processing of waste products, and the subsequent development of drusen (*Burns, 1980; Green et al, 1985, Ishibashi et al, 1986*).

A second theory of drusen development is that components originate from the blood in the choriocapillaris (*Friedman et al, 1963*). The analysis of the vesicular components of drusen has supported this hypothesis, demonstrating a high concentration of cholesterols similar to those found in atherosclerosis (*Curcio et al, 2001*). Further evidence is provided by animal experiments, which have shown ingested lipids to accumulate in Bruch's membrane (*Curcio et al, 2001*). In view of the conflicting evidence, a third possibility is that drusen are derived from a mixture of both sources (*Pauleikhoff et al, 2004*).

3.2.2   Abnormalities of the Retinal Pigment Epithelium

Clinically evident pigmentary abnormalities, such as focal hyper- and hypo- pigmentation of the RPE, are frequently seen in early AMD. More advanced degenerative changes of the RPE, culminate in areas of geographic atrophy.

3.2.2.1 Focal Hyperpigmentation

Focal hyperpigmentation is clinically visible as regions of pigment clumping. Histologically this has been identified as an increased concentration of melanin in the pigment epithelial cells, a proliferation of the cells themselves, or the migration of pigment epithelial cells into the subretinal space or outer retina (*Bressler et al, 1994*). Focal pigment clumping is often seen overlying soft drusen, but may also be found in eyes with hard drusen only (*Bressler et al, 1990*). The presence of focal hyperpigmentation has been identified as a risk factor in the subsequent development of choroidal neovascular changes (*Bressler et al, 1990*).

3.2.2.2 Focal Hypopigmentation

Focal hypopigmentation of the RPE manifests as small areas of mottled pigmentation. This RPE depigmentation occurs in areas of reduced retinal pigment epithelial melanin density. This may be caused by RPE atrophy, thinning of the RPE overlying drusen, or by a reduction in the melanin content of individual RPE cells (*Pauleikhoff et al, 2004*).

3.2.2.3 Geographic Atrophy

Geographic atrophy constitutes the end stage of dry AMD. It is characterised by a well-demarcated area of RPE atrophy, which is accompanied by the degeneration of overlying photoreceptors, and increased visibility of the underlying choroidal circulation. There may also be regions of altered pigmentation surrounding the area of atrophy. The initial stages of atrophy are often characterised by a sparing of the foveal retina, with parafoveal and perifoveal localised regions of RPE atrophy becoming confluent to form a horseshoe pattern (*Sarks et al, 1988; Schatz, 1989*). Dense scotomas are found to correspond with these areas of atrophy (*Sunness et al, 1995*). Although visual acuity may be maintained whilst the foveal centre is intact, the loss of paracentral vision can make reading and face recognition difficult. Eventually the fovea is also involved, with a consequent reduction in visual function.

3.2.3   Choroidal Neovascularisation

Choroidal neovascularisation usually occurs in the presence of basal laminar and linear deposits in the retina. Capillaries initially grow through Bruch's membrane into the sub-RPE space, where they grow and differentiate into arterioles and venules. This is accompanied by the development of fibrous tissue surrounding the new vessels. The response of the RPE to this new growth differs between individuals. Sometimes the new vessels will be enclosed by a proliferation of the RPE, preventing further neovascular growth (*Miller, 1986*) whilst, in other cases, the RPE will give way to the new vessel development. In some cases the vessels will then penetrate the RPE, to form a subretinal portion to the neovascular membrane.

The neovascular growth may be seen ophthalmoscopically as a greenish grey lesion. The fragile nature of the new vessels means that leakage and haemorrhage is common, and thus neovascularisation is often accompanied by sub- or intraretinal haemorrhages, hard exudates, or pigment epithelial detachment. Symptoms accompanying the growth of these new vessels include metamorphopsia and blurred vision. Although the clinical signs and symptoms described will often indicate the presence of choroidal neovascularisation, it is generally investigated and classified by means of fluorescein angiography.

3.2.3.1 Fluorescein Angiography

Fluorescein angiography is a technique, which involves the intravenous injection of a fluorescent dye. It was initially developed to assess the status of the inner retinal vasculature, but has also been found to be of value in the evaluation of the choroidal circulation, the integrity of the RPE, the distribution of drusen, and the presence of subretinal fluid or haemorrhage.

Sodium fluorescein is a substance which fluoresces when exposed to blue light. Intravenous injection of the dye is therefore followed by illumination of the retina with blue light, and the fluorescence emitted is recorded on a series of fundus photographs. In this way, the dispersal of fluorescein through the retina may be monitored. Fluorescein molecules are able to freely move out of the fenestrated capillaries of the choroidal circulation, but the tight junctions between adjacent retinal capillary cells prevents the egress of the dye from the inner retinal circulation. Furthermore, the healthy retinal pigment epithelium acts as a barrier to prevent the movement of fluorescein from the choroid to the retina. A glow of fluorescence is therefore

seen from the underlying choroid, which is interrupted only by the presence of melanin in the RPE, and macular pigment at the fovea.

Defects of the RPE, Bruch's membrane, or the choriocapillaris are often visualised as fluorescein angiographic abnormalities, manifesting as areas of hypo- or hyperfluorescence. Hypofluorescence is caused when substances such as lipid, haemorrhagic blood, or pigmentation block the normal level of fluorescence. It may also reflect a vascular abnormality, indicating the non-perfusion of choroidal vessels due to vessel closure or atrophy.

Hyperfluorescence may be caused by a reduction in melanin and intraretinal pigment, which block the transmission of fluorescence from the choroidal circulation. This is referred to as a transmission, or window defect, and can be caused by death or attenuation of RPE cells, or a reduced density of melanin within existing cells. Soft drusen may also cause hyperfluorescence through damage to the overlying RPE, as well as through fluorescein pooling within fractures in the deposits. Hyperfluorescence may also indicate choroidal neovascularisation, or breaks within the RPE, allowing the pooling of fluorescein within the subretinal space.

Choroidal neovascularisation can be classified according to the location and nature of the hyperfluorescence. Classic choroidal neovascularisation is seen as a well-defined hyperfluorescent area during the early stages of fluorescein angiography, which becomes enlarged and indistinct in the later phases due to leakage. Histologically this pattern of hyperfluorescence reflects a neovascular membrane, which has proliferated between the RPE and the neurosensory retina. Occult choroidal neovascularisation shows a less regular pattern of hyperfluorescence, which has consistently indistinct borders. This reflects the growth of new vessels between the RPE and Bruch's membrane. Combined occult and classic choroidal neovascularisation may occur in the same eye.

3.2.4   *Pigment Epithelial Detachment*

A detachment of the retinal pigment epithelium (PED) is clinically visible as a well demarcated, round elevation of the retina. It is usually confined to the macular region, and is caused by the accumulation of fluid between the retinal pigment epithelium and Bruch's membrane. This is a further manifestation of exudative AMD.

Occult choroidal neovascularisation has been found to underlie the formation of a pigment epithelial detachment in 28-58% of cases (*Lim et al, 1997*). Fluid may leak from the fragile new vessels, or rupture may lead to a haemorrhagic detachment. The fibrovascular membrane itself may cause a PED by mechanically raising the retinal pigment epithelium. Hard exudates, subretinal fluid, or subretinal haemorrhage will often be associated with a vascular PED.

The formation of a serous PED is usually preceded by the confluence of soft drusen. Distinguishing between vascular and avascular PEDs may be facilitated by fluorescein angiography, whereupon an avascular, or serous PED will be seen as an area of early hyperfluorescence, which does not expand with time, and maintains a well-defined border. In contrast, a PED associated with occult choroidal neovascularisation will show an irregular filling of the PED, often with blurred edges, and a leakage in the later photographic frames.

The PED may spontaneously flatten over time, although tearing of the RPE may also occur in about 10% of patients (*Chuang & Bird, 1988; Pauleikhoff et al, 2002*). The end stage tends to be either subretinal fibrosis or geographic atrophy, and the visual acuity outcome is usually poor (*Caswell et al, 1985*).

3.2.5   Disciform Scar

The formation of a disciform scar constitutes the end-stage of exudative age-related macular degeneration. Upon ophthalmoscopy the scar may vary in colour from yellow, white, brown, or even black. It may also be associated with blood, lipids or exudates. The formation of a disciform scar leads to an irreparable loss of vision.

This subretinal or sub-RPE fibrous tissue develops as a consequence of choroidal neovascular vessel haemorrhage and leakage, which leads to the proliferation of a fibrovascular membrane beneath the RPE. Any scar tissue, which forms above the RPE tends to be avascular and results from RPE hyperplasia. The sub-RPE scar tissue may contract, causing a rip of the RPE, thus allowing subretinal and sub-RPE fibrous tissue to become continuous (*Green & Enger, 1993*).

3.3   Classification of Age-Related Macular Degeneration

Many clinical and epidemiological studies have been carried out into age-related macular degeneration. Various definitions and severity scales have been used in these different studies. For example, the Framingham Eye Study (*Sperduto & Siegel, 1980*), a population based epidemiological study, relied on visual acuity and ophthalmological opinion. By comparison, the Beaver Dam Eye Study (*Klein et al, 1997*) used the Wisconsin Grading Scale (*Klein, 1991*), a system involving the grading of specified pathological features, using stereo fundus photographs. This variation in grading and classification may be problematic in the comparison of results from different study groups.

In an effort to address this problem, The International ARM Epidemiological Study Group published a report describing a standardised grading system (*Bird et al, 1995*). According to this system, the classification of early and late ARM is solely based on fundus appearance, as assessed by stereo photographs. Table 3.1 summarises the diagnostic criteria outlined in the International Classification and Grading System for the classification of AMD.

Condition	Diagnostic Features
Early ARM	Drusen with or without associated pigment and/or focal hypopigmentation of the RPE
Late AMD (Dry)	Area of geographic atrophy > 175μm in diameter
Late AMD (Wet)	One or more of the following: RPE detachment SubRPE/Subretinal neovascular membrane Disciform scar Subretinal Haemorrhage Hard exudates

Table 3.1. A summary of the classification of AMD according to the International Classification System (*Bird et al, 1995*).

3.4   Pathogenesis of Age-Related Macular Degeneration

3.4.1   Pattern of Photoreceptor Loss in Ageing and AMD

Post-mortem examination of the retinas of donor eyes has provided some insight into the pattern of cell loss associated with normal ageing. Curcio et al (*1993*) studied 24 eyes aged

27-90 years, and recorded the spatial density of cones and rods subserving the central 43° of vision. No consistent age-related changes in cone density were found at any retinal location, and the total number of foveal cones appeared to be constant throughout all age groups. In the case of rods, however, density was found to decrease by 30% within the central 28.5° of retina with increasing age through the range tested. The initial locus of rod loss was found to be within a parafoveal ring, extending from 3.5-10° from fixation, and beginning in the inferior retina. No gaps were found in the photoreceptor mosaic, but surrounding rod outer segments were enlarged to fill spaces vacated by dying rods. This ensured constant rod coverage and rhodopsin density throughout eyes of all ages. The selective loss of rod photoreceptors appeared to apply to the central retina only.

To determine whether the preferential loss of rod photoreceptors might be part of a continuum which eventually manifests as AMD, Curcio conducted a further post-mortem study (*Curcio et al, 1996*). Thirteen donor eyes were harvested and examined, all of which showed signs of mid to late AMD.

The foveal cone mosaic of eyes with non-exudative AMD appeared normal. However, in the parafovea distinct abnormalities were noted, such as areas (up to 30 μm in diameter) in which cone inner segments were adjacent to each other without intervening rods - a situation rarely found in the parafovea of healthy eyes. In the areas of retina overlying RPE atrophy, both rod and cone loss were discovered, with few rods being detected at all in these areas. Photoreceptor loss was found in all cases to be greatest in the parafoveal retina.

In eyes with exudative AMD few rods survived adjacent to areas of RPE disruption. Rod loss was particularly notable in areas overlying active neovascularisation. In total, 6 out of 10 eyes showed more extensive rod loss than cone loss in this study. Curcio et al (*1996*) suggested that rod loss occurs physiologically in older eyes, but in some eyes the RPE becomes dysfunctional, secondary to which rod loss continues past the stage noted in healthy older eyes, and cones also become involved. Eventually only small islands of cones remain, which may be sufficient to sustain vision for some time. Ultimately, all photoreceptors may disappear from the affected region if geographic atrophy or disciform degeneration develops.

This study also highlighted the fact that greatest cell loss in ARM and AMD appeared to occur within the parafoveal/perifoveal region, extending from 1.5-10° from fixation. This is consistent with the theory that this area is the site of earliest non-exudative AMD involvement (*Schatz et al, 1989*). Defects in visual function are reported in non-exudative patients

particularly in the region from 5-10° from fixation (*Sunness et al, 1995, Owsley et al, 2000, Curcio et al, 2000*), and this is also the region in which the incidence of RPE atrophy is at its greatest (*Aschero et al, 1993*).

If rods are preferentially affected by AMD, the next question might be why the death and degeneration of cones invariably follows. The same situation is seen in retinitis pigmentosa, in which there is an initial phase of rod loss, followed by a second wave of cone cell death - even when the mutant gene affects rod structural proteins alone. Cone loss appears to be, therefore, spatially and temporally correlated with rod loss (*Cideciyan et al, 1998*). One theory is that rods may produce a chemical signal which is required for the continued survival of neighbouring cones, and that the deprivation of this signal from the cones results in the triggering of a degeneration process (*Hicks and Sahel, 1999*). Evidence for this hypothesis is provided by studies on the retinal degeneration (rd) mouse, which exhibits mutations in the gene coding for the β subunit of rod cGMP phosphodiesterase (a defect seen in some human forms of retinitis pigmentosa). In this animal, rod degeneration is rapid and almost total by 1 month after birth (*Carter-Dawson et al, 1978*). Thus, if a retina is taken from the rd mouse 1 month after birth, a rod-free state is assumed to exist. In the normal state cones are lost shortly after rod loss is complete. However, when fragments of retina are taken from a normal mouse and transplanted into the subretinal spaces of the rod-free retina, cone loss is significantly reduced in the host retina (*Mohand-Said et al, 1997*). A further study indicated that, if an rd mouse retina is separated from a normal mouse retina by a semi-permeable membrane, more cones survive in the target retina than in age-matched controls (*Mohand-Said, 1998*). This suggests that a diffusable substance produced by rods is responsible for maintaining cone vitality in the healthy retina.

3.4.2 Changes to the Retinal Pigment Epithelium

Age-related changes to the retinal pigment epithelium appear to play an important role in the pathogenesis of age-related macular degeneration. One major function of the RPE is the phagocytosis of the tips of photoreceptor outer segments, and the processing of the waste components. This material is subsequently released into the choroidal circulation. Any disturbance of this cycle may lead to the incomplete degradation of phagocytosed material, and its accumulation within the retinal pigment epithelium as lipofuscin (*Boulton et al, 1989*).

One factor, which may predispose towards the formation of lipofuscin is the peroxidation of lipids in photoreceptor outer segments as a result of oxidative stress. The retina is particularly vulnerable to photo-oxidative damage conferred by a high oxygen demand, prolonged light exposure, and the presence of polyunsaturated fatty acids (*Beatty et al, 2000*).

Free radicals are formed in response to normal metabolic activity in the mitochrondria of cells (*Hagen et al, 1997*). Photosensitive molecules also produce free radicals in response to light absorption (*Spaide et al, 2003*). Free radicals react with other molecules in order to scavenge electrons, causing molecular damage to proteins, carbohydrates and lipids. The oxidation of lipids by these free radicals results in the formation of peroxidised lipids, which themselves oxidise other lipids in a self-propagating reaction. These active molecules also cross-link with other molecules to form advanced lipoxidation end products (*Spaide et al, 2003*). These abnormal molecules are difficult for the RPE to break down (*Brunk & Collins, 1981*). Indigestible material is stored within the RPE as lipofuscin granules (*Bazan et al, 1990; Wiegand et al, 1983; Katz et al, 1996*), or extruded into Bruch's membrane (*Rungger-Brandle et al, 1987*).

RPE cell density also declines with age (*Panda-Jonas et al, 1996*), with surrounding cells spreading to compensate. The debris produced by the death of these cells may add to the accumulation of deposits in Bruch's membrane (*Burns & Feeney Burns, 1980*), as well as increasing the metabolic load on remaining cells. Although lipofuscin is believed to be primarily a by-product of the breakdown of photoreceptor outer segments, there is also evidence to suggest that material from the autophagy of apoptotic RPE cells may contribute (*Schutt et al, 2002*).

Such factors predispose towards the age-related accumulation of lipofuscin in the RPE. At the age of 80, the amount of RPE cytoplasmic space filled with lipofuscin has increased to 90%, from only 8% at the age of 40 years (*Feeney-Burns et al, 1980*). The distribution of lipofuscin granules in the human retina increases with decreasing retinal eccentricity, forming a peak in a perifoveal ring in the macula, with a well-defined dip at the fovea (*Wing et al, 1978*). This distribution might be expected in view of the higher ratio of photoreceptors to RPE cells in the macular region than the periphery, which places a greater metabolic load on the individual cells (*Dorey et al, 1989*).

The damage caused to the RPE cells by this substance is not purely mechanical, but also toxic. Lipofuscin has been shown to have the toxic effect of inhibiting lysosomal enzymes

(*Holz et al, 1999*), and RPE antioxidants (*Shamsi & Boulton, 2001*), and also has detergent properties, which may cause cell death through the disintegration of organelle membranes (*Schutt et al, 2002*). Furthermore, lipofuscin is a photosensitive compound, which produces free radicals on absorption of light (*Boulton et al, 1993, Wassall et al, 1999*). This process propagates oxidative damage to the RPE (*Galliard et al, 1995*). It has been suggested that there is a threshold lipofuscin concentration in the RPE, above which macular degeneration occurs (*Sohal & Donato, 1978; Boulton & Marshall, 1986*). This is supported by previous findings that the annular pattern of macular degeneration is well correlated with the area of greatest lipofuscin concentration (*Weiter et al, 1988; Holtz et al, 2001*). Further evidence for a pathogenic role for lipofuscin is found in other macular conditions, such as Best's and Stargardt's disease, which also show increased lipofuscin concentration in the pathogenic macular area.

3.4.3   Changes to Bruch's Membrane

Bruch's membrane consists of collagen and elastic fibres, which form a sieve-like structure. It provides support and anchorage for the RPE, and also forms a semi-permeable membrane which allows the passage of biomolecules, up to a certain size, between the choriocapillaris and the RPE. Nutrients, oxygen and retinoids pass from the choroidal circulation to the outer retina. Metabolic waste products from the photoreceptors and RPE traverse the membrane in the opposite direction to reach the choroidal circulation (*Guymer et al, 1998*).

There are a number of age-related changes, which occur to Bruch's membrane. Changes occuring to the collagen fibres of Bruch's membrane include increased cross-linkage, denaturisation, and chemical changes, such as glycosylation. The effect of these changes is to greatly reduce the solubility of the collagen (*Karwatowski et al, 1995*), and also to render the fibres less susceptible to collagenolytic enzymes of the RPE, resulting in a less efficient turnover of collagen (*Guymer et al, 1998*). Changes also occur to the elastic layer of Bruch's membrane, which increases in density, undergoes calcification, and becomes basophilic, thus making the layer more brittle (*Loeffler et al, 1986*).

The increased density of the fibrous components of the membrane, and the deposition of material in the inner layers of Bruch's (basal laminar and linear deposits), mean that the membrane becomes more resistant to the passage of materials from the RPE to the choriocapillaris. This is accompanied by a reduction in the basal infoldings of the RPE plasma

membrane, which also results in a progressive decline in active transport with age (*Sarks et al,* *1988*). Furthermore, an age-related increase in the inter-fibril concentration of the proteoglycan heparin sulphate in Bruch's membrane could impede the passage of negatively charged macromolecules between the choroidal circulation and outer retina (*Marshall, 1987;* *Guymer et al, 1998*). Bruch's membrane therefore begins to alter in its filtration properties, predisposing towards the accumulation of further waste products internal to the membrane, and forming a barrier to normal metabolic exchange.

Water permeability of Bruch's membrane also decreases with age (*Pauleikhoff et al, 1990*), a characteristic which may be caused by age-related lipid accumulation (*Pauleikhoff et al,* *1994*). This lipid accumulation is higher in the macula than the peripheral retina (*Holz et al,* *1994*). The ratio of neutral lipids to polar phospholipids in Bruch's membrane also becomes greater with age (*Sheraidah et al, 1993*), which could further impact upon the diffusion properties of the membrane.

There is a general age-related increase in the thickness of Bruch's membrane, from approximately 2 μm at birth, to 4-6 μm in the tenth decade of life (*Ramratten et al, 1994*). This thickening is attributed to accumulation of RPE-derived debris in the inner collagenous layer and, later, in the elastic layer (*Farkas et al, 1971*). Changes in thickness are also associated with the changes in collagen composition and cross-linkage, increase in glycosaminoglycan size, increased lipid deposition and impaired ability to degrade extracellular material such as collagen and elastin (*Zarbin, 2004*). A linear relationship has been found between lipofuscin accumulation in the RPE and Bruch's membrane thickness, suggesting that the two factors may be associated (*Okubo et al, 1999*).

3.4.4 Changes to the Choroidal Circulation

The choriocapillaris also undergoes age-related changes. Increasing age leads to a reduction in vessel diameter and an increase in intercapillary spaces. The choriocapillaris density decreases by 45% over 10 decades of life (*Ramratten et al, 1994*). There is also a decline in the number of choroidal capillaries (*Olver et al, 1990*). These factors, combined with a reduction in the thickness of the vascular layer (*Ramratten et al, 1994*), have the effect of reducing blood flow, which may contribute to RPE dysfunction (*Holz et al, 2004*).

It is not known whether changes to the choroidal circulation precede, or are a result of abnormalities of Bruch's membrane. It is possible that the age-related changes to Bruch's

membrane might form a barrier to diffusable agents produced by the RPE which regulate the morphology of the choriocapillaris (*Guymer et al, 1998*). Conversely, the abnormality of the choroidal circulation might constitute the primary defect, and could be responsible for impeding the removal of material from Bruch's membrane, resulting in the accumulation of waste products in that layer (*Guymer et al, 1998*).

3.4.5 Choroidal Neovascularisation

Histological examination has suggested some possible causes of the development of choroidal neovascularisation, although the precise mechanism remains unknown. One theory is that new vessel growth is instigated by an inflammatory type of reaction. This is supported by the finding of macrophages and leukocytes within the damaged area of Bruch's membrane (*Penfold et al, 1985; Killingsworth et al, 1990*), and within drusen (*Mullins et al, 2001*). Alterations to retinal microglia are seen in early AMD, which together with the presence of soluble transmitters, cytokines, provides further support for an immunological basis to choroidal neovascularisation (*Penfold et al, 1997; 2001*). This immune response may be instigated by the destruction of Bruch's membrane (*Feeney-Burns & Ellersieck, 1985; Killingsworth et al, 1990*), by chemical substrates such as phospholipids (*Pauleikhoff et al, 1990*), or by advanced glycation end products.

A further theory is that an alteration in the permeability of Bruch's membrane, caused by lipid deposits, is responsible for the onset of choroidal neovascularisation (*Pauleikhoff et al, 1992*). It has been suggested that a reduction in the permeability of Bruch's membrane impedes the diffusion of growth factors from the RPE to the choriocapillaris (*Moore et al, 1995*). A well-regulated balance of factors from the RPE is necessary for the healthy function of the choriocapillaris. These include pigment epithelial derived factor (PEDF), Angioprotein (Ang1), and vascular endothelial growth factor (VEGF). VEGF is a survival factor required by the choriocapillaris. A reduction in the level of VEGF reaching the choriocapillaris therefore results in degenerative changes.

It has been hypothesised that outer retinal ischaemia induced by changes to the choroidal circulation in AMD might result in an increased production and expression of the growth factor VEGF by the RPE. This has been supported by findings of increased VEGF levels in the vitreous of patients with ischaemic retinal disease, and also in excised choroidal neovascular membranes (*Aiello et al, 1994; Lopez et al, 1996*). A resultant imbalance in levels

of angiogenic VEGF, and antiangiogenic PEDF may be responsible for choroidal neovascular changes. Animal models indicate that increased secretion of VEGF by RPE cells can induce neovascularisation (*Spilsbury et al, 2000*). However, less than 1% of available oxygen is extracted from the choroidal circulation by the RPE (*Spaide et al, 2003*), which may leave a wide margin before ischaemic changes impact on RPE function.

Another source of increased levels of VEGF may be the response of the RPE to oxidative damage. The response of the RPE to the formation of advanced glycation and lipoxidation end products is for macrophage scavenger receptors such as CD-36 to bind to the abnormal molecules (*Ryeom et al, 1996; Smedsrod et al, 1997*). This process triggers an increased expression of VEGF, and also the expression of factors which allow vascular endothelial cells to form capillary tubes more efficiently (*Spaide et al, 2003*).

It seems likely that a combination of these factors may be involved in the process of choroidal neovascularisation.

3.4.6 Pigment Epithelial Detachment

Serous or avascular PEDs are often associated with basal laminar and basal linear deposits. These deposits result in a decrease in the adhesive forces between the RPE and Bruch's membrane (*Pauleikhoff et al, 2002*). The water permeability of Bruch's membrane also decreases with age, and the resulting impediment to the net flow of fluids from the retina towards the choroidal circulation may result in the accumulation of fluid in the sub RPE space (*Bird & Marshall, 1986*). A detachment of the RPE and its basement membrane from the remaining layers of Bruch's membrane ensues (*Green et al, 1985*).

3.4.7 Geographic Atrophy

Geographic atrophy is caused by the death of RPE and outer retinal cells. Excessive lipofuscin accumulation has been linked to cell death in these regions. Areas of atrophy have been found to correspond well with the location of lipofuscin deposition (*Holtz et al, 2001*).

Histologically, the underlying choriocapillaris is often found to be sclerosed or atrophied, suggesting a possible involvement of vascular abnormalities in the pathogenesis of geographic atrophy (*Green & Harlan Jr, 1999*). Basal laminar and linear deposits are also usually present

in eyes with geographic atrophy. These deposits within Bruch's membrane may lead to RPE cell damage and drusen formation (*Young, 1987*).

Healthy photoreceptor function requires the provision of metabolites and vitamin A (retinol) by the choroidal circulation. A combination of choriocapillaris atrophy and reduced permeability of Bruch's membrane could therefore compromise photoreceptor function, leading eventually to cell death and retinal atrophy (*Guymer et al, 1998; Curcio et al, 2000*).

Geographic atrophy can also develop secondary to the regression of drusen, the flattening of a pigment epithelial detachment, or choroidal neovascularisation.

3.4.8   Haemodynamic Model for the Pathogenesis of AMD

Most hypotheses regarding the pathogenesis of dry AMD suggest that a primary defect in the RPE layer is the instigator of subsequent pathologic changes (*Eagle, 1984; Bird, 1997*). The haemodynamic model, however, theorises that AMD is a vascular disorder, which is characterised by changes to the choroidal circulation (*Friedman, 2004*). According to this model, choroidal vascular resistance is increased due to progressive infiltration of lipids into ocular tissues (*Friedman, 1989*) and blood flow is reduced due to age-related changes to the choriocapillaris. The resultant impairment in the choroidal circulation and perfusion hinders the removal of waste from the RPE, leading to drusen formation, RPE changes, geographic atrophy and Bruch's membrane changes. A combination of elevated choroidal pressure, breaks in Bruch's membrane, and an imbalance in the production and diffusion of growth factors from the RPE is postulated to be responsible for the development of choroidal neovascularisation.

Evidence supporting his hypothesis lies in the strong link between AMD and risk factors predisposing to systemic atherosclerosis (*Friedman, 2000*). There have also been reports suggesting that the fellow, healthy eye of patients with unilateral exudative AMD still exhibits choroidal circulatory abnormalities, in the absence of gross RPE changes (*Dimitrova, 2002*). The implication of this is that slowed choroidal perfusion may precede RPE changes.

3.4.9   Genetic Involvement in the Development of AMD

There is strong evidence to suggest that genetic factors may contribute to the development of AMD (see section 3.5.2). A complex condition such as AMD, however, is inevitably

mediated by a combination of factors, which may involve a number of gene loci, as well as environmental influences. In order to determine which genes may be involved in the development of AMD, comparisons have been made with monogenic conditions, which exhibit similar phenotypic traits.

One gene, which has been the source of considerable debate with regard to AMD is the ATP-binding cassette transporter (ABCA₄). This gene is located in photoreceptor outer segments (*Papermaster et al, 1978*), and has been shown to be mutated in Stargardt's disease (*Allikmets et al, 1997a*). Given the phenotypic similarities between Stargardt's disease and AMD, there have been several studies of the possible role of this gene in the pathogenesis of AMD. One study suggested that ABCA₄ may be involved in as many as 16% of AMD cases (*Allikmets et al, 1997b*), although a number of subsequent reports have been unable to support this finding (*Stone et al, 1998; De La Paz et al, 1999; Guymer et al, 2001; Webster et al, 2001*).

Another way of identifying the locus of genetic involvement in AMD is to investigate the biochemical pathways, which might logically be affected in the disease process. For example, paraoxonase-1 (PON₁) is a gene which prevents low-density lipoprotein oxidation (*Ikeda et al, 2001*). Another gene which helps protect tissues against oxidative stress is mitochondrial superoxide dismutase-2 (SOD₂) (*Kimura et al, 2000*). Apolipoprotein E (APOE) is a gene which is associated with the monogenic disease hyperlipoproteinemia. Its involvement in AMD is suspected in view of its role in lipid mobilisation and redistribution, and in the maintenance and repair of neural cell membranes (*Mahley, 1988; Boyles et al, 1989, Klaver et al, 1998; Schmidt et al, 2000*). Although mutation of these genes may have a role in the pathogenesis of AMD, this remains to be proven.

3.5   Risk Factors for the Development of Age-Related Macular Degeneration

Changes to the outer retina, RPE, Bruch's membrane, and choriocapillaris occur in every eye as a function of age, but only in some individuals do these changes culminate in the development of AMD. Certain factors have been identified through epidemiological, prospective and cross-sectional studies as being influential in the progression of these physiological changes to a pathological end-stage.

3.5.1   Age

The strong relationship between age and AMD has been well documented. The Beaver Dam study, for example, demonstrated that during the 5 year period of the study, people aged 75 or older at baseline were six times more likely to develop early AMD than those aged between 43 and 54 years (*Klein et al, 1997*).

3.5.2   Genetic

Studies into the epidemiology of AMD have found a very definite familial effect on the incidence of AMD. One large study based on maternal and sibling records, for example, reported that a family history of AMD was the strongest predictor of the onset of the disease (*Hyman et al, 1983*). Another report based on twins found 100% concordance rate of AMD in 23 monozygotic twin pairs, and 25% in 8 dizygotic pairs, suggesting a strong genetic predisposition to AMD (*Myers, 1994*). Evidence has also been found for a genetic predisposition towards drusen development (*Piguet et al, 1993*). As yet the exact locus of the predisposing genetic factors is unknown.

3.5.3   Race

A number of studies have indicated that black people are at less risk of developing late AMD than white people. For example, Gregor and Joffe (*1978*) compared a group of 1000 South African black people with 380 white people, and found that exudative macular degeneration was diagnosed in 0.1% of the eyes of the black group, and 3.5% of the eyes of the white group. Another study in East Baltimore found that 30% of bilateral blindness in whites was due to AMD, whereas none of the black group had lost the sight of both eyes through the condition (*Sommer, 1991*). This difference may be due to melanin, which provides a protective effect, although genetic differences may also be involved.

Other studies of the prevalence of AMD in Hispanics have produced mixed results. Two studies indicated a possible reduced prevalence among Hispanics compared to non-Hispanic whites, but the populations studied were small, and possibly unrepresentative (*Cruickshanks et al, 1997; Klein, 1995*).

3.5.4 Gender

Studies into the epidemiology of AMD in various communities have reached different conclusions regarding the influence of gender as a risk factor for the development of AMD. Smith et al (*1997*) pooled data from three other studies i.e. Beaver Dam (*Klein et al, 1997*), Rotterdam (*Vingerling et al, 1995a*), and Blue Mountains (*Mitchell et al, 1995*). They reported that women had a higher frequency of later AMD than men (odds ratio [OR] 1.15, 95% confidence interval [CI] 1.1 to 1.2). A recent comparison of a large number of population based prevalence studies also found a slightly increased risk for women of developing any type of AMD (OR 1.13, 95% CI 1.01, 1.26) (*Evans, 2001*). One reason for this difference may be the menopause, which eliminates the protective effect of oestrogens against atherosclerotic changes (*Witteman et al, 1989*). This theory is supported by reports that an early onset of the menopause is associated with an increase in the risk of late AMD (*Vingerling et al, 1995b*), whilst a delayed menopause is conversely associated with a decreased risk (*Smith et al, 1997*). Furthermore, it appears that women using oestrogen replacement are at a lower risk of choroidal neovascularisation than those who are not (*The Eye-Disease Case-Control Study Group, 1992*).

3.5.5 Vascular

There is strong evidence to suggest that atherosclerosis of the choroidal circulation is a risk factor for the development of AMD (*Verhoeff & Grossman, 1937; Vingerling et al, 1995d*). Factors predisposing towards atherosclerotic changes, such as hypertension, cigarette smoking and dyslipidaemias, have been found to confer an increased risk of AMD (*Vingerling et al, 1995c*).

Diabetes mellitus may also increase the risk of AMD, as hyperglycaemia has been reported to have an effect upon the functioning of the choroidal circulation, the RPE, and Bruch's membrane (*Kohner et al, 1995*). However, the epidemiologic data on the link between diabetes and AMD is inconsistent (*Klein et al, 1992b*).

3.5.6 Ocular Variables

It has been hypothesised that melanin has a protective effect against retinal photodamage (*Young, 1988; Jampol et al, 1992*). The Blue Mountains Eye study did find an increased risk

associated with blue eyes (*Mitchell et al, 1998*), but this was not supported by findings in the Beaver Dam Eye Study (*Klein et al, 1998*).

The relationship between refractive error and AMD is also unclear. Several case-control studies have suggested an association between hypermetropia and AMD (*Hyman et al, 1983, Eye Disease Case-Control Study Group, 1992*). However, although this was supported by findings in the Blue Mountains Eye Study (*Wang et al, 1998*), other epidemiological studies found no link, or even suggested that hypermetropia may exert a protective effect (*Klein et al, 1998*).

Opinion is also divided as to whether cataracts might be a risk factor. In the Beaver Dam Eye Study there was a correlation between early AMD and nuclear sclerosis (*Klein et al, 1994*), but no longitudinal evidence of increased incidence of AMD in people with cataracts (*Klein et al, 1998*). The Framingham Eye Study, however, found a decreased frequency of AMD in the presence of nuclear sclerosis, and an increased frequency in the presence of cortical lens changes (*Sperduto et al, 1981*).

A stronger association has been found between cataract extraction and the development of neovascular AMD. A prospective study of patients with bilateral early ARM, and unilateral cataract extractions found that the operated eye was at a significantly higher risk of developing choroidal neovascularisation (*Pollack et al, 1996*). This finding was supported by longitudinal data from the Beaver Dam Eye Study (*Klein et al, 1998*). The precise cause of the increased risk following cataract surgery is not fully understood, but could be due to post-operative inflammatory reactions or to photic damage to the retina during surgery.

3.5.7 Environmental

The possible involvement of environmental factors in the pathogenesis of AMD is supported by epidemiological studies, which have found marked differences in the prevalence of the disease in genetically similar communities. For example, there is a low prevalence of AMD in rural communities of Southern Italy when compared to other European communities (*Pagliarini et al, 1997*), despite the genetic homogeneity of Europe (*Cavalli-Sforza et al, 1994*).

3.5.7.1 Light Exposure

It has been suggested that exposure to UV radiation, or bright sunlight may cause changes in the RPE which mimic those seen in AMD (*Young, 1988; West et al, 1989*). Most studies have failed to find an association between light exposure and AMD (*Hyman et al, 1983; West, 1989; Cruickshanks, 1993*). The Beaver Dam Eye Study did, however, find a relationship between the amount of time spent outdoors in the summer with the presence of exudative macular degeneration and pigmentary changes (*Cruickshanks et al, 1993*). A follow-up study has also found a link between time spent outdoors in early life and the development of early ARM (*Cruickshanks et al, 2001*). An epidemiological study of watermen who work on the Chesapeake bay similarly found an association between high levels of exposure to blue and visible light over the preceding 20 years and a diagnosis of advanced AMD (*Taylor et al, 1990*).

3.5.7.2 Smoking

The relationship between smoking and an increased risk of developing AMD was first suggested by Paetkau et al (*1978*), who noticed an earlier age of onset of advanced AMD in smokers vs. non-smokers. The majority of reports published since then have supported this finding (*Hyman et al, 1983; Eye-Disease Case-Control Study Group, 1992; Vinding et al, 1992; Smith et al, 1996; Vingerling et al, 1996; Delcourt et al, 1998; Age-Related Eye Disease Study, 2001*). The association appears to be greatest with neovascular age-related macular degeneration (*Vingerling et al, 1996*).

One possible mechanism to explain the increased risk of AMD linked to cigarette smoking is that the associated reduction in serum antioxidants may extend to a reduction in retinal antioxidant enzymes. These have a protective effect against damage caused by free radicals produced during light exposure (*Beatty et al, 2000*). This is combined with a reported reduction in levels of the UV screening, antioxidant macular pigment in smokers (*Hammond et al, 1996*). The effect of cigarette smoking on choroidal blood flow may also be implicated in the early onset of AMD (*Solberg, 1998*).

3.5.7.3 Diet

There is evidence to suggest that the retina is particularly prone to photo-oxidative damage (*Beatty et al 2000*). Retinal antioxidant enzymes, macular pigment, and vitamins all help to minimise this damage. Furthermore, antioxidants are postulated to protect against atherosclerosis, another potential risk factor for AMD (*Diaz et al, 1997*). Studies have been conducted to investigate the hypothesis that an increase in serum levels of antioxidants might provide a protective effect against the onset and development of AMD (*Sperduto, 1990*).

Animal models would suggest that this might be the case. Vitamin A and E deficiency in primates has been found to lead to photoreceptor disruption (*Hayes, 1974*), whilst vitamin C has been found to have a protective effect against retinal photic injury in rats (*Organisciak et al, 1985*).

Results from cross-sectional studies have been inconclusive. The first National Health and Nutrition Examination Survey (NHANES- I) suggested that a diet low in vitamin A is related to an increased risk of AMD (*Goldberg et al, 1988*). The follow-up NHANES III, however, found no overall association between dietary or supplementary intake of antioxidant carotenoids lutein and zeaxanthin and ARM (*Mares-Perlman et al, 2001*). The Eye Disease Case Control Study Group found a significant association between low levels of serum carotenoids and neovascular degeneration, but found no such links with vitamins C and E (*Eye Disease Case-Control Study Group, 1993*). Similarly, a further report by the Eye Disease Case-Control Study Group indicated that a high dietary intake of carotenoids was related to a decreased risk of choroidal neovascularisation (*Seddon et al, 1994*). This finding was in accordance with the hypothesis that an increased intake of dietary carotenoids leads to an increase in macular pigment, which has a protective effect against retinal photo-oxidative damage (*Koh et al, 2004*). No association was found between the development of exudative AMD, and the intake of vitamins A, C or E (*Seddon et al, 1994*). Other studies have suggested, however, individuals with ARM have low serum levels of vitamin E (*West, 1994; Delcourt et al, 1999; VandenLangenberg et al, 1998*).

Of the large, population based studies, the Australian Blue Mountains Eye Study found no association between dietary antioxidants and any form of AMD (*Smith et al, 1999*). The American Beaver Dam population similarly failed to show any connection between the intake of vitamin C or E or carotenoids and the prevalence of early or late AMD (*Mares-Perlman et al, 1996*). A nested case-control study within the Beaver Dam population did, however, find

an association between low serum levels of the carotenoid lycopene and an increased risk of AMD (*Mares-Perlman et al, 1995*).

Zinc is another dietary element which may have a role in protecting against AMD. It is found in high concentrations in the retina, RPE and choroid, and acts as a cofactor for enzymes such as retinol dehydrogenase and catalase (*Galin et al, 1962*). An early longitudinal study indicated that zinc supplements did result in a better visual outcome in 151 subjects with early to late AMD over a period of 12-24 months (*Newsome et al, 1988*). Further prospective studies, however, were unable to support this finding (*Stur et al, 1996; Christen et al, 1999; Cho et al, 2001*). The Beaver Dam Eye study also indicated a weakly protective effect of a history of dietary zinc supplements, which was confirmed by the results of a 5 year incidence study in the same population (*Mares-Perlman, 1996; VandenLangenberg et al, 1998*). No association was found, however, between prevalence of AMD and zinc intake or serum concentration in either the Eye Disease Case-Control Study Group (*1992*), or the Blue Mountains Eye Study (*Smith et al, 1999*).

A large prospective study (the Age-Related Eye Disease Study, AREDS) was initiated in an attempt to resolve the contradictory results from earlier studies. The AREDS study was a randomised placebo-controlled trial involving 3640 individuals with various levels of AMD. Participants were given supplements of either high doses of vitamins C and E and beta carotene, high doses of zinc, a combination of both, or a placebo. The follow-up results indicated that the group taking antioxidants plus zinc showed a significant reduction in risk of development of advanced AMD. The effect of either of these supplements separately was non-significant. The recommendation of the group was that individuals with signs of early AMD, or unilateral late AMD, should be advised to take antioxidant and zinc supplements (*Age-Related Eye Disease Study, 2001*).

High dietary levels of certain fats such as saturated fat (*Mares-Perlman et al, 1995*) vegetable fats, mono- and poly-unsaturated fats, linoleic acid (*Seddon et al, 2001; Cho et al, 2001*), and cholesterol (*Mares-Perlman et al, 1995; Smith et al, 2000*) may also be significant in increasing the risk of developing AMD. However, it has been proposed that an increased intake of omega-three fatty acids and fish might have a protective effect, indicating that it is the nature of the fats ingested which is relevant to increased risk, rather than merely the quantity consumed (*Smith et al, 2000; Seddon et al, 2001; Cho et al, 2001*).

3.5.8   Socio-economic

Studies have not identified social deprivation as a risk factor in AMD. The Eye Disease Case Control Study Group, for example, investigated the prevalence of neovascular AMD in two groups, one having completed less than 12 years of school, and one having completed more than 12 years. After controlling for other risk factors, such as cigarette smoking, no significant increased risk was linked to level of education (*The Eye Disease Case-Control Study Group, 1992*).

3.5.9   Funduscopic Risk Factors

Not all patients with bilateral drusen go on to develop severe visual loss. Gass (*1973*) observed 49 patients with bilateral drusen over an average of 4.9 years. Of these only 9 developed severe visual loss in at least one eye. It has been noted, however, that certain characteristics predispose towards progression to late AMD. Large, soft, confluent drusen, and focal RPE hyperpigmentation are two primary high-risk fundus features (*Gass, 1973; Smiddy & Fine, 1984; Bressler et al, 1990; Klein et al, 2002*). The development of unilateral late AMD in the fellow eye has also been identified as a strong risk factor for severe visual loss in the previously unaffected eye. Estimates for the risk of developing choroidal neovascularisation in the second eye have ranged between 4% and 18% per annum (*Chandra et al, 1974; Roy & Kaiser-Kupfer, 1990; Macular Photocoagulation Study Group, 1993*).

For a comprehensive review of risk factors in AMD see Evans 2001.

3.6   Treatment of Age-Related Macular Degeneration

3.6.1   Laser Photocoagulation

In the 1990s, the only established treatment for AMD was laser photocoagulation of new choroidal vessels – an approach only applicable to the exudative form of the disease. The Macular Photocoagulation Study Group evaluated the effectiveness of this treatment (*MPS Group, 1986a; 1986b; 1993a; 1993b*). Eyes with well-defined extrafoveal choroidal neovascularisation were assigned randomly to either treatment or no-treatment groups. A three year follow-up of 208 eyes indicated a relative risk of severe visual loss in untreated eyes of 1.4 (95% confidence interval 1.1-1.9) compared to eyes treated with laser

photocoagulation (*MPS Group, 1986a*). A further study reported that 47% of 83 eyes, which were not treated at baseline for subfoveal choroidal neovascularisation had lost 6 or more lines of visual acuity over the subsequent 4 years. This figure was 22% (17 out of 77) for eyes treated with laser photocoagulation (*MPS Group, 1993b*). The group also investigated the rate of recurrence of choroidal neovascularisation following treatment. Of 119 eyes with extrafoveal choroidal neovascularisation treated with laser photocoagulation, 70 (59%) developed recurrent lesions over 3 years, with most occurring during the first year after laser treatment (*MPS group, 1986b*). These results indicate an improved prognosis for long term visual acuity following laser photocoagulation of classic choroidal neovascularisation, although rate of recurrence of new vessel growth remains high.

Freund et al (*1993*) reported, however, that 58 out of every 67 patients newly diagnosed with exudative AMD (unilateral) did not meet the Macular Photocoagulation Study Group guidelines for laser photocoagulation. A further disadvantage of this mode of treatment lies in the nonselective necrotic damage inflicted on the area where the laser is applied. In the subfoveal area this damage may result in immediate reduction in visual acuity, particularly in patients with relatively good visual acuity prior to treatment (*MPS Group, 1993a*). Laser photocoagulation remains the preferred treatment for choroidal neovascularisation which does not involve the fovea, but in recent years a new treatment for exudative AMD has emerged - photodynamic therapy.

3.6.2 Photodynamic Therapy

Photodynamic therapy (PDT) involves the use of a non-toxic light-sensitive compound, a photosensitiser. This compound is intravenously administered and subsequently activated by exposure to light, to produce photochemical effects in the target area (*Henderson & Doughtery, 1992*). The advantage of this, when compared to traditional thermal photocoagulation, lies in its selectivity. Firstly, the photosensitiser is preferentially concentrated in the target tissue, and secondly, the light irradiation is directed towards and confined to the specific target area.

The actual biological mechanism underlying PDT appears to be similar for all photosensitising agents (*Ochsner, 1997*). It can follow one of two pathways. A type I reaction involves the absorption of light energy by the photosensitiser, which is transformed from its ground singlet state (S_0), to an excited triplet state (T_1). T_1 may then initiate photochemical

reactions directly by generating reactive, cytotoxic free radicals. In the type II reaction, T_1 acts indirectly by transferring its energy to ground state oxygen. The excited state oxygen then causes photo-oxidative damage to biological targets. It is this type II pathway that is believed to form the primary mechanism in PDT for most sensitisers.

The PDT technique was developed for use in the treatment of solid tumours, but the introduction of photosensitising agents with improved selectivity and activity has allowed the expansion of use into other areas of medicine. In the treatment of choroidal neovascularisation secondary to AMD, the compound verteporfin is used (*Boyle & Dolphin, 1996*). Verteporfin is a chemically stable compound which can be activated with light from a low-power, nonthermal laser at wavelengths which can penetrate blood, melanin, and fibrotic tissue (*Richter et al, 1987*). This photosensitising agent has been found to principally target lysosomes in the affected area, resulting in hydrolytic enzyme leakage and intracellular lysis (*Jori & Reddi, 1993*). This may be why it is so effective in the targeting of the RPE, which has a high level of lysosomal activity. Another advantage of verteporfin as a photosensitizing agent is that it is also rapidly and selectively taken up by neovascular endothelium (*Roberts & Hasan, 1992*).

The aim of verteporfin therapy in patients with choroidal neovascularisation secondary to AMD is to occlude or destroy the new vessels selectively, whilst maintaining perfusion in the deeper, larger choroidal vessels and overlying retinal tissue and retinal vessels. This ensures the continuing health and function of the choroid and overlying retina in the treated area.

Two identically designed randomised controlled multicentre trials have been carried out to investigate the efficacy and safety of PDT in the treatment of subfoveal choroidal neovascularisation (*TAP Study Group, 1999*). Patients were randomised in the ratio 2:1 for verteporfin treatment or placebo. The combined study included a total of 609 eyes, 402 of which received verteporfin PDT treatment.

Results showed that, at one year, the average visual acuity in treated eyes was 6/48+2 compared to 6/60 in the untreated eyes. The average loss of vision from baseline was 2.2 lines in the treated group, and 3.5 lines in the placebo group. Compared with the control group, more treated patients had improvements of one or more lines (16% vs. 7%), and fewer treated patients had losses of six lines or more (15% vs. 24%). The treatment was found to be most effective in those eyes with predominantly classic CNV (*TAP Study Group, 1999*). A follow-up TAP report, after 2 years of treatment, found that in the subgroup with predominantly

classic CNV, 59% of the eyes which received verteporfin treatment had lost fewer than 15 letters of vision, compared to 31% of the control eyes. There were, however, no statistically significant differences between treated and placebo groups with minimally classic CNV (*Bressler, 2001*).

Another important consideration is the need for repeated treatment over a 12 month period, although retreatment does not appear to affect vision adversely. In the TAP study, participants in the verteporfin group received an average of 5.5 treatments over the two year period.

In order to determine the possible application of this PDT treatment, one American study group investigated 'Medicare' Health Care Financing Administration (HCFA) Data, which outlines the number of treatments billed for various medical procedures every year (*Margherio et al, 2000*). The overall number of US patients diagnosed annually with neovascular AMD is estimated to be around 200,000 (*Bressler, 1997*). Based on an estimate of patients treated with photocoagulation, and a retrospective review of 1000 consecutive records of new patients with AMD referred to the Associated Retinal Consultants practices during 1998, estimates were made of how many patients would be eligible for verteporfin therapy. If this patient population was representative of the general population, approximately 84,000 patients would have been eligible for verteporfin therapy in 1998, compared with 42,000 for laser photocoagulation (*Margherio et al, 2000*).

These reports suggest that photodynamic therapy may play an important role in the treatment of subfoveal, classic choroidal neovascularisation. Its application still appears to be restricted, however, to a relatively small patient sub-group.

3.6.3 Transpupillary Thermotherapy

Transpupillary thermotherapy technique (TTT) is a laser photocoagulation technique, which exposes the retina to significantly lower temperatures than the standard laser photocoagulation techniques. Infrared light is delivered through the pupil, and absorbed by the retinal pigment epithelium, before being released as thermal energy (*Berger, 1997*). This is a technique which is widely used in the treatment of choroidal melanomas (*Shields et al, 1996*). Early reports suggested that TTT may have a therapeutic effect in the management of occult choroidal neovascularisation secondary to AMD (*for example, Reichel et al, 1999; Newsom et al, 2001*), whilst incurring less chorioretinal atrophy than conventional photocoagulation. Recent clinical trials in India have found TTT to be successful in treating both classic and occult

CNV, with vision stabilising or improving after treatment in between 60% (*Agarwal et al,* *2004*) and 72 % of cases (*Nagpal et al, 2003; Verma et al, 2004*). However, a recent study on Caucasian eyes (*Haas et al, 2003*) found only 14% of eyes stabilised after treatment. It has been suggested that Indian eyes respond to lower energy levels than Caucasian eyes (*Nagpal,* *2003*).

3.6.4   Prophylactic Laser Treatment

One possible avenue of treatment for AMD, which has generated a considerable amount of interest, is laser prophylaxis. In reports in 1971 and 1973, Gass commented on the resolution of drusen following laser photocoagulation treatment of existing CNV or RPE detachments. Also, low-intensity ruby laser photocoagulation applied to individual large drusen was seen to cause them to disappear, often restoring the fundus to near normal colour without affecting visual acuity. It has since also been reported that application of perifoveal laser photocoagulation may result in the resolution of not only the treated drusen, but also other macular drusen, with an associated improvement in visual function (*Sigelman, 1991*).

One aim of prophylactic laser treatment is to reduce the risk of development of advanced AMD in eyes with high risk drusen characteristics (*The CNV Prevention Trial Research* *Group, 1998*). Prospective studies have not demonstrated a protective effect, and there is evidence that the risk of developing choroidal neovascularisation may be increased by laser induced drusen regression (*The CNV Prevention Trial Research group, 1998; Owens, 1999*). However one recent report describing the 8 year follow-up of 29 patients with soft drusen, 13 of which were treated with prophylactic laser photocoagulation, describes a significantly higher incidence of exudative complications in the untreated group (*Frennesson, 2003*)

3.6.5   Radiation Therapy

Investigation into radiation therapy has been based on the fact that the endothelial cells of proliferating vessels are susceptible to radiation. It has been demonstrated that the proliferation of new vessels may be thus inhibited (*Johnson, 1982; Joussen, 2000*). Further support for the potential value of this treatment is provided by the success of radiation therapy in treating proliferative benign vascular tumours, such as choroidal hemangiomas (*Scott et al,* *1991*). Clinical trials of radiation therapy for choroidal neovascularisation have, however, proved inconclusive. Although there have been reports indicating a positive effect in slowing

neovascular growth, or causing regression of existing new vessels (*Chakravarthy et al, 1993*; *Haas et al, 2000*), these were non-randomised clinical trials incorporating few patients. Other studies have reported no such therapeutic benefits. The Radiation Therapy in Age-Related Macular Degeneration Study (*RAD Study, 1999*), for example, enrolled 205 patients in a randomised, double-blind study involving a control group undergoing sham treatment. After a 12 month follow-up they found no apparent improvement in the radiation treatment group compared to the control group.

3.6.6   Pharmacologic Therapy

Antiangiogenic pharmacologic therapy is based on the principle that choroidal neovascularisation is initiated by an imbalance between positive and negative growth factors. The inhibition of growth stimulating factors such as VEGF, or the application of inhibitory factors such as PEDF, would be expected to correct this balance. The main concern with this mode of treatment is that it has the potential to interfere with other physiological mechanisms such as wound healing. Research is also being carried out into the protective effects of other drugs against choroidal neovascularisation, including statins, aspirin, thalidomide and prednisolone (*Kaven, 2001; Ciardella et al, 2002; Wilson, 2004*).

3.6.7   Surgical Treatment

A number of potential surgical treatments for AMD have been considered. These include macular translocation, transplantation of retinal pigment epithelial cells, and extraction of subretinal neovascular membranes. Of these procedures, macular translocation appears to hold the most promise for a positive visual outcome. The technique involves a 360° retinotomy and macular rotation, thus moving the macula to overlie a healthier region of the RPE (*Machemer & Steinhorst, 1983*), or a scleral folding technique (*de Juan et al, 1998*). A number of reports have suggested a post-operative recovery in central vision following macular translocation (*Eckardt et al, 1999; Kirchof, 2002*). Potential complications are numerous, however, and may include diplopia, retinal detachments, corneal oedema, haemorrhage or recurrence of choroidal neovascularisation.

CHAPTER 4 : OCULAR ELECTROPHYSIOLOGY

4.1   The Electroretinogram

The electroretinogram (ERG) is an objective means of assessing retinal function. It relies on the presence of a potential difference (pd) across the retina, and the changes in this pd which take place when a visual stimulus is presented. The first ERG was recorded from enucleated frog eyes by Holmgren (*1865*). Several years later retinal electrical signals were recorded from the eyes of living organisms (*Dewar and McKendrick, 1873*).

The ERG consists of a characteristic waveform, with each change in polarity of the response corresponding loosely to the activity of a different group of retinal neurones. Einthoven & Jolly (*1908*) first described the three main features of the flash ERG. An initial negative deflection was labelled the 'a' wave, and was followed by a large positive 'b' wave. The final, slow developing positive component was termed the 'c' wave.

The temporal and amplitude characteristics of the waveform are dependent on the stimulus parameters used, and also on the state of adaptation. Figure 4.1 shows two ERGs recorded from the same individual under photopic (A) and scotopic (B) conditions. It may be seen that the shape of the waveform is very different in the two cases. Under photopic conditions the cone response is smaller and faster than the mixed response elicited from the dark-adapted eye.
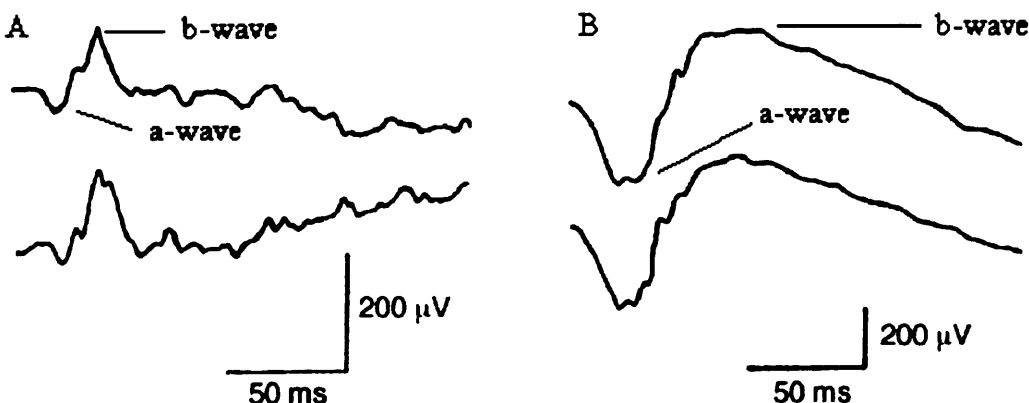
Figure 4.1. Transient ERG responses recorded from a single individual to the same stimulus under light-adapted (A) and dark-adapted (B) conditions. A faster response of smaller amplitude is recorded from the light-adapted eye (*Perlman, 2003*).

Extensive research has been invested into determining the exact population of retinal cells, which is responsible for each part of the ERG waveform. An understanding of the precise

origins of each component of the ERG would allow an assessment of the integrity of each retinal layer. However, such an analysis is difficult because the ERG itself is a composite of numerous retinal events. Changes in electrical activity are slow to develop and recede, and thus tend to overlap. Therefore, each ERG waveform represents the summed electrical activity of disparate retinal elements.

One means of locating the origin of an ERG component is through the recording of intraretinal responses using a current source density analysis technique or local ERG (*Brown et al, 1961*). This is achieved by placing a microelectrode at a specific retinal locus and recording the current, which flows between this and a reference electrode. This technique provides information regarding the electrical activity of cells adjacent to the microelectrode. By adjusting the position of reference and active electrodes, it is possible to obtain information regarding the activity of a specific population of cells.

Pharmacological agents that block synapses between various groups of retinal neurones can also be used in the analysis of the ERG. For example, early investigations into the contribution of photoreceptors to the ERG used aspartate to block post-photoreceptoral activity (*Faber, 1969*). The advantage of this technique is that it allows the analysis of a summed response from the whole population of a particular retinal cell type.

4.2   Components of the Flash Electroretinogram

4.2.1   Granit's Analysis

The first analysis of the retinal origins of the ERG was published by Granit in 1933. He observed changes in the cat ERG as the animal was placed under ether anaesthesia. The ERG waveform was separated into its component processes according to the order in which they were extinguished as the state of anaesthesia deepened. As a result of the work, three components were isolated, and then later a fourth was introduced. Granit termed these PI (the first process to be suppressed by anaesthesia), PII, and PIII (the most resistant to anaesthesia). These components are shown in Figure 4.2.
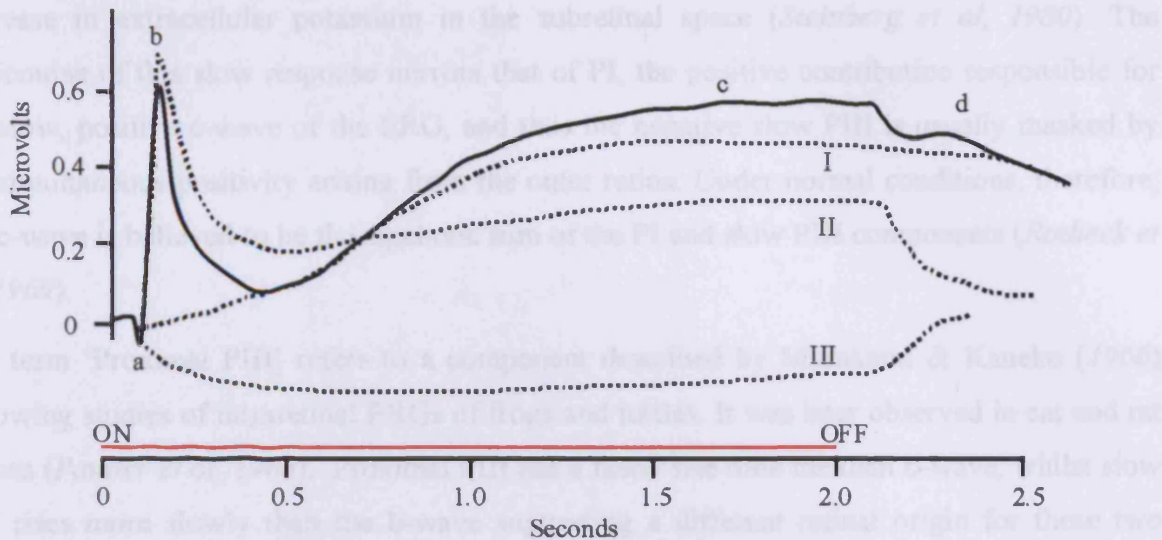
Figure 4.2. Diagram illustrating Granit's component analysis of the ERG (*Granit, 1933*). The solid line shows a classic ERG waveform, whilst the dotted lines indicate PI, PII, and PIII component processes.

Process PI has a positive polarity and a long implicit time. This process contributes to the formation of the c-wave of the ERG (*Rodieck, 1969*). The positive waveform of process PII has a shorter implicit time, and is responsible for the b-wave. The a-wave is formed by the leading edge of negative going PIII, the component with the shortest implicit time. However, PIII has been subclassified since Granit's original analysis in 1933, and is now believed to be a composite of three processes.

Granit (*1962*) noted that PIII appeared to be divisible into 'fast' and 'slow' components, so termed because of the disparity in the speed at which the negativity dissipated following the termination of the stimulus. These two processes were originally believed to reflect the different timing of rod and cone activity, with the rod receptor potential showing a slower rise at stimulus onset, and a slower fall at offset than the cone receptor potential (*Arden et al, 1965*). However, the slow recovery of the rod receptor potential is only apparent at high stimulus intensities, above the level at which the rod receptoral amplitude is saturated (*Baylor et al, 1982*), and yet the slow recovery of PIII is present at much dimmer stimulus intensities. More recently this slow-recovering component of PIII has been attributed to the Slow Negative Response from the inner retina, which occurs even at the relatively low intensities at which the rod receptor potential does not contribute to the ERG (*Frishman, 1990*).

To further confuse the terminology, the term 'slow PIII' is now applied to a negative potential of Müller cell origin, which is slower to arise and recover than the rod receptor potential. It is considered to arise from a hyperpolarisation of the Müller cells in response to a light-evoked

decrease in extracellular potassium in the subretinal space (*Steinberg et al, 1980*). The timecourse of this slow response mirrors that of PI, the positive contribution responsible for the slow, positive c-wave of the ERG, and thus the negative slow PIII is usually masked by the simultaneous positivity arising from the outer retina. Under normal conditions, therefore, the c-wave is believed to be the algebraic sum of the PI and slow PIII components (*Rodieck et al, 1969*).

The term 'Proximal PIII' refers to a component described by Murakami & Kaneko (*1966*) following studies of intraretinal ERGs of frogs and turtles. It was later observed in cat and rat retinas (*Pautler et al, 1968*). Proximal PIII has a faster rise time the than b-wave, whilst slow PIII rises more slowly than the b-wave suggesting a different retinal origin for these two negative components (*Murakami & Kaneko, 1966*). Furthermore, aspartate blocks proximal PIII but not slow PIII (*Hanitzsch, 1973*). Proximal PIII has been suggested to reflect horizontal cell activity, mediated by Müller cells (*Hanitzsch, 1973; Falk & Shiells, 1986; Shiells & Falk, 1999*).

4.2.2 The Early Receptor Potential (ERP)

The early receptor potential (ERP) was discovered by Brown and Murakami in 1964, and is the fastest occurring wave in the ERG. It is only visible in response to an extremely bright flash of less than 1ms duration. The biphasic waveform consists of an initial, small, positive, cone-dominated component (R1), followed by a larger negative phase (R2), which has both rod and cone contributions (*Yonemura et al, 1966*). The ERP begins 0.7ms after stimulus onset (*Cone, 1964*), and is complete within 1.5ms (*Berson, 1987*). As a result of the very short implicit time of this waveform, the ERP is believed to be due to the charge displacement occurring in photoreceptor outer segments during the photochemical reactions caused by quanta hitting the photopigment (*Cone et al, 1969*).

4.2.3 The a-wave

The a-wave is a negative trough, which constitutes the first waveform visible in the conventional ERG (*see Figure 4.3*). The appearance of the negative deflection is dependent on the state of adaptation of the eye, the photopic response being smaller and faster than the scotopic waveform. The intensity of the stimulus also affects the magnitude of the a-wave response, with the largest amplitude response elicited by the brightest stimuli (*Berson, 1987*).
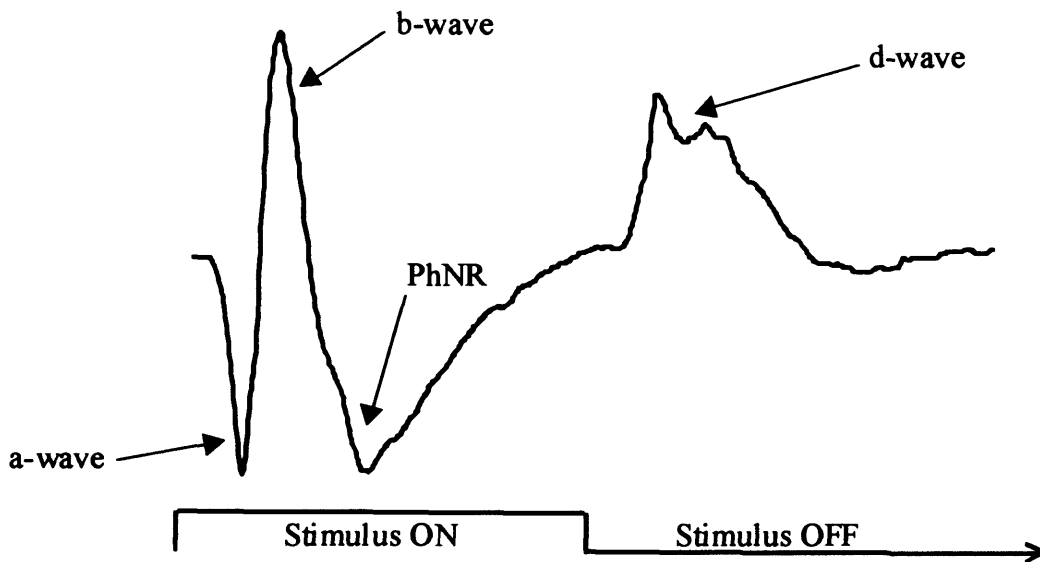
Figure 4.3. Typical ERG response from the L- and M- cones illustrating components. Long duration stimulus (200ms) ensures a separation of ON- and OFF- responses.

Current source density analysis has demonstrated that the light-evoked extracellular current flow around photoreceptors is comparable in timecourse and waveform to the ERG a-wave (*Penn & Hagins, 1969*). It is therefore believed that the a-wave is at least partially attributable to the electrical activity of photoreceptors. Photoreceptors are unlikely, however, to be the sole generators of the response. Tomita (*1963*) hypothesised that the a-wave consists of various potentials arising from the activity of different retinal layers, and suggested that the relative dominance of each of these components is species dependent.

Robson and Frishman (*1999*) reviewed experiments on macaques and cats designed to identify the contributions of various cell types to the dark adapted ERG. They noted that the implicit time of the a-wave is always less than 25ms, and shorter at high stimulus energies. This does not reflect the timing of the rod photocurrent peak, which generally occurs considerably later.

The average number of photons absorbed by the rod outer segments from a flash of light is directly proportional to the energy of the stimulus. Experiments on the electrical activity of individual rods have also shown that the reduction in the circulating current of each rod is proportional to the number of photons absorbed (*Lamb et al, 1981*). Each rod, therefore, shows a decrease in the dark current, which is proportional to an increase in flash energy, until a saturated level is reached beyond which any further increase in the intensity of the stimulus will not change the magnitude of the rod response. If the a-wave were to be attributable to this change in the rod photocurrent, therefore, then the amplitude of the ERG at

any fixed time following the presentation of the stimulus would increase in direct proportion to the flash energy and show the same saturation characteristics as isolated rods. This, in fact, only applies to the earliest part of the a-wave (10ms or less after the flash stimulus). Thereafter, the increase in amplitude of the response as a function of stimulus energy no longer follows the time-course of the activity of individual rods. At times greater than 10ms after flash onset, the amplitude of the a-wave is at its maximum at a stimulus intensity significantly lower than the saturation level expected from the time-course of the response of individual rods. When the flash energy is further increased past this point there is actually a reduction in the amplitude of the negative potential measured (*Robson and Frishman, 1999*).

These results suggest that the earliest part of the dark-adapted ERG is due to the rod photocurrent alone, and thereafter a net positive contribution must be added to the ERG, presumably from the inner retina. It is assumed that the a-wave peak occurs when the relatively slow-rising negative signal from the rods is overtaken by the more-delayed but faster rising positive response of other, higher-order retinal neurones.

The cornea positive contribution of rod bipolar cells to the dark-adapted ERG is represented by Granit's PII. It might be supposed that the a-wave of the scotopic ERG consists of the sum of the negative contribution of the rod photocurrent response, and the more delayed corneal positive contribution of the rod bipolar response. Robson and Frishman (*1996*), however, found that the a-wave can only be well approximated by the sum of rod (*Lamb & Pugh, 1992*) and rod bipolar (*Robson & Frishman, 1995*) activity when inner retinal responses are substantially reduced. This may be done either by pharmacological means, or by the use of a weak adapting background to selectively suppress the proximal neurones. This indicates a further proximal contribution to the a-wave of the scotopic ERG.

The source of the proximal retinal contribution to the dark-adapted a-wave is uncertain. At low stimulus intensities a corneal negative response believed to originate from amacrine or ganglion cells – the scotopic threshold response (STR) – has been described in the dark-adapted ERG (*Sieving, 1986; 1988*). The maximum amplitude of the STR, however, is too small to account for the proximal contribution to the a-wave at higher flash intensities (*Robson and Frishman, 1996*), suggesting a further inner retinal contribution.

It has also been suggested that the leading edge of the scotopic a-wave is a sum of rod photoreceptor activity, rod bipolar cell activity and a proximal PIII component derived from horizontal cell (H-cell) activity (*Shiells & Falk, 1999*). The pharmacological agent glutamate

analogue 2-amino-4-phosphobutyric acid (APB) blocks the activity of depolarising bipolar cells (DBCs), including rod bipolars. ERGs recorded on the dogfish retina in the presence of APB showed a vitreal negative wave of larger amplitude than the a-wave, as would be expected after the elimination of the PII component. The amplitude of this negative response was reduced upon the instillation of kainate, an agent which blocks H-cell responses, indicating a direct or indirect negative contribution of H-cells to the rod ERG a-wave. The direct contribution of H-cells to the ERG is unlikely, as these cells are tangentially orientated and thus would not be able to create a pd across the retina. It has therefore been suggested that the closure of cation channels in H-cells results in a decrease in the extracellular concentration of potassium ions in the outer plexiform layer, which results in a voltage drop across Müller cells. Müller cells are therefore implicated in the generation of this negative component.

However, the possibility of a contribution to the a-wave from a more proximal source is indicated by previous intraretinal microelectrode recordings, which have demonstrated the presence of negative field potentials at the level of the inner plexiform layer. These potentials have been shown to increase in magnitude with stimulus energy up to two times the size of the saturated STR amplitude (*Sieving et al, 1986*). This negative contribution at high stimulus intensities is likely to be due to amacrine, not ganglion cell activity because ganglion cell responses saturate at fairly low light levels (*Sakmann et al, 1969*), and the signal persists when ganglion cell degeneration has occurred (*Sieving et al, 1991*).

The origins of the light-adapted (photopic) ERG a-wave have also been studied. Brown and Wantabe (*1962*) concluded from the recording of local ERGs in monkeys that the a-wave of the photopic ERG is also derived to some extent from photoreceptor activity. Further studies, using extracellular electrodes positioned at the level of the cone photoreceptors, confirmed that the characteristics of the photopic a-wave concurred with the kinetics of the late receptor potential recorded from monkeys (*Brown et al, 1965; Heynen & Van Norren, 1985*). However, the possibility of a proximal retinal contribution to the waveform, such as that identified in the scotopic ERG by Robson and Frishman (*1996; 1999*), has also been evaluated.

Glutamate analogue 2-amino-4-phosphobutyric acid (APB) has been used to eliminate the b-wave of the photopic ERG by blocking block synaptic transmission from photoreceptors to depolarising ON-centre bipolar cells (*Knapp & Schiller, 1984; Evers & Gouras, 1986; Falk et al 1986*). After injection of APB a negative wave is observed which is larger than the a-wave and lasts for the duration of the stimulus. Evers & Gouras (*1986*) attributed this increased

negativity to the activity of hyperpolarizing OFF-centre bipolars (HBC). However, Knapp & Schiller (*1984*) suggested that it is horizontal cells which contribute to the more negative ERG revealed after APB injection.

Bush and Sieving (*1994*) further investigated the proximal negative contribution to the photopic a-wave by recording ERGs from monkeys using both APB to block DBCs, and cis-2,3-piperidine-dicarboxylic acid (PDA), which blocks transmission between photoreceptors and HBCs, as well as inhibiting the synapse between bipolar cells and third order neurones. The injection of the two drugs completely eliminated post-receptoral ON and OFF pathways and resulted in an a-wave that was significantly smaller than that recorded in control monkeys, and in monkeys injected with APB alone. This finding supported the hypothesis that there is a post-receptoral cornea-negative contribution to the standard photopic a-wave.

Bush and Sieving (*1994*) also recorded an intensity-response function from monkeys under various conditions. The decrease in the amplitude of the a-wave after the instillation of APB and PDA was proportionally greatest for dimmer stimulus intensities, indicating that the relative influence of the inner retinal contribution to the a-wave is lessened with increasing stimulus intensity. Moreover, after instillation of APB and PDA, no appreciable a-wave could be recorded from the monkey eye until the flash intensity was more than 1 log unit above the control a-wave threshold. This suggests that at low intensities the contribution of the outer retina to the a-wave is minimal.

APB alone did not affect the early part of the leading edge of the a-wave. This suggested that, as in the scotopic ERG, the cornea-positive contribution from the DBCs does not influence the first 10ms or so of the a-wave amplitude.

4.2.4 The b-wave

The b-wave first appears at low stimulus intensities, below those at which the negative a-wave first becomes apparent. It is the first major positive deflection of the ERG, and also the most prominent component of the ERG over a wide range of stimulus conditions (*see Figure 4.3*). The component process which underlies the b-wave is Granit's PII (*Granit, 1933*). There is a long established belief that the major generator of PII, and the ERG b-wave is the ON-bipolar cell (*e.g. Newman, 1980; Newman & Odette, 1984; Stockton & Slaughter, 1989*). This is supported by the fact that the pharmacological blockade of DBCs, using the pharmacological

agent APB, largely extinguishes PII (*Massey et al, 1983; Porciatti et al, 1987; Müller et al, 1988; Smith et al, 1989; Stockton & Slaughter, 1989; Shiells & Falk, 1999*).

Until recently it was supposed that the relationship between b-wave amplitude and depolarising ON-bipolar cell (DBC) activity was an indirect one. Models of b-wave generation suggested that the light-evoked response of DBCs resulted in an extrusion of potassium (K+) into the extracellular space, leading to a local depolarisation of Müller cell membranes (*Newman & Odette, 1984*). It was the summed Müller cell transmembrane potential, which was believed to be responsible for the b-wave. Evidence for this lay in the similarity of the waveform of intracellular recordings of the Müller cell depolarisation in response to light, and the waveform of the ERG b-wave; also in current source density analyses of the intraretinal sources and sinks (*Faber 1969; Miller & Dowling, 1970*).

However, recent evidence suggests that the b-wave is largely a direct measure of DBC activity. Shiells & Falk (*1999*) recorded ERGs from the dark-adapted retina of the dog fish before and after the instillation of APB. The subtraction of the post-APB response from the pre-APB response allowed the isolation of the b-wave from the photoreceptoral negative contribution. The intensity response function of this isolated b-wave showed an excellent agreement with the IR function of rod bipolar cells, indicating that DBCs are responsible for b-wave generation. This was supported by the findings of Green and Kapousta-Bruneau (*1999*), who recorded ERGs from the isolated cone-free rat retina. The introduction of Barium (Ba^{2+}) to the retina, blocking the potassium conductance of Müller cells, was found to cause an increase rather than a reduction in the amplitude of the ERG b-wave. This strongly suggested that the b-wave recorded from the rat retina was directly generated by the current flow from ON bipolar cell activity rather than the indirect activity of Müller cells.

Other recent reports have suggested that, although the ERG b-wave appears to be principally generated by DBC activity, there are contributions arising from other retinal loci (e.g. *Sieving et al, 1994; Hood & Birch, 1996*). Recordings from isolated ON-bipolar cells from dogfish (*Ashmore & Falk, 1980*), and cats (*Robson & Frishman, 1995*) show a linear intensity response function at low stimulus intensities. The cat b-wave, however, does not show such linearity (*Robson & Frishman, 1995*).

The non-linearity of the b-wave intensity response function at low stimulus intensities has been ascribed to the presence of a negative component from the proximal retina. This proximal component is the scotopic threshold response (STR), which is elicited by very dim

stimuli, and saturates at low stimulus intensities. Although the STR is much smaller than PII, reaching at saturation only 5% of the maximum PII amplitude (*Robson & Frishman, 1995*), it can alter the leading edge of PII, and may totally obscure it at lower flash intensities where PII is expected to be linear (*Hood & Birch, 1996*). In addition to this proximal negative contribution to the b-wave, the negative fast PIII component derived from photoreceptoral activity also plays a role in shaping the b-wave, especially at high stimulus intensities.

Hood & Birch obtained a derived PII from the human scotopic ERG by subtracting a computational model of PIII from an ERG recorded using a dim adapting background to suppress the STR. The isolated PII was found to be described fully by the intensity/response function fitted by Ashmore & Falk (*1980*) to DBC activity in these conditions. Subtraction of pharmacologically derived photoreceptoral and inner retinal contributions to the cat ERG has confirmed that the leading edge of PII accurately represents DBC activity at all stimulus intensities (*Robson & Frishman, 1999*). However, the trailing edge of this signal demonstrates both fast and slow components. It has been suggested that the faster signal reflects DBC recovery, whilst the second, slower component reflects Müller cell activity (*Robson & Frishman, 1999*).

Consequently there is only a limited range of stimulus intensities over which b-wave amplitude gives an accurate representation of DBC activity (*Hood and Birch, 1996*). The outer retinal contribution of photoreceptors is particularly important at high stimulus intensities, whilst the inner retinal input of the STR influences the waveform at low intensities.

Evers & Gouras (*1986*) provided indirect evidence that there is a further contribution to the photopic ERG b-wave from hyperpolarising second order neurones. It was demonstrated that APB (which blocks DBC activity) affects the S-cone ERG differently to L- and M- cone ERGs. L- and M-cone pathways have ON- and OFF- centre processing, whilst the S-cones synapse primarily with ON-centre bipolars. This suggests that HBCs may have some influence on the ERG waveform. In order to investigate this further, Sieving et al (*1994*) used the glutamate antagonists, cis-2, 3-piperidine dicarboxylic acid (PDA) and kynurenic acid (KYN) on macaque monkeys to block the light activity of hyperpolarizing second order neurones (HBCs and horizontal cells) without diminishing the response from DBCs. APB was also used to block DBC activity. ERGs were recorded before and after the intravitreal injection of the drugs to isolate the various components of the light-adapted ERG b-wave.

The control ERG showed an initial negative deflection (the a-wave) followed by a large positive b-wave. A plateau of overall negative polarity followed, linking the b- and d-waves, which gradually rose back towards the baseline during the light flash (*See Figure 4.4, A*). Instillation of PDA and KYN, together blocking the light-response of HBCs, horizontal cells, and third order neurones, had a profound effect upon the ERG waveform. The a-, b- and d-waves were completely obscured by a large and positive response sustained for the duration of the flash. Only the initial rising edge of the b-wave, and the trailing edge of the d-wave were preserved (*See Figure 4.4, B*). When APB was added to the eye to suppress the response of depolarising bipolar cells, the normal negative cone receptor potential underlying the large, positive, sustained response was revealed (*See Figure 4.4, C*).
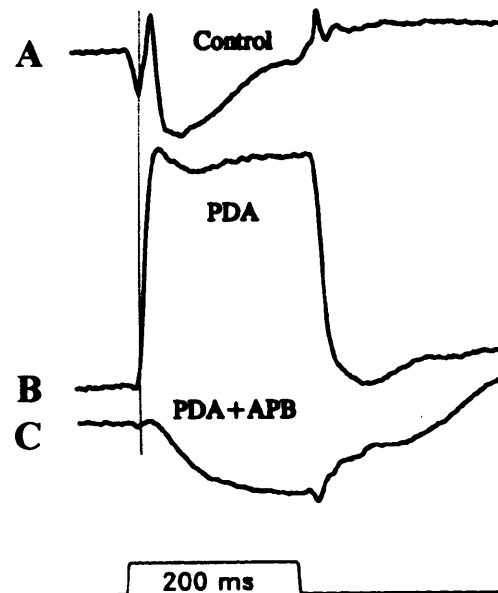
Figure 4.4. Effects of PDA and APB on the photopic ERG of a monkey eye. Drugs were given by serial intravitreal injections. The 200 ms flash was 3.76 log td presented against a steady background of 3.3 log td (*Bush & Sieving, 1994*).

In order to demonstrate that the influence of PDA and KYN on the photopic ERG waveform lay in their suppression of the hyperpolarizing second order neurones, rather than in their secondary effect of suppressing of the activity of third order neurones, ERGs were repeated with the instillation of N-methyl-D-aspartate (NMDA) alone (an agent which makes third order neurones unresponsive to light). The blockade of third order neurones was found to have little effect on the ERG b-wave, thus indicating that the substantial changes to the ERG

b-wave in the presence of PDA and KYN were explained principally by the suppression of HBC and H-cell activity by these drugs.

These results suggest that DBCs contribute a large, positive and sustained potential, which is curtailed by the HBC/horizontal cell activity. It therefore appears that DBC activity is required to produce the photopic b-wave, but that the phasic shape is dependent on the activity of hyperpolarizing neurones (*Sieving et al, 1994*).

4.2.5 The Oscillatory Potentials (OPs)

The oscillatory potentials (OPs) are a series of up to seven rhythmic wavelets superimposed on the rising phase of the b-wave. They were first reported by Granit and Munsterhjelm (*1937*) in the frog ERG, but it was not until 1953 that similar wavelets were observed in the human ERG (*Cobb and Morton, 1953*). The OPs have a higher dominant frequency (90-160 Hz) than the a- and b-waves, which are dominated by components at a frequency of around 25 Hz (*Algvere and Wachtmeister, 1972*). When the ERG is recorded with standard high- and low- bandpass frequency filters the OPs are difficult to discern, but judicial filtering can be used to isolate them effectively from the lower frequency components. The International Society for the Clinical Electrophysiology of Vision (ISCEV) standard suggests bandpass filtering of 100-1000Hz (*Marmor & Zrenner, 1999*).

Optimal recording of the OPs requires specific adaptational conditions. The OPs have been shown to reflect both photopic and scotopic activity (*Wachtmeister et al, 1974*), and thus mesopic conditions are found to be the most effective in eliciting OPs. Such conditions are best obtained by a period of total dark adaptation, followed by a 'conditioning' flash (*Wachtmeister, 1973*).

The origin of these responses has been the source of some contention. Both rod and cone systems are known to contribute to the OPs (*Peachey et al, 1987*), but there is uncertainty regarding the precise retinal generators. Current source density profiles have indicated that OPs originate from a proximal locus i.e. the inner plexiform layer (*Ogden, 1973; Wachtmeister & Dowling, 1978; Heynen et al, 1985*). The proximal retinal origin is further indicated by the suppression of OPs in cases of experimental (*Brown, 1968*) and pathologic (*Yonemura et al, 1962*) central retinal artery occlusion.

Early and late OPs appear to have distinct origins. The use of dopamine modulating drugs (reserpine and haloperidol) has shown that dopaminergic neurones, possibly dopaminergic

amacrine cells, are involved in the generation of the early OPs. The later OPs are also affected by these drugs, but to a lesser extent (*Gutierrez & Spiguel, 1973; Hempel, 1972; Wachtmeister & Dowling, 1978, Wachtmeister, 1981; Pourcho, 1996*). Other studies have found the application of GABA antagonists to result in a substantial reduction or abolition of the early OPs (*Wachtmeister, 1980*). GABA is an amino acid, which is also part of the negative feedback process at the level of the amacrine cells (*Burchartd, 1972; Nakamura et al, 1979*) and interplexiform cells (*Nakamura et al, 1980*).

The later OPs are reduced by the glycine antagonist strychnine (*Wachtmeister, 1980*). Glycine is an inhibitory neurotransmitter which is only found in the inner plexiform layer of the retina, and is involved in the processing of the OFF-pathway, mediated by hyperpolarising bipolars (*Cunningham and Miller, 1980*). The earlier OPs therefore seem be related to the rod-mediated GABA-nergic ON-pathway, and the later ones to the glycine sensitive OFF-pathway. The last OP has been found to be consistently time-locked to stimulus offset, supporting this supposition (*Kojima & Zrenner, 1978*). The possible rod-mediated origin of the earlier OPs (OP2 and OP3) has been further supported by studies demonstrating a selective reduction in the amplitude of these peaks when the eye is stimulated by light flickering at a frequencies too fast for the rod system to process (*Lachapelle et al, 1983*). Other reports have suggested that OP3 and OP4 are rod dominated. Janaky et al (*1996*), for example, used blue flashes against a dark background to elicit rod mediated OPs, and found that they corresponded well with OPs 3 and 4 recorded in response to a standard white flash. It has also been noted that retinopathies resulting in a differential dysfunction in the rod system lead to a decrease in the amplitude of the earlier OPs, whilst it is the later OPs which are principally affected by loss of cone function (*Wachtmeister, 1998*).

Further evidence suggesting distinct retinal origins for the OPs comes from depth profile studies (*Wachtmeister and Dowling, 1978*). The first OP appears to have the most proximal origin, while the second and third are localised more distally, and the fourth and fifth are located in the outer lamina of the inner plexiform layer. These findings are consistent with the theory that OPs are generated by a series of inhibitory feedback systems operating at different levels within the retina (*Brown, 1968*).

Pharmacological studies have also suggested that OPs reflect the activity of the inhibitory feed-back circuits within the inner retina, driven by amacrine, and possibly interplexiform cells (*Wachtmeister, 1998*). This is further supported by intracellular recordings from amacrine (*Marchiafava & Weiler, 1982*) and interplexiform cells (*Hashimoto et al, 1980*),

which demonstrate oscillations in their light-evoked responses. The amacrine cells, however, have a tangential orientation, and are thus unlikely to cause a trans-retinal potential. Although this suggests that they do not directly generate the OPs, there is still likely to be some underlying amacrine involvement (*Wachtmeister, 1998*). Interplexiform cells, which form both pre- and post- synaptic connections with amacrine cells, are more radial in orientation than amacrines (*Boycott et al, 1975*), and may be implicated in OP generation.

Evidence against ganglion cells being directly involved in the generation of OPs is provided by studies which have demonstrated that OPs are not affected in patients with optic nerve atrophy (*Wanger & Persson, 1983; Wachtmeister & el Azazi, 1985*). Furthermore, pharmacological investigation has shown that the administration of tetradoxin, which blocks ganglion cell action potentials, has a minimal effect on primate OPs (*Ogden*, 1973). However, other studies report a reduction in OP amplitude in patients with glaucoma or optic nerve diseases (*Gur et al, 1987; Vaegan et al, 1995*). The extent of any involvement of the ganglion cells in the generation of the OPs is as yet uncertain, but would seem to be small.

4.2.6   The Photopic Negative Response (PhNR)

The PhNR is a slow-developing corneal negative response, elicited under photopic conditions, which follows the b-wave (*Viswanathan et al, 1999; see Figure 4.3*). Recent studies on macaque monkeys with experimental glaucoma have demonstrated a reduction in the PhNR even when visual field defects are relatively mild, and there is no significant attenuation in the a- or b-waves of the response (*Viswanathan et al, 1999*). Other reports have described the suppression of the PhNR when using tetradoxin to suppress the action potentials of retinal ganglion cells in macaque monkeys (*Viswanathan, 1999, 2000*). These studies indicate that the source of this potential is probably in the spiking activity of retinal ganglion cells, but the slow timing of the response raises the possibility that it could be mediated by glial cells. Preliminary studies suggest that the PhNR may be of value in assessing inner retinal function in diseases such as primary open angle glaucoma (*Viswanathan et al, 2001*). A recent study (*Drasdo et al, 2001*) has indicated that the s-cone PhNR is more sensitive even than the pattern ERG for this purpose.

4.2.7   The Scotopic Threshold Response (STR) and the Slow Negative Response

When a very dim stimulus is presented to the dark adapted mammalian eye, just above ERG threshold, a response is recorded which is cornea-negative in polarity (*Schweitzer et al, 1965; Sieving et al, 1988, Saszic, 2002*). This negative response has since been split into two negative components, one which has a short implicit time, the scotopic threshold response, and a slower developing negativity which follows it, and is termed the slow negative response (*Sieving et al, 1986*). The human STR has been found to be similar in characteristics to the STR of the cat and monkey, which have been shown to originate from retinal loci proximal to the photoreceptors (*Sieving, 1986*), and is thus thought to reflect post-receptor processing in the retina (*Sieving et al, 1988*). Further, pharmacological evidence has indicated that the STR is strongly influenced by cells which release GABA or glycine in the dark, indicating a possible third order neuron origin to the response (*Naarendorp and Sieving, 1991*).

4.2.8   The c-wave

The c-wave is a positive phase of the ERG, which usually peaks between 2 and 10 seconds after stimulus presentation, depending on flash intensity and duration. It is generally considered to be the sum of the positive PI component, originating from the RPE, and the simultaneously occurring negative slow PIII component from Müller cells. Both are caused by the decrease in concentration of extracellular potassium occurring in the subretinal space during light stimulation. This potassium change results in a difference in hyperpolarisation between the apical and basal membranes of the RPE, and also a hyperpolarisation of the apical membrane of the Müller cells (*Steinberg et al, 1970*).

The c-wave is largely dependent on rod photoreceptor cell activity, and is most apparent in dark-adapted conditions. It also has the spectral sensitivity function of rods, and is absent in cone dominated retinas (*Arden, 1955*). Other reports, however, have described a cone-driven c-wave recorded in cone-dominated duplex retinas (*Wioland et al, 1984*).

In the case of disease or damage of the RPE, the PI component is impaired, and thus the negative slow PIII becomes dominant and a decrease in the amplitude of the positive c-wave results. This was illustrated by Nilsson et al (*1977*), who intravenously injected an agent toxic to the RPE, sodium iodate, into the sheep retina to demonstrate the almost immediate replacement of the c-wave by a negative potential. Generalised photoreceptor death and dysfunction, however, will also result in a reduction in c-wave amplitude. A report by

Mayhew et al (*1985*), for example, describes a juvenile visual dysfunction, Batten's disease, in which the earliest stage of retinal involvement is marked by photoreceptor outer segment dysfunction, followed by photoreceptor death. At this early stage in the disease progression, the RPE and proximal retinal layers remain in tact, but the primary deficit noted on the ERG is a diminished c-wave, which is eventually replaced by a negative potential.

Some studies have suggested a third, more proximal component to the c-wave. In an electroretinogram recorded in the absence of the RPE, it would be expected that the positive PI would be abolished, leaving in the place of the c-wave a negative waveform attributable to the slow PIII. Zeumer et al (*1994*), however, recorded a slow cornea-positive potential from an isolated frog retina, detached from the RPE, and deduced that this was due to a proximal increase in potassium concentration, generating a potential in the vitreal endfeet of the Müller cells. Another study, which recorded electrophysiological responses from the isolated human retina (extracted from enucleated eyes), similarly reported the existence of a proximal, corneal positive component in the human c-wave (*Hanitzsch & Lichtenberger, 1997*). Further evidence of such an inner retinal contribution to the human c-wave is provided by reports of a reduced c-wave following occlusion of the central retinal artery, in which condition the photoreceptor-RPE interface is undisturbed (*Textorius, 1978*).

The presence of a cornea-positive proximal retinal contribution to the human c-wave could potentially limit the value of this signal in assessing RPE integrity. The utility of the c-wave as an index of RPE function is further compromised by the reduction in amplitude caused by generalised photoreceptor loss and dysfunction. In the assessment of reduced c-wave amplitude it is beneficial, therefore, to consider the integrity of the other ERG waveforms in order to provide a differential diagnosis. Photoreceptor abnormalities, for example, may often be ruled out by the presence of normal a- and b-waves.

4.2.9   The d-wave

The d-wave, or off-response, is a cornea positive potential, which may be recorded at the offset of a bright, long duration stimulus (*Granit, 1933; Arden & Tansley, 1955; see Figure 4.3*). When shorter duration stimuli are used the d-wave is not separable from the b-wave. Sometimes the separation of the components is incomplete, and a small positive wave is recorded at the end of the descending limb of the b-wave. This has been termed the 'i-wave'

to signify that it is a result of interference between the ON- and OFF- responses (*Nagata, 1963*).

The d-wave is specific to the cone off-pathway. A positive wave at light offset has been recorded in the scotopic ERG of some species, but a prolonged implicit time of the response indicates that in these cases it is not a true d-wave (*Brown, 1969*). The cone off-pathway is believed to begin at the synapse between cones and hyperpolarising bipolar cells (HBCs). Work by Stockton and Slaughter (*1989*) into the retina of the mudpuppy suggests that in cold blooded retinas changes in potassium currents within the HBCs at light offset lead to a Müller cell response, which is responsible for the d-wave. A current source density analysis in the frog retina (*Xu et al, 1995*) supported the involvement of the HBCs in the d-wave, but a relative insensitivity of the current to Ba2+ suggested that Müller cells may not mediate the d-wave generation. There also appears to be HBC involvement in the d-wave of the primate retina, with a selective extinction of the d-wave recorded upon instillation of PDA, a pharmacological agent which suppresses responses of the HBCs and horizontal cells whilst leaving depolarising bipolar cells (DBCs) in tact (*Sieving et al, 1994*). These results do not exclude, however, the possibility of a horizontal cell contribution to the d-wave. Xu et al (1995) also found a current within the photoreceptor layer to be contributing to the d-wave. This is most significant during the very beginning of the d- wave, and supports the theory that the initial rising phase of the d-wave reflects the fast decay of the cone receptor potential (*Kawasaki et al, 1980*).

4.3   Recording the Electroretinogram

4.3.1   International Standards for Clinical Electrophysiology

With any clinical technique, it is desirable to have basic international standards, which allow comparison of data recorded from different laboratories. The International Society for Clinical Electrophysiology of Vision (ISCEV) proposed such a standard for the most commonly recorded responses in 1989 (*Marmor et al, 1989*), which has since been updated with developments in the field (*Marmor et al, 1995; Marmor & Zrenner, 1999*). Standards include recommendations for electrodes, light sources, calibration, electronic recording equipment, subject preparation and the clinical protocols for the recording and measurement of five basic

ERG responses. Specialised types of ERG response are excluded at this stage from the ISCEV standards.

4.3.2 Electrodes

The recording of an electroretinogram requires the placement of three electrodes: active, reference and earth. The difference in voltage between the active and reference electrodes is detected and amplified by a differential amplifier. Upon the presentation of a visual stimulus, both active and reference electrodes will detect background noise and myogenic activity, whilst only the active electrode will measure the electrical response directly linked to retinal activity. Differential amplification therefore isolates the signal generated in response to visual stimulation from extraneous electrical signals.

The development of practically viable active electrodes provided a great step forward in the evolution of clinical electrophysiology. The first corneal electrodes consisted of a scleral contact lens containing a silver ring, which recorded electrical signals from the underlying tear film (*Riggs, 1941*). The contact lens electrode continues to be widely employed in electroretinography (*Fishman, 2002*), providing large and repeatable signals (*Marmor, 1977*). The need for corneal anaesthesia and lubrication, however, remains a disadvantage of the use of this type of electrode. The duration of the recording session is also limited. The Burian Allen contact lens electrode, for example (*Burian & Allen, 1954*) should not be used for more than 30 minutes. A further disadvantage of this type of electrode is that it disrupts the optics of the eye, which is particularly problematic when trying to record pattern evoked responses.

More recently, alternatives to the contact lens electrode have been developed. The gold foil electrode, described by Arden et al (*1979*), consists of a polyethylene film (Mylar), which is coated on one side with gold foil. This is curved into a 'J' shape, the tail of which sits in the lower fornix. This electrode leaves the optics of the eye unaffected, and may be used without corneal anaesthesia, although some patients will experience irritation and tearing. The gold foil electrode may also fall out of the eye during recording.

The Dawson, Trick, and Litzkow (DTL) electrode addresses some of these limitations (*Dawson et al, 1979*). It consists of 7 strands of silver-impregnated nylon fibre. For maximal signal measurement this is placed along the tear prism, above the lower lid, although it may give better patient comfort if placed in the lower fornix. Since the electrode will often be blinked down into the lower fornix during recording, resulting in a signal of reduced

amplitude, it may be beneficial to begin with the electrode in this position to improve the repeatability of results (*Hebert et al, 1999*). In most cases the patient is unaware of the presence of the electrode when properly positioned. The optics of the eye are also unaffected. Signals recorded with the DTL and Gold Foil electrodes tend to be smaller in amplitude, however, than a comparable response measured with a contact lens electrode (*Vaegan, 1996*).

A skin electrode, placed over the infraorbital ridge below the lower eyelid, may be used in place of a corneal electrode in certain circumstances e.g. in the testing of small children. Signals recorded in this way have been found to be approximately 50% the size of those recorded using the DTL electrode (*Coupland & Janaky, 1989*), making it a generally undesirable technique. ISCEV standards strongly recommend active recording electrodes that contact the cornea or bulbar conjunctiva (*Marmor & Zrenner, 1999*).

A 9mm silver-silver chloride disc electrode, located at the ipsilateral outer canthus position, usually constitutes the reference electrode. The earth electrode may be placed at the mid-frontal or vertex locations, or may take the form of a crocodile clip attached to the earlobe.

4.3.3   Computer Averaging Equipment

The amplitude of the signal detected by ERG electrodes is very small in comparison to background electrical activity evoked by neurological and myogenic activity. Various means are employed by computer recording systems to enhance the recorded signal to minimise the effect of background noise. Differential amplification is necessary initially to render the signal of sufficient amplitude to be detectable by recording equipment. This is often followed by a bandpass filtering system, which allows the isolation of activity at a particular frequency, eliminating other electrical responses falling outside this range.

In view of the small amplitude of many retinal responses, it is often desirable to average a number of responses, thus cancelling out any contaminating oscillations, which are not time-locked to the presentation of the stimulus. Furthermore, many averaging systems may be programmed with an 'artefact reject' setting, whereby a recorded signal which is greater than a predetermined amplitude is rejected by the computer and not included in the averaging process. This helps to eliminate any ERG traces contaminated by large amplitude signals evoked by muscular activity, such as blinks or eye movements. These factors will greatly improve the signal-to-noise ratio of the electroretinogram.

4.3.4   The Full-Field / Ganzfeld Electroretinogram

The full-field electroretinogram is generally recorded in response to a flash presented within a Ganzfeld bowl. This is a large diameter dome, which is illuminated homogenously by a flash stimulator, such that the central 120° of the retina are illuminated when the patient's head is positioned on a chin rest at the base of the dome (*Kooijman, 1986*). The advantage of this form of retinal stimulation is that less variability is incurred by small fluctuations in patient fixation. The ganzfeld bowl also eliminates complications which may arise from the intraocular light scatter of a small diameter stimulus.

4.3.5   The Focal Electroretinogram

The full-field electroretinogram provides a measure of the mass response from the whole retina, and will exhibit a reduction in amplitude in the presence of diffuse retinal dysfunction. In diseases such as age-related macular degeneration the full-field ERG might not be expected to be sensitive to early pathological changes because the whole macular region (20° diameter) only accounts for 9% of the total retinal cone population (*Curcio et al, 1990*). Therefore, even the total absence of macular cone function would only have a modest effect on the amplitude of the summed full-field ERG. The focal ERG has therefore been developed as a means of targeting and assessing the integrity of the central retina.

The recording of a focal ERG can be hampered by practical considerations. Improved recording techniques have helped to eliminate the problem of recording small amplitude signals. The second problem arises from indirect stimulation of the peripheral retina caused by intraocular light scatter. The effect of stray light on the recording of a focal electroretinogram was demonstrated by Asher (*1951*) and Boynton & Riggs (*1951*), who showed that the ERG produced in response to a small focal stimulus centred on the optic disc was of the same size as that produced by the same stimulus directed at the fovea.

One means of eliminating this problem has been to use a reversing checkerboard pattern stimulus, set on a screen within a luminance-averaged surround, thus removing the effect of stray light by maintaining a constant space-averaged luminance (*Riggs et al, 1964*). The waveform of the pattern reversal ERG is illustrated in Figure 4.5. It may be seen to consist of 2 principal components, a positive wave with an implicit time of approximately 50ms (P50), and a negative wave with an implicit time of approximately 95ms (N95). The N95 component has been shown to be dominated by ganglion cell activity, whilst the P50 component reflects

both ganglion cell response to the patterned stimulus, and a distal retinal response to local changes in luminance (*Arden et al, 1982; Dawson et al, 1982; Drasdo et al, 1990*).
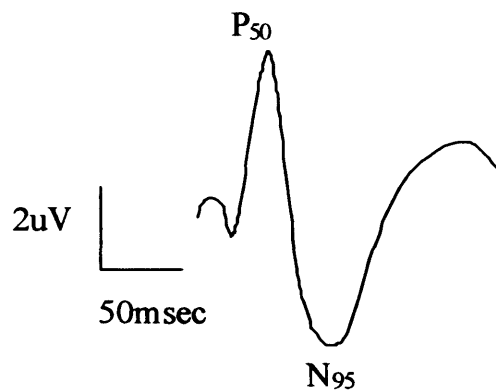
Figure 4.5. The waveform of the pattern reversal electroretinogram

In view of the inner retinal contribution to the pattern ERG, and its sensitivity to optical defocus, attempts have also been made to isolate a focal response from the retina to a flash stimulus, which might more directly reflect outer retinal dysfunction. One way of removing the problem of indirect stimulation of the peripheral retina is through the use of an adapting surround. This desensitises the peripheral retina and thereby minimises any scattered light response (*Armington et al, 1961; Brindley & Westheimer, 1965*).

Various means of presenting the focal stimuli have been developed, including a hand-held stimulator-ophthalmoscope (*Sandberg & Ariel, 1977*), and an infrared retinal camera monitoring system and stimulator (*Miyake & Awaya, 1984*). Both of these allow the accurate centration of the stimulus, and the monitoring of fixation. Other studies have relied on the patient's stable fixation, and have simply presented a flashing target at the centre of a ganzfeld surround (e.g. *Seiple et al, 1986*).

Research has been carried out to identify the optimal stimulus size for focal ERG recording. Although a stimulus of only 1-2° diameter can elicit a recordable ERG, a minimum of 3-4° diameter is necessary to allow for a reduction in focal ERG amplitude with disease that can still be distinguished from the normal recording noise level (*Jacobson et al, 1969*). Larger focal stimuli may also be used, depending on the retinal area perceived to be at risk from a particular disorder. In age-related macular degeneration, for example, recent reports have suggested that the initial locus of the disease is the region extending to 10° either side of fixation (*Curcio et al, 1996; 2000*). A stimulus of 20° diameter might therefore be more appropriate in investigating the early stages of AMD than a foveal stimulus.

4.3.6 The Multifocal Electroretinogram

Multifocal electroretinography was developed by Erich Sutter in the early 1990s (*Sutter & Tran, 1992; Sutter & Bearse 1999; 2000*). It is a technique, which simultaneously assesses the activity of numerous discrete regions of the retina. The multifocal ERG (mfERG) usually produces 61 or 103 focal responses from the cone-driven retina within 7 minutes or less of recording.

The stimulator display usually stimulates 21-25° of the central retina, and consists of an array of hexagons, which are scaled in size to inversely correspond to the variation in cone density with eccentricity (*See Figure 4.6, A*). This means that focal responses should be of a comparable size from each hexagon in the normal subject (*Sutter & Tran, 1992*). The programme modulates each hexagon to flash white and black according to an apparently random sequence. In fact, all the hexagons are following a pattern called the m-sequence, with each hexagon starting at a different point in the sequence. The frame display typically changes at a rate of 75 Hz, with each hexagon having a 50% chance of being white or black at any given time. Whilst these stimuli are being simultaneously presented, the summed retinal response is recorded in the usual way by a single earth, reference and active electrode. Responses derived from the stimulation of each individual hexagon can be determined by adding all the ERG responses following times at which that particular hexagon is white, and subtracting the ERG responses when the hexagon is black. In this way, responses immediately following the presentation of a white hexagon to a given area are accumulated, whilst eliminating all responses associated with the stimulation of other regions. This derived response is known as the first order kernel of the mfERG (*Sutter, 2000*).
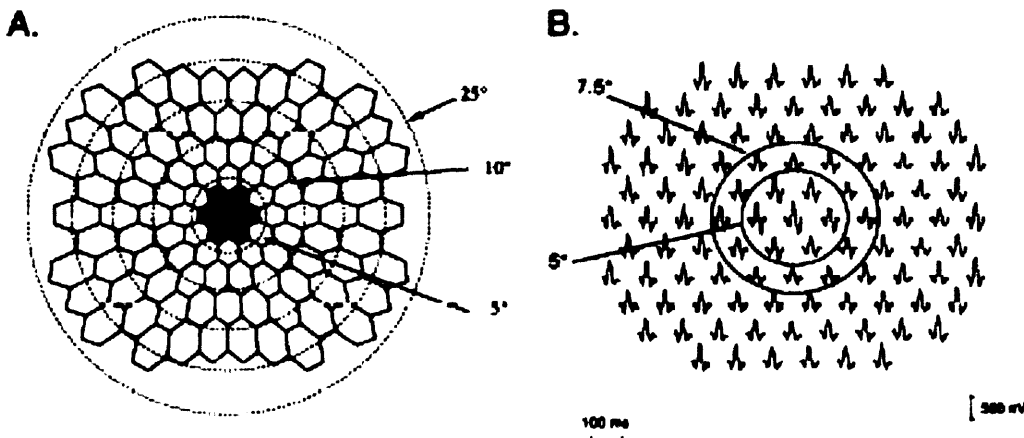
Figure 4.6. Sample display employed in multifocal ERG recording (A). Circles with radii as indicated are shown for reference. Multifocal ERG response recorded from healthy control subject (B) (*From Hood et al, 1998*).

The first order mfERG responses are typically displayed as a topographic representation of the miniature waveforms in relation to their retinal origin (*see Figure 4.6, B*). This allows an immediate visual assessment of any areas of particularly depressed response amplitude. It is equally important, however, to look for delays in the implicit time of responses. Some patients with significantly reduced visual field sensitivity in retinitis pigmentosa have been found to have large amplitude but greatly delayed mfERG responses (*Hood et al, 1998*).

In addition to the basic first order kernel responses, further information can be gained from the mfERG by assessment of the second order kernel. The second order kernel is effectively a measure of the effect of adaptation on each measured local response.

4.3.7 Transient and Steady State Electroretinograms

If visual stimuli are well enough spaced out that the electrical activity arising from one stimulus is completed before the next occurs, the individual ERG waveforms described in section 4.2 may be discerned i.e. a 'transient' response is obtained. If, however, the frequency of flash presentation is increased, the responses to successive stimuli may overlap, resulting in a periodic waveform, or 'steady-state' response. The steady-state response to any stimulus flickering at a frequency greater than about 20 Hz must be the result of cone activity, as rods are unable to respond to temporal frequencies higher than this (*Fleishmann, 1922; Hecht & Schlaer, 1936*). The 30 Hz flicker ERG is a well-recognised clinical test designed to assess cone activity (*Marmor & Zrenner, 1999*). However, the steady-state 30 Hz response reflects solely L- and M- cone activity, as it is too fast for the S-cones to discern (*Stockman et al, 1991*).

4.3.8 Isolating Responses From Rods and Cones

As mentioned in section 4.3.7, it is possible to isolate cone responses simply by employing a high frequency stimulus. However, in order to analyse the individual components of the ERG it is necessary to use a lower frequency stimulus. ISCEV standards (*Marmor & Zrenner, 1999*) suggest that for a single flash cone response, a steady adapting background should be used to suppress rod responses, and that a 10 minute adaptational period should be allowed prior to ERG recording. A frequency of 2 Hz or less is recommended.

In order to obtain a response reflecting the integrity of the rod system alone, ISCEV standards recommend a period of at least 20 minutes dark adaptation, followed by a dim white or blue flash. The frequency of stimulation should be 0.5 Hz or less (*Marmor & Zrenner, 1999*).

4.4   The Electroretinogram in Age-Related Macular Degeneration

4.4.1   The Ganzfeld Electroretinogram in AMD

Sunness et al (*1985*) investigated full-field retinal function in 21 subjects with age-related macular degeneration (AMD) and visual acuity better than 6/18, whose contralateral eyes were at various stages of disease progression. Ganzfeld ERGs were recorded to a range of stimulus intensities, following 45 minutes dark adaptation. The ERG parameters were found to be normal in all subjects, regardless of the extent of macular damage conferred by AMD. Even those eyes with disciform scars secondary to choroidal neovascularisation still maintained full-field ERG responses which fell within the normal range of values. The only reduced ERG responses recorded came from the treated eye of those subjects who had undergone laser photocoagulation. In these subjects the maximum response amplitude in the treated eye was marginally smaller than that of control subjects, although still within the normal range. These results indicated that even at the end stage of the AMD disease process, peripheral retinal function abnormalities are minimal.

Holopigian et al (*1997*) recorded photopic and scotopic ERGs and flicker ERGs from ten patients with early AMD (visual acuity better than 6/7.5), and normal control subjects. The only abnormality found throughout this electrophysiological assessment was a slightly reduced rod-dominated b-wave amplitude in two out of the ten subjects with AMD, and a slightly raised semi-saturation constant (logK) in the scotopic intensity-response functions of a further 2 subjects. In general, the conclusion of this paper was to support previous findings that peripheral vision is largely unaffected in early AMD.

One report investigating visual function in 66 subjects with AMD (*Walter et al, 1999*) did find significant deficits in the group averaged full-field ERG responses recorded. Rod-dominated a- and b-waves were found to be significantly delayed and reduced in amplitude in the AMD group compared to age-matched controls. The b-wave recorded to a bright flash presented to the dark-adapted eye was also significantly smaller than in control subjects. A delay was also found in the timing of OP2. The 30 Hz flicker ERG was found to be normal,

but photopic a- and b-waves recorded to a bright flash were abnormally small, with a significantly increased implicit time of the a-wave. These results suggested a significant dysfunction in both rod and cone activity across the retina. However, it should be noted that the 66 subjects tested were very diverse in the extent of disease progression.

In summary, therefore, the effect of AMD on the full-field electroretinogram is equivocal. There is evidence that the latter stages of the disease may have a sufficient effect on a wide enough area of retina that the visual function deficit may impact upon the amplitude or implicit time of the resultant full-field ERG. Both cone and rod systems appear to be affected. Nonetheless, studies restricted to subjects with early ARM indicate that the full-field ERG is not a sensitive measure of early macular changes.

4.4.2. The Pattern Electroretinogram in AMD

The reversing checkerboard stimulus, by virtue of its constant mean luminance, allows electroretinographic assessment of central retinal function which is not distorted by the effects of scattered light. A number of studies have therefore considered the possible utility of the pattern ERG in the assessment of macular disease (*Arden et al, 1984; Celesia & Kaufman, 1984; Niermann, 1989; Birch et al, 1993; Junghardt et al, 1995; Holder, 1997*). There is a general finding in all these reports that macular disease originating distal to the retinal ganglion cells results in a reduction in amplitude of the P50 component, with a possible increase in latency. Holder further (*1997*) reported that the majority of 223 eyes with macular disease showed no reduction in the N95:P50 amplitude ratio, indicating that there is no selective loss of the N95 component. This is in accordance with evidence suggesting that the N95 component is largely ganglion cell derived, whilst the P50 component comprises both ganglion cell and distal retinal contributions (*Drasdo et al, 1990*).

Holder (*1997*) made comparisons between pattern reversal VEP implicit time and the amplitude of the P50 component of the pattern ERG, and found that a reduced P50 amplitude in macular disease was usually reflected in a delayed VEP response. In optic nerve disease the P50 component of the pattern ERG usually remains intact, whilst the pattern VEP P100 component is delayed. The use of the PERG was advocated by Holder as a means of differentiating between sub-clinical macular disease and optic nerve disease in the case of a delayed VEP.

There has not been wide-scale use of the pattern ERG in the assessment of age-related macular degeneration, possibly as a result of limitations pertaining to the sensitivity of the pattern ERG to optical defocus, and the prevalence of media opacities in the age group susceptible to AMD. However, Birch et al (*1993*) demonstrated the potential value of the pattern ERG in the longitudinal monitoring of macular function in 42 patients with AMD in order to assess the efficacy of laser treatment intervention. The reduction in pattern ERG P50 amplitude was found to be more highly correlated with both the growth of subfoveal membrane and the area of post-laser scarring than measurements of visual acuity.

4.4.3   The Focal Electroretinogram in AMD

Studies using small diameter, foveal stimuli have generally found a good correlation in eyes with AMD between visual acuity and amplitude of focal ERG response (*Biersdorf & Diller, 1969; Birch & Fish, 1988*). However, it would be desirable for a focal ERG to be sensitive to smaller changes in retinal function, which are not always reflected in a reduction in visual acuity. One means of assessing this is to grade the funduscopic signs of AMD in the subjects tested, and to look for correlations with the extent of disruption to the focal ERG response.

Falsini et al (*1999*) evaluated the focal ERG as an objective indicator of outer retinal function in non-exudative AMD. Twenty-five subjects with bilateral dry AMD were graded according to the Wisconsin Age-Related Maculopathy Grading System (*Klein et al, 1991*). Focal ERGs were then recorded to a 9° diameter flicker stimulus, modulated sinusoidally at 32 Hz, the resultant traces were fourier analysed, and the fundamental component assessed. It has been suggested that the fundamental component of the flicker ERG is photoreceptoral in origin (*Zrenner et al, 1987, Porciatti et al, 1989; Falsini et al, 1995*), and may therefore be effective in the assessment of a disorder such as AMD, which is believed to primarily affect the outer retina. The analysis of this parameter showed a mean focal ERG amplitude reduction of 57% in the AMD group compared to controls, although the mean phase remained constant between groups (*Falsini et al, 1999*). A correlation was also found between the severity of the Wisconsin grading score and the decrease in ERG amplitude. These findings suggested that the 32 Hz focal flicker stimulus was effective at assessing the extent of AMD-related retinal changes. Further studies (*Remulla et al, 1995; Falsini et al, 2000*) suggested that a 41 - 42 Hz flicker ERG is even more effective at analysing outer retinal function in AMD. The 41 Hz

stimulus gives a higher amplitude fundamental component than the 32 Hz, less distorted by the 2nd harmonic, which is thought to have a more proximal origin (*Porciatti et al, 1989*).

Remulla et al (*1995*) used a 42 Hz focal ERG stimulus ($4°$ diameter) on 67 patients with unilateral neovascular AMD, but only macular drusen in the test eye. Subjects were classified according to the presence or absence of a choroidal perfusion defect on fluorescein angiography in the test eye. The group of subjects with prolonged choroidal filling times (n = 28) were found to have significant phase delays of the fundamental component of the focal flicker electroretinogram compared to those with normal choroidal filling characteristics, although there was no significant difference in response amplitudes. Remulla (*1995*) hypothesised that this result indicated a link between choroidal vascular abnormalities, with possible outer retinal ischaemia, and delayed foveal ERG implicit times. Previous reports have suggested a weak link between choroidal perfusion abnormalities and the development of choroidal neovascularisation in AMD (*Zhao et al, 1995*). Of further interest, therefore, is whether the delay in the foveal ERG response is also associated with an increased risk of exudative retinal changes.

One means of assessing whether this might be the case is to perform baseline focal ERG tests on the high-risk 'good' eye of patients with unilateral neovascularisation, and to determine the visual outcome of these individuals over a period of time. Sandberg et al (*1993*) recorded foveal electroretinograms to a $4°$ stimulus flickering at 42 Hz on 127 patients, who were then followed up for a period of up to 4.5 years to determine their outcome measure. A preliminary report stated that approximately 20% of the subjects showed a relatively delayed foveal ERG in their non-exudative eye at baseline (*Sandberg et al, 1993*). Delayed implicit time at baseline did not prove to be an independent indicator of an increased risk of choroidal neovascularisation over the course of the longitudinal study (*Sandberg et al, 1998*). It was found, however, that within the subset of patients who did develop CNV, longer delays in baseline ERG timing were associated with earlier onset of exudative changes. It was suggested that these results indicated that a slower foveal ERG implicit time might be a sign of retinal ischaemia, and a forerunner of choroidal neovascularisation.

4.4.4   The Multifocal Electroretinogram in AMD

A number of studies have considered the effect of AMD on the first order kernel responses of the mfERG (*Kretschmann et al, 1998; Huang et al, 2000; Li, 2001; Heinemann-Vernaleken,*

2001). Li et al (*2001*) evaluated the mFERG in 15 patients with early AMD and good VA. Each subject was tested using a mfERG paradigm involving 103 hexagons. Responses were grouped and averaged according to nasal/temporal, and superior/inferior retinal location, and also into 6 concentric rings centred on the fovea. No significant difference was found in the responses from the nasal vs. temporal retinal location, or the superior vs. inferior groupings in either the AMD or control groups. However, analysis of the concentric rings of responses indicated that there was a significant difference between the amplitude of the average foveal responses in AMD and pre-AMD subjects compared to age-matched controls. A longer implicit time of both N1 and P1 responses was also recorded in the AMD and pre-AMD subjects. Furthermore, a similar change was also reported in the responses from the other, asymptomatic eye of subjects with unilateral AMD. As AMD is usually a bilateral condition, this suggests that the foveal mfERG response may be sensitive indicator of these very early, pre-clinical retinal changes in AMD. Similar changes in amplitude and implicit time of the mfERG responses have been reported in wet AMD (*Huang et al, 2000; Jurklies, 2002*), and in atrophic AMD (*Kretschmann et al, 1998; Huang et al, 2000*). In these more advanced cases the amplitude reductions extend into extrafoveal regions, and delayed responses are found throughout the area tested by the mfERG.

Knowledge of the precise retinal originators of the P1 and N1 components is not yet sufficient to allow a full understanding of the locus of damage resulting in these mfERG abnormalities. The P1 amplitude of the central fovea has, however, been strongly linked to cone photoreceptoral function (*Marmor et al, 1999; Kretschmann, 1999*). The reduction in mfERG P1 amplitude in AMD studies is, therefore, consistent with the expected reduction in cone number and function. Li et al (*2001*) point out, however, that there is also a postulated inner retinal contribution to the mfERG (*Hood et al, 1999*). The delays in implicit time of the positive and negative components found in AMD subjects may, therefore, reflect not only outer retinal damage, but potentially also a deficit in more proximal layers.

4.4.5 Electrophysiological Evaluation of Therapeutic Interventions in Age-Related Macular Degeneration

Focal (*Falsini et al, 2003*) and multifocal ERGs (*Palmowski et al, 2002; Ruther et al, 2003; Moschos et al, 2003*) have also been used to assess the effect of treatment on AMD. This allows a more precise determination of the efficacy of surgical or medical intervention than

the standard measures of visual acuity and fundus appearance. In a study by Palmowski et al (*2002*) for example, the multifocal ERG was used to assess retinal function in AMD following photodynamic therapy. It was found that an improvement in parafoveal visual function could be demonstrated using this electrophysiological technique, even when the patient's visual acuity remained unchanged after treatment.

4.5   The Electro-Oculogram (EOG)

The electro-oculogram (EOG) is a technique used to measure the standing potential that exists between the cornea and Bruch's membrane (*Marg, 1951*). The voltage at the cornea is positive in relation to the posterior pole. The amplitude of the eye's standing potential varies with retinal illumination.

Following light onset the standing potential of the eye oscillates. This oscillation has two components, one being much faster than the other. The fast oscillation is evoked by a delayed hyperpolarisation of the basal membrane of the RPE, following the initial hyperpolarisation of the apical membrane, which is responsible for the c-wave (*Steinberg et al, 1983*). The fast oscillation develops approximately 1 minute after light onset, and is recorded using a modified EOG technique, whereby the eye is exposed to periods of light and dark, each 75 seconds in duration. The slow oscillation produces a 'light peak' approximately 5-10 minutes after light onset (*Kris, 1958*). The 'light peak' is generated by the gradual depolarisation of the basal membrane of the RPE (*Linsenmeier & Steinberg, 1982; Griff & Steinberg, 1982; Valeton & Van Norren, 1982*). Following the 'light peak', the standing potential of the eye declines before rising again over time to form a second peak. This slow oscillation has been shown to have a frequency of approximately 2 cycles per hour (*Kolder, 1991*).

Clinically, the EOG is measured under alternating conditions of light and dark, each of 15 minutes duration, using standardised horizontal eye movements to produce a shift in potential difference measured by skin electrodes positioned at the inner and outer canthus. The standing potential is measured in this way at regular intervals through the periods of light and dark adaptation. A ratio is recorded of the maximum amplitude of the standing potential in the light, i.e. the 'light peak', to the minimum amplitude in the dark i.e. the 'dark trough'. The ratio of 'light peak', to the preceding 'dark trough' is known as the Arden Ratio (*Arden & Fojas, 1962*) and is an objective means of assessing RPE integrity, which is unaffected by interindividual variations in absolute values.

Although the EOG is severely reduced in many diffuse abnormalities of the RPE, like the c-wave, healthy photoreceptor function is also required to elicit a normal response. Furthermore, the mechanism behind the light peak is believed to be an adrenaline activation of the apical α 1- adrenergic receptors, resulting in an increase in the concentration of calcium ions in RPE cells, which act as a secondary messenger to increase basal membrane chloride conductance (*Joseph & Miller, 1992*). Therefore, any dysfunction which decreases the release of either the primary (adrenaline), or secondary (calcium ions) messenger will also result in an EOG abnormality. Consequently the EOG is not a specific indicator of RPE pathology.

4.6   The Electro-oculogram in AMD

The EOG is a mass response, and is unmeasurable if less than 30° solid angle of the retina is illuminated (*Linsenmeier & Steinberg, 1982; Steinberg et al, 1985*). As with the ganzfeld ERG, the EOG is unaffected by small lesions, or functional deficits confined to the macular region. Sunness et al (*1985*) and Holopigian et al (*1997*) both used the EOG to investigate the possibility of diffuse retinal dysfunction in patients with early signs of AMD. The Arden ratio was found to be normal in all AMD subjects, supporting previous findings by Marcus et al (*1983*). The more diverse group of AMD subjects participating in a similar study by Walter et al (*1997*) did, however, demonstrate significantly lower group averaged values for the light peak, dark trough and Arden Ratio than the age-matched normals. This was found to be most marked in subjects with geographic atrophy, and not significant in those who had solely hard or mixed drusen.

Arden & Wolf (*2003*) speculated that the mixed evidence pertaining to EOG results from individuals with AMD could be related to the variability of the clinical EOG. By increasing the period of pre-dark adaptation prior to the presentation of the EOG light stimulus, they attempted to minimise this variability and provide a more precise measure of the effects of AMD on the EOG response. This technique, performed on 17 patients with AMD, demonstrated a delay and slight reduction in the amplitude of the light peak of the patient group compared to normal controls.

A further aspect of this investigation was to consider EOGs recorded in response to ethanol. It has been shown that small quantities of alcohol, when taken orally, can induce a change in the standing potential of the eye which is indistinguishable from the slow oscillations evoked by light stimulation (*Skoog et al, 1975*). Arden & Wolf (*2003*) demonstrated this effect by

performing both techniques on normal control subjects, as well as on individuals with AMD. The alcohol EOG was found to be markedly more reduced and delayed than the light EOG in AMD subjects. Even those with only minor fundal changes and no loss of acuity demonstrated some loss in the light-rise, and the extent of this deficit was found to correlate with the grading of RPE changes. It was suggested that this change was due to an inability of alcohol to stimulate the RPE. This could be due to basal laminar deposit within and below Bruch's membrane, obstructing the passage of water-soluble molecules from the choroid to the RPE. Whatever the precise mechanism, these results imply a widespread change to the physiology of the RPE occurring even at an early stage of AMD.

4.7   The Visual Evoked Potential

The visual evoked potential (VEP) is a signal which originates in the visual cortex following the presentation of visual stimuli. The signal is recorded at the scalp via surface electrodes, which detect the open electrical fields generated by synchronous slow potentials in apical dendrites of the visual cortex (*Wood, 1982*). Like the ERG, the VEP can be recorded either to pattern or flash stimuli.

4.8   Recording the Visual Evoked Potential

4.8.1   Electrodes and Electrode Positioning

In the recording of a VEP it is necessary to ensure that electrodes are attached in the same position relative to the visual cortex in all subjects. All electrode placement systems rely on measurements taken from easily identifiable 'bony landmarks' on the skull i.e. the nasion (the bony ridge just above the nose), the inion (the ridge slightly above the base of the skull), and the preauricular notches (depressions located anterior to either ear). Some clinicians will position the electrodes at fixed measurements from these points, with the active electrode placed 5cm above the inion along the midline (*Halliday et al, 1979*). However, this does not allow for interindividual variability in head sizes. The more commonly used 10-20 system instead places electrodes according to a predetermined percentage of the distance between the bony landmarks (*Harding, 1991*). Different numbers and locations of electrodes may be used to record different signals, but this system is consistent for all head sizes, and controls some

of the intersubject variability inherent in VEP recording. Variability in responses can still be high, however, as a result of individual differences in cortical topography.

4.8.2 Pattern Stimuli

Pattern VEPs are generally recorded in response to a checkerboard, although sine- and square-wave stimuli may also be used. The checkerboard pattern VEP may be phase-reversed, such that white squares become black, and vice versa, at a rate determined by the stimulus frequency. The pattern may also be presented and then removed, to be replaced by a background of the same mean luminance as the pattern. In both cases the mean luminance of the display remains constant, ensuring that the VEP recorded is a visual response to the pattern itself, uncontaminated by luminance responses. Furthermore, since there is no change in the mean luminance of the pattern stimulus, there is no excitation of the peripheral retina by time-locked stray light. Consequently, the pattern VEP response originates from the area of the retina stimulated by the checkerboard, with no scattered light response.

The VEP evoked to a pattern reversal checkerboard stimulus consists of three major components, the N75, P100, and N135 (*See Figure 4.7*). The initial letter denotes the polarity of the response (positive or negative), and the number indicates the approximate implicit time of the peak. The P100 is the most prominent, and most commonly assessed pattern VEP parameter.

Responses to patterned stimuli are strongly affected by optical factors, such as pupil diameter (the technique is performed undilated), refractive error and lens opacities.
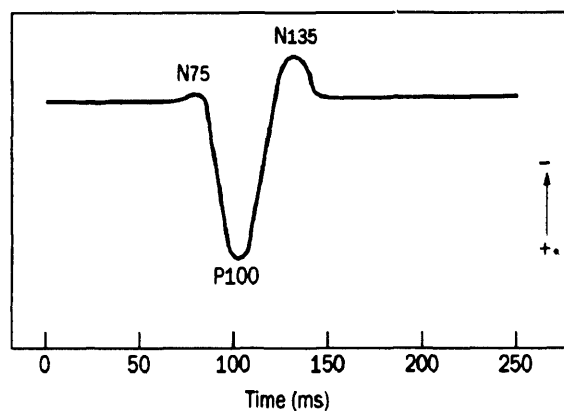
Figure 4.7. The waveform of the pattern-reversal VEP (*Brigell, 2001*).

4.8.3   Flash Stimuli

Unlike the pattern VEP, the flash VEP is relatively unaffected by media opacities, as most opacities will scatter rather than absorb light. An amplitude reduction greater than 50%, or a response implicit time greater then 15 ms is, therefore, highly suggestive of central visual field dysfunction (*Brigell, 2001*). This makes the flash VEP a valuable tool in the assessment of retinal function in elderly patients with cataract.

The major disadvantage of the VEP recorded to a flash stimulus is the complexity of the waveform. The flash VEP consists of four negative, and three positive peaks, labelled N1, P1, N2, P2, N3, P3, N4, P4 (*See Figure 4.8*). As the flash VEP is often variable in waveform between individuals, it can be difficult to identify and analyse homologous waves.
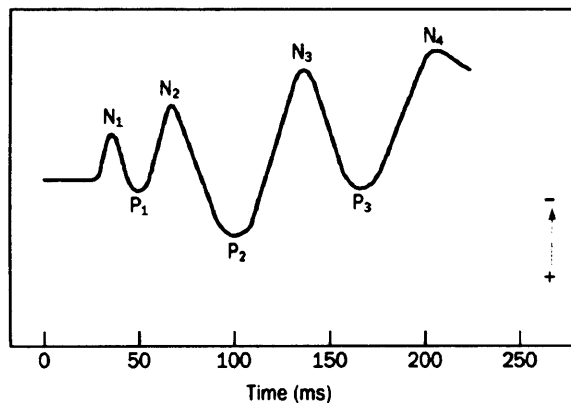
Figure 4.8. The waveform of the flash VEP (*Brigell, 2001*).

4.8.4   The Assessment of Visual Evoked Potentials

Even when the components of the VEP are identified, assessment of the amplitude of each response can be unreliable, with up to 25% intrasubject variability on different recording sessions (*DeVoe, 1968*). The implicit time of the components, however, is found to be a more reliable indicator of dysfunction within the visual pathway. Normal intrasubject variability for implicit time of the pattern VEP P100 component is between 2 and 5% (*Oken et al, 1987*). Although a prolonged implicit time of VEP components is generally associated with nerve demyelinating conditions of the visual pathway, such as multiple sclerosis, resulting in slowed signal transduction (*Asselman et al, 1975*), an increase is also reported in other conditions, such as central serous retinopathy (*Sherman et al, 1986*). In this case the increased implicit time is believed to be due to reduced efficacy of cones in the absorption of photons of light, rather than in a slowed transmittance through the visual pathway (*Smith et al, 1978*).

4.8.5　Transient and Steady State Visual Evoked Potentials

The frequency of stimulus presentation of a VEP will also effect the waveform of the response. As with the ERG, a response recorded to a high frequency stimulus (above 6-10 Hz) will be a steady state response. The transient VEP is recorded to lower stimulus frequencies, allowing analysis of individual components.

4.8.6　The Multifocal Visual Evoked Potential

This is a technique which has been developed as a means of assessing localised defects in the visual field (*Sutter, 1992*). A pseudorandom sequence of stimuli (the m-sequence) is presented to record independent responses from multiple areas of the visual field. These responses are then used to derive linear and non-linear components of the VEP.

Betsuin et al (*2001*) recorded multifocal VEPs from 20 controls, and 6 subjects with AMD. When responses were analysed within the four quadrants of the visual field tested, it was found that results corresponded to measured perimetric defects. A similar congruity between multifocal VEP and perimetry results has been reported previously (*Klistorner et al, 1998*). This suggests a possible value of the multifocal VEP in assessing localised defects of the central visual field.

4.8.7　The Dynamic Visual Evoked Potential

A further way in which the VEP has been used in the assessment of macular integrity is in the monitoring of the recovery of visual function following exposure to an intense light source. Parisi (*2001*) described an increased time to peak, and decreased amplitude of the major P100 component following a photopigment bleach. Both amplitude and implicit time can be recorded over time after the bleach until the VEP regains its baseline parameters. The recovery of VEP amplitude has been shown to take several times longer than the return of baseline visual acuity following a bleach. Both VEP and acuity recovery times have been shown to be age-dependent (*Lovasik, 1983*).

It has been claimed that the recovery time is dependent on the speed with which photopigment can regenerate. Any disease, therefore, which compromises the integrity of, or limits the supply of metabolites to the photoreceptor/RPE complex is likely to prolong recovery.

Parisi (*2001*) described the dynamic VEP as being an objective, but not specific test of macular function as VEP recovery is found to be affected not only in diseases of the outer retina, such as Stargardt's disease (*Parisi, 2002*), and diabetes (*Parisi, 1994*), but also in conditions which have an effect on the inner retina or optic nerve head such as multiple sclerosis (*Parisi et al, 1998*), and primary open angle glaucoma (*1992*). The technique has not been used on subjects with age-related macular degeneration.

4.9 The Visual Evoked Potential in Age-Related Macular Degeneration

The VEP is of particular interest in the assessment of AMD because of cortical magnification i.e. more than 50% of cells in the primary visual cortex have receptive fields in the central 10° of visual angle (*Daniel & Whitteridge, 1961; Horton & Hoyt, 1991*).

Information from the central visual field is processed nearest to the surface at the occipital pole (and so nearest to the skin electrodes recording the signal), whereas the peripheral visual field is represented at a location deep within the calcarine sulcus (*Holmes, 1931*). As a result, the relative influence of macular activity on the VEP is further enhanced. The VEP is, therefore, a means of obtaining information regarding central retinal function, without the problems associated with recording a focal retinal response.

One recent study (*Perlman, 2001*) investigated both flash and pattern-reversal visual evoked potentials in twenty patients with varying degrees of age-related macular degeneration. It was found that flash VEPs were apparently normal in patients with AMD. When both eyes of a patient with unilateral late AMD were tested monocularly, however, there was a slightly reduced amplitude in the response from the eye with more advanced retinal changes. The authors suggested that the lack of sensitivity to early AMD changes might reflect the focal nature of the disorder, which is masked by the magnitude of the full-field flash response. It was therefore hypothesised that that a focal flash VEP response might be a more sensitive indicator of macular disease. This was supported by findings that the focal pattern reversal VEP was significantly delayed and reduced in amplitude in AMD, even in cases of normal, or near normal visual acuity (*Perlman et al, 2001*). The sensitivity of the pattern reversal VEP to early macular changes suggests a potential utility of the technique in the monitoring of visual function before and after treatment for AMD (*Cohen et al, 1994; Brunner et al., 2000*).

CHAPTER 5 : VISUAL PSYCHOPHYSICS

5.1   Introduction

In the clinic, AMD is typically evaluated by ophthalmoscopic examination of the central retina and by the assessment of visual acuity. Although of value in the clinic, these techniques only provide information about gross changes in retinal form and function. In recognition of the need for the development of more sophisticated measures, numerous studies have been undertaken to evaluate the diagnostic and prognostic value of alternative techniques. However, evaluation of these studies is complicated by the variety of study designs and outcome variables used by different research groups.

Some cross-sectional studies use subjects with neovascular AMD in the non-study eye and only drusen in the test eye (for example *Eisner et al, 1991*) because these 'healthy' eyes are considered to be at high risk of exudative outcome (*Strahlman, 1983*). Comparisons between the results of these patients and those with bilateral drusen may highlight tests which are sensitive to early pre-exudative retinal changes. However, it is not known exactly which of these subjects will go on to develop exudative changes, and thus the true prognostic value of any test cannot be confirmed. This may only be assessed by means of a longitudinal study where visual function is measured at baseline in a group of subjects, and followed up over a prolonged period.

There are also differences in the methods used to evaluate outcome variables. In some cases group averaged data is compared (for example *Collins & Brown, 1989; Kleiner et al, 1988*). Whilst this may give an insight into the mechanisms underlying the disease process, a difference in group means does not signify that a test has any clinical value. Other studies have looked for correlations between the extent of macular fundus changes (e.g. number and morphology of drusen, percentage area of hyper-/hypo-pigmentation of RPE) and the severity of functional deficits.

Given the difference in study designs, it is not easy to compare results. However, trends in the data do suggest that certain visual functions are significantly affected in early AMD.

The following chapter reviews the psychophysical literature as relates to AMD. References were collected using the Web of Science, and PubMed literature search engines. Particular

emphasis has been placed on studies involving large groups of subjects, and on longitudinal studies which have assessed visual outcome over prolonged periods of time.

5.2 Visual Acuity

5.2.1 Introduction

Visual acuity (VA) is a measure of the finest resolvable detail in a high contrast pattern. Clinically it is determined by the identification of letters on a chart. VA may also be assessed by the use of less complex stimuli, such as sine wave gratings, where the spatial frequency content of the task is well defined.

Excluding cortical effects, visual acuity is primarily a measure of central retinal integrity, determined by cone photoreceptor function. Standard measurements of acuity do not provide information about peripheral or scotopic vision. Furthermore, the classic representation of 6/6 snellen acuity as representing 'normal' foveal function must be questioned. Elliott et al. (*1995*) assessed visual acuity in 223 subjects with no ocular pathology, ranging in age from 18-80 years of age. They found the average visual acuity of subjects aged 18-24 years to be 6/4.5, declining to 6/6+1 in subjects aged 75+ years. It is clear from this normative data that the assumption that a subject with 6/6 acuity has fully functioning foveal cones is flawed, as an acuity of 6/6 clearly represents a considerable reduction in foveal function in a subject previously achieving 6/4.5. Indeed, Frisen and Frisen (1979) estimated that an acuity of 6/6 can be obtained with only 45% of the foveal cones in working order. Classic measures of visual acuity must therefore be regarded as providing only limited information about retinal function.

5.2.2 Clinical Measures of Visual Acuity

Visual acuity is typically measured with the Snellen Letter Chart, which was designed in 1862 (*see Figure 5.1 A*). The conventional test contains ten lines of letters which gradually decrease in size whilst the number of letters on each line increases. Snellen assumed that the average eye could resolve detail of 1 minute of arc. Hence each line is annotated with the distance at which the limb width of the letters subtends 1 minute of arc. Although many other letter charts have been designed since, Snellen's terminology remains widely used.

$$\text{Visual Acuity} = \frac{\text{Viewing Distance}}{\text{Distance at which smallest detail resolved subtends 1 minute of arc}}$$
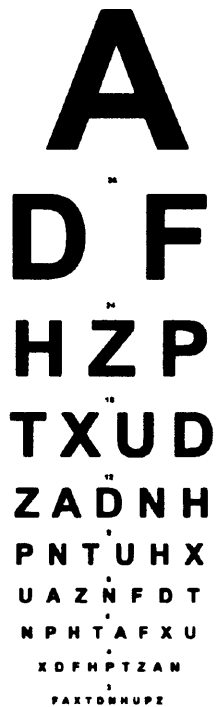
A   **B**
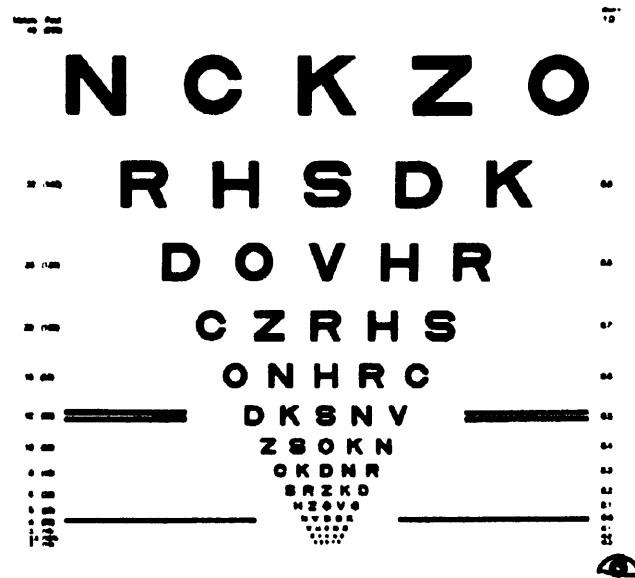
Figure 5.1. Samples of Snellen (A) and Bailey Lovie (B) visual acuity charts.

The Bailey-Lovie visual acuity chart (*Bailey & Lovie, 1976*) was designed to address some design limitations of the Snellen Chart (*see Figure 5.1 B*). There is an equal number of letters on each line, with one letter-width spacing between each character. The inter-row spacing is equal to the letter height of the lower row. These modifications help to standardise the effects of crowding. It also provides more large letters on the rows for the assessment of patients with low vision.

Visual acuity assessed using the Bailey Lovie Chart is recorded as the log of the minimum angle of resolution (logMAR). The Snellen 6/6 fraction, which indicates a minimum angle of resolution of 1 minute of arc, therefore has a logMAR value of 0.

Low contrast versions of standard letter charts are also available (*see for example Regan &* *Neima, 1983*).

5.2.3   *Visual Acuity and AMD*

Most investigations use visual acuity as the basis for the classification and grading of subjects with AMD, thus the selection criteria used often preclude the assessment of the relationship between disease severity and visual acuity.

Cheng & Vingrys (*1993*), for example, measured VA with high (90%) and low (10%) contrast Bailey-Lovie charts on 11 subjects with early ARM, 11 with pre-ARM, and 8 age-matched controls. A significant difference was found in the VA of the groups, but this was undoubtedly biased by the selection procedure, in which subjects were classified according to fundus appearance and high contrast VA. Low contrast VA was found to correlate well with high contrast VA, and gave little extra information regarding retinal function. This finding was in agreement with previous findings (*Lovie-Kitchin, 1989*).

Brown et al (*1983; 1984*) investigated variations in VA under different conditions of luminance and retinal eccentricity in subjects with AMD and age-matched controls. Subjects with AMD were found to adapt more slowly to variations in background luminance (*Brown et al, 1983*), and experienced greater difficulty than controls in performing visual acuity tasks in low luminance (*Brown et al, 1984*). Furthermore Sunness et al (*1997*) found visual acuity to be disproportionately reduced with a reduction in luminance in 153 subjects with geographic atrophy in comparison to subjects with bilateral drusen, indicating that the extent of this deficit is dependent on the severity of retinal changes.

Eisner et al (*1991*) evaluated the prognostic value of VA measurement in subjects at risk of developing neovascular AMD. Forty-one subjects with unilateral exudative AMD in the non-test eye were investigated, and were classified as being at high- or low-risk of exudative outcome according to fundus appearance in the test eye. It was found that a high risk fundus appearance in the test eye was associated with reduced VA in the fellow eye. Longitudinal studies, however, have not illustrated any link between baseline VA and a neovascular outcome.

Sunness et al (*1997*) used visual acuity as an outcome measure in a longitudinal study to determine the relative changes in visual function which occurred in 13 subjects with bilateral drusen and 153 subjects with geographic atrophy over a 2 year follow-up period. The median

worsening in visual acuity of the geographic atrophy group was found to be 3 lines, compared to a median of 3 letters in the drusen group. Subjects with drusen in the test eye, and geographic atrophy in the fellow eye fell between the two in terms of visual acuity loss.

The widespread use of VA measures in the assessment of AMD is defended by the suggestion that object and pattern perception depend almost exclusively on the perception of fine detail. However, low spatial frequency information has been shown to be equally important for object recognition and detection (*Marron et al, 1982*). In order to fully evaluate the sensitivity of the visual system to spatial variations in luminance, it is necessary to measure the contrast sensitivity function.

5.3 Spatial Contrast Sensitivity

5.3.1 Introduction

The contrast sensitivity function is determined by measuring the contrast threshold for detection of sinusoidal gratings at various spatial frequencies. In normal subjects the result is a band-pass function, with the highest contrast sensitivity in the mid-spatial frequency range - approximately 2-6 cycles/degree (*Campbell & Green, 1965*).

The characteristics of this curve vary with changes in luminance level and retinal location. As luminance is reduced from photopic to mesopic levels, there is a general decrease in contrast sensitivity. Maximum contrast sensitivity and the high-frequency cut-off (corresponding to visual acuity) shift to lower spatial frequencies (*Patel, 1966*). At low scotopic levels the low frequency attenuation in contrast sensitivity is not apparent. The same trends can be seen with increasing retinal eccentricity (*Rovamo et al, 1978*). This indicates the importance of stating all parameters used for contrast sensitivity measurements.

Contrast sensitivity measurement is more time-consuming than recording of visual acuity, but provides more information. In some disorders high-spatial frequency sensitivity can remain intact whilst low spatial frequency sensitivity is significantly attenuated. In studies into visual performance in AMD, therefore, it has been important to record contrast sensitivity functions in order to determine whether it is purely high spatial frequency sensitivity which has been lost, or whether there is a more widespread deficit in spatial visual function.

5.3.2   Contrast Sensitivity and AMD

The largest study to date was carried out by Alexander et al (*1988*). They discovered a reduction in the peak contrast sensitivity below the minimum of elderly controls in 80% of 100 subjects with AMD. However, the subject group employed in this study had advanced retinal changes, and visual acuity ranging from 6-30 – 6/384. Furthermore, the test parameter consisted of an estimate of peak contrast sensitivity based on the visibility of 4 equally sized letters (6/405) presented at gradually reduced contrast. Changes to the contrast sensitivity function were therefore not fully characterised, and the study did not investigate the earliest changes occurring in AMD.

Sjostrand et al (*1977*) recorded contrast sensitivity functions to sinusoidal gratings ranging in spatial frequency from 0.7-38 cycles/deg. Eleven subjects with macular disease (3 with AMD) were investigated, and 10 healthy controls (aged 19-61). This study demonstrated that subjects with AMD show most marked reduction in contrast sensitivity for high and intermediate spatial frequencies, with contrast sensitivity almost unaffected below 2 cycles/degree. However, one subject with more advanced AMD showed a more marked impairment across the whole spatial frequency range. A further study (*Sjostrand et al, 1979*) on a larger subject group (n = 22) showed similar results. Sjostrand suggested that this indicates a sparing of the peripheral part of the test field (more sensitive to lower spatial frequencies) when an overall reduction in contrast sensitivity at all spatial frequencies might suggest the involvement of a wider retinal area (as in those subjects with advanced AMD).

However, these studies did not age-match their controls. The significance of this is highlighted by Owsley et al (*1990*) who demonstrated a small but significant reduction in spatial contrast sensitivity with age in control subjects, especially at high spatial frequencies. The same pattern of loss was noted in subjects with early AMD (*Owsley et al, 1990*), but to a greater extent (*See Figure 5.2*). Once again the major locus of sensitivity loss in AMD subjects was in the high and mid spatial frequency mechanisms. Other studies have supported this finding (*Brown & Lovie-Kitchin, 1987; Stangos et al, 1995*).

Although group averaged data suggest a reduction in contrast sensitivity in individuals with AMD compared to age-matched controls, no significant difference has been found between those subjects with bilateral drusen, and those with monocular exudative AMD in the non-text eye. This indicates that this test is not sensitive to increased risk of neovascularisation (*Stangos et al, 1995*).

0.001

0.010 —

CONTRAST

0.100 —

1.000

C   B   A

SPATIAL FREQUENCY
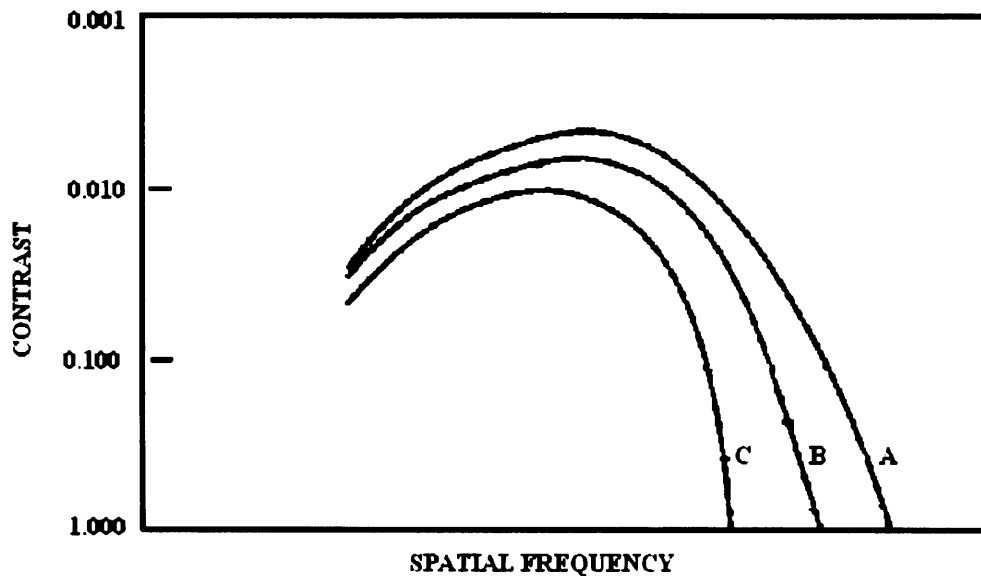
Figure 5.2. Schematic plot illustrating three hypothetical contrast sensitivity functions from young adult (A), older adult (B), and individual with non-exudative AMD (C). The reduction in contrast sensitivity for the subject with AMD is similar to that observed with normal ageing, but more pronounced (Owsley et al, 1990).

Brown & Garner (*1983*) evaluated the effect of luminance on the contrast sensitivity function in people with AMD. Results from both control subjects, and those with AMD showed a generalised decrease in contrast sensitivity for all spatial frequencies as luminance decreased, and a shift in peak contrast sensitivity towards lower spatial frequencies. The contrast sensitivity function was found to be significantly depressed in the AMD group compared to the control group at the higher luminance levels, with only a small difference between groups at the lowest luminance level.

The implication of these studies is that measurements of contrast sensitivity will allow a greater discrimination between AMD and control subjects at high levels of luminance and high spatial frequencies. High spatial frequencies are only detectable by the visual system at high contrast levels, where the task is very similar to that of visual acuity measurement. The recording of a full contrast sensitivity function may not, therefore, provide any additional information in the assessment of patients with AMD than basic acuity tasks. Owsley et al (*1990*) illustrated this by evaluating the visual acuity of 15 subjects with AMD (VA ranging from 6/7.5-6/18), and 30 elderly controls using the Regan low contrast letter charts (100%, 84%, 40%, 25%, and 12% contrast). They found that the greatest acuity losses for AMD subjects were detected using the high contrast charts. Other studies however have found the lower contrast charts to be more effective at discriminating between AMD subjects and controls (*Greeves et al, 1988, Kleiner et al, 1988*).

5.4 Temporal Resolution

5.4.1 Critical Flicker Frequency

The critical flicker frequency (CFF) describes the highest temporal frequency at which a stimulus is still perceived as flickering. The CFF of the visual system is dependent on stimulus and adaptive parameters (see *Brown, 1965* for review). Importantly, the CFF also changes with age. Domey (*1964*) stated that the average CFF changes from 44.8 Hz at age 13-19 years to 33.1 Hz at age 80-89 years. This emphasises the importance of age-matching in comparisons of subject and control groups.

5.4.2 Critical Flicker Frequency and AMD

Brown & Lovie-Kitchin (*1987*) investigated CFF to a square wave stimulus (100% modulation) in nine subjects with ARM, 8 pre-ARM subjects, and 10 age-matched controls. Values were found to be reduced in the ARM group compared to control and pre-ARM groups. Pre-ARM subjects showed a marginal reduction compared to controls. The implication of these results was that temporal aspects of visual function are significantly affected even in early AMD.

5.4.3 Temporal Contrast Sensitivity

De Lange (*1952*) extended the concept of the CFF function based on work by Ives (*1922*) to plot, for a range of temporal frequencies, the contrast threshold at which flicker is just perceivable. The temporal CSF resembles the spatial CSF curve in showing both high and low frequency attenuation. An observer will see any combination of frequency and modulation depth below the function as flicker, whilst any point lying above the curve is perceived as steady light.

5.4.4 Temporal Contrast Sensitivity and AMD

The recording of temporal contrast sensitivity is time consuming. Several studies have therefore limited their evaluation to the contrast threshold for flicker perception at a pre-determined frequency. Haegerstrom-Portnoy et al (1988) investigated flicker sensitivity to a

25 Hz stimulus at different wavelengths (630nm, 570nm, 480nm) in 10 subjects with early ARM, 8 pre-ARM subjects, and 9 elderly controls. Results showed flicker sensitivity to be reduced in ARM subjects compared to controls for the 570nm and 630nm stimuli. However, the test did not seem to be sensitive to very early retinal changes.

Eisner et al (*1992*) assessed sensitivity to a 20 Hz flickering stimulus in a prospective study on a group of 47 subjects with exudative AMD in the fellow (non-test) eye, and only early retinal changes in the study eye. Eleven of the 47 subjects developed neovascular AMD in the test eye over the 18 month follow-up period. Results showed no evidence of a relationship between flicker sensitivity and an exudative outcome. Although 20 Hz flicker sensitivity in AMD patients was shown to be an unreliable risk indicator on the limited group tested (*Eisner et al, 1992*), Mayer et al (*1992; 1994*) widened the investigation to determine the prognostic value of the measurement of a complete temporal contrast sensitivity function.

Mayer et al (*1992*) initially measured temporal contrast sensitivity functions in 13 subjects with unilateral CNV in the non-test eye, and compared with results from an age-matched control group, and from a younger control group. Overall temporal contrast sensitivity was reduced in both older groups compared to younger eyes, but the group at risk of exudative changes demonstrated greater sensitivity losses than the older controls. This was most marked at mid-temporal frequencies (10 – 14 Hz), and slightly less so at the lower temporal frequencies. At high temporal frequencies (40-50 Hz) there was considerable overlap between the two study groups. This echoes results found by Brown and Lovie-Kitchin in a smaller study (*Brown & Lovie-Kitchin, 1987*).

Mayer et al (*1992; 1994*) also collected longitudinal data to determine the value of the temporal contrast sensitivity function in predicting CNV development. After 4 years follow-up, of sixteen eyes tested at baseline, seven had converted to exudative AMD (*Mayer et al, 1994*). The converted eyes showed a greater sensitivity loss at baseline than those AMD eyes which didn't develop CNV over the duration of the study. Sensitivity to 5 and 10 Hz showed the greatest separation at baseline between those eyes which would develop exudative changes and those which would not (*see Figure 5.3*).
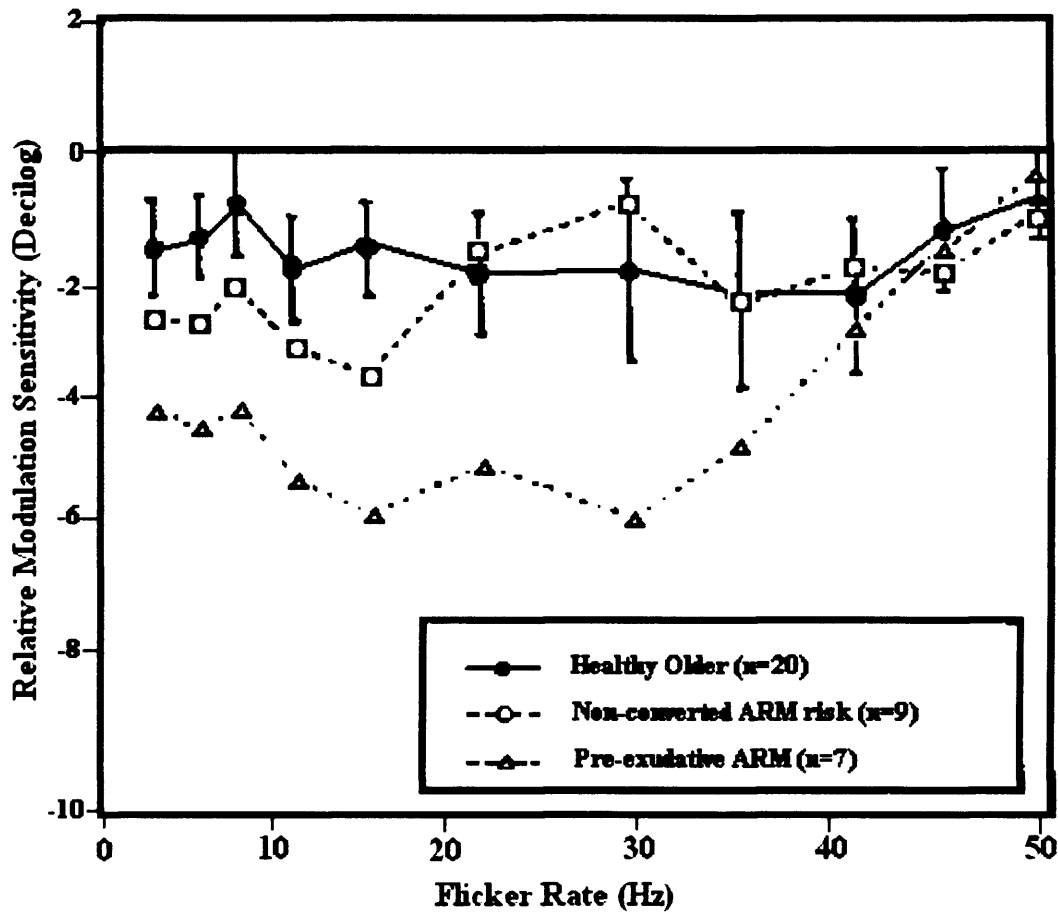
Figure 5.3. Diagram showing temporal contrast sensitivity for healthy older, non-converted ARM risk and pre-exudative ARM eyes at baseline. Relative modulation sensitivity is calculated by taking the ratio of actual modulation sensitivity to predicted sensitivity based on results from 30 younger adults. A clear separation between groups is seen at mid-low temporal frequencies (*Mayer et al, 1994*).

When sensitivity to 5 and 10 Hz was combined, and a cut-off point selected, baseline results were found to separate between the two groups with 100% accuracy. Whilst this result appears impressive, the sample size was too small to draw any definitive conclusions. Furthermore, given the number of test parameters and combinations that could be evaluated, it is not clear whether this finding is due to a type I statistical error.

5.5   Colour Vision

5.5.1   Introduction

Colour vision is clinically defined as the ability to differentiate between two equiluminant stimuli on the basis of spectral composition alone. Acquired colour vision defects arise in a

range of ocular pathologies of both retinal and post-retinal origin. Francois and Verriest (*1968*) identified 92 conditions in 1179 patients which gave rise to acquired colour vision defects.

At the level of the outer retina, human colour vision is determined by the differential absorption of light by three cone photoreceptor types, most sensitive to short- (425nm), medium- (535nm) and long- (565nm) wavelength light. Figure 5.4 illustrates the absorption spectra of these three systems. The scotopic luminosity function of the rod photoreceptors is also illustrated.
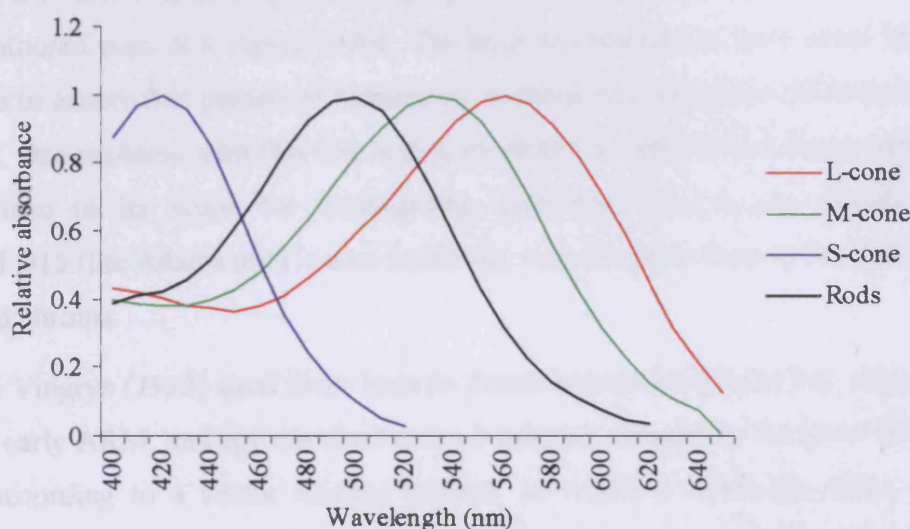
Figure 5.4. The absorption spectra of L-, M- and S- cones and rods (*Dartnall et al, 1983*).

Studies into age-related changes in colour vision have shown that hue discrimination deteriorates with age, with blue-yellow colour discrimination most affected (*Knoblauch et al, 1987; Verriest et al, 1962*). Although this effect is largely explained by age-related changes in the ocular media (*Moreland, 1993; Verriest et al, 1962*) age-related changes in the S-cone pathway also play a role (*Knoblauch et al, 1987; Schefrin, 1992*).

5.5.2 *Colour Vision and AMD*

Köllner (*1912*) noted that colour vision defects in patients with retinal disease are usually blue-yellow in origin, compared to the red-green deficiencies noted in congenital defects and in optic nerve disorders. On this basis, an acquired colour vision defect in AMD may be expected to be tritanopic in origin. This finding would also be consistent with the parafoveal

locus of damage in the disease, as it is in this region that S-cones are at their greatest density (*Curcio et al, 1991*).

Reports from as far back as 1942 (*Sloan, 1942*) have detected tritan defects in patients with AMD. More recent studies have focused on the prognostic potential of colour vision testing in AMD (*Eisner et al, 1992*), and on its ability to monitor changes in the disease process by comparing groups with different levels of disease severity, or by correlating with fundus appearance (*Eisner et al 1991; Cheng & Vingrys 1993*).

Various colour vision tests have been used in the assessment of AMD patients. The Farnsworth D15 test is most frequently employed (*Farnsworth, 1943*). Patients are required to place 16 coloured caps in a logical order. The hues are selected to have equal Munsell value and chroma to ensure that perceived luminance, contrast and saturation differences cannot aid the subject. One problem with this test is that its ability to demonstrate tritan defects is weak in comparison to its scope for highlighting significant protan and deutan defects. A desaturated D15 (the Adams test) is also available, with the same hues at the Farnsworth D15, but reduced chroma.

Cheng and Vingrys (*1993*) used these tests to detect acquired losses in hue discrimination in pre-ARM, early ARM, and age-matched control subjects. Results to the panel D15 tests were analysed according to a vector scoring method, in which a confusion index (C-index) is calculated to represent the extent of colour vision loss, and a scatter index (S-index) to indicate the randomness of the arrangement. The vector angle classifies the type of defect. The 98th percentile of the C-index results of controls was adopted as the pass criterion. On this basis 1 pre-ARM, and 6 ARM subjects failed the D15 test. Results from the desaturated D15 test showed more variability in both the control and ARM groups, and the separation between the groups was therefore less marked than with the standard D15 test. Thus, with the criteria used only 2 ARM, and 1 pre-ARM subject could be considered abnormal.

The expected tritan defect was observed in all the subjects that failed the D15 tests, but sensitivity was not high and most pre-ARM subjects passed both tests. Atchison et al (*1990*) similarly found the desaturated D15 test to be insensitive to early retinal changes in ARM. In contrast, Collins et al (*1986*) found the desaturated panel D15 test to be effective in detecting changes in colour vision in patients with ARM, and visual acuity of 6/6 or better (*Collins, 1986*). This study was assessed on the basis of group means, however, which could account for the difference in outcome.

Eisner et al (*1991, 1992*) considered the prognostic value of the panel D15 test. In a cross-sectional study 41 subjects with unilateral neovascular AMD in the untested eye were classified as high or low risk of exudative outcome in the test eye according to fundus appearance (*Eisner et al, 1991*). Seventeen of 32 high-risk eyes failed the D15 test, and all eyes with low-risk fundi passed (*according to Adams' pass/fail criterion, 1982*). A subsequent longitudinal study followed 47 subjects with neovascular AMD for at least 18 months (*Eisner et al, 1992*). Failure of the D15 test at baseline was found to be a sensitive indicator of exudative changes (8 of 11 eyes which developed CNV failed the panel D15 test at baseline). Specificity was poor however, as 12 out of 32 eyes which did not develop advanced AMD during the follow-up period also failed the D15 test at baseline.

A more sensitive measure of hue discrimination can be obtained with the Farnsworth-Munsell 100 hue test (FM 100 hue; *Farnsworth 1943*). This test consists of 85 movable colour samples arranged in four boxes of 21 or 22 colours each. The colour samples form a natural hue circle, representing perceptually equal steps of hue difference.

Midena et al (*1997*) used the FM 100 hue test to evaluate 47 patients with early AMD and 36 age-matched controls. On the basis of comparisons made with Verriest's ranges of normality (*Verriest et al, 1982*), no subjects were found to exhibit abnormal hue discrimination in this study. However, Bowman et al (*1980*) found the FM 100 hue test to be more sensitive than the D15 test at detecting early retinal changes in subjects with AMD. This difference could be accounted for partially by the difference in outcome variable, with Bowman (*1979*) assessing differences in group means rather than using the test as a diagnostic measure. The selection criteria in Midena's study (*1997*) were also more stringent, with all subjects having a VA of 6/7.5 or better, compared to a range of 6/6-6/12 in Bowman's early AMD group (*Bowman, 1979*).

Cheng and Vingrys (1993) used the Isovalue colour vision test to investigate perception of colour saturation in ARM. Results showed a significant difference in group means between the ARM and age-matched normal group, but could not distinguish between the early ARM and pre-ARM groups. The Isovalue test was found to be less sensitive than the D15 to early ARM, but results did support claims that colour saturation capabilities are affected in acquired dyschromatopsias (*Frisen & Kalm, 1981; Frisen,1990*).

In addition to tests of hue discrimination in AMD, other studies have considered the effect of the disease on colour matching (*Smith et al, 1988; Eisner et al, 1987; 1991; 1992*). A

bipartite field is used in such studies, and subjects are required to adjust the relative proportions of red and green in the mixture field in order to match the hue of the test field. A comparison can be made of the ratio of green to red in the mixture field for small and large test fields (Log G:R [small field] : Log G:R [large field]). This is termed the 'colour match area effect'.

Smith et al (*1988*) tested 10 subjects with ARM in this way. Results showed that the first apparent abnormality to develop in ARM was a smaller log G:R value for the smallest test field, with this defect extending to the larger fields as the disease progressed. The 'colour match area effect' also tended to be reduced with increased disease severity.

In previous studies, the shift towards a lower log G:R ratio has been associated with a decrease in the optical density of photopigment (*Pokorny et al, 1980; Smith et al, 1978*). This finding has been ascribed to photoreceptor disorientation (*Pokorny et al, 1980*). The decreased 'colour match area effect' suggests that the abnormality is more marked in the central retina, with the decrease in log G:R ratio being greater for the small field than the large field.

Eisner et al (1987) found the 'colour match area effect' to be smaller in subjects with unilateral neovascular AMD in the non-test eye, than in those with bilateral drusen. They also reported that abnormal colour matching was very specific for a high-risk fundus appearance indicative of imminent neovascular changes (*Eisner et al, 1991*). This finding suggested that the 'colour match area effect' might be a sensitive predictor of impending CNV. However, a subsequent longitudinal study (*Eisner et al, 1992*) did not find baseline colour-matching results to be a successful risk indicator of development of exudative changes over an 18 month follow-up period.

In conclusion, no single test of colour vision appears to have accurate diagnostic or prognostic value. There is, however, a definite trend towards tritan colour vision defects in patients with AMD, even at an early stage in the disease process. This finding suggests that the short-wavelength sensitive pathway is selectively sensitive to disruption early in the disease process. This could be related to the increased vulnerability of S-cones to damage by toxins (*DeMonasterio et al, 1981*). S-cones are also less adept at recovering from intense bleaches than L- and M-cones (*Harwerth and Sperling, 1975*) and are liable to suffer light damage when exposed to repeated brief flashes of short wavelength light or as a secondary effect of continuous exposure to higher luminance levels (*Ham et al, 1978; Sperling et al, 1980*).

5.6   Visual Field

5.6.1   Introduction

The visual field has been defined as 'all the space that one eye can see at any given instant' (*Tate et al, 1977*). The sensitivity of the eye varies with eccentricity, adaptation level, and the nature of the test stimulus. The studies discussed below all involve static, rather than kinetic, techniques of quantifying the visual field. In full-threshold techniques, stimulus intensity or size is altered in order to determine the sensitivity of various retinal loci. Suprathreshold techniques also involve the presentation of stimuli at predetermined positions in the visual field, but at a fixed level above the estimated eccentricity-adjusted threshold. The Amsler chart (*Amsler, 1947*), used to check for distortions or blind spots (scotomas) in the central 20° of visual field, may be considered to be a form of suprathreshold strategy.

One possible confounding factor in the analysis of visual field data is the age-related reduction in the eye's sensitivity. This is attributable to the age-related reduction of pupil size, the transmission of the ocular media, and the sensitivity of the retina and visual pathways. Johnson et al (*1989*) concluded that the majority of the loss is due to the latter explanation. This age-dependent variation in retinal sensitivity means that comparison with age-matched controls is important in investigating pathological changes in the visual field.

5.6.2   The Visual Field and AMD

The efficacy of high and low contrast Amsler charts in evaluating AMD has been investigated by Cheng & Vingrys (*1993*). Eleven subjects with ARM participated in the study, as well as 11 subjects with normal VA but early macular changes (classified as 'pre-ARM'), and 8 age-matched controls. The low-contrast Amsler was found to be more sensitive at detecting early ARM-related changes than the high-contrast chart. Two-thirds of subjects with ARM, and one-third of pre-ARM subjects were found to fail the low contrast test, whilst 5 of the ARM subjects who failed the low contrast test passed the high contrast one. Specificity was 100%, with no controls failing either Amsler test. Cheng suggested that the high contrast test may be less sensitive due to a 'fill in' effect, which is reduced with a decrease in contrast.

In studies of AMD, visual field evaluation has largely been confined to the macular area. To assess the validity of limiting the investigation to this region Sunness et al (*1985*) examined

peripheral retinal function in 21 subjects with AMD and visual acuity of 6/18 or better in the test eye. Results showed a loss in dark-adapted sensitivity in the central 20° of the visual field in patients with AMD to red and blue test stimuli, but only a small decrease in sensitivity in the periphery, which was for the short-wavelength stimulus only. The peripheral loss was attributed to increased yellowing of the lens in older individuals. The conclusion was that peripheral retinal function is normal in people with AMD.

Several studies have compared photopic central field sensitivity in subjects with AMD (*Cheng & Vingrys, 1993; Midena et al, 1997*). Cheng and Vingrys (*1993*), for example, analysed the central 10° of visual field using the Humphrey Field Analyser (HFA) 10-2 programme. A red test spot was included to isolate early losses in cone sensitivity. Mean field sensitivity was found to be reduced in the ARM group compared to age-matched controls and pre-ARM subjects, but not significantly so. Midena et al (*1997*) used the same test parameters (excluding the red test spot) on 47 patients with early AMD in the test eye, and 36 age-matched controls. They found the reduction in central 10° mean field sensitivity in the AMD group to be significant in terms of group means. The AMD group was further subdivided into those with bilateral early AMD (34 of 47 subjects), and those with unilateral neovascular AMD in the fellow eye (13 out of 47 patients). In this case no significant difference was found between the two groups, indicating that the ability of the test to identify eyes at increased risk of developing neovascular AMD was poor.

Owsley et al (*2000*) included evaluation of dark-adapted sensitivity of the central retina in their assessment of 80 patients with AMD. Static threshold perimetry was carried out at 51 extrafoveal loci within the central 38° of visual field. Orange stimuli were used in the light-adapted state (600nm), and blue-green stimuli in the dark-adapted state (500nm). The effect of pre-retinal absorption on the blue-green light was calculated using a heterochromic flicker technique. The mean sensitivity of the central retina was calculated from the results.

Dark adapted mean field sensitivity was found to be significantly lower for patients with AMD than for age-matched controls. Light-adapted sensitivity was also reduced, but the magnitude of the dark-adapted mean field sensitivity loss was greater in 39 of 44 patients. Dark-adapted sensitivity impairment was most significant in the parafoveal region of the field, between 2 - 8.5° eccentricity. Similar findings were reported in a follow-up study involving patients with milder retinal changes (*Owsley et al, 2001*). This finding is consistent with

recent anatomical studies, which suggest a selective loss of parafoveal rod photoreceptors in early AMD (*Curcio et al, 1996, Medeiros et al, 2001*).

Sparing of foveal sensitivity continues as the disease process progresses. A study by Sunness et al (*1994*), mapped the relative and absolute scotomas of 60 patients with geographic atrophy and found visual loss to reflect patterns of atrophy. Geographic atrophy develops in discrete foci (usually in the parafovea) which gradually enlarge and coalesce to form a horseshoe of atrophy around the foveal centre. This then develops into a ring, and the foveal centre is eventually involved (*Sarks et al, 1988*).

Midena et al (*1994, 1997*) further investigated the relationship between fundus appearance and visual field sensitivity in AMD. They found that drusen number was not related to mean photopic field sensitivity. However, drusen morphology did seem to have a significant effect on the visual field. The presence of larger drusen and a greater proportion of soft drusen were independently linked to reduced central retinal sensitivity.

Such results are consistent with the report of Sunness et al (*1988*), in which a fundus camera stimulator was used to determine static dark-adapted thresholds of drusen and drusen-free areas equidistant from the fovea in 8 patients with drusen. No significant difference was found between retinal sensitivity over drusen and non-drusen areas in the case of both confluent and discrete drusen at various eccentricities. This suggests that the presence of drusen themselves does not mediate sensitivity loss, but that they are a side-effect of more diffuse RPE and retinal dysfunction which is responsible for the impairment in visual function. The association between drusen morphology and central mean field sensitivity could indicate that the presence of soft drusen, for example, signifies a more advanced state of retinal and RPE dysfunction than hard drusen alone.

However, Sunness et al (*1988*) also found that a discrete area of sensitivity loss was detected over even very small areas of focal RPE atrophy. Sensitivity was found to recover rapidly outside the atrophic area. Tolentino et al (*1994*) similarly found a relation between central visual field defects and the extent of RPE atrophy in a more extensive study involving 59 patients with dry AMD, and visual acuity of 6/12 or better.

In a longitudinal study, Sandberg et al (*1998*) used letter recognition perimetry on 127 subjects with macular drusen, and neovascular AMD in the non-tested eye. The number of deficits within the central 10 x 10 degrees of visual field was recorded at baseline. A total of 27 eyes converted to neovascular AMD during the 3 year follow-up of the study, but baseline

perimetry results were not found to be a significant predictor of development of choroidal neovascularisation. However, a longitudinal study by Sunness et al (*1997*), which involved an assessment of scotoma size in 74 subjects with geographic atrophy, did find that greater visual field loss at baseline was related to marked visual acuity loss over the 2 year follow up period.

The value of the analysis of the dark-adapted visual field in determining those individuals most at risk of developing advanced forms of AMD has not yet been investigated in a longitudinal study. Investigations specifically targeting those aspects of retinal sensitivity found to be altered in individuals with AMD e.g. parafoveal rod function, are most likely to be of value.

5.7   Dark Adaptation

5.7.1   Introduction

The classic dark adaptation curve measures the recovery of retinal sensitivity following exposure to a bright light. After adaptation to a strong bleaching light source this recovery is found to be biphasic (*Hecht et al, 1935*). The initial rapid recovery is attributable to an increase in cone sensitivity. After approximately 10 minutes rod threshold falls below that of cones, and a second, slower component of recovery is observed. Full recovery of sensitivity, following a 100% bleach, takes more than 40 minutes (*Hart, 1987*).

A dark adaptation curve is ordinarily obtained following adaptation to a bleaching light. The subject's head is fixed by chin and brow rests, one eye is covered, and the other monocularly fixates a small red target. The recovery of retinal sensitivity is determined at the desired retinal locus by means of a flashing test stimulus, altered in intensity by a neutral density wedge until just detected by the subject. A plot of log threshold vs. time is thereby obtained. The use of different parameters and test locations allows the differential plotting of rod and cone adaptation curves. A foveal dark adaptation curve will give a measure of purely cone photoreceptor recovery, whilst the use of a short wavelength stimulus at 10 degrees eccentricity will target rod recovery. Figure 5.5 shows a representation of the classic dark adaptation curve.
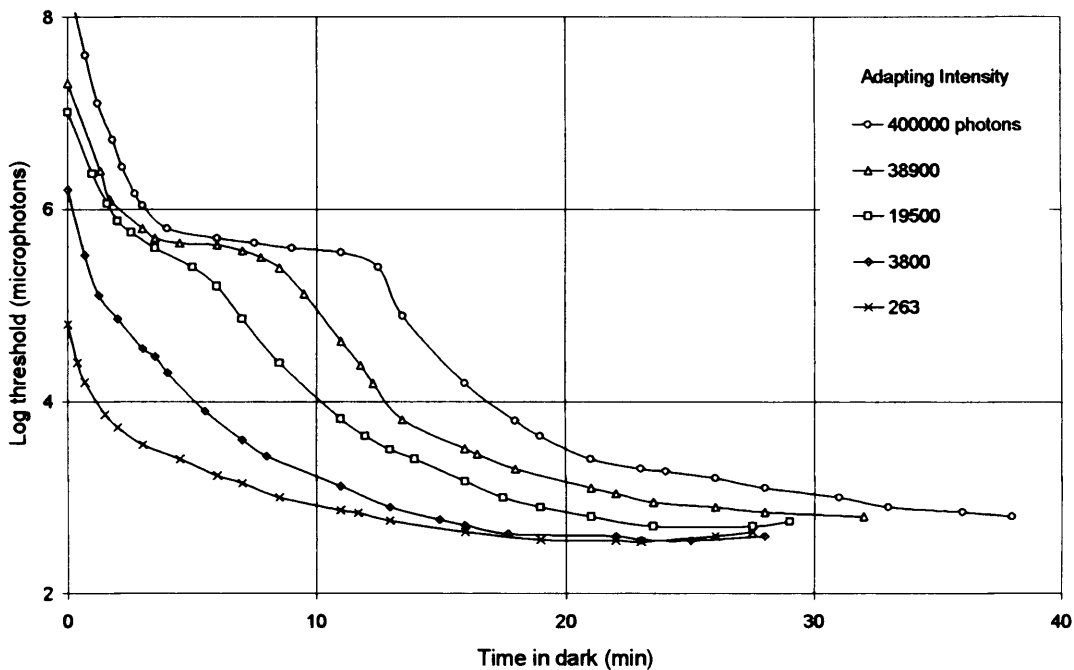
Figure 5.5. Dark adaptation curves from a normal observer. From Hecht, 1937.

When using this technique to investigate disease-related changes in visual function, some caution must be exercised regarding the age of the subject groups as there is substantial evidence that dark-adaptation parameters change with age (*Eisner et al, 1987; Coile & Baker, 1992*). Coile & Baker (*1992*) measured foveal dark adaptation in 58 subjects ranging in age from 10-78 years. Data were corrected for age-related yellowing of the lens according to Said and Weale's values (*1959*). The data showed a slight age-related decline in rate of adaptation before the age of 50, followed by a greater decline in subsequent decades. A parallel increase was noted in foveal pigment regeneration time constants, consistent with the idea that the change in pigment regenerative ability contributes to the change in dark adaptation rate.

5.7.2 Dark Adaptation and AMD

The photochemical theory of dark adaptation states that the concentration of bleached rhodopsin in the outer segments of rod photoreceptors controls the mechanism which establishes the threshold level during dark adaptation (*Rushton, 1965*). The regeneration of rhodopsin requires retinoids and metabolites to be delivered to the RPE by the choroidal circulation (*Leibrock et al, 1998*). The abnormal material deposited in Bruch's membrane in AMD contains a high proportion of hydrophobic neutral lipids (*Starita et al, 1996*), which could form a barrier to the movement of these substrates from choriocapillaris to RPE.

Atrophy of the choriocapillaris has also been reported in AMD (*Ciulla et al, 1999; Friedman et al, 1995; Chen, 1992*), and is another factor which could limit the supply of metabolites to the RPE and photoreceptors.

The importance of the RPE in the regeneration of visual pigment was demonstrated as far back as the 1800s, with experiments showing that the frog retina could regenerate bleached visual pigment only when in contact with the RPE (*Boll, 1876*). It has since been discovered that the RPE is vital in the regeneration of *11-cis* retinal from its bleached *all-trans* configuration (See *Saari 2000, for review*). Since the RPE is seen to be a locus of dysfunction in early AMD (demonstrated clinically by focal hyper- and hypo- pigmentation), there are good reasons to suspect that dark adaptation may be affected in the disease process.

There is some evidence, however, that the visual cycle may be different in cone photoreceptors. Goldstein demonstrated that the amplitude of the cone, but not the rod early receptor potential reaches a steady state in an illuminated frog retina isolated from the RPE. This suggests that cones can regenerate their visual pigment in the absence of the RPE in the frog retina (*Goldstein 1967; 1970; Goldstein & Wolf, 1973*). An explanation for this seems to lie in the metabolic activity of the Müller cells. Cultured chick Müller cells have been shown to take up exogenous all-trans retinol, and convert it to 11-*cis* retinol (*Das et al, 1992*). No oxidation to 11-*cis* retinal has been observed, but other studies have shown that isolated amphibian cone cells resensitise with exogenous 11-*cis* retinol (*Leibrock et al, 1998*). Jin et al (*1994*) demonstrated that, whilst cone photoreceptors can take up retinal from surrounding extracellular medium and use it to resensitise photopigment, rods cannot. This shows that retinal can move freely along the cone photoreceptor, whilst exogenous retinal is either not taken up by the rod cell body, or cannot move from the rod cell body to the rod outer segment. Jin (*1994*) postulated that the free transfer of retinal along cone but not along rod photoreceptors could explain the access of cones to an intraretinal store of 11-*cis* retinal not available to rods.

This evidence strongly suggests that cones may have a separate locus of visual pigment regeneration in the retina. Therefore AMD might have a differential effect on rod and cone dark adaptation processes.

One of the simplest means of assessing cone recovery following a partial photopigment bleach is the macular photostress test. Sloan et al (*1968*) describe a technique whereby VA is measured prior to a bleaching flash. Following the flash, the subject is then encouraged to

read as far as possible down the letter chart, and the time taken to recover baseline VA following the bleach is recorded. Variations of this technique have been used in a number of subsequent studies investigating macular function in AMD (*Cheng & Vingrys, 1993; Sandberg et al, 1995; Midena et al, 1997, Wu et al, 1990*).

The sensitivity of the photostress test to early pathological changes was highlighted by Sandberg et al (*1995*), who used letters flashed onto a computer screen to assess macular recovery time following a 94% bleach of cone photopigment. Of the 133 subjects with macular drusen and unilateral neovascular AMD in the fellow eye, 62% showed a recovery delayed beyond the upper limit for normal derived from age-matched controls. Sixteen of the subjects with delayed recovery had an initial visual acuity of 6/6 or better. This suggests that changes in the kinetics of cone adaptation precede loss of visual acuity in the AMD disease process.

The visual acuity task is a useful criterion of recovery, as it is quick to perform and the letter recognition task is easy for the subject to understand. It does have limitations in that cone recovery alone is investigated and the only parameter assessed in most cases is the total time taken for recovery. There is also inter-subject variability in letter recognition tasks engendered by the reluctance of some subjects to guess at letters of which they are uncertain.

Other studies have carried out more detailed investigations of rod and cone photoreceptor recovery following a bleach, by plotting curves of retinal sensitivity as a function of time after initiation of dark-adaptation (*Brown & Lovie-Kitchin, 1983; Brown et al, 1986; Collins & Brown, 1989; Eisner et al, 1987; 1991; 1992; Steinmetz et al, 1993; Owsley et al, 2001*). Eisner et al (*1987*), for example, used a 660nm foveal target to the plot cone dark adaptation in 21 subjects with unilateral exudative AMD in the non-test eye, and 130 with bilateral early AMD. The time constant of recovery was found to be greater for subjects with unilateral CNV than those with bilateral drusen. This indicated a possible prognostic role for the monitoring of foveal cone recovery functions. This finding was reinforced by a later study which demonstrated a correlation between retinal signs indicating a high risk of neovascular AMD, and a prolonged recovery time of photopic dark adaptation (*Eisner et al, 1991*).

Histological reports have suggested that rod photoreceptors may be affected earlier in the AMD disease process than cones (*Curcio et al, 1996*). Psychophysical measures of the visual field (*Owsley et al, 2000, 2001*) have also suggested that parafoveal rod function may be compromised before that of cones. Investigations of rod dark adaptation in AMD have

similarly found a significant effect on rod recovery even at an early stage of the disease process (*Brown et al, 1983; Owsley et al, 2001*).

Owsley et al (*2001*) assessed rod dark adaptation in 20 subjects with early ARM. Pre-bleach sensitivity was measured following 30 minutes dark-adaptation then subjects were exposed to a strong adapting light. Recovery was monitored with a 500nm target presented 12° inferior to the fovea. Five minutes after the adapting flash, threshold measurements began, and continued until the subject was within 0.3 log units of baseline sensitivity. Figure 5.6 shows the dark adaptation data obtained from 3 people with ARM, with the recovery curve of a normal older adult for comparison.
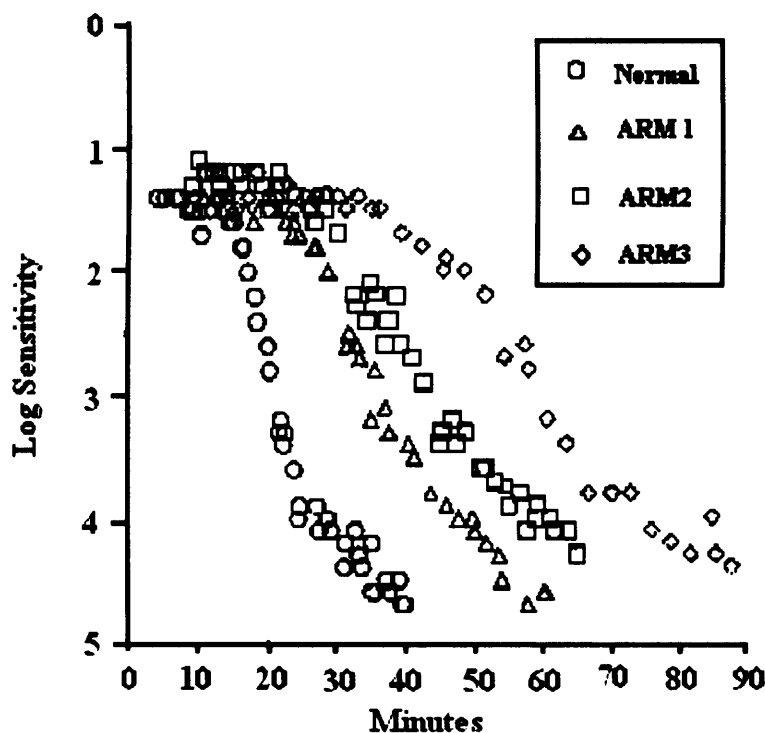
Figure 5.6. The dark adaptation functions recorded by Owsley et al (2001) for three subjects with ARM, and one healthy older adult. All subjects had visual acuity of 6/7.5 or better.

Parameters calculated were time to rod-cone break, time to recovery to within 0.3 log units of baseline sensitivity, and the kinetics of the 2nd and 3rd components of rod recovery (as it is these components which are largely dictated by rate of rhodopsin recovery: *see Rushton, 1955; Lamb, 1981*).

The rod-cone break was significantly delayed in ARM subjects, by an average of 10 minutes. This supported previous findings on a smaller study group by Brown & Lovie-Kitchin (*1983*). The ARM group also showed a slower rate of recovery during the second component of rod adaptation than did the normal group. Recovery during the third component was not

significantly different between groups. The ARM group took an average of 17 minutes longer to return to within 0.3 log units of baseline sensitivity, and the time constant of rod recovery was an average of 15 minutes longer than for controls.

These group-averaged results strongly indicate a marked alteration in the kinetics of rod function, even in the earliest stages of AMD disease progression. A small study by Brown et al (*1986*) on 4 subjects with early ARM suggested that the kinetics of rod recovery following a bleach are affected before abnormalities are recorded in cone adaptation. In contrast, however, Steinmetz et al (*1993*) found rod and cone kinetics to be equally affected in 10 subjects with early ARM.

These studies support the theory that outer retinal changes related to the development of ARM result in widespread alterations of rod and cone visual cycle kinetics, with some suggestion that the magnitude of rod dysfunction may be greater. The question remains as to whether this information has clinical potential as a means of monitoring AMD, or identifying those at risk of developing advanced AMD.

A number of studies have looked for associations between fundus appearance and retinal function in AMD (*Collins & Brown, 1989; Eisner et al, 1991; Cheng & Vingrys, 1993; Midena et al, 1997; Sandberg et al, 1995*). Sandberg et al (*1995*) used a letter perimetry technique to monitor macular cone recovery of 133 subjects with ARM and found a correlation between log recovery time and the presence of RPE pigmentary degenerative changes. This finding was supported by other studies, which used different techniques to monitor macular recovery (*Collins & Brown, 1989; Cheng and Vingrys, 1993*). In contrast, Eisner et al (*1991*), measuring the dark-adaptation of foveal cone photoreceptors of 41 subjects with ARM, found a reduced rate of dark-adaptation to be strongly associated with the presence of high-risk drusen, but not with focal hyperpigmentation or atrophy. Midena et al (*1997*), who monitored the recovery of central cone function using a visual acuity task, found increased number and confluence of drusen, presence of focal hyperpigmentation and presence of focal RPE atrophy to all be independently associated with an increased photostress recovery time. Further research will be required to determine the exact relationship between these various funduscopic signs of AMD, and the effects on dynamic retinal function.

Eisner et al (*1992*) conducted a longitudinal study to investigate the value of dark adaptation assessment as an indicator of imminent neovascular changes. Forty-seven individuals with

early AMD in the test eye and CNV in the fellow eye were tested at baseline. A foveally centred, 660nm target within an annular 580nm surround was used to plot the recovery of foveal cone function following a 3 minute exposure to a 20 000 td, 580nm bleaching light. Eleven of the 47 subjects developed neovascular changes in their test eye over the 18 month follow-up period. The time constant of cone dark adaptation at baseline was not found to be an effective risk indicator of the development of CNV when considered independently of other factors. Eisner et al (*1992*) suggested that this could be because high-risk eyes also have a low effective photopigment density, and thus the bleaching stimulus could be effectively dim for these eyes, giving a spuriously normal dark adaptation function. Smiddy & Fine (*1984*) in a prospective study of 71 subjects with bilateral drusen similarly found photostress recovery time to be an insignificant risk indicator of exudative changes over a 2.5 year follow-up period.

However, conflicting results were found by a much larger longitudinal study incorporating 127 subjects with macular drusen in the test eye, and CNV in the fellow eye (*Sandberg et al, 1998*). Subjects were exposed to a 94% bleach of cone photopigment, and glare recovery was assessed using a computer-controlled letter recognition task. Twenty-seven subjects developed CNV during a 3 year follow-up period, and prolonged recovery time was found to be a significant age-adjusted predictor of an exudative outcome. Each minute prolongation of glare recovery time increased the relative risk by 30%. The disparity between this result and the previous longitudinal studies could be accounted for by the larger sample size, and the greater number who went on to develop exudative AMD.

The literature therefore supports the hypothesis that dark adaptation kinetics are affected at an early stage of AMD. It also suggests that a glare recovery technique may act as a prognostic test to determine those individuals with early ARM who are most likely to develop exudative changes (*Sandberg et al, 1998*). No definitive argument has been presented for the exact cause of the delayed dark-adaptation seen in AMD. However there seems to be more than one factor which may be responsible for these functional changes (*see section 5.6.1*).

5.8   Absolute Threshold

5.8.1   Introduction

Absolute threshold is a measure of the smallest amount of radiation, which can be perceived by the visual system. In order to measure the absolute visual threshold it is necessary that the eye undergo a sufficient period of dark adaptation i.e. approximately 45 minutes for rods (although many studies will abbreviate this as the bulk of adaptation occurs in the first 15-20 minutes).

The significance of age in the measurement of absolute threshold of normals is debatable. Domey et al (*1960*) studied 241 observers aged between 16 and 89 years and found the absolute thresholds of the elderly to be almost 250 times higher than those of the young observers. When results are corrected for lenticular changes and re-evaluated, it can be seen that rod threshold, measured after 40 minutes dark adaptation, remains almost constant through the first 6 decades of life, and then begins to rise. The cone threshold does not show the same age-related decline. The age-matching of subjects in comparisons between thresholds of AMD and normal groups is, therefore, of importance in the consideration of rod sensitivity.

5.8.2   Absolute Threshold and AMD

Brown & Lovie-Kitchin (*1983*) measured rod sensitivity at an eccentricity of 10°, following 20 minutes dark adaptation. The average threshold of the 8 AMD subjects tested was found to be significantly elevated compared to age-matched controls, by an average of 0.33 log units. However, the subjects with AMD used in this study were very wide-ranging in the extent of their visual deficit, with visual acuity ranging from 6/9 to 6/120. The group-averaged results do not indicate to what extent absolute threshold is affected in the early stages of AMD. Recent work by Jackson et al (*1998*) suggested that, whilst there is an age-related loss in absolute sensitivity of older individuals, rod sensitivity is not significantly different in subjects of a similar age with and without early ARM.

There are more studies of the loss of absolute sensitivity in the cone pathway in AMD. Steinmetz et al (*1993*) investigated the dark-adapted foveal sensitivity of 12 individuals with ARM. Foveal thresholds were found to be more variable in the ARM group compared to age-

matched controls, and were depressed by at least 10 dB in 6 of the 12 subjects. However, there was no relationship between the number of drusen and the magnitude of scotopic sensitivity loss. Similar losses in cone sensitivity in individuals with AMD have been reported in other studies (*Brown & Lovie-Kitchin, 1983; Brown et al, 1986*). The parafovea appears to be particularly vulnerable to functional deficit (*Brown et al, 1986*)

Eisner et al (*1987; 1991; 1992*) evaluated the prognostic value of cone thresholds. An initial cross-sectional study (*Eisner et al, 1987*) investigated cone sensitivity in 21 individuals with unilateral neovascular AMD in the non-test eye, and compared this with results taken from 130 subjects with bilateral drusen. Eisner found absolute cone thresholds to be lower for the subjects with unilateral exudative AMD in the contralateral eye, thus indicating that this parameter may be a potential risk indicator for future neovascular changes in an eye with drusen. Furthermore, a second cross-sectional study (*Eisner et al, 1991*) found raised cone thresholds to be related to a fundus appearance indicative of a high risk of CNV. A prospective study to further investigate this finding involved the baseline assessment of cone threshold in forty-seven subjects with exudative AMD in the non-test eye (*Eisner et al, 1992*). Eleven of the 47 subjects developed neovascular changes over the 18 month follow-up period. Absolute cone sensitivity in this case, however, did not help to predict the outcome after the effects of age had been removed.

Another longitudinal study (*Sunness et al, 1989*) followed 18 individuals with ARM over a period of 45 months. Sunness found that, at baseline, those individuals who were to develop advanced retinal changes (n=5) had a significantly reduced dark-adapted foveal sensitivity compared to those who remained unconverted throughout the study. With an optimal cut-off point in baseline foveal threshold it was possible to predict with 100% sensitivity, and 92% specificity the outcome of the subjects over the follow-up period. The significance of these results was limited, however, by the small subject group involved. The study also differed from Eisner's (*1992*) in that it did not discriminate between a dry and an exudative advanced AMD outcome, possibly explaining the disparity in results. However, a further longitudinal study by Sunness et al (*1997*) followed a larger group of 74 subjects with dry AMD, and visual acuity of 6/15 or better. The foveal dark-adapted threshold once again showed some promise at predicting outcome, with a reduced foveal dark adapted sensitivity at baseline accounting for an increased risk of a doubling of the minimum angle of resolution over the 2 year follow-up.

5.8.3   S-Cone Sensitivity and AMD

In addition to general measurements of rod and cone absolute thresholds, further studies have investigated the sensitivity of the S-cone pathway in AMD. In humans, S-cones only comprise 5-10% of the cone mosaic, with the greatest density falling in the parafoveal region (*See Calkins et al, 2001, for review*). It is this region which has been suggested to be vulnerable to early AMD (*see Curcio, 1996*). S-cone photoreceptors are also believed to be more susceptible to metabolic damage than L- and M-cones (*Hood & Greenstein, 1988*). Colour-vision studies have suggested that the earliest defects recorded in people with AMD are tritanopic in nature (*e.g. Cheng & Vingrys, 1993; Collins & Brown, 1989; Haegerstrom-Portnoy et al, 1988*), again suggesting an early involvement of the S-cone pathway in the disease process.

Eisner et al (*1991*) investigated S-cone function in a cross-sectional study of 41 individuals with drusen in the study eye and unilateral exudative AMD in the fellow eye. The subjects were classified as being at high- and low-risk of developing exudative AMD in their test eye, according to retinal appearance. High-risk eyes appeared to have a lower S-cone mediated sensitivity than low-risk eyes. To ameliorate the possible confounding effect of age on the S-cone sensitivities measured in the two groups, a further comparison was made within a limited age range of 66-74 years, the difference remained significant (P<0.05). A similar study by Sunness et al (*1989*), investigating S-cone sensitivity in 31 individuals with drusen, also found that the 13 eyes with high-risk drusen had reduced sensitivity compared to eyes with low risk drusen, although there was considerable overlap between the groups.

DeMonasterio et al (*1985*) reported that the spatial density of S-cones decreased in the central fovea for old female, but not for old male macaques, which would suggest that gender should be taken into account when analysing the effects of age and AMD on the S-cone system. In Eisner's study (*1991*), the high-risk eyes of men had a significantly lower S-cone mediated sensitivity than the low-risk eyes, whereas this comparison was not significant for women, although this was possibly linked to the smaller number of women in the study.

Eisner's longitudinal study (*1992*) into the prognostic value of the measurement of retinal sensitivity in AMD suggested that S-cone sensitivity is better able predict the onset of CNV than absolute sensitivity. When S-cone sensitivity was plotted against age for those eyes which did not develop CNV over the 18 months of the study, 6 of 11 exudative outcome eyes fell below the curve.

These results support the theory that S-cones may be sensitive to damage in AMD. It appears that measurements of S-cone sensitivity may be of possible use in assessing the likelihood of an individual developing advanced AMD, but further investigations on a larger group of subjects would be required to determine the precise cut-off point in threshold of high-risk eyes. Eisner (*1992*) also highlighted the fact that S-cone sensitivity is highly dependent on age and media absorption, factors making it a complicated predictor of retinal changes.

5.9   Test Combinations

In addition to reports discussing the effect of AMD on individual aspects of visual function, some studies have considered the power of certain test combinations in detecting and monitoring the disease process. Associations have been found between results of various tests. For example, Cheng and Vingrys (*1993*) reported a significant correlation in their study between the vector score recorded on the panel D15 test for colour vision, and a central visual field anomaly detected with the low-contrast Amsler chart. Such correlations suggest that the functions tested are reflecting the same retinal dysfunction. In this case Cheng & Vingrys suggested that a parafoveal photoreceptor loss might be responsible for abnormalities in both tests.

In other situations two aspects of visual function can be found to be independently abnormal in a study group of AMD subjects, both highlighting anomalies of retinal function in AMD without being related to each other. In such a situation these two measures appear to reflect different aspects of the functional change caused by AMD. A combined analysis of the results to two such tests may provide the key to a diagnostic/prognostic tool of greater efficacy than a single measure.

An example of this is provided by Eisner et al (*1992*) in their longitudinal study of 47 individuals with drusen in the test eye and contralateral neovascular changes. Eleven eyes converted to exudative AMD during the 18 month follow-up period. The strongest prognostic indicator of outcome was found to be a combination of the results of two baseline tests - the dark adaptation constant, and the colour-match-area effect. This predicted neovascular outcome with an odds ratio of 26 (*Eisner et al, 1992*).

Eisner et al (1992) suggested that patients with AMD might have a reduced quantal absorption by foveal cones compared to normal subjects. This would mean that the bleaching stimulus used for dark adaptation was effectively dim for those eyes, resulting in a spuriously

normal dark adaptation time in some abnormal eyes due to an incomplete initial bleach. The 'colour match area effect' is strongly related to the quantum catching ability, or effective photopigment density of the foveal cones (*Smith et al, 1988*). A small 'colour match area effect' indicates that the effective photopigment density of the fovea is low compared to that of the parafoveal cones. Thus those subjects with spuriously normal dark adaptation functions conferred by a reduced foveal photopigment density should be highlighted by an abnormally small colour-match-area-effect.

Other studies pairing results of dark-adaptation functions with other measures of static retinal function have found strong diagnostic possibilities. Cheng & Vingrys (*1993*) for example, used a combination of photostress recovery time and panel D15 results. The subject was considered to 'fail' if either parameter was abnormal. Using these criteria, (9/11) 82% of ARM subjects would fail the test, but only 27% of pre-ARM subjects would be detected (3/11). By including results to the low-contrast Amsler chart the sensitivity was increased, with 100% of ARM, and 36% (4/11) of the pre-ARM subjects correctly identified by results to the test combination. Specificity remained at 100%.

However, caution must be exerted in placing too much weight on post-hoc analyses of data. Multiple data comparisons such as this may lead to type I statistical errors.

5.10   Conclusion

In most clinics the assessment of individuals with AMD is limited to fundus appearance, visual acuity and the Amsler chart. This chapter has indicated that, whilst these tests undoubtedly provide useful information, further measures of visual function hold the potential to further our understanding of AMD.

Published data suggest that the measurement of temporal contrast sensitivity functions may prove a useful prognostic tool in identifying those individuals who are liable to develop exudative AMD. Contrast sensitivity measurements at a combination of two temporal frequencies were found to predict at baseline with 100% sensitivity and specificity those subjects who would go on to develop choroidal neovascularisation (*Mayer et al 1992; 1994*). However, longitudinal data was only obtained from a small group of subjects, of which only 7 individuals developed choroidal neovascularisation. Furthermore, extensive post hoc statistical testing to determine the combination which provided the optimal separation

between groups may have artificially inflated the prognostic value of the test. Further research is necessary to fully explore the potential value of this technique in a clinical setting.

Measurement of colour vision also appears to be effective in the assessment of subjects with AMD. The advantage of the routine use of the D15 colour vision test is that it is fast and simple to employ in a clinical setting. Acquired colour deficiencies in AMD are invariably tritanopic in nature, but diagnosis relying on colour vision tests may yield a poor specificity as a number of other conditions also lead to acquired tritanopic defects (*Francois & Verriest, 1968*). Studies such as that of Cheng and Vingrys (*1993*) suggest that the value of measures of colour vision may be increased by combining colour vision test results with results from other tests, such as dark adaptation.

There is a solid theoretical foundation for the belief that dark adaptation is impaired in AMD. Some studies have suggested that this dysfunction is greater with regard to rod recovery than cone recovery (*Brown et al, 1986*), although this has been disputed (*Steinmetz et al, 1993*). Differences in the nature of the bleach and test stimulus could explain this discrepancy. It does seem that measurement of recovery of visual acuity does not elicit maximal information regarding retinal function. Histological (*Curcio et al, 1996*) and psychophysical (*Owsley et al, 2001; Vingrys et al, 1990; Hart et al, 1983*) evidence suggests that the recovery of sensitivity in an extrafoveal location may provide a more sensitive indictor of retinal changes.

Static perimetric data suggests that mean central visual field sensitivity is reduced in AMD (*Cheng & Vingrys, 1993; Owsley et al, 2001*), but differences in group averaged results have little practical application, as overlap between the normal and AMD populations may still be high. However, preliminary studies do suggest that visual field data may have a role in the assessment of patient prognosis (*Sunness et al, 1997; Chen et al, 1992*). The Amsler test remains a useful tool in the assessment of patients with AMD, with low-contrast charts being more sensitive diagnostically (*Cheng & Vingrys, 1993*).

The literature discussed suggests that many aspects of visual function are affected in AMD, and that there may be the potential to develop clinical tests which detect and monitor retinal changes with greater sensitivity than visual acuity measurement. However, in terms of diagnostic and prognostic value, it is debatable whether any of the tests discussed approach the sensitivity of certain funduscopic signs. Bressler et al (*1990*) graded the macular features of 127 individuals with unilateral choroidal neovascularisation in the fellow eye, and then followed the visual outcome of these subjects over 5 years. Thirty individuals developed

neovascular AMD in this time. It was found that 60% of individuals with large drusen and RPE hyperpigmentation in the test eye developed neovascular AMD over this follow-up period, compared to only 10% of those who did not show these signs. Similarly, the Macular Photocoagulation Study Group (*1997*) found the presence of a combination of 4 factors i.e. focal hyperpigmentation, large drusen, more than 5 drusen within the macular region, and systemic hypertension, to be associated with an annual risk of 18% of developing choroidal neovascularisation in the second eye for subjects with unilateral neovascular AMD. This was compared to an annual risk of less than 2% for those individuals with unilateral choroidal neovascularisation who lacked all of these signs in their fellow eye.

Based on histopathological work by Sarks (*1980*), Bressler et al (*1990*) postulated that focal hyperpigmentation and large drusen were both indicative of diffuse thickening of the inner aspect of Bruch's membrane, predisposing towards the development of neovascular ingrowth through breaks in Bruch's membrane. Eisner et al (*1992*) suggested that their combination of foveal dark adaptation constant and 'colour match area effect' was comparable to the assessment of the summed area of macular confluent drusen and RPE focal hyperpigmentation as a risk indicator for choroidal neovascularisation over an 18 months follow-up. This may be because this combination of factors is reflecting the same changes to Bruch's membrane as the funduscopic signs discussed. In order to achieve such sensitivity in the assessment of AMD using clinical tests, it is necessary to develop test parameters which similarly target those subclinical changes which histopathological and anatomical studies have highlighted.

CHAPTER 6 : ELECTRORETINOGRAM TECHNIQUE DEVELOPMENT

Previous chapters have presented evidence which suggests that certain aspects of visual function are particularly vulnerable in patients with ARM. The electroretinogram provides an objective and easily quantifiable means of assessing these changes. In order to optimise electrophysiological evaluation of this group of patients it is desirable to use test parameters which selectively target the areas of visual function most likely to be affected by ARM.

This chapter describes the development of ERG protocols which are likely to be sensitive to early retinal changes in AMD. This includes ERG techniques to assess the function of rods and cones of the central retina (focal rod and cone ERGs), the integrity of the retinal circulation and inner layers of the central retina (focal OPs), the integrity of the RPE (C-wave), the activity of the S-cone pathway (the S-cone ERG), and cone photopigment regeneration (the dynamic ERG).

6.1   General Techniques used for ERG and VEP Recording

6.1.1   Instillation of Mydriatic

It was necessary for subjects to be dilated prior to all ERG and VEP procedures used in this study. Before instilling the mydriatic, the subject's susceptibility to closed-angle glaucoma was assessed by measuring intraocular pressure and anterior chamber depth (according to Van Herick's technique), and by asking questions about family history. Provided that pressures were below 21 mmHg, the anterior chamber was deep (grade 2-4), and there was no family history of closed-angle glaucoma, 1 drop of 1.0% tropicamide hydrochloride was instilled into each eye. Twenty minutes were allowed for mydriasis and then the diameter of the pupil was measured.

6.1.2   Electrode Placement for ERG Recording

For ERG recording the earth electrode was positioned at the mid-frontal location i.e. approximately 5cm vertically above the nasion. The reference electrode was placed at the ipsilateral outer canthus i.e. at the notch at the end of the supraorbital ridge. Prior to the

application of the electrodes, the underlying area was gently cleaned with an exfoliating gel, Nuprep (*D.O. Weaver & Co., Aurora, USA*). This removes dead skin cells and grease which may increase the resistance of the skin-electrode interface.

A 30mm length of Blenderm tape (*3M Health Care, St Paul, USA*) was attached to the back of each silver-silver chloride skin electrode. Each electrode cup was then filled with TECA electrode conductivity gel (*Oxford Instruments Medical Inc., New York, USA*), using a syringe and blunt needle. The electrode was attached to the prepared areas of skin using the Blenderm tape. A hole pierced through the Blenderm tape into the electrode cup allowed the electrode gel to be replenished during the experiment should the resistance of the electrode-skin interface become unacceptably high.

Following the positioning of the reference and earth electrodes, a Dawson-Trick-Litzkow (DTL) active electrode was prepared. The end of a 70mm length of DTL fibre was wound around a metal holder encased in a non-conductive sheath. The sheath was then pushed into place over the end of the fibre to keep it in place. The holder was positioned at the outer canthus of the test eye, and attached using a length of Blenderm tape. The DTL fibre was then draped along the lower fornix of the test eye as the patient looked upwards. Although a larger signal is obtained if the fibre lies along the lid margin (*Lachapelle et al, 1993*), positioning deep within the lower-lid conjunctival sac prevents the electrode from being blinked out of position, and therefore achieves a repeatable response (*Herbert et al, 1999*). Lower noise levels have also been reported with the electrode positioned in this way (*Vaegan, 1996*).

Figure 6.1. Subject who has been prepared for ERG recording.

Following electrode attachment, the resistance of the skin-electrode interface in each position was assessed. It was ensured that resistance was approximately equal for all electrodes, and if possible below 4 KΩ, thus minimising contamination of the traces by extraneous artefacts.

6.1.3   Electrode Placement for VEP Recording

The positioning of electrodes for VEP recording was in accordance with the 10-20 electrode placement system (*see section 4.8.1*). Two additional silver-silver chloride skin electrodes were employed to record VEPs, with the mid-frontal electrode acting as a common earth for both VEP and ERG recording. The active electrode was placed over the occipital cortex i.e. 15% up from the inion along the vertical midline. The reference electrode was positioned at the vertex, at 50% of the inion-nasion distance. Subjects were prepared and the electrodes applied in the same way as in ERG recording.

6.1.4   Equipment

The computer averaging system used in all ERG and VEP recording was a Medelec Synergy EP system (*Oxford Instruments Medical, Surrey; See Figure 6.2*).

Several parameters must be programmed into the computer averaging system prior to recording:

- The high and low frequency filters (which determine the frequency of signals which will be averaged by the system);
- The amplification of the recording system;
- The sensitivity of the artefact reject setting;
- The number of responses to be averaged;
- The timebase (which is the period of time over which each response is recorded).

These parameters were varied between protocols according to the nature of the signal recorded.
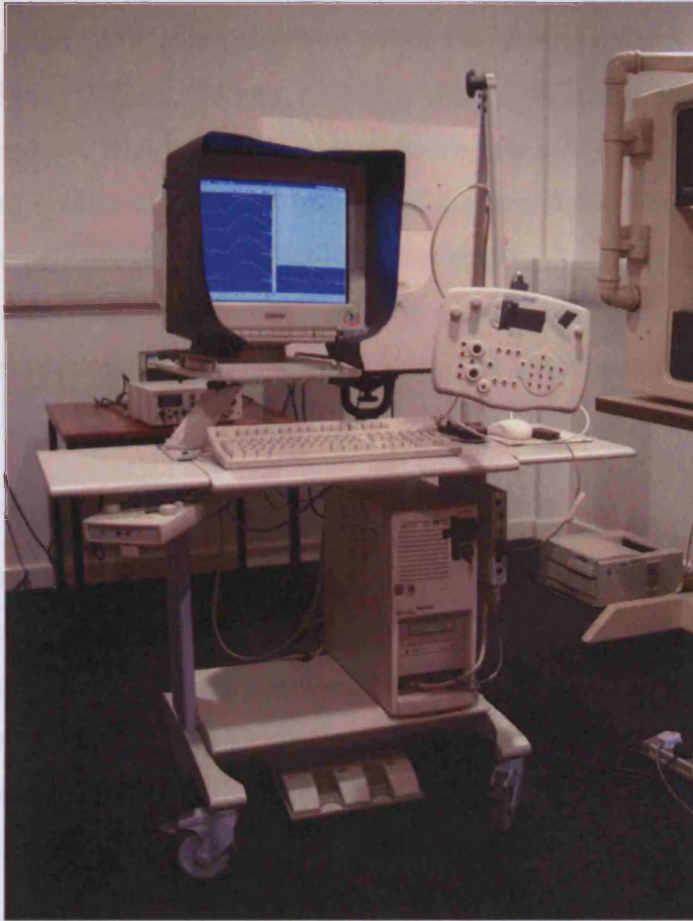
Figure 6.2. Medelec Synergy computer averaging system

All flash stimuli used in ERG and VEP recording were generated by a light emitting diode (LED) miniature ganzfeld stimulator (*CH electronics, Kent; See Figure 6.3*).

Figure 6.3. LED miniature ganzfeld stimulator

The head stage of the stimulator comprised a tube containing an array of LEDs of 4 different wavelengths (454nm, 525nm, 595nm, 664nm), with a diffusing screen mid way along the tube, and a hemispheric translucent diffuser at the far end of the tube. A further diffusing filter was added to the system to further homogenise the test field. The LEDs were driven by a controller which permits the manipulation of intensity, duration, and temporal frequency. When the stimulator was held immediately adjacent to the eye, a ganzfeld stimulus was provided. Focal responses were obtained by holding the stimulator 14cm from the eye.

6.1.5   Measurement of Responses

The International Society for the Clinical Electrophysiology of Vision (ISCEV) have made recommendations regarding the measurement of implicit time and amplitude of the a-wave and b-wave of transient ERG responses, and the implicit time and amplitude of steady state ERGs (see Figure 6.4). These standards were used in the measurement of both focal and full-field responses in this study.
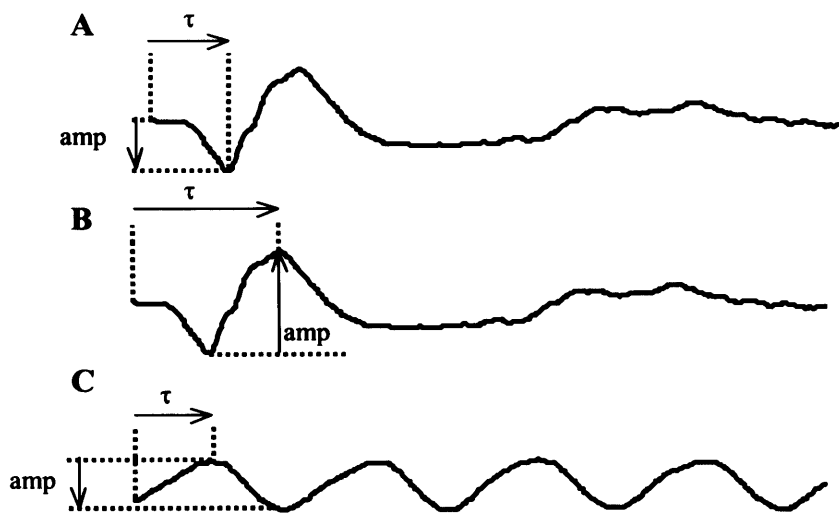
Figure 6.4. Diagram illustrating how to measure the amplitude and implicit time (τ) of the a-wave (A) and b-wave (B) of the transient ERG, and the steady state ERG (C) according to ISCEV standards (Marmor et al, 1989; 1995; 1999).

There is no standardised technique for measuring the oscillatory potentials (OPs). The technique used in this study, shown in Figure 6.5, is based on a method where peak-to-trough differences are summed (*Severns, 1994*).
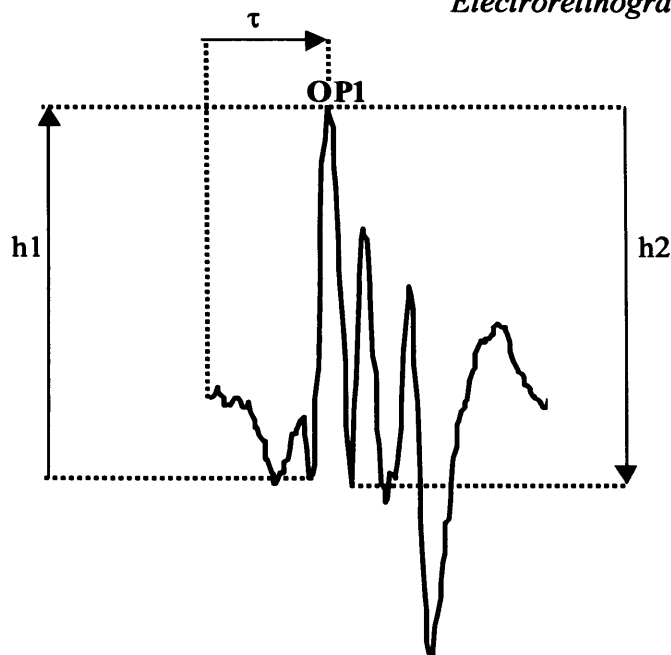
Figure 6.5. Illustrating the summed peak-to-trough method of measuring OP amplitude and implicit time (τ) from isolated OPs. In the diagram above, OP1 amplitude is h1 + h2

6.2   The Focal Rod Electroretinogram

6.2.1 Introduction

The recording of a focal rod ERG is more problematic than the recording of a focal cone response. Unlike cones, rods lack directional sensitivity (*Pirenne, 1962*), and are therefore prone to stimulation by scattered light.

Sandberg et al (*1996*) demonstrated the effect of scattered light on the focal rod ERG by recording a response from the dark-adapted eye to a 30° diameter blue flash of 2.1 log scot tds.sec^{-1}. The ERG elicited by this stimulus has a double b-wave. The first b-wave results from the direct focal stimulation of the macula. The second, larger response comes from the peripheral retina in response to intraocular light scatter. There is some overlap of the two responses i.e. the a-wave of the scattered light response is coincident with the b-wave of the focal response. This means that any direct measurement of the amplitude of the focal response is difficult to interpret.

There are several ways to isolate the focal rod ERG. Sandberg et al (*1996*) hypothesised that the stray light component of the double-peaked focal flash response could be matched by the full-field response to a dimmer flash. A preliminary experiment demonstrated that the signal recorded in response to a full-field, uniform stimulus could be matched by an ERG recorded

to a stimulus composed of bands of non-uniform intensity, still providing the same overall mean retinal illuminance. Having demonstrated this, it was possible to record a range of full-field ERGs to various stimulus intensities, and to identify one response which exactly matched the amplitude and temporal characteristics of the scattered light response. By mathematically subtracting this full-field trace from the initial double b-wave, the focal response was isolated (*see Figure 6.6*).
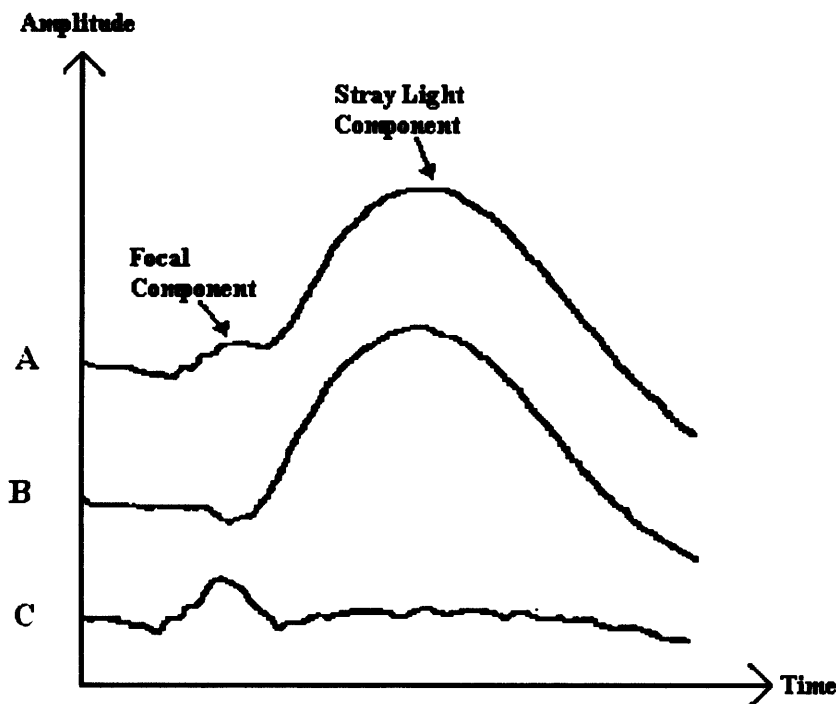
Figure 6.6. ERG recorded by Sandberg et al (*1996*) to a 30° diameter blue flash of 2.1 log scot td.sec^{-1} (A), a full-field ERG elicited by blue flash of 0.4 log scot td.sec^{-1} (B), and the subtraction of (B) from (A) to leave a focal response (C).

A second approach to the elimination of the scattered light component of the focal rod ERG is to suppress the peripheral rods using background illumination. This technique was evaluated during multifocal rod ERG recording by Hood et al (*1998b*). They found that the use of an adapting surround was sufficient to extinguish the b-wave elicited by scattered light, to leave an isolated focal response.

A third means of eliminating the scattered light response is to merely use a very small, dim stimulus (*Horiguchi et al, 1991; Chosi et al, 2003*). A blue stimulus of size 5° diameter was found to elicit no response when imaged on the optic disc if less than 1.5 cd.m^{-2} (for a 10ms flash), indicating that the scattered light effect was minimal. Horiguchi et al (*1991*) suggested that any small response from the peripheral retina would be negated by the adaptational

effects of the diffuse red light which was produced by their fundus monitor. However, the disadvantage of using a low intensity stimulus is that small amplitude responses reduce the signal to noise ratio, making the technique less sensitive to minor changes in retinal function.

Despite these studies, no electrophysiological technique has yet become established as the means of assessing central rod function.

There have been no studies of the effect of age-related macular degeneration on the focal rod ERG. However, histopathological evidence indicates the possibility of a selective loss of rod photoreceptors from the parafoveal retina in the early stage of the AMD disease process (*Curcio et al, 1996, Curcio et al, 2000, Medeiros et al, 2001*). This suggests that a technique to isolate a response from rod photoreceptors within this region may be a valuable way to further investigate the differential loss of rods and cones in early AMD.

Given that the focal rod ERG may be sensitive to early changes in AMD, it was decided that a pilot study should be conducted to assess the relative merits of the subtraction and background adaptation techniques. However, at the outset there were reasons for questioning the suitability of both the wavelength and luminance of the focal stimulus used by Sandberg et al (*1996*).

6.2.2 Development of Stimulus Parameters

Preliminary investigations were conducted to determine the most effective stimulus parameters for recording the focal rod ERG.

In order to prevent progressive retinal adaptation, ISCEV recommendations suggest a minimum interstimulus interval of 2 secs when recording rod ERGs (*Marmor et al 1989, 1995, 1999*). A temporal frequency of 0.5 Hz was therefore used in all rod ERG recording in this study. In order to effectively assess the parafoveal region suspected to be targeted by early AMD, the stimulus diameter chosen was 20° (*Curcio et al, 1996; Curcio et al, 2000; Owsley et al, 2000; Medeiros et al, 2001; Owsley et al, 2001*).

The ISCEV standard for the recording of a rod ERG states that the flash intensity must be at least 2.5 log units below the standard ISCEV flash intensity (*Marmor et al, 1989, 1995, 1999*). The standard flash is $1.5 - 4.5$ cd.m^{-2}.sec^{-1}, and consequently a flash of 0.0142 cd.m^{-2}.sec^{-1} or less is recommended for scotopic recording. The focal rod ERG technique described by Sandberg et al (*1996*) used a 5ms, 440nm, flash of

2.1 log scot tds.sec^{-1}. Using values supplied by Wyszeki & Stiles (*1982; see Appendix VI*) to convert scotopic to photopic trolands, it was determined that this stimulus had an equivalent photopic luminance of 0.07 cd.m^{-2}.sec^{-1} (assuming a pupil diameter of 8mm). The flash used by Sandberg et al (*1996*) was therefore more intense than the ISCEV recommendation, leading to the possibility that Sandberg's focal rod response was contaminated by cone signals.

To ensure that an ERG response is purely rod-driven, a technique has been described (*Birch & Fish, 1987*) in which a red flash is presented to the dark adapted eye, which is of the same photopic luminance as the blue flash used to elicit the rod ERG. Rods are extremely insensitive to long-wavelength light and therefore any response obtained originates in the cone pathway. If no response is recorded to such a red flash, there can also be no cone response to a photopically matched blue stimulus.

This technique was used to determine whether the response recorded by Sandberg et al (*1996*) might have been contaminated by cone signals. When a focal (20° diameter) red flash of the same photopic luminance as the blue stimulus used in Sandberg's experiment (0.07 cd.m^{-1}.sec^{-1}) was presented to the dark adapted eye of control subject BC, a repeatable response was recorded. This may be seen in the bottom trace of Figure 6.7. This finding suggested that cone signals may have contaminated Sandberg's focal rod ERG.
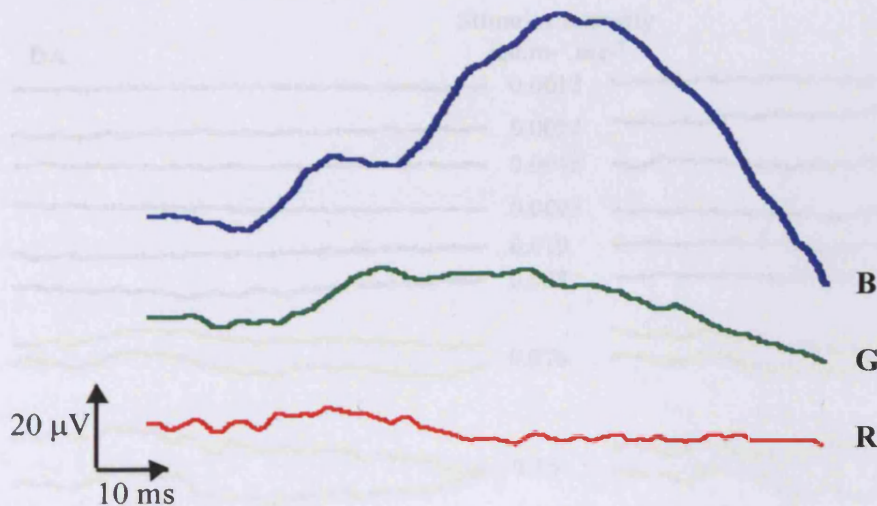
Figure 6.7. ERG responses elicited by blue (454nm, B), green (525nm, G) and red (664nm, R) focal stimuli (20° diameter, 5ms, 0.5 Hz, 0.07 cd.m^{-2}.sec^{-1}) after 30 mins dark adaptation. It can be seen in the top trace that the response to the blue flash has the characteristic double peaked response expected (B). A clear, but much smaller response is elicited by the green flash (G), whilst the red flash produces a small, but repeatable ERG (R).

In order to determine the appropriate intensity of flash to use in this study, responses were recorded from the dark-adapted eye of 2 healthy control subjects, DA and AB, in response to a series of red flashes that differed in luminance.

- The luminance of the red LED array was set at 61 cd.m^{-2}, and was attenuated using eight 0.3 log neutral density filters to achieve a luminance of 0.23 cd.m^{-2}.

- The red LEDs were modulated to flash at 0.5 Hz, with a stimulus duration of 5ms providing an effective flash intensity of 0.0012 cd.m^{-2}.

- The subject was dark adapted for 30 minutes.

- Thirty responses were recorded, bandpass filtered from 1-100 Hz, and averaged on a 200 ms timebase.

- Further responses were then recorded to stimuli of increasing intensity. Removal of one 0.3 log neutral density filter between each recording resulted in a doubling of flash luminance.

The ERG traces recorded from both subjects are shown in Figure 6.8. No repeatable responses were recorded in either subject to a red flash with a luminance of less than 0.038 cd.m^{-2}.sec^{-1}. Above this level, however, a response from the dark-adapted retina was clearly visible, with a b-wave of repeatable latency. This was assumed to be due to L- and M- cone activity.
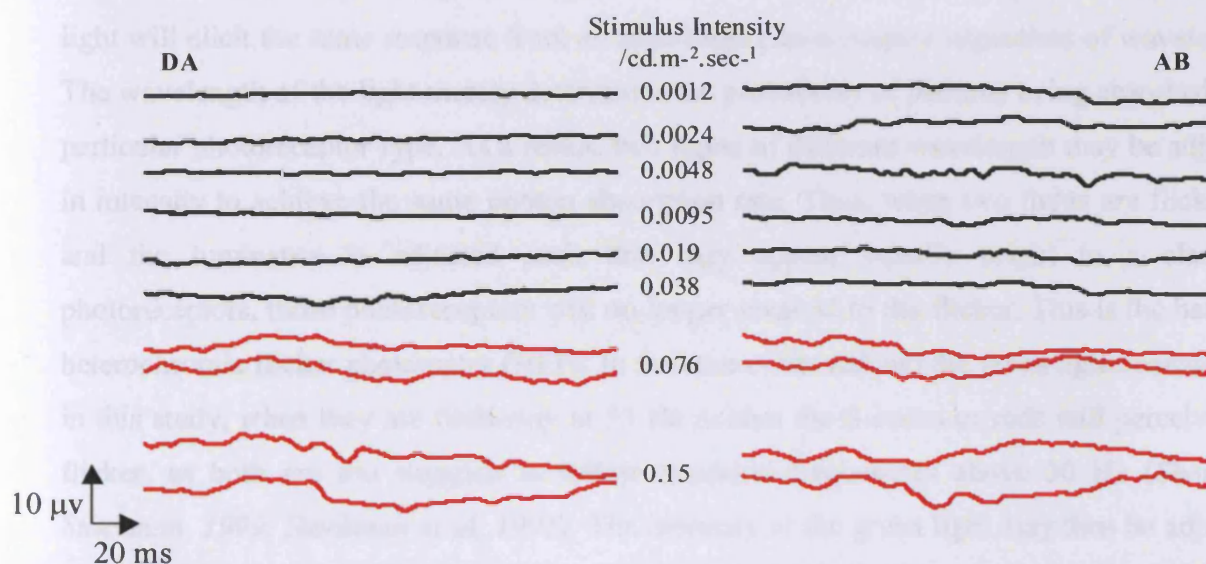
Figure 6.8. Dark-adapted responses recorded from subjects DA and AB to a red flash stimulus of increasing intensity. No response was elicited to red flashes of time-averaged luminance of 0.038 cd.m^{-2}.sec^{-1} or less. The red traces demonstrate that a repeatable response was recorded when the flash luminance was 0.076 cd.m^{-2}.sec^{-1} or greater.

It was therefore decided that flash luminance for rod experiments in this study should be 0.038 cd.m^{-2}.sec^{-1}. This exceeds the ISCEV recommendations, but is lower than the intensity judged by Sandberg (*1996*) to elicit a minimal cone response from the dark-adapted eye.

Using the blue (454nm) LED array, assuming an 8mm pupil diameter, this equates to a time averaged scotopic illuminance of 1.7 log scotopic tds.sec^{-1} (*calculated using values supplied by Wyszecki and Stiles, 1982, see Appendix VI*). In contrast, if a green (525nm) flash is used at 0.038 cd.m^{-2}.sec^{-1} then the scotopic illuminance provided is only 0.73 log scotopic tds.sec^{-1}. Thus a blue flash elicits a larger ERG response from the dark-adapted eye than a photopically matched green stimulus (*see Figure 6.7, B and G*).

However, another consideration is that light from the blue LED is more susceptible to scatter and absorption by the ocular media than the green LED (*Wyszecki & Stiles, 1982*), a factor of particular importance in an elderly patient group with age-related media changes. It is also of concern that the blue LED has a peak wavelength, which is close to the maximum absorption of the S-cone. It is important to be confident that the response elicited is rod-driven, and not contaminated by S-cone activity.

Another stimulus option which would minimise these concerns would be a green flash, alternating with a photopically matched red 'off' phase. The theory behind this lies in the fact that each individual class of photoreceptors is colour blind i.e. the absorption of a photon of light will elicit the same response from an individual photoreceptor regardless of wavelength. The wavelength of the light merely determines the probability of photons being absorbed by a particular photoreceptor type. As a result, two lights of different wavelength may be adjusted in intensity to achieve the same photon absorption rate. Thus, when two lights are flickering and the luminance is adjusted such that they appear equally bright to a class of photoreceptors, those photoreceptors will no longer respond to the flicker. This is the basis of heterochromic flicker photometry (HFP). In the case of the red and the green lights considered in this study, when they are flickering at 33 Hz neither the S-cones or rods will perceive the flicker, as both are too sluggish to follow temporal frequencies above 30 Hz (*Sharp & Stockman, 1999; Stockman et al, 1991*). The intensity of the green light may then be adjusted by an observer, until a minimum of flicker is perceived. At this point the red and green lights are balanced in such a way that they are of the same effective luminance to the L- and M-cones. The balance cannot be perfect, as two groups of photoreceptors are being considered, but it can minimise the stimulus provided to these photoreceptors. When the temporal frequency of the flicker is then reduced to 0.5 Hz, the response elicited is mainly from the

rods and the S-cones. Since the green LED has a peak wavelength of 525nm it is a poor stimulus to the S-cones (see Figure 5.1 for S-cone absorption spectrum). It may therefore be assumed that the red and green lights are principally eliciting a rod response.

A further pilot experiment was therefore carried out to compare the response obtained with a focal blue stimulus (20° diameter, 5ms flash, 0.5 Hz, 1.7 log scotopic tds.sec^{-1}) to the ERG recorded in response to a focal green flash, with a red 'off' phase. The red LED was set at its maximum of 30 cd.m^{-2}, and HFP used at 33 Hz to set the luminance of the green LED array. This resulted in a green luminance of around 30 cd.m^{-2}. With a flash duration of 12 ms (frequency 0.5 Hz), the illuminance of the green flash was approximately 1.7 log scotopic tds.sec^{-1}, and should therefore have provided the same stimulus to the scotopic system as the blue flash.

The responses in Figure 6.9 were recorded from control subjects JC and BC, aged 26, in response to the stimuli described above.
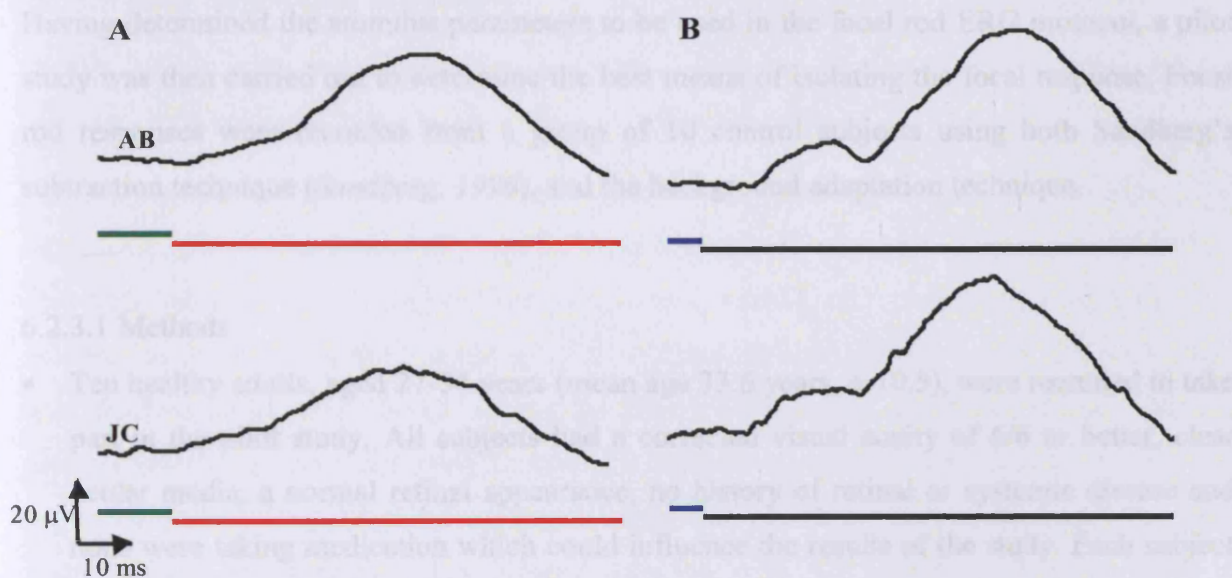
Figure 6.9. Dark-adapted ERG response recorded to a focal green flash (20° diameter, 12 ms duration , 0.5 Hz, 1.7 log scotopic tds.sec^{-1}) presented against red 'off' phase (A). Response recorded to a focal blue flash (20° diameter, 5 ms duration , 0.5 Hz, 1.7 log scotopic tds.sec^{-1}) (B). The broken horizontal lines describe stimulus duration.

It may be seen that, whilst the green and blue flashes are of the same scotopic intensity, the focal element of the response elicited by the blue flash is larger in both subjects, and more clearly exhibits the double b-wave (*see Figure 6.9, B*). Only a slight flattening in the ascending slope of the b-wave recorded to the green flash indicates that a focal response might be present (*see Figure 6.9, A*). This smaller focal response may be due to the presence of the red 'off' phase. Although rods are insensitive to the long wavelength (664nm) light,

there may be a slight desensitising effect. The larger diffuse scattered light response seen in (B) than (A) may be due to greater scatter of the shorter wavelength blue stimulus than the longer wavelength green stimulus presented in (A).

The green stimulus was therefore rejected on the basis of the larger focal response elicited by the blue flash. A further disadvantage of the technique was the time consumed in the process of determining flash luminance through heterochromic flicker photometery (HFP).

On the basis of these preliminary studies it was decided that, when evaluating the two methods of isolating focal rod responses (the subtraction and background adaptation techniques), the most appropriate stimulus would be a 20° diameter, 1.7 log scotopic tds.sec^{-1}, blue (454nm) flash of 5 ms duration, modulated at a temporal frequency of 0.5 Hz.

6.2.3 *Comparison of Subtraction and Background Adaptation Techniques*

Having determined the stimulus parameters to be used in the focal rod ERG protocol, a pilot study was then carried out to determine the best means of isolating the focal response. Focal rod responses were recorded from a group of 10 control subjects using both Sandberg's subtraction technique (*Sandberg, 1996*), and the background adaptation technique.

6.2.3.1 Methods

- Ten healthy adults, aged 27-54 years (mean age 33.6 years, ± 10.5), were recruited to take part in the pilot study. All subjects had a corrected visual acuity of 6/6 or better, clear ocular media, a normal retinal appearance, no history of retinal or systemic disease and none were taking medication which could influence the results of the study. Each subject gave their informed consent after being provided with a full description of the procedures involved.

- Each subject was dilated with 1.0% tropicamide, and prepared for ERG recording in the manner described in section 6.1.

- Subjects were dark-adapted for 30 minutes.

- The stimulus was a 20° diameter, blue (454nm) 5 ms flash of 1.7 log scotopic tds sec^{-1}, presented at a temporal frequency of 0.5 Hz. The subjects were asked to fixate the centre of the flash.

Subtraction Technique

- Thirty ERG responses were elicited in response to the stimulus, and averaged on a 200 ms timebase, bandpass filtered from 1-100 Hz.

- The LED stimulator was then held adjacent to the subject's eye, to provide a ganzfeld stimulus.

- A series of full-field ERGs was then recorded in response to a blue flash (454nm, 5ms, 0.5 Hz), whose luminance was altered systematically to obtain an ERG b-wave which matched the amplitude and implicit time of the second b-wave obtained with the focal stimulus.

- The matching full-field response was mathematically subtracted from the initial double-peaked trace to isolate the focal component.

Background Adaptation Technique

In this technique, a desensitising green (525nm) surround was employed to minimise the scattered light response from rods in the peripheral retina.

The photograph in Figure 6.10 shows the apparatus that was constructed for this study. The equipment allowed the presentation of the focal blue stimulus at the back of a ganzfeld bowl. The bowl was an acetate hemisphere, which was treated with sandblasting equipment to achieve the desired opacity. A circle of 12 evenly spaced high intensity green LEDs (525nm) was attached to an MDF board behind the bowl. These LEDs could be adjusted using a dimmer switch, and provided even illumination across the ganzfeld bowl. A hole was cut into the board, and a tube inserted, which was attached centrally to the back of the bowl. The head stage of the LED stimulator was inserted into this tube. To prevent light from the focal stimulus from being reflected throughout the bowl a cone was attached to the inside of the bowl. The aperture in the cone subtended 20° at the eye of a subject positioned on the chin rest. A schematic diagram is shown in Figure 6.11. The general protocol for this technique is described below.

- Thirty ERG responses were elicited by the blue flash presented in the centre of the ganzfeld bowl, bandpass filtered from 1-100 Hz, and averaged on a 200 ms timebase.

- A steady, diffuse green (525nm) background light was then introduced and further ERGs recorded.

- The luminance of the background was altered systematically and its effect on the ERG waveform noted.
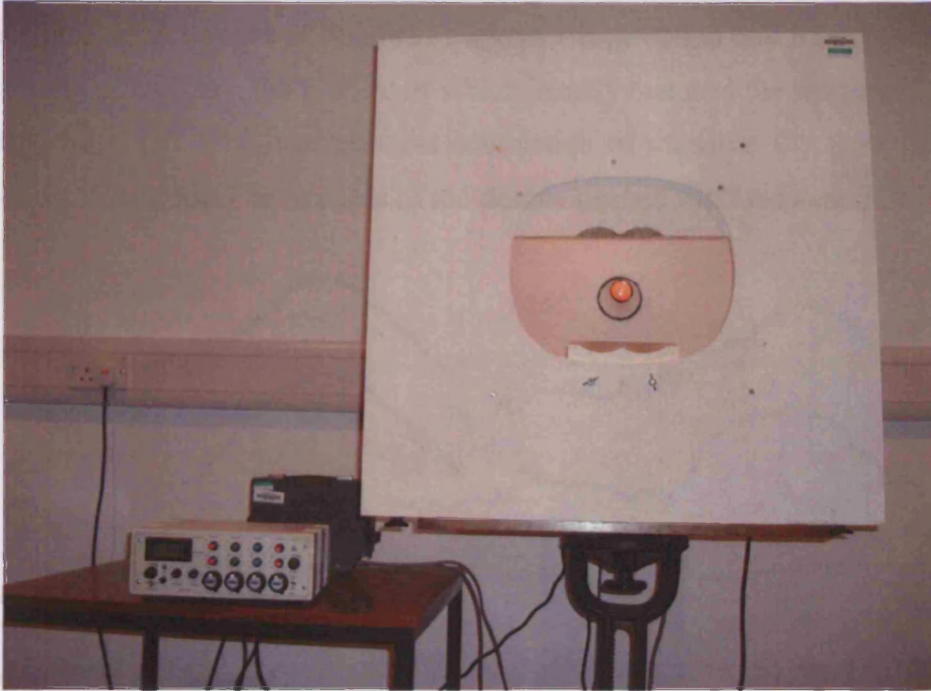
Figure 6.10. Equipment constructed for the recording of focal ERGs by a background adaptation technique.
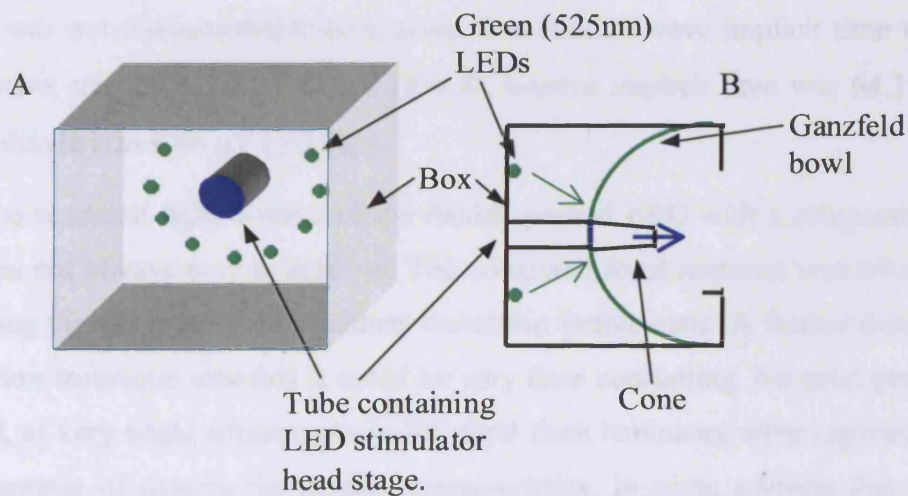
Figure 6.11. Schematic diagram showing the internal construction of the apparatus used to record a focal rod ERG using the background adaptation technique. Panel A illustrates the positioning of the head stage of the LED stimulator and green LEDs, without the ganzfeld bowl in place. Panel B is a cross-sectional diagram. The inside of the box was painted white, to aid the even distribution of background illumination.

6.2.3.2 Results

Figure 6.12 shows typical ERG responses recorded using the subtraction technique. The initial trace (*A*) demonstrates the double b-wave expected in response to focal stimulation of the dark-adapted eye. A series of full-field responses recorded to dim blue flashes culminated in the recording of an ERG, the b-wave of which exactly matched the scattered light response of the initial trace (*B*). The mathematical subtraction of response (*B*) from (*A*) resulted in isolation of the direct, focal component of the double-peaked ERG response.
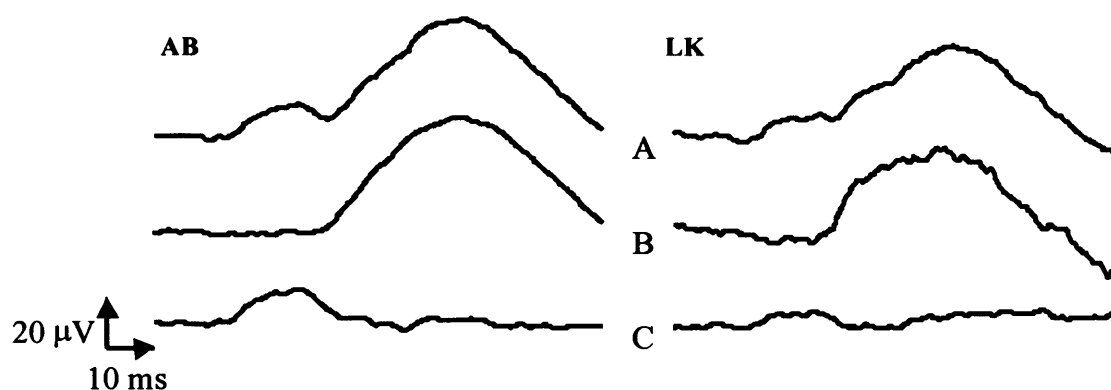
Figure 6.12. Focal rod responses elicited from subjects AB (aged 26) and LK (aged 29) using the subtraction technique. The upper trace was obtained in response to the focal blue stimulus (A), the middle trace is a full-field response whose amplitude and latency matched that of the scattered light response (B), and the lower trace is the result of the subtraction of B from A (C).

A focal response was obtained from all 10 subjects using the subtraction technique, although the a-wave was not distinguishable in 6 cases. The mean a-wave implicit time was 29.1 ms (± 3.4), a-wave amplitude was 0.48 μV (± 0.8), b-wave implicit time was 64.3 ms (± 3.2), b-wave amplitude was 9.86 μV (± 2.7).

Matching the scattered light b-wave of the double peaked ERG with a comparable full-field response was not always easy to achieve. The computed focal response was often noisy as a result, making the analysis of the resultant waveform problematic. A further disadvantage of the subtraction technique was that it could be very time consuming. No strict protocol could be followed, as very slight adjustments in full-field flash luminance were required in order to obtain a response of exactly the correct characteristics. In some subjects this was readily achieved, in others many ERGs were recorded in order to obtain the required response. Typically, the recording period lasted for 30 minutes in addition to time taken for dark adaptation.

Figure 6.13 shows typical focal ERG responses recorded using the background adaptation technique. A double b-wave is seen in the first trace of each data set, in response to focal stimulation with no background. The subsequent traces demonstrate the reduction in the amplitude of the second b-wave as the intensity of background illumination is increased. In both cases illustrated, a background luminance of 1.46 log scot tds was sufficient to completely extinguish the scattered light response, leaving the focal rod response isolated. Any further increase in the intensity of background illuminance had little effect on the waveform of the isolated focal response.
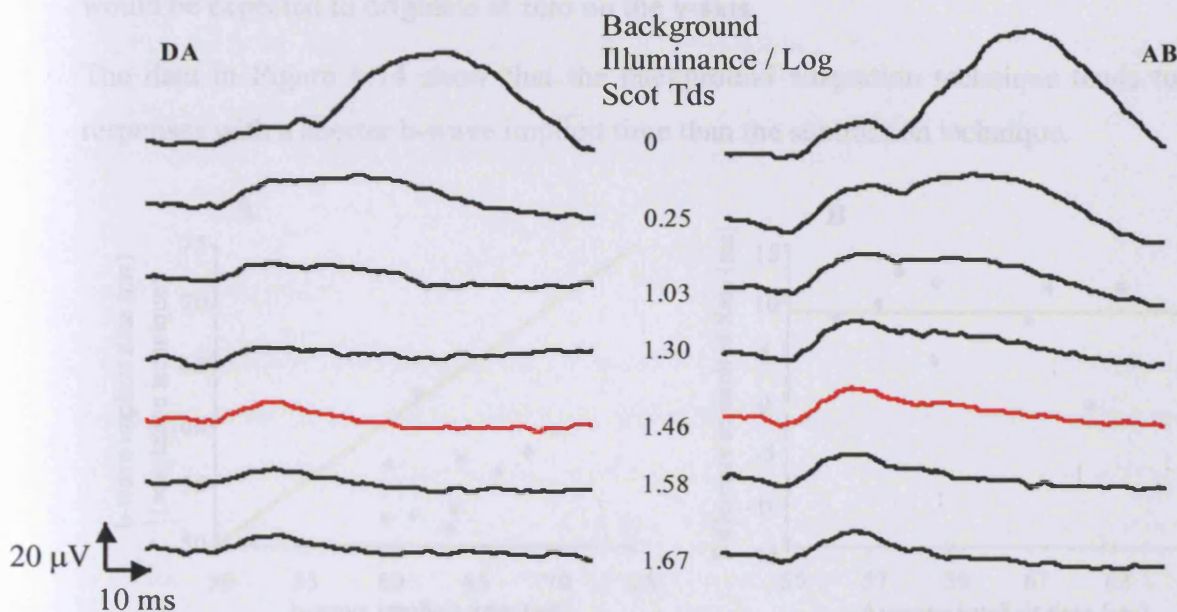
Figure 6.13. Focal rod responses obtained from subjects DA (aged 26) and AB (aged 26) using the background adaptation technique. The top trace shows the ERG recorded in response to focal stimulation, with no adapting background. The intensity of the background increases down the column of responses. The red traces indicate the isolated focal response.

Clear focal responses were recorded from all ten subjects using this technique. In only one individual (HT) was the a-wave too small to be measured. The mean a-wave implicit time was 27.8 ms ($\pm$ 3.3), a-wave amplitude was 1.48 μV ($\pm$ 0.78), b-wave implicit time was 55.9 ms ($\pm$ 3.5), and b-wave amplitude was 7.58 μV ($\pm$ 2.9).

Although there was a small amount of variation in the level of background illuminance required to completely suppress the response from the peripheral retina, in all subjects 1.67 log scot tds was sufficient to completely extinguish the second b-wave. This level of background illuminance was therefore chosen for further experiments using the background adaptation technique. The technique was quick to perform, and a standardised protocol produced satisfactory results from all subjects.

6.2.4   Comparison of Techniques

In order to assess the agreement of the two techniques, b-wave implicit time (*Figure 6.14*) and amplitude (*Figure 6.15*) have been compared graphically. Panel (A) in each case shows a scatter diagram of the data. Panel (B) shows the differences between the two techniques plotted against the average of the two measurements. In a situation in which the two techniques showed perfect agreement, the points would be expected to lie along the line of equality, shown in red. In the plot in panel (B) the line describes the bias i.e. the mean difference between the two techniques. If there was no bias between the two then this line would be expected to originate at zero on the y-axis.

The data in Figure 6.14 show that the background adaptation technique tends to produce responses with a shorter b-wave implicit time than the subtraction technique.
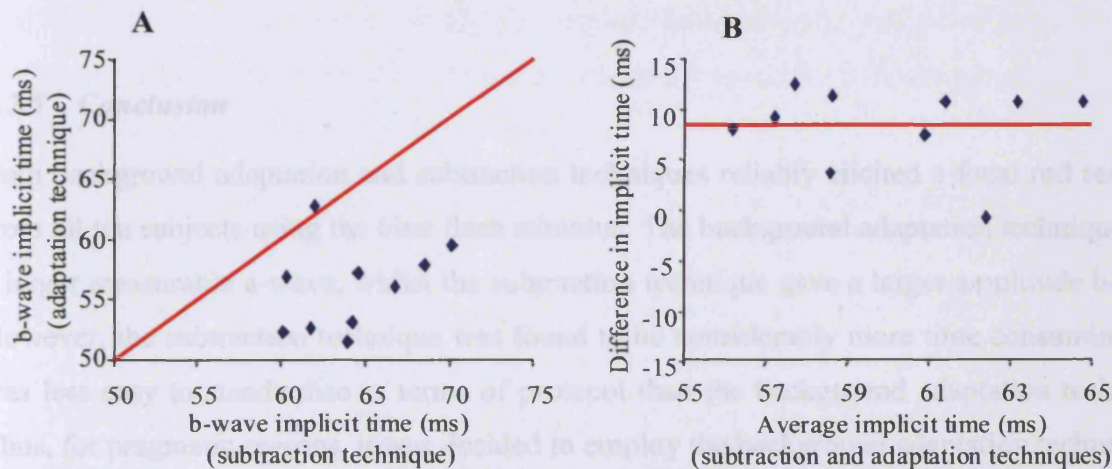
Figure 6.14. Scatter plot of focal rod b-wave implicit time recorded using the adaptation technique and subtraction techniques (A); graph showing differences between implicit times using the two techniques (subtraction – background adaptation technique) against the average of the two techniques (B).

Figure 6.15 shows that the agreement between amplitude measurements for the two techniques is relatively good. In panel A, the points of the scatter plot are all seen to lie below the line of equality. This represents a bias in the results, which may be seen in panel (B), in which the line of equality falls at a point 2.28 µv above zero. This indicates that the b-wave amplitude tends to be greater when using the subtraction technique.

The smaller, faster b-wave recorded using the background adaptation technique is indicative of a more light-adapted status, possibly due to the scatter of light from the adapting surround onto the central retina.
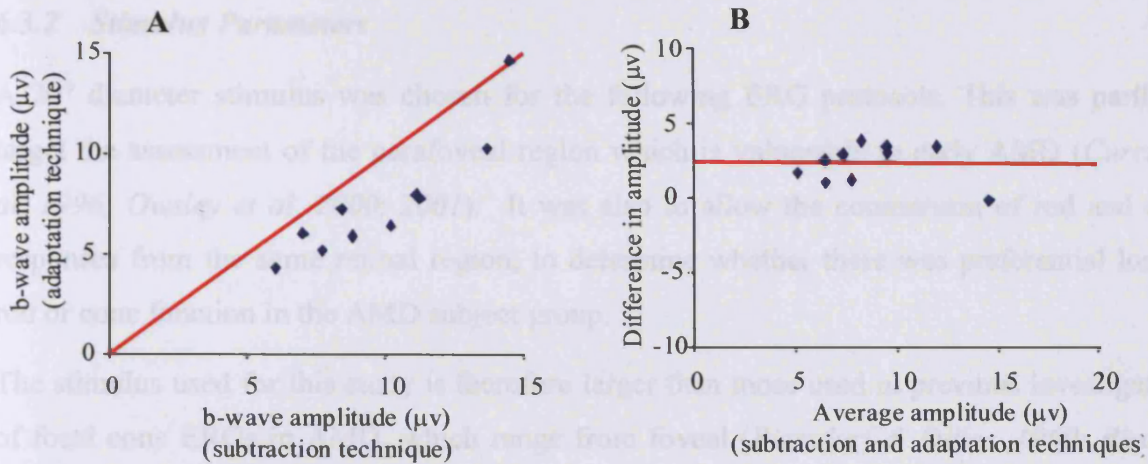
Figure 6.15. Scatter plot of focal rod b-wave amplitude recorded using the adaptation and subtraction techniques (A); graph showing differences between amplitudes using the two techniques (subtraction – background adaptation technique) against the average of the two techniques (B). In both cases red line indicates line of equality.

6.2.5   Conclusion

Both background adaptation and subtraction techniques reliably elicited a focal rod response from all ten subjects using the blue flash stimulus. The background adaptation technique gave a larger measurable a-wave, whilst the subtraction technique gave a larger amplitude b-wave. However, the subtraction technique was found to be considerably more time consuming, and was less easy to standardise in terms of protocol than the background adaptation technique. Thus, for pragmatic reasons, it was decided to employ the background adaptation technique in the general protocol of this study.

6.3   The Focal Cone Electroretinogram

6.3.1   Introduction

The focal cone ERG (*see section 4.3.5*) has been employed in the assessment of central retinal function in many studies of age-related macular degeneration (*Biersdorf & Diller, 1969; Birch & Fish, 1988; Sandberg et al, 1993; Remulla et al, 1995; Sandberg et al, 1998; Falsini et al 1999; Falsini et al, 2000*).

The following section describes the development of a focal cone protocol to maximise sensitivity to the changes expected in early ARM.

6.3.2 Stimulus Parameters

A 20° diameter stimulus was chosen for the following ERG protocols. This was partly to target the assessment of the parafoveal region which is vulnerable to early AMD (*Curcio et al, 1996; Owsley et al, 2000, 2001*). It was also to allow the comparison of rod and cone responses from the same retinal region, to determine whether there was preferential loss of rod or cone function in the AMD subject group.

The stimulus used for this study is therefore larger than those used in previous investigations of focal cone ERGs in AMD, which range from foveal (*Biersdorf & Diller, 1969; Birch & Fish, 1988*) up to 9° (*Falsini et al, 1999*) in diameter.

In order to assess the transient ERG, a frequency of 5 Hz was chosen. This was found to produce clear separation of the ON and OFF components of the response, allowing easy analysis of the a- and b- waves. At higher temporal frequencies the individual wavelets of the ERG were found to be less distinct, at lower temporal frequencies a longer period of time was required to average the same number of responses

In addition to recording a transient cone response, it was also decided to investigate the steady state ERG response in subjects with AMD. Previous reports, using smaller stimuli, have suggested that temporal and amplitude characteristics of this response may be affected by early ARM, and may have prognostic value at identifying those who will develop advanced AMD (*Remulla et al, 1995; Sandberg et al, 1998; Falsini et al, 1999, Falsini et al, 2000*). It has been suggested that the first harmonic of the steady state cone ERG reflects primarily outer retinal activity (*Porciatti et al, 1989*), and that a high, 41 Hz, temporal frequency will be dominated by this first harmonic (*Remulla et al, 1995; Falsini et al, 2000*). Since the photoreceptor layer is targeted early in the disease process, a response dominated by outer retinal activity is ideal for the purposes of this study, and the 41 Hz stimulus was selected for the final protocol.
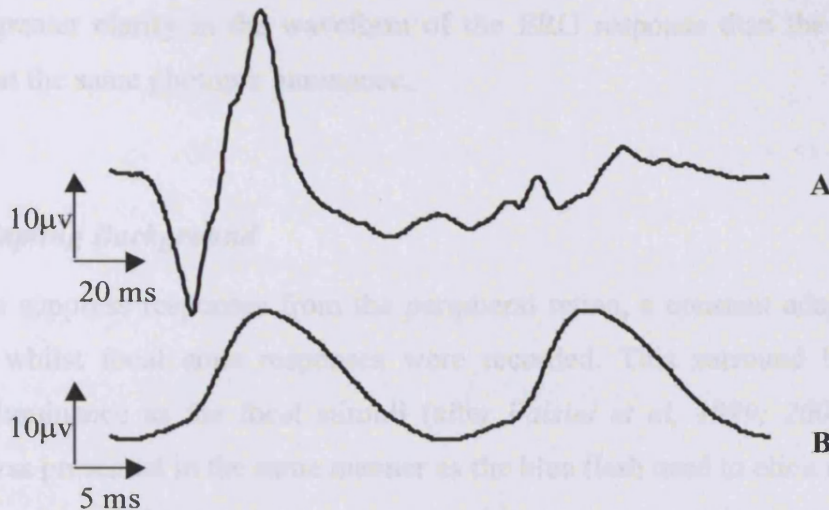
Figure 6.16. Sample full-field 5 Hz (A) and 41Hz (B) cone responses recorded from subject LG (aged 55). Stimulus consisted of 30 cd.m^{-2}.sec^{-1} amber (595nm) square wave flicker. For each trace two hundred responses were averaged on a 200 ms timebase, and bandpass filtered from 1-100 Hz.

A long wavelength flash is ideal for recording a focal cone response, as it will strongly stimulate the L- and M- cones, whilst being relatively unaffected by scatter and absorption by the ocular media than shorter wavelength stimuli. A comparison was made of ERG responses elicited by the red (664nm), green (525nm), and amber (595nm) stimuli available. This may be seen in Figure 6.17, which illustrates focal cone responses elicited by different wavelength stimuli from 2 healthy young subjects.
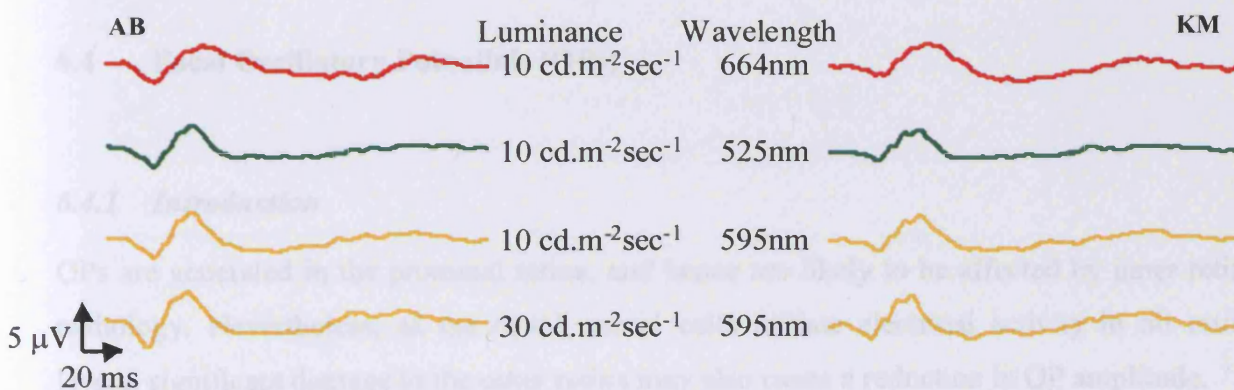
Figure 6.17: The top three traces show focal ERG responses elicited by equiluminant red (664nm), green (525nm) and amber (595nm) square wave stimuli (5 Hz, 10 cd.m^{-2}.sec^{-1}) from subject AB (aged 26), and KM (aged 28). The final trace illustrates the response recorded to the amber flash at maximum intensity (30 cd.m^{-2}.sec^{-1}).

Of the wavelengths provided by the LED stimulator, the largest amplitude cone response was elicited by the amber flash at maximum intensity (30 cd.m^{-2}.sec^{-1}). The amber flash also

provided greater clarity in the waveform of the ERG response than the other wavelengths presented at the same photopic luminance.

6.3.3 Adapting Background

In order to suppress responses from the peripheral retina, a constant adapting surround was presented whilst focal cone responses were recorded. This surround had the same time averaged luminance as the focal stimuli (after *Falsini et al, 1999; 2000*). The focal cone stimulus was presented in the same manner as the blue flash used to elicit focal rod responses, at the back of a ganzfeld bowl. Homogenous white background illumination was provided by 8 daylight bulbs that illuminated the bowl.

6.3.4 Conclusion

Two focal cone protocols were developed for inclusion in the electrophysiological study of ARM. The first elicited a transient response, through the presentation of a 5 Hz square wave stimulus (595 nm, 20° diameter, 30 cd.m^{-2}.sec^{-1}). The second response was a steady state signal recorded in response to a 41 Hz stimulus (595nm, 20° diameter, 30 cd.m^{-2}.sec^{-1}). A ganzfeld white surround of 30 cd.m^{-2}.sec^{-1} was used in both cases.

6.4   Focal Oscillatory Potentials (OPs)

6.4.1 Introduction

OPs are generated in the proximal retina, and hence are likely to be affected by inner retinal pathology. Nevertheless, as the distal retinal cells initiate electrical activity in all retinal layers, significant damage to the outer retina may also cause a reduction in OP amplitude.

Miyake et al (*1990*) described the use of a focal white stimulus, modulated to a rectangular wave flicker of frequency 5 Hz to elicit focal cone OPs. In all cases 3-4 OPs were elicited from normal subjects, with an inter-peak interval of approximately 6.5 ms. This technique may be of value in the investigation of age-related macular degeneration.

6.4.2   *Stimulus Parameters*

Miyake et al (*1990*) investigated focal OPs recorded using both 5° and 15° diameter stimuli, and found the amplitude of the response recorded using the smallest stimulus to be disproportionately small. This implies that the cells generating the OPs are relatively sparse in the fovea. A 20° diameter stimulus was chosen for this study in order to target the retinal area affected in early AMD, and to elicit a relatively large OP response from controls.

In order to evaluate the effect of stimulus wavelength on OP characteristics, a series of focal OPs was recorded from two control subjects, AB (26), and KM (28), using the 5 Hz, square wave stimulus. As in the previous study, responses were recorded to red (664nm), amber (595nm) and green (525nm) flashes to assess the relative size of the OPs elicited. All stimuli were presented at the back of the ganzfeld bowl, with an equiluminant white surround to minimise responses from the peripheral retina. Data were bandpass filtered from 100-1000 Hz, in order to extract the OPs.

Figure 6.18 shows the OP responses recorded. In all cases three OPs are clearly visible. A comparison of the first three traces, recorded to equiluminant stimuli of different wavelengths, indicates that the amber flash provides the clearest signal from the central retina. The bottom trace shows the response to the brightest amber flash available (30 cd.m^{-2}.sec^{-1}), a small amplitude fourth OP is just visible at this intensity for subject KM. The mean interpeak interval for focal OPs elicited by the amber flash (30 cd.m^{-2}.sec^{-1}) was 7.7 ms.
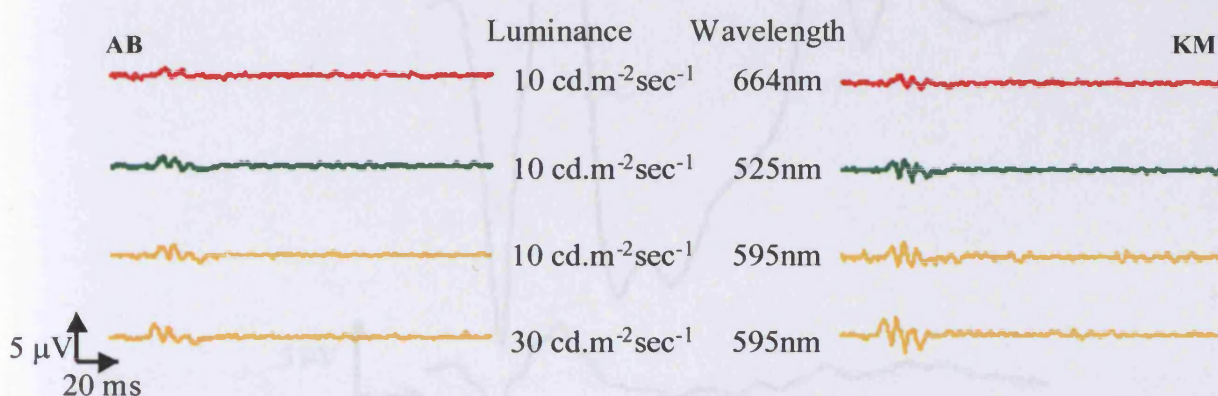
Figure 6.18. Top three traces show focal OP responses elicited by equiluminant red (664nm), green (525nm) and amber (595nm) square wave stimuli (5 Hz, 20° diameter, 10 cd.m^{-2}.sec^{-1}) from subject AB (aged 26) and KM (aged 28). The final trace illustrates the response recorded to the amber flash at maximum intensity (30 cd.m^{-2}.sec^{-1}). Data were bandpass filtered from 100-1000 Hz, and 200 responses were averaged for each trace. The timebase was 200 ms.

6.4.3   Conclusion

Clear focal OPs were elicited from the parafovea using the same 20° diameter, 5 Hz amber flash that elicited the best a- and b- waves. By bandpass filtering data on two channels from 1-100 Hz, and 100-1000 Hz it will be possible to simultaneously record both the transient 5 Hz focal ERG and the OPs in the final protocol.

6.5   Focal vs. Full-Field Responses

ARM affects the central retina, and it is therefore expected that focal ERG signals may be attenuated in individuals with the condition. Intersubject variability in ERG amplitudes is a confounding factor however, and may reduce the sensitivity of the tests. To overcome this problem, full-field rod and cone signals were also recorded. By evaluating a ratio of the focal to full-field response amplitudes the sensitivity of the tests may be increased by minimising variability within normal subjects.

This technique is illustrated in Figure 6.19, which shows sample focal and full-field 5Hz cone responses recorded from subject AB (aged 26). The Figure legend below demonstrates the calculation of the amplitude ratio.
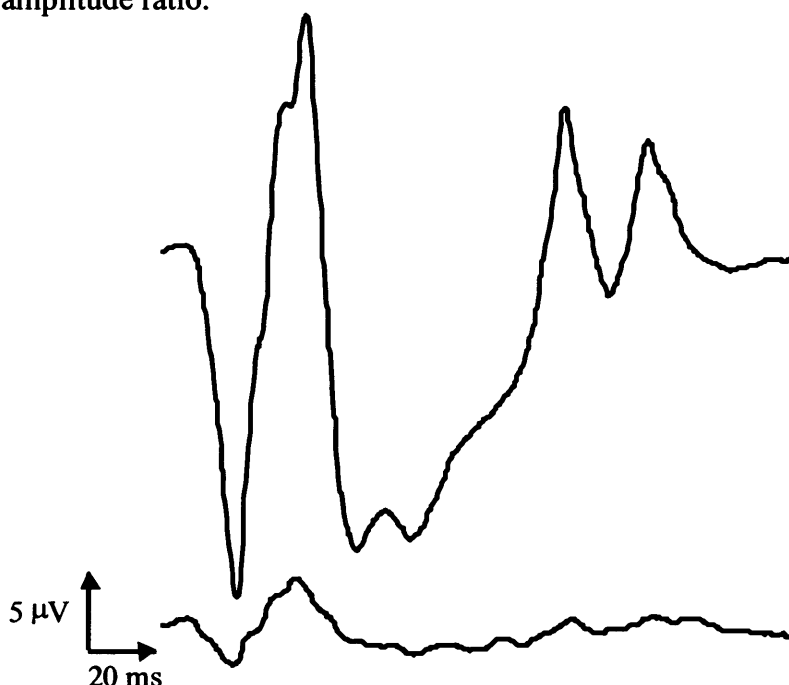
Figure 6.19. Full-field (top) and focal (bottom) photopic ERG responses recorded from subject AB to square wave flash (595nm, 30 cd.m^{-2}.sec^{-1}, 5 Hz). The amplitude of the a-wave was 2.4 µv (focal) and 21.0 µv (full-field), resulting in a focal : full-field ratio of 0.11. The amplitude of the b-wave was 5.4 µv (focal) and 34.6 µv (full-field), resulting in a focal : full-field amplitude ratio of 0.16.

It can be seen in Figure 6.19 that the waveform of the focal response is similar to that of the full-field response. In order to provide further evidence that the focal responses recorded do originate solely from the central retina, a further series of ERGs was recorded from a subject, PS (age 78), with bilateral disciform AMD. Visual field analysis indicated the presence of a central scotoma in each eye.

Figure 6.20 shows the focal and full-field rod and transient cone responses recorded from this subject. Both focal cone and rod responses are unmeasurable, whilst the full-field responses are clearly recorded. The implication is that the peripheral retina of PS is functional, and responding to ganzfeld flashes. This suggests that the rod and cone focal responses are uncontaminated by peripheral retinal activity.
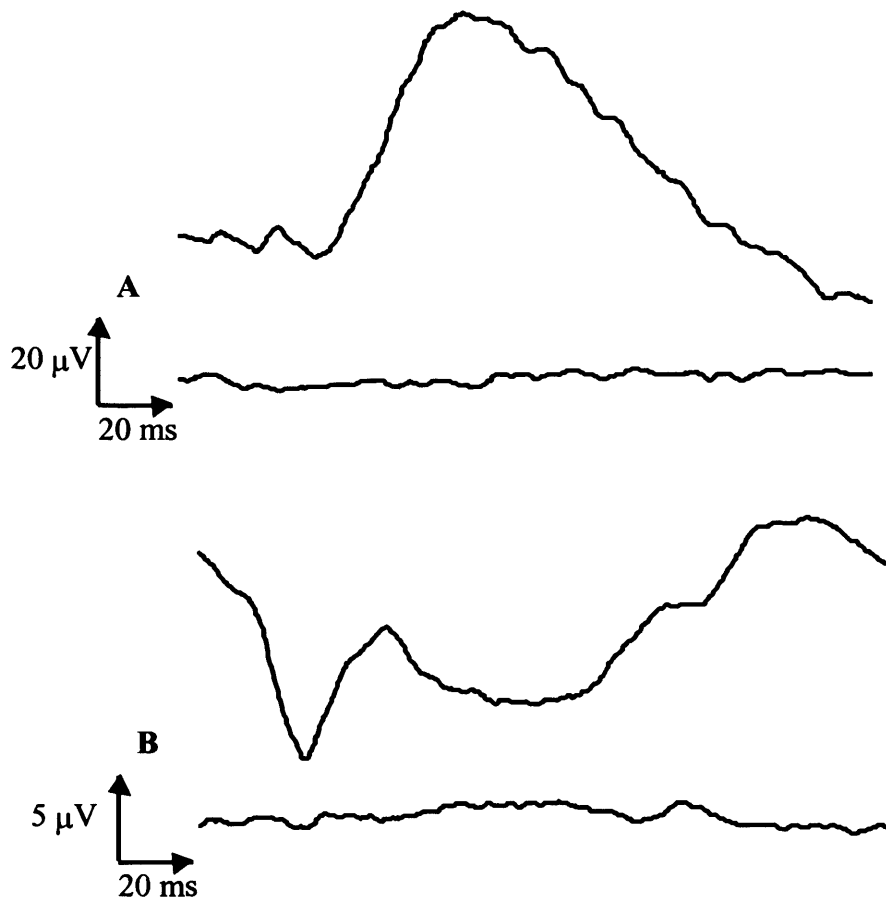
Figure 6.20. ERG responses recorded from subject PS who has a central scotoma in both eyes. The upper traces show rod responses (A). The lower traces show cone responses (B). The upper trace in each pair of signals is obtained in response to full-field stimulation and the lower trace is the focal signal. No measurable response is elicited by the focal stimuli.

6.6 The c-wave

6.6.1 Introduction

The c-wave is a slow developing corneal positive ERG response, which is believed to reflect the integrity of the retinal pigment epithelium (*see section 4.2.8*). The RPE and outer retina are affected at an early stage in AMD, and thus the c-wave may have diagnostic potential. There have been no previous reports of the effect of early AMD on the c-wave, but abnormalities in the waveform have been recorded in dogs and humans with diffuse RPE abnormality, whilst the a- and b-waves remain within normal limits (*Nilsson & Wrigstad, 1997*).

The ERG c-wave may be recorded from the cornea of humans, but is so slow to peak that the signal may be contaminated by electrode drift. Special non-polarisable electrodes can be used to counteract this problem, and the signal recorded on a DC amplifier. However, performing ERG recordings with DC amplification is technically difficult (*Nilsson & Anderson, 1988*). Hamasaki et al (*1997*) compared c-waves recorded using DC and AC equipment, and found that both systems would record a measurable response, although the amplitude of the c-wave was larger with the DC system. They recommended that AC amplifiers should have a low pass filter of 0.1 Hz or below.

Moschos et al (*1993*) successfully recorded the c-wave, using AC amplification, from 48 healthy controls and 15 subjects with cone dysfunction syndrome. The stimulus consisted of a 300 asb (95.4 cd.m^{-2}) intensity flash of 1.25 secs duration, presented to the dark-adapted eye. The time window of recording was 5 seconds, and a ten minute interstimulus interval maintained the level of retinal adaptation. All controls showed a recordable c-wave of mean amplitude 530.18 μV at a mean implicit time of 1928.64 ms. Fourteen of the 15 subjects with cone dysfunction syndrome also produced a recordable c-wave, but of reduced amplitude and prolonged implicit time.

The optimal recording conditions to elicit a c-wave of maximal amplitude involve long duration, high intensity stimuli presented to the dark adapted eye (*Skoog & Nilsson, 1974; Hamasaki et al, 1997*). A long timebase is required to record the peak of the response, which occurs within 2-10 seconds after stimulus onset.

The aim of this study was to determine whether a practicable technique for reliably eliciting the ERG c-wave from healthy control subjects could be devised, within the confines of the AC amplification equipment available.

6.6.2   Recording the c-wave

A pilot experiment was carried out to determine whether it was possible to replicate the results of Moschos et al (*1993*). Responses were recorded from subject JB (age 56), who was dilated with 1.0% tropicamide, and prepared for ERG recording in the manner described in section 6.1. White flash stimuli were generated by a combination of red, green, blue and amber LEDs driven by the LED stimulator. Flash luminance was adjusted to 95.4 cd.m^{-2}, with a flash duration of 1.25 secs. An interstimulus interval of 10 minutes was used. Figure 6.21 shows three consecutive ERG traces recorded on a 3 second timebase and bandpass filtered from 0.1-100 Hz.

Figure 6.21. ERG responses recorded from subject JB, in response to a full-field white flash (95.4 cd.m^{-2}, 1.25 sec duration). Responses were recorded on a 3 second timebase, and bandpass filtered from 0.1-100 Hz. Trace A is a single (not averaged) ERG obtained after 30 mins dark adaptation. Traces B and C were recorded 10 and 20 minutes later respectively.

A large positive going waveform can be seen following the b-wave in all three traces in Figure 6.20. This does not peak within the 3 second time window, but rather appears to continue rising. The amplitude of this positive response, measured at 3 secs after stimulus onset, becomes progressively smaller in consecutive traces. The first ERG recorded shows the greatest amplitude of response (1103.6 μV), with smaller signals seen in the second (686.5 μV) and third (293.3 μV) traces. The timing of this positive response suggests that it is

the c-wave described by Moschos (*1993*), although no sample traces were included in the original article, and consequently a direct comparison was not possible.

6.6.3   Conclusion

The progressive decrease in the amplitude of the response in successive traces indicated that the ten minute interstimulus interval used in this protocol was insufficient to allow the level of retinal adaptation to return to baseline between flashes.

A further problem encountered in the recording of the c-wave response using this technique was the difficulty experienced by the subject in avoiding blinking and eye movements in response to a long duration flash presented to a dark adapted eye. This was accentuated by the long timebase, with the subject having to maintain stable fixation for 3 seconds to prevent contamination of the trace by extraneous signals. A number of responses were rejected due to such eye movements. This made the process particularly time consuming as a further period of dark adaptation was required before the next flash could be presented.

Attempts to repeat the recording on a further two control subjects, DA and AB (both aged 26) were unsuccessful. In both cases this was due to rejection of the ERG traces due to blinking. The instillation of a topical anaesthetic did not remedy the problem.

A large physiologic variability in the size of the c-wave has been reported. It has been suggested that 10-15% of normal subjects fail to have a recordable response (*Hock & Marmor, 1983*). The repeatability of the c-wave is also found to be poor, with a same-day intrasubject variability of 23-40% found in one study (*Hamasaki et al, 1997*). In view of such reports, and the problems experienced in eliciting this response from healthy adults, it was decided not to use the technique in this study.

6.7   The S-Cone Electroretinogram

6.7.1   Introduction

The first colour vision defects recorded in individuals with early AMD are tritanopic in nature (*e.g. Cheng & Vingrys, 1993; Collins & Brown, 1989; Haegerstrom- Portnoy & Brown, 1988*). Studies of retinal sensitivity in AMD have also suggested a selective disruption of the

S-cone pathway, which may be predictive of choroidal neovascularisation (*Eisner et al, 1987; 1991; 1992; Sunness et al, 1989*).

The S-cone ERG would be a means of objectively assessing S-cone function in subjects with early AMD. In humans, S-cones only comprise 5-10% of the cone mosaic (*Curcio et al, 1991*), and thus very precise recording conditions are required to elicit a response from the S-cones, which is uncontaminated by L- and M- cone and rod activity. The S-cones are maximally stimulated by short wavelength stimuli, but even at 450nm there is overlap in the sensitivity spectra of the three cone types.

One means of minimising intrusion from other classes of photoreceptor is to provide an adapting background, of a wavelength which will selectively desensitise the L- and M- cones, and an intensity greater than 2000 scotopic trolands, in order to suppress any rod response (*Aguilar & Stiles, 1954*). However, under these conditions the S-cone response is partially superimposed on a preceding b-wave reflecting residual L- and M- cone activity (*Gouras & Mackay, 1990; Gouras et al, 1993*). This results in difficulties in analysing the amplitude of the S-cone b-wave, and completely disguises the presence of any S-cone a-wave. Recent reports have suggested that S-cones are better isolated using a technique that involves a short wavelength flash presented against a high intensity yellow or amber background (*Horiguchi et al, 1995; Simonsen & Rosenberg, 1996; Suzuki et al, 1998; Arden et al, 1999*). However, this high intensity background can be uncomfortable for the patient, and may cause some desensitisation of the S-cones.

A further technique to isolate the S-cone ERG was developed to overcome these problems. The 'silent substitution' technique of recording the S-cone ERG (*Sawusch et al, 1987; Swanson et al, 1993*) involves heterochromic flicker photometry, the theory of which is described in section 6.2.2. A continuous full-field long wavelength background is used to desensitise L-cones. Full-field medium and short wavelength lights are then superimposed, and modulated to flicker in counterphase at a frequency of 33 Hz. This frequency is too fast for rods or S-cones to perceive the flicker (*Sharp & Stockman, 1999; Stockman et al, 1991*). Since the L-cones have been desensitised by the adapting background, the M-cones alone are responsible for flicker perception. The brightness of either medium or short wavelength lights is then adjusted to the point at which the two colours are equiluminant to the M-cones, and thus no flicker is perceived. When the temporal frequency of the square wave flicker is subsequently reduced, the medium and short wavelength lights now provide a stimulus to the S-cones. Since the combined luminance of the stimulus and background is sufficient to

desensitise the rods, the response elicited should be purely S-cone in nature. This technique has been shown to produce a response of higher amplitude than the adaptation technique, and shows less evidence of intrusion from L- and M- cone activity (*Chiti et al, 2003*).

The silent substitution technique was chosen for this study in order to produce S-cone responses of maximal amplitude. A further benefit of this technique lies in its ability to allow for individual differences in optical media. The short wavelength light is more prone to absorption and scatter than the medium wavelength. A subject with greater media absorption will therefore require a higher luminance short wavelength light in order to balance the medium wavelength. This should partially compensate for differences in media absorption between individuals.

6.7.2   Stimulus Parameters

The specific stimulus parameters used in this study were developed in our lab by Drasdo et al (*2001; 2002*), and have been shown to evoke an uncontaminated S-cone response.

Wavelength	Presentation	Luminance / $cd.m^{-2}.sec^{-1}$	Illuminance / $tds.sec^{-1}$
Red (664nm)	Continuous	120	6000
Blue (454nm)	'On' phase	Matched to green in heterochromic flicker photometry at 33 Hz.	
Green (525nm)	'Off' phase	12	1200

Table 6.1. S-cone ERG recording parameters.

Following the process of heterochromic flicker photometry, the temporal frequency of the square wave green and blue flicker was reduced and modulated at 1.67 Hz. The exact nature of the OFF- pathway of S-cones, if one does indeed exist, is not fully understood. However, a recent report has demonstrated an input from the S-cones to the magnocellular OFF- pathway (*Chattergee & Callaway, 2002*). A long duration stimulus at 1.67 Hz will provide a good separation of any ON- and OFF-components of the S-cone response (*Drasdo et al, 2001*).

Figure 6.22. Full-field S-cone ERG recorded from subjects JB (aged 56) using silent substitution technique (red background 120 $cd.m^{-2}$; green 12 $cd.m^{-2}.sec^{-1}$; blue matched to green in heterochromic flicker photometry, frequency 1.67 Hz). Two hundred responses were averaged on a 500ms timebase, and bandpass filtered from 1-100 Hz.

Attempts were made on three control subjects to record a focal S-cone response, by presenting a 20° diameter stimulus (parameters as above), set within a 25 $cd.m^{-2}$ white adapting surround. In each case the response was so small as to be unmeasurable, even after averaging 300 responses.

6.8 The Dynamic Focal Cone Electroretinogram

6.8.1 Introduction

Over the last fifty years many studies have evaluated outer retinal function by exposing the eye to an intense, bleaching light source and measuring the time taken for visual function to return to a pre-bleach level (*Balliart, 1954; Severin et al, 1963; Glaser et al, 1977; Collins & Brown, 1989; Sandberg et al, 1998*). Recovery of visual function after exposure to an intense source is primarily dependent on the speed with which photopigment can regenerate. Therefore, any disease compromising the integrity of, or limiting the supply of metabolites to the photoreceptor / RPE complex is likely to prolong recovery time. This is exemplified by the observation of extended recovery times in age-related macular degeneration. There are limitations however, to the basic clinical 'photostress test'.

One limitation relates to the bleach itself. The percentage of photopigment bleached is affected by factors such as pupil size, media opacification and, for short bleaches of low intensity, modest timing errors (*Margrain & Thompson, 2002*). Another limitation relates to the belief that the test can differentiate outer retinal from inner retinal disorders (*Glaser et al, 1977*). More recent studies have reported prolonged photostress recovery times (PSRT) in diseases such as primary open angle glaucoma (*Sherman & Henkind, 1988; Parisi & Bucci, 1992; Horiguchi et al, 1998*) and optic neuritis (*Campos et al, 1980; Parisi et al, 1998*).

These findings suggest that recovery of visual function obtained during conventional photostress testing may be influenced by inner and post retinal activity.

The greatest limitation of this clinical test is its subjective nature. Visual acuity measurement is prone to intersubject variability inherent in the nature of the task. Inter-individual differences in the speed of reading letters, inclination to guess at uncertain letters and maximum acuity are all factors which may increase variability in the recovery times recorded in normal subjects (*Amos, 1991*). The effect of learning and increased confidence in the task involved may also mean a variable result from a single subject over several visits.

In order to overcome this limitation a number of studies have monitored the recovery of visual function objectively using the visual evoked potential (*Lovasik, 1983; Franchi et al, 1987; Parisi & Bucci, 1992; Parisi et al, 1994; Parisi et al, 1995; Parisi et al, 1998; Parisi et al, 2002*). Although this technique provides a means of obtaining an objective assay of the recovery of visual function, it does not give a direct measure of outer retinal activity. Hence, its value in the detection of conditions which exclusively disrupt outer retinal function, such as early age-related macular degeneration, may be limited. In this study, therefore, a protocol was developed to enable the objective monitoring of the recovery of outer retinal function following a photopigment bleach.

A pilot study was conducted to determine whether the recovery of visual function following exposure to a bleaching light could be evaluated using the 41Hz focal cone electroretinogram in a group of healthy adults. The 41Hz focal cone ERG appeared to be particularly well suited to the task for two reasons. Firstly because the signal, or more specifically the first harmonic of the signal, is dominated by receptoral activity (*Falsini et al, 2000*), and secondly because this high frequency, steady state signal would facilitate the substantial averaging necessary to improve the post-bleach signal-to-noise ratio.

6.8.2 Method

- Ten healthy adults, aged 27-54 years (mean age 30.4 years, ± 9.2 SD), were recruited to the study. All subjects had a corrected visual acuity of 6/6 or better, clear ocular media, a normal retinal appearance, no history of retinal or systemic disease and, none were taking medication which could influence the results of the study. Each subject gave their informed consent after being provided with a full description of the procedures involved.

- Each subject was dilated with 1.0% tropicamide, and prepared for ERG recording in the manner described in section 6.1.

- A 20° diameter, amber (595 nm) stimulus, with a luminance of 30 cd.m^{-2}.sec $^{-1}$, flickering at a temporal frequency of 41 Hz, was presented in the centre of a ganzfeld bowl. Subjects were required to fixate the centre of the stimulus, which was surrounded by a white (30 cd.m^{-2}) adaptational background.

- A pre-bleach 41 Hz focal cone ERG was recorded as a baseline measure. One hundred ERG responses were averaged on a 50 ms timebase, and bandpass filtered from 1-100 Hz.

- The test eye was subsequently light-adapted to a bright white background (5.6 log trolands) for a period of 2 minutes, resulting in an 86% bleach of cone visual pigment (*Hollins & Alpern, 1973*). This bleaching light was presented within the ganzfeld bowl.

- The 41 Hz focal cone ERG was then recorded at 20 second intervals for a period of approximately 4 minutes.

6.8.3　*Data Analysis*

In order to objectify amplitude measurements, individual traces were modelled using a cosine function (1), which was fitted to the data on a least squares basis.

$$Amp(t) = (m.t + c) + ([Amp/2] \times \cos [k/t]) \qquad (1)$$

Where t = time in ms, m = constant allowing for drift, c = constant allowing for bias, Amp = amplitude in μv, and k = 543.2 (constant to convert ms to radians).

This technique was particularly valuable at early times post-bleach, when the signal-to-noise ratio was relatively low. The recovery of outer retinal function was evaluated by plotting these amplitude measurements as a function of time post-bleach.

Traditionally, it has been assumed that photopigment regeneration, which underlies the recovery of outer retinal function, proceeds as a first order chemical reaction and therefore it may be appropriate to summarise the amplitude recovery data using an exponential function in the form:

$$Amp(t) = a.(1-\exp(-0.693(t-x)/\tau) \qquad (2)$$

Where a is the pre-bleach amplitude, τ is a time constant, x is the time at which the recovery first starts and t is the time after the bleach. However, a recent study has shown that the

exponential time constant varies with bleaching level (Paupoo et al, 2000). This finding is inconsistent with a 'first order' process and it has been suggested that the recovery is instead 'rate-limited'. An alternative model based on Michaelis Menton kinetics has therefore been proposed:

$$Amp(t) = 1 - K_m.W\{B/K_m \exp(B/K_m) \exp\text{-}r(1+K_m)/K_m\} \qquad (3)$$

where K_m is the Michaelis constant, W is the 'Lambert W function', B is the initial bleach, and r is the maximum rate of recovery (*Mahroo et al., 2003; Paupoo et al. 2000; Lamb, 2003 personal communication*).

In order to determine if the amplitude recovery data agreed with a 'first order' or 'rate limited' reaction the recovery data was modelled using both equations (2) and (3).

6.8.4   Results

Figure 6.23 shows a typical set of recovery data.
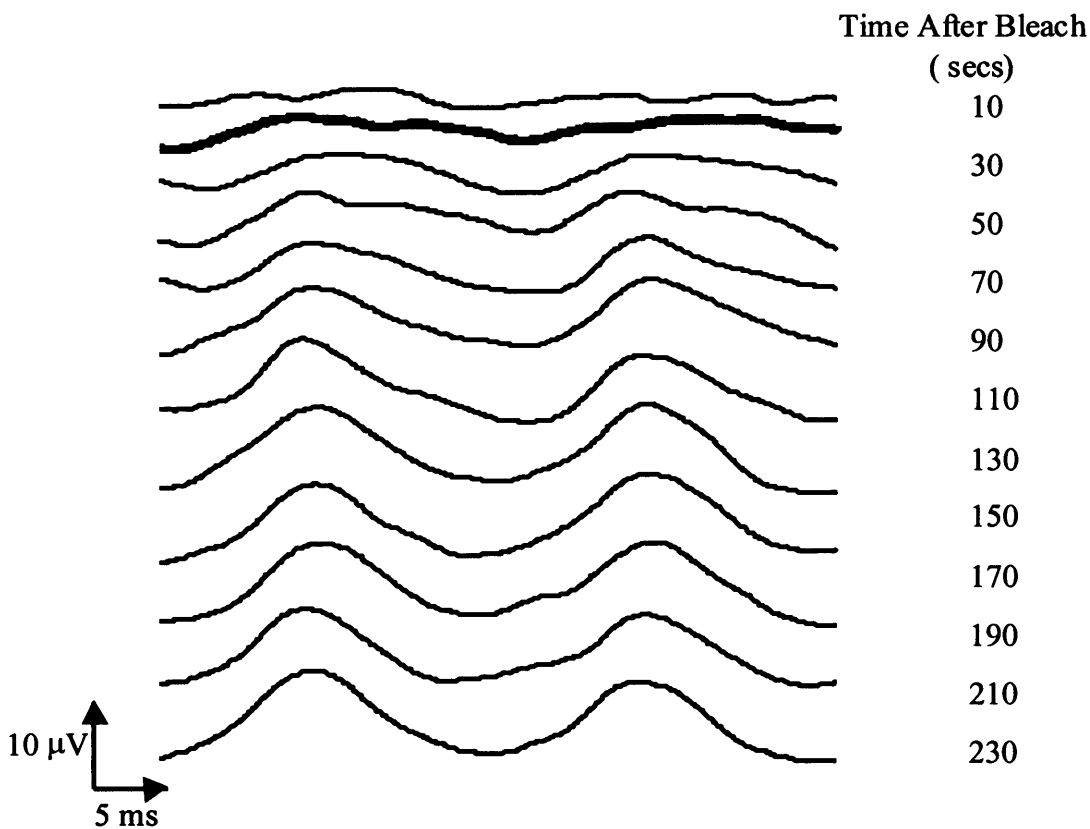
Figure 6.23. Typical set of traces recorded from subject FJ after 2 minutes adaptation to a bright adapting light. The amplitude of the 41 Hz focal cone ERG is negligible 10 seconds after the bleach but returns there after.

It may be seen that the first trace obtained 10 seconds after exposure to the bleaching light was very nearly a flat line. Thereafter, the amplitude of the 41Hz focal ERG gradually increased and in all cases had reached pre-bleach levels within the 4 minute recording period.

The cosine fitting procedure is exemplified in Figure 6.24, which shows the how the model (equation 1) was fitted to the data obtained 30 seconds after the bleach (see the bold trace in Figure 6.23). This procedure allowed standardisation of the assessment of the amplitude of the fundamental component of the signal thereby minimising the effects of noise and higher harmonics.
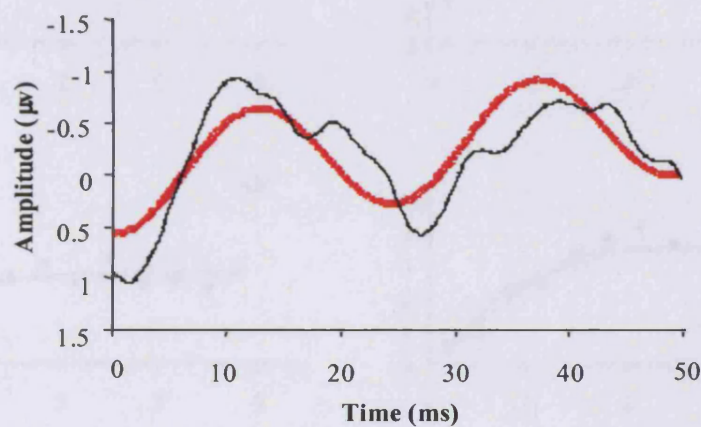
Figure 6.24. Demonstrates how an objective estimate of the amplitude of the first harmonic of each trace was obtained i.e. by fitting a cosine function. The trace used in this example is the one obtained 30 seconds after the bleach for subject FJ (see bold trace in Figure 6.23).

The resulting peak to trough amplitude data was plotted as a function of time after bleach. Figure 6.25 shows the results obtained with the Dynamic Focal Cone ERG for each of the ten subjects. Both the 'first order' and 'rate limited' models provided a good fit of the data. The mean values for x and τ for the 'first order' model were -0.06 min (SD 0.17) and 0.87 min (SD 0.48) respectively. The mean values for Km, r and B in the 'rate limited' model were 0.18 (SD 0.05), 0.68 (SD 0.21) and 0.95 (SD 0.05) respectively. A visual inspection of the data showed that there was little to choose between the two models. Evaluation of the residual standard deviation (RSD), which provides a measure of the goodness of fit suggests that the 'rate limited' model (i.e. the one based on Michaelis Menton kinetics) is better able to describe our data ('rate limited' RSD = 0.32μV; 'first order' RSD = 0.35μV). However, the 'rate limited' model includes more free parameters and a superior fit may be expected on this basis alone.
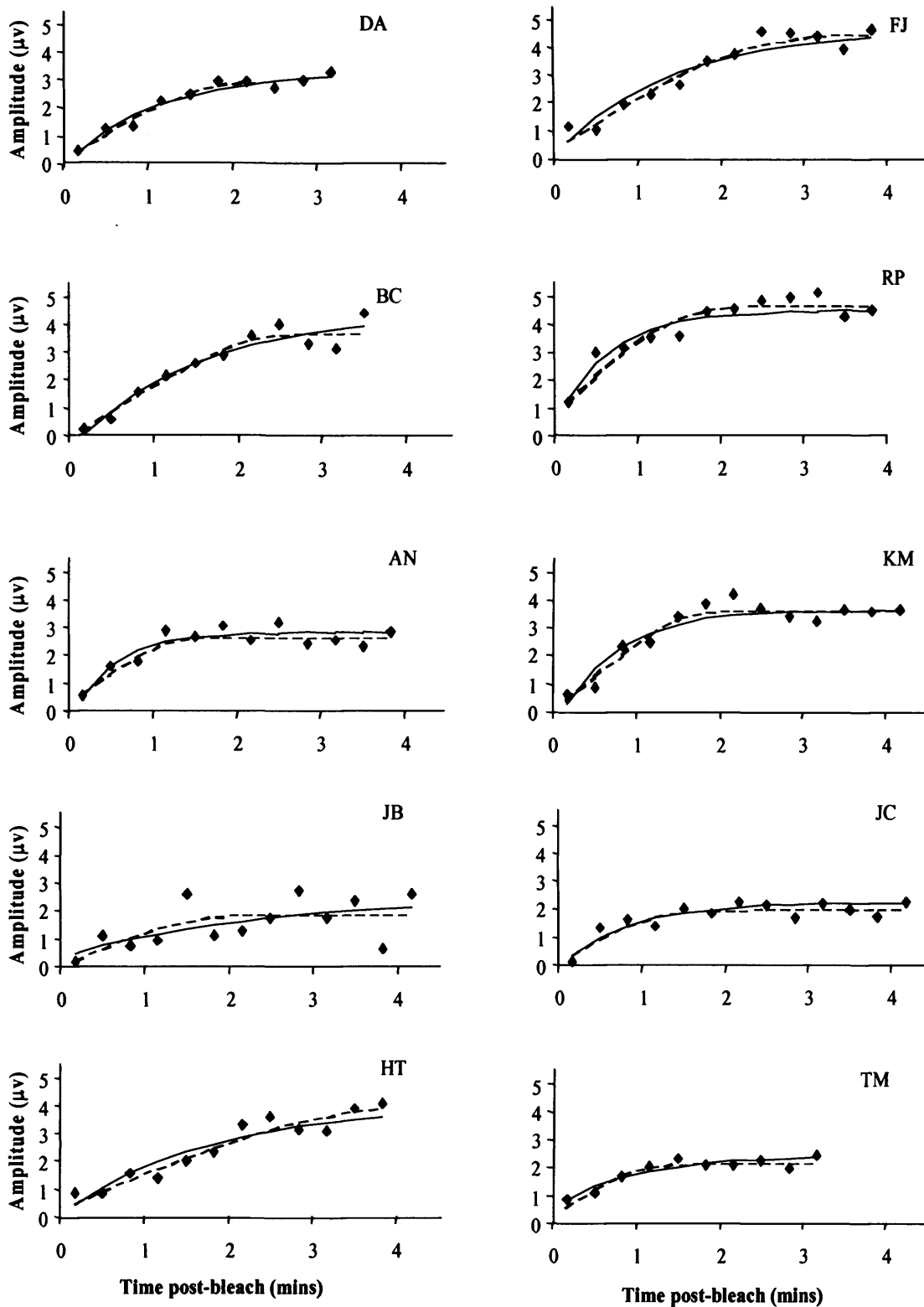
Figure 6.25. Recovery data obtained using the Dynamic Focal Cone ERG for each of our subjects. The dashed line is best fitting 'first order' model (equation 1) and the solid line the best fitting 'rate limited' model (equation 2).

The Akaike criterion is a statistic that may be used to determine if the inclusion of additional parameters is warranted on the basis of their ability to improve the description of the data (*Carson et al, 1983*). The most appropriate model has the lowest Akaike criterion. The mean Akaike criterion values determined for the 'first order' and 'rate limited' models were 17.2 and 17.3 respectively. On the basis of this analysis there was no significant improvement from the addition of an extra parameter.

6.8.5 Discussion

The results of this study suggest that the Dynamic Focal Cone ERG may be used to evaluate the recovery of outer retinal function following exposure of the eye to intense illumination. The electrophysiological data was objective, thus overcoming problems associated with visual acuity measurement in the traditional photostress test (*Amos, 1991*). Interpretation of the data was objectified by the use of a cosine model, thus providing an estimate of the amplitude of the fundamental frequency of the signal.

An evaluation of the Akaike criterion suggests that there is no difference in goodness of fit between the 'rate limited' and 'first order' models of macular recovery and thus the first order model has been chosen for the analysis of subsequent data, as the model has fewer variables. The values obtained for the free parameters in the model will be used to compare the results of subjects in the subsequent study on people with AMD.

6.9 Conclusion

A series of pilot studies has led to the development of a battery of electrophysiological techniques that may be of value in the early detection of ARM and the assessment of visual function in people who suffer from the condition.

The focal rod ERG protocol was developed in response to reports that parafoveal rod photoreceptor loss occurs at an early stage in ARM, and appears to precede cone loss (*Curcio et al, 1996; 2000; Medeiros et al, 2001*). Preliminary investigation indicated that the 2.1 log scot tds.sec^{-1} stimulus employed by Sandberg et al (*1996*) in the recording of the focal rod ERG might elicit a signal contaminated by cone response. An intensity-response series was therefore recorded, and it was determined that the maximum intensity of blue flash which would not result in a response from the cones was 1.7 log scot tds sec^{-1}. The stimulus was 20°

in diameter, thus effectively targeting the area most vulnerable to ARM related changes (*Curcio et al, 1996, 2000*). Results of a pilot study comparing two techniques for recording the focal rod ERG indicated that a background adaptation technique would be most suitable for this study, reliably eliciting both a- and b-waves.

The focal cone ERG was included in this study as a means of assessing central retinal cone function. The response recorded to a 5 Hz stimulus in a preliminary study showed distinct a- and b-waves, and bandpass filtering from 100-1000 Hz provided good isolation of the macular OPs. In addition to this technique, a 41 Hz flickering stimulus was included to produce a steady state focal cone response. The first harmonic of this signal has been hypothesised to strongly reflect outer retinal function (*Porciatti et al, 1989; Remulla et al, 1995; Falsini et al, 2000*). It therefore has the potential to provide a direct assay of the retinal layers affected at an early stage by ARM. Both of these stimuli were 20° in diameter, again targeting the entire macular region shown to be affected in early ARM.

A preliminary assessment was made of a C-wave recording technique described by Moschos et al (*1994*). It was hoped that this could provide a means of investigating the integrity of the RPE in subjects with ARM. However the C-wave protocol has been excluded from this study on the basis of the variability of results recorded from control subjects in the preliminary investigation, and in published literature (*Hamasaki et al, 1997; Hock & Marmor, 1983*).

The literature suggests the occurrence of selective dysfunction of S-cone function in early ARM (*e.g. Eisner et al, 1987; Haegerstrom- Portnoy et al, 1988; Sunness et al, 1989; Eisner et al 1991; 1992; Cheng & Vingrys, 1993; Collins & Brown, 1989*). A protocol was therefore included in this study to allow electrophysiological assessment of the integrity of the short-wavelength sensitive pathway in ARM. The technique chosen was an established full-field silent substitution technique (*Drasdo et al 2001; Chiti et al, 2003; Drasdo et al 2002*). Attempts to elicit a focal response to this stimulus resulted in a signal too small to be reliably recorded and measured even in young control subjects.

The final protocol described in this chapter was the dynamic ERG – a technique designed to objectively assess the recovery of cone function following a photopigment bleach. There is much evidence to suggest that photostress recovery is abnormal in subjects with ARM, but this has previously been assessed by psychophysical techniques (*Balliart, 1954; Severin et al, 1963; Glaser et al, 1977; Collins & Brown, 1989; Sandberg et al, 1998*). The protocol

developed for this study employs the amplitude recovery of the 41 Hz ERG to more directly assess outer retinal activity.

The following chapters describe the study in which these techniques were applied to a group of subjects with ARM, and a group of age matched controls. Further psychophysical tests were also included to allow a full assay of retinal function in these subjects.

CHAPTER SEVEN : GENERAL EXPERIMENTAL TECHNIQUES

7.1 Subjects

7.1.1 Subjects with Age-Related Macular Degeneration and Age-Related Maculopathy

Subjects with Age-related Maculopathy (ARM) were recruited by Mr Chris Blyth from the retinal clinic at The University of Wales College of Medicine. Subjects were also obtained through recruitment by optometrists, and via Cardiff University Eye Clinic.

Subjects over the age of 55 were enrolled in the study on the basis of a diagnosis of ARM in either or both eyes, according to the 1995 international classification system (*Bird et al, 1995*). A corrected visual acuity of 6/18 (0.5 logMAR) or better was required in the test eye of each subject. The contralateral eye could be of any status. The subjects with ARM were sub-classified according to the retinal appearance of the fellow eye, as shown in table 7.1.

Group	Classification
1	Fellow eye ARM
2	Fellow eye exudative AMD
3	Fellow eye dry AMD

Table 7.1. The sub-classification of subjects with ARM according to status of fellow eye.

7.1.2 Control Subjects

Control subjects were recruited from advertisements, by referral from optometrists, and from friends and spouses of subjects with ARM. The control group had the same mean age and gender balance as the ARM group.

Eligibility criteria included a corrected visual acuity of 6/9 or better (logMAR 0.2) and no diagnosis of ARM or AMD. Control subjects were permitted to have up to 20 small (<63μm) hard drusen within the macular area.

7.1.3   Exclusion Criteria

For both control and ARM groups, subjects were excluded from the study on the basis of a history of systemic pathology or medication, which may have an effect on retinal function. Similarly, no individuals were included who had been diagnosed with ocular pathology (other than AMD), which was likely to affect retinal performance.

Further exclusion criteria included a history of photosensitive epilepsy, shallow filtration angles (grades 0 and 1) as determined by the Van Herick technique and the presence of any media opacities in the test eye which would be detrimental to the quality of fundus photographs.

7.1.4   Ethical Permission

Ethical permission was obtained from the departmental ethical committee, and from Bro Taff Health Authority.

Each subject was provided with written information about the study at least 2 days before attending the clinic, and signed a consent form acknowledging that they had read and understood the information sheet, and were willing to participate in the study.

The study adhered to the tenets of the Declaration of Helsinki.

7.2   Visual Acuity

A Bailey-Lovie logMAR chart (*Bailey & Lovie, 1976*) was used to assess distance visual acuity of all subjects monocularly in each eye prior to pupil dilation. The chart was illuminated to the recommended level of 168 cd.m^{-2} (*Ferris & Sperduto, 1982*), and viewed through any distance prescription required.

7.3   Fundus Photography

According to the 1995 International Classification System (*Bird et al., 1995*), stereo fundus photographs are required for the classification and grading of subjects with AMD. The requirements are for a system providing colour 30° or 35° stereoscopic transparencies centred on the fovea.

All fundus photographs were obtained using the Nidek 3-Dx stereo disc camera (*Nidek Co. Ltd., Japan*), which is a simultaneous stereo fundus camera i.e. 2 images are simultaneously captured on 1 photographic frame. The two images are separated by 3 mm, achieving a constant level of stereopsis in all photographs. The retinal angle subtended by the picture is 32° diagonally, allowing an assessment of the whole macular area. Kodak Elite Chrome 200 (*Kodak Ltd.*) film was used for all photographs.

In order to achieve the 3 mm separation between the two photographic images, it was necessary to dilate the subject's pupil to a diameter of at least 4mm. Before instilling a mydriatic, the subjects' susceptibility to closed-angle glaucoma was assessed by measurement of intraocular pressure and anterior chamber angle (according to the Van Herrick technique), and an evaluation of family history. Provided that the pressure was below 21 mmHg, the angle of drainage was grade 2-4, and there was no family history of closed-angle glaucoma, 1 drop of 1.0% tropicamide hydrochloride was instilled into each eye. Twenty minutes were allowed for mydriasis and the diameter of the pupil was measured. Following pupillary dilation, the retinas of both eyes of each subject were photographed.

7.4   Fundus Grading

All stereo fundus photographs were developed, and then digitised using Nidek Scan software (*Nidek Co. Ltd., Japan*). Digitised photographs were then graded according to the severity of retinal signs of AMD, using the system described in the 1995 International Classification System (*Bird et al., 1995*). Fundus appearance was evaluated using a grid consisting of three concentric opaque circles on a transparent background, which was superimposed and centred on the foveola of one of the two stereoimages of each eye. The macula was thereby divided into central, middle, and outer subfields. Four oblique radial lines, segmenting each subfield into superior, inferior, nasal, and temporal portions, further dissected these zones (*see Figure 7.1*).

Five open circles of various sizes were used to estimate drusen diameter within each subfield. According to the International Classification System, retinas were assessed and assigned a numeric value according to parameters including predominant drusen size and drusen type, number of drusen, main location of drusen, and an estimate of the area covered by drusen. Fundi were also graded according to the presence and extent of other lesions, including

pigmentary abnormalities of the retinal pigment epithelium, geographic atrophy, and neovascular changes. The grading scale is provided in full in Appendix II, Table AII.1.

Outer Subfield

Middle Subfield

Central Subfield

1000 um

3000 um

6000 um
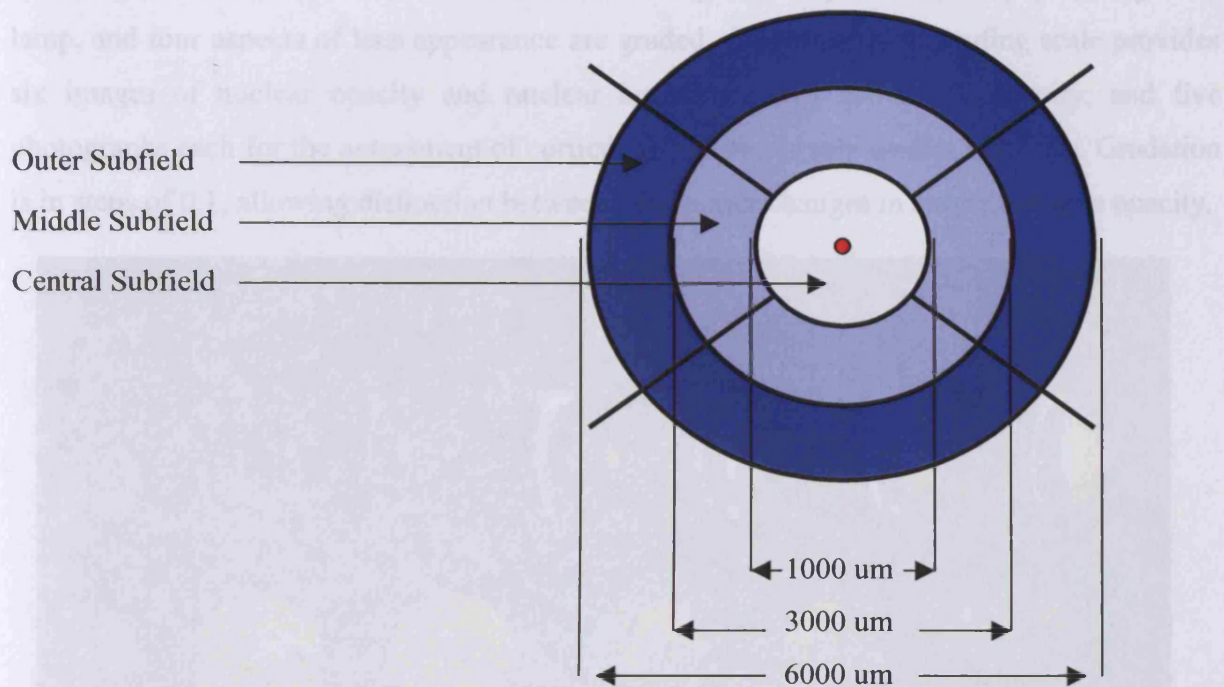
Figure 7.1. Schematic diagram illustrating grading grid for fundus photographs (according to International Classification System).

Images were also viewed stereoscopically to exclude the possibility of undetected pigment epithelial detachment or subretinal fibrovascular proliferation resulting in an elevation of the retina.

7.5   Lens Opacity Grading

It has already been stated that the presence of any media opacities, which might have a detrimental effect on the clarity of fundus photographs constitutes one of the exclusion criteria for recruitment to this study (*see section 7.1.3*). However, in any research on elderly subjects a certain extent of lens opacification is almost inevitable. It is therefore necessary to quantify and grade minor lens opacities in a consistent fashion between individuals.

Lens opacities of all subjects involved in this study were evaluated using the LOCS III grading system.

The Lens Opacities Classification System (LOCS) has been used in epidemiological studies of cataract natural history, as well as in the evaluation of the effect of lens opacities on visual

function, since it was published in its first form in 1988 (*Chylack et al., 1988*). Since this time, the system has been modified twice (*Chylack et al, 1989; 1993*), with the current scale referred to as LOCS III. The lens is assessed through the subject's dilated pupil using a slit lamp, and four aspects of lens appearance are graded. A photographic grading scale provides six images of nuclear opacity and nuclear brunescence of increasing severity, and five photographs each for the assessment of cortical and posterior subcapsular opacities. Gradation is in steps of 0.1, allowing distinction between very minor changes in severity of lens opacity.
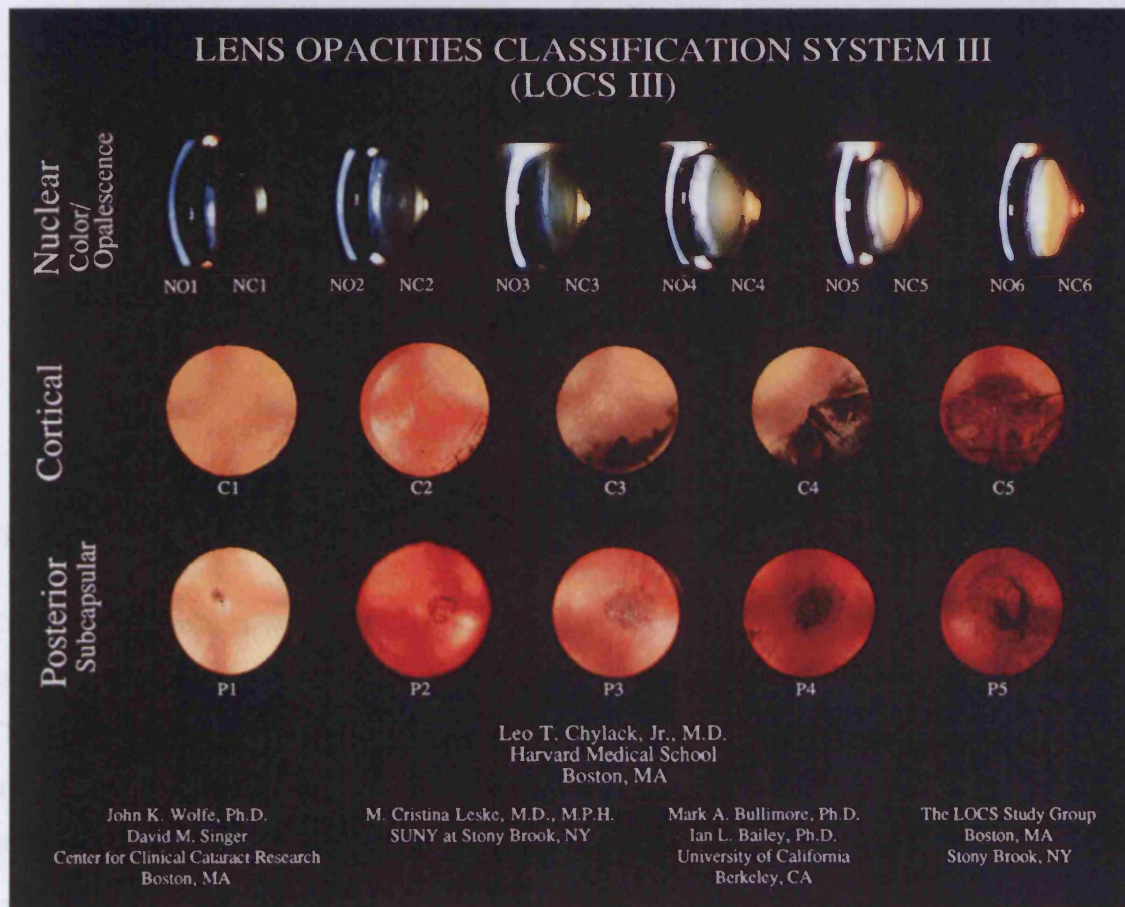
Figure 7.2. Photographic grading scale for LOCS III lens classification system (*Chylack et al, 1993*).

7.6　Colour Vision Testing

The colour vision of each subject was assessed monocularly in the test eye using the Farnsworth D15 test (*Farnsworth, 1943*) and the Lanthony desaturated D15 test (*Lanthony, 1978*), according to the manufacturers recommendations. Colour vision tests were performed

under simulated daylight illumination, provided within a box by an artificial daylight bulb at 615 lux illumination (Artificial daylight bulb, Thorn, 20W).
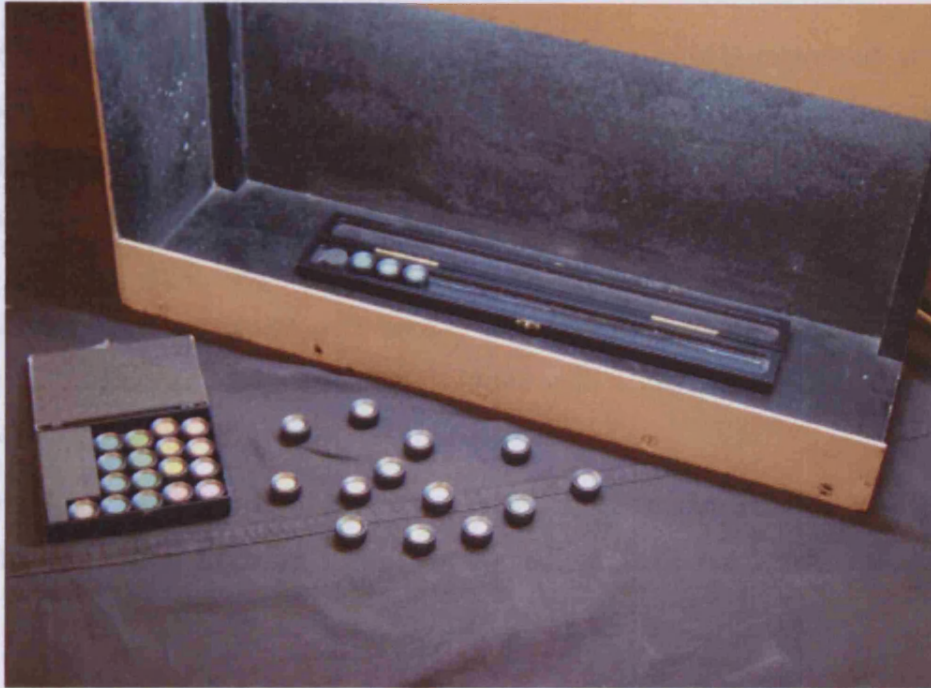
Figure 7.3. Saturated and Desaturated D15 tests within daylight-illuminated box.

Colour vision results were analysed using a Qbasic computer programme by Vingrys & King–Smith (*1988*), designed to allow the standardised assessment of the results of any panel test. This system is based on a vector scoring method, whereby relative colour difference vectors are plotted from a common origin, and the length and angle of vectors are analysed to give a quantification of the severity, type and selectivity of a colour vision defect.

The angle of the major radius of the vector lines is an estimation of the type of the colour vision defect, and is known as the confusion angle. Vingrys & King-Smith (*1988*), on the basis of the assessment of 53 normal subjects and 66 with congenital colour defects, found the confusion angle of protan subjects to range between +3° to +17°, the corresponding range for deutanomolous individuals was -4° to -11°. Subjects with definite tritan defects were classified as having confusion angles between –70 to -90°. Controls had an angle of around +60°.

The severity of the colour vision anomaly may be assessed by the total error score (TES), or by normalising results to a perfect cap arrangement to obtain the Confusion index (C-index).

The C-index also allows a comparison of performance across different tests, for example the saturated and desaturated D15 test. The C-index and TES of a normal subject are 1.0 and 11.4 respectively for the D15 test, with a higher value indicating a more severe colour vision defect.

The degree of scatter or selectivity of the arrangement of caps is expressed as the Scatter index (S-index). A low S-index (1.09-1.38) represents a non-polarised or random arrangement, and is indicative of either a normal observer, or one producing an anarchic arrangement of caps. Conversely, a high S-index of 4.74 or above suggests a congenital dichromat, with a high degree of polarity of test cap arrangement. A congenital dyschromatopsia tends to present with high C- and S- indices, whilst acquired colour vision defects are often characterised by a high C- index with a lower S- index (*Vingrys & King-Smith, 1988*).

Vingrys and King-Smith (*1988*) recommend that three parameters be assessed for the complete characterisation of colour vision for any individual i.e. confusion angle, C-index and S-index.

7.7   Dark Adaptation

Dark adaptation curves were assessed monocularly in the test eye of all subjects, following pupillary dilation, using an adapted Humphrey Field Analyser (*See Figure 7.4*).

Prior to dark adaptation, all subjects were adapted to a bright white background (8,200 cd.m^{-2}) for 2 minutes, achieving an approximately 85% bleach of cone pigment (*Hollins & Alpern, 1973*). The stimulus used to assess retinal sensitivity following the bleach was a Goldmann size V target, of wavelength 490nm, located at a position 8° in the inferior visual field. Threshold was determined using a staircase method. The subject fixated a central red LED, and was instructed to press a button every time the blue stimulus appeared below the fixation target. Fixation was monitored using an infra-red camera system. Each assessment of sensitivity took approximately 50 seconds to complete, and the subject was then given 1 minute to relax before the target was presented once again. Dark adaptation continued until the rod-cone break had been passed and a plateau of sensitivity achieved. The maximum duration of dark adaptation was 1 hour.
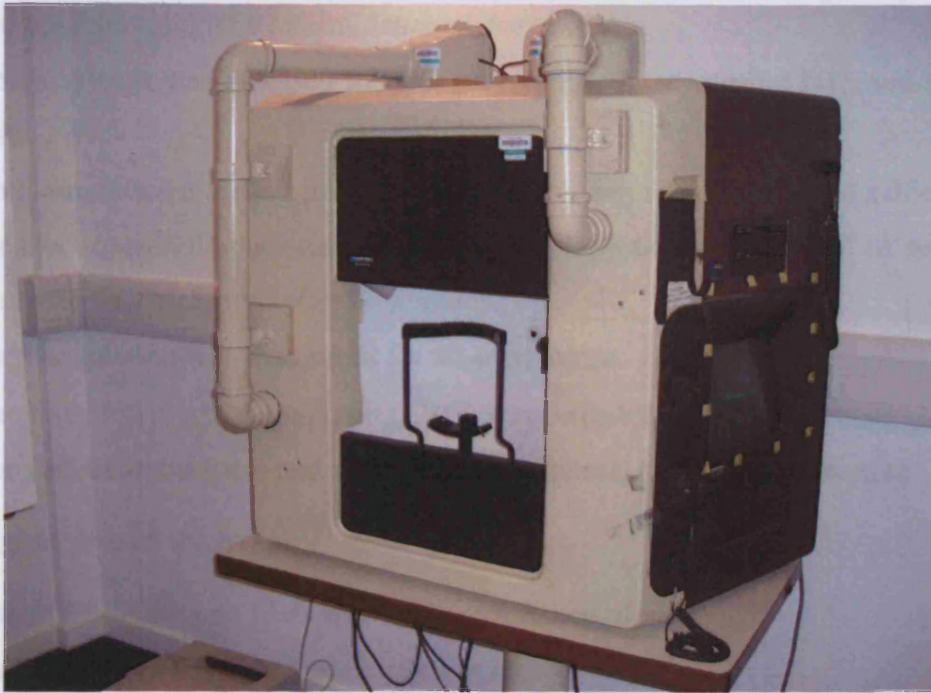
Figure 7.4. Adapted Humphrey Field Analyser used for measurement of dark adaptation functions.

7.8   Outline of Experimental Procedure

All subjects received an information letter which described the study. They were informed that the whole process would take 3 hours to complete, and that time was allowed for a tea break.

Each session began with a discussion of the patient's ocular health, general health, medication and family medical history. This was followed by a general discussion of the tests to follow and each patient was given time to ask any questions they might have before being asked to sign a consent form. The remainder of the visit followed the outline set out below.

- Preliminary fundus photographs were taken of both eyes using a non-mydriatic digital camera.

- Intraocular pressures were measured (using the Topcon CT40 non-contact tonometer)

- A slit lamp biomicroscope was used to assess the anterior chamber angle of drainage (according to Van Herick's system). Also preliminary assessment was carried out of media opacities.

- Visual acuity was tested monocularly in each eye.

- The test eye was identified according to visual acuity, lens opacities, fundus appearance, and ophthalmologist's referral letter where available.

- Colour vision was assessed monocularly in the test eye using D15 and desaturated D15 tests.

- Both pupils were dilated using 1 drop of 1.0% tropicamide, and the subject was prepared for electrophysiological tests, according to the procedure outlined in section 6.1. Pupil diameter was measured after 25 minutes.

- Dark adaptation was monitored for 30-60 minutes.

- The focal rod electroretinogram (ERG) was recorded.

- The full-field rod ERG and visual evoked potential (VEP) were recorded

Lights on and tea break

- The full-field S-cone ERG and VEP were recorded.

- The full-field 41 Hz photopic ERG was recorded.

- The full-field 5 Hz photopic ERG was recorded.

- The focal 5 Hz photopic ERG was recorded.

- The focal 41 Hz photopic ERG was recorded.

- The dynamic focal cone ERG was recorded.

- Electrodes were removed and stereo fundus photographs taken of each eye using the Nidek 3-Dx stereo disc camera.

- Lens opacities were graded according to LOCS III system.

7.9 Statistical Analysis of Results

All data were averaged within the control and ARM groups in order to assess differences in group means. Unless otherwise specified, group-averaged data presented within the following chapters is accompanied in brackets by the standard error of the mean (SEM), allowing an assessment of the certainty of the mean.

Results were checked for normality using the Shapiro-Wilkes W test. Normally distributed data were compared between groups using the unpaired student t-test, or the one way ANOVA. The non-parametric Mann-Whitney U test or the Kruskal-Wallis test was used to compare data which did not have normal distribution. A 5% probability level was taken as significant.

The assessment of group means provides information as to the general trend in retinal function, but provides little information about the clinical potential of a test. For each test, therefore, the parameter which showed the greatest difference between group means was further assessed by plotting a Receiver Operating Characteristics (ROC) curve. This provides a measure of the sensitivity and specificity of a test in distinguishing between the control and ARM groups.

In the context of this study, sensitivity may be defined as the proportion of subjects with ARM correctly identified by a test. Conversely, specificity is the proportion of control subjects correctly identified as not having ARM. The ROC curve plots sensitivity against 1-specificity for every possible cut off point for a stated parameter.

Assessment of the area under the ROC curve is one way of quantifying the capacity of a technique to correctly identify individuals (*Altman & Bland, 1994*). The test may be analysed to determine whether the area under the curve is significantly different from 0.5. In a curve which rises rapidly towards the upper left hand corner of the graph, indicating a high sensitivity rate for a low 1-specificity rate, the area under the curve is large. If the area is 1.0, then the test is ideal, and achieves 100% sensitivity and 100% specificity. If the area is 0.5, then the test achieves only 50% sensitivity and 50% specificity i.e. is no more accurate at distinguishing between the two groups than chance alone.

The co-ordinates of the ROC curves were also assessed to determine an optimal cut-off for each parameter, which would separate between the control and ARM groups with maximum accuracy. However, there is no statistical means of determining the best cut-off point to adopt in the application of a test as a diagnostic indicator. This decision must be made on a clinical basis, and with regard to the consequences of a false diagnosis.

Literature suggests that the second eye of a person with unilateral exudative AMD is at a greater risk of developing choroidal neovascularisation than an eye of similar retinal appearance with only drusen in the contralateral eye (*Strahlman et al, 1983; Roy & Kaiser-Kupfer, 1990*). It has also been reported that eyes with unilateral geographic atrophy are at an increased risk of developing atrophy in the fellow eye (*Klein, 1997*). Previous reports have compared results between subjects with bilateral drusen, and those with choroidal neovascularisation in the fellow eye on the basis that a test which distinguishes between these groups may be sensitive to pre-neovascular changes in retinal function (*Eisner et al, 1987; 1991; Stangos et al, 1995; Midena et al, 1997*).

Accordingly, the subjects with ARM in this study were categorised as described in section 7.1 as either having bilateral ARM, unilateral dry AMD in the non-test eye, or unilateral choroidal neovascularisation. A comparison of averaged test results between these groups was carried out. A finding of significantly worse performance by the group with dry or wet AMD in the fellow eye might suggest that a particular parameter is sensitive to changes in retinal function which precede the development of late AMD. However, it is important to stress that the only accurate means of assessing the prognostic value of a test is to undertake a longitudinal study.

CHAPTER 8 - RESULTS OF PSYCHOPHYSICAL EVALUATION

8.1   Introduction

This chapter presents the results of the psychophysical tests conducted in this study. Subject details and biometric data have also been included.

8.2   Subjects

Thirty-one subjects with ARM participated in the study, of whom 16 (62%) were female. The mean age of subjects with ARM was 72.4 years (± 7.99 SD; range 57-86 years). The mean logMAR visual acuity of the ARM group was 0.20 (± 0.15 SD; range 0-0.5). This corresponds to a maximum snellen acuity of 6/6, a minimum of 6/18, and a mean of approximately 6/9.

Subjects with ARM were subdivided according to the status of the contralateral eye, with group 1 consisting of individuals with bilateral drusen, group 2 being composed of subjects with unilateral wet AMD in the fellow eye, and group 3 subjects having dry AMD in the fellow eye. In total, 12 subjects fell into group 1, 11 into group 2, and 8 into group 3. There was no significant difference in age (ANOVA; $F(2,28) = 0.853$; $p = 0.437$) or visual acuity (Kruskal Wallis; $\chi^2(2) = 0.461$; $p = 0.794$) between any of the ARM sub-groups.

Twenty-eight control subjects participated in the study, of whom 13 (46%) were female. The mean age of control subjects was 71.7 years (± 7.07 SD; range 57-84 years). Importantly, there was no significant difference in age between the control and ARM groups (student t-test; $t(58) = -0.38$; $p = 0.71$). The mean logMAR visual acuity of the control subjects was 0.04 (± 0.07 SD; range 0-0.2). This corresponds to a maximum Snellen acuity of 6/6, a minimum of 6/9, and a mean of approximately 6/7. Visual acuity was significantly worse in the ARM group than controls (Mann-Whitney U test; $z = -4.457$, $p < 0.001$), as would be expected on the basis of the recruitment criteria.

Details of all subjects who participated in the study are summarised in Appendix I, Tables AI.1 and AI.2.

8.2.1   Power Calculations

The power of a study may be defined as the probability that a real difference in the magnitude of results between groups will be detected as statistically significant. A power of between 80 and 90% is generally considered necessary for the results of a study to be considered as reliable (*Altman, 1982*). A study will have increased power if it involves a larger sample size, if it is detecting a larger difference of interest, or if the standard deviation of results is small.

Altman (*1982*) devised a nomogram whereby the power of a study is related to sample size and a measure called 'standardised difference'. The standardised difference is obtained by dividing the smallest difference of interest for a test by the standard deviation. This study was capable of detecting a standardised difference of 0.72 with 80% power at the 5% level.

8.3   Fundus Grading

Photographs were taken of the test eye of each subject, and graded according to the International Classification System (*Bird et al, 1995*), as described in section 7.5, to confirm subject status. The fellow eye was photographed where possible, although in several subjects this was precluded by the presence of media opacities. In these cases the contralateral eye was assessed with a volk lens, and categorised as healthy, ARM, wet or dry AMD according to retinal appearance. Figures 8.1 to 8.4 show typical fundus photographs obtained from one control subject, and three subjects with ARM in the test eye.
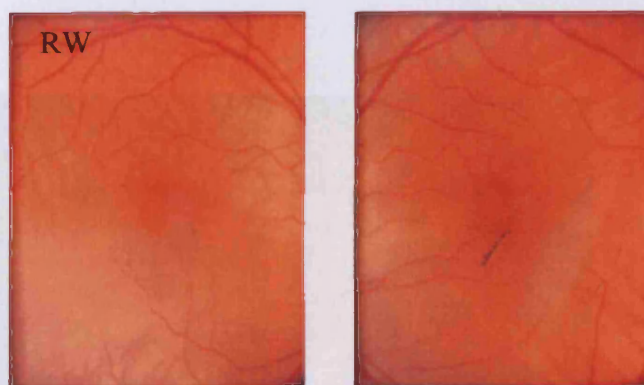
Figure 8.1. Fundus photographs from R and L eye of control subject (RW).

Figure 8.2. Fundus photographs from R and L eye of subject (ERee) with bilateral drusen.
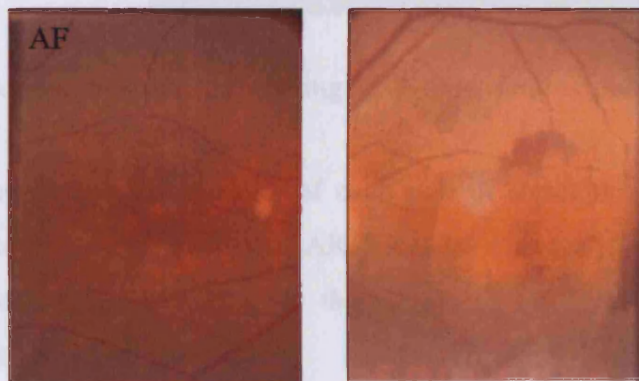
Figure 8.3. Fundus photographs from subject (AF) with large soft drusen (R eye) and extensive macular disciform scarring (L eye).
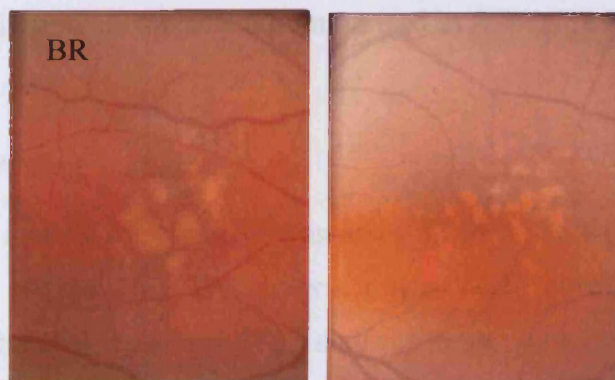
Figure 8.4. Fundus photographs from subject (BR) with dry AMD (R eye) and large, soft drusen (L eye).
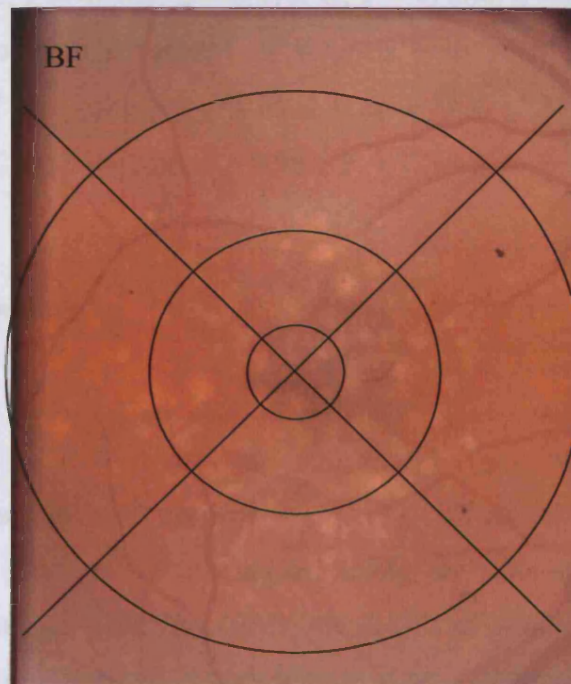
Figure 8.5. Superimposition of grading grid onto fundus photograph of subject (BF) with drusen.

A grid was superimposed onto one of each pair of stereophotographs (*as shown in Figure 8.5*), in order to grade the severity of ARM related changes (*Bird et al, 1995*). The scaling of the grid was calculated according to the advice of Dr Tunde Peto who runs the Reading Centre at Moorfields Eye Hospital.

Each photograph was graded for drusen morphology, number, size, location, area covered, and for the presence and location of focal pigmentary changes (*see Appendix II, Table AII.1 for grading scale*).

The fundus grading of all subjects is summarised in Appendix II, Tables AII.2 and AII.3.

8.4   Lens Grading

The crystalline lens of each subject was assessed in the test eye according to the LOCS III procedure (*see section 7.6*). The criteria graded were nuclear opalescence (NO), nuclear colour (NC), cortical opacities (C), and posterior subcapsular opacities (P). The lens classification of each subject is summarised in Appendix I, Tables AI.1 and AI.2.

Statistical analysis indicated that there was no significant difference between ARM and control groups for any of the four lens grading parameters (Man Whitney U Test; NO,

z = -1.04, p = 0.299; NC, z = -0.558, p = 0.577; C, z = -0.864, p = 0.388; P, z = -0.822, p = 0.411). Furthermore, the three subgroups of subjects with ARM were also shown to be homologous in terms of lens opacities (Kruskal Wallis; NO, $\chi^2(2)$ = 4.55, p = 0.103; NC, $\chi^2(2)$ = 4.75, p = 0.093; C, $\chi^2(2)$ = 2.50, p = 0.287; P, $\chi^2(2)$ = 2.76, p = 0.252).

8.5   Colour Vision Testing

8.5.1   Results

Colour vision results were obtained from the test eye of all subjects for both saturated and desaturated D15 tests. Results were analysed using the Qbasic computer programme developed by Vingrys and King-Smith (*1988*), the details of which are discussed in section 7.6. Three parameters were assessed for each subject i.e. confusion angle, C-index and S-index. To summarise, the confusion angle provides information as to the nature of the colour vision defect (i.e. protan, deutan, tritan), the C-index indicates the extent of the abnormality, and the S-index indicates the level of randomness or selectivity of the hue confusion. A higher C- and S- index are indicative of a more pronounced congenital colour defect. Acquired dyschromatopsias often present with a lower S-index than congenital defects (*Vingrys & King-Smith, 1988*).

The scatter plots in Figure 8.6 show the confusion angles calculated for the saturated and desaturated D15 tests for control subjects, and those with ARM. It may be seen that the number of subjects showing an abnormal confusion axis is greater when using the desaturated D15 than the standard D15 test. The ARM group exhibited tritan style defects only, with three subjects being classed as tritanomolous according to the standard D15 (WT, DF, MP), and 4 according to the desaturated D15 (JW, ER, MP, DC). One control subject exhibited a tritan tendency on the saturated D15 test (RC), and two were found to show tritan confusion angles on the desaturated D15 (DJ, PS). One control subject (WF) was classified by both tests as being protanomolous. A further subject (KM) was shown by the desaturated test to be deutanomolous, but displayed no specific type of defect on the saturated test.
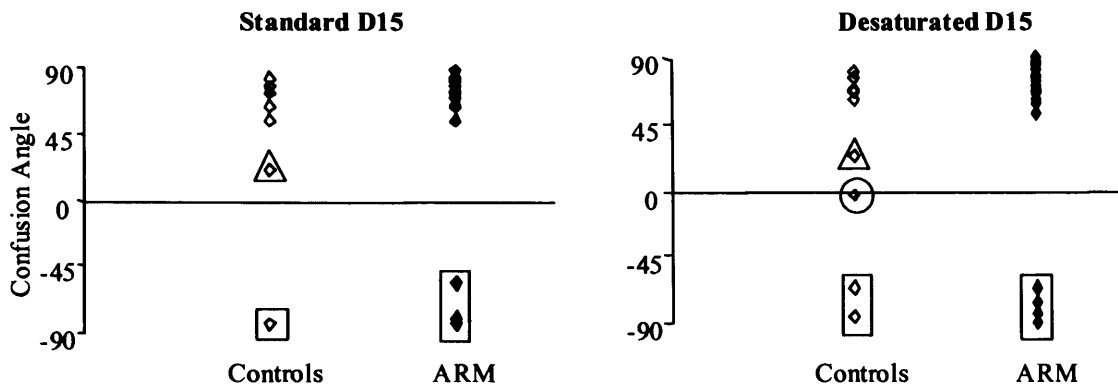
Figure 8.6. Scatter diagram illustrating spread of confusion angles for control and ARM subjects assessed using the standard and desaturated D15 tests. The data points enclosed in a rectangle indicate those subjects whose angle corresponds with a tritan defect, the circle indicates a deutan defect, and the triangle signals a protan defect.

In their retrospective analysis of subjects with congenital colour defects, Vingrys and King-Smith (*1988*) found the C-indices of normal subjects ranged from 1 to 1.77 for the standard D15 test. Three control subjects from our study had a C-index above this range (WF, DJ and KM). One of these, WF, had a protan angle of confusion for both the saturated and the desaturated tests. For the saturated test WF had a C-index of 1.85, and an S-index value of 1.62. According to the data of Vingrys and King-Smith (*1988*) these values suggest a very mild congenital colour vision defect. DJ and KM showed no definite tendency towards any type of colour deficiency on the saturated test.

The C- and S- indices for control subjects and subjects with ARM are plotted in Figures 8.7 and 8.8.
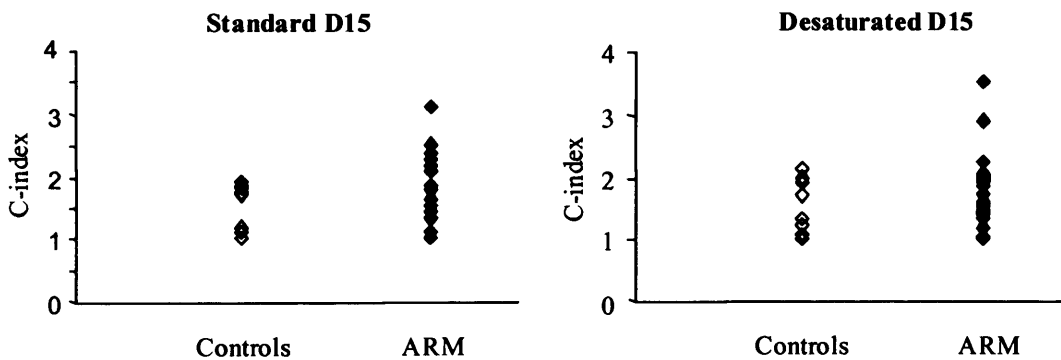
Figure 8.7. Scatter diagram illustrating the spread of C-indices for control and ARM subjects assessed using the standard and desaturated D15 tests.
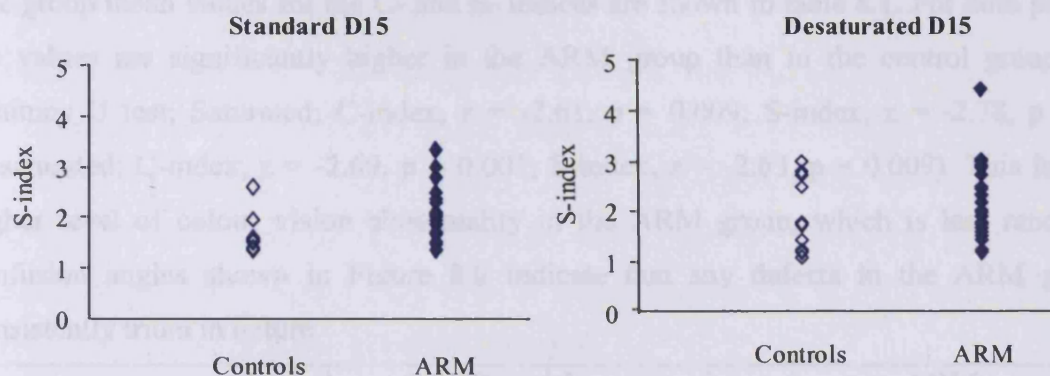
Figure 8.8. Scatter diagram illustrating the spread of S-indices for control and ARM subjects assessed using the standard D15 and desaturated D15 tests.

The one subject (MP) who showed a definite tendency towards a tritan defect on both saturated and desaturated D15 tests also had the highest C-index for both tests (Saturated, C-index = 3.08; Desaturated, C-index = 3.53). A moderately high S- index on both tests was indicative of an acquired colour vision defect (Saturated, S = 2.35; Desaturated, S = 2.91). The results of this subject are illustrated in Figure 8.9 by a plot of cap arrangement for both the standard D15 test (A) and the desaturated version (B), and show the expected configuration for a tritanopic observer. Subject MP is in the ARM group and has neovascular AMD in her contralateral eye, and thus may be considered to be at increased risk of developing choroidal neovascularisation in her test eye (*Strahlman et al, 1983*).
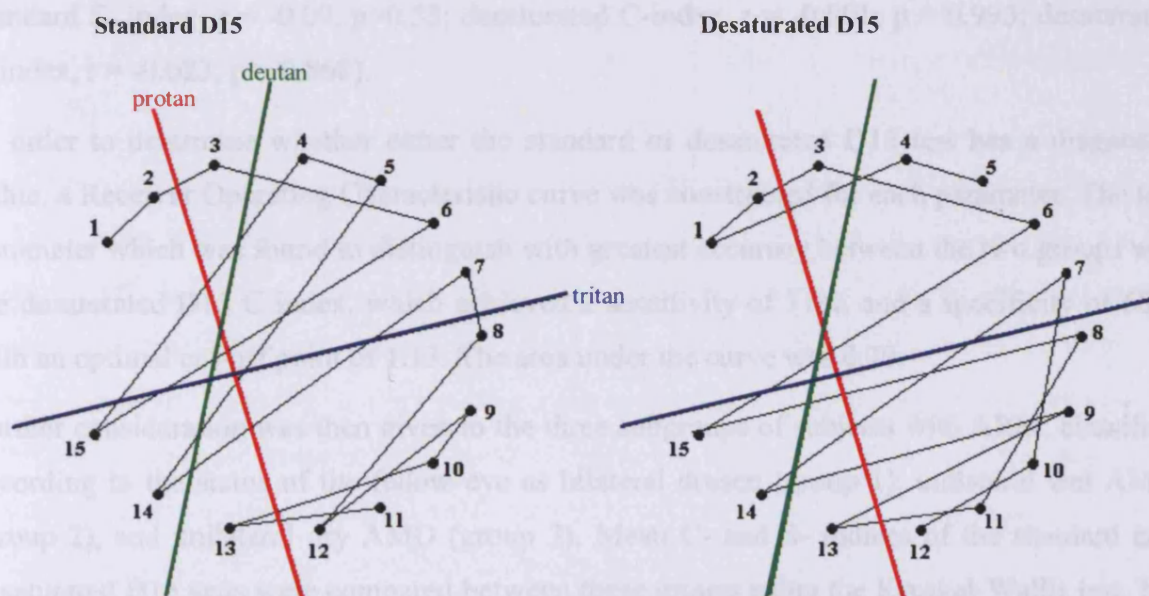
Figure 8.9. Illustration of tritanopic defect of subject MP (with ARM and unilateral choroidal neovascularisation), recorded using both the standard and desaturated D15 tests and plotted in accordance with Farnsworth, 1947.

The group mean values for the C- and S- indices are shown in table 8.1. For both parameters the values are significantly higher in the ARM group than in the control group (Mann-Whitney U test; Saturated; C-index, z = -2.61, p = 0.009; S-index, z = -2.78, p = 0.005; Desaturated; C-index, z = -2.69, p = 0.007; S-index, z = -2.63, p = 0.009). This indicates a higher level of colour vision abnormality in the ARM group, which is less random. The confusion angles shown in Figure 8.6 indicate that any defects in the ARM group are consistently tritan in nature.

		Control	**ARM**
Standard	C-index	**1.16 (± 0.06)**	**1.47 (± 0.10)**
	S-index	**1.51 (± 0.06)**	**1.86 (± 0.10)**
Desat.	C-index	**1.26 (± 0.08)**	**1.64 (± 0.11)**
	S-index	**1.65 (± 0.10)**	**2.02 (± 0.13)**

Table 8.1. Average values for C- and S- indices of saturated and desaturated D15 tests for ARM and control groups. Values in bold were significantly different between groups. Values in parentheses describe the magnitude of the SE.

No significant correlation was found between standard or desaturated colour vision C- and S-indices and LOCS nuclear colour grading (Pearson's; standard C-index, r = 0.02, p = 0.90; standard S- index, r = -0.09, p=0.53; desaturated C-index, r = -0.001; p = 0.993; desaturated S-index, r = -0.023, p = 0.868).

In order to determine whether either the standard or desaturated D15 test has a diagnostic value, a Receiver Operating Characteristic curve was constructed for each parameter. The test parameter which was found to distinguish with greatest accuracy between the two groups was the desaturated D15 C-index, which achieved a sensitivity of 71%, and a specificity of 68% with an optimal cut-off point of 1.13. The area under the curve was 0.70.

Further consideration was then given to the three subgroups of subjects with ARM, classified according to the status of the fellow eye as bilateral drusen (group 1), unilateral wet AMD (group 2), and unilateral dry AMD (group 3). Mean C- and S- indices of the standard and desaturated D15 tests were compared between these groups using the Kruskal-Wallis test. No significant difference was found between the three groups.

8.5.2   Discussion of Colour Vision Results

The control group in this study performed less well than that of Vingrys and King-Smith (*1988*) on the standard D15 test. In this study 3 control subjects had a C-index above the maximum 1.77 reported for the 53 control subjects whose data were analysed by Vingrys and King-Smith (*1988*). Vingrys and King-Smith (*1988*) reported perfect cap alignment for the standard D15 test in 85% of their control subjects, compared to the 75% of healthy normals who showed perfect cap arrangement in this study.

However, their control group was much younger, with a median age of 33 years. Studies into age-related changes in colour vision have shown that hue discrimination deteriorates with age, with blue-yellow colour discrimination most affected (*Knoblauch et al, 1987; Verriest et al, 1962*). The results of only one subject, WF, were consistent on both tests with a red-green colour vision deficiency, but low values for the C- and S- index indicated that this was a mild anomaly.

These colour vision results show a higher level of hue discrimination abnormality in the group of subjects with ARM, than in control subjects. Anomalies were shown to be along a tritan colour confusion axis, as would be expected from previous reports of colour vision in ARM and AMD (*Bowman, 1980; Collins, 1986; Collins et al, 1989; Cheng & Vingrys, 1993*). The tritanopic nature of the defect suggests a selective disruption of the short-wavelength sensitive visual pathway. This might be explained by the vulnerability of the S-cones to factors such as photo-toxic (*Ham et al, 1978; Sperling et al, 1980*) and metabolic damage (*DeMonasterio et al, 1981*).

There was no significant difference between the colour vision results of the three subgroups of individuals with ARM, classified according to the condition of the fellow eye. As the subjects with unilateral AMD are considered to be at increased risk of developing the condition in the fellow eye (*Strahlman et al, 1983; Klein, 1997*), a difference between the groups would be indicative of a prognostic value to the test. However, the low subject number in each of these groups means that a small difference in outcome could remain undetected by this analysis. Furthermore, not all subjects with unilateral wet AMD or geographic atrophy will imminently develop the condition in the second eye.

In this study only one subject with ARM (MP) showed a significant tritan colour vision defect on both the saturated and desaturated D15 tests. This subject had choroidal neovascularisation in her second eye. A longitudinal study would determine whether this subject, and subjects

WT, DF, JW, ER and DC who showed tritan defects on either the saturated or desaturated test, are at an increased risk of developing advanced AMD. Such a finding would be in accordance with Eisner et al (*1992*) who used the standard D15 for a baseline assessment of colour vision in a prospective study of subjects with unilateral exudative AMD. These subjects were subsequently followed-up over a minimum of 18 months. It was found that failure of the D15 test at baseline identified those who would imminently develop choroidal neovascularisation with 73% sensitivity, although specificity was only 62%.

The diagnostic value of the saturated and desaturated D15 tests at distinguishing between subjects with ARM, and control subjects was also assessed. The desaturated D15 C-index was found to show the greatest promise in this respect, but only achieved a sensitivity of 71%, and a specificity of 68% with an optimal cut-off of 1.13. However, this is based on the assumption that fundus grading achieves 100% accuracy in distinguishing between healthy subjects and those with ARM.

The finding that the desaturated D15 has the greater diagnostic value of the two tests concurs with the findings of Collins et al (*1986*), but is contrary to some studies (*Aitchison et al, 1990; Cheng & Vingrys, 1993*). However, the study by Aitchison et al (*1990*) specifies that subjects had no pathology in the contralateral eye, and neither Cheng & Vingrys (*1993*) or Collins et al (*1986*) described the pathology of the second eye. It is possible that the inclusion of subjects with advanced AMD in their fellow eye in this study might account for the difference in outcome. The problem reported by Cheng and Vingrys (*1993*) in the application of the desaturated D15 was the variability in the results of the control group. Those subjects who showed the most pronounced tritan defect on the desaturated D15 test (JW, ER, MP, DC), all had unilateral late AMD. It could be that the inclusion of such subjects widened the difference between the control and ARM groups, and negated the effect of random confusions in control subjects.

8.6   Dark Adaptation Functions

8.6.1. Results

Dark adaptation functions were obtained in the manner described in section 7.7. It was not possible to obtain results from 2 control subjects (GO, BB), and 2 subjects with ARM (WT, DF). This was due to equipment failure.

The biphasic dark adaptation function is classically considered to be the sum of two exponential functions, reflecting the cone- and rod- dependent aspects of dark adaptation. The crossing point of these two functions is known as the rod-cone break, and reflects the point at which the sensitivity of rods surpasses that of cones. In their study of ARM-related changes in dark adaptation kinetics, Owsley et al (*2001*) modelled data according to a single exponential, double linear model based on Lamb's model of rod-mediated dark adaptation (*Leibrock et al, 1998; McGwin et al, 1999*). The two linear portion of the model represents the second and third components of rod recovery, which are believed to be largely dictated by the rate of rhodopsin regeneration .

In order to evaluate the ability of this single exponential, double linear model to provide a better description of dark adaptation than a double exponential model, the dark adaptation data of ten of the control subjects enrolled in this study were modelled using both a double exponential (equation 1), and a single exponential, double-linear model (equation 2). These ten subjects were selected alphabetically.

$$S(t) = (S + a.exp(-\tau 1.t)) + (b.exp(-\tau 2([max(t-knot1,0]))) \tag{1}$$

In which S(t) = sensitivity at time t, S = final sensitivity, a = constant relating to initial cone sensitivity, $\tau 1$ = time constant of cone recovery, t = time (mins), b = constant relating to initial rod sensitivity, $\tau 2$ = time constant of rod recovery, knot 1 = time of rod-cone break (mins).

$$S(t) = ((S + a.exp(-\tau 1.t)) + (c.([max(t-knot1,0]))) + (d.(max(t- knot2,0)])) \tag{2}$$

In which, S(t) = sensitivity at time t, a = final cone sensitivity, b = constant relating to initial cone sensitivity, $\tau 1$ = time constant for cone recovery, t = time (mins), knot 1 = time of rod-cone break (mins), c = slope of first component, d = slope of second component, knot 2 = time of transition between second and third components of rod-mediated dark adaptation (mins).

Data were fit on a least squares basis, and the two models were assessed according to the Akaike criterion i.e. a statistic which helps determine an appropriate model. The most suitable model for a set of data will be indicated by a lower Akaike criterion value (*Carson et al, 1983*).

Figure 8.10 shows the dark adaptation data for two typical control subjects, and the fit obtained with both models. The mean Akaike criterion calculated for the double exponential

model was 66.67 (± 29.47 SD), and for the single exponential, double linear model was 65.89 (± 25.46 SD). This suggests that there was little difference in the ability of the models to describe the data, and therefore the double exponential model (equation 1) was chosen for the analysis of data from all subjects. The parameters assessed were final sensitivity (dB), time to rod-cone break (mins), and the time constants of the first ($\tau1$) and second ($\tau2$) exponential functions, corresponding to cone and rod function respectively.
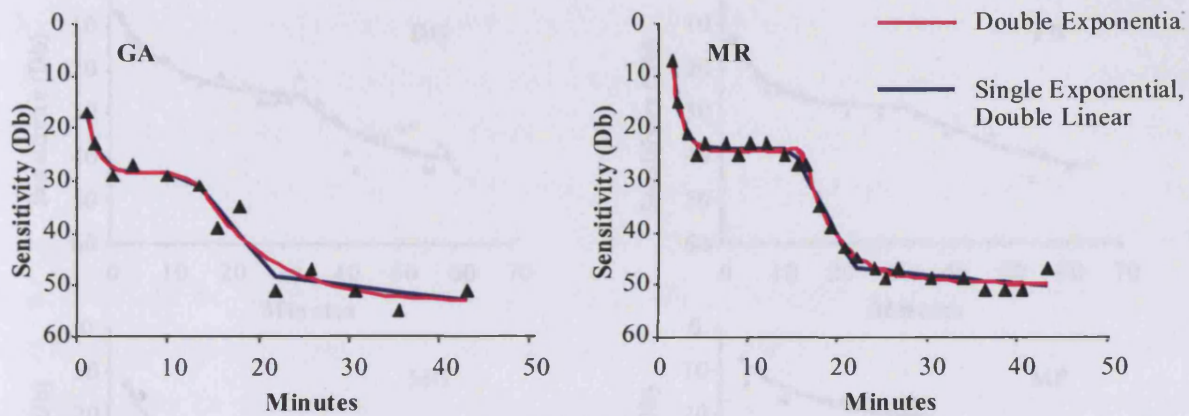
Figure 8.10. Typical dark adaptation curves from 2 healthy control subjects, fit with double exponential (equation 1) and single exponential, double linear (equation 2) models.

Figure 8.11 shows typical dark adaptation curves from six subjects with ARM. The data of 3 subjects with ARM could not be analysed for $\tau2$, as these subjects failed to show a rod-cone break within the 60 minute testing period. In the following analyses their rod-cone break time has been included as a conservative value of 60 minutes. Two of these subjects were classified as having wet AMD in the fellow eye (BJ and ER), the third had bilateral drusen (KS). One such data set, for subject BJ, may be seen in Figure 8.11.

The group averaged dark adaptation recovery parameters for control and ARM groups are shown in table 8.2. The two factors which were found to be significantly different between controls and subjects with ARM, even at the 1% significance level, were final sensitivity (Mann-Whitney U test, z = -3.54; p < 0.001), and the time to rod-cone break (Mann-Whitney U test, z = -4.164, p < 0.001).

Figure 8.11. Typical dark adaptation curves from 6 subjects with ARM, modelled with a double exponential function (equation 1).

Table 8.2. Group-averaged values for the parameters of dark-adaptation of control and ARM subjects, modelled using a double exponential function (equation 1). Values in bold were significantly different between groups. Values in parentheses describe the magnitude of the SE.

	Controls	**ARM**
Final Sensitivity (Db)	**50.3 (± 0.61)**	**45.45 (± 1.18)**
Time to Rod-Cone Break (mins)	**18.0 (± 1.88)**	**32.54 (± 2.47)**
Time Constant of Cone Recovery (τ1)	**0.66 (± 0.17)**	**0.37 (± 0.09)**
Time Constant of Rod Recovery (τ2)	0.35 (± 0.11)	0.23 (± 0.06)

A higher time constant was indicative of a faster rate of recovery. For both cone and rod recovery the average time constants are higher for the control than the ARM group. However, the intersubject variability for the time constants was high in both controls and subjects with ARM, and the difference between the two groups marginally failed to reach significance at the 5% level for the time constant of rod recovery ($\tau2$, Mann-Whitney U test, $z = -1.83$; $p = 0.067$). For the time constant of cone recovery ($\tau1$) the difference just reached significance ($z = -1.96$; $p = 0.050$).

The difference in group means between the control and ARM groups were highly significant for both final sensitivity and time to rod-cone break. Further consideration was therefore given to the diagnostic potential of these tests i.e. the sensitivity and specificity with which they were able to distinguish between subjects with ARM and control subjects. This was assessed by plotting a receiver operating characteristics (ROC) curve. Time to rod-cone break was found to be the more sensitive indicator, and at an optimal cut-off of 19.05 mins discriminated between groups with a sensitivity of 83% and a specificity of 80%. The ROC curve for time to rod-cone break may be seen in Figure 8.12. The area under the curve was 0.83.
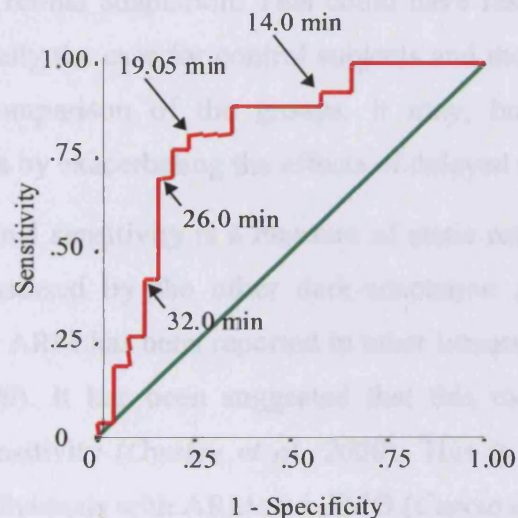
Figure 8.12. ROC curve showing sensitivity and 1-specificity of time to rod-cone break in distinguishing between subjects with and without ARM. Arrows indicate cut-off criteria of the curve.

It would also be desirable to assess the capacity of the dark adaptation function to identify those subjects with ARM who will go on to develop late AMD in the test eye. The only means of accurately determining this is to follow the outcome of subjects over a period of months after baseline testing. However, a preliminary assessment of prognostic value was undertaken

by subdividing the subjects with ARM according to the status of their fellow eye i.e. group 1 = bilateral ARM, group 2 = unilateral wet AMD, group 3 = unilateral dry AMD, and comparing dark adaptation performance between the three groups. It was found that the rod-cone break time showed a significant difference between the groups (Kruskal-Wallis, χ^2 (2) = 7.347, p = 0.025). Further analysis indicated that subjects in group 2, with unilateral choroidal neovascularisation had a significantly prolonged rod-cone break time (38.95 mins ($\pm$ 3.79)) compared to subjects in group 1 with bilateral ARM (26.91 mins ($\pm$ 3.84)). This finding remained significant when the Bonferroni correction for multiple comparisons was applied (Mann Whitney U Test, z = -2.649, p = 0.024).

8.6.2 Discussion of Dark Adaptation Results

All parameters of the double exponential model indicated a delayed recovery in ARM subjects, with reduced final sensitivity.

Threshold at all times after cessation of the bleach was determined using a staircase method. It should be noted that the presentation of suprathreshold stimuli using this technique may, in itself, have caused slight retinal adaptation. This could have resulted in prolonged recovery times. Since this was equally the case for control subjects and those with ARM, this does not present a problem in comparison of the groups. It may, however, have increased the separation between groups by exacerbating the effects of delayed recovery in the ARM group.

The finding of reduced final sensitivity is a measure of static retinal function, as opposed to the dynamic function assessed by the other dark-adaptation parameters. A reduction in absolute rod sensitivity in ARM has been reported in other literature (*Brown & Lovie-Kitchin; 1983; Owsley et al, 2000*). It has been suggested that this rod dysfunction may precede abnormalities in cone sensitivity (*Owsley et al, 2000*). This is consistent with findings of preferential rod loss in individuals with ARM and AMD (*Curcio et al, 1996*).

The lower values for both $\tau 1$ and $\tau 2$ in the ARM group indicated a generally more delayed recovery function for rods and cones in subjects with ARM compared to age-matched controls. This finding reached significance for the cone recovery function ($\tau 1$), but marginally failed to do so for the rod recovery function ($\tau 2$). One explanation for this may be that all subjects reached a plateau of cone sensitivity within the testing time, whilst the 60 minutes was inadequate for some subjects to reach their final rod threshold. This conferred greater

variability on the modelling of the rod mediated component of the dark adaptation curve. Another possible explanation for the greater abnormality seen in the cone mediated portion of the curve is that the cone recovery is more rapid, and may therefore place greater demands on the substrates of photopigment regeneration than the slower rod recovery.

A delayed dark adaptation function in ARM has been reported in a number of studies (*Brown et al, 1986; Eisner et al, 1987; 1991; Owsley et al, 2001; Steinmetz et al, 1993*). This slowed adaptation may be a consequence of increased deposition of substances rich in neutral lipids at the level of Bruch's membrane (*Bird, 1992; Feeney-Burns & Ellersieck, 1985; Starita et al, 1996*), causing it to become hydrophobic. Such deposits would constitute a barrier to the passage of metabolites and retinoids to the photoreceptors from the choroidal circulation. The consequent limitation in the availability of 11-cis retinal to rod outer segments would slow rhodopsin regeneration, and decrease the rate of recovery of bleached photopigment.

The delay of the rod-cone break in subjects with ARM was shown to be the parameter providing the greatest separation between controls and subjects with ARM. In particular, three subjects with ARM failed to exhibit a rod-cone break during the 60 minutes over which dark adaptation was monitored. Other reports have similarly found a significantly delayed rod-cone break in subjects with ARM (*Brown et al, 1986; Owsley et al, 2001*), and our results were consistent with one study suggesting that abnormalities of the dynamic aspects of retinal function precede static sensitivity loss in AMD (*Owsley et al, 2001*).

Diagnostically, a cut-off of 19.05 mins for the rod-cone break distinguished between subjects with ARM and controls with a sensitivity of 83%, and a specificity of 80%. The finding of a specificity of 80% indicates that 20% of control subjects would be falsely identified as having ARM on the basis of the timing of the rod-cone break. However, this is not necessarily the case, because some of the control subjects identified by the test may actually be at a pre-clinical stage of ARM. Figure 8.13 shows a scatter plot of rod-cone break up times. It may be seen that the results of 5 control subjects fall clearly above the cut-off determined by the ROC curve. A longitudinal study would reveal whether those control subjects will actually be seen to develop retinal signs of ARM.
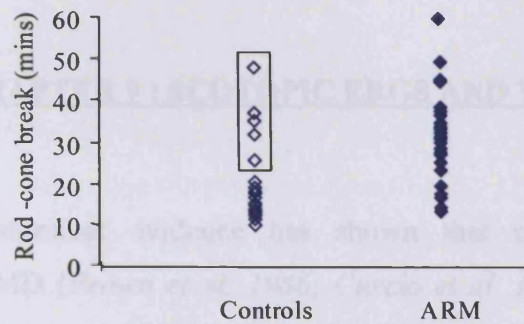
Figure 8.13. Scatter diagram illustrating spread of rod-cone break times for control and ARM subjects. The data points enclosed in the rectangle indicate control subjects with a rod-cone break exceeding the cut-off determined by the ROC curve (subjects AS, JC, VB, VE, WT).

Comparison between subgroups of subjects with ARM classified according to the status of the fellow eye indicated that the rod-cone break is significantly delayed in subjects with unilateral choroidal neovascularisation compared to those with bilateral ARM. Individuals with unilateral exudative AMD are more likely to develop the condition in the fellow eye than those with bilateral ARM (*Strahlman et al, 1983*). The findings of this study may therefore suggest that a prolonged rod-cone break is indicative of imminent neovascular changes.

A further indication that the timing of the rod-cone break is sensitive to retinal changes that precede the development of advanced AMD is provided by the evaluation of the data of individual subjects. Of the 6 subjects with rod-cone breaks of 40 mins or longer, 4 had unilateral exudative AMD (ER, AF, BJ, WD). Furthermore, two of the three individuals who failed to show a rod-cone break within the 60 minute testing period had unilateral exudative AMD. One of these (ER) developed choroidal neovascularisation in her second eye several weeks after participating in the study. Fundus photographs of her test eye showed no signs of wet AMD on the day of her visit, but the grossly delayed dark-adaptation function recorded may provide further evidence that this test is sensitive to incipient neovascular changes. A longitudinal study would determine whether those individuals with markedly delayed rod-cone breaks went on to develop neovascular changes over the follow-up period.

Eisner et al (*1992*) did not find the dark adaptation function alone to be a significant risk indicator in their longitudinal study of 42 subjects with unilateral choroidal neovascularisation. They postulated that this was because the bright adapting light presented prior to dark adaptation was relatively dim to some abnormal subjects with reduced cone quantum absorption, resulting in a spuriously normal dark adaptation function. However, their study only investigated cone dark adaptation parameters. A longitudinal study to evaluate the prognostic potential of rod-mediated dark-adaptation, or rod-cone break time has yet to be carried out.

CHAPTER 9 : SCOTOPIC ERGS AND VEPS

Psychophysical and anatomical evidence has shown that central rod dysfunction is characteristic of early AMD (*Brown et al, 1986; Curcio et al, 1996, Steinmetz et al, 1993; Jackson et al, 1998; Owsley et al, 2000, Curcio et al, 2000; Medeiros et al, 2001*). Owsley et al (*2000*), for example, found mean scotopic sensitivity loss within the central 18° of visual field to exceed photopic sensitivity loss in 87% of subjects with early ARM. Curcio et al (*1996*) found the foveal cone mosaic of eyes with large drusen to be relatively intact, but parafoveal cones were seen to be abnormally large, and few rods remained in this region. In eyes with late AMD, virtually all surviving photoreceptors were cones. Such reports suggest that central rod dysfunction is likely to be associated with early AMD.

This rod loss, seen at an early stage of ARM, could have implications which extend beyond the scotopic visual dysfunction reported in psychophysical studies. Studies performed on mouse retinas in vitro have suggested that rods may produce a chemical signal which is required for the continued survival of neighbouring cones, and that the deprivation of this signal triggers cone death (*Mohand-Said et al, 1997; Mohand-Said, 1998, Hicks and Sahel, 1999*). It may be the case, therefore, that rod loss is the factor which triggers cone degeneration in AMD. An understanding of changes which occur to the scotopic visual system in early ARM may be the key to preventing the subsequent dysfunction of the photopic visual system (*Curcio et al, 2000*).

This chapter describes the results obtained with the focal rod ERG and the rod VEP from subjects with ARM and control subjects. The development of these techniques has been described in chapter 6. There is no literature regarding the effect of ARM on these signals, but the psychophysical and anatomical evidence discussed above would suggest that an abnormal response is likely.

9.1   Methods

The general methods have been described in detail in chapters 6 and 7. The experimental parameters are summarised below.

- Each subject was dilated and dark adapted prior to ERG recording. Dark adaptation was monitored according to the technique described in section 7.7 until a steady level of retinal sensitivity was reached following the rod-cone break, up to a maximum of 60 minutes.

- Focal ERGs were then recorded in response to a blue (494nm), 20° diameter stimulus with an illuminance of 1.7 log scot tds sec^{-1}, flashing for 5 ms at a temporal frequency of 0.5 Hz. The stimulus was presented within a green (525 nm) ganzfeld surround, with an illuminance of 1.67 log scot tds.

- Thirty ERG responses were recorded, bandpass filtered from 1-100 Hz, and averaged on a 200 ms timebase.

- Full-field ERGs were then recorded to the same stimulus (494nm, 1.7 log scot tds sec^{-1}, duration 5 ms at a temporal frequency of 0.5 Hz). Full-field VEPs were simultaneously recorded on a separate channel, and also filtered from 1-100 Hz.

- The amplitudes and implicit times of ERG a- and b- waves were measured for focal and full-field responses. Absolute values were assessed, as well as the focal to full-field amplitude ratio.

- VEP responses were group averaged off-line, and the implicit time and amplitude of major peaks and troughs compared between control and experimental groups.

9.2   Results

9.2.1   ERG Results

Figure 9.1 shows typical focal rod ERGs recorded from 5 control subjects and 5 subjects with ARM.

Focal rod a-waves were small in amplitude, and not present in all responses recorded. However, a distinct b-wave was recorded in all subjects except one individual with ARM, VW, whose focal rod ERG was unmeasurably small.

The amplitude and implicit time of the focal rod b-wave of individual subjects may be seen in Figure 9.2. This graph illustrates a considerable spread in b-wave response characteristics of subjects within both groups.
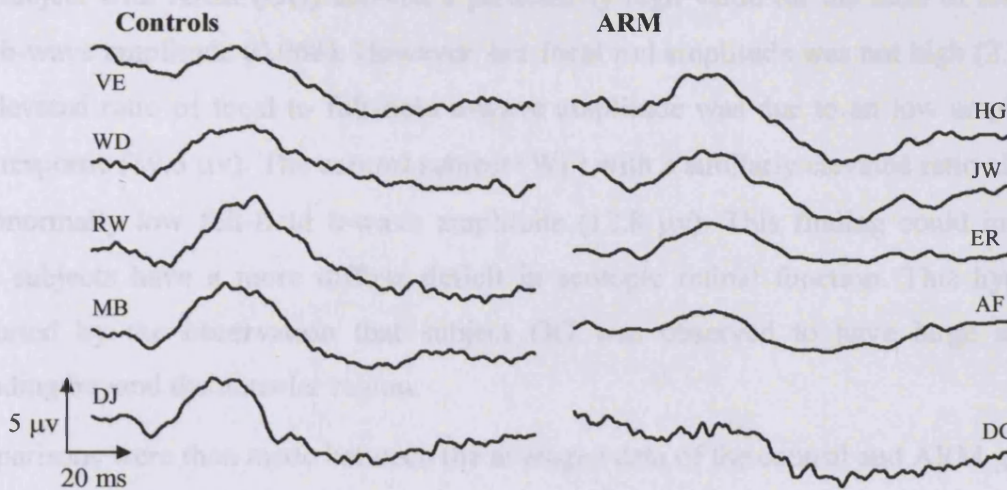
Controls   ARM

Figure 9.1. Typical focal rod ERG traces recorded from 5 control subjects and 5 subjects with ARM.
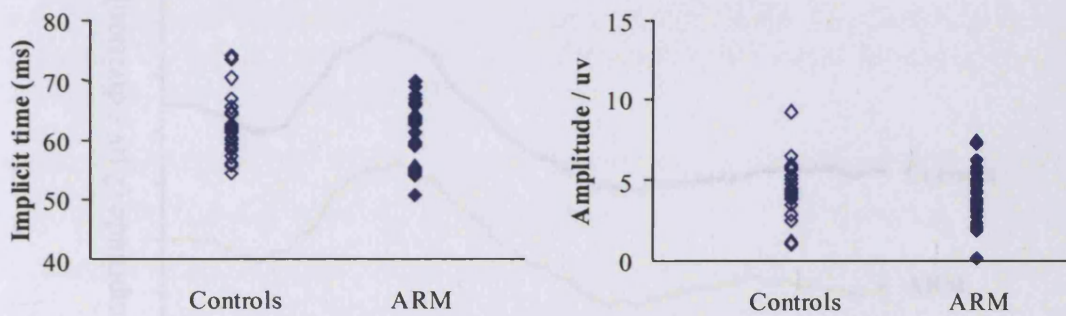
Figure 9.2. Scatter plots showing implicit times and amplitudes of focal rod ERG b-waves recorded from control subjects and subjects with ARM.

The ratio of focal to full-field b-wave response amplitude was then calculated for each subject. The ratios calculated for individual subjects may be seen in Figure 9.3. There is still considerable variability in the control data, but the ratios of the ARM subjects are now seen to be grouped around lower values than those of the control subjects.
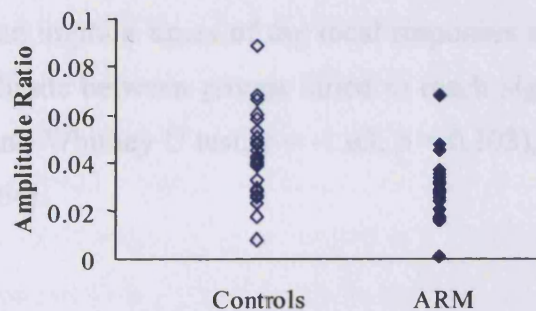
Figure 9.3. Scatter plot showing ratio of focal to full-field b-wave amplitude calculated in control subjects, and in subjects with ARM.

One subject with ARM (OG) showed a particularly high value for the ratio of focal to full-field b-wave amplitude (0.068). However, her focal rod amplitude was not high (2.7 μv), and the elevated ratio of focal to full-field b-wave amplitude was due to an low amplitude full-field response (39.5 μv). The control subject (WF) with a similarly elevated ratio also showed an abnormally low full-field b-wave amplitude (12.8 μv). This finding could indicate that these subjects have a more diffuse deficit in scotopic retinal function. This hypothesis is supported by the observation that subject OG was observed to have large soft drusen extending beyond the macular region.

Comparisons were then made between the averaged data of the control and ARM groups. The group averaged focal ERG responses may be seen in Figure 9.4.
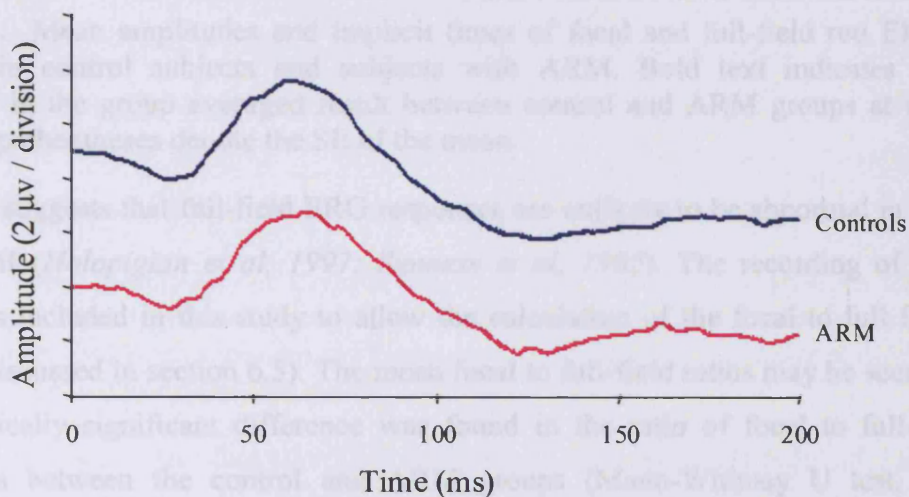
Figure 9.4. Group averaged focal rod ERG responses from controls and subjects with ARM.

Table 9.1 describes the average amplitude and implicit time of the focal and full-field ERG responses recorded from control subjects and those with ARM. As expected, the mean amplitude of the focal response is larger in the control group than the ARM group for both a- and b-waves. The mean implicit times of the focal responses are almost identical. However, the difference in amplitude between groups failed to reach significance at the 5 % level for either the a-wave (Mann-Whitney U test, z = -1.63; p = 0.103), or b-wave (Mann-Whitney U test, z = -1.39; p = 0.164).

		Controls	**ARM**
Full-Field	a-wave implicit time (ms)	32.59 (± 0.45)	32.48 (± 0.31)
	a-wave amplitude (μv)	15.06 (± 1.48)	15.87 (± 1.30)
	b-wave implicit time (ms)	65.46 (± 1.54)	63.46 (± 0.71)
	b-wave amplitude (μv)	112.95 (± 7.20)	122.65 (± 0.46)
Focal	a-wave implicit time (ms)	29.02 (± 0.90)	31.16 (± 1.08)
	a-wave amplitude(μv)	1.22 (± 0.17)	0.93 (± 0.17)
	b-wave implicit time (ms)	62.03 (± 1.03)	61.40 (± 0.95)
	b-wave amplitude (μv)	4.31 (± 0.31)	3.94 (± 0.46)
Ratio	Focal to full a-wave amp.	0.084 (± 0.012)	0.068 (± 0.018)
	Focal to full-field b-wave amp.	**0.042 (± 0.004)**	**0.032 (± 0.003)**

Table 9.1. Mean amplitudes and implicit times of focal and full-field rod ERG responses recorded in control subjects and subjects with ARM. Bold text indicates a significant difference in the group averaged result between control and ARM groups at the 5% level. Values in pathentheses denote the SE of the mean.

Literature suggests that full-field ERG responses are unlikely to be abnormal in subjects with early ARM (*Holopigian et al, 1997; Sunness et al, 1985*). The recording of ganzfeld rod ERGs was included in this study to allow the calculation of the focal to full field response ratio (as discussed in section 6.5). The mean focal to full-field ratios may be seen in table 9.1. No statistically significant difference was found in the ratio of focal to full-field a-wave amplitudes between the control and ARM groups (Mann-Whitney U test, z = -1.552; p = 0.121). However, the ratio of focal to full-field b-wave amplitudes was larger in the control group than the ARM group, with the difference reaching significance at the 5% level (Mann Whitney U test; z = -2.34; p = 0.019).

Results were then considered with regard to the three subsets of subjects with ARM i.e. those with bilateral ARM (group 1), those with unilateral wet AMD in the fellow eye (group 2), and those with unilateral dry AMD in the fellow eye (groups 3). The mean amplitude and implicit time of focal and full-field responses within the three groups may be seen in table 9.2. The only parameter which showed a significant difference between the three groups was the focal b-wave amplitude (Kruskal-Wallis, $\chi^2(2)$ = 6.346; p = 0.042). Further analysis showed the difference to be between subjects with bilateral drusen (group 1) and those with unilateral dry AMD (group 3) (Mann-Whitney U test, z = -2.136; p = 0.021). However, when the

Bonferroni correction was applied to minimise the risk of type I error incurred by multiple comparisons this difference was no longer significant (p = 0.063).

		ARM		
		Group 1	*Group 2*	*Group 3*
Full-Field	a-wave implicit time(ms)	32.15 (± 0.58)	32.22 (± 0.55)	33.28 (± 0.32)
	a-wave amplitude (μv)	16.27 (± 3.33)	11.91 (± 1.31)	20.26 (± 2.34)
	b-wave implicit time (ms)	62.85 (± 1.53)	64.30 (± 0.94)	63.23 (± 1.06)
	b-wave amplitude (μv)	129.83 (± 11.13)	122.98 (± 8.77)	112.36 (± 14.57)
Focal	a-wave implicit time (ms)	29.49 (± 1.54)	33.33 (± 2.06)	31.31 (± 2.13)
	a-wave amplitude(μv)	1.38 (± 0.36)	0.50 (± 0.15)	0.92 (± 0.31)
	b-wave implicit time (ms)	62.25 (± 1.33)	59.08 (± 1.65)	63.26 (± 2.02)
	b-wave amplitude (μv)	**5.36 (± 0.92)**	**3.32 (± 0.45)**	**2.65 (± 0.65)**
Ratio	Focal to full a-wave amp.	0.11 (± 0.044)	0.042 (± 0.012)	0.049 (± 0.017)
	Focal to full b-wave amp.	0.041 (± 0.006)	0.025 (± 0.004)	0.023 (± 0.005)

Table 9.2. Mean amplitude and implicit times of focal and full-field scotopic ERG responses recorded in the three groups of subjects with ARM, sub-classified according to the status of the fellow eye. Bold text indicates the parameters found to be significantly different between groups. Values in parentheses denote the SE of the mean.

Statistical analysis of the data therefore suggests that the only parameter of the rod ERG to show a significant difference between the control and ARM groups is the group averaged ratio of focal to full-field b-wave amplitude. Although this finding is of interest, lending weight to suggestions in the literature of early focal rod dysfunction in ARM, comparison of group-averaged results is of little value in the clinic. In order to determine the potential diagnostic value of this ratio, sensitivity and specificity were calculated using a Receiver Operating Characteristic (ROC) curve to identify the optimal cut-off point.

Figure 9.5 shows the ROC curve calculated for this parameter. According to this analysis, a cut-off point of 0.38 achieved a diagnostic sensitivity of 83 %, and a specificity of 61%. The area under the curve was 0.71.
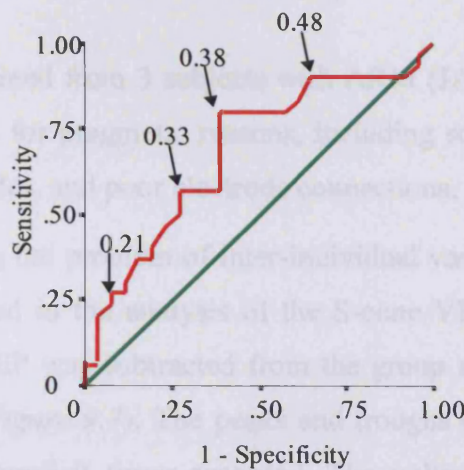
Figure 9.5. ROC curve showing sensitivity and 1-specificity of focal to full-field b-wave amplitude ratio of rod ERG in distinguishing between subjects with and without ARM. Arrows indicate cut-off criteria of curve.

9.2.2 VEP Results

Figure 9.6 shows scotopic VEPs recorded from 5 control subjects. It may be seen that there was great variability in the shape of rod VEP responses recorded from different individuals, to the extent that a straightforward comparison of amplitudes and implicit times of responses was inappropriate. However, the group averaged VEPs did show a clearly defined series of peaks and troughs (*see Figure 9.7*).
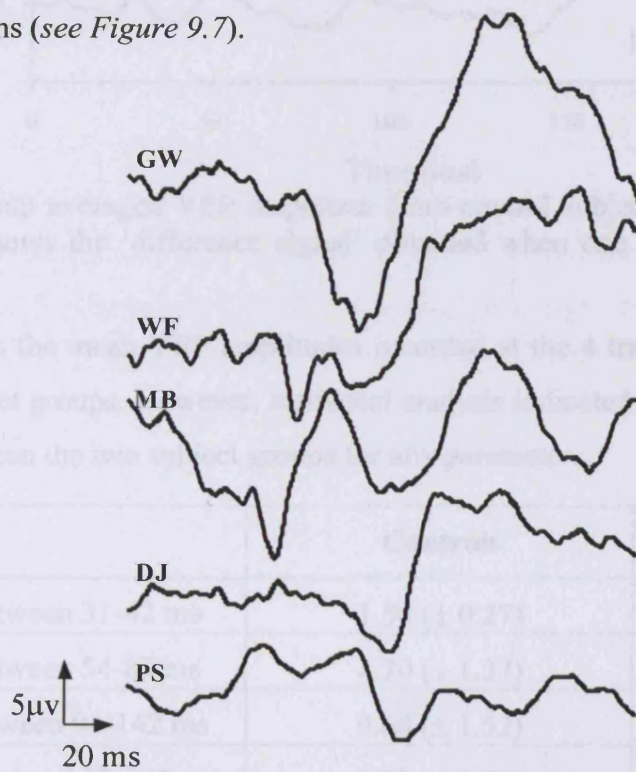
Figure 9.6. Typical rod VEPs recorded from 5 healthy control subjects.

Rod VEPs were not obtained from 3 subjects with ARM (JA, MP, DG) and from 3 controls (PG, CD, VB). This was for pragmatic reasons, including scalp conditions which precluded the application of electrodes, and poor electrode connections.

As a means of combating the problem of inter-individual variability in response, a technique was used that is described in the analysis of the S-cone VEP by Drasdo et al (*2002*). The group averaged ARM VEP was subtracted from the group averaged control VEP to elicit a 'difference signal' (*see Figure 9.7*). The peaks and troughs of this subtracted response were then cursored, and the implicit times recorded. The voltage changes at these times were assessed in individual VEP traces, regardless of whether they coincided with an apparent peak or trough of that particular response. On this basis, four transitional times were assessed in each VEP. These were 31–42ms, 54–83 ms, 94–142 ms, and 142-170 ms.
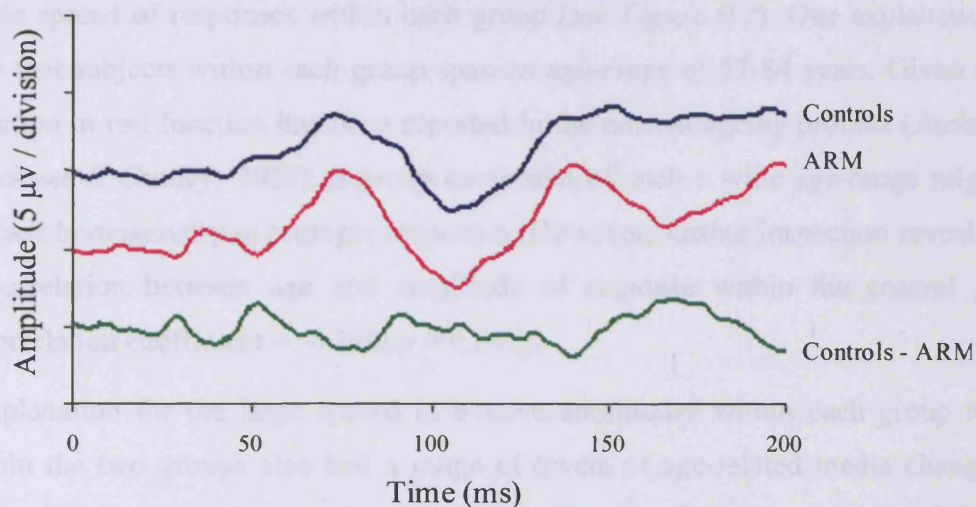
Figure 9.7. Group averaged VEP responses from control subjects, and subjects with ARM. Bottom trace shows the 'difference signal' obtained when one trace is subtracted from the other.

Table 9.3 shows the mean VEP amplitudes recorded at the 4 transitional times from control and ARM subject groups. However, statistical analysis indicated that there was no significant difference between the two subject groups for any parameter.

	Controls	**ARM**
Amplitude between 31-42 ms	1.50 ($\pm$ 0.27)	1.79 ($\pm$ 0.21)
Amplitude between 54-83 ms	4.70 ($\pm$ 1.37)	4.97 ($\pm$ 0.85)
Amplitude between 94-142 ms	9.64 ($\pm$ 1.52)	8.20 ($\pm$ 1.23)
Amplitude between 142-170 ms	4.82 ($\pm$ 0.78)	5.03 ($\pm$ 0.88)

Table 9.3. Mean VEP response amplitudes measured at predetermined times. The values in parentheses denote the SE of the mean.

9.3   Discussion

The group averaged results showed a reduction in both a- and b-wave amplitudes in subjects with ARM compared to control subjects. This finding was in accordance with previous psychophysical studies which described a differential loss in rod function in individuals with early ARM (*Brown et al, 1986; Curcio et al, 1996, Steinmetz et al, 1993; Jackson et al, 1998; Owsley et al, 2000*). However, the difference in amplitude failed to reach significance.

The lack of a significant difference in amplitude is likely to be attributable to the fact that the focal signals were small, even in control subjects. Thus the signal to noise ratio is relatively poor, and likely to mask any differences in amplitude between the groups.

Examination of individual focal b-wave amplitudes within the control and ARM groups reveals a wide spread of responses within each group (*see Figure 9.2*). One explanation for this could be that subjects within each group span an age-range of 57-84 years. Given that a general reduction in rod function has been reported in the normal ageing process (*Jackson et al, 1998; Jackson & Owsley, 2000*), a group composed of such a wide age-range might be expected to lack homogeneity in scotopic responses. However, further inspection revealed no significant correlation between age and amplitude of response within the control group (Pearson's correlation coefficient = -0.229, p = 0.242).

A further explanation for the large spread in b-wave amplitudes within each group is that subjects within the two groups also had a range of levels of age-related media changes. It would be expected that individuals with a higher level of nuclear sclerosis would exhibit smaller focal rod amplitudes due to scatter and absorption of the short-wave length stimulus by ocular media. A scatter plot of b-wave amplitude against extent of lens nuclear opacity (graded according to LOCS III standards, *Chylack et al, 1993*) in the control subjects may be seen in Figure 9.8. A significant negative correlation was found between amplitude and lens grading (Pearson's correlation co-efficient = -0.397; p = 0.036). This supported the hypothesis that lens changes may have accounted for some of the intersubject variability in focal rod response.

A regression line was fitted to the amplitude vs. nuclear opacity grading data, and the equation of this line used to correct b-wave amplitude data for both subjects with ARM and age-matched controls. However, the subsequent comparison of the adjusted b-wave data still showed no significant difference between the ARM and control groups. This finding reflects the matching of the two groups for lens status.
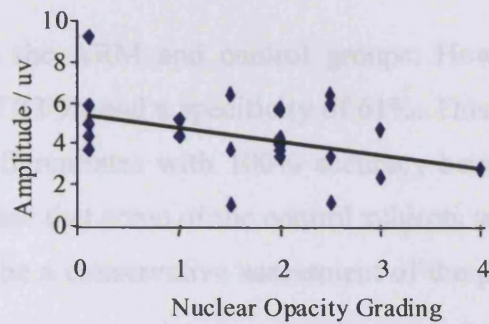
Figure 9.8. Scatter plot showing relationship between focal rod b-wave amplitude and LOCS III nuclear opacity grading for control subjects. A regression line has been added to the plot (equation $y = -0.667x + 5.49$; $R^2 = 0.1578$).

Of the scotopic ERG parameters assessed in this study only one, the ratio of focal to full-field b-wave amplitude, was found to be significantly different between the control and ARM groups in terms of group means. A high focal to full-field ratio, as observed in the control group, is indicative of a relatively large response amplitude from the macula, compared to the response elicited by the stimulation of the whole retina. A low amplitude ratio would therefore be expected in the differential loss of central retinal function reported in ARM and AMD. Therefore, the significantly lower ratio for the ARM group supports the hypothesis of selective central rod dysfunction.

In the recording of ERG responses there is inherent variability conferred by inter-subject anatomical differences in factors such as retinal pigmentation (*Wali & Leguire, 1992*) and axial length (*Chan & Mohidin, 2003*). In this study the ratio of focal to full-field amplitude was assessed as a novel means of increasing the sensitivity of ERG tests by reducing this variability. Each subject is effectively acting as a control for their own responses, and thus the inter-subject variability is likely to be reduced.

However, examination of the scatter plot in Figure 9.3 shows that, even when the ratio of focal to full-field b-wave amplitude is considered, there is still a considerable spread in the data of control subjects. It has been hypothesised that AMD constitutes the end point of a continuum of retinal changes which occur in apparently healthy individuals as a function of age (*Curcio et al, 1996*). The range of central retinal rod function observed in control subjects in this study may reflect this continuum. Although none of these individuals exhibit photographic signs of ARM, assessment of the 'healthy controls' over a period of time may show that some are actually at a pre-clinical level of the disease process.

When the ROC curve was used to assess the diagnostic value of the ratio of focal to full-field rod b-wave amplitude, the test was found to be significantly more effective than chance at

discriminating between the ARM and control groups. However, the optimal cut-off only achieved a sensitivity of 83 %, and a specificity of 61%. This is based on the assumption that fundus classification differentiates with 100% accuracy between control subjects and those with ARM. If it is the case that some of the control subjects are actually at a pre-clinical stage of ARM then this may be a conservative assessment of the potential diagnostic value of this test.

Comparisons were also made between the group averaged results of the ARM subgroups discussed in chapter 7 (*see table 7.1*). On the basis that the subjects with unilateral advanced AMD in the fellow eye (groups 2 and 3) are more likely to develop choroidal neovascularisation in their test eye than subjects with bilateral drusen (group 1), differences in mean responses between the groups might have prognostic significance. There was a significant difference in b-wave amplitude between subjects with bilateral drusen and those with advanced dry AMD in the fellow eye. However, multiple comparisons of this nature incur the risk of a type 1 error. The Bonferroni correction is a conservative way of correcting for multiple comparisons (*Altman, 1997*). The difference between groups ceased to be significant after correction.

The rod VEP was recorded at the same time as the full-field rod ERG. Visual evoked potentials are dominated by macular activity even when elicited by a full-field stimulus because of 'cortical magnification'. The rod VEP was therefore incorporated in this study as a second means of assessing central retinal rod function.

Flash VEPs are inherently complex in waveform, and show great intersubject variability (*Brigell, 2001*). The problem of inherent variability was compounded in this study because the VEPs were, for pragmatic reasons, based on only 30 sweeps. This is significantly less than the 64 averages recommended by Harding et al (*1996*). The variability in the rod VEPs meant that a direct comparison of implicit times and amplitudes of specific VEP waveforms was not possible. An alternative approach, involving the identification of a 'difference signal' was little better. The lack of any significant difference between groups was likely to be due to the variability in VEP amplitude. Furthermore, although the VEP does reflect central retinal function, it is a signal from the visual cortex and any subtle abnormalities of outer retinal function may be disguised by the considerable processing of the signal which occurs along the visual pathway.

There is, to date, no published literature discussing the effect of ARM and AMD on the focal rod ERG. However the findings in this study are in agreement with anatomical (*Curcio et al, 1996*) and psychophysical (*Brown et al, 1986; Steinmetz et al, 1993; Jackson et al, 1998; Owsley et al, 2000*) studies suggesting that rods are vulnerable at an early stage of AMD. One explanation for a possible differential loss of rods over cones in AMD has been offered by Curcio et al (*2000; 2001*). The visual cycle is dependent on the regeneration of 11-*cis*-retinal from the bleached all-*trans* isomer after a photopigment bleach. This process occurs in photoreceptors and the RPE following the supply of all-*trans* precursors by the choroidal bloodstream via plasma proteins in Bruch's membrane (*Saari, 2000*). The importance of the supply of retinoids, not only in the visual cycle, but in the continued vitality of the retina, is apparent in the rod outer segment degeneration and photoreceptor death which is seen in a situation of vitamin A deficiency (*Katz et al, 1991; Katz et al, 1993*). Lack of vitamin A primarily affects the rod photoreceptors, although cone death occurs at a later stage (*Kemp et al, 1989*). This selective disruption of rod survival is could be due to an alternative pathway of retinoid delivery available to the cones but not to rods (*Goldstein 1967; 1970; Goldstein et al, 1973; Das et al, 1992; Jin et al, 1994; Leibrock et al, 1998*).

It has been proposed that the abnormal material deposited in Bruch's membrane in AMD forms a barrier to the movement of metabolites and retinoids from the choriocapillaris to the RPE (*Starita et al, 1996*). This could effectively result in a localised vitamin A deficiency responsible not only for selective rod loss and dysfunction, but also explaining the abnormalities reported in the kinetics of rod adaptation in individuals with AMD (*Owsley et al, 2001*). Since age-related changes have been reported in Bruch's membrane in the absence of clinical signs of AMD (*Pauleikhoff et al, 1994*), this explanation would also be in keeping with the fact that the rod loss and functional change seen in AMD is effectively a more extreme form of age-related changes seen in healthy older adults.

CHAPTER 10 : PHOTOPIC ERGS AND VEPS

The healthy function of the central cones is vital to our appreciation of colour and visual detail. As discussed in chapter 5, psychophysical evidence suggests that the macular cones are affected in early ARM, but electrophysiological investigation provides an opportunity to objectively assess the nature and extent of this deficiency. Chapter 6 describes the development of protocols designed to record transient and steady state ERGs from the macular cones. This chapter presents the results obtained from subjects with ARM and from age-matched controls using these techniques.

10.1   The 5 Hz ERG

10.1.1 Introduction

Abnormalities of central retinal cone function in ARM and AMD have been highlighted by psychophysical tests investigating visual acuity (*Brown et al, 1983; Brown et al, 1984; Sunness et al, 1997*), absolute cone threshold (*Brown et al, 1986; Eisner et al, 1987; Steinmetz et al, 1993*), visual field (*Cheng & Vingrys, 1993; Midena et al, 1994; Midena et al, 1997*), and contrast sensitivity (*Alexander et al, 1988; Kleiner et al, 1988; Collins et al, 1989; Mayer et al, 1992; Midena et al, 1997*). Studies investigating focal cone ERGs in subjects with AMD have also highlighted abnormalities in macular function.

Electrophysiological techniques to objectively assess macular function have largely targeted the central 10° of the retina (*Biersdorf & Diller, 1969; Birch & Fish, 1988, Sandberg et al, 1993; Remulla et al, 1995, Sandberg et al, 1998; Falsini et al, 1999; 2000*). Evidence suggests, however, that functional (*Sunness, 1985; Owsley et al, 2000*), and anatomical (*Curcio et al, 1996; Curcio et al, 2000; Medeiros et al, 2001*) cone abnormalities in AMD stretch throughout the macula, to 10° either side of fixation.

Recent studies have focussed principally on the steady state response elicited by a stimulus flickering at a temporal frequency greater than 30Hz (*Birch & Fish, 1988, Sandberg et al, 1993; Remulla et al, 1995, Sandberg et al, 1997; Falsini et al, 1999; 2000*). Unlike the steady state signal, the ERG recorded in response to a 5 Hz stimulus shows a distinct waveform, made up of components reflecting the activity of different retinal layers. As discussed in

chapter 4, the photopic a-wave is considered to primarily reflect the activity of the cone photoreceptors (*Brown et al, 1965; Heynen & Van Norren, 1985*), although there is also believed to be an inner retinal contribution (*Knapp & Schiller, 1984; Evers & Gouras, 1986; Falk & Shiells, 1986; Bush and Sieving, 1994*). The b-wave of the transient photopic ERG has been shown to derive from the activity of both depolarising and hyperpolarising second order neurones (*Evers & Gouras, 1986; Sieving et al, 1994*). The oscillatory potentials may also be extracted from the 5 Hz ERG. The origins of the OPs are not precisely understood, but they have been shown to originate from a proximal retinal source (*Heynen et al, 1985*), probably from cells located within the inner plexiform layer (*Ogden, 1973; Wachtmeister & Dowling, 1978; Wachtmeister, 1998*).

An assessment of the characteristics of the focal 5 Hz waveform therefore allows an assay of the function of different retinal cell populations. At the outset it was hypothesised that the a-wave would be most affected by the ARM disease process, as it primarily reflects the function of the outer retina.

The ratio of focal to full-field response amplitude was also calculated for each subject. In view of the differential loss of central retinal function expected in individuals with ARM, it was hypothesised that these subjects would have a reduced ratio compared to age-matched controls.

10.1.2 Method

The general methods have been described in detail in chapters 6 and 7. The experimental parameters are summarised below.

- Focal ERGs were recorded in response to an amber (595nm), 20° diameter stimulus with a luminance of 30 cd.m^{-2}.sec^{-1} (1500 phot tds), flashing for 100 ms, at a temporal frequency of 5 Hz. The stimulus was presented within a white ganzfeld surround, with a luminance of 30 cd.m^{-2}.sec^{-1}.

- Two hundred ERG responses were recorded, bandpass filtered from 1-100 Hz, and averaged on a 200 ms timebase. A separate channel simultaneously averaged responses bandpass filtered from 100-1000 Hz, thus extracting the oscillatory potentials.

- Full-field ERGs were then recorded to the same stimulus (595nm, 30 cd.m^{-2}.sec^{-1}, duration 100 ms, at a temporal frequency of 5 Hz).

- The amplitude and implicit time of the a- and b- waves were measured for focal and full-field responses. Absolute values were assessed, as well as the focal to full-field amplitude ratio.

- The amplitude and implicit time of the oscillatory potentials were also measured for both focal and full-field responses. The implicit time of individual OPs, summed OP amplitude, and the focal to full-field summed amplitude ratio were assessed.

10.1.3 Results

10.1.3.1 a- and b-waves

Figure 10.1 shows typical focal cone ERGs recorded from 5 control subjects, and five subjects with ARM. Distinct a- and b- waves were recorded from most subjects, however signals recorded from subjects with ARM typically appeared smaller and less well defined.
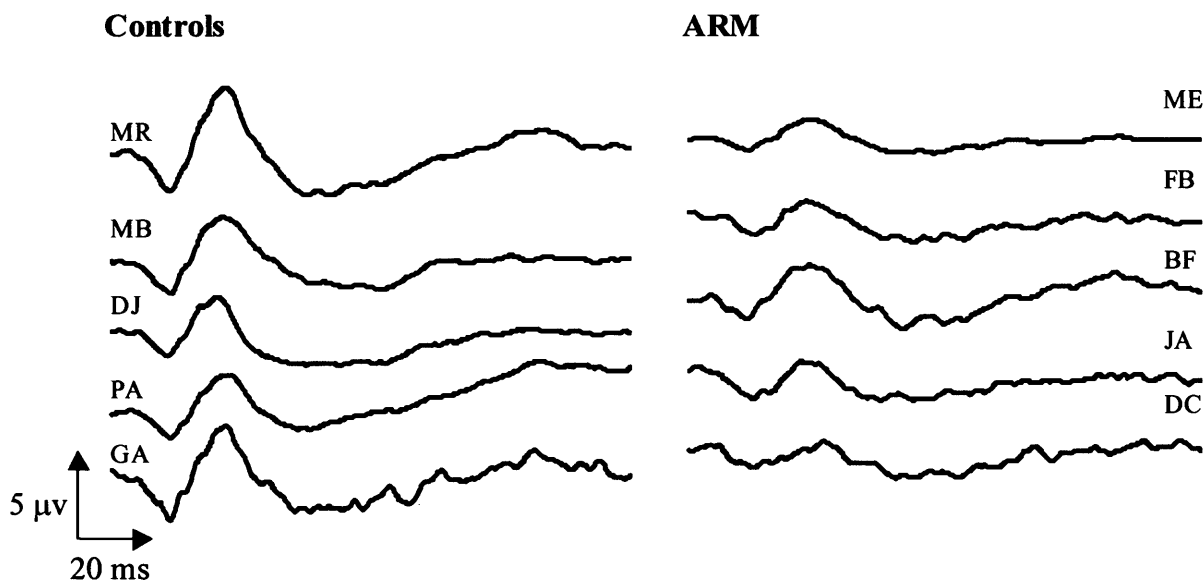
Figure 10.1. Typical 5 Hz focal cone ERG responses recorded from 5 control subjects, and 5 subjects with ARM.

The amplitude and implicit time of a- and b-waves of individuals within both groups may be seen in Figures 10.2 and 10.3. These scatter plots illustrate a considerable spread in the amplitude data within each group for a- and b- wave amplitudes. However, the implicit time data shows less variability, and there is a trend towards shorter implicit times for a- and b-waves in control subjects compared to subjects with ARM.
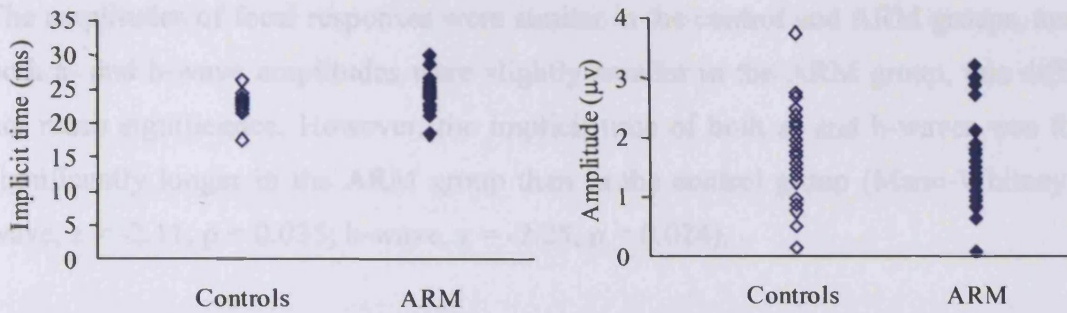
Figure 10.2. Scatter plots showing implicit times and amplitudes of 5Hz focal cone ERG a-waves recorded from control subjects and subjects with ARM.
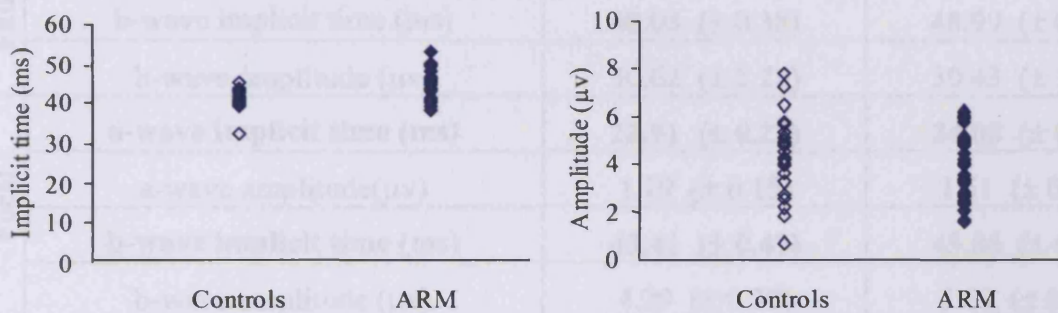
Figure 10.3. Scatter plots showing implicit times and amplitudes of 5Hz focal cone ERG b-waves recorded from control subjects and subjects with ARM.

In order to further assess differences in amplitude and implicit time between the two groups, group-averaged results were then considered. The group-averaged 5 Hz focal cone ERG traces are shown in Figure 10.4.
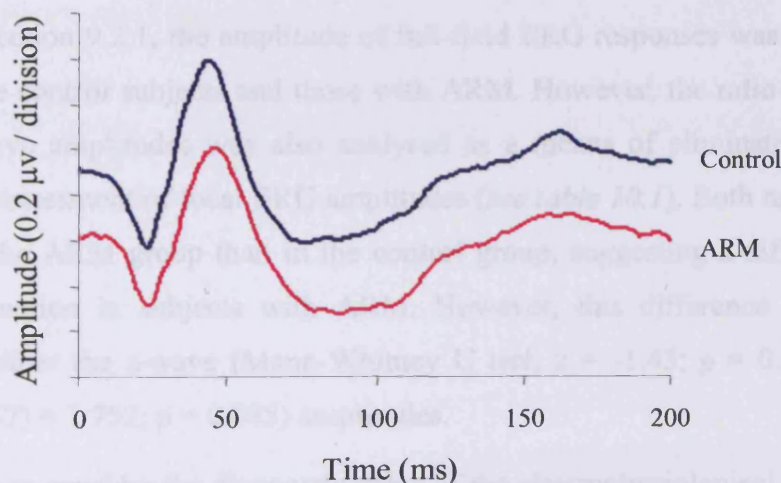
Figure 10.4. Group averaged 5Hz focal cone ERG responses

Table 10.1 describes the group-averaged amplitude and implicit time of a- and b-waves for the focal and full-field ERG responses recorded from control subjects and those with ARM.

The amplitudes of focal responses were similar in the control and ARM groups, and although both a- and b-wave amplitudes were slightly smaller in the ARM group, this difference did not reach significance. However, the implicit time of both a- and b-waves was found to be significantly longer in the ARM group than in the control group (Mann-Whitney U test; a-wave, $z = -2.11$, $p = 0.035$; b-wave, $z = -2.25$, $p = 0.024$).

		Controls	**ARM**
Full-Field	a-wave implicit time (ms)	25.79 (± 0.22)	26.3 (± 0.33)
	a-wave amplitude (µv)	14.72 (± 1.04)	14.59 (± 0.71)
	b-wave implicit time (ms)	48.05 (± 0.38)	48.99 (± 0.51)
	b-wave amplitude (µv)	30.62 (± 2.22)	30.43 (± 1.75)
Focal	**a-wave implicit time (ms)**	**22.91 (± 0.27)**	**24.08 (± 0.43)**
	a-wave amplitude(µv)	1.79 (± 0.15)	1.51 (± 0.13)
	b-wave implicit time (ms)	**43.41 (± 0.47)**	**45.86 (± 0.68)**
	b-wave amplitude (µv)	4.29 (± 0.30)	3.69 (± 0.25)
Ratio	Focal : full-field a-wave amplitude	0.13 (± 0.01)	0.10 (± 0.01)
	Focal : full-field b-wave amplitude	0.15 (± 0.07)	0.13 (± 0.08)

Table 10.1. Mean amplitudes and implicit time of focal and full-field 5 Hz cone ERG a- and b-wave responses recorded from control subjects and subjects with AMD. The values in parentheses denote the SE of the mean. Bold text indicates parameters which were significantly different between groups.

As discussed in section 9.2.1, the amplitude of full-field ERG responses was not expected to differ between the control subjects and those with ARM. However, the ratio of focal to full-field a- and b-wave amplitudes was also analysed as a means of eliminating inter-subject variability in the assessment of focal ERG amplitudes (*see table 10.1*). Both ratios were found to be smaller in the ARM group than in the control group, suggesting a differential loss of central retinal function in subjects with ARM. However, this difference failed to reach significance for either the a-wave (Mann-Whitney U test; $z = -1.43$; $p = 0.152$) or b-wave (student t-test, $t(57) = 1.752$; $p = 0.085$) amplitudes.

It is also desirable to consider the diagnostic value of the electrophysiological tests. The mean implicit time of the 5 Hz focal cone b-wave was the parameter which showed the greatest difference between the ARM and control groups. In order to assess the diagnostic value of

this test, an ROC curve was plotted. When an optimal cut-off of 42.9 ms was employed, this parameter achieved a sensitivity of 74% and a specificity of 64%.

Consideration was then given to the characteristics of ERGs recorded in the three different ARM groups i.e. bilateral ARM (group 1), unilateral wet AMD (group 2), and unilateral dry AMD (group 3). The mean amplitude and implicit time of focal and full-field responses within the groups may be seen in table 10.2. No significant difference was found between the three groups for any parameter.

		ARM		
		Group 1	*Group 2*	*Group 3*
Full-Field	a-wave implicit time (ms)	26.53 (± 0.74)	26.36 (± 0.39)	25.95 (± 0.40)
	a-wave amplitude (μv)	14.03 (± 0.87)	14.72 (± 1.18)	15.26 (± 1.92)
	b-wave implicit time (ms)	48.73 (± 1.21)	49.47 (± 0.44)	48.70 (± 0.57)
	b-wave amplitude (μv)	27.91 (± 2.04)	33.17 (± 3.36)	30.43 (± 4.00)
Focal	a-wave implicit time (ms)	23.40 (± 0.88)	24.20 (± 0.49)	24.95 (± 0.73)
	a-wave amplitude(μv)	1.50 (± 0.20)	1.56 (± 0.18)	1.47 (± 0.33)
	b-wave implicit time (ms)	45.03 (± 0.92)	46.69 (± 1.23)	45.98 (± 1.55)
	b-wave amplitude (μv)	3.88 (± 0.38)	4.04 (± 0.39)	2.91 (± 0.51)
Ratio	Focal : full-field a-wave amplitude	0.11 (± 0.001)	0.11 (± 0.01)	0.093 (±0.02)
	Focal : full-field b-wave amplitude	0.14 (± 0.01)	0.13 (± 0.01)	0.10 (± 0.02)

Table 10.2. Mean amplitude and implicit times of focal and full-field 5 Hz ERG responses recorded in the three groups of subjects with ARM, sub-classified according to the status of fellow eye i.e. bilateral ARM (group 1), unilateral wet AMD (group 2), unilateral dry AMD (group 3). Values in parentheses denote the SE of the mean.

10.1.3.2 Oscillatory Potentials

Oscillatory potentials were also extracted from the 5 Hz ERG through bandpass filtering responses from 100-1000 Hz. Typical focal OP responses may be seen in Figure 10.5.

Up to 4 OPs were extracted from the full-field ERG of most subjects. The implicit time of the 4 wavelets was measured in each individual. The peak to trough amplitude of all discernible OPs was also measured and the summed amplitude calculated for each subject. The number of

OPs elicited by the focal stimulus was more variable. Ten subjects with ARM, and 1 control subject failed to show any repeatable wavelets, and only 2 subjects with ARM, and 6 control subjects showed the complete 4 macular OPs described by Miyake (1990). In the absence of any recordable OPs, a summed amplitude of 0 µv was ascribed to the individual.
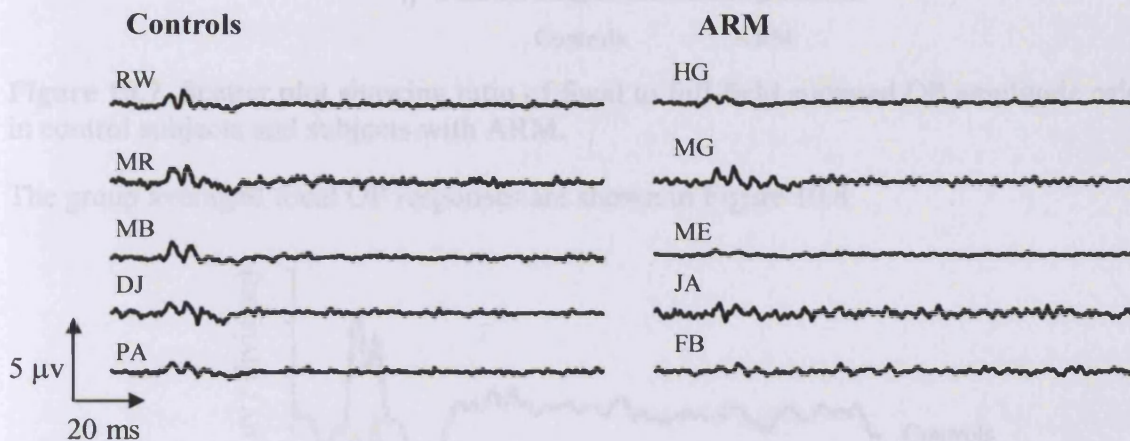
Figure 10.5. Typical focal OP responses recorded from 5 control subjects, and 5 subjects with ARM.

The summed amplitude data is shown in Figure 10.6. It may be seen that there is great variability in summed OP amplitude, with considerable overlap between the data of subjects with ARM and controls.
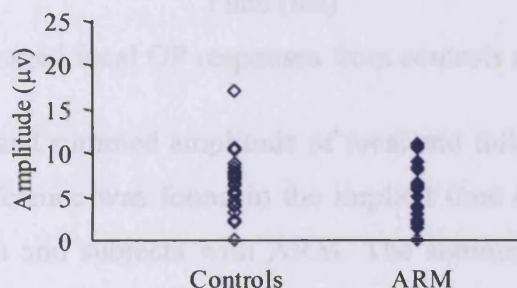
Figure 10.6. Scatter plot showing summed focal OP amplitudes recorded from control subjects and subjects with ARM.

In order to decrease the intersubject variability seen in the summed OP amplitude data, the focal to full-field amplitude ratio was also calculated. The data points for all subjects may be seen in Figure 10.7. There remains a considerable spread within the results of each group, but a trend towards lower ratio values may be seen in subjects with ARM compared to age-matched controls.
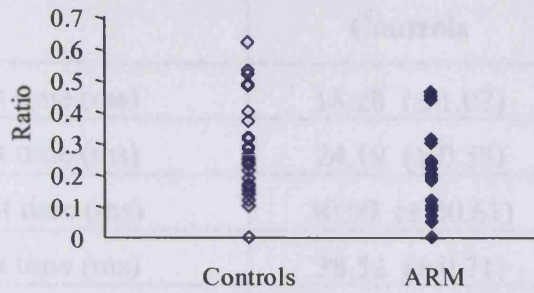
Figure 10.7. Scatter plot showing ratio of focal to full-field summed OP amplitude calculated in control subjects and subjects with ARM.

The group averaged focal OP responses are shown in Figure 10.8.
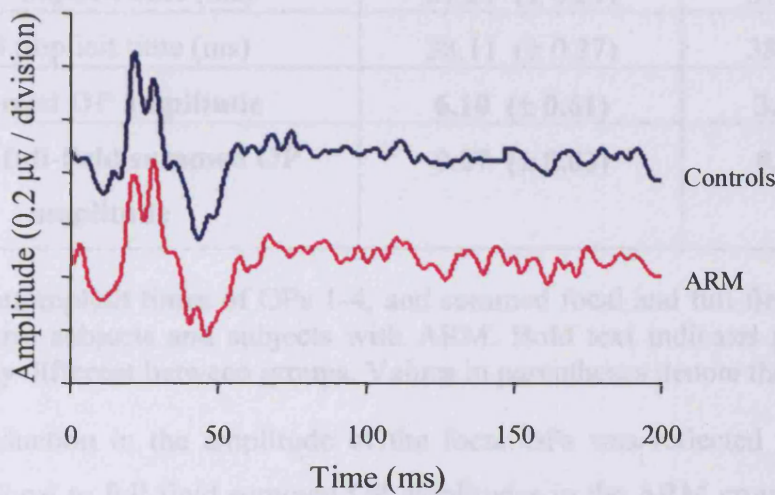
Figure 10.8. Group averaged focal OP responses from controls and subjects with ARM.

The mean implicit time and summed amplitude of focal and full-field OPs are shown in table 10.3. No significant difference was found in the implicit time of the focal or full-field OPs between control subjects and subjects with ARM. The summed amplitude of full-field OP wavelets was also found, as expected, to be equivalent between the two groups. However, the mean summed amplitude of the focal OPs was found to be larger in the control group than the ARM group. This difference was statistically significant even at the 1% level (Mann-Whitney U test, z = -2.62; p = 0.01). The magnitude of this difference was greater than would be anticipated from visual inspection of the group-averaged traces, this finding is considered further in the discussion section (*section 10.1.4*).

		Controls	**ARM**
Full-Field	OP1 implicit time (ms)	18.28 (± 1.07)	19.35 (± 0.73)
	OP2 implicit time (ms)	24.19 (± 0.58)	27.00 (± 0.45)
	OP3 implicit time (ms)	30.99 (± 30.61)	34.27 (± 0.47)
	OP4 implicit time (ms)	38.52 (± 0.71)	42.63 (± 0.58)
	Summed OP amplitude	24.41 (± 1.97)	25.46 (± 2.21)
Focal	OP1 implicit time (ms)	19.03 (± 0.37)	17.27 (± 2.08)
	OP2 implicit time (ms)	24.79 (± 0.20)	25.26 (± 0.41)
	OP3 implicit time (ms)	31.27 (± 0.29)	31.61 (± 0.60)
	OP4 implicit time (ms)	38.11 (± 0.27)	38.55 (± 1.01)
	Summed OP amplitude	**6.10 (± 0.61)**	**3.74 (± 0.66)**
Ratio	**Focal : full-field summed OP amplitude**	**0.27 (± 0.03)**	**0.15 (± 0.03)**

Table 10.3. Mean implicit times of OPs 1-4, and summed focal and full-field OP amplitudes recorded in control subjects and subjects with ARM. Bold text indicates parameters which were significantly different between groups. Values in parentheses denote the SE of the mean.

The selective reduction in the amplitude of the focal OPs was reflected in a significantly smaller ratio of focal to full-field summed OP amplitudes in the ARM group than in controls (Mann-Whitney U test, z = -3.0; p = 0.003). This amplitude ratio showed the greatest difference between the results of control and ARM groups. In order to assess the sensitivity and specificity of this parameter, an ROC curve was constructed (*see Figure 10.9*). For an optimal cut-off of 0.23, a sensitivity of 74% and specificity of 61% was obtained.
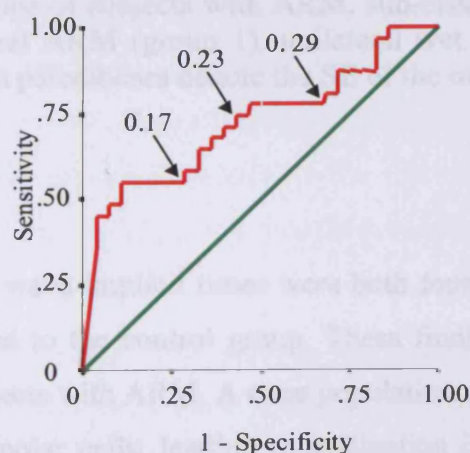
Figure 10.9. ROC curve showing sensitivity and specificity of the focal to full-field summed OP amplitude ratio in distinguishing between subjects with and without ARM. Arrows indicate cut-off criteria of curve.

Comparisons were then made between the three sub-groups of subjects with ARM i.e. those with bilateral ARM (group 1), those with unilateral wet AMD (group 2), and those with unilateral dry AMD (group 3). Table 10.4 shows the implicit times of OPs 1-4, and the summed OP amplitudes when averaged between these three groups. None of the differences between groups approached significance for any parameter.

		ARM		
		Group 1	*Group 2*	*Group 3*
Full-Field	OP1 implicit time (ms)	19.53 (± 0.46)	18.34 (± 2.04)	20.20 (± 0.52)
	OP2 implicit time (ms)	26.93 (± 0.61)	26.65 (± 1.04)	27.58 (± 0.60)
	OP3 implicit time (ms)	34.69 (± 0.60)	33.67 (± 1.09)	34.53 (± 0.57)
	OP4 implicit time (ms)	42.08 (± 0.90)	42.35 (± 1.15)	43.86 (± 0.70)
	Summed OP amplitude	23.17 (± 3.21)	26.59 (± 3.74)	27.33 (± 5.27)
Focal	OP1 implicit time (ms)	/	15.40 (± 1.60)	/
	OP2 implicit time (ms)	25.19 (± 0.92)	25.03 (± 0.57)	25.72 (± 0.66)
	OP3 implicit time (ms)	32.03 (± 0.89)	30.43 (± 1.12)	32.65 (± 1.07)
	OP4 implicit time (ms)	39.25 (± 1.24)	36.72 (± 2.12)	40.15 (± 1.35)
	Summed OP amplitude	3.15 (± 0.86)	5.04 (± 1.40)	2.84 (± 1.04)
Ratio	Focal : full-field summed OP amplitude	0.13 (± 0.03)	0.21 (± 0.06)	0.11 (± 0.04)

Table 10.4. Mean implicit times of OPs 1-4, and summed focal and full-field OP amplitudes recorded in the three groups of subjects with ARM, sub-classified according to the status of the fellow eye i.e. bilateral ARM (group 1), unilateral wet AMD (group 2), unilateral dry AMD (group 3). Values in parentheses denote the SE of the mean.

10.1.4 Discussion

The focal 5 Hz a- and b- wave implicit times were both found to be significantly delayed in the ARM group compared to the control group. These findings may be explained by cone photoreceptor loss in subjects with ARM. A cone population of reduced density would lead to a smaller input to the bipolar cells, leading to a situation in which the bipolar cells were relatively less light adapted in subjects with ARM compared to control subjects. This in turn could result in a prolonged implicit time of the b-wave response. As the peak of the a-wave is

hypothesised to be shaped by the rising edge of the positive response of the depolarising ON bipolars (*Robson & Frishman, 1999; Bush & Sieving, 1994*), a slowed bipolar response may also cause a delay in the a-wave implicit time.

Although the amplitude of focal a- and b- waves and the ratio of focal to full-field amplitudes were higher in all cases in the control group than the ARM group, this difference did not reach significance at the 5 % level. This may be partially explained by the variability in the amplitude of the focal ERG responses, which may be seen in Figures 10.2 and 10.3. This is in accordance with previous studies, which have suggested that the amplitude of ERG responses but not the implicit time is affected by factors such as axial length (*Chan & Mohidin, 2003*) and fundus pigmentation (*Wali & LeGuire, 1992*). The calculation of a ratio of focal to full-field response amplitude was a novel approach to reducing this inter-subject variability. The difference in the ratio of focal to full-field b-wave amplitude between groups did approach significance, with a p value of 0.085, suggesting that there was a differential loss of central cone function in the ARM group, which might have been shown to be statistically significant with a larger subject group. However, even after the calculation of a ratio, a considerable spread was seen in the data of subjects within each group. It must be remembered that the subject groups were classified on the basis of fundus appearance. The intersubject variability in response amplitude is suggestive of an underlying heterogeneity in the levels of cone function within each group, which may not be reflected in the severity of fundus changes.

The b-wave implicit time showed the greatest difference between the groups, but only achieved a diagnostic sensitivity of 74% and specificity of 64% with an optimal cut-off. This is due to considerable overlap in the averaged data of the two groups.

Comparison of the results of subjects with bilateral drusen (group 1) and those with unilateral wet (group 2) and dry (group 3) AMD showed no significant difference between groups for any parameter. Although, on the basis of the assumption that subjects in group 2 are more likely to develop choroidal neovascularisation in the test eye, this suggests that there is no evidence of a prognostic value to this test, a longitudinal study would be required to confirm this finding.

In previous studies of the transient focal ERG in AMD, small diameter, foveal stimuli have been used to look for correlations between ERG parameters and visual acuity (*Biersdorf & Diller, 1969*). The aim of this study was to assess a wider retinal area encompassing the entire macular region in order to highlight changes in function which precede visual acuity loss. The

results suggest that there are differences in central cone function between the ARM and control groups, which most likely reflect cone photoreceptor loss. However, these differences are relatively mild, and fail to reach significance with regard to amplitude measurements. This suggests that any changes in cone function which occur in early ARM are relatively modest.

Although the diagnostic and prognostic value of the test used in this study remains uncertain, it does provide a simple means of objectively assessing the integrity of the central retina, and holds potential as a means of longitudinally monitoring a subject's macular cone function.

In addition to consideration of the main components of the transient ERG waveform, band pass filtering was also used to isolate the oscillatory potentials. The assessment of the summed amplitude of focal OPs in this study indicated a significantly reduced amplitude of response in the ARM group compared to controls. The differential reduction in the amplitude of the macular OPs in subjects with ARM was reflected in a reduced mean ratio of focal to full-field summed OP amplitude, suggesting a selective loss of central retinal function.

In view of the proximal origin of the oscillatory potentials (*Ogden, 1973; Wachtmeister & Dowling, 1978; Heynen et al, 1985*), diseases affecting the inner retinal layers might be considered to be more likely to have an effect on the response recorded. For example, a reduction in OP amplitude is seen in diseases affecting the inner retinal circulation such as diabetic retinopathy, (*Hennekes, 1986, Bresnick, 1987, Drasdo et al, 2002*) and central retinal vein occlusion (*Yu et al, 1998*). Some dystrophies and degenerations, such as retinitis pigmentosa (*Cideciyan & Jacobsen, 1993*) and congenital stationary night blindness (*Heckenlively et al, 1983*), also affect OPs. However, a delay in the implicit time of OP2, and a reduction in amplitude of OP3 has also been noted in Stargardt's disease (*Lachapelle et al, 1989*), a disease with some phenotypic similarities to AMD (*Allikmetz et al, 1997; Fishman et al, 1991; Birnbach et al, 1994*). The effect of AMD on OPs has not previously been established in the literature, although one abstract has suggested that OP1 and OP2 may be reduced in the full-field ERG (*Zhang, 1994*).

The focal OPs recorded in this study showed a marked reduction in amplitude in subjects with early ARM to an extent that they were completely unmeasurable in 10 of the 32 subjects, compared to only 1 of the control subjects. However, the large intersubject variability in summed OP amplitude shown in Figure 10.6 makes this test unlikely to be useful diagnostically. Even the calculation of the ratio of focal to full-field response only partially

eliminated this variability, which is likely to be due to the small response amplitude, and poor signal to noise ratio. This rendered the test poor at discriminating between the subject groups.

Figure 10.8 shows the group averaged focal OP traces of subjects with ARM and age-matched controls. It may be seen that the large difference found in the mean summed amplitude data from the two groups is not reflected in the appearance of the group averaged traces. One explanation for this reduced difference would be that those subjects whose traces showed no measurable OPs, and thus whose summed amplitude was considered to be 0, did have small responses which were not distinguishable above noise level, but which were nonetheless present. When all the traces were averaged such time-locked signals would have been emphasised by constructive interference, whilst the random noise would have been diminished. Thus the 10 subjects with ARM whose summed OP amplitude was considered to be 0 µv, may have contributed to the amplitude of the focal OPs seen in the ARM group-averaged trace. The summed amplitude of the group-averaged trace was found to be 1.5 µv for subjects with ARM, and 1.6 µv for age-matched controls, thus the ARM group continued to show a reduced amplitude compared to the control group.

A comparison was also made between groups of the implicit time of the first 4 focal OPs, and no significant difference was found. This may be explained partially by the fact that the number of focal OPs measurable in each subject was very variable. In the assessment of focal OP1, only 8 control subjects, and 3 subjects with ARM actually exhibited a measurable response, although the number of subjects exhibiting OP2 (n = 27 and 20), OP3 (n = 27 and 17), and OP4 (n = 21 and 12) was greater. Furthermore, the OPs were numbered according to their approximate implicit time, but in a subject showing only 2 measurable OPs it is possible, for example, that a delayed OP2 would be assessed as an early OP3.

The finding in this study of reduced focal summed OP amplitude in subjects with ARM, and of a reduced focal to full-field summed amplitude ratio is suggestive of inner retinal spread of dysfunction in the disease. Literature also suggests that the oscillatory potentials are sensitive to abnormalities in the inner retinal circulation (*Speros & Price, 1981*), which is reflected in reports of OP abnormalities in vascular conditions such as diabetic retinopathy (*Hennekes, 1986, Bresnick, 1987, Drasdo et al, 2002*), systemic hypertension (*Ravilicio et al, 1995, Müller et al, 1984*), and vascular occlusions (*Yu et al, 1998*).

There is strong evidence to suggest that the choroidal circulation is affected in ARM and AMD. Abnormal choroidal filling characteristics in fluorescein angiography have been

reported in subjects with ARM, (*Pauleikhoff et al, 1990, Chen et al, 1992*), and measures of ocular blood flow velocity have indicated a reduced choroidal blood flow in both exudative and non-exudative AMD (*Friedman, 1995; Grunwald et al, 1998; Mori et al, 2001*). It has been hypothesised that age and diet-related atherosclerotic changes to the choroidal circulation are responsible for an increased vascular resistance, resulting in reduced blood flow (*Verhoeff & Grossman, 1937; Friedman et al, 1989; Vingerling et al, 1995d; Friedman 2004*). This hypothesis has been supported by histopathologic studies of donor eyes with ARM (*Green & Key, 1977; Green et al, 1985*). Furthermore, conditions which predispose toward atherosclerotic changes are also risk factors for the development of ARM and AMD (*Vingerling et al, 1995c; Friedman, 2000*). The finding of reduced amplitude OPs in individuals with ARM may suggest that vascular abnormalities extend to the inner retinal circulation.

10.2   The 41 Hz ERG

10.2.1 *Introduction*

This section describes the use of the 41 Hz focal ERG to assess central retinal function in subjects with ARM and control subjects.

Age-related macular degeneration primarily affects the outer retina, with the RPE and photoreceptor layer showing abnormalities at an early stage of the disease process (*Sarks, 1976; Green & Enger, 1993*). It has been suggested that the first harmonic of the steady state cone ERG reflects primarily outer retinal activity (*Porciatti et al, 1989*). Abnormalities in the focal 41 Hz ERG, which is dominated by this first harmonic, may therefore be expected in early ARM.

Studies using the focal 41 Hz ERG to assess outer retinal integrity in people with ARM have shown the test to be sensitive to early retinal changes (*Sandberg et al, 1993; Remulla et al, 1995; Sandberg et al, 1998; Falsini et al, 1999, Falsini et al, 2000*). In this study a protocol was developed to record a focal 41 Hz ERG from the central 20° of the retina of subjects with ARM and age-matched controls. This involved a larger stimulus than those used in previous studies, which might better reflect changes occurring across the whole macular region.

Full-field responses were also recorded in order to assess the focal to full-field amplitude ratio. It was hypothesised that subjects with ARM would show a reduction in the magnitude of this ratio as a result of the central retinal damage conferred by the disease.

10.2.2 Method

The general methods have been described in detail in chapters 6 and 7. The experimental parameters are summarised below.

- Focal ERGs were recorded in response to an amber (595nm), 20° diameter stimulus of 30 $cd.m^{-2}.sec^{-1}$ (1500 phot tds), flickering with a stimulus duration 12 ms, at a temporal frequency of 41 Hz. The stimulus was presented within a white ganzfeld surround, with a luminance of 30 $cd.m^{-2}.sec^{-1}$.

- Two hundred ERG responses were recorded, bandpass filtered from 1-100 Hz, and averaged on a 50 ms timebase.

- Full-field ERGs were then recorded to the same stimulus (595nm, 30 $cd.m^{-2}.sec^{-1}$, duration 12 ms, at a temporal frequency of 41 Hz).

- Peak to trough amplitude and implicit time were measured. Absolute values were assessed, as well as the ratio of focal to full field amplitude.

10.2.3 Results

Figure 10.10 shows typical focal 41 Hz ERGs recorded from 5 controls subjects and 5 subjects with ARM.
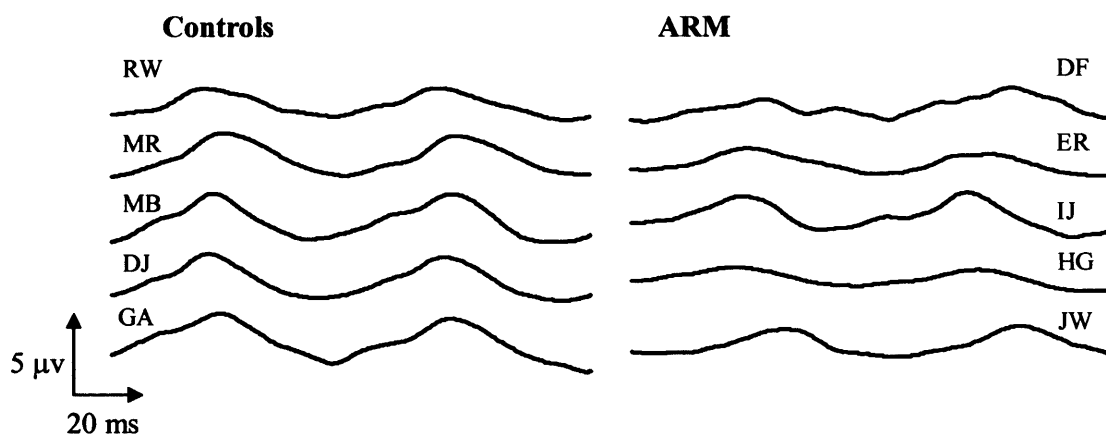
Figure 10.10. Typical focal 41 Hz responses recorded from 5 control subjects and 5 subjects with ARM.

The signal recorded approximates a sine wave showing two distinct peaks, and a trough. The parameters assessed for each subject were the peak-to-trough amplitude of the response, and the implicit time (time to first peak).

The amplitudes and implicit times obtained from each subject are shown in Figure 10.11. One subject with ARM (DG) had an unmeasurable focal 41 Hz response, and is therefore shown to have an amplitude of 0 μv.
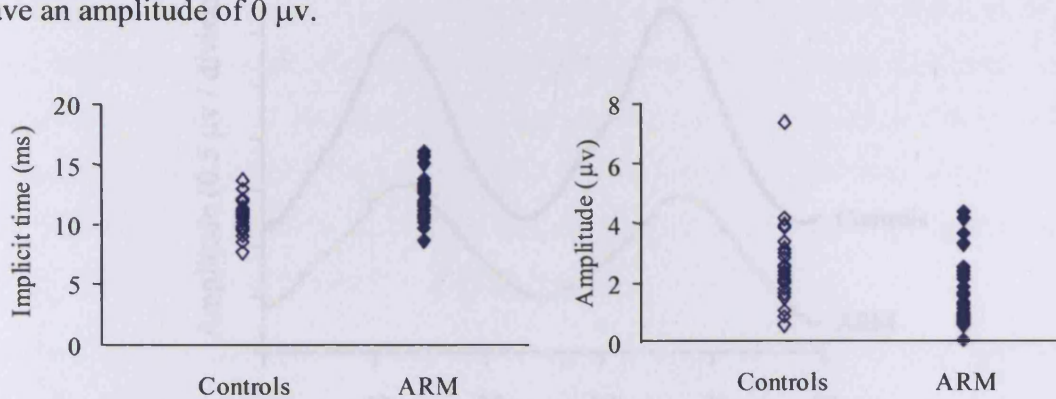
Figure 10.11. Scatter plots showing amplitude and implicit time of focal 41 Hz ERG recorded from control subjects and subjects with ARM.

Once again, considerable variability is seen in the amplitude of the response for both control and experimental groups. One control subject (DJ) had a focal response which was considerably larger than the other subjects, with an amplitude of 7.3 μv. In order to reduce the variability of amplitude results, the focal to full-field amplitude ratio was calculated. This data is shown in Figure 10.12.
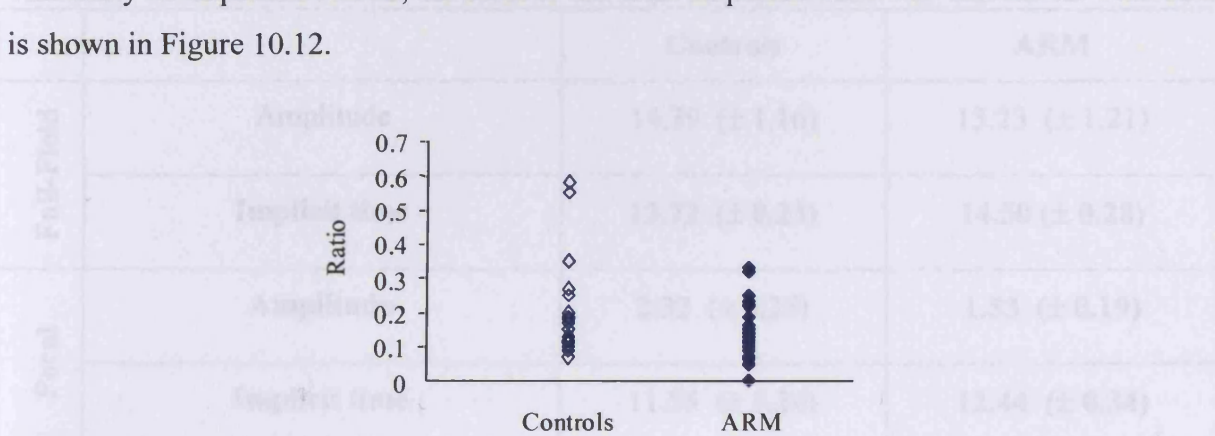
Figure 10.12. Scatter plot showing the focal to full-field 41 Hz ERG amplitude ratio, for control subjects and those with ARM.

The implicit time data shown in Figure 10.11 is considerably less variable within groups than the amplitude data. Although there is still considerable overlap between the data of individuals within the groups, there are 5 subjects with ARM (WT, JW, VW, DC, MG) whose implicit times fall completely outside the range of the control data i.e. have an implicit time longer than 14.0 ms. Three of these individuals had exudative AMD in the fellow eye.

Results were then averaged in order to assess any difference in the mean response characteristics between the control and ARM groups. Figure 10.13 shows the group-averaged focal responses recorded from control and ARM groups. The response of the ARM group is seen to be markedly smaller and more delayed than the signal of control subjects.
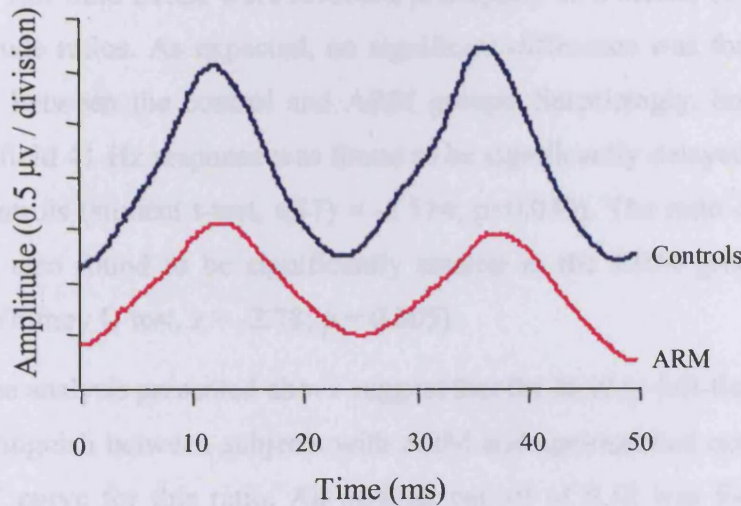
Figure 10.13. Group-averaged focal 41 Hz cone ERGs.

The group averaged amplitude and implicit time of the focal and full-field 41 Hz ERG responses from control subjects and subjects with ARM are shown in table 10.5.

		Controls	**ARM**
Full-Field	Amplitude	14.39 (± 1.16)	13.23 (± 1.21)
	Implicit time	**13.72 (± 0.23)**	**14.50 (± 0.28)**
Focal	**Amplitude**	**2.32 (± 0.25)**	**1.53 (± 0.19)**
	Implicit time	**11.55 (± 0.26)**	**12.44 (± 0.34)**
Ratio	**Focal : full-field amplitude**	**0.19 (± 0.02)**	**0.12 (± 0.01)**

Table 10.5. Mean implicit time and amplitude of 41 Hz ERG responses recorded in control subjects and subjects with ARM. Bold text indicates parameters which are significantly different between groups. Values in parentheses denote the SE of the mean.

Table 10.5 shows that the control group had a faster focal response of larger amplitude than the ARM group. This difference was found to be statistically significant with respect to both amplitude (Mann-Whitney U test, z = -2.73; p = 0.006) and implicit time (student t-test, t(57) = -2.082; p = 0.042).

Once again, the full-field ERGs were recorded principally as a means of calculating focal to full-field amplitude ratios. As expected, no significant difference was found in the full-field ERG amplitude between the control and ARM groups. Surprisingly, however, the implicit time of the full-field 41 Hz response was found to be significantly delayed in the ARM group compared to controls (student t-test, t(57) = -2.114; p=0.039). The ratio of focal to full-field amplitudes was also found to be significantly smaller in the ARM group than the control group (Mann-Whitney U test, z = -2.78; p = 0.005).

The results of the analysis presented above suggest that the focal to full-field amplitude data is best able to distinguish between subjects with ARM and age-matched controls. Figure 10.14 shows the ROC curve for this ratio. An optimal cut-off of 0.12 was found to differentiate between groups with a sensitivity of 65 % and a specificity of 79%.
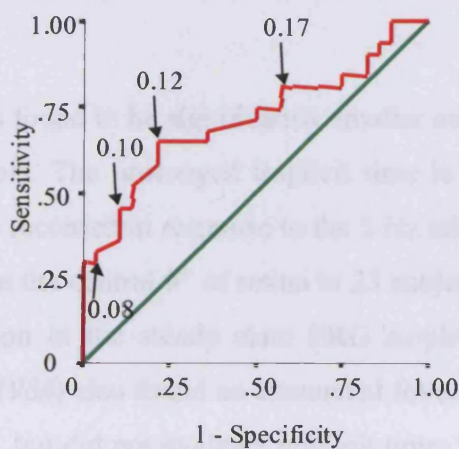
Figure 10.14. ROC curve showing sensitivity and specificity of the focal to full-field 41 Hz ERG amplitude ratio in distinguishing between subjects with and without ARM. Arrows indicate cut-off criteria of curve.

Table 10.6 shows the group averaged 41 Hz ERG data for subjects with ARM when subclassified according to the status of the fellow eye i.e. bilateral ARM (group 1), unilateral wet AMD (group 2), and unilateral dry AMD (group 3). Comparison of response amplitude and implicit times, and the focal to full-field amplitude ratio all showed no significant difference between the three groups (Kruskal-Wallis, χ2(2) = 0.45; p = 0.80; ANOVA, F(2,28) = 1.83; p = 0.18; ANOVA, F(2,28) = 1.46; p = 0.25).

		ARM		
		Group 1	*Group 2*	*Group 3*
Full-Field	Amplitude	11.64 (± 1.30)	12.84 (± 1.50)	16.14 (± 3.74)
	Implicit time	13.95 (± 0.58)	15.19 (± 0.37)	14.36 (± 0.31)
Focal	Amplitude	1.74 (± 0.35)	1.39 (± 0.35)	1.39 (± 0.27)
	Implicit time	11.70 (± 0.58)	13.18 (± 0.49)	12.53 (± 0.68)
Ratio	Focal : full-field amplitude	0.15 (± 0.03)	0.11 (± 0.03)	0.097 (±0.01)

Table 10.6. Mean amplitude and implicit time of focal and full-field 41 Hz ERG responses recorded in the three groups of subjects with ARM, sub-classified according to the status of the fellow eye i.e. bilateral ARM (group 1), unilateral wet AMD (group 2), and unilateral dry AMD (group 3). Values in parentheses denote the SE of the mean.

10.2.4 Discussion

The focal 41 Hz ERG was found to be significantly smaller and more delayed in subjects with ARM compared to controls. The prolonged implicit time is in accordance with the slowed focal cone a- and b-waves recorded in response to the 5 Hz stimulus. Falsini et al (*1999*), used the 32 Hz ERG to evaluate the central 9° of retina in 25 subjects with bilateral dry AMD, and similarly found a reduction in the steady state ERG amplitude compared to age-matched controls. Birch and Fish (*1988*) also found an attenuated foveal steady state ERG amplitude in 49 individuals with AMD, but did not evaluate implicit time. However, Sandberg et al (*1993*) found a significantly delayed 42 Hz ERG response in subjects with unilateral choroidal neovascularisation in the fellow eye.

The 41 Hz ERG is dominated by the first harmonic of the steady state response (*Remulla et al, 1995; Falsini et al, 2000*), which has been attributed to outer retinal activity (*Porciatti et al, 1989*). As the outer retina is the primary locus of dysfunction in ARM, this response might be expected to be sensitive to early changes in macular function. The a-wave of the transient ERG also originates in the outer retina, but is smaller in amplitude than the peak to trough amplitude of the steady state ERG, leading to a poor signal to noise ratio. Furthermore,

although the a-wave of the photopic ERG largely reflects photoreceptoral activity, it has been shown that both depolarising and hyperpolarising second order neurones also contribute to the waveform (*Knapp et al, 1984; Evers et al, 1986; Bush & Sieving, 1994*). The 41 Hz may therefore provide a stronger measure of outer retinal activity. This may explain why the difference in the 41 Hz ERG amplitude reached significance, while the difference in the 5 Hz ERG amplitude did not.

A more surprising finding was the significant delay in implicit time found for the full-field 41 Hz ERG in the ARM group compared to controls. This could be attributable to a deficit in outer retinal function which extends beyond the macular region. However, there was no significant difference in the amplitude of the full-field responses between groups, and the larger focal to full-field amplitude ratio in control subjects supported a preferential loss of macular function in individuals with ARM.

The focal to full-field amplitude ratio was the parameter of the 41 Hz ERG which best distinguished between subjects with ARM and control subjects. Diagnostically it was shown to have a sensitivity of 65% and a specificity of 79% with an optimal cut-off point. The ratio might be expected to be more sensitive to early retinal changes than absolute amplitude values, through the minimisation of inter-subject variability conferred by extraneous factors such as axial length and fundus pigmentation. However, there is considerable overlap between the two groups in the response ratios of individuals (as illustrated in Figure 10.12), which reflects a true range in the level of macular function within the two groups.

None of the parameters showed a significant difference between the subgroups of subjects with ARM. However, examination of the focal 41 Hz ERG implicit times of individual subjects did show 5 subjects with ARM whose results fell outside the range of responses of the control group. Three of these individuals had exudative AMD in the second eye. This suggests that certain individuals within the unilateral choroidal neovascularisation subgroup are showing a more abnormal level of retinal function than others within that group. A follow-up of these individuals over a period of time would determine whether the prolonged implicit times of these three subjects are indicative of impending neovascular changes.

The finding that the 41 Hz focal cone ERG implicit time may have value in identifying subjects vulnerable to neovascular changes is supported by previous reports (*Remulla et al, 1995; Sandberg et al, 1998*). Remulla et al (*1995*) used a 42 Hz stimulus of 4° diameter to assess retinal function in 67 subjects with macular drusen in the test eye and unilateral wet

AMD in the fellow eye. A delayed ERG was reported in those subjects assessed by fluorescein angiography to be at high risk of developing choroidal neovascularisation in their second eye. Sandberg (*1998*) also found a prolonged implicit time in approximately 20% of 127 subjects with unilateral choroidal neovascularisation. After a 4.5 year follow-up period it seemed that longer delays in the baseline ERG timing were associated with an earlier onset of neovascularisation in those subjects who went on to develop bilateral exudative AMD. Sandberg (*1998*) suggested that the slowed foveal ERG implicit time might be a sign of retinal ischaemia preceding choroidal neovascularisation.

10.3   The S-Cone ERG and VEP

10.3.1 Introduction

The S-cone photoreceptors are believed to be vulnerable to damage in macular disease. This finding has been ascribed to a vulnerability of these receptors to light and oxidative damage (*Ham et al, 1978; Sperling et al, 1980*) and a susceptibility to metabolic damage (*DeMonasterio et al, 1981*).

The presence of tritanopic colour vision defects (*Bowman et al, 1979; Collins et al, 1986; Eisner et al, 1991; Cheng & Vingrys, 1993*), and reduced S-cone sensitivity (*Sunness et al, 1989; Eisner et al, 1991*), as discussed in chapter 5, are indicative of a selective disruption of the short wavelength sensitive pathway in early ARM. Furthermore, there is evidence to suggest that an elevation of S-cone thresholds may be indicative of incipient neovascular changes in these individuals (*Eisner et al, 1992*), although the sensitivity and specificity of this parameter as a predictive test were poor. There is no published literature regarding the effect of AMD on the S-cone electroretinogram or VEP.

The aim of this study was to assess the integrity of the S-cone pathway using electrophysiological techniques. As well as a measurement of the a- and b-wave amplitudes, allowing an assay of outer retinal and bipolar cell function, the PhNR was also measured. The PhNR is believed to originate from the retinal ganglion cells (*Viswanathan, 1999, 2000*) and a recent study suggested that the S-cone PhNR was sensitive to ganglion cell loss in glaucoma (*Drasdo et al, 2001*). Anatomical studies have found the ganglion cell layer to be preserved in non-exudative AMD (*Medeiros et al, 2001*). However, the PhNR is the largest amplitude waveform of the S-cone ERG, and thus provides the best signal to noise ratio. Any marked

abnormality in photoreceptor cell function will also be reflected in a reduced signal at the level of the ganglion cells.

This section describes the recording of full-field S-cone ERGs and VEPs from control subjects, and subjects with ARM.

10.3.2 Method

Chapter 6 has described the development of the full-field S-cone ERG protocol used in this study. The same stimulus was also used to record simultaneous VEP responses. Since the VEP is dominated by central retinal function, this was included as a means of highlighting changes in central S-cone function. S-cone ERGs and VEPs were recorded from the control and ARM groups. The experimental parameters are summarised below.

- The red (664nm) LEDs of the LED stimulator were set to a continuous luminance of 120 cd.m^{-2}. In addition, the green (535nm) and blue (454nm) LEDs were modulated to flicker in counterphase at a frequency of 33 Hz, with the blue light illuminated for 50% of the time in the 'ON' phase, and the green light illuminated in the 'OFF' phase. The luminance of the green LEDs was set at 12 cd.m^{-2}.sec^{-1}.

- The required luminance of the blue LEDs was then determined individually for each subject by heterochromic flicker photometry. The subject held the head stage of the LED stimulator adjacent to their eye, providing a full-field visual stimulus. The luminance of the blue LEDs was set to a level above or below the flicker balance, at which point a flicker was obvious to the subject. The luminance was then gradually shifted towards the flicker balance point, and the subject was instructed to inform the investigator of the precise moment at which the flicker appeared to cease. The luminance of the blue LEDs at this point was recorded. This process was repeated twice starting at a luminance above the flicker balance, and twice starting below the flicker balance. The 4 end points were averaged, and the luminance of the blue LEDs was set at this value.

- The frequency at which the blue and green LEDs flickered was then reduced to 1.67 Hz, whilst maintaining the 50% duty cycle.

- Two hundred ERG and VEP responses were then amplified, bandpass filtered from 1-100 Hz, and averaged on a 500 ms timebase.

- The amplitude and implicit time of the a- and b- waves and the PhNR were assessed for each subject. Absolute values were assessed, as well as the ratio of a to b wave amplitude.

- VEP responses were group averaged off-line, and the implicit time and amplitude of major peaks and troughs compared between control and subject groups.

10.3.3 ERG Results

Figure 10.15 shows typical S-cone ERGs recorded from 5 control subjects and five subjects with ARM. It may be seen that the amplitude of the a-wave was generally small, but a distinct b-wave and PhNR were recorded from most subjects. S-cone ERGs were not obtained from 5 subjects with ARM (JA, JW, KG, FB, BR) and 5 controls (GO, PA, GW, VB, BB) for pragmatic reasons, explained in the discussion.
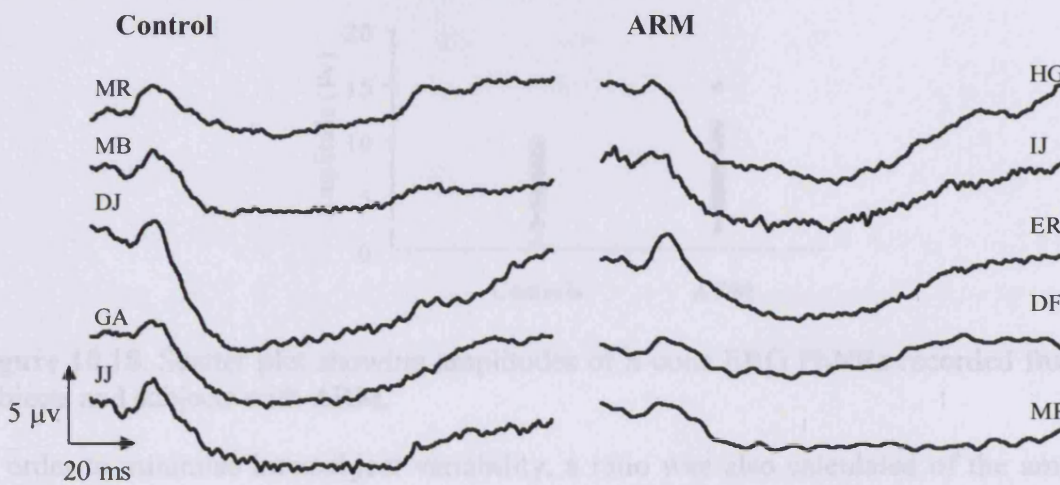
Figure 10.15. Typical S-cone ERG responses recorded from 5 control subjects and 5 subjects with ARM.

The inter-subject variability in both implicit times and amplitudes of the a- wave, b-wave and PhNR was considerable within both groups. This is illustrated in Figures 10.16, 10.17, and 10.18, which show the characteristics of the a-wave, b-wave and PhNR of subjects within both groups.
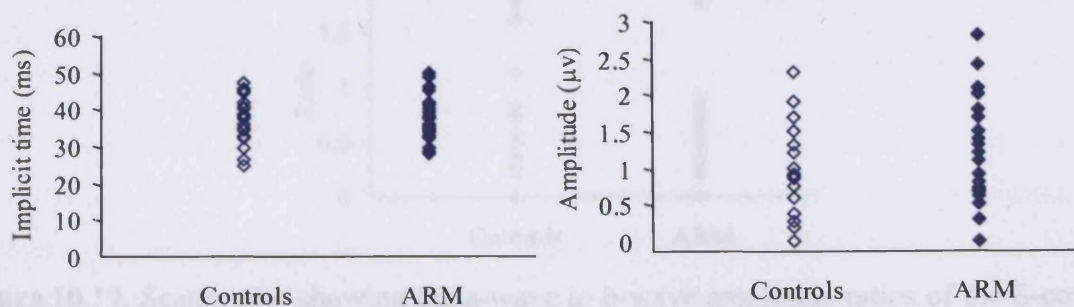
Figure 10.16. Scatter plots showing amplitudes and implicit times of S-cone ERG a-waves recorded from control subjects and subjects with ARM.
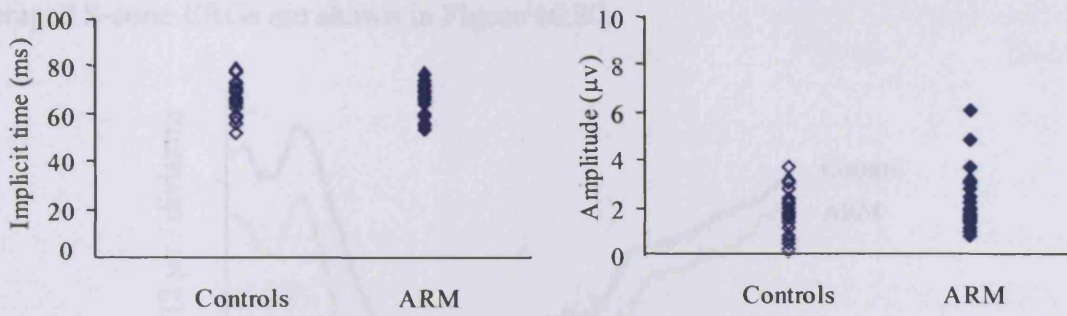
Figure 10.17. Scatter plots showing amplitudes and implicit times of S-cone ERG b-waves recorded from control subjects and subjects with ARM.
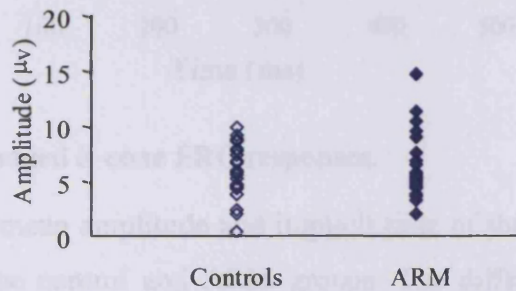
Figure 10.18. Scatter plot showing amplitudes of S-cone ERG PhNRs recorded from control subjects and subjects with ARM.

In order to minimise intersubject variability, a ratio was also calculated of the amplitude of the a-wave to the amplitude of the b-wave. The scatter plot in Figure 10.19 shows the spread of ratios calculated for subjects in both groups. There remains considerable variability in the responses within the groups. In some cases the a-wave was unrecordable, and the ratio calculated was 0, whilst in others the a-wave was almost double the size of the b-wave, resulting in a ratio approaching 2.
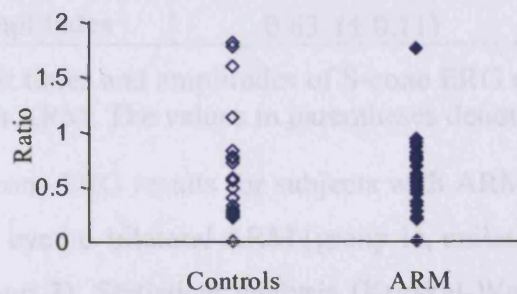
Figure 10.19. Scatter plot showing the a-wave to b-wave amplitude ratios of the S-cone ERG recorded in control subjects and subjects with ARM.

Comparisons were then made between the control and ARM mean ERG responses. The group averaged S-cone ERGs are shown in Figure 10.20.
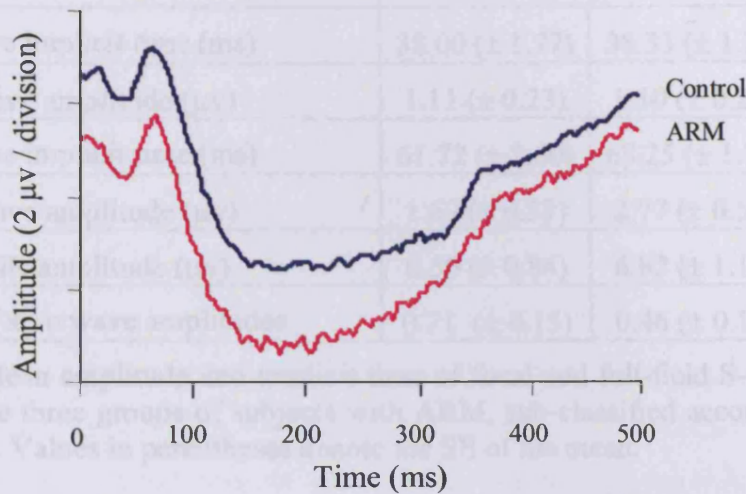
Figure 10.20. Group-averaged S-cone ERG responses.

Table 10.7 describes the mean amplitude and implicit time of the a-wave, b-wave and PhNR of the S-cone ERG of the control and ARM groups. The differences between control and ARM groups failed to approach significance for any parameter, including the a- to b-wave amplitude ratio.

	Controls	**ARM**
a-wave implicit time (ms)	37.55 (± 1.42)	37.90 (± 1.21)
a-wave amplitude (μv)	0.92 (± 0.12)	1.15 (± 0.14)
b-wave implicit time (ms)	65.24 (± 1.42)	65.52 (± 1.31)
b-wave amplitude (μv)	1.74 (± 0.18)	2.23 (± 0.26)
PhNR amplitude (μv)	5.79 (± 0.48)	6.35 (± 0.56)
Ratio of a : b wave amplitudes	0.63 (± 0.11)	0.58 (± 0.69)

Table 10.7. Mean implicit times and amplitudes of S-cone ERG responses recorded in control subjects and subjects with ARM. The values in parentheses denote the SE of the mean.

Table 10.8 shows the S-cone ERG results for subjects with ARM, when regrouped according to the status of the fellow eye i.e. bilateral ARM (group 1), unilateral wet AMD (group 2), and unilateral dry AMD (group 3). Statistical analysis (Kruskal-Wallis) indicated no significant difference in the S-cone ERG parameters between the three sub-groups.

	ARM		
	Group 1	*Group 2*	*Group 3*
a-wave implicit time (ms)	38.00 (± 1.77)	38.33 (± 1.26)	37.08 (± 3.93)
a-wave amplitude (µv)	1.11 (± 0.23)	1.10 (± 0.24)	1.28 (± 0.25)
b-wave implicit time (ms)	61.72 (± 2.60)	68.25 (± 1.74)	66.67 (± 1.39)
b-wave amplitude (µv)	1.69 (± 0.33)	2.77 (± 0.54)	2.22 (± 0.28)
PhNR amplitude (µv)	6.50 (± 0.84)	6.82 (± 1.18)	5.32 (± 0.37)
Ratio of a : b wave amplitudes	0.71 (± 0.15)	0.46 (± 0.10)	0.58 (± 0.08)

Table 10.8. Mean amplitude and implicit time of focal and full-field S-cone ERG responses recorded in the three groups of subjects with ARM, sub-classified according to the status of the fellow eye. Values in parentheses denote the SE of the mean.

10.3.4 VEP Results

The S-cone VEP responses were complex, and showed great inter-individual variability in the implicit time and amplitude of peaks and troughs, even within the control group of subjects (*see Figure 10.21*). This prevented the direct comparison of the amplitude and latency of the components of different individuals' waveforms. It was not possible to obtain S-cone VEPs from 5 subjects with ARM (JA, JW, MP, VW, BR) and 5 controls (GO, CD, PA, BB, VB).

A similar problem was encountered in the assessment of the rod VEPs (*see section 9.2.2*), and the same technique was employed in both cases to assess the responses.
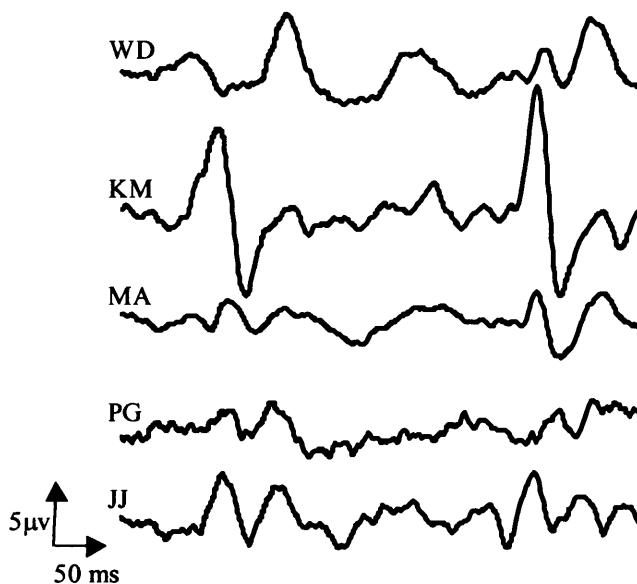
Figure 10.21. Typical S-cone VEP responses recorded from 5 control subjects. The inter-individual variation in response waveform may clearly be seen.

Following the protocol described by Drasdo et al (*2003*), the individual VEP responses were group-averaged, and the mean ARM response was subtracted from the mean control response. The group-averaged S-cone VEP consisted of a complex but well-defined waveform (*see Figure 10.22*). The subtraction of the averaged ARM waveform from the averaged control response elicited a 'difference signal' consisting of peaks and troughs at implicit times corresponding to amplitude differences between the two group-averaged VEP responses. These implicit times were measured and marked upon each subject's VEP trace, regardless of whether these points corresponded to a peak or trough of that particular response. Each individual response was then assessed for amplitude changes between these time points. The times of greatest amplitude change in the 'difference signal' were measured to be at 44.5 – 92.5 ms and 133.5 – 166.5 ms (ON- response), and 344.5 – 394.5 and 430.5 – 462.5 ms (OFF- response). Table 10.9 shows the average amplitude change between these points for the ARM and control groups. Statistical analysis showed no significant difference between groups in these measurements.
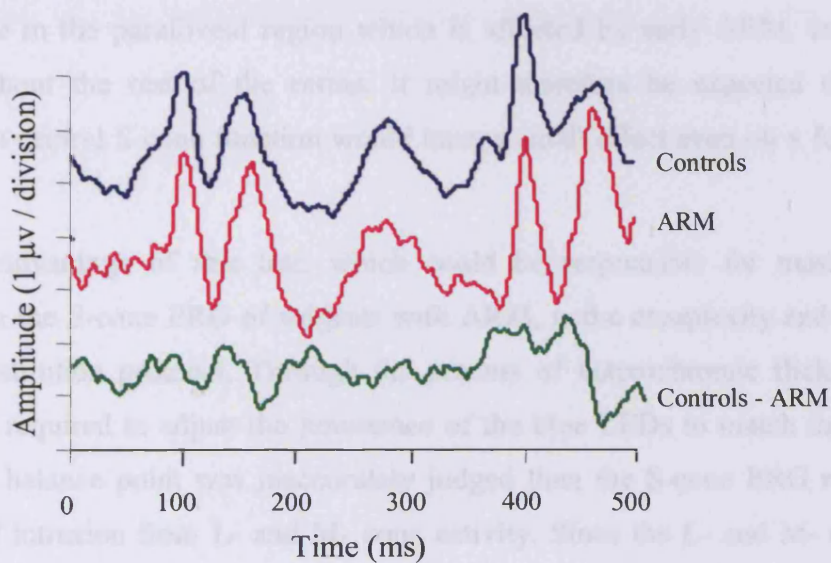
Figure 10.22. Group-averaged S-cone VEP responses, and the subtraction of one from the other to obtain a 'difference signal'.

	Controls	**ARM**
Amplitude between 44.5-92.5 ms	2.65 (± 0.38)	2.41 (± 0.40)
Amplitude between 133–166.5 ms	2.90 (± 0.60)	2.70 (± 0.52)
Amplitude between 344-394.5 ms	3.43 (± 0.49)	2.83 (± 0.40)
Amplitude between 430-462.5 ms	3.20 (± 0.57	3.56 (± 0.70)

Table 10.9. Mean S-cone VEP response amplitudes measured at predetermined times.

10.3.5 Discussion

This study found no significant difference in any parameter between the control and ARM groups for the S-cone ERG or VEP.

No previous studies have considered the effect of ARM on the S-cone ERG response, although psychophysical evidence does suggest a selective dysfunction of the short-wavelength pathway early in the disease process (*Eisner et al, 1987; Haegerstrom- Portnoy et al, 1988; Collins & Brown, 1989; Sunness et al, 1989; Eisner et al, 1991; 1992, Cheng & Vingrys, 1993*). However, colour vision tests and psychophysical assessment of foveal S-cone sensitivity all assess the function of the central retina, rather than the pan-retinal S-cone activity measured in the ERG.

For pragmatic reasons the S-cone ERG was recorded in this study in response to a full-field stimulus. This could explain the fact that no significant difference was found for any parameter between the control and experimental groups. However, the S-cone population is at its most dense in the parafoveal region which is affected by early ARM, and is relatively sparse throughout the rest of the retina. It might therefore be expected that any major abnormality in central S-cone function would have a small effect even on a full-field S-cone ERG.

A further disadvantage of this test, which could be responsible for masking any such abnormality in the S-cone ERG of subjects with ARM, is the complexity and subjectivity of the silent substitution protocol. Through the process of heterochromic flicker photometry, subjects were required to adjust the luminance of the blue LEDs to match that of the green LEDs. If this balance point was inaccurately judged then the S-cone ERG recorded would show signs of intrusion from L- and M- cone activity. Since the L- and M- cone responses overlap with the S-cone response, the amplitude and implicit time of the ERG waveforms may have been distorted by this intrusion. It may be seen in the group-averaged S-cone ERG responses in Figure 10.20 that there is a second peak on both traces at approximately 350 ms. The OFF response of the S-cone system, if it does exist at a retinal level, is not seen in the pure S-cone ERG. This late peak is therefore likely to reflect M-cone intrusion. In the elderly subject group assessed in this study, it was difficult to obtain a good heterochromic flicker balance.

Six subjects were unable to perform the heterochromic flicker balance at all. The data of a further 3 subjects were rejected due to problems associated with the large number of averages

required, and the long timebase. Traces were either contaminated by eye movements, or rejected by the artefact reject setting such that an insufficient number of averages was obtained.

The S-cone VEP was also assessed in this study as a means of assessing central retinal function. The great inter-subject variability in waveform, reported previously in our lab by Drasdo et al (*2003*), as well as the difficulty in achieving an accurate heterochromic flicker balance may have contributed to the inability of this test to find any significant difference between the control and ARM groups for S-cone function. Furthermore, as with the rod VEP, it must be remembered that the S-cone VEP is a reflection of the cortical processing of a signal. The modification of the visual information as it passes from photoreceptor to visual cortex might mask any small abnormalities in outer retinal function.

In summary this study has found no electrophysiological evidence of an S-cone abnormality in individuals with ARM, but this may be due to problems associated with the extent of the retina stimulated and the application of the silent substitution technique to an elderly test group.

CHAPTER 11 : THE DYNAMIC FOCAL CONE ERG

11.1   Introduction

This chapter describes the use of the dynamic focal ERG technique to assess photostress recovery in subjects with ARM and controls.

Previous reports have indicated that the macular recovery function is delayed following exposure to a bright light in subjects with AMD (*Smiddy and Fine, 1984; Collins and Brown, 1989; Sandberg and Gaudio, 1995; Midena et al., 1997; Phipps et al., 2003; Wu et al., 1990*). In these studies recovery has been defined as the return of visual acuity. The time reported for the return of visual acuity in control subjects and subjects with ARM has varied depending on the nature of the acuity task, the extent of cone photopigment bleached, and the characteristics of the test group. For example, Cheng & Vingrys (*1993*) found controls to have a recovery time of 20-45 seconds, whilst the range of recovery times for subjects with ARM was 15-165 seconds. In contrast, Sandberg & Gaudio (*1995*) found the upper limit for normal controls to be 100 seconds, with ARM subjects taking between 17-600 seconds for full recovery. However, the ARM group in Sandberg's study consisted of 133 subjects with exudative AMD in the fellow eye (*Sandberg & Gaudio, 1995*), compared to only 11 subjects with early ARM who participated in the study by Cheng & Vingrys (*1993*).

Techniques involving the use of an acuity task to monitor retinal recovery are hindered by the variability conferred by the subjective nature of the task. In this study an objective electroretinographic measure of visual function was used to assess retinal recovery. There is no literature describing the use of the electroretinogram to monitor photostress recovery, although the use of the pattern VEP for this purpose has been reported (*Lovasik, 1983; Franchi et al, 1987; Parisi & Bucci, 1992; Parisi et al, 1995; Parisi et al, 1998; Parisi et al, 2002*). The VEP photostress recovery technique has not been evaluated in subjects with ARM or AMD, but literature suggests that the normal amplitude and latency recovery time in control subjects ranges from 68-78 seconds (*Parisi et al, 2001*). Lovasik (*1983*) reported that VEP recovery took longer for most control subjects than the return of baseline visual acuity.

Although the monitoring of VEP recovery does provide an objective means of assessing retinal adaptation following exposure to a bright adapting light, it does not allow a direct assessment of outer retinal function. An abnormal recovery time has been reported using the standard photostress recovery test, and the VEP photostress recovery test in diseases such as

237

primary open angle glaucoma (*Parisi & Bucci, 1992; Horiguchi et al, 1998; Sherman, 1988*) and optic neuritis (*Campos et al, 1980; Parisi et al, 1998*). This suggests that previously documented photostress recovery techniques, whilst obviously largely reflecting the integrity of the distal retina, are also influenced by inner retinal function and optic nerve activity.

Section 6.7 has described the development of a protocol designed to allow an objective assessment of retinal adaptation following exposure to a high intensity light. In this technique the recovery of the 41 Hz ERG following a photopigment bleach was assessed by modelling amplitude data with an exponential function. The 41 Hz ERG signal is dominated by the first harmonic, which is believed to reflect photoreceptoral activity (*Porciatti et al, 1989; Remulla et al, 1995; Falsini et al, 2000*). The recovery of this response should therefore provide a more direct measure of photoreceptor recovery than the psychophysical and VEP techniques previously employed.

11.2   Method

The general methods have been described in detail in chapters 6 and 7. The experimental parameters are summarised below.

- Focal ERGs were recorded in response to a 20° diameter, square wave amber (595 nm) stimulus with a luminance of 30 $cd.m^{-2}.sec^{-1}$, flickering at a temporal frequency of 41 Hz. This was presented within a white ganzfeld surround with a luminance of 30 $cd.m^{-2}$.

- A pre-bleach 41 Hz focal cone ERG was recorded as a baseline measure. One hundred ERG responses were recorded, bandpass filtered from 1-100 Hz, and averaged on a 50 ms timebase.

- The test eye was subsequently light-adapted to a bright white background (5.6 log trolands) for a period of 2 minutes, resulting in an approximately 85% bleach of cone visual pigment (*Hollins & Alpern, 1973*). The light-adapting background subtended a circular area of 40 degrees diameter. It consisted of extra halogen bulb illumination of the lower portion of the ganzfeld bowl. There was a fixation cross in the centre of the adapting background.

- Following light adaptation the bright background was turned off, and the subject asked to fixate the centre of the flickering amber LED stimulus directly ahead of them, at the centre of the bowl.

- The 41 Hz focal cone ERG was then recorded at 20 second intervals for a period of 5 minutes. One hundred responses were averaged each time, which took approximately 10 seconds. The subject then had 10 seconds to relax before the next signal was recorded. Figure 11.1 illustrates the timecourse of the recording.

- In order to objectify the amplitude measurements, individual traces were modelled using a cosine function in the form:

  Amp(t) = (m.t + c) + ([Amp/2] x cos [k/t]) , in which t = time in ms, m = constant allowing for drift, c = constant allowing for bias, Amp = amplitude in μv, and k = 543.2 (constant to convert ms to radians).

- Amplitude recovery data were also modelled with an exponential function in the form:

  Amp(t) = a.(1-exp(-0.693(t-x) /τ), in which a = final amplitude in μv, t = time, x = x-axis intersect, τ = time constant of recovery. Final amplitude was designated as the pre-bleach ERG amplitude, and the other parameters were adjusted to achieve the best fit to the data, on a least squares basis. The x-axis intersect was constrained to be equal to, or greater than 0.
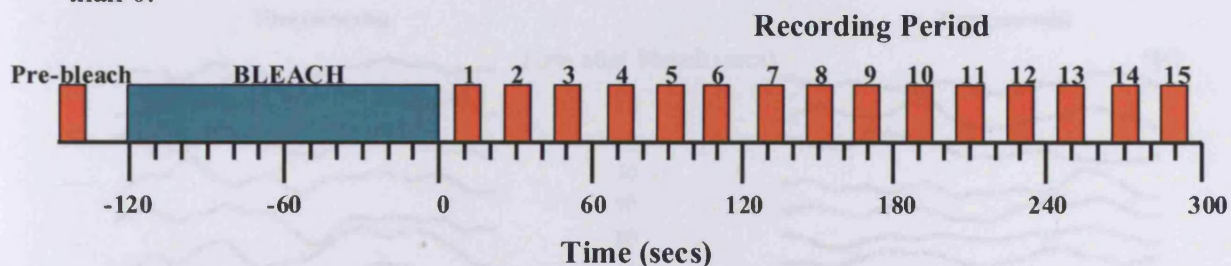
Figure 11.1. Timeline showing sequence of events in the recording of the dynamic focal cone ERG.

11.3   Results

All data were modelled as described above, and the time constant of recovery extracted from the exponential model. Nine subjects with ARM, and 1 control subject (PS) failed to show any appreciable recovery of the ERG amplitude over the five minutes (300 seconds) during which 41 Hz ERG amplitude was monitored. Two of these individuals had bilateral drusen (ERe, DB), five had wet AMD in the fellow eye (JW, ER, MP, AF, DG), and two had dry AMD in the fellow eye (PB, DF). The results of these subjects have not been included in subsequent analysis of group averaged data.

Figure 11.2 shows typical ERG responses and recovery curves for 2 control subjects (top traces), and 2 subjects with ARM (lower 2 traces).
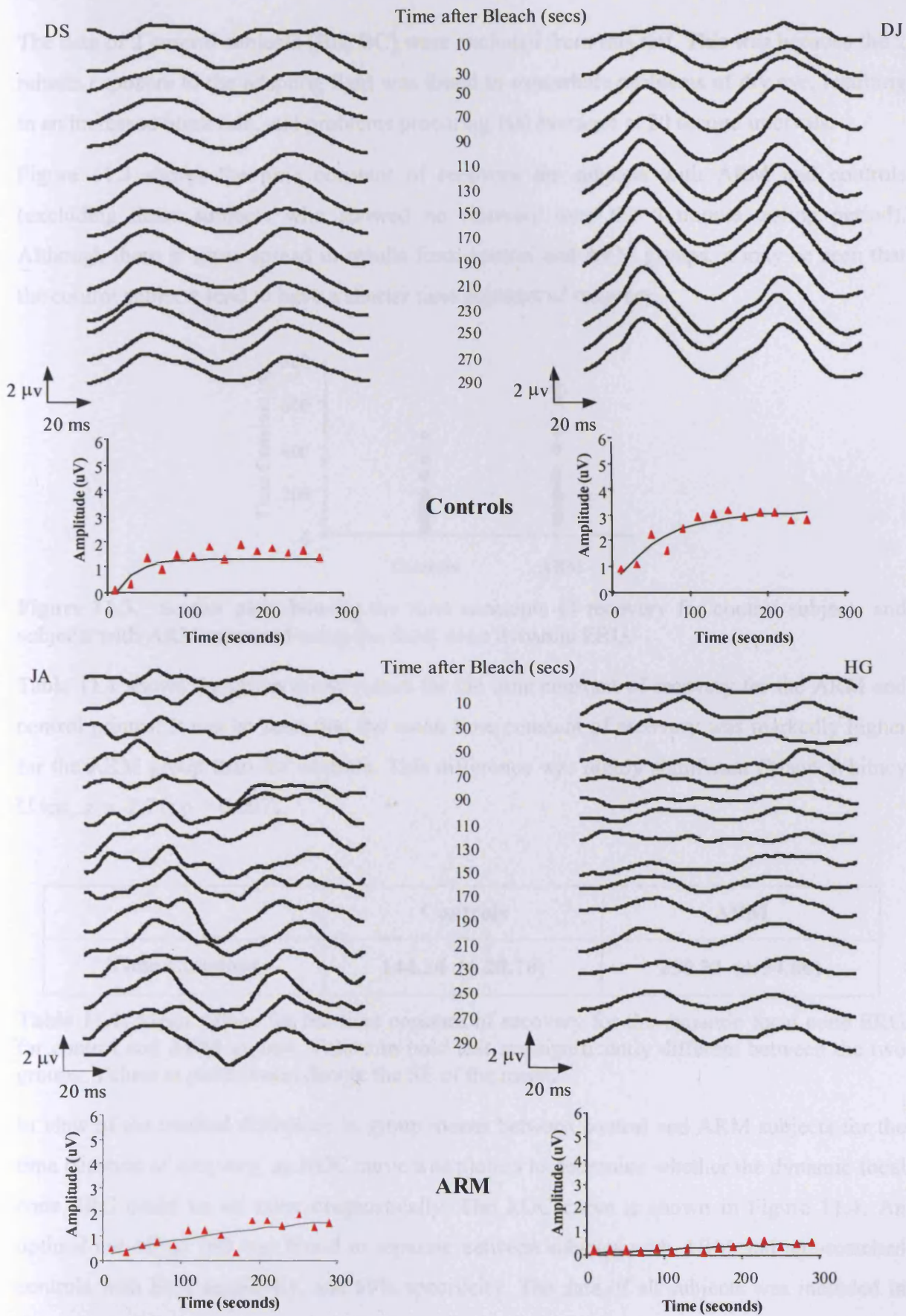
Figure 11.2. Typical dynamic focal cone ERG recovery data from two control subjects (upper traces) and two subjects with ARM (lower traces).

The data of 2 control subjects (BB, BC) were excluded from this test. This was because the 2 minute exposure to the adapting light was found to exacerbate problems of dry eye, resulting in an increased blink rate, and problems procuring 100 averages at 20 second intervals.

Figure 11.3 shows the time constant of recovery for subjects with ARM and controls (excluding those subjects who showed no recovery over the 5 minute testing period). Although there is some spread in results from control and ARM groups, it may be seen that the control subjects tend to have a shorter time constant of recovery.
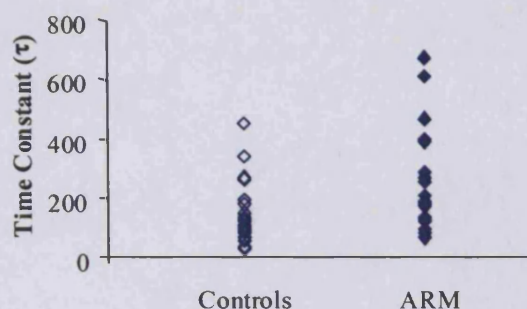
Figure 11.3. Scatter plot showing the time constants of recovery for control subjects and subjects with ARM, assessed using the focal cone dynamic ERG.

Table 11.1 shows the group mean values for the time constant of recovery for the ARM and control groups. It can be seen that the mean time constant of recovery was markedly higher for the ARM group than for controls. This difference was highly significant (Mann Whitney U test, $z = -2.71$; $p = 0.007$).

	Controls	**ARM**
Time Constant	**144.24 ($\pm$ 20.78)**	**250.23 ($\pm$ 34.80)**

Table 11.1. Mean values for the time constant of recovery for the dynamic focal cone ERG for control and ARM groups. Values in bold text are significantly different between the two groups. Values in parentheses denote the SE of the mean.

In view of the marked difference in group means between control and ARM subjects for the time constant of recovery, an ROC curve was plotted to determine whether the dynamic focal cone ERG could be of value diagnostically. The ROC curve is shown in Figure 11.4. An optimal cut-off of 160 was found to separate between subjects with ARM and age-matched controls with 81% sensitivity, and 69% specificity. The data of all subjects was included in this calculation, with those who failed to show recovery in 5 minutes being classified as having a time constant of recovery longer than the cut-off determined by the ROC curve.
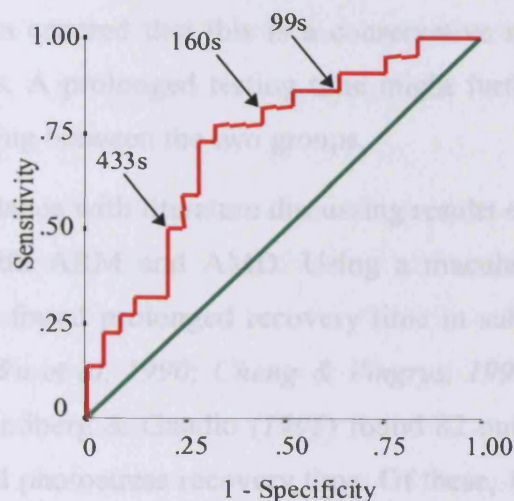
Figure 11.4. ROC curve showing sensitivity and specificity of time constant of dynamic ERG recovery in distinguishing between subjects with and without ARM. Arrows indicate cut-off criteria of curve.

The data were then recategorised according to the status of the fellow eye of subjects with ARM i.e. bilateral ARM (group 1), unilateral wet AMD (group 2), unilateral dry AMD (group 3). The mean values for the time constant of recovery within these groups may be seen in table 11.2. Statistical analysis indicated that there was no significant difference between the 3 groups (ANOVA; $F(2,19) = 0.380$, $p = 0.689$).

	ARM		
	Group 1	*Group 2*	*Group 3*
Time Constant	244.08 (± 56.41)	213.73 (± 56.34)	297.00 (± 72.16)

Table 11.2. Mean values for the time constant of recovery of the dynamic focal cone ERG recorded in the three groups of subjects with ARM, sub-classified according to the status of the fellow eye i.e. bilateral ARM (group 1), unilateral wet AMD (group 2), unilateral dry AMD (group 3). Values in parentheses denote the SE of the mean.

11.4   Discussion

The mean time constant of recovery for the dynamic focal cone ERG was found to be significantly higher in the ARM group than the control group. This indicates a prolonged time

course of glare recovery in subjects with ARM. The exclusion of data from 9 subjects with ARM who failed to show appreciable recovery of the ERG response amplitude over the 5 minutes testing time has ensured that this is a conservative measure of the true difference between the two groups. A prolonged testing time might further increase the power of this technique in distinguishing between the two groups.

This finding is in accordance with literature discussing results of psychophysical tests of glare recovery in subjects with ARM and AMD. Using a macular photostress recovery test, a number of studies have found prolonged recovery time in subjects with ARM compared to age-matched controls (*Wu et al, 1990; Cheng & Vingrys, 1993; Sandberg & Gaudio, 1995; Midena et al, 1997*). Sandberg & Gaudio (*1995*) found 82 out of 133 subjects with macular drusen to have a delayed photostress recovery time. Of these, 16 had a visual acuity of 6/6 or better. In accordance with the findings of Sandberg & Gaudio (*1995*), 4 of the subjects with ARM which were identified in this study as having abnormal time constants of recovery also had a visual acuity of 6/6 or better, and a further four had a visual acuity of 6/7.5. This suggests that glare recovery time is a more sensitive indicator of early retinal changes than visual acuity alone.

These findings may be explained by histopathological changes to the outer retina reported in AMD. The process of retinal adaptation following exposure to a high intensity light is dependent on the regeneration of bleached photopigment. This requires the delivery of retinoids and metabolites from the choroidal circulation to the RPE and photoreceptors via Bruch's membrane (*Leibrock et al, 1998*). Structural changes to Bruch's membrane which occur in ARM and AMD, such as thickening and the accumulation of hydrophobic deposits (*Starita et al, 1996*), have been postulated to limit the supply of these essential molecules to the outer retina (*Marshall et al, 1998; Curcio et al, 2000; Owsley et al, 2001*). This effect is exacerbated by the atrophy of the choriocapillaris reported in AMD (*Ciulla et al, 1999, Friedman et al, 1995; Chen,* 1992). A further factor which is vital to the process of retinal adaptation is the healthy functioning of the RPE, as this cell monolayer is essential in the conversion of all-*trans* retinal to its pre-bleach 11-*cis* configuration (*See Saari 2000 for review*). Since the RPE is believed to show abnormalities at an early stage in AMD (*Young, 1987*), which is reflected in focal pigmentary changes (*Bressler et al, 1994*), this may also affect the rate of retinal recovery following light adaptation.

When an ROC curve was plotted for the time constant of recovery for the 41 Hz ERG amplitude, an optimal cut-off point of 160 was found to distinguish between subjects with

ARM and age-matched controls with a sensitivity of 81% and a specificity of 69%. This indicates that the time constant of recovery may have some diagnostic potential in distinguishing between subjects with ARM and age-matched controls.

In this study no difference was found in the time constant of recovery between subjects with bilateral drusen, those with unilateral wet AMD in the fellow eye, and those with unilateral dry AMD in the fellow eye. This supported the findings of Midena et al (*1997*), who similarly found no difference in the macular recovery function of 34 subjects with bilateral early ARM and 13 subjects with unilateral exudative AMD in the fellow eye. A prolonged recovery time in those subjects with unilateral choroidal neovascularisation might have been indicative of a prognostic application of the test, as the 'healthy eyes' of such subjects are considered to be at an increased risk of developing neovascular changes (*Strahlman, 1983*).

However, it may be noted that 5 of the 11 subjects with exudative AMD who participated in this study showed no measurable amplitude recovery during the 5 minutes testing time, whilst only 2 out of 8 individuals with GA, and 2 out of 12 with bilateral drusen showed a similar delay. The fact that no significant difference was found between the unilateral exudative AMD group and the other two groups may reflect a split in the function of the group with neovascular changes. It is possible that the 5 subjects showing a markedly abnormal recovery time are actually at an increased risk of developing the condition in their fellow eye, compared to other subjects in the group who showed normal recovery times.

Sandberg et al (*1998*) followed 127 individuals with macular drusen, and unilateral wet AMD in the non-test eye for a minimum of 3 years. Glare recovery time was found to be an age-adjusted predictor of choroidal neovascularisation. A longitudinal follow-up of the patients enrolled in this study would be desirable to determine whether the dynamic focal cone ERG also holds prognostic potential.

As discussed above, the prolonged retinal recovery seen in AMD following exposure to a bright light source may be attributable to a change in the filtration properties of Bruch's membrane conferred by age- and ARM- related changes. An alteration to the permeability of Bruch's membrane in AMD has also been linked to the onset of choroidal neovascularisation, through the disruption of the transport of RPE derived growth factors to the choriocapillaris via Bruch's membrane (*Moore et al, 1995*). This common causal factor may explain the link between prolonged photostress recovery time and incipient choroidal neovascularisation found by Sandberg et al (*1998*). This is supported by the fact that a delay in retinal adaptation

has also been associated with increased confluence of drusen (*Midena et al, 1997*), a retinal sign which is also associated with a thickening of Bruch's membrane (*Curcio et al, 1999; Sarks et al, 1980*) and an increased risk of choroidal neovascularisation (*Bressler et al, 1990*). This would be in accordance with a possible prognostic role for the assessment of recovery of retinal function following a photopigment bleach.

As discussed above, the time constant of recovery of the modelled data shows promise as a diagnostic test. In view of the findings of previous longitudinal studies (*Sandberg et al, 1998*), there may also be a prognostic application for this technique. The important question is whether the dynamic ERG has any advantages not conferred by the assessment of glare recovery using a standard visual acuity task. The objectivity of the technique is one obvious benefit. The ERG is not reliant on an individual's response to a subjective task, and is therefore unhindered by sources of variability such as inter-subject differences in willingness to guess at letters if uncertain and speed of response, both of which are factors affecting an individual's performance on a letter recognition task (*Amos, 1991*). Previous versions of the photostress test have achieved objectivity through the use of the VEP to record recovery (*Lovasik, 1983; Franchi et al, 1987; Parisi & Bucci, 1992; Parisi et al, 1995; Parisi et al, 1998; Parisi et al, 2002*). The advantage of the 41 Hz ERG over this technique is that it achieves a more direct assay of the function of the outer retina than the VEP. It would therefore be expected that the 41 Hz ERG would be more sensitive to the earliest changes occurring in dynamic retinal function in AMD.

CHAPTER 12 : GENERAL DISCUSSION, CONCLUSIONS AND FURTHER WORK

12.1   General Discussion

The aims of this study were to develop a battery of electrophysiological tests to investigate visual function in people with ARM, and to determine which of these techniques were most sensitive to the earliest functional changes to occur in the disease.

Chapter 6 describes the development of these protocols. In all cases the stimulus and recording parameters chosen were based on two considerations. The primary concern was to develop techniques which would be particularly sensitive to the earliest changes which occur in ARM, but it was also important that the techniques be applicable to the elderly subject group participating in the study. These subjects are described in chapter 8. Thirty one subjects with ARM, and 28 age-matched controls took part. It is important to note that the ARM and control groups were matched with respect to age, gender balance, and lens opacity grading.

Literature describing anatomic studies of donor retinas suggests that the rod and cone loss seen in early ARM is greatest in the region extending from 3-10° either side of fixation (*Curcio et al, 1996; Curcio et al, 2000; Medeiros et al, 2001*). Similarly, psychophysical studies have found functional loss to extend throughout the macula (*Sunness et al, 1985; Owsley et al, 2000; 2001*), indicating that ERG stimuli of 20° in diameter would be optimal for detecting the rod and cone losses seen in eyes with early ARM.

The technique developed for the recording of the focal rod ERG was designed to elicit a response of maximum amplitude without intrusion from the cone system. A short-wavelength (454nm) stimulus was found to be most appropriate for this purpose. The ERG recorded in response to a 20° diameter stimulus presented to the dark-adapted eye consisted of an initial small peak corresponding to the focal stimulation of the central retina, followed by a larger peak elicited by diffuse stimulation of the peripheral retina by scattered light. On the basis of a pilot study to compare two techniques for the isolation of the focal component of this response, a background adaptation protocol was adopted, whereby a dim green (565nm) background light was used to suppress the peripheral rods. The background adaptation technique was found to be a reliable

method of eliciting a response from the ten controls who participated in the pilot study, as well as involving minimal time expenditure.

Chapter 9 describes the results of the focal rod ERG and the rod VEP. The amplitudes of both a- and b-waves of the focal rod ERG were reduced in the ARM group compared to controls. This finding agreed with reports of psychophysical studies describing abnormal macular rod function in people with ARM (*Brown et al, 1985; Steinmetz et al, 1993; Owsley et al, 2000; Curcio et al, 2000*). However, the amplitude difference failed to reach significance, probably because there was a high level of inter-subject variability in the response amplitudes. The focal to full-field b-wave amplitude ratio, which helped to minimise this variability, was found to be significantly different between the two groups, suggesting a central rod defect in subjects with ARM. The rod VEP results showed marked intersubject variability, and no difference was found between subjects with ARM and controls. The recording of a larger number of averages, reducing noise levels in the traces, could have increased the power of this test.

Protocols were also designed for the recording of both transient and steady-state focal cone ERGs. The transient ERG was recorded in response to a 100 ms stimulus presented at 5 Hz. This response showed clearly defined a- and b- waves in control subjects. Band-pass filtering from 100-1000 Hz also allowed the extraction of macular OPs from this response, as described by Miyake et al (*1990*). The steady state ERG was elicited by a square wave stimulus flickering at 41 Hz. This 41 Hz response is dominated by the first harmonic of the signal (*Remulla et al, 1995; Falsini et al, 2000*), which reflects outer retinal activity (*Porciatti et al, 1989*). A white background of the same average luminance as the stimulus was used in both cases to suppress the response of the peripheral retina to scattered light.

The focal cone ERG results are described in chapter 10. The transient ERG showed a smaller and more delayed response in subjects with ARM than in controls. However, this difference only reached significance for the implicit times. A delay was similarly found in the focal steady state ERG recorded in response to a 41 Hz flicker. This could be explained by diffuse photoreceptoral loss, leading to a relatively less light-adapted state of the bipolars, and a subsequently slowed PII component. The amplitude of the focal 41 Hz ERG was also found to be significantly reduced in subjects with ARM, a finding that was in agreement with previous studies using a flicker

stimulus to investigate focal cone function (*Birch & Fish, 1988; Falsini et al, 1999*). This was also reflected in a significantly reduced focal to full-field amplitude in the ARM group.

The amplitudes of both the 41 Hz cone ERG, and the a-wave of the 5 Hz cone ERG are dominated by outer retinal activity, which raises the question of why a significant difference was found between groups in the steady state but not the transient ERG parameter. Bush and Sieving (*1994*) suggested that the a-wave response to a stimulus of less than 4.06 log tds.sec^{-1} is strongly influenced by a post-receptoral contribution, probably from horizontal cells, or hyperpolarising bipolars. The stimulus used in this study was 3.18 log tds.sec^{-1} in luminance. Furthermore, it has been suggested that even under optimal stimulus conditions only the first 10 ms of the a-wave directly represents the photocurrent of the receptors (*Robson & Frishman, 1999*). It may be, therefore, that the 41 Hz ERG response provides a more direct assay of a receptoral deficit.

The analysis of photopic macular OPs, extracted from the 5 Hz ERG response, showed a significant reduction in summed amplitude in subjects with ARM compared to age-matched controls. Ten of the subjects with ARM failed to show any measurable focal OPs, as opposed to 1 control subject. Similarly, the ratio of focal to full-field summed OP amplitude was reduced in subjects with ARM, indicating that there is a differential loss of central function in these subjects. Although the OPs have been shown to be generated by cells in the inner plexiform layer (*Ogden, 1973; Wachtmeister & Dowling, 1978; Heynen et al, 1985*) a reduction in amplitude has been reported in individuals with Stargardt's disease (*Lachapelle et al, 1989*), a disease which is phenotypically similar to AMD.

Studies have shown the OPs to be affected by conditions such as diabetic retinopathy, systemic hypertension, and vascular occlusions, which are characterised by abnormal inner retinal blood flow (*Speros & Price, 1981; Müller et al, 1984; Hennekes, 1986, Bresnick & Palta, 1987, Ravilicio et al, 1995, Yu et al, 1998; Drasdo et al, 2002*). Although the pathogenesis of AMD is not fully understood, it has been postulated that artherosclerosis of the choroidal vasculature is an important contributing factor (*Verhoeff & Grossman, 1937; Friedman et al, 1989; Vingerling et al, 1995d; Friedman 2004*). This hypothesis has been supported by histopathologic studies of donor eyes with ARM (*Green & Key, 1977; Green et al, 1985*), by the recording of choroidal perfusion abnormalities in fluorescein angiography (*Pauleikhoff et al, 1990, Chen et al, 1992*), and also by laser doppler measures of ocular blood flow velocity, which indicate a reduced

choroidal blood flow in ARM (*Friedman, 1995; Grunwald et al, 1998; Mori et al, 2001*). Furthermore, conditions which predispose toward atherosclerotic changes are also risk factors for the development of ARM and AMD (*Vingerling et al, 1995c; Friedman, 2000*). The finding of reduced amplitude OPs in individuals with ARM may suggest that this vascular sclerosis extends to the inner retinal circulation.

The S-cone ERG protocol described in Chapter 6 was based on an established silent substitution technique (*Drasdo et al, 2001; 2003*). The technique involved heterochromic flicker photometry to minimise M-cone intrusion, whilst using adapting lights to silence the L- cones and rods, leaving the S-cone response isolated. The full-field S-cone VEP was also included as a means of assessing the integrity of the short-wavelength pathway of the central retina.

Results of the S-cone ERG and VEP are described in chapter 10. Previous psychophysical studies have suggested that the S-cone pathway is particularly vulnerable to dysfunction in early ARM (*Eisner et al, 1987; Haegerstrom- Portnoy et al, 1988; Collins & Brown, 1989; Sunness et al, 1989; Eisner et al, 1991; 1992, Cheng & Vingrys, 1993*). However, in this study no evidence was found of an S-cone abnormality in ARM. This finding may be attributed to the full-field nature of the ERG stimulus, which could have disguised focal changes in macular function. Pragmatic reasons may also have been responsible, such as the problems associated with obtaining an accurate heterochromic flicker balance from the elderly cohort, and the variability inherent in the recording of a flash VEP.

The final technique described in Chapter 6 was the dynamic focal cone ERG, which was used to monitor central cone recovery following exposure to a bright adapting light. This was a novel technique which was deemed particularly appropriate for this study on the basis of literature reporting abnormal photostress recovery in individuals with ARM (*Smiddy and Fine, 1984; Collins and Brown, 1989; Sandberg and Gaudio, 1995; Midena et al., 1997; Phipps et al., 2003; Wu et al., 1990*). The focal 41 Hz ERG was chosen for the purpose of this test as many responses could be averaged rapidly, producing a clear response with a good signal to noise ratio within a short period of time. Furthermore, as this response has been shown to reflect outer retinal function (*Porciatti et al, 1989*) it should provide a direct measure of photoreceptoral recovery. One hundred responses were averaged every 20 seconds following the cessation of the bleaching light. By fitting each trace with a cosine model, an objective analysis of the amplitude of the first

harmonic of the response was obtained. The amplitude data could then be plotted as a function of time after bleach, and modelled with an exponential function in order to assess recovery.

Chapter 11 describes the results of the dynamic focal cone ERG. The time constant of recovery was found to be significantly delayed in subjects with ARM compared to age-matched controls, supporting the findings of previous psychophysical studies. Nine subjects with ARM, and one control subject failed to show any appreciable recovery during the 5 minute testing period.

In addition to the electrophysiological tests described in chapter 6, several psychophysical tests were included in order to provide a more complete assessment of visual function in individuals with ARM. On the basis of literature suggesting that these tests may be sensitive to early functional changes, the standard and desaturated D15 tests were incorporated into the study, as was the recording of a full dark adaptation curve for each subject.

The results of the psychophysical tests are presented in chapter 8. The saturated and desaturated D15 tests were both assessed using a vector scoring method devised by Vingrys & King-Smith (*1988*). The Confusion index (C-index) and Scatter index (S-index) calculated provided a measure of the extent of the colour vision defects recorded in each subject, and the degree of randomness of the arrangement. The angle of confusion indicated the nature of the colour vision defect i.e. tritan, deutan or protan. Results showed that the ARM group performed worse than control subjects on both the standard and desaturated version of the D15 test, with regard to both C- and S-indices. The confusion angle of subjects indicated that those in the ARM group with a defined colour vision defect were all tritanomolous. This finding is consistent with previous reports of tritanopic colour vision deficiencies in individuals with early ARM and AMD (*Bowman, 1980; Collins, 1986; Collins et al, 1989; Cheng & Vingrys, 1993*). An explanation for this finding may be the relative susceptibility of S-cones to photo-oxidative damage (*Ham et al, 1978; Sperling et al, 1980*), and metabolic damage (*DeMonasterio et al, 1981*).

Dark adaptation data are also shown in chapter 8. Retinal sensitivity at a point 8° in the inferior visual field was measured until a steady threshold was reached, or 1 hour had elapsed. Sensitivity was then plotted against time, and the data points were fitted with a mathematical model in order to assess the time constants of rod and cone recovery, time to rod-cone break and the final rod sensitivity. A double exponential model was selected over a single exponential, double linear model advocated by Owsley et al (*2001*) on the basis of the assessment of ten sets of data from

control subjects using both models. The dark adaptation function was found to be generally delayed in the ARM group compared to controls in both the cone and rod mediated portions of recovery. This was reflected in the group-averaged time constants of recovery, and also in a delayed rod-cone break time in the ARM group. However, of these dynamic factors only the timing of the rod-cone break reached significance at the 1% level. The delayed recovery seen in the ARM subjects supported the findings of previous studies (*Brown et al, 1986; Eisner et al, 1987; 1991; Owsley et al, 2001; Steinmetz et al, 1993*).

The final rod sensitivity was also shown to be reduced in subjects with ARM compared to age-matched controls, as reported in other studies of scotopic sensitivity in ARM (*Brown et al, 1983; Brown et al, 1986; Owsley et al, 2000, 2001*). However, the difference between groups was not as significant as the timing of the rod-cone break when assessed for sensitivity and specificity.

For each test, an ROC curve was constructed for the parameter which showed the greatest difference between the ARM and control groups. In this way an optimal cut-off was determined which would separate the two groups with maximum sensitivity and specificity. A summary of these results may be seen in table 12.1

Test	Parameter	Optimal Cut-Off	Sensitivity	Specificity
Desaturated D15 Colour Vision Test	C-index	1.13	71%	68%
Dark Adaptation Function	Time to rod-cone break	19.05 mins	83%	80%
Focal Rod ERG	Focal to full-field amplitude ratio	0.38	83%	61%
5 Hz Focal Cone	b-wave implicit time	42.9 ms	74%	64%
Macular OPs	Focal to full-field summed amplitude ratio	0.23	74%	61%
41 Hz Focal Cone	Focal to full-field amplitude ratio	0.12	65%	79%
Dynamic ERG	Time constant of Recovery	160	81%	69%

Table 12.1. Summary of the sensitivity and specificity of the parameters which best distinguished between control subjects and those with ARM.

A high sensitivity and specificity indicates a successful diagnostic test which will accurately identify those subjects who have ARM. Of the two psychophysical parameters the time to rod-cone break of the dark-adaptation function is seen to give the best results. It is the time constant of recovery of the dynamic ERG which provides the best separation between groups of the electrophysiological tests.

It is of particular interest that both factors which show the strongest diagnostic potential reflect the kinetic function of the retina. This study therefore concurs with the results of Owsley et al (*2001*) who compared final sensitivity of the dark adaptation function with parameters such as the time constant of rod recovery, and time to rod-cone break. They similarly found a greater effect of ARM on the kinetic aspects of rod function.

This delayed recovery has been postulated to be a result of histopathological changes to the outer retina in early ARM. The process of retinal adaptation is dependent on the regeneration of bleached photopigment in the photoreceptors. This requires the delivery of *all-trans* retinol and metabolites from the choroidal circulation to the RPE and photoreceptors via Bruch's membrane (*Leibrock et al, 1998*). The ARM related thickening of Bruch's membrane, and the deposition of hydrophobic lipids limit the passage of retinoids and metabolites to the photoreceptors from the choroidal circulation, consequently slowing the rate of pigment regeneration (*Bird, 1992; Feeney-Burns & Ellersieck, 1985; Starita et al, 1996; Marshall et al, 1998; Curcio et al, 2000; Owsley et al, 2001*). This effect may be exacerbated by the atrophy of the choriocapillaris reported in AMD (*Ciulla et al, 1999, Friedman et al, 1995; Chen, 1992*), and degeneration of the retinal pigment epithelium, where a vital process in the regeneration of visual pigment occurs (*See Saari 2000 for review*). The findings of this study would suggest that this process of slowed retinal recovery precedes the photoreceptoral loss which is likely to be responsible for changes in static visual function in ARM.

A further point of interest in Table 12.1 is that for three of the four ERG tests assessing static measures of visual function, the parameter which showed greatest separation between subjects with ARM and control subjects was the focal to full-field amplitude ratio. The scatter diagrams included in each chapter demonstrate that the spread of amplitude data within each group shows considerable variability. The calculation of the amplitude ratio was a novel technique designed to reduce the intersubject variability conferred by extraneous factors such as axial length (*Chan &*

Mohidin, 2003) and fundus pigmentation (*Wali & Leguire, 1992*). This proved to be successful in decreasing variability, and increasing the separation between the results of the two groups.

However, even when the ratio was calculated there often remained a variability within both ARM and control groups which could no longer be accounted for by the factors discussed above. It has been hypothesised that AMD constitutes the end point of a continuum of retinal changes which occur in apparently healthy individuals as a function of age (*Young, 1987; Curcio et al, 1996*). The range of retinal function observed in control subjects in this study may reflect this continuum. Although none of these individuals exhibit retinal signs of ARM, assessment of 'healthy controls' over period of months may indicate that some are actually at a pre-clinical level of the ARM disease process. A longitudinal study would reveal whether control subjects who show more abnormal results do go on to develop signs of ARM.

The sensitivity and specificity ascribed to each test assumes that the photographic fundus grading is 100% accurate. If functional abnormality does precede the retinal changes associated with ARM, and some subjects who are classified as controls according to the International Classification System (*Bird et al, 1995*) in fact have early ARM, the actual diagnostic value of the tests in this study may be higher than calculated.

Literature suggests that a person with unilateral AMD is at a greater risk of developing the same condition in the fellow eye than a person of similar retinal appearance with bilateral ARM (*Strahlman et al, 1983; Roy & Kaiser-Kupfer, 1990; Klein, 1997*). Previous reports have compared the visual function of subjects with bilateral drusen to that of subjects with choroidal neovascularisation in the fellow eye (*Eisner et al, 1987; 1991; Stangos et al, 1995; Midena et al, 1997*), the assumption being that those individuals with unilateral wet AMD may be at a sub-clinical stage of the disease in their fellow eye at the time of testing. A test which was sensitive to pre-neovascular changes might therefore show a difference between the two groups. On this basis, the subjects with ARM in this study were divided into three groups according to the status of their second eye. Group 1 was composed of subjects with bilateral drusen, group 2 contained those with unilateral wet AMD in the fellow eye, and subjects in group 3 had dry AMD in the fellow eye. Comparisons between the visual functions of these three groups were included as a means of assessing the possible prognostic value of each test.

The rod-cone break of the dark-adaptation function was markedly delayed in subjects with unilateral exudative AMD compared to those with unilateral dry AMD or bilateral ARM. This could indicate that this test is sensitive to the retinal changes which precede the development of advanced AMD.

However, there are problems associated with this analytical approach. In this study only 12 subjects fell into group 1, 11 into group 2, and 8 into group 3. The power of the comparison of results for these three groups was reduced by the small subject numbers. In view of the general inter-subject variability even between control subjects it would be expected that only a marked difference between groups would be detected by comparison of group means.

 A further consideration is that not all subjects with unilateral advanced AMD go on to develop the condition in the study eye. Bressler et al (*1990*) followed 127 individuals with unilateral exudative AMD over a period of 5 years, and found that only 30 (24%) of these developed bilateral choroidal neovascularisation. On the basis of this figure, it might be assumed that only 3 of the 11 subjects enrolled in this study with unilateral CNV would develop neovascular changes in the test eye over a 5 year follow up.

If a test did highlight functional changes which precede choroidal neovascularisation, it might be expected that there would be a split in the results of subjects with unilateral exudative AMD. Those individuals who will develop exudative AMD in the test eye over the following months would show notably abnormal results to such prognostic tests, while those who are not in a pre-neovascular state would show no marked reduction in function compared to those with bilateral ARM. In four tests there was a very definite trend for some subjects with exudative AMD to show markedly abnormal results. Of the three subjects who showed no rod-cone break in the 60 minute dark adaptation testing period, two had exudative AMD in the fellow eye. One of these subjects (ER) actually reported that she developed choroidal neovascular changes in her fellow eye in the weeks following the study. Three of the four subjects with the most marked tritan defects on the desaturated D15 test also had unilateral exudative AMD. Similarly, of the five subjects who showed a focal 41 Hz implicit time which was extended beyond the range of the control subjects, three had exudative AMD in the fellow eye. The subjects who performed worst on the dynamic ERG test also tended to have unilateral exudative AMD, with 5 out of 9 subjects

who showed no measurable recovery of ERG amplitude over the 5 minute recording period being diagnosed as having choroidal neovascularisation in the fellow eye.

A longitudinal follow-up of the retinal status of these subjects would determine whether they are more likely to develop exudative AMD in the test eye that the other subjects with unilateral choroidal neovascularisation. Previous longitudinal studies have found a delayed latency of the 42 Hz ERG (*Sandberg et al, 1998*) and an abnormal photostress recovery time (*Sandberg et al, 1998*) to be risk factors for choroidal neovascularisation. Cone dark adaptation was not found to be an independent risk factor by Eisner et al (*1992*), in a longitudinal study of 42 people with unilateral choroidal neovascularisation. A prospective study of rod-mediated dark adaptation as a predictor of exudative changes has yet to be published.

12.2   Conclusions

The rationale for conducting this study was to achieve a better understanding of the aspects of visual function affected at the earliest stage in ARM through electrophysiological investigation, and to determine the potential clinical value of these tests.

A battery of tests was developed and modified to target the areas most vulnerable to early changes in ARM. Rod, cone and dynamic retinal function were all shown to be affected in subjects with ARM. The results suggested that tests measuring the regeneration of rod and cone photopigment following adaptation to a bright adapting light best distinguished between those subjects classified as having ARM, and age-matched controls. There was also evidence to suggest that these tests may also have some value in highlighting subjects at an increased risk of developing exudative AMD. The advantage of the dynamic ERG in this respect is that it is markedly less time consuming than the recording of a full dark adaptation function, and provides a fully objective measure of retinal recovery.

Diagnostically none of the tests were able to accurately distinguish between those subjects with ARM and those without. Therefore in terms of identifying people according to the existing classification criteria they are only of limited value in the clinic. However, the focal rod and cone ERG techniques could both have value as a means of longitudinally monitoring visual function. This could be useful in the assessment of the efficacy of new modes of treatment.

12.2   Further Work

The focal rod technique and the dynamic ERG were both novel tests designed for the purpose of this study. Both showed promise as clinical tools, being simple to perform, and not too time-consuming. Furthermore, both showed some limited diagnostic potential in the evaluation of ARM. A larger scale assessment of these techniques on a wider group of subjects with ARM and AMD would be desirable to further assess their clinical potential, as well as a study to determine the test-retest repeatability of these procedures. With regard to the dynamic ERG, it would also be of interest to prolong the test to assess recovery over a longer period. In this way the retinal function of subjects who showed no recovery in the 5 minute testing time could be assessed more accurately.

Further analysis which might be of interest would be an assessment of how strong the association is between the outcome of these functional tests, and the severity of retinal changes (gauged by drusen size, number, type etc.). It would also be possible to assess whether any correlations exist between the outcomes of the different tests, possibly allowing distinction between tests which assess different or similar pathological processes. Analysis to determine whether a combination of test outcomes could improve the diagnostic power of these tests would also be of value.

A recurring theme to arise in this thesis was the dilemma of how to accurately classify subjects. Subjects were assigned to the control or ARM group on the basis of retinal appearance alone. Those who showed no retinal signs of disease were assumed to be healthy and placed in the control group. However, how can we be sure that some of the control subjects were not at a pre-clinical stage of the disease process? How do we know which subjects with ARM will go on to develop exudative AMD? In short, how can we be sure that our groups were in fact homogeneous?

A longitudinal follow-up of the retinal status of subjects in the months following the baseline collection of data would be the most appropriate way of addressing these questions. It would be possible to retrospectively re-group subjects based on outcome, and to re-analyse the data accordingly. In this way the true diagnostic and prognostic value of each test could be accurately determined.

Furthermore, having accurately classified the status of each subject at baseline, it would then be possible to use Logistic Regression Analysis to determine how the variables assessed in this

study combine to predict whether or not a subject has ARM or pre-exudative AMD. For example, the results of the rod-cone break time, absolute rod sensitivity, and the focal to full-field rod b-wave amplitude ratio could be assessed with respect to whether or not a subject has ARM.

Age-related macular degeneration is not a homogenous disease, but a group of disorders consisting of many different phenotypes, with different visual outcomes. In view of this it might be expected that individuals would show a different pattern of functional loss, which was dependent on the nature of their disorder. The use of factor analysis might allow the identification of variables that characterise the different types of AMD. Improved classification of subjects at an early stage might allow more effective assessment of which subjects are liable to respond well to treatment, and what the expected visual outcome might be.

REFERENCES

• Adams, A.J., Rodic, R., Husted, R., Stamper, R. (1982). Spectral sensitivity and color discrimination changes in glaucoma and glaucoma-suspect patients. *Invest Ophthalmol Vis Sci,* **23**(4): 516-524.

• Agarwal, M., Shanmugam M. P., Gopal, L., Shetty, N., Bhende, M., Sharma, T., Thakur, S., Raman, R., Nizamuddin, S. H., Moorthy, K. R. (2004). Transpupillary thermotherapy for choroidal neovascular membrane in age related macular degeneration. *Indian J Ophthalmol,* **52**(1): 45-49.

• Aguilar, M., Stiles, W.S. (1954). Saturation of the rod mechanism of the retina at high levels of stimulation. *Optica Acta,* **1**: 59-65.

• Ahnelt, P. and Kolb, H. (1994). Horizontal cells and cone photoreceptors in human retina: a Golgi-electron microscopic study of spectral connectivity. *J Comp Neurol,* **343**(3): 406-427.

• Ahnelt, P.K., Kolb, H., Pflug, R. (1987). Identification of a subtype of cone photoreceptor, likely to be blue sensitive, in the human retina. *J Comp Neurol,* **255**(1): 18-34.

• Ahnelt, P., Keri, C., Kolb, H. (1990). Identification of pedicles of putative blue-sensitive cones in the human retina. *J Comp Neurol,* **293**(1): 39-53.

• Aiello, L.P., Avery, R.L., Arrigg, P.G., Keyt, B.A., Jampel, H.D., Shah, S.T., Pasquale, L.R., Thieme, H., Iwamoto, M.A., Park, J.E. (1994). Vascular endothelial growth factor in ocular fluid of patients with diabetic retinopathy and other retinal disorders. *N Engl J Med,* **331**(22): 1480-1487.

• Aiello, L.P., Pierce, E.A., Foley, E.D., Takagi, H., Chen, H., Riddle, L., Ferrara, N., King, G.L., Smith, L.E. (1995). Suppression of retinal neovascularization in vivo by inhibition of vascular endothelial growth factor (VEGF) using soluble VEGF-receptor chimeric proteins. *Proc Natl Acad Sci U S A,* **92**(23): 10457-10461.

• Albright, T.D., Desimone, R., Gross, C.G. (1984). Columnar organisation of directionally selective cells in visual area MT of the macaque. *J Neurophysiol,* **51**: 16-31.

• Alexander, M.F., Maguire, M.G., Lietman, T.M., Snyder, J.R., Elman, M.J., Fine, S.L. (1988). Assessment of visual function in patients with age-related macular degeneration and low visual acuity. *Arch Ophthalmol,* **106**(11): 1543-1547.

• Algvere, P. and Wachtmeister, L. (1972). On the oscillatory potentials of the human electroretinogram in light and dark adaptation. II. Effect of adaptation to background light and subsequent recovery in the dark. A Fourier analysis. *Acta Ophthalmol (Copenh),* **50**(6): 837-862.

• Allikmets, R. (1997a). A photoreceptor cell-specific ATP-binding transporter gene (ABCR) is mutated in recessive Stargardt macular dystrophy. *Nat Genet,* **17**(1): 122.

• Allikmets, R., Shroyer, N.F., Singh, N., Seddon, J.M., Lewis, R.A., Bernstein, P.S., Peiffer, A., Zabriskie, N.A., Li, Y., Hutchinson, A., Dean, M., Lupski, J.R., Leppert, M.

(1997b). Mutation of the Stargardt disease gene (ABCR) in age-related macular degeneration. *Science*, **277**(5333): 1805-1807.

- Alm, A. (2003). Ocular Circulation. In: P.L. Kaufman, A. Alm, Eds. *Adlers Physiology of the Eye*. St Louis: Mosby. 747-786.

- Altman, D.J. (1982). How large a sample? In: S.M. Gore, D.G. Altman, Eds. *Statistics in Practice*. London: British Medical Association. 6-8.

- Altman, D. J. (1997). *Practical statistics for Medical Research*. London: Chapman & Hall.

- Altman, D.J. and Bland, J.M. (1994). Diagnostic tests 3: receiver operating characteristic plots. *Br Med J*, **309**: 188.

- Amos, J.F. (1991). Patient History. In: J. Eskridge, Ed. *Clinical Procedures in Optometry*. Philadelphia: Lippincott. 26-29.

- Amsler, M. (1947). L'examen qualitatif de la function maculaire. *Ophthalmologica*, **26**: 1458-1462.

- Anderson, D.H., Fisher, S.K., Steinberg, R.H. (1978). Mammalian cones: disc shedding, phagocytosis, and renewal. *Invest Ophthalmol Vis Sci*, **17**(2): 117-133.

- Arden, G. and Brown, K. (1965). Some properties of the cat electroretinogram revealed by local recording under oil. *J Physiol*, **176**: 429-461.

- Arden, G., Carter, R. M., Macfarlan, A. (1984) Pattern and Ganzfeld electroretinograms in macular disease. *Br J Ophthalmol*. **68**: 878-884.

- Arden, G. and Fojas, M. (1962). Electrophysiological abnormalities in pigmentary degenerations of the retina. *Arch Ophthalmol*, **68**: 369-389.

- Arden, G. and Tansley, K. (1955). The spectral sensitivity of the pure cone retina of the grey squirrel (sciurus carolinensis leucotis). *J Physiol*, **127**: 592-602.

- Arden, G., Wolf, J., Berninger, T., Hogg, C.R., Tzekov, R., Holder, G.E. (1999). S-cone ERGs elicited by a simple technique in normals and in tritanopes. *Vis Res*, **39**(3): 641-650.

- Arden, G.B., Carter, R.M., Hogg, C., Siegel, I.M., Margolis, S. (1979). A gold foil electrode: extending the horizons for clinical electroretinography. *Invest Ophthalmol Vis Sci*, **18**(4): 421-426.

- Arden, G.B., Vaegan, Hogg, C.R. (1982). Clinical and experimental evidence that the pattern electroretinogram (PERG) is generated in more proximal retinal layers than the focal electroretinogram (FERG). *Ann N Y Acad Sci*, **388**: 580-607.

- Arden, G.B. and Wolf, J.E. (2003). Differential effects of light and alcohol on the electro-oculographic responses of patients with age-related macular disease. *Invest Ophthalmol Vis Sci*, **44**(7): 3226-3232.

259

• Age-Related Eye Disease Study (2001). A randomized, placebo-controlled, clinical trial of high-dose supplementation with vitamins C and E, beta carotene, and zinc for age-related macular degeneration and vision loss: AREDS report no. 8. *Arch Ophthalmol*, **119**(10): 1417-1436.

• Ariel, M. and Daw, N.W. (1982). Pharmacological analysis of directionally sensitive rabbit retinal ganglion cells. *J Physiol*, **324**: 161-185.

• Armington, J.A., Tepas, D.I., Kropfl, W.J., Hengst, W.H. (1961). Summation of retinal potentials. *J Opt Soc Am A*, **51**: 877-886.

• Aschero, M., Lacapria, A., Staurenghi, G., Lonati, C., Orzalesi, W. (1993). Map distribution of initial atrophy and drusen in patients with age-related macular degeneration. *Invest Ophthalmol Vis Sci*, **34**: 1163.

• Asher, J. (1951). The electroretinogram of the blind spot. *J Physiol*, **114**:112-140.

• Ashmore, J.F. and Falk, G. (1980). Responses of rod bipolar cells in the dark-adapted retina of the dogfish, Scyliorhinus canicula. *J Physiol*, **300**: 115-150.

• Asselman, P., Chadwick, D.W., Marsden, D.C. (1975). Visual evoked responses in the diagnosis and management of patients suspected of multiple sclerosis. *Brain*, **98**(2): 261-282.

• Atchison, D.A., Lovie-Kitchin, J.E., Swann, P.G. (1990). Investigation of central visual fields in patients with age-related macular changes. *Optom Vis Sci*, **67**(3): 179-183.

• Attwell, D., Mobbs, P., Tessier-Lavigne, M., Wilson, M. (1987). Neurotransmitter-induced currents in retinal bipolar cells of the axolotl, Ambystoma mexicanum. *J Physiol*, **387**: 125-161.

• Bailey, I.L. and Lovie, J.E. (1976). New design principles for visual acuity letter charts. *Am J Optom Physiol Opt*, **53**(11): 740-745.

• Balliart, J. (1954). Examen Fonctionnel de la macula. *Bulletin Societie d'Ophthalmologe Francaise*, **4**: 1.

• Bauer, P.J. (2002). The complex of cGMP-gated channel and Na+/Ca2+, K+ exchanger in rod photoreceptors. *Adv Exp Med Biol*, **514**: 253-274.

• Baylor, D. and Lamb, T. (1982). Local effects of bleaching in retinal rods of the toad. *J Physiol*, **328**: 49-71.

• Baylor, D.A., Fuortes, M.G., O'Bryan, P.M. (1971). Receptive fields of cones in the retina of the turtle. *J Physiol*, **214**(2): 265-294.

• Baylor, D.A., Lamb, T.D., Yau, K.W. (1979). The membrane current of single rod outer segments. *J Physiol*, **288**: 589-611.

• Bazan, H.E., Bazan, N.G., Feeney-Burns, L., Berman, E.R. (1990). Lipids in human lipofuscin-enriched subcellular fractions of two age populations. Comparison with rod outer segments and neural retina. *Invest Ophthalmol Vis Sci*, **31**(8): 1433-1443.

• Beatty, S., Koh, H., Phil, M., Henson, D., Boulton, M. (2000). The role of oxidative stress in the pathogenesis of age-related macular degeneration. *Surv Ophthalmol*, **45**(2): 115-134.

• Berger, J.W. (1997). Thermal modelling of micropulsed diode laser retinal photocoagulation. *Lasers Surg Med*, **20**(4): 409-415.

• Bernstein, P.S. (1999). Macular Biology. In: J.W., Berger, S.L. Fine, M.G. Maguire, Eds. *Age-Related Macular Degeneration*. St Louis; London: Mosby. 1-16.

• Berson, E.L. (1987). Electrical phenomena in the retina. In: Moses, R.A., Ed. *Adler's Physiology of The Eye*. St. Louis: Mosby. 506-564.

• Betsuin, Y., Mashima, Y., Ohde, H., Inoue, R., Oguchi, Y. (2001). Clinical application of the multifocal VEPs. *Curr Eye Res*, **22**(1): 54-63.

• Biersdorf, W.R. and Diller, D.A. (1969). Local electroretinogram in macular degeneration. *Am J Ophthalmol*, **68**(2): 296-303.

• Birch, D.G., Anderson, J.L., Fish, G.E., Jost, B.F. (1993) Pattern-reversal electroretinographic follow-up of laser photocoagulation for subfoveal neovascular lesions in age-related macular degeneration. *Am J Ophthalmol*, **116**: 148-155.

• Birch, D.G. and Fish, G.E. (1987). Rod ERGs in retinitis pigmentosa and cone-rod degeneration. *Invest Ophthalmol Vis Sci*, **28**(1): 140-150.

• Birch, D.G. and Fish, G.E. (1988). Focal cone electroretinograms: aging and macular disease. *Doc Ophthalmol*, **69**(3): 211-220.

• Bird, A.C. (1991). Doyne Lecture. Pathogenesis of retinal pigment epithelial detachment in the elderly; the relevance of Bruch's membrane change. *Eye*, **5**(1): 1-12.

• Bird, A.C. (1992). Bruch's membrane change with age. *Br J Ophthalmol*, **763**: 166-168.

• Bird, A.C. (1997). What is the future of research in age-related macular disease? *Arch Ophthalmol*, **115**(10): 1311-1313.

• Bird, A.C., Bressler, N.M., Bressler, S.B., Chisholm, I.H., Coscas, G., Davis, M.D., de Jong, P.T., Klaver, C.C., Klein, B.E., Klein, R. (1995). An international classification and grading system for age-related maculopathy and age-related macular degeneration. The International ARM Epidemiological Study Group. *Surv Ophthalmol*, **39**(5): 367-374.

• Bird, A.C. and Marshall, J. (1986). Retinal pigment epithelial detachments in the elderly. *Trans Ophthalmol Soc U K*, **105**(6): 674-682.

• Birnbach, C.D., Jarvelainen, M., Possin, D.E., Milam, A.H. (1994). Histopathology and immunocytochemistry of the neurosensory retina in fundus flavimaculatus. *Ophthalmology*, **101**(7): 1211-1219.

• Bloomfield, S.A. and Miller, R.F. (1986). A functional organization of ON and OFF pathways in the rabbit retina. *J Neurosci*, **6**(1): 1-13.

• Boll, F. (1876). Zur anatomie und physiologie der retina. *Monatsber Akad Wissensch*, **23**: 783-787.

• Boulton, M., Dontsov, A., Jarvis-Evans, J., Ostrovsky, M., Svistunenko, D. (1993). Lipofuscin is a photoinducible free radical generator. *J Photochem Photobiol B*, **19**(3): 201-204.

• Boulton, M. and Marshall, J. (1986). Effects of increasing numbers of phagocytic inclusions on human retinal pigment epithelial cells in culture: a model for aging. *Br J Ophthalmol*, **70**: 808.

• Boulton, M., McKechnie, N.M., Breda, J., Bayly, M., Marshall, J. (1989). The formation of autofluorescent granules in cultured human RPE. *Invest Ophthalmol Vis Sci*, **30**(1): 82-89.

• Bowman, K.J. (1980). The clinical assessment of colour discrimination in senile macular degeneration. *Acta Ophthalmol (Copenh)*, **58**(3): 337-346.

• Boycott, B.B. and Dowling, J.E. (1969). Organisation of the primate retina: Light microscopy. *Philos Trans R Soc Lond B*, **255**: 109-194.

• Boycott, B.B., Dowling, J.E., Fisher, S.K., Kolb, H., Laties, A.M. (1975). Interplexiform cells of the mammalian retina and their comparison with catecholamine-containing retinal cells. *Proc R Soc Lond B Biol Sci*, **191**(1104): 353-368.

• Boycott, B.B. and Hopkins, J.M. (1991). Cone bipolar cells and cone synapses in the primate retina. *Vis Neurosci*, **7**(1): 49-60.

• Boycott, B.B. and Kolb, H. (1973). The connections between bipolar cells and photoreceptors in the retina of the domestic cat. *J Comp Neurol*, **148**(1): 91-114.

• Boycott, B.B. and Wassle, H. (1974). The morphological types of ganglion cells of the domestic cat's retina. *J Physiol*, **240**(2): 397-419.

• Boycott, B.B. and Wassle, H. (1991). Morphological Classification of Bipolar Cells of the Primate Retina. *Eur J Neurosci*, **3**(11): 1069-1088.

• Boyle, R.W. and Dolphin, D. (1996). Structure and biodistribution relationships of photodynamic sensitizers. *Photochem Photobiol*, **64**(3): 469-485.

• Boyles, J.K., Zoellner, C.D., Anderson, L.J., Kosik, L.M., Pitas, R.E., Weisgraber, K.H., Hui, D.Y., Mahley, R.W., Gebicke-Haerter, P.J., Ignatius, M.J. (1989). A role for apolipoprotein E, apolipoprotein A-I, and low density lipoprotein receptors in cholesterol transport during regeneration and remyelination of the rat sciatic nerve. *J Clin Invest*, **83**(3): 1015-1031.

• Boynton, R.M. and Riggs, L.A. (1951). The effect of stimulus area and intensity upon the human retinal response. *J Exp Psychol*, **42**: 217-226.

• Bresnick, G.H. and Palta, M. (1987). Oscillatory potential amplitudes. Relation to severity of diabetic retinopathy. *Arch Ophthalmol*, **105**(7): 929-933.

• Bressler, N.M. (1997). Submacular surgery. New information, more questions. *Arch Ophthalmol*, 115(8): 1071-1072.

• Bressler, N.M. (2001). Photodynamic therapy of subfoveal choroidal neovascularization in age-related macular degeneration with verteporfin: two-year results of 2 randomized clinical trials-tap report 2. *Arch Ophthalmol*, 119(2): 198-207.

• Bressler, N.M., Bressler, S.B., West, S.K., Fine, S.L., Taylor, H.R. (1989). The grading and prevalence of macular degeneration in Chesapeake Bay watermen. *Arch Ophthalmol*, 107(6): 847-52.

• Bressler, N.M., Silva, J.C., Bressler, S.B., Fine, S.L., Green, W.R. (1994). Clinicopathologic correlation of drusen and retinal pigment epithelial abnormalities in age-related macular degeneration. *Retina*, 14(2): 130-142.

• Bressler, S.B., Maguire, M.G., Bressler, N.M., Fine, S.L. (1990). Relationship of drusen and abnormalities of the retinal pigment epithelium to the prognosis of neovascular macular degeneration. The Macular Photocoagulation Study Group. *Arch Ophthalmol*, 108(10): 1442-1447.

• Brigell, M.G. (2001). The Visual Evoked Potential. In: G. A. Fishman, Ed. *Electrophysiologic Testing*. San Francisco: Foundation of the American Academy of Ophthalmology. 237-279.

• Brindley, G.S. and Westheimer, G. (1965). The spatial properties of the human electroretinogram. *Am J Ophthalmol*, 179: 518.

• Brown, B., Adams, A.J., Coletta, N.J., Haegerstrom-Portnoy, G. (1986). Dark adaptation in age-related maculopathy. *Ophthalmic Physiol Opt*, 6(1): 81-84.

• Brown, B. and Garner, L.F. (1983). Effects of luminance on contrast sensitivity in senile macular degeneration. *Am J Optom Physiol Opt*, 60(9) 788-793.

• Brown, B. and Lovie-Kitchin, J.E. (1983). Dark adaptation and the acuity-luminance response in senile macular degeneration. *Am J Optom Physiol Opt*, 61: 265-270.

• Brown, B. and Lovie-Kitchin, J.E. (1987). Contrast sensitivity in central and paracentral retina in age-related maculopathy. *Clinical and Experimental Optometry*, 70: 145-148.

• Brown, B. and Lovie-Kitchin, J.E. (1987). Temporal function in age-related maculopathy. *Clinical and Experimental Optometry*, 70: 112-116.

• Brown, B., Tobin, C., Roche, N., Wolanowski, A. (1986). Cone adaptation in age-related maculopathy. *Am J Optom Physiol Opt*, 63(6): 450-454.

• Brown, B., Zadnik, K., Bailey, I.L., Colenbrander, A. (1984). Effect of luminance, contrast, and eccentricity on visual acuity in senile macular degeneration. *Am J Optom Physiol Opt*, 61(4): 265-270.

• Brown, J.L. (1965). Flicker and intermittent stimulation. In: C.H.Graham, Ed. *Vision and Visual Perception*. New York; London: Wiley.

- Brown, K. and Wantabe, K. (1962). Isolation and identification of a receptor potential from the pure cone fovea of the monkey retina. *Nature*, **193**: 958-960.

- Brown, K. and Wiesel, T. (1961). Localisation of origins of electroretinogram components by intraretinal recording in the intact cat eye. *J Physiol*, **158**: 257-280.

- Brown, K.T. (1968). The electroretinogram: its components and their origins. *Vision Res*, **8**(6): 633-677.

- Brown, K.T. (1969). The electroretinogram: its components and their origins. *UCLA Forum Med Sci*, **8**: 319-378.

- Brown, K.T. and Murakami, M. (1964). A new receptor potential of the monkey retina wih no detectable latency. *Nature*, **201**: 626-628.

- Brown, K.T., Watanabe, K., Murakami, M. (1965). The early and late receptor potentials of monkey cones and rods. *Cold Spring Harb Symp Quant Biol*, **30**: 457-482.

- Brunk, U. and Collins, V.P. (1981). Lysosomes and age pigments in cultured cells. In: R.S. Sohal, Ed. *Age Pigments*. Elsever/North Holland Biomedical Press. 243-265.

- Brunner, R., Widder, R.A., Walter, P., Luke, C., Godehardt, E., Bartz-Schmidt, K.U., Heimann, K., Borberg, H. (2000). Influence of membrane differential filtration on the natural course of age-related macular degeneration: a randomized trial. *Retina*, **20**(5): 483-491.

- Burchardt, D.A. (1972). The effects of picrotoxin and strychnine upon electrical activity of the proximal retina. *Brain Res*, **43**: 246-249.

- Burian, H.M. and Allen, L. (1954). A speculum contact lens electrode for electroretinography. *Electroencephalogr Clin Neurophysiol*, **6**:509-511.

- Burns, R.P. and Feeney-Burns, L. (1980). Clinico-morphologic correlations of drusen of Bruch's membrane. *Trans Am Ophthalmol Soc*, **68**: 206-225.

- Bush, R.A. and Sieving, P.A. (1994). A proximal retinal component in the primate photopic ERG a-wave. *Invest Ophthalmol Vis Sci*, **35**(2): 635-645.

- Cajal, S.R. (1892). The Structure of the Retina. Springfield: Thomas.

- Calderone, J.B. and Jacobs, G.H. (1995). Regional variations in the relative sensitivity to UV light in the mouse retina. *Vis Neurosci*, **12**(3): 463-468.

- Calkins, D.J. (2001). Seeing with S cones. *Prog Retin Eye Res*, **20**(3): 255-287.

- Campbell, F.W. and Green, D.G. (1965). Optical and retinal factors affecting visual resolution. *J Physiol*, **181**(3): 576-593.

- Campos, E.C., Enoch, J.M., Fitzgerald, C.R., Benedetto, M.D. (1980). A simple psychophysical technique provides early diagnosis in optic neuritis. *Doc Ophthalmol*, **49**(2): 325-335.

• Carr, R.E. (1968). Chloroquine and organic changes in the eye. *Dis Nerv Syst* **29**(3): 36-39.

• Carson, E.R., Cobelli, C., Finkelstein, L. (1983). The mathematical modelling of metabolic and endocrine systems. New York: Wiley.

• Carter-Dawson, L.D., LaVail, M.M., Sidman, R.L. (1978). Differential effect of the rd mutation on rods and cones in the mouse retina. *Invest Ophthalmol Vis Sci*, **17**(6): 489-498.

• Casagrande, V.A. (1994). A third parallel visual pathway to primate area V1. *Trends Neurosci*, **17**(7): 305-310.

• Casagrande, V.A. and Ichida, J.M. (2003). The Primary Visual Cortex. In: P.L. Kaufman, A. Alm., Eds., *Adler's Physiology of the Eye*. St Louis: Mosby. 669-685.

• Caswell, A.G., Cohen, D.S., Bird, A.C. (1985). Retinal pigment epithelial detachments in the elderly: Classification and outcome. *Br J Ophthalmol*, **69**: 397-403.

• Cavalli-Sforza Menozzi, P., Liazza, A. (1994). The History and Geography of Human Genes. Princeton: Princeton University Press.

• Celesia, G. and Kaufman, D. (1984) Pattern ERGs and VEPs in maculopathies and optic nerve disease. *Invest Ophthalmol Vis Sci*, **26**: 726-735.

• Chabre, M. (1998). Molecular aspects of phototransduction in retinal rods. *Med Sci*, **14**(12): 1315-1321.

• Chakravarthy, U., Houston, R.F., Archer, D.B. (1993). Treatment of age-related subfoveal neovascular membranes by teletherapy: a pilot study. *Br J Ophthalmol*, **77**(5): 265-273.

• Chan, H.L. and Mohidin, N. (2003). Variation of multifocal electroretinogram with axial length. *Ophthalmic Physiol Opt*, **23**(2): 133-140.

• Chandra, S.R., Gragoudas, E.S., Friedman, E., Van Buskirk, E.M., Klein, M.L. (1974). Natural history of disciform degeneration of the macula. *Am J Ophthalmol*, **78**(4): 579-582.

• Chattergee, S. and Callaway, E.M. (2002). S-cone contributions to the magnocellular visual pathway in the macaque monkey. *Neuron*, **35**: 1135-1146.

• Chen, J.C., Fitzke, F.W., Pauleikhoff, D., Bird, A.C. (1992). Functional loss in age-related Bruch's membrane change with choroidal perfusion defect. *Invest Ophthalmol Vis Sci*, **33**(2): 334-340.

• Cheng, A.S. and Vingrys, A.J. (1993). Visual losses in early age-related maculopathy. *Optom Vis Sci*, **70**(2): 89-96.

• Chiti, Z., North, R.V., Mortlock, K.E., Drasdo, N. (2003). The S-cone electroretinogram: a comparison of techniques, normative data and age-related variation. *Ophthalmic Physiol Opt*, **23**(4): 370-376.

• Cho, E., Hung, S., Willett, W.C., Spiegelman, D., Rimm, E.B., Seddon, J.M., Colditz, G.A., Hankinson, S.E. (2001). Prospective study of dietary fat and the risk of age-related macular degeneration. *Am J Clin Nutr*, 73(2): 209-218.

• Cho, E., Stampfer, M.J., Seddon, J.M., Hung, S., Spiegelman, D., Rimm, E.B., Willett, W.C., Hankinson, S.E. (2001). Prospective study of zinc intake and the risk of age-related macular degeneration. *Ann Epidemiol*, 11(5): 328-336.

• Choroidal Neovascularization Prevention Trial Research Group (1998). Laser treatment in eyes with large drusen. Short-term effects seen in a pilot randomized clinical trial. Choroidal Neovascularization Prevention Trial Research Group. *Ophthalmology*, 105 (1) 11-23.

• Chosi, T., Matsumoto, C.S., Nakatsuka, K. (2003). Rod-driven focal macular electroretinogram. *Jap J Ophthalmol*, 47(4): 356-361.

• Christen, W.G., Ajani, U.A., Glynn, R.J., Manson, J.E., Schaumberg, D.A., Chew, E.C., Buring, J.E., Hennekens, C.H. (1999). Prospective cohort study of antioxidant vitamin supplement use and the risk of age-related maculopathy. *Am J Epidemiol*, 149(5): 476-484.

• Chuang, E.L. and Bird, A.C. (1988). The pathogenesis of tears of the retinal pigment epithelium. *Am J Ophthalmol*, 105(3): 285-290.

• Chun, M.H. and Wassle, H. (1989). GABA-like immunoreactivity in the cat retina: electron microscopy. *J Comp Neurol*, 279: 55-67.

• Chylack, L.T., Jr., Leske, M.C., McCarthy, D., Khu, P., Kashiwagi, T., Sperduto, R. (1989). Lens opacities classification system II (LOCS II). *Arch Ophthalmol*, 107(7): 991-997.

• Chylack, L.T., Jr., Leske, M.C., Sperduto, R., Khu, P., McCarthy, D. (1988). Lens Opacities Classification System. *Arch Ophthalmol*, 106(3): 330-334.

• Chylack, L.T., Jr., Wolfe, J.K., Singer, D.M., Leske, M.C., Bullimore, M.A., Bailey, I.L., Friend, J., McCarthy, D., Wu, S.Y. (1993). The Lens Opacities Classification System III. The Longitudinal Study of Cataract Study Group. *Arch Ophthalmol*, 111(6): 831-836.

• Ciardella, A.P., Donsoff, I.M., Guyer, D.R., Adamis, A., Yannuzzi, L.A. (2002). Antiangiogenesis agents. *Ophthalmol Clin North Am,* 15(4): 453-458.

• Cideciyan, A.V., Hood, D.C., Huang, Y., Banin, E., Li, Z.Y., Stone, E.M., Milam, A.H., Jacobson, S.G. (1998). Disease sequence from mutant rhodopsin allele to rod and cone photoreceptor degeneration in man. *Proc Natl Acad Sci U S A*, 95(12): 7103-7108.

• Cideciyan, A.V. and Jacobson, S.G. (1993). Negative electroretinograms in retinitis pigmentosa. *Invest Ophthalmol Vis Sci*, 34(12): 3253-3263.

• Ciulla, T.A., Harris, A., Chung, H.S., Danis, R.P., Kagemann, L., McNulty, L., Pratt, L.M., Martin, B.J. (1999). Color Doppler imaging discloses reduced ocular blood flow velocities in nonexudative age-related macular degeneration. *Am J Ophthalmol*, 128(1): 75-80.

• Cleland, B.G., Dubin, M.W., Levick, W.R. (1971). Sustained and transient neurones in the cat's retina and lateral geniculate nucleus. *J Physiol*, 217(2): 473-496.

• Cobb, W. and Morton, H. (1953). A new component of the human electrretinogram. *Journal of Physiology*, **123**: 36-37.

• Cohen, A.I. (1992). The Retina. In: M.J. Hart, Ed. *Adler's Physiology of the Eye*. St. Louis: Mosby Year Book. 579.

• Cohen, S.Y., Le Gargasson, J.F., Guez, J.E., Rigaudiere, F., Coscas, G.J., Grall, Y. (1994). Focal visual evoked potentials generated by scanning laser ophthalmoscope in patients with age-related macular degeneration treated by perifoveal photocoagulation. *Doc Ophthalmol*, **86** (1): 55-63.

• Coile, D.C. and Baker, H.D. (1992). Foveal dark adaptation, photopigment regeneration, and aging. *Vis Neurosci*, **8**(1): 27-39.

• Collins, M. (1989). The onset of prolonged glare recovery with age. *Ophthalmic Physiol Opt*, **9**(4): 368-371.

• Collins, M. and Brown, B. (1989). Glare Recovery and Age-Related Maculopathy. *Clin Vis Sci*, **4**(2): 145-153.

• Collins, M. and Brown, B. (1989). Glare Recovery and its relation to other clinical findings in Age-Related Maculopathy. *Clin Vis Sci*, **4**(2): 155-163.

• Collins, M.J. (1986). Pre age-related maculopathy and the desaturated D15 colour vision test. *Clin Exp Optom*, **69**: 223-227.

• Collins, M.J. and Brown, B. (1989). Glare recovery and age-related maculopathy. *Clin Vis Sci*, **4**: 145-153.

• Collins, M.J. and Brown, B. (1989). Glare recovery and its relation to other clinical findings in age-related maculopathy. *Clin Vis Sci*, **4**: 155-163.

• Cone, R.A. (1964). Early receptor potential of the vertebrate retina. *Nature*, **204**: 736-749.

• Cone, R.A. and Cobbs, W.H. (1969). The rhodopsin cycle in the living eye of the rat. *Nature*, **221**: 820-822.

• Copenhagen, D.R. and Jahr, C.E. (1989). Release of endogenous excitatory amino acids from turtle photoreceptors. *Nature*, **341**: 536-539.

• Coupland S.G., Janaky, M. (1989). ERG electrode in pediatric patients: comparison of DTL fiber, PVA-gel, and non-corneal skin electrodes. *Doc Ophthalmol*, **71**(4): 427-33.

• Cowey, A, Stoerig, P. (1991). The neurobiology of blindsight. *Trends Neurosci*, **14**: 140.

• Cruickshanks, K.J., Hamman, R.F., Klein, R., Nondahl, D.M., Shetterly, S.M. (1997). The prevalence of age-related maculopathy by geographic region and ethnicity. The Colorado-Wisconsin Study of Age-Related Maculopathy. *Arch Ophthalmol*, **115**(2): 242-250.

• Cruickshanks, K.J., Klein, R., Klein, B.E. (1993). Sunlight and age-related macular degeneration. The Beaver Dam Eye Study. *Arch Ophthalmol*, **111**(4): 514-518.

• Cruikshanks, K.J., Klein, R., Klein, B.E., Nondahl, D.M. (2001). Sunlight and the 5-year incidence of early age-related maculopathy: the beaver dam eye study. *Arch Ophthalmol* **119**(2): 246-50.

• Cunningham, R. and Miller, R.F. (1980). Electrophysiological analysis of taurine and glycine action on neurons of the mudpuppy retina. I. Intracellular recording. *Brain Res*, **197**(1): 123-138.

• Curcio, C.A., Allen, K.A., Sloan, K.R., Lerea, C.L., Hurley, J.B., Klock, I.B., Milam, A.H. (1991). Distribution and morphology of human cone photoreceptors stained with anti-blue opsin. *J Comp Neurol*, **312**(4): 610-624.

• Curcio, C.A., Medeiros, N.E., Millican, C.L. (1996). Photoreceptor loss in age-related macular degeneration. *Invest Ophthalmol Vis Sci*, **37**(7): 1236-1249.

• Curcio, C.A. and Millican, C.L. (1999). Basal linear deposit and large drusen are specific for early age-related maculopathy. *Arch Ophthalmol*, **117**(3): 329-339.

• Curcio, C.A., Millican, C.L., Allen, K.A., Kalina, R.E. (1993). Aging of the human photoreceptor mosaic: evidence for selective vulnerability of rods in central retina. *Invest Ophthalmol Vis Sci*, **34**(12): 3278-3296.

• Curcio, C.A., Millican, C.L., Bailey, T., Kruth, H.S. (2001). Accumulation of cholesterol with age in human Bruch's membrane. *Invest Ophthalmol Vis Sci*, **42**(1): 265-274.

• Curcio, C.A. (2001). Photoreceptor topography in ageing and age-related maculopathy. *Eye*, **15**(3): 376-83.

• Curcio, C.A., Owsley, C., Jackson, G.R. (2000). Spare the rods, save the cones in aging and age-related maculopathy. *Invest Ophthalmol Vis Sci*, **41**(8): 2015-2018.

• Curcio, C.A., Sloan, K.R., Jr., Packer, O., Hendrickson, A.E., Kalina, R.E. (1987). Distribution of cones in human and monkey retina: individual variability and radial asymmetry. *Science*, **236**(4801): 579-582.

• Curcio, C.A., Sloan, K.R., Kalina, R.E., Hendrickson, A.E. (1990). Human photoreceptor topography. *J Comp Neurol*, **292**(4): 497-523.

• Dacey, D., Packer, O.S., Diller, L., Brainard, D., Peterson, B., Lee, B. (2000). Center surround receptive field structure of cone bipolar cells in primate retina. *Vision Res*, **40**(14): 1801-1811.

• Dacey, D., Peterson, B., Gamlin, P.D., Robinson, F.R. (2001). Retrograde photofilling reveals the complete morphology of diverse new ganglion cell types that project to the lateral geniculate nucleus in macaque monkey. *Invest Ophthalmol Vis Sci*, **42**(4): S617.

• Dacey, D.M. (1999). Primate retina: cell types, circuits and color opponency. *Prog Retin Eye Res*, **18**(6): 737-763.

• Dacey, D.M. and Lee, B.B. (1994). The 'blue-on' opponent pathway in primate retina originates from a distinct bistratified ganglion cell type. *Nature*, **367**(6465): 731-735.

• Dacey, D.M., Lee, B.B., Stafford, D.K., Pokorny, J., Smith, V.C. (1996). Horizontal cells of the primate retina: cone specificity without spectral opponency. *Science*, 271(5249): 656-659.

• Daniel, P.M. and Whitteridge, W. (1961). The representation of the visual field on the cerebral cortex in monkeys. *J Physiol*, 159: 302-321.

• Dartnall, H.J., Bowmaker, J.K., Mollon, J.D. (1983). Human visual pigments: microspectrophotometric results from the eyes of seven persons. *Proc R Soc Lond B Biol Sci*, 220(1218): 115-130.

• Das, S.R., Bhardwaj, N., Kjeldbye, H., Gouras, P. (1992). Muller cells of chicken retina synthesise 11-cis retinol. *Biochem J*, 285: 907-913.

• Dawson, W.W., Maida, T.M., Rubin, M.L. (1982). Human pattern-evoked retinal responses are altered by optic atrophy. *Invest Ophthalmol Vis Sci*, 22(6): 796-803.

• Dawson, W.W., Trick, G.L., Litzkow, C.A. (1979). Improved electrode for electroretinography. *Invest Ophthalmol Vis Sci*, 18(9): 988-991.

• de Juan, E., Jr., Loewenstein, A., Bressler, N.M., Alexander, J. (1998). Translocation of the retina for management of subfoveal choroidal neovascularization II: a preliminary report in humans. *Am J Ophthalmol*, 125(5): 635-646.

• De La Paz, M.A., Guy, V.K., Abou-Donia, S., Heinis, R., Bracken, B., Vance, J.M., Gilbert, J.R., Gass, J.D., Haines, J.L., Pericak-Vance, M.A. (1999). Analysis of the Stargardt disease gene (ABCR) in age-related macular degeneration. *Ophthalmology*, 106(8): 1531-1536.

• De Lange, H. (1952). Experiments on flicker and some calculations on an electrical analogue of the foveal systems. *Physica*, 18: 935-950.

• DeGuillebon, H. and Zauberman, H. (1972). Experimental retinal detachment. Biophysical aspects of retinal peeling and stretching. *Arch Ophthalmol*, 87(5): 545-548.

• Deigner, P.S., Law, W.C., Canada, F.J., Rando, R.R. (1989). Membranes as the energy source in the endergonic transformation of vitamin A to 11-cis-retinol. *Science*, 244(4907): 968-971.

• Delcourt, C., Cristol, J.P., Tessier, F., Leger, C.L., Descomps, B., Papoz, L. (1999). Age-related macular degeneration and antioxidant status in the POLA study. POLA Study Group. Pathologies Oculaires Liees a l'Age. *Arch Ophthalmol*, 117(10): 1384-1390.

• Delcourt, C., Diaz, J.L., Ponton-Sanchez, A., Papoz, L. (1998). Smoking and age-related macular degeneration. The POLA Study. Pathologies Oculaires Liees a l'Age. *Arch Ophthalmol*, 116(8): 1031-1035.

• DeMonasterio, F.M., McCrane, E.P., Newlander, J.K., Schein, S.J. (1985). Density profile of blue-sensitive cones along the horizontal meridian of macaque retina. *Invest Ophthalmol Vis Sci*, 26(3): 289-302.

• DeMonasterio, F.M., Schein, S.J., McCrane, E.P. (1981). Staining of blue-sensitive cones of the macaque retina by a fluorescent dye. *Science*, 213(4513): 1278-1281.

• Dessauer, C.W., Posner, B.A., Gilman, A.G. (1996). Visualizing signal transduction: receptors, G-proteins, and adenylate cyclases. *Clin Vis Sci*, 91(5): 527-537.

• Deterre, P., Bigay, J., Forquet, F., Robert, M., Chabre, M. (1988). cGMP phosphodiesterase of retinal rods is regulated by two inhibitory subunits. *Proc Natl Acad Sci U S A*, 85(8): 2424-2428.

• DeVoe, R.C., Ripps, H., Vaughan, H.G., Jr. (1968). Cortical responses to stimulation of the human fovea. *Vision Res*, 8(2): 135-147.

• Dewar, J. and McKendrick, J. (1873). On the physiological action of light. *Trans R Soc Edinb*, 27:141-166.

• Diaz, M.N., Frei, B., Vita, J.A., Keaney, J.F., Jr. (1997). Antioxidants and atherosclerotic heart disease. *N Engl J Med*, 337(6): 408-416.

• Dick, E., Miller, R.F., Bloomfield, S. (1985). Extracellular K+ activity changes related to electroretinogram components. II. Rabbit (E-type) retinas. *J Gen Physiol*, 85(6): 911-31.

• Dimitrova, G., Tamaki, Y., Kato, S. (2002). Retrobulbar circulation in patients with age-related maculopathy. *Eye*, 16(5): 580-6.

• Ding, Y., Casagrande, V.A. (1997). The distribution and morphology of LGN K pathway axons within the layers and CO blobs of owl monkey V1. *Vis Neurosci*, 14(4): 691-704.

• Domey, R.G. (1964). Statistical Properties of Foveal Cff as Function of Age, Light/Dark Ratio, and Surround. *J Opt Soc Am*, 54: 394-398.

• Domey, R.G., MacFarland, R.A., Chadwick, E. (1960). Dark adaptation as a function of age and time. II. A derivation. *J Gerontol*, 15: 267-279.

• Donders, F.C. (1854). Beitrage zur pathologischen anatomie des auges. *Arch Ophthalmol*, 1:106.

• Dorey, C.K., Wu, G., Ebenstein, D., Garsd, A., Weiter, J.J. (1989). Cell loss in the aging retina. Relationship to lipofuscin accumulation and macular degeneration. *Invest Ophthalmol Vis Sci*, 30(8): 1691-1699.

• Dowling, J.E. and Boycott, B.B. (1966). Organization of the primate retina: electron microscopy. *Proc R Soc Lond B Biol Sci*, 166(2) 80-111.

• Drasdo, N., Aldebasi, Y.H., Chiti, Z., Mortlock, K.E., Morgan, J.E., North, R.V. (2001). The s-cone PHNR and pattern ERG in primary open angle glaucoma. *Invest Ophthalmol Vis Sci*, 42(6) 1266-1272.

• Drasdo, N., Aldebasi, Y.H., Mortlock, K.E., Chiti, Z., Morgan, J.E., North, R.V., Wild, J.M. (2002). Ocular optics, electroretinography and primary open angle glaucoma. *Ophthalmic Physiol Opt*, 22(5): 455-462.

• Drasdo, N., Chiti, Z., Owens, D.R., North, R.V. (2002). Effect of darkness on inner retinal hypoxia in diabetes. *Lancet*, **359**(9325): 2251-2253.

• Drasdo N., Thompson, D.A., Arden, G.B. (1990) A comparison of pattern ERG amplitudes and nuclear layer thickness in different zones of the retina. *Clin Vis Sci*, **5**: 412-420.

• Eagle, R.C., Jr. (1984). Mechanisms of maculopathy. *Ophthalmology*, **91**(6): 613-625.

• Eckardt, C., Eckardt, U., Conrad, H.G. (1999). Macular rotation with and without counter-rotation of the globe in patients with age-related macular degeneration. *Graefes Arch Clin Exp Ophthalmol*, **237**(4): 313-325.

• Einthoven, W. and Jolly, W. (1908). The form and magnitude of the electrical response of the eye to stimulation by light at various intensities. *J Exp Physiol*, **1**: 373-416.

• Eisner, A., Fleming, S.A., Klein, M.L., Mauldin, W.M. (1987). Sensitivities in older eyes with good acuity: cross-sectional norms. *Invest Ophthalmol Vis Sci*, **28**(11): 1824-1831.

• Eisner, A., Fleming, S.A., Klein, M.L., Mauldin, W.M. (1987). Sensitivities in older eyes with good acuity: eyes whose fellow eye has exudative AMD. *Invest Ophthalmol Vis Sci*, **28**(11): 1832-1837.

• Eisner, A., Klein, M.L., Zilis, J.D., Watkins, M.D. (1992). Visual function and the subsequent development of exudative age-related macular degeneration. *Invest Ophthalmol Vis Sci*, **33**(11): 3091-3102.

• Eisner, A., Stoumbos, V.D., Klein, M.L., Fleming, S.A. (1991). Relations between fundus appearance and function. Eyes whose fellow eye has exudative age-related macular degeneration. *Invest Ophthalmol Vis Sci*, **32**(1): 8-20.

• Elliott D.B., Yang, K.C., Whitaker, D. (1995) Visual acuity changes through adulthood in normal healthy eyes: seeing beyond 6/6. *Optom Vis Sci*, **72**: 186-91.

• Enroth-Cugell, D. and Robson, J.G. (1966). The contrast sensitivity of retinal ganglion cells of the cat. *J Physiol*, **187**: 517.

• Evans, J.R. (2001). Risk factors for age-related macular degeneration. *Prog Retin Eye Res*, **20**(2): 227-253.

• Evers, H.U. and Gouras, P. (1986). Three cone mechanisms in the primate electroretinogram: two with, one without off-center bipolar responses. *Vision Res*, **26**(2): 245-254.

• Eye Disease Case-Control Study Group (1992). Risk factors for neovascular age-related macular degeneration. The Eye Disease Case-Control Study Group. *Arch Ophthalmol*, **110**(12): 1701-1708.

• Eye Disease Case-Control Study Group (1993). Antioxidant status and neovascular age-related macular degeneration. Eye Disease Case-Control Study Group. *Arch Ophthalmol*, **111**(1): 104-109.

• Faber, D. (1969). Analysis of the slow trans-retinal potentials in response to light (PhD Thesis). Buffalo NY: State University of New York at Buffalo.

• Falk, G. and Shiells, R.A. (1986). Do horizontal cell responses contribute to the electroretinogram (ERG) in dog fish? *J Physiol*, **381**: 113.

• Falsini, B., Fadda, A., Iarossi, G., Piccardi, M., Canu, D., Minnella, A., Serrao, S., Scullica, L. (2000). Retinal sensitivity to flicker modulation: reduced by early age-related maculopathy. *Invest Ophthalmol Vis Sci*, **41**(6): 1498-1506.

• Falsini, B., Focosi, F., Molle, F., Manganelli, C., Iarossi, G., Fadda, A., Dorin, G., Mainster, M.A. (2003). Monitoring retinal function during transpupillary thermotherapy for occult choroidal neovascularization in age-related macular degeneration. *Invest Ophthalmol Vis Sci*, **44**(5): 2133-2140.

• Falsini, B., Porciatti, V., Fadda, A., Merendino, E., Iarossi, G., Cermola, S. (1995). The first and second harmonics of the macular flicker electroretinogram: differential effects of retinal diseases. *Doc Ophthalmol*, **90**(2): 157-167.

• Falsini, B., Serrao, S., Fadda, A., Iarossi, G., Porrello, G., Cocco, F., Merendino, E. (1999). Focal electroretinograms and fundus appearance in nonexudative age-related macular degeneration. Quantitative relationship between retinal morphology and function. *Graefes Arch Clin Exp Ophthalmol*, **237**(3): 193-200.

• Famiglietti, E.V., Jr. and Kolb, H. (1975). A bistratified amacrine cell and synaptic cirucitry in the inner plexiform layer of the retina. *Brain Res*, **84**(2): 293-300.

• Famiglietti, E.V., Jr. and Kolb, H. (1976). Structural basis for ON-and OFF-center responses in retinal ganglion cells. *Science*, **194** (4261): 193-195.

• Farkas, T.G. (1971). Drusen of the retinal pigment epithelium. *Surv Ophthalmol*, **16**: 75-87.

• Farnsworth, D. (1943). The Farnsworth-Munsell 100 hue and dichotomous test for colour vision. *J Opt Soc Am*, **33**: 568-578.

• Fatt, I. and Shantinath, K. (1971). Flow conductivity of retina and its role in retinal adhesion. *Exp Eye Res*, **12**(2): 218-226.

• Feeney-Burns, L., Berman, E.R., Rothman, H. (1980). Lipofuscin of human retinal pigment epithelium. *Am J Ophthalmol*, **90**(6): 783-791.

• Feeney-Burns, L. and Ellersieck, M.R. (1985). Age-related changes in the ultrastructure of Bruch's membrane. *Am J Ophthalmol*, **100**(5): 686-697.

• Felleman, D.J., Burkhelter, A., Van Essen, D.C. (1997). Cortical connections of areas V3 and VP of macaque monkey extrastriate visual cortex. *J Comp Neurol*, **379**: 21-47.

• Ferris, F.L., 3rd (1983). Senile macular degeneration: review of epidemiologic features. *Am J Epidemiol*, **118**(2): 132-151.

• Ferris, F.L., 3rd, Fine, S.L., Hyman, L. (1984). Age-related macular degeneration and blindness due to neovascular maculopathy. *Arch Ophthalmol*, 102(11): 1640-1642.

• Ferris, F. L., 3rd and R. D. Sperduto (1982). Standardized illumination for visual acuity testing in clinical research. *Am J Ophthalmol*, 94(1): 97-98.

• Fesenko, E.E., Kolesnikov, S.S., Lyubarsky, A.L. (1985). Induction by cyclic GMP of cationic conductance in plasma membrane of retinal rod outer segment. *Nature*, 313(6000): 310-313.

• Fine, B.S. and Yanoff, M. (1979). The Retina. In: B.S. Fine, and M. Yanoff, Eds. *Ocular Histology*. Hagerstown, MD: Harper & Row. 59.

• Fishman, G.A. (2002). The Electroretinogram. In: G. A. Fishman, Ed. *Electrophysiologic Testing*. San Francisco: Foundation of the American Academy of Ophthalmology. 1-155.

• Fishman, G.A., Farbman, J.S., Alexander, K.R. (1991). Delayed rod dark adaptation in patients with Stargardt's disease. *Ophthalmology*, 98(6): 957-962.

• Fleishmann, L. (1922). Gesundheitsschadenlichkeit der Magnet-Wechselfelder. *Naturwissenschaften*, 10: 434.

• Franchi, A., Magni, R., Lodigiani, L., Cordella, M. (1987). VEP pattern after photostress: an index of macular function. *Graefes Arch Clin Exp Ophthalmol*, 225(4): 291-294.

• Francois, J. and Verriest, G. (1968). Nouvelles observations de deficiencies acquises de la discrimination chromatique. *Annales d'occuliste*, 201: 1097-1114.

• Frennesson, C.I. (2003). Prophylactic laser treatment in early age-related maculopathy: an 8-year follow-up in a randomized pilot study shows a reduced incidence of exudative complications. *Acta Ophthalmol Scand*, 81(5): 449-54.

• Freund, K.B., Yannuzzi, L.A., Sorenson, J.A. (1993). Age-related macular degeneration and choroidal neovascularization. *Am J Ophthalmol*, 115(6): 786-791.

• Friedman, E. (2000). The role of the atherosclerotic process in the pathogenesis of age-related macular degeneration. *Am J Ophthalmol*, 130: 658-663.

• Friedman, E. (2004). Update of the vascular model of AMD. *Br J Ophthalmol*, 88: 161-163.

• Friedman, E., Ivry, M., Ebert, E. (1989). Increased scleral rigidity and age-related macular degeneration. *Ophthalmology*, 96: 104-108.

• Friedman, E., Krupsky, S., Lane, A.M., Oak, S.S., Friedman, E.S., Egan, K., Gragoudas, E.S. (1995). Ocular blood flow velocity in age-related macular degeneration. *Ophthalmology*, 102 (4) 640-646.

• Friedman, E., Smith, T.R., Kuwabara, T. (1963). Senile choroidal vascular patterns and drusen. *Arch Ophthalmol*, 69: 220-30.

• Frisen, L. (1990). Clinical Tests of Vision. New York: Raven Press.

• Frisen, L. and Frisen, M. (1979). Micropsia and visual acuity in macular edema. A study of the neuro-retinal basis of visual acuity. *Albrecht Von Graefes Arch Klin Exp Ophthalmol*, 210(2): 69-77.

• Frisen, L. and Kalm, H. (1981). Sahlgren's saturation test for detecting and grading acquired dyschromatopsia. *Am J Ophthalmol*, 92(2): 252-258.

• Frishman, L.J. and Steinberg, R.H. (1990). Origin of negative potentials in the light-adapted ERG of cat retina. *J Neurophysiol*, 63(6): 1333-1346.

• Fukada, Y. (1971). Receptive field organization of cat optic nerve fibers with special reference to conduction velocity. *Vision Res*, 11(3): 209-226.

• Fukuda, Y. and Stone, J. (1974). Retinal distribution and central projections of Y-, X-, and W-cells of the cat's retina. *J Neurophysiol*, 37(4): 749-772.

• Fung, B.K., Young, J.H., Yamane, H.K., Griswold-Prenner, I. (1990). Subunit stoichiometry of retinal rod cGMP phosphodiesterase. *Biochemistry*, 29(11): 2657-64.

• Galin, M.A., Nano, H.D., Hall, T. (1962). Ocular zinc concentration. *Invest Ophthalmol*, 1: 142-148.

• Galliard, E.R., Atherton, S.J., Eldred, G.E., Dillon, J. (1995). Photophysical studies on human retinal lipofuscin. *Photochem Photobiol*, 61: 448-453.

• Gass, J.D. (1971). Photocoagulation of macular lesions. *Trans Am Acad Ophthalmol Otolaryngol*, 75(3): 580-608.

• Gass, J.D. (1973). Drusen and disciform macular detachment and degeneration. *Arch Ophthalmol*, 90(3): 206-217.

• Gass, J.D., Jallow, S., Davis, B. (1985). Adult vitelliform macular detachment occurring in patients with basal laminar drusen. *Am J Ophthalmol*, 99(4): 445-459.

• Glaser, J.S., Savino, P.J., Sumers, K.D., McDonald, S.A., Knighton, R.W. (1977). The photostress recovery test in the clinical assessment of visual function. *Am J Ophthalmol*, 83(2): 255-260.

• Goldberg, J., Flowerdew, G., Smith, E., Brody, J.A., Tso, M.O. (1988). Factors associated with age-related macular degeneration. An analysis of data from the first National Health and Nutrition Examination Survey. *Am J Epidemiol*, 128(4): 700-710.

• Goldstein, E.B. (1967). Early receptor potential of the isolated frog (Rana pipiens) retina. *Vision Res*, 7(11): 837-845.

• Goldstein, E.B. (1970). Cone pigment regeneration in the isolated frog retina. *Vision Res*, 10(10): 1065-1068.

• Goldstein, E.B. and Wolf, B.M. (1973). Regeneration of the green-rod pigment in the isolated frog retina. *Vision Res*, 13(3): 527-534.

• Goodchild, A.K., Chan, T.L., Grunert, U. (1996). Horizontal cell connections with short-wavelength-sensitive cones in macaque monkey retina. *Vis Neurosci*, 13(5): 833-845.

• Gouras, P. (1984). Colour Vision. *Prog Retin Eye Res*, 3: 227-261.

• Gouras, P. (1991). Precortical physiology of colour vision. In: P. Gouras, Eds. *Vision and Visual Dysfunction, Vol 6*. London: Macmillan. 163-178.

• Gouras, P. (1992). Retinal circuitry and its relevance to diagnostic psychophysics and electrophysiology. *Current Opinion in Ophthalmology*, 3(803-812).

• Gouras, P. (2001). Colour Vision. In www.webvision.med.utah.edu.

• Gouras, P. and MacKay, C.J. (1990). Electroretinographic responses of the short-wavelength-sensitive cones. *Invest Ophthalmol Vis Sci*, 31(7): 1203-1209.

• Gouras, P., MacKay, C.J., Yamamoto, S. (1993). The human S-cone electroretinogram and its variation among subjects with and without L and M-cone function. *Invest Ophthalmol Vis Sci*, 34(8): 2437-2442.

• Granit, R. (1933). The components of the retinal action potential in mammals and their relation to the discharge of the optic nerve. *J Physiol*, 77: 207-239.

• Granit, R. (1962). Neurophysiology of the Retina. In : H Davidson, Ed. *The Eye*. New York: Academic Press. 575-691.

• Granit, R.L. and Munsterhjelm, A. (1937). The electrical response of the dark-adapted frog's eye to monochromatic stimuli. *J Physiol*, 88: 436-458.

• Green, D.G. and Kapousta-Bruneau, N.V. (1999). A dissection of the electroretinogram from the isolated rat retina with microelectrodes and drugs. *Vis Neurosci*, 16(4): 727-741.

• Green, R.W. and Harlan, J.B.J. (1999). Histopathologic Features. In: J.W. Berger, S.L. Fine, Maguire, M.G. Eds. *Age-Related Macular Degeneration*. St Louis; London: Mosby. 81-154.

• Green, W.R. and Enger, C. (1993). Age-related macular degeneration histopathologic studies. The 1992 Lorenz E. Zimmerman Lecture. *Ophthalmology*, 100(10): 1519-1535.

• Green, W.R. and Key, S.N., 3rd (1977). Senile macular degeneration: a histopathologic study. *Trans Am Ophthalmol Soc*, 75:180-254.

• Green, W.R., McDonnell, P.J., Yeo, J.H. (1985). Pathologic features of senile macular degeneration. *Ophthalmology*, 92(5): 615-627.

• Greeves, A.L., Cole, B.L., Jacobs, R.J. (1988). Assessment of contrast sensitivity of patients with macular disease using reduced contrast near visual acuity charts. *Ophthalmic Physiol Opt*, 8(4): 371-377.

• Gregor, Z. and Joffe, L. (1978). Senile macular changes in the black African. *Br J Ophthalmol*, **62** (8) 547-550.

• Griff, E.R. and Steinberg, R.H. (1982). Origin of the light peak: in vitro study of Gekko gekko. *J Physiol*, **331**: 637-652.

• Grunert, U. and Wassle, H. (1990). GABA-like immunoreactivity in macaque monkey retina: a light and electron microscopic study. *J Comp Neurol*, **297**: 509-524.

• Grunwald, J.E., Hariprasad, S.M., DuPont, J., Maguire, M.G., Fine, S.L., Brucker, A.J., Maguire, A.M., Ho, A.C. (1998). Foveolar choroidal blood flow in age-related macular degeneration. *Invest Ophthalmol Vis Sci*, **39**(2): 385-390.

• Gur, M., Zeevi, Y.Y., Bielik, M., Neumann, E. (1987). Changes in the oscillatory potentials of the electroretinogram in glaucoma. *Curr Eye Res*, **6**(3): 457-466.

• Gutierrez, O. and Spiguel, R.D. (1973). Oscillatory potentials of the cat retina: effects of adrenergic drugs. *Life Sci*, **13**(7): 991-999.

• Guymer, R.H., Luthert, P., Bird, A.C. (1998). Changes in Bruch's membrane and related structures with age. *Prog Retin Eye Res*, **18**(1): 59-90.

• Guymer, R.H., Heon, E., Lotery, A.J., Munier, F.L., Schorderet, D.F., Baird, P.N., McNeil, R.J., Haines, H., Sheffield, V.C., Stone, E.M. (2001). Variation of codons 1961 and 2177 of the Stargardt disease gene is not associated with age-related macular degeneration. *Arch Ophthalmol*, **119**(5): 745-751.

• Haab, O. (1888). Ueber die Erkrankung der macula lutea. *Periodischer Internationaler Opthalmologen Congress, Heidelberg, Germany*, 429-437.

• Haas, A., Feigl, B., Weger, M. (2003). Transpupillary thermotherapy in exudative, age-related macular degeneration. *Ophthalmologe*, **100**(2): 111-114.

• Haas, A., Papaefthymiou, G., Langmann, G., Schrottner, O., Feigl, B., Leber, K.A., Hanselmayer, R., Pendl, G. (2000). Gamma knife treatment of subfoveal, classic neovascularization in age-related macular degeneration: a pilot study. *J Neurosurg*, **93**(3): 172-176.

• Hack, I., Peichl, L., Brandstatter, J. H. (1999). An alternative pathway for rod signals in the rodent retina: rod photoreceptors, cone bipolar cells, and the localization of glutamate receptors. *Proc Natl Acad Sci USA*, **96**(24): 14130-14135.

• Haegerstrom-Portnoy, G., Adams, A. J., Brown, B., Jampolsky, A. (1983). Dynamics of visual adaptation are altered in vascular disease. In: G.M. Breinin and I.M. Siegel, Eds. *Advances in Diagnostic Visual Optics. Proceedings of the 2nd International Symposium on Visual Optics*. New York: Springer-Verlag.

• Haegerstrom-Portnoy, G. and Brown, B. (1988). Two-colour increment threshold in early age-related macular degeneration. *Clin Vis Sci*, **4**: 165-172.

• Hageman, G.S., Marmor, M.F., Yao, X.Y., Johnson, L.V. (1995). The interphotoreceptor matrix mediates primate retinal adhesion. *Arch Ophthalmol*, 113(5): 655-660.

• Hagen, T.M., Yowe, D.L., Bartholomew, J.C., Wehr, C.M., Do, K.L., Park, J.Y., Ames, B.N. (1997). Mitochondrial decay in hepatocytes from old rats: membrane potential declines, heterogeneity and oxidants increase. *Proc Natl Acad Sci U S A*, 94(7): 3064-3069.

• Hagins, W.A., Penn, R.D., Yoshikami, S. (1970). Dark current and photocurrent in retinal rods. *Biophys J*, 10(5): 380-412.

• Halliday, A.M., Barrett, G., Blumhardt, L.D., Kriss, A. (1979). The macular and paramacular subcomponents of the pattern evoked response. In : D. Lehmann, E. Calloway, Eds. *Human Evoked Potentials: Applications and Problems*. New York: Plenum Publishing Corp. 135-51.

• Ham, W.T., Jr., Ruffolo, J.J., Jr., Mueller, H.A., Clarke, A.M., Moon, M.E. (1978). Histologic analysis of photochemical lesions produced in rhesus retina by short-wave-length light. *Invest Ophthalmol Vis Sci*, 17(10): 1029-1035.

• Hamasaki, D.I., Korabathina, K., Patel, S.R., Liu, M., Lam, B.L. (1997). The c-wave of the electroretinogram recorded under clinical conditions from rabbits. *Doc Ophthalmol*, 94(4): 365-381.

• Hammond, B.R., Jr., Wooten, B.R., Snodderly, D.M. (1996). Cigarette smoking and retinal carotenoids: implications for age-related macular degeneration. *Vision Res*, 36(18): 3003-3009.

• Hanitzsch, R. (1973). Intraretinal isolation of P3 subcomponents in the isolated rabbit retina after treatment with sodium aspartate. *Vision Res*, 13(11): 2093-2102.

• Hanitzsch, R. and Lichtenberger, T. (1997). Two neuronal retinal components of the electroretinogram c-wave. *Doc Ophthalmol*, 94(3): 275-285.

• Harding, G.F., Odom, J.V., Spileers, W., Spekreijse, H. (1996). Standard for visual evoked potentials 1995. The International Society for Clinical Electrophysiology of Vision. *Vision Res*, 36(21): 3567-3572.

• Harding, G.F.A. (1991). Visual Evoked Cortical Potentials: Basic Recording. In J.R. Heckenlively, G.B. Arden, Eds. *Principles and Practice of Clinical Electrophysiology*. St Louis: Mosby Year Book. 399-424.

• Hart, W.M., Jr. (1987). Acquired dyschromatopsias. *Surv Ophthalmol*, 32(1): 10-31.

• Hart, W.M., Jr. and Burde, R.M. (1983). Three-dimensional topography of the central visual field. Sparing of foveal sensitivity in macular disease. *Ophthalmology*, 90(8): 1028-1038.

• Hart, W.M.J. (1987). Visual Adaptation. In: R.A. Moses, W.M.J. Hart, Eds. *Adler's Physiology of the Eye*. St Louis: Mosby. 389-414.

- Harwerth, R.S. and Sperling, H.G. (1975). Effects of intense visible radiation on the increment-threshold spectral sensitivity of the rhesus monkey eye. *Vision Res,* **15**(11): 1193-1204.

- Hashimoto, Y., Abe, M., Inokuchi, M. (1980). Identification of the interplexiform cell in the dace retina by dye-injection method. *Brain Res,* **197**(2): 331-40.

- Hayden, S.A., Mills, J.W., Masland, R.M. (1980). Acetylcholine synthesis by displaced amacrine cells. *Science,* **210**(4468): 435-437.

- Hayes, K.C. (1974). Retinal degeneration in monkeys induced by deficiencies of vitamin E or A. *Invest Ophthalmol,* **13**(7): 499-510.

- Hayreh, S.S. (1962). The ophthalmic artery, III, Branches. *Br J Ophthalmol,* **46**: 212.

- Hayreh, S.S. (1963). The central artery of the retina: its role in the blood supply of the optic nerve. *Br J Ophthalmol,* **47**: 651.

- Hebert, M., Vaegan, Lachapelle, P. (1999). Reproducibility of ERG responses obtained with the DTL electrode. *Vision Res,* **39**(6): 1069-1070.

- Hecht, S. (1937). Rods, cones, and the chemical basis of vision. *Physiol Rev,* **17**: 239-290.

- Hecht, S., Haig, C., Wald, G. (1935). Dark adaptation of retinal fields of different size and location. *J Gen Physiol,* **19**: 321.

- Hecht, S. and Schlaer, S. (1936). Intermittent stimulation by light. V. The relation between intensity and critical frequency for different parts of the specturm. *J Gen Physiol,* **19**: 965.

- Hecht, S., Schlaer, S., Pirenne, M.H. (1942). Energy, quanta and vision. *J Gen Physiol,* **25**: 819-840.

- Heckenlively, J.R., Martin, D.A., Rosenbaum, A.L. (1983). Loss of electroretinographic oscillatory potentials, optic atrophy, and dysplasia in congenital stationary night blindness. *Am J Ophthalmol,* **96**(4): 526-534.

- Heinemann-Vernaleken, B., Palmowski, A.M., Allgayer, R., Ruprecht, K.W. (2001). Comparison of different high resolution multifocal electroretinogram recordings in patients with age-related maculopathy. *Graefes Arch Clin Exp Ophthalmol,* **239**(8): 556-561.

- Hempel, F.G. (1972). Modification of the rabbit electroretinogram by reserpine. *Ophthal Res,* **4**: 65-67.

- Henderson, B.W. and Dougherty, T.J. (1992). How does photodynamic therapy work? *Photochem Photobiol,* **55**(1): 145-157.

- Hendry, S.H. and Reid, R.C. (2000). The koniocellular pathway in primate vision. *Ann Rev Neurosci,* **23**: 127-53.

- Hennekes, R. (1986). Oscillatory potentials as an indicator of functional changes in diabetic retinopathy. *Klin Monatsbl Augenheilkd,* **189**(5): 372-373.

• Henson, D.B. (1993). Visual Fields. New York: Oxford University Press Inc.

• Herbert, M., Vaegan, Lachapelle, P. (1999). Reproducibility of ERG responses obtained with the DTL electrode. *Vision Res*, **39**(6): 1069-1070.

• Heynen, H. and van Norren, D. (1985a). Origin of the electroretinogram in the intact macaque eye-I. Principal component analysis. *Vision Res*, **25**(5): 697-707.

• Heynen, H., Wachtmeister, L., van Norren, D. (1985b). Origin of the oscillatory potentials in the primate retina. *Vision Res*, **25**(10): 1365-1373.

• Hicks, D. and Sahel, J. (1999). The implications of rod-dependent cone survival for basic and clinical research. *Invest Ophthalmol Vis Sci*, **40**(13): 3071-3074.

• Hock, P.A. and Marmor, M.F. (1983). Variability of the human c-wave. *Doc. Ophthalmol. Proc. Series*, **37**: 151-157.

• Hogan, M.J. and Alvarado, J.A. (1971). Retina. In: M.J. Hogan, J.A Alvarado, Eds. *Histology of the Human Eye*. Philadelphia: Saunders. 393.

• Holder, G. (1997) The pattern electroretinogram in anterior visual pathway dysfunction and its relationship to the pattern VEP: A personal clinical review of 743 eyes. *Eye*, **11**: 924-934.

• Hollins, M. and Alpern, M. (1973). Dark adaptation and visual pigment regeneration in human cones. *J Gen Physiol*, **62**(4): 430-447.

• Hollyfield, J.G., Varner, H.H., Rayborn, M.E. (1990). Regional variation within the interphotoreceptor matrix from fovea to the retinal periphery. *Eye*, **4**(2): 333-339.

• Holmes, G. (1931). A contribution to the cortical respresentation of vision. *Brain*, **52**: 470-479.

• Holmgren, F. (1865). Method att objectivera effecten afljusintryk pa retina. *Upsala Lakarforenings Forhandlingar*, **1**: 184-198.

• Holopigian, K., Seiple, W., Greenstein, V., Kim, D., Carr, R.E. (1997). Relative effects of aging and age-related macular degeneration on peripheral visual function. *Optom Vis Sci*, **74**(3): 152-159.

• Holtz, F.G., Schutt, F., Pauleikhoff, D., Bird, A.C. (2004). Pathophysiology. In: F.G. Holz, Pauleikhoff, D., Spaide, R.F., Bird, A.C., Eds. *Age-Related Macular Degeneration*. Berlin: Springer. 32-44.

• Holz, F.G., Bellmann, C., Staudt, S., Schutt, F., Volcker, H.E. (2001). Fundus autofluorescence and development of geographic atrophy in age-related macular degeneration. *Invest Ophthalmol Vis Sci*, **42**: 1051.

• Holz, F.G., Schutt, F., Kopitz, J., Eldred, G.E., Kruse, F.E., Volcker, H.E., Cantz, M. (1999). Inhibition of lysosomal degradative functions in RPE cells by a retinoid component of lipofuscin. *Invest Ophthalmol Vis Sci*, **40**(3): 737-743.

• Holz, F.G., Sheraidah, G., Pauleikhoff, D., Bird, A.C. (1994). Analysis of lipid deposits extracted from human macular and peripheral Bruch's membrane. *Arch Ophthalmol*, 112(3): 402-406.

• Holz, F.G., Wolfensberger, T.J., Piguet, B., Gross-Jendroska, M., Wells, J.A., Minassian, D.C., Chisholm, I.H., Bird, A.C. (1994). Bilateral macular drusen in age-related macular degeneration. Prognosis and risk factors. *Ophthalmology*, 101: 1522-1528.

• Hood, D.C. and Birch, D.G. (1996). B-wave of the scotopic (rod) electroretinogram as a measure of the activity og human on-bipolar cells. *J Opt Soc Am A*, 13: 613-633.

• Hood, D.C. and Greenstein, V. (1988). Blue (S) cone pathway vulnerability : a test of a fragile receptor hypothesis. *Applied Optics*, 27: 1025-1029.

• Hood, D.C., Greenstein, V., Frishman, L., Holopigian, K., Viswanathan, S., Seiple, W., Ahmed, J., Robson, J.G. (1999). Identifying inner retinal contributions to the human multifocal ERG. *Vision Res*, 39(13): 2285-2291.

• Hood, D.C., Holopigian, K., Greenstein, V., Seiple, W., Li, J., Sutter, E.E., Carr, R.E. (1998). Assessment of local retinal function in patients with retinitis pigmentosa using the multi-focal ERG technique. *Vision Res*, 38(1): 163-179.

• Hood, D.C., Wladis, E.J., Shady, S., Holopigian, K., Li, J., Seiple, W. (1998). Multifocal rod electroretinograms. *Invest Ophthalmol Vis Sci*, 39(7): 1152-1162.

• Horiguchi, M., Ito, Y., Miyake, Y. (1998). Extrafoveal photostress recovery test in glaucoma and idiopathic central serous chorioretinopathy. *Br J Ophthalmol*, 82(9): 1007-1012.

• Horiguchi, M., Miyake, Y., Fujii, Y. (1991). Human focal rod ERG. *Invest Ophthalmol Vis Sci*, 32: S926.

• Horiguchi, M., Miyake, Y., Kondo, M., Suzuki, S., Tanikawa, A., Koo, H.M. (1995). Blue light-emitting diode built-in contact lens electrode can record human S-cone electroretinogram. *Invest Ophthalmol Vis Sci*, 36(8): 1730-1732.

• Horton, J.C. (1992). The Central Visual Pathways. In: W.M.J. Hart, Ed. *Adler's Physiology of the Eye*. St. Louis: Mosby. 728.

• Horton, J.C. and Hoyt, W.F. (1991). The representation of the visual field in human striate cortex. A revision of the classic Holmes map. *Arch Ophthalmol*, 109(6): 816-824.

• Huang, S., Wu, D., Jiang, F., Ma, J., Wu, L., Liang, J., Luo, G. (2000). The multifocal electroretinogram in age-related maculopathies. *Doc Ophthalmol*, 101(2): 115-124.

• Hubel, D. H. (1988). Eye, Brain and Vision. London: W.H. Freeman.

• Hubel, D.H. and Wiesel, T.N. (1972). Laminar and columnar distribution of geniculo-cortical fibers in the macaque monkey. *J Comp Neurol*, 146(4): 421-450.

• Hubel, D.H., Wiesel, T.N., Stryker, M.P. (1977). Orientation columns in macaque monkey visual cortex demonstrated by the 2-deoxyglucose autoradiographic technique. *Nature*, **269**(5626): 328-30.

• Hudspeth, A.J. and Yee, A.G. (1973). The intercellular junctional complexes of retinal pigment epithelia. *Invest Ophthalmol*, **12**(5): 354-365.

• Hyman, L.G., Lilienfeld, A.M., Ferris, F.L., 3rd, Fine, S.L. (1983). Senile macular degeneration: a case-control study. *Am J Epidemiol*, **118**(2): 213-227.

• Ikeda, T., Obayashi, H., Hasegawa, G., Nakamura, N., Yoshikawa, T., Imamura, Y., Koizumi, K., Kinoshita, S. (2001). Paraoxonase gene polymorphisms and plasma oxidized low-density lipoprotein level as possible risk factors for exudative age-related macular degeneration. *Am J Ophthalmol*, **132**(2): 191-195.

• Ishibashi, T., Patterson, R., Ohnishi, Y., Inomata, H., Ryan, S.J. (1986). Formation of drusen in the human eye. *Am J Ophthalmol*, **101**(3): 342-353.

• Ives, H.E. (1922). Critical frequency relations in scotopic vision. *J Opt Soc Am*, **6**: 254-268.

• Jackson, G.R. and Owsley, C. (2000). Scotopic sensitivity during adulthood. *Vision Res*, **40**(18): 2467-2473.

• Jackson, G.R., Owsley, C., Cordle, E.P., Finley, C.D. (1998). Aging and scotopic sensitivity. *Vision Res*, **38**(22): 3655-3662.

• Jacobson, J.H., Kawasaki, K., Hirose, T. (1969). The human electroretinogram and occipital potential in response to focal illumination of the retina. *Invest Ophthalmol*, **8**(5): 545-556.

• Jampol, L.M. and Tielsch, J. (1992). Race, macular degeneration, and the Macular Photocoagulation Study. *Arch Ophthalmol*, **110**(12): 1699-1700.

• Janaky, M., Goupland, S.G., Benedek, G. (1996). Human oscillatory potentials: components of rod origin. *Ophthalmologica*, **210**(6): 315-318.

• Jin, J., Jones, G.J., Cornwall, M.C. (1994). Movement of retinal along cone and rod photoreceptors. *Vis Neurosci*, **11**(2): 389-399.

• Johnson, C.A., Adams, A.J., Lewis, R.A. (1989). Evidence for a neural basis of age-related visual field loss in normal observers. *Invest Ophthalmol Vis Sci*, **30**(9): 2056-2064.

• Johnson, L.K., Longenecker, J.P., Fajardo, L.F. (1982). Differential radiation response of cultured endothelial cells and smooth myocytes. *Anal Quant Cytol*, **4**(3): 188-198.

• Jonas, J.B., Schmidt, A.M., Muller-Bergh, J.A., Schlotzer-Schrehardt, U.M., Naumann, G.O. (1992). Human optic nerve fiber count and optic disc size. *Invest Ophthalmol Vis Sci*, **33**(6): 2012-2018.

• Jori, G. and Reddi, E. (1993). The role of lipoproteins in the delivery of tumour-targeting photosensitizers. *Int J Biochem*, **25**(10): 1369-1375.

• Jorzic, J.J., Schmitz-Valckenberg, S., Chen, J., Unnebrink, K., Holtz, F.G., Group, F.-S. (2002). Reticular pseudodrusen and peripapillary atrophy associated with geographic atrophy in advanced ARMD. ARVO conference abstract.

• Joseph, D.P. and Miller, S.S. (1992). Alpha-1-adrenergic modulation of K and Cl transport in bovine retinal pigment epithelium. *J Gen Physiol*, **99**(2): 263-290.

• Joussen, A.M., Kruse, F.E., Oetzel, D., Voelcker, H.E. (2000). Irradiation for inhibition of endothelial cell growth in vitro. *Ophthalmic Res*, **32**(5) 222-228.

• Junghardt, A., Wildberger, H., Torck, B. (1995). Pattern electroretinogram, visual evoked potential and psychophysical functions in maculopathy. *Doc Ophthalmol*, **90**: 229-245.

• Jurklies, B., Weismann, M., Husing, J., Sutter, E.E., Bornfeld, N. (2002). Monitoring retinal function in neovascular maculopathy using multifocal electroretinography - early and long-term correlation with clinical findings. *Graefes Arch Clin Exp Ophthalmol*, **240**(4): 244-264.

• Kamermans, M. and Spekreijse, H. (1999). The feedback pathway from horizontal cells to cones. A mini review with a look ahead. *Vision Res*, **39**(15): 2449-2468.

• Karwatowski, W.S., Jeffries, T.E., Duance, V.C., Albon, J., Bailey, A.J., Easty, D.L. (1995). Preparation of Bruch's membrane and analysis of the age-related changes in the structural collagens. *Br J Ophthalmol*, **79**(10): 944-952.

• Katz, M.L., Gao, C.L., Rice, L.M. (1996). Formation of lipofuscin-like fluorophores by reaction of retinal with photoreceptor outer segments and liposomes. *Mech Ageing Dev*, **92**(2): 159-174.

• Katz, M.L., Gao, C.L., Stientjes, H.J. (1993). Regulation of the interphotoreceptor retinoid-binding protein content of the retina by vitamin A. *Exp Eye Res*, **57**(4): 393-401.

• Katz, M.L., Kutryb, M.J., Norberg, M., Gao, C.L., White, R.H., Stark, W.S. (1991). Maintenance of opsin density in photoreceptor outer segments of retinoid-deprived rats. *Invest Ophthalmol Vis Sci*, **32**(7): 1968-1980.

• Kaven, C., Spraul, C.W., Zavazava, N., Lang, G.K., Lang, G.E. (2001). Thalidomide and prednisolone inhibit growth factor-induced human retinal pigment epithelium cell proliferation in vitro. *Ophthalmologica,* **215**(4): 284-9.

• Kawasaki, K., Yonemura, D., Nakazato, H., Wakabayashi, K., Shirao, Y., Sakai, N. (1980). Analysis of rapid off-response in electroretinogram major participation of receptor potential (author's transl). *Nippon Ganka Gakkai Zasshi*, **84**(10): 1574-1580.

• Kemp, C.M., Jacobson, S.G., Borruat, F.X., Chaitin, M.H. (1989). Rhodopsin levels and retinal function in cats during recovery from vitamin A deficiency. *Exp Eye Res*, **49**(1): 49-65.

• Killingsworth, M.C., Sarks, J.P., Sarks, S.H. (1990). Macrophages related to Bruch's membrane in age-related macular degeneration. *Eye*, **4**(4): 613-621.

• Kimura, K., Isashiki, Y., Sonoda, S., Kakiuchi-Matsumoto, T., Ohba, N. (2000). Genetic association of manganese superoxide dismutase with exudative age-related macular degeneration. *Am J Ophthalmol*, **130**(6): 769-773.

• Kirchhof, B. (2002). Macular translocation. Improved prognosis for age-related macular degeneration. *Ophthalmologe*, **99**(3): 143.

• Kita, M. and Marmor, M.F. (1991). Systemic mannitol increases the retinal adhesive force in vivo. *Arch Ophthalmol*, **109**(10): 1449-1450.

• Kita, M. and Marmor, M.F. (1992). Effects on retinal adhesive force in vivo of metabolically active agents in the subretinal space. *Invest Ophthalmol Vis Sci*, **33**(6): 1883-1887.

• Klaver, C.C., Wolfs, R.C., Assink, J.J., van Duijn, C.M., Hofman, A., de Jong, P.T. (1998). Genetic risk of age-related maculopathy. Population-based familial aggregation study. *Arch Ophthalmol*, **116**(12): 1646-1651.

• Klein, R., Davis, M.D., Magli, Y.L., Segal, P., Klein, B.E., Hubbard, L. (1991). The Wisconsin age-related maculopathy grading system. *Ophthalmology*, **98**(7): 1128-1134.

• Klein, R., Klein, B.E., Jensen, S.C., Cruickshanks, K.J. (1998). The relationship of ocular factors to the incidence and progression of age-related maculopathy. *Arch Ophthalmol*, **116**(4): 506-513.

• Klein, R., Klein, B.E., Jensen, S.C., Meuer, S.M. (1997). The five-year incidence and progression of age-related maculopathy: the Beaver Dam Eye Study. *Ophthalmology*, **104**(1): 7-21.

• Klein, R., Klein, B.E., Moss, S.E. (1992b). Diabetes, hyperglycemia, and age-related maculopathy. The Beaver Dam Eye Study. *Ophthalmology*, **99**(10): 1527-1534.

• Klein, R., Klein, B.E., Moss, S.E., Linton, K.L. (1992a). The Beaver Dam Eye Study. Retinopathy in adults with newly discovered and previously diagnosed diabetes mellitus. *Ophthalmology*, **99**(1): 58-62.

• Klein, R., Klein, B.E., Tomany, S.C., Meuer, S.M., Huang, G.H. (2002). Ten-year incidence and progression of age-related maculopathy: The Beaver Dam eye study. *Ophthalmology*, **109**(10): 1767-1779.

• Klein, R., Klein, B.E., Wang, Q., Moss, S.E. (1994). Is age-related maculopathy associated with cataracts? *Arch Ophthalmol*, **112**(2): 191-196.

• Klein, R., Rowland, M.L., Harris, M.I. (1995). Racial/ethnic differences in age-related maculopathy. Third National Health and Nutrition Examination Survey. *Ophthalmology*, **102**(3): 371-381.

• Klein, R., Klein, B.E., Cruickshanks, K.J. (1999). The prevalence of age-related maculopathy by geographic region and ethnicity. *Prog Retin Eye Res*, **18**(3): 371-89.

• Kleiner, R.C., Enger, C., Alexander, M.F., Fine, S.L. (1988). Contrast sensitivity in age-related macular degeneration. *Arch Ophthalmol*, **106**(1): 55-57.

• Klistomer, A.I., Graham, S.L., Grigg, J.R., Billson, F.A. (1998). Multifocal topographic visual evoked potential: improving objective detection of local visual field defects. *Invest Ophthalmol Vis Sci*, **39**(6): 937-950.

• Knapp, A.G. and Schiller, P.H. (1984). The contribution of on-bipolar cells to the electroretinogram of rabbits and monkeys. A study using 2-amino-4-phosphonobutyrate (APB). *Vision Res*, **24**(12): 1841-1846.

• Knoblauch, K., Saunders, F., Kusada, M., Hynes, R., Podor, M., Higgins, K.E., De Monasterio, F.M. (1987). Age and illuminance effects in the Farnsworth-Munsell 100-hue test. *Applied Optics*, **26**: 1441-1448.

• Koh, H-H, Murray, I.J., Nolan, D., Carden, D., Feather, J., Beatty, S. (2004). Plasma and macular responses to lutein supplement in subjects with and without age-related mculopathy: a pilot study. *Exp Eye Res*, **79**: 21-27.

• Kohner, E.M., Patel, V., Rassam, S.M. (1995). Role of blood flow and impaired autoregulation in the pathogenesis of diabetic retinopathy. *Diabetes*, **44**(6): 603-607.

• Kojima, M. and Zrenner, E. (1978). Off-components in response to brief light flashes in the oscillatory potential of the human electroretinogram. *Albrecht Von Graefes Arch Klin Exp Ophthalmol*, **206**(2): 107-120.

• Kolb, H. (1970). Organisation of the outer plexiform layer of the primate retina: Electron microscopy of Golgi-impregnated cells. *Philos Trans R Society Lond B*, **258**: 261-283.

• Kolb, H. (1991). The neural organization of the human retina. In: J.R Heckenlively, G.B. Arden, Eds. *Principles and Practice of Clinical Electrophysiology of Vision*. St Louis: Mosby Year Book. 26-27.

• Kolb, H., Boycott, B.B., Dowling, J.E. (1969). A second type of midget bipolar cell in the primate retina. Appendix. *Philos Trans R Soc Lond B*, **255**: 177-184.

• Kolb, H., Cuenca, N., Wang, H.H., Dekorver, L. (1990). The synaptic organization of the dopaminergic amacrine cell in the cat retina. *J Neurocytol*, **19**(3): 343-366.

• Kolb, H. and Dekorvar, L. (1991). Midget ganglion cells of the parafovea of the human retina: a study by electron microscopy and serial section reconstructions. *J Comp Neurol*, **303** (4): 617-636.

• Kolb, H., Fernandez, E., Nelson, R. (2001). The Outer Plexiform Layer. In: www.webvision.med.utah/edu.

• Kolb, H., Fernandez, E., Nelson, R. (2003). Simple Anatomy of the Retina. In: www.webvision.med.utah/edu.

• Kolb, H., Goede, P., Roberts, S., McDermott, R., Gouras, P. (1997). Uniqueness of the S-cone pedicle in the human retina and consequences for color processing. *J Comp Neurol*, **386** (3): 443-460.

• Kolb, H., Fernandez, E., Schouten, J., Ahnelt, P., Linberg, K.A., Fisher, S.K. (1994). Are there three types of horizontal cell in the human retina? *J Comp Neurol*, **343**(3): 370-86.

• Kolb, H., Linberg, K.A., Fisher, S.K. (1992). Neurons of the human retina: a Golgi study. *J Comp Neurol*, **318**(2): 147-187.

• Kolb, H., Mariani, A., Gallego, A. (1980). A second type of horizontal cell in the monkey retina. *J Comp Neurol*, **189**(1): 31-44.

• Kolb, H. and Marshak, D. (2003). The midget pathways of the primate retina. *Doc Ophthalmol*, **106**(1): 67-81.

• Kolb, H., Nelson, R. (1993). OFF-alpha and OFF-beta ganglion cells in cat retina: II. Neural circuitry as revealed by electron microscopy of HRP stains. *J Comp Neurol*, **329**(1): 85-110.

• Kolb, H., Nelson, R., Mariani, A. (1981). Amacrine cells, bipolar cells and ganglion cells of the cat retina: a Golgi study. *Vision Res*, **21**(7): 1081-1114.

• Kolb, H. and West, R.W. (1977). Synaptic connections of the interplexiform cell in the retina of the cat. *J Neurocytol*, **6**(2): 155-170.

• Kolder, H.E. (1991). Electro-oculography. In: J.R. Heckenlively, and G.B. Arden, Eds. *Principles and Practice of Clinical Electrophysiology of Vision*. St Louis: Mosby Year Book. 291-313.

• Kollner, H. (1912). *Die Storungendes Farbenisinnes: ihre Klinische Bedeutung und ihre Diagnose*. Berlin: Karger.

• Kooijman, A.C. and Witmer, F.K. (1986). Ganzfield light distribution on the retina of human and rabbit eyes: calculations and in vitro measurements. *J Opt Soc Am A*, **3** (12) 2116-20.

• Kouyama, N. and Marshak, D.W. (1992). Bipolar cells specific for blue cones in the macaque retina. *J Neurosci*, **12**(4): 1233-1252.

• Kretschmann, U., Seeliger, M., Ruether, K., Usui, T., Zrenner, E. (1998). Spatial cone activity distribution in diseases of the posterior pole determined by multifocal electroretinography. *Vision Res*, **38**(23): 3817-3828.

• Kretschmann, U., Stilling, R., Ruther, K., Zrenner, E. (1999). Familial macular cone dystrophy: diagnostic value of multifocal ERG and two-color threshold perimetry. *Graefes Arch Clin Exp Ophthalmol*, **237**(5): 429-432.

• Krinsky, N.I. (1958). The enzymatic esterification of vitamin A. *J Biol Chem*, **232**(2): 881-894.

• Kris, C.H. (1958). Corneo-fundal potential variations during light and dark adaptation. *Nature*, **182**: 1027-1028.

• Kuhne, W. (1977). Chemical processes in the retina. *Vision Res*, **17**(11): 1269-1316.

• Lachapelle, P., Benoit, J., Little, J.M., Lachapelle, B. (1993). Recording the oscillatory potentials of the electroretinogram with the DTL electrode. *Doc Ophthalmol*, **83**(2): 119-130.

• Lachapelle, P., Little, J.M., Polomeno, R.C. (1983). The photopic electroretinogram in congenital stationary night blindness with myopia. *Invest Ophthalmol Vis Sci*, **24**(4): 442-450.

• Lachapelle, P., Little, J.M., Roy, M.S. (1989). The electroretinogram in Stargardt's disease and fundus flavimaculatus. *Doc Ophthalmol*, **73**(4): 395-404.

• Lachica, E.A. and Casagrande, V.A. (1993). The morphology of collicular and retinal axons ending on small relay (W-like) cells of the primate lateral geniculate nucleus. *Vis Neurosci*, **10**(3): 403-418.

• Lamb, T.D. (1981). The involvement of rod photoreceptors in dark adaptation. *Vision Res*, **21**(12): 1773-1782.

• Lamb, T.D., McNaughton, P.A., Yau, K.W. (1981). Spatial spread of activation and background desensitization in toad rod outer segments. *J Physiol*, **319**: 463-496.

• Lamb, T.D. and Pugh, E.N., Jr. (1992). A quantitative account of the activation steps involved in phototransduction in amphibian photoreceptors. *J Physiol*, **449**: 719-758.

• Lanthony, P. (1978). The desaturated panel D-15. *Doc Ophthalmol*, **46**(1): 185-189.

• Lasansky, A. (1969). Basal junctions at synaptic endings of turtle visual cells. *J Cell Biol*, **40**(2): 577-81.

• Leibowitz, H.M., Krueger, D.E., Maunder, L.R., Milton, R.C., Kini, M.M., Kahn, H.A., Nickerson, R.J., Pool, J., Colton, T.L., Ganley, J.P., Loewenstein, J.I., Dawber, T.R. (1980). The Framingham Eye Study monograph: An ophthalmological and epidemiological study of cataract, glaucoma, diabetic retinopathy, macular degeneration, and visual acuity in a general population of 2631 adults, 1973-1975. *Surv Ophthalmol*, **24**(Suppl): 335-610.

• Leibrock, C.S., Reuter, T., Lamb, T.D. (1998). Molecular basis of dark adaptation in rod photoreceptors. *Eye*, **12**(3): 511-520.

• LeVay, S., Wiesel, T.N., Hubel, D.H. (1980). The development of ocular dominance columns in normal and visually deprived monkeys. *J Comp Neurol*, **191**(1): 1-51.

• Li, J., Tso, M.O., Lam, T.T. (2001). Reduced amplitude and delayed latency in foveal response of multifocal electroretinogram in early age related macular degeneration. *Br J Ophthalmol*, **85**(3): 287-290.

• Lim, J.I., Aaberg, T.M.S., Capone, A.J., Sternberg, P.J. (1997). Indocyanine green angiography-guided photocoagulation of choroidal neovascularisation associated with retinal pigment epithelial detachment. *Am J Ophthalmol*, **123**: 524-532.

• Linberg, K.A. and Fisher, S.K. (1986). An ultrastructural study of interplexiform cell synapses in the human retina. *J Comp Neurol*, **243**(4): 561-576.

• Linsenmeier, R.A. and Steinberg, R.H. (1982). Origin and sensitivity of the light peak in the intact cat eye. *J Physiol*, **331**: 653-673.

• Lion, F., Rotmans, J.P., Daemen, F.J.M. (1975). Biochemical aspects of the visual process, XXVII, Stereospecificity of ocular retinol dehydrogenases and the visual cycle. *Biochem Biophys Acta*, **384**: 282.

• Loeffler, K.U. and Lee, W.R. (1986). Basal laminar deposit in the human macula. *Graefe's Arch Clin Exp Ophthalmol*, **224**: 493-501.

• Loeffler, K.U. and Lee, W.R. (1992). Is basal laminar deposit unique for age-related macular degeneration? *Arch Ophthalmol*, **110**(1): 15-16.

• Lopez, P.F., Sippy, B.D., Lambert, H.M., Thach, A.B., Hinton, D.R. (1996). Transdifferentiated retinal pigment epithelial cells are immunoreactive for vascular endothelial growth factor in surgically excised age-related macular degeneration-related choroidal neovascular membranes. *Invest Ophthalmol Vis Sci*, **37**(5): 855-868.

• Lovasik, J.V. (1983). An electrophysiological investigation of the macular photostress test. *Invest Ophthalmol Vis Sci*, **24**(4): 437-441.

• Lovie-Kitchin, J.E. (1989). High contrast and low contrast visual acuity in age-related macular degeneration. *Clin Exp Optom*, **72**: 79-83.

• Machemer, R. and Steinhorst, U.H. (1993). Retinal separation, retinotomy, and macular relocation: II. A surgical approach for age-related macular degeneration? *Graefes Arch Clin Exp Ophthalmol*, **231**(11): 635-641.

• Macular Photocoagulation Study Group (1986a). Argon laser photocoagulation for neovascular maculopathy. Three-year results from randomized clinical trials. Macular Photocoagulation Study Group. *Arch Ophthalmol*, **104**(5): 694-701.

• Macular Photocoagulation Study Group (1986b). Recurrent choroidal neovascularization after argon laser photocoagulation for neovascular maculopathy. Macular Photocoagulation Study Group. *Arch Ophthalmol*, **104**(4): 503-512.

• Macular Photocoagulation Study Group (1993a). Five-year follow-up of fellow eyes of patients with age-related macular degeneration and unilateral extrafoveal choroidal neovascularization. Macular Photocoagulation Study Group. *Arch Ophthalmol*, **111**(9): 1189-1199.

• Macular Photocoagulation Study Group (1993b). Laser photocoagulation of subfoveal neovascular lesions of age-related macular degeneration. Updated findings from two clinical trials. Macular Photocoagulation Study Group. *Arch Ophthalmol*, **111**(9): 1200-1209.

• Macular Photocoagulation Study Group (1997). Risk factors for choroidal neovascularization in the second eye of patients with juxtafoveal or subfoveal choroidal

neovascularization secondary to age-related macular degeneration. Macular Photocoagulation Study Group. *Arch Ophthalmol*, **115**(6): 741-747.

• Mahley, R.W. (1988). Apolipoprotein E: cholesterol transport protein with expanding role in cell biology. *Science*, **240**(4852): 622-630.

• Mahroo, O.A., Hussain, N., Mehta, H., Patel, A., Lamb, T.D. (2003). Recovery of the human cone electroretinogram a-wave following bleaching exposures: a measure of pigment regeneration in vivo. ARVO Conference Abstract.

• Marchiafava, P.L. and Weiler, R. (1982). The photoresponses of structurally identified amacrine cells in the turtle retina. *Proc R Soc Lond B Biol Sci*, **214**(1196): 403-415.

• Marcus, M., Merin, S., Wolf, M., Feinsod, M. (1983). Electrophysiologic tests in assessment of senile macular degeneration. *Ann Ophthalmol*, **15**(3): 235-238.

• Mares-Perlman, J.A., Brady, W.E., Klein, R., Klein, B.E., Bowen, P., Stacewicz-Sapuntzakis, M., Palta, M. (1995). Serum antioxidants and age-related macular degeneration in a population-based case-control study. *Arch Ophthalmol*, **113**(12): 1518-1523.

• Mares-Perlman, J.A., Brady, W.E., Klein, R., VandenLangenberg, G.M., Klein, B.E., Palta, M. (1995). Dietary fat and age-related maculopathy. *Arch Ophthalmol*, **113**(6): 743-748.

• Mares-Perlman, J.A., Fisher, A.I., Klein, R., Palta, M., Block, G., Millen, A.E., Wright, J.D. (2001). Lutein and zeaxanthin in the diet and serum and their relation to age-related maculopathy in the third national health and nutrition examination survey. *Am J Epidemiol*, **153**(5): 424-432.

• Mares-Perlman, J.A., Klein, R., Klein, B.E., Greger, J.L., Brady, W.E., Palta, M., Ritter, L.L. (1996). Association of zinc and antioxidant nutrients with age-related maculopathy. *Arch Ophthalmol*, **114**(8): 991-997.

• Marg, E. (1951). Development of electro-oculography. *Arch Ophthalmol*, **45**: 169-185.

• Margherio, R.R., Margherio, A.R., DeSantis, M.E. (2000). Laser treatments with verteporfin therapy and its potential impact on retinal practices. *Retina*, **20**(4): 325-330.

• Margrain, T.H. and Thomson, D. (2002). Sources of variability in the clinical photostress test. *Ophthalmic Physiol Opt*, **22**(1): 61-67.

• Mariani, A.P. (1984). Bipolar cells in monkey retina selective for the cones likely to be blue-sensitive. *Nature*, **308**(5955): 184-186.

• Mariani, A.P. (1990). Amacrine cells of the rhesus monkey retina. *J Comp Neurol*, **301**(3): 382-400.

• Marmor, M.F. (1977). Unsedated corneal electroretinograms from children. *Doc Ophthalmol Proc Series*, **13**: 349-355.

• Marmor, M.F. (1995). An updated standard for clinical electroretinography. *Arch Ophthalmol*, 113(11): 1375-1376.

• Marmor, M.F., Abdul-Rahim, A.S., Cohen, D.S. (1980). The effect of metabolic inhibitors on retinal adhesion and subretinal fluid resorption. *Invest Ophthalmol Vis Sci*, 19(8): 893-903.

• Marmor, M.F., Arden, G.B., Nilsson, S.E., Zrenner, E. (1989). Standard for clinical electroretinography. *Arch Ophthalmol*, 107: 816-819.

• Marmor, M.F., Tan, F., Sutter, E.E., Bearse, M.A., Jr. (1999). Topography of cone electrophysiology in the enhanced S cone syndrome. *Invest Ophthalmol Vis Sci*, 40(8): 1866-1873.

• Marmor, M.F. and Zrenner, E. (1999). Standard for clinical electroretinography (1999 update). International Society for Clinical Electrophysiology of Vision. *Doc Ophthalmol*, 97(2): 143-156.

• Marron, J.A. and Bailey, I.L. (1982). Visual factors and orientation-mobility performance. *Am J Optom Physiol Opt*, 59(5): 413-426.

• Marshall, J. The ageing retina: physiology or pathology. *Eye*, 1(2): 282-95.

• Marshall, J., Hussain, A.A., Starita, C., Moore, D.J., Patmore, A.L. (1998). Aging and Bruch's membrane. In: M.F. Marmor, T.J. Wolfensberger, Eds. *The Retinal Pigment Epithelium: Function and Disease*. New York: Oxford University Press. 669-692.

• Masland, R.H. and Ames, A. III (1976). Responses to acetylcholine of ganglion cells in an isolated mammalian retina. *J Neurophysiol*, 39(6): 1220-1235.

• Massey, S.C., Redburn, D.A., Crawford, M.L. (1983). The effects of 2-amino-4-phosphonobutyric acid (APB) on the ERG and ganglion cell discharge of rabbit retina. *Vision Res*, 23(12): 1607-1613.

• Mayer, M.J., Spiegler, S.J., Ward, B., Glucs, A., Kim, C.B. (1992). Foveal flicker sensitivity discriminates ARM-risk from healthy eyes. *Invest Ophthalmol Vis Sci*, 33(11): 3143-3149.

• Mayer, M.J., Spiegler, S.J., Ward, B., Glucs, A., Kim, C.B. (1992). Mid-frequency loss of foveal flicker sensitivity in early stages of age-related maculopathy. *Invest Ophthalmol Vis Sci*, 33(11): 3136-3142.

• Mayer, M.J., Spiegler, S.J., Ward, B., Glucs, A., Kim, C.B. (1992). Preliminary evaluation of flicker sensitivity as a predictive test for exudative age-related maculopathy. *Invest Ophthalmol Vis Sci*, 33(11): 3150-3155.

• Mayer, M.J., Ward, B., Klein, R., Talcott, J.B., Dougherty, R.F., Glucs, A. (1994). Flicker sensitivity and fundus appearance in pre-exudative age-related maculopathy. *Invest Ophthalmol Vis Sci*, 35(3): 1138-1149.

• Mayhew, I.G., Jolly, R.D., Pickett, B.T., Slack, P.M. (1985). Ceroid-lipofuscinosis (Batten's disease). pathogenesis of blindness in the ovine model. *Neuropathol Appl Neurobiol*, 11(4): 273-290.

• McGwin, G., Jr., Jackson, G.R., Owsley, C. (1999). Using nonlinear regression to estimate parameters of dark adaptation. *Behav Res Methods Instrum Comput*, 31 (4): 712-7.

• Medeiros, N.E. and Curcio, C.A. (2001). Preservation of ganglion cell layer neurons in age-related macular degeneration. *Invest Ophthalmol Vis Sci*, 42(3): 795-803.

• Merigan, W.H. (1989). Chromatic and achromatic vision of macaques: role of the P pathway. *J Neurosci*, 9(3): 776-783.

• Midena, E., Angeli, C.D., Blarzino, M.C., Valenti, M., Segato, T. (1997). Macular function impairment in eyes with early age-related macular degeneration. *Invest Ophthalmol Vis Sci*, 38(2) 469-477.

• Midena, E., Segato, T., Blarzino, M.C., Degli Angeli, C. (1994). Macular drusen and the sensitivity of the central visual field. *Doc Ophthalmol*, 88(2): 179-185.

• Miller, H., Miller, B., Ryan, S.J. (1986). The role of retinal pigment epithelium in the involution of subretinal neovascularization. *Invest Ophthalmol Vis Sci*, 27(11): 1644-1652.

• Miller, R.F. and Dowling, J.E. (1970). Intracellular responses of the Muller (glial) cells of mudpuppy retina: their relation to b-wave of the electroretinogram. *J Neurophysiol*, 33(3): 323-341.

• Missotten, L. (1965). The Ultrastructure of the Human Retina. Brussels: Arscia Uitgaven.

• Mitchell, P., Smith, W., Attebo, K., Wang, J.J. (1995). Prevalence of age-related maculopathy in Australia. The Blue Mountains Eye Study. *Ophthalmology*, 102 (10) 1450-1460.

• Mitchell, P., Smith, W., Wang, J.J. (1998). Iris color, skin sun sensitivity, and age-related maculopathy. The Blue Mountains Eye Study. *Ophthalmology*, 105(8) 1359-1363.

• Miyake, Y. (1990). Macular oscillatory potentials in humans. Macular OPs. *Doc Ophthalmol*, 75(2): 111-124.

• Miyake, Y. and Awaya, S. (1984). Stimulus deprivation amblyopia. Simultaneous recording of local macular electroretinogram and visual evoked response. *Arch Ophthalmol*, 102(7): 998-1003.

• Mohand-Said, S., Deudon-Combe, A., Hicks, D., Simonutti, M., Forster, V., Fintz, A.C., Leveillard, T., Dreyfus, H., Sahel, J.A. (1998). Normal retina releases a diffusible factor stimulating cone survival in the retinal degeneration mouse. *Proc Natl Acad Sci U S A*, 95(14): 8357-8362.

• Mohand-Said, S., Hicks, D., Simonutti, M., Tran-Minh, D., Deudon-Combe, A., Dreyfus, H., Silverman, M.S., Ogilvie, J.M., Tenkova, T., Sahel, J. (1997). Photoreceptor transplants

increase host cone survival in the retinal degeneration (rd) mouse. *Ophthalmic Res*, 29(5): 290-297.

- Moore, D.J., Hussain, A.A., Marshall, J. (1995). Age-related variation in the hydraulic conductivity of Bruch's membrane. *Invest Ophthalmol Vis Sci*, 36(7): 1290-1297.

- Moreland, J. D. (1993). Lens-equivalent age controls for diabetics. *Invest Ophthalmol Vis Sci*, 34(2): 281-2.

- Mori, F., Konno, S., Hikichi, T., Yamaguchi, Y., Ishiko, S., Yoshida, A. (2001). Pulsatile ocular blood flow study: decreases in exudative age related macular degeneration. *Br J Ophthalmol*, 85(5): 531-533.

- Moschos, M., Brouzas, D., Papantonis, F., Chatzis, V. (1993). C-wave study in cone dysfunction syndrome. *Ophthalmologica*, 207(1): 37-41.

- Moschos, M.N., Panayotidis, D., Moschos, M.M., Bouros, C., Theodossiadis, P.G., Theodossiadis, G.P. (2003). A preliminary assessment of macular function by MF-ERG in myopic eyes with CNV with complete response to photodynamic therapy. *Eur J Ophthalmol*, 13(5): 461-467.

- Movshon, J.A., Newsome, W.T. (*1996*). Visual response properties of striate cortical neurones projecting to area MT in macaque monkeys. *J Neurosci*, 16: 7733.

- Mullen, K.T. and Kingdom, F.A.A. (1991). Colour contrast in form perception. In: P. Gouras, Eds. *Vision and Visual Dysfunction*. London: Macmillan. 198-217.

- Muller, F., Wassle, H., Voigt, T. (1988). Pharmacological modulation of the rod pathway in the cat retina. *J Neurophysiol*, 59(6): 1657-1672.

- Muller, W., Gauss, J., Spittel, U., Duck, K., H. (1984). Oscillatory potentials in cases of systemic hypertension. *Doc Ophthalmol*, 40: 167-171.

- Mullins, R.F., Aptsiauri, N., Hageman, G.S. (2001). Structure and composition of drusen associated with glomerulonephritis: implications for the role of complement activation in drusen biogenesis. *Eye*, 15(3): 390-395.

- Murakami, M. and Kaneko, A. (1966). Differentiation of PIII subcomponents in cold-blooded vertebrate retinas. *Vision Res*, 6: 627-636.

- Myers, S.M. (1994). A twin study on age-related macular degeneration. *Trans Am Ophthalmol Soc*, 92: 775-844.

- Naarendorp, F. and Sieving, P.A. (1991). The scotopic threshold response of the cat ERG is suppressed selectively by GABA and glycine. *Vision Res*, 31(1): 1-15.

- Nagata, M. (1963). Studies on the photopic ERG of the human retina. *Japanese Journal of Ophthalmology*, 7 96-124.

• Nagpal, M., Nagpal, K., Sharma, S., Puri, J., Nagpal, P.N. (2003). Transpupillary thermotherapy for treatment of choroidal neovascularization secondary to age-related macular degeneration in Indian eyes. *Indian J Ophthalmol,* 51(3): 243-50.

• Nakamura, Y., McCurie, B., Sterling, P. (1979). Selective uptake of [3H] gamma-amino butyric acid (GABA) and [3H] gamma-glycine by neurons of the amacrine layer of cat retina. Abstracts of Neuroscience Meeting, Toronto .

• Nakamura, Y., McGuire, B.A., Sterling, P. (1980). Interplexiform cell in cat retina: identification by uptake of gamma-[3H]aminobutyric acid and serial reconstruction. *Proc Natl Acad Sci U S A,* 77(1): 658-661.

• Nelson, R. (1977). Cat cones have rod input: a comparison of the response properties of cones and horizontal cell bodies in the retina of the cat. *J Comp Neurol,* 172(1): 109-135.

• Nelson, R. and Kolb, H. (1983). Synaptic patterns and response properties of bipolar and ganglion cells in the cat retina. *Vision Res,* 23(10): 1183-1195.

• Nelson, R. and Kolb, H. (1985). A17: a broad-field amacrine cell in the rod system of the cat retina. *J Neurophysiol,* 54(3): 592-614.

• Newman, E.A. (1980). Current source-density analysis of the b-wave of frog retina. *J Neurophysiol,* 43(5): 1355-1366.

• Newman, E.A. and Odette, L.L. (1984). Model of electroretinogram b-wave generation: a test of the K+ hypothesis. *J Neurophysiol,* 51(1): 164-182.

• Newsom, R.S., McAlister, J.C., Saeed, M., McHugh, J.D. (2001). Transpupillary thermotherapy (TTT) for the treatment of choroidal neovascularisation. *Br J Ophthalmol,* 85(2): 173-178.

• Newsome, D.A., Swartz, M., Leone, N.C., Elston, R.C., Miller, E. (1988). Oral zinc in macular degeneration. *Arch Ophthalmol,* 106(2): 192-198.

• Niermann, F., Lorenz, R. Heider, W. (1989) P-ERG and P-VECP in maculopathy: a comparison with other sensory tests. *Fortschr Ophthalmol,* 86: 54-58.

• Nilsson, S.E. and Anderson, B.E. (1988). Corneal DC recordings of slow ocular potential changes such as the ERG c-wave and the light peak in clinical work. *Doc Ophthalmol,* 68: 313-325.

• Nilsson, S.E., Knave, B., Persson, H.E. (1977). Changes in ultrastructure and function of the sheep pigment epithelium and retina induced by sodium iodate. II. Early effects. *Acta Ophthalmol (Copenh),* 55(6): 1007-1026.

• Nilsson, S.E. and Wrigstad, A. (1997). Electrophysiology in some animal and human hereditary diseases involving the retinal pigment epithelium. *Eye,* 11(5): 698-706.

• Ochsner, M. (1997). Photophysical and photobiological processes in the photodynamic therapy of tumours. *J Photochem Photobiol B,* 39(1): 1-18.

- Ogden, T.E. (1973). The oscillatory waves of the primate electroretinogram. *Vision Res*, 13(6): 1059-1074.

- Ohyama, T., Hackos, D.H., Frings, S., Hagen, V., Kaupp, U.B., Korenbrot, J.I. (2000). Fraction of the dark current carried by Ca(2+) through cGMP-gated ion channels of intact rod and cone photoreceptors. *J Gen Physiol*, 116(6): 735-754.

- Oken, B.S., Chiappa, K.H., Gill, E. (1987). Normal temporal variability of the P100. *Electroencephalogr Clin Neurophysiol*, 68(2): 153-156.

- Okubo, A., Rosa, R.H., Jr., Bunce, C.V., Alexander, R.A., Fan, J.T., Bird, A. C, Luthert, P.J. (1999). The relationships of age changes in retinal pigment epithelium and Bruch's membrane. *Invest Ophthalmol Vis Sci*, 40(2): 443-9.

- Olver, J., Paileikhoff, D., Bird, A.C. (1990). Morphometric analysis of age changes in the choriocapillaris. *Invest Ophthalmol Vis Sci*, 31: 47.

- O'Malley, D.M. and Masland, R.H. (1989). Co-release of acetylcholine and gamma-aminobutyric acid by a retinal neuron. *Proc Natl Acad Sci U S A*, 86(9): 3414-3418.

- Organisciak, D.T., Wang, H.M., Li, Z.Y., Tso, M.O. (1985). The protective effect of ascorbate in retinal light damage of rats. *Invest Ophthalmol Vis Sci*, 26 (11): 1580-1588.

- Osterberg, G. (1935). Topography of the layer of rods and cones in the human retina. *Acta Ophthalmol (Suppl.)*, 6: 1-103.

- Owens, S.L., Guymer, R.H., Gross-Jendroska, M., Bird, A.C. (1999). Fluorescein angiographic abnormalities after prophylactic macular photocoagulation for high-risk age-related maculopathy. *Am J Ophthalmol*, 127(6): 681-687.

- Owsley, C., Jackson, G.R., Cideciyan, A.V., Huang, Y., Fine, S.L., Ho, A.C., Maguire, M.G., Lolley, V., Jacobson, S.G. (2000). Psychophysical evidence for rod vulnerability in age-related macular degeneration. *Invest Ophthalmol Vis Sci*, 41(1): 267-273.

- Owsley, C., Jackson, G.R., White, M., Feist, R., Edwards, D. (2001). Delays in rod-mediated dark adaptation in early age-related maculopathy. *Ophthalmology*, 108(7): 1196-1202.

- Owsley, C., Sloane, M.E., Skala, H.W., Jackson, C.A. (1990). A comparison of the Regan low-contrast letter charts and contrast sensitivity testing in older patients. *Clin Vis Sci*, 5: 325-334.

- Paetkau, M.E., Boyd, T.A., Grace, M., Bach-Mills, J., Winship, B. (1978). Senile disciform macular degeneration and smoking. *Can J Ophthalmol*, 13(2): 67-71.

- Pagliarini, S., Moramarco, A., Wormald, R.P., Piguet, B., Carresi, C., Balacco-Gabrieli, C., Sehmi, K.S., Bird, A.C. (1997). Age-related macular disease in rural southern Italy. *Arch Ophthalmol*, 115(5): 616-22.

- Palmowski, A.M., Allgayer, R., Heinemann-Vernaleken, B., Ruprecht, K.W. (2002). Influence of photodynamic therapy in choroidal neovascularization on focal retinal function

assessed with the multifocal electroretinogram and perimetry. *Ophthalmology*, **109**(10): 1788-1792.

• Panda-Jonas, S., Jonas, J.B., Jakobczyk-Zmija, M. (1996). Retinal pigment epithelial cell count, distribution, and correlations in normal human eyes. *Am J Ophthalmol*, **121**(2): 181-189.

• Papermaster, D.S., Schneider, B.G., Zorn, M.A., Kraehenbuhl, J.P. (1978). Immunocytochemical localization of a large intrinsic membrane protein to the incisures and margins of frog rod outer segment disks. *J Cell Biol*, **78**(2): 415-425.

• Parisi, V. (2001). Electrophysiological evaluation of the macular cone adaptation: VEP after photostress. A review. *Doc Ophthalmol*, **102**(3): 251-262.

• Parisi, V. and Bucci, M.G. (1992). Visual Evoked-Potentials after Photostress in Patients with Primary Open-Angle Glaucoma and Ocular Hypertension. *Invest Ophthalmol Vis Sci*, **33**(2): 436-442.

• Parisi, V., Canu, D., Iarossi, G., Olzi, D., Falsini, B. (2002). Altered recovery of macular function after bleaching in Stargardt's disease-fundus flavimaculatus: Pattern VEP evidence. *Invest Ophthalmol Vis Sci*, **43**(8): 2741-2748.

• Parisi, V., Pierelli, F., Restuccia, R., Spadaro, M., Parisi, L., Colacino, G., Bucci, M.G. (1998). Impaired VEP after photostress response in multiple sclerosis patients previously affected by optic neuritis. *Evoked Potentials - Electroencephalogr Clin Neurophysiol*, **108**(1): 73-79.

• Parisi, V., Uccioli, L., Monticone, G., Parisi, L., Durola, L., Pernini, C., Neuschuler, R., Menzinger, G., Bucci, M.G. (1995). Visual-Evoked Potentials after Photostress in Newly-Diagnosed Insulin-Dependent Diabetes Patients. *Graefes Arch Clin Exp Ophthalmol*, **233**(10) :601-604.

• Parisi, V., Uccioli, L., Monticone, G., Parisi, L., Menzinger, G., Bucci, M.G. (1994). Visual evoked potentials after photostress in insulin-dependent diabetic patients with or without retinopathy. *Graefes Arch Clin Exp Ophthalmol*, **232**(4): 193-198.

• Park, S.S., Sigelman, J., Gragoudas, E.S. (1994). The Anatomy and Cell Biology of the Retina. In: W. Tasman, E.A. Jaeger, Eds. *Duane's Foundations of Clinical Ophthalmology (Vol 1)*. Philadelphia: Lippincott. 1.

• Patel, A.S. (1966). Spatial resolution by the human visual system. The effect of mean retinal illuminance. *J Opt Soc Am*, **56**(5): 689-694.

• Pauleikhoff, D., Chen, J.C., Chisholm, I.H., Bird, A.C. (1990). Choroidal perfusion abnormality with age-related Bruch's membrane change. *Am J Ophthalmol*, **109**(2): 211-217.

• Pauleikhoff, D., Harper, C.A., Marshall, J., Bird, A.C. (1990). Aging changes in Bruch's membrane. A histochemical and morphologic study. *Ophthalmology*, **97**(2): 171-178.

• Pauleikhoff, D., Hermans, P., Holz, F.G., Bird, A.C. (2004). Histopathology. In: F.G. Holz, D. Pauleikhoff, R.F. Spaide, A.C. Bird, Eds. *Age-Related Macular Degeneration*. Berlin: Springer. 48-64.

• Pauleikhoff, D., Loffert, D., Spital, G., Radermacher, M., Dohrmann, J., Lommatzsch, A., Bird, A.C. (2002). Pigment epithelial detachment in the elderly. Clinical differentiation, natural course and pathogenetic implications. *Graefes Arch Clin Exp Ophthalmol*, 240(7): 533-538.

• Pauleikhoff, D., Sheraidah, G., Marshall, J., Bird, A.C., Wessing, A. (1994). Biochemical and histochemical analysis of age related lipid deposits in Bruch's membrane. *Ophthalmologe*, 91(6): 730-734.

• Pauleikhoff, D., Zuels, S., Sheraidah, G.S., Marshall, J., Wessing, A., Bird, A.C. (1992). Correlation between biochemical composition and fluorescein binding of deposits in Bruch's membrane. *Ophthalmology*, 99(10): 1548-1553.

• Pautler, E.L., Murakami, M., Nosaki, H. (1968). Differentiation of P 3 subcomponents in isolated mammalian retinas. *Vision Res*, 8(4): 489-91.

• Paupoo, A.A., Mahroo, O.A., Friedburg, C., Lamb, T.D. (2000). Human cone photoreceptor responses measured by the electroretinogram a-wave during and after exposure to intense illumination. *J Physiol*, 529(2): 469-482.

• Peachey, N.S., Alexander, K.R., Fishman, G.A. (1987). Rod and cone system contributions to oscillatory potentials: an explanation for the conditioning flash effect. *Vision Res*, 27(6): 859-866.

• Penfold, P.L., Killingsworth, M.C., Sarks, S.H. (1985). Senile macular degeneration: the involvement of immunocompetent cells. *Graefes Arch Clin Exp Ophthalmol*, 223(2): 69-76.

• Penfold, P.L., Liew, S.C., Madigan, M.C., Provis, J.M. (1997). Modulation of major histocompatibility complex class II expression in retinas with age-related macular degeneration. *Invest Ophthalmol Vis Sci*, 38(10): 2125-2133.

• Penfold, P.L., Madigan, M.C., Gillies, M.C., Provis, J.M. (2001). Immunological and aetiological aspects of macular degeneration. *Prog Retin Eye Res*, 20(3): 385-414.

• Penn, R.D. and Haggins, W.A. (1969). Signal transmission along retinal rods and the origin of the a-wave. *Nature*, 223: 201-205.

• Perlman, I. (2003). The Electroretingram: ERG. In: www.webvision.med.utah/edu.

• Perlman, I., Segev, E., Mazawi, N., Merhav-Armon, T., Lei, B., Leibu, R. (2001). Visual evoked cortical potential can be used to differentiate between uncorrected refractive error and macular disorders. *Doc Ophthalmol*, 102(1): 41-62.

• Perry, V.H., Oehler, R., Cowey, A. (1984). Retinal ganglion cells that project to the dorsal lateral geniculate nucleus in the macaque monkey. *Neuroscience*, 12(4): 1101-23.

• Phipps, J.A., Guymer, R.H., Vingrys, A.J. (2003). Loss of cone function in age-related maculopathy. *Invest Ophthalmol Vis Sci*, **44**(5): 2277-2283.

• Piguet, B., Wells, J.A., Palmvang, I.B., Wormald, R., Chisholm, I.H., Bird, A.C. (1993). Age-related Bruch's membrane change: a clinical study of the relative role of heredity and environment. *Br J Ophthalmol*, **77**(7): 400-403.

• Pirenne, M.H. (1962). Directional sensitivity of the rods and cones. In: H. Davidson, Ed. *The Eye, Vol. 2. New York: Academic Press.*

• Pokorny, J., Smith, V.C., Ernest, J.T. (1980). Macular color vision defects: specialized psychophysical testing in acquired and hereditary chorioretinal diseases. *Int Ophthalmol Clin*, **20**(1): 53-81.

• Pollack, A., Marcovich, A., Bukelman, A., Oliver, M. (1996). Age-related macular degeneration after extracapsular cataract extraction with intraocular lens implantation. *Ophthalmology*, **103**(10): 1546-54.

• Polyak, S.L. (1941). The Retina. Chicago: University of Chicago Press.

• Porciatti, V., Bagnoli, P., Alesci, R. (1987). ON- and OFF- activity in the retinal and tectal responses to focal stimulation with uniform or patterned stimuli. *Clin Vis Sci*, **2**: 93-102.

• Porciatti, V., Falsini, B., Fadda, A., Bolzani, R. (1989). Steady-state analysis of the focal ERG to pattern and flicker: relationship between ERG components and retinal pathology. *Clin Vis Sci*, **4**: 323-332.

• Pourcho, R.G. (1996). Neurotransmitters in the retina. *Curr Eye Res*, **15**(7): 797-803.

• RAD (1999). A prospective, randomized, double-masked trial on radiation therapy for neovascular age-related macular degeneration (RAD Study). Radiation Therapy for Age-related Macular Degeneration. *Ophthalmology*, **106**(12): 2239-2247.

• Ramrattan, R.S., van der Schaft, T.L., Mooy, C.M., de Bruijn, W.C., Mulder, P.G., de Jong, P.T. (1994). Morphometric analysis of Bruch's membrane, the choriocapillaris, and the choroid in aging. *Invest Ophthalmol Vis Sci*, **35**(6): 2857-2864.

• Rando, R.R. (1990). The chemistry of vitamin A and vision. *Angew Chem Int Ed Engl*, **29**: 461-480.

• Rappaport, D.H. (1995). Genesis of the retinal pigment epithelium in the macaque monkey. *J Comp Neurol*, **363**: 359-376.

• Ravilico, G., Rinaldi, G., Solimano, N. (1995). Oscillatory potentials in subjects with treated hypertension. *Ophthalmologica*, **209**: 187-189

• Raviola, E. and Gilula, N.B. (1975). Intramembrane organization of specialized contacts in the outer plexiform layer of the retina. A freeze-fracture study in monkeys and rabbits. *J Cell Biol*, **65**(1): 192-222.

• Regan, D. (1989). Human Brain Electrophysiology. New York: Elsevier Science Publishing Co Ltd. 327.

• Regan,D. and Neima, D. (1983). Low-contrast letter charts as a test of visual function. *Ophthalmology*, **90**(10): 1192-1200.

• Reichel, E., Berrocal, A.M., Ip, M., Kroll, A.J., Desai, V., Duker, J.S., Puliafito, C.A. (1999). Transpupillary thermotherapy of occult subfoveal choroidal neovascularization in patients with age-related macular degeneration. *Ophthalmology*, **106**(10): 1908-1914.

• Remulla, J.F., Gaudio, A.R., Miller, S., Sandberg, M.A. (1995). Foveal electroretinograms and choroidal perfusion characteristics in fellow eyes of patients with unilateral neovascular age-related macular degeneration. *Br J Ophthalmol*, **79**(6): 558-561.

• Richter, A.M., Kelly, B., Chow, J., Liu, D.J., Towers, G.H., Dolphin, D., Levy, J.G. (1987). Preliminary studies on a more effective phototoxic agent than hematoporphyrin. *J Natl Cancer Inst*, **79**(6): 1327-1332.

• Rickman, D.W. and Brecha, N.C. (1989). Morphologies of somatostatin-immunoreactive neurons in the rabbit retina. In: R. Weiler, N.N. Osbourne, Eds. *Neurobiology of the Inner Retina*. Berlin: Springer-Verlag. 461-468.

• Riggs, L.A. (1941). Continuous and reproducible records of the electrical activity of the human retina. *Proc Soc Exp Biol Med*, **48**: 204-207.

• Riggs, R.A., Johnson, E.P., Schick, A.M.L. (1964). Electrical responses of the human eye to moving stimulus patterns. *Science*, **144**: 567.

• Roberts, W.G. and Hasan, T. (1992). Role of neovasculature and vascular permeability on the tumor retention of photodynamic agents. *Cancer Res*, **52**(4): 924-930.

• Robson, J.G. and Frishman, L.J. (1995). Response linearity and kinetics of the cat retina: the bipolar cell component of the dark-adapted electroretinogram. *Vis Neurosci*, **12**(5): 837-850.

• Robson, J.G. and Frishman, L.J. (1996). Photoreceptor and bipolar cell contributions to the cat electroretinogram: a kinetic model for the early part of the flash response. *J Opt Soc Am A*, **13**(3): 613-622.

• Robson, J.G. and Frishman, L.J. (1999). Dissecting the dark-adapted electroretinogram. *Doc. Ophthalmol*, **95**: 187-215.

• Rodieck, R. (1973). The Vertebrate Retina: Principles of Structure and Function. San Francisco: WH Freeman & Co.

• Rodieck, R.W., Binmoeller, K.F., Dineen, J. (1985). Parasol and midget ganglion cells of the human retina. *J Comp Neurol*, **233**(1): 115-32.

• Rodieck, R. and Ford, R. (1969). The cat local electroretinogram to incremental stimuli. *Vision Res*, **9**: 1-24.

• Roe, A.W. and Ts'o, D.Y. (1995). Visual topography in primate V2: multiple representation across functional stripes. *J Neurosci*, **15**: 3689.

• Rovamo, J., Virsu, V., Nasanen, R. (1978). Cortical magnification factor predicts the photopic contrast sensitivity of peripheral vision. *Nature*, **271**(5640): 54-56.

• Roy, M. and Kaiser-Kupfer, M. (1990). Second eye involvement in age-related macular degeneration: a four-year prospective study. *Eye*, **4** (6): 813-818.

• Rungger-Brandle, E., Englert, U., Leuenberger, P.M. (1987). Exocytic clearing of degraded membrane material from pigment epithelial cells in frog retina. *Invest Ophthalmol Vis Sci*, **28**(12): 2026-2037.

• Rushton, W.A.H. (1955). The bleaching and regeneration of rhodopsin in the living eye of the albino rabbit and of man. *Optica Acta*, **1**:183-190.

• Rushton, W.A.H. (1965). The Ferrier Lecture 1962: Visual Adaptation. *Proc R Soc*, **162**: 20-46.

• Ruther, K., Breidenbach, K., Schwartz, R., Hassenstein, A., Richard, G. (2003). Testing central retinal function with multifocal electroretinography before and after photodynamic therapy. *Ophthalmologe*, **100**(6): 459-464.

• Ryeom, S.W., Sparrow, J.R., Silverstein, R.L. (1996). CD36 participates in the phagocytosis of rod outer segments by retinal pigment epithelium. *J Cell Sci*, **109**(2): 387-395.

• Saari, J.C. (2000). Biochemistry of visual pigment regeneration: the Friedenwald lecture. *Invest Ophthalmol Vis Sci*, **41**(2): 337-348.

• Said, F.S. and Weale, R.A. (1959). The variation with age of the spectral transmissivity of the living human crystalline lens. *Gerontologia*, **3**: 213-231.

• Sakman, B. and Creutzfeld, O.D. (1969). Scotopic and mesopic light adaptation in the cats retina. *Pflugers Arch*, **313**: 168-185.

• Sandberg, M.A. and Ariel, M. (1977). A hand-held, two-channel stimulator-ophthalmoscope. *Arch Ophthalmol*, **95**(10): 1881-1882.

• Sandberg, M.A. and Gaudio, A.R. (1995). Slow photostress recovery and disease severity in age-related macular degeneration. *Retina*, **15**(5): 407-412.

• Sandberg, M.A., Miller, S., Gaudio, A.R. (1993). Foveal cone ERGs in fellow eyes of patients with unilateral neovascular age-related macular degeneration. *Invest Ophthalmol Vis Sci*, **34**(12): 3477-3480.

• Sandberg, M.A., Pawlyk, B.S., Berson, E.L. (1996). Isolation of focal rod electroretinograms from the dark-adapted human eye. *Invest Ophthalmol Vis Sci*, **37**(5): 930-934.

• Sandberg, M.A., Weiner, A., Miller, S., Gaudio, A.R. (1998). High-risk characteristics of fellow eyes of patients with unilateral neovascular age-related macular degeneration. *Ophthalmology*, 105(3): 441-447.

• Sarks, S.H., Arnold, J.J., Killingsworth, M. C., Sarks, J.P. (1999). Early drusen formation in the normal and aging eye and their relation to age related maculopathy: a clinicopathological study. *Br J Ophthalmol*, 83(3): 358-68.

• Sarks, J.P., Sarks, S.H., Killingsworth, M.C. (1988). Evolution of geographic atrophy of the retinal pigment epithelium. *Eye*, 2(5): 552-577.

• Sarks, J.P., Sarks, S.H., Killingsworth, M.C. (1994). Evolution of soft drusen in age-related macular degeneration. *Eye*, 8(3): 269-283.

• Sarks, S.H. (1976). Ageing and degeneration in the macular region: a clinico-pathological study. *Br J Ophthalmol*, 60(5): 324-341.

• Sarks, S.H. (1982). Drusen patterns predisposing to geographic atrophy of the retinal pigment epithelium. *Aust J Ophthalmol*, 10 (2) 91-97.

• Sarks, S.H., Van Driel, D., Maxwell, L., Killingsworth, M. (1980). Softening of drusen and subretinal neovascularization. *Trans Ophthalmol Soc U K*, 100(3): 414-422.

• Sarraf, D., Gin, T., Yu, F., Brannon, A., Owens, S.L., Bird, A.C. (1999). Long-term drusen study. *Retina*, 19(6): 513-519.

• Saszik, S.M., Robson, J.G., Frishman, L.J. (2002). The scotopic threshold response of the dark-adapted electroretinogram of the mouse. *J Physiol*, 543(3): 899-916.

• Sawusch, M., Pokorny, J., Smith, V.C. (1987). Clinical electroretinography for short wavelength sensitive cones. *Invest Ophthalmol Vis Sci*, 28(6): 966-974.

• Schatz, H. and McDonald, H.R. (1989). Atrophic macular degeneration. Rate of spread of geographic atrophy and visual loss. *Ophthalmology*, 96(10): 1541-1551.

• Schefrin, B.E., Werner, J.S., Plach, M., Utlaut, N., Switkes, E. (1992). Sites of age-related sensitivity loss in a short-wave cone pathway. *J Opt Soc Am A*, 9(3): 355-363.

• Schertler, G.F., Villa, C., Henderson, R. (1993). Projection structure of rhodopsin. *Nature*, 362(6422): 770-772.

• Schmidt, S., Saunders, A.M., De La Paz, M.A., Postel, E.A., Heinis, R.M., Agarwal, A., Scott, W.K., Gilbert, J.R., McDowell, J.G., Bazyk, A., Gass, J.D., Haines, J.L., Pericak-Vance, M.A. (2000). Association of the apolipoprotein E gene with age-related macular degeneration: possible effect modification by family history, age, and gender. *Mol Vis*, 6: 287-293.

• Schmolesky, M. (2000). The Primary Visual Cortex. In: www.webvision.med.utah/edu.

- Schutt, F., Bergmann, M., Holz, F.G., Kopitz, J. (2002). Isolation of intact lysosomes from human RPE cells and effects of A2-E on the integrity of the lysosomal and other cellular membranes. *Graefes Arch Clin Exp Ophthalmol*, **240**(12): 983-988.

- Schutt, F., Ueberle, B., Schnolzer, M., Holz, F.G., Kopitz, J. (2002). Proteome analysis of lipofuscin in human retinal pigment epithelial cells. *FEBS Lett*, **528**(1-3): 217-221.

- Schweizer, N.M.J. and Troelestra, A. (1965). A negative component in the b-wave of the human ERG. *Ophthalmologica*, **149**: 230-235.

- Scott, T.A., Augsburger, J.J., Brady, L.W., Hernandez, C., Woodleigh, R. (1991). Low dose ocular irradiation for diffuse choroidal hemangiomas associated with bullous nonrhegmatogenous retinal detachment. *Retina*, **11**(4): 389-393.

- Seddon, J.M., Ajani, U.A., Sperduto, R.D., Hiller, R., Blair, N., Burton, T.C., Farber, M.D., Gragoudas, E.S., Haller, J., Miller, D.T. (1994). Dietary carotenoids, vitamins A, C, and E, and advanced age-related macular degeneration. Eye Disease Case-Control Study Group. *JAMA*, **272**(18): 1413-1420.

- Seddon, J.M., Rosner, B., Sperduto, R.D., Yannuzzi, L., Haller, J.A., Blair, N.P., Willett, W. (2001). Dietary fat and risk for advanced age-related macular degeneration. *Arch Ophthalmol*, **119**(8): 1191-1199.

- Seiple, W.H., Siegel, I.M., Carr, R.E., Mayron, C. (1986). Evaluating macular function using the focal ERG. *Invest Ophthalmol Vis Sci*, **27**(7): 1123-1130.

- Severin, S.L. (1980). Qualitative photostress testing for the diagnosis of cystoid macular edema. *J Am Intraocul Implant Soc*, **6**(1): 25-27.

- Severin, S.L., Harper, J.Y., Culver, J.F. (1963). Photostress test for the evaluation of macular function. *Arch Ophthalmol*, **70**: 593.

- Severns, M.L., Johnson, M.A., Bresnick, G.H. (1994). Methodologic dependence of electroretinogram oscillatory potential amplitudes. *Doc Ophthalmol*, **86**(1): 23-31.

- Shamsi, F.A. and Boulton, M. (2001). Inhibition of RPE lysosomal and antioxidant activity by the age pigment lipofuscin. *Invest Ophthalmol Vis Sci*, **42**(12): 3041-3046.

- Sharpe, L.T. and Stockman, A. (1999). Rod pathways: the importance of seeing nothing. *Trends Neurosci*, **22**(11): 497-504.

- Sheraidah, G., Steinmetz, R., Maguire, J., Pauleikhoff, D., Marshall, J., Bird, A.C. (1993). Correlation between lipids extracted from Bruch's membrane and age. *Ophthalmology*, **100**(1): 47-51.

- Sherman, J., Bass, S.J., Noble, K.G., Nath, S., Sutija, V. (1986). Visual evoked potential (VEP) delays in central serous choroidopathy. *Invest Ophthalmol Vis Sci*, **27**(2): 214-221.

- Sherman, M.D. and Henkind, P. (1988). Photostress recovery in chronic open angle glaucoma. *Br J Ophthalmol*, **72**(9): 641-645.

• Shields, C.L., Shields, J.A., DePotter, P., Kheterpal, S. (1996). Transpupillary thermotherapy in the management of choroidal melanoma. *Ophthalmology*, 103(10): 1642-50.

• Shiells, R. A. and G. Falk (1999). Contribution of rod, on-bipolar, and horizontal cell light responses to the ERG of dogfish retina. *Vis Neurosci*, 16(3): 503-11.

• Shiells, R.A., Falk, G., Naghshineh, S. (1981). Action of glutamate and aspartate analogues on rod horizontal and bipolar cells. *Nature*, 294(5841): 592-594.

• Sieving, P.A. (1991). Retinal ganglion cell loss does not abolish the STR of the cat and human ERG. *Clin Vis Sci*, 6: 149-158.

• Sieving, P.A., Frishman, L.J., Steinberg, R.H. (1986). Scotopic threshold response of proximal retina in cat. *J Neurophysiol*, 56(4): 1049-1061.

• Sieving, P.A., Murayama, K., Naarendorp, F. (1994). Push-pull model of the primate photopic electroretinogram: a role for hyperpolarizing neurons in shaping the b-wave. *Vis Neurosci*, 11(3): 519-532.

• Sieving, P.A. and Nino, C. (1988). Scotopic threshold response (STR) of the human electroretinogram. *Invest Ophthalmol Vis Sci*, 29(11): 1608-1614.

• Sigelman, J. (1991). Foveal drusen resorption one year after perifoveal laser photocoagulation. *Ophthalmology*, 98(9): 1379-1383.

• Sigleman, J. and Ozanics, V. (1982). Retina. In: F.A. Jakobiec, Ed. *Ocular Anatomy, Embryology, and Teratology; Vol 15*. Philadelphia: Harper & Row. 441.

• Simonsen, S.E. and Rosenberg, T. (1996). Reappraisal of a short-wavelength-sensitive (S-cone) recording technique in routine clinical electroretinography. *Doc Ophthalmol*, 91(4): 323-332.

• Sjostrand, J. (1979). Contrast sensitivity in macular disease using a small-field and a large-field TV-system. *Acta Ophthalmol (Copenh)*, 57(5): 832-846.

• Sjostrand, J. and Frisen, L. (1977). Contrast sensitivity in macular disease. A preliminary report. *Acta Ophthalmol (Copenh)*, 55(3): 507-514.

• Skoog, K.O. and Nilsson, S.E. (1974). The c-wave of the human D.C. registered ERG. I. A quantitative study of the relationship between c-wave amplitude and stimulus intensity. *Acta Ophthalmol (Copenh)*, 52(5): 759-773.

• Skoog, K.O., Textorius, O., Nilsson, S.E. (1975). Effects of ethyl alcohol on the directly recorded standing potential of the human eye. *Acta Ophthalmol (Copenh)*, 53(5): 710-720.

• Sloan, L.L. (1942). The use of pseudo-isochromatic charts in detecting central scotomas due to lesions in the conducting pathways. *Am J Ophthalmol*, 25: 1352-1356.

• Sloan, P.G. (1968). Clinical application of the photostress test. *Am J Optom Arch Am Acad Optom*, 45(9): 617-623.

• Smedsrod, B., Melkko, J., Araki, N., Sano, H., Horiuchi, S. (1997). Advanced glycation end products are eliminated by scavenger-receptor-mediated endocytosis in hepatic sinusoidal Kupffer and endothelial cells. *Biochem J*, **322**(2). 567-573.

• Smiddy, W.E. and Fine, S.L. (1984). Prognosis of patients with bilateral macular drusen. *Ophthalmology*, **91**(3): 271-277.

• Smith, E.L., 3rd, Harwerth, R.S., Crawford, M.L., Duncan, G.C. (1989). Contribution of the retinal ON channels to scotopic and photopic spectral sensitivity. *Vis Neurosci*, **3**(3): 225-239.

• Smith, V.C., Pokorny, J., Diddie, K.R. (1978). Color matching and Stiles-Crawford effect in central serous choroidopathy. *Mod Probl Ophthalmol*, **19**: 284-295.

• Smith, V.C., Pokorny, J., Diddie, K.R. (1988). Color matching and the Stiles-Crawford effect in observers with early age-related macular changes. *J Opt Soc Am A*, **5**(12): 2113-2121.

• Smith, V.C., Pokorny, J., Ernest, J.T., Starr, S.J. (1978). Visual function in acute posterior multifocal placoid pigment epitheliopathy. *Am J Ophthalmol*, **85**(2): 192-199.

• Smith, W., Mitchell, P., Leeder, S.R. (1996). Smoking and age-related maculopathy. The Blue Mountains Eye Study. *Arch Ophthalmol*, **114**(12): 1518-1523.

• Smith, W., Mitchell, P., Leeder, S.R. (2000). Dietary fat and fish intake and age-related maculopathy. *Arch Ophthalmol*, **118**(3): 401-404.

• Smith, W., Mitchell, P., Wang, J.J. (1997). Gender, oestrogen, hormone replacement and age-related macular degeneration: results from the Blue Mountains Eye Study. *Aust N Z J Ophthalmol*, **25**(1): S13-15.

• Smith, W., Mitchell, P., Webb, K., Leeder, S.R. (1999). Dietary antioxidants and age-related maculopathy: the Blue Mountains Eye Study. *Ophthalmology*, **106**(4): 761-767.

• Snell, R.S. and Lemp, M.A. (1998). Clinical Anatomy of the Eye. Oxford: Blackwell Science.

• Snodderly, D.M. (1995). Evidence for protection against age-related macular degeneration by carotenoids and antioxidant vitamins. *Am J Clin Nutr*, **62**(6): 1448S-1461S.

• Snodderly, D.M., Brown, P.K., Delori, F.C., Auran, J.D. (1984). The macular pigment. I. Absorbance spectra, localization, and discrimination from other yellow pigments in primate retinas. *Invest Ophthalmol Vis Sci*, **25**(6): 660-673.

• Sohal, R.S. and Donato, H. (1978). Effects of experimentally altered life spans on the accumulation of flourescent age pigment in the housefly, Musca domestica. *Exp Gerontol*, **13**(5): 335-341.

• Solberg, Y., Rosner, M., Belkin, M. (1998). The association between cigarette smoking and ocular diseases. *Surv Ophthalmol*, **42**(6): 535-547.

- Sommer, A., Tielsch, J.M., Katz, J., Quigley, H.A., Gottsch, J.D., Javitt, J.C., Martone, J.F., Royall, R.M., Witt, K.A., Ezrine, S. (1991). Racial differences in the cause-specific prevalence of blindness in east Baltimore. *N Engl J Med*, 325(20): 1412-1417.

- Soucy, E., Wang, Y., Nirenberg, S., Nathans, J., Meister, M. (1998). A novel signaling pathway from rod photoreceptors to ganglion cells in mammalian retina. *Neuron*, 21(3): 481-493.

- Spaide, R.F., Armstrong, D., Browne, R. (2003). Continuing medical education review: choroidal neovascularization in age-related macular degeneration-what is the cause? *Retina*, 23(5): 595-614.

- Sperduto, R.D., Ferris, F.L., 3rd, Kurinij, N. (1990). Do we have a nutritional treatment for age-related cataract or macular degeneration? *Arch Ophthalmol*, 108(10): 1403-5.

- Sperduto, R.D., Hiller, R., Seigel, D. (1981). Lens opacities and senile maculopathy. *Arch Ophthalmol*, 99(6): 1004-1008.

- Sperduto, R.D., Seigel, D. (1980). Senile lens and senile macular changes in a population-based sample. *Am J Ophthalmol*, 90(1): 86-91.

- Sperling, H.G., Johnson, C., Harwerth, R.S. (1980). Differential spectral photic damage to primate cones. *Vision Res*, 20(12): 1117-1125.

- Speros, P. and J. Price (1981). Oscillatory potentials. History, techniques and potential use in the evaluation of disturbances of retinal circulation. *Surv Ophthalmol*, 25(4): 237-52.

- Spilsbury, K., Garrett, K.L., Shen, W.Y., Constable, I.J., Rakoczy, P.E. (2000). Overexpression of vascular endothelial growth factor (VEGF) in the retinal pigment epithelium leads to the development of choroidal neovascularization. *Am J Pathol*, 157(1): 135-144.

- Spraul, C.W. and Grossniklaus, H.E. (1997). Characteristics of Drusen and Bruch's membrane in postmortem eyes with age-related macular degeneration. *Arch Ophthalmol*, 115(2): 267-273.

- Stangos, N., Voutas, S., Topouzis, F., Karampatakis, V. (1995). Contrast sensitivity evaluation in eyes predisposed to age-related macular degeneration and presenting normal visual acuity. *Ophthalmologica*, 209(4): 194-198.

- Starita, C., Hussain, A.A., Pagliarini, S., Marshall, J. (1996). Hydrodynamics of ageing Bruch's membrane: implications for macular disease. *Exp Eye Res*, 62(5): 565-572.

- Steinberg, R., Oakley, B.I., Neimeyer, G. (1980). Light-evoked changes in [K+]0 in the retina of intact cat eye. *J Neurophysiol*, 44: 897-921.

- Steinberg, R.H., Linsenmeier, R.A., Griff, E.R. (1983). Three light-evoked responses of the retinal pigment epithelium. *Vision Res*, 23(11): 1315-1323.

- Steinberg, R.H., Linsenmeier, R.A., Griff, E.R. (1985). Retinal pigment epithelial cell contributions to the electroretinogram and electrooculogram. *Prog Retin Eye Res*, 4: 33-66.

• Steinberg, R.H., Schmidt, R., Brown, K.T. (1970). Intracellular responses to light from cat pigment epithelium: origin of the electroretinogram c-wave. *Nature*, 227(259): 728-730.

• Steinmetz, R.L., Haimovici, R., Jubb, C., Fitzke, F.W., Bird, A.C. (1993). Symptomatic abnormalities of dark adaptation in patients with age-related Bruch's membrane change. *Br J Ophthalmol*, 77(9): 549-554.

• Stirling, C.E. and Lee, A. (1980). Ouabain-H-3 autoradiography of frog retina. *J Cell Biol*, 85(2): 313-324.

• Stockman, A., MacLeod, D.I., DePriest, D.D. (1991). The temporal properties of the human short-wave photoreceptors and their associated pathways. *Vision Res*, 31(2): 189-208.

• Stockton, R.A. and Slaughter, M.M. (1989). B-wave of the electroretinogram. A reflection of ON bipolar cell activity. *J Gen Physiol*, 93(1): 101-122.

• Stone, E.M., Webster, A.R., Vandenburgh, K., Streb, L.M., Hockey, R.R., Lotery, A.J., Sheffield, V.C. (1998). Allelic variation in ABCR associated with Stargardt disease but not age-related macular degeneration. *Nat Genet*, 20(4): 328-329.

• Stone, J. and Dreher, Z. (1987). Relationship between astrocytes, ganglion cells, and vasculature of the retina. *J Comp Neurol*, 255: 35-49.

• Stone, J. and Fukuda, Y. (1974). Properties of cat retinal ganglion cells: a comparison of W-cells with X- and Y- cells. *J Neurophysiol*, 37: 722.

• Strahlman, E.R., Fine, S.L., Hillis, A. (1983). The second eye of patients with senile macular degeneration. *Arch Ophthalmol*, 101(8): 1191-1193.

• Strettoi, E., Raviola, E., Dacheux, R.F. (1992). Synaptic connections of the narrow-field, bistratified rod amacrine cell (AII) in the rabbit retina. *J Comp Neurol*, 325(2): 152-68.

• Stur, M., Tittl, M., Reitner, A., Meisinger, V. (1996). Oral zinc and the second eye in age-related macular degeneration. *Invest Ophthalmol Vis Sci*, 37(7): 1225-1235.

• Sunness, J.S., Bressler, N.M., Maguire, M.G. (1994). Scanning laser ophthalmoscopic analysis of the pattern of visual loss in age-related geographic atrophy of the macula. *Am J Ophthalmol*, 119(2): 143-151.

• Sunness, J.S., Johnson, M.A., Massof, R.W., Marcus, S. (1988). Retinal sensitivity over drusen and nondrusen areas. A study using fundus perimetry. *Arch Ophthalmol*, 106(8): 1081-1084.

• Sunness, J.S., Massof, R.W., Bressler, N.M., Bressler, S.B. (1989). S cone pathway sensitivity in eyes with high risk and low risk drusen characteristics. *Appl Opt*, 28: 1158-1164.

• Sunness, J.S., Massof, R.W., Johnson, M.A., Bressler, N.M., Bressler, S.B., Fine, S.L. (1989). Diminished foveal sensitivity may predict the development of advanced age-related macular degeneration. *Ophthalmology*, 96(3): 375-381.

• Sunness, J.S., Massof, R.W., Johnson, M.A., Finkelstein, D., Fine, S.L. (1985). Peripheral retinal function in age-related macular degeneration. *Arch Ophthalmol*, 103(6): 811-816.

• Sunness, J.S., Rubin, G.S., Applegate, C.A., Bressler, N.M., Marsh, M.J., Hawkins, B.S., Haselwood, D. (1997). Visual function abnormalities and prognosis in eyes with age-related geographic atrophy of the macula and good visual acuity. *Ophthalmology*, 104(10): 1677-1691.

• Sunness, J.S., Schuchard, R.A., Shen, N., Rubin, G.S., Dagnelie, G., Haselwood, D.M. (1995). Landmark-driven fundus perimetry using the scanning laser ophthalmoscope. *Invest Ophthalmol Vis Sci*, 36(9): 1863-1874.

• Sutter, E. (2000). The interpretation of multifocal binary kernels. *Doc Ophthalmol*, 100(2): 49-75.

• Sutter, E.E. (1992). A deterministic approach to non-linear systems analysis. In: R.B. Pinter, B. Nabet, Eds. *Nonlinear Vision*. Cleveland: CRC Press. 171-220.

• Sutter, E.E. and Bearse, M.A., Jr. (1999). The optic nerve head component of the human ERG. *Vision Res*, 39(3): 419-436.

• Sutter, E.E. and Tran, D. (1992). The field topography of ERG components in man-I. The photopic luminance response. *Vision Res*, 32(3): 433-446.

• Suzuki, S., Horiguchi, M., Tanikawa, A., Miyake, Y., Kondo, M. (1998). Effect of age on short-wavelength sensitive cone electroretinogram and long- and middle-wavelength sensitive cone electroretinogram. *Jpn J Ophthalmol*, 42(5): 424-430.

• Swanson, W.H., Birch, D.G., Anderson, J.L. (1993). S-cone function in patients with retinitis pigmentosa. *Invest Ophthalmol Vis Sci*, 34(11): 3045-3055.

• Tate, G.W. and Lynn, J.R. (1977). Principles of Quantitative Perimetry. New York: Grune and Stratton.

• Taylor, H.R., Munoz, B., West, S., Bressler, N.M., Bressler, S.B., Rosenthal, F.S. (1990). Visible light and risk of age-related macular degeneration. *Trans Am Ophthalmol Soc*, 88: 163-168.

• Textorius, O. (1978). The c-wave of the human electroretinogram in central retinal artery occlusion. *Acta Ophthalmol (Copenh)*, 56(5): 827-836.

• Tolentino, M.J., Miller, S., Gaudio, A.R., Sandberg, M.A. (1994). Visual field deficits in early age-related macular degeneration. *Vision Res*, 34(3): 409-413.

• Tomita, T. (1963). Electrical activity in the vertebrate retina. *Acta Soc Ophthalmol Jap*, 70: 766-768.

• Toussaint, D., Kuwabara, T., Cogan, D.G. (1961). Retinal vascular patterns. II. Human retinal vessels studied in three dimensions. *Arch Ophthalmol*, 65: 575-581.

• Treatment of Age-Related Macular Degeneration with Photodynamic Therapy (TAP) Study Group (1999). Photodynamic therapy of subfoveal choroidal neovascularization in age-related macular degeneration with verteporfin: one-year results of 2 randomized clinical trials--TAP report.. *Arch Ophthalmol*, 117(10): 1329-1345.

• Turner, D.L. and Cepko, C.L. (1987). A common progenitor for neurons and glia persists in rat retina late in development. *Nature*, 328(6126): 131-136.

• Van Gisbergen, J. (2004). Neurophysiology of the Visual System. In: www.mbfys.kun.nl/mbfys/education/medical/webteach.

• Vaegan (1996). Electrode standards in electroretinography. *Doc Ophthalmol*, 92(3): 243-245.

• Vaegan, Graham, S.L., Goldberg, I., Buckland, L., Hollows, F.C. (1995). Flash and pattern electroretinogram changes with optic atrophy and glaucoma. *Exp Eye Res*, 60(6): 697-706.

• Valeton, J.M. and van Norren, D. (1982). Intraretinal recordings of slow electrical responses to steady illumination in monkey: isolation of receptor responses and the origin of the light peak. *Vision Res*, 22(3): 393-399.

• VandenLangenberg, G.M., Mares-Perlman, J.A., Klein, R., Klein, B.E., Brady, W.E., Palta, M. (1998). Associations between antioxidant and zinc intake and the 5-year incidence of early age-related maculopathy in the Beaver Dam Eye Study. *Am J Epidemiol*, 148(2): 204-214.

• Vaney, D.I. (1986). Morphological identification of serotonin-accumulating neurons in the living retina. *Science*, 233(4762): 444-446.

• Verhoeff, F.H. and Grossman, H.P. (1937). Pathogenesis of disciform degeneration of the macula. *Arch Ophthalmol*, 18: 561-585.

• Verma, L., Tewari, H.K., Nainiwal, S., Ravindranathan, J. (2004). Transpupillary thermotherapy in subfoveal choroidal neovascular membrane secondary to age-related macular degeneration. *Indian J Ophthalmol*, 52(1): 35-40.

• Verriest, G., Van De Velde, R., Vanderdonck, R. (1962). Etude quantitative de l'effet qu'exerce sur la discrimination chromatique une absorption selective de la partie froide de spectre visible. *Rev Opt (Paris)*, 41: 109-118.

• Verriest, G., Van Laethem, J., Uvijls, A. (1982). A new assessment of the normal ranges of the Farnsworth-Munsell 100-hue test scores. *Am J Ophthalmol*, 93(5): 635-642.

• Verriest, G., Vandervyver, R., Vanderdonck, R. (1962). Nouvelle recherche se rapportant a'l'influence du sexe et de l'age sur la discrimination chromatique, ainsi qu'a la signification practique du test 100 hue de Farnsworth-Munsell. *Rev Opt (Paris)*, 41: 499-509.

• Vinding, T., Appleyard, M., Nyboe, J., Jensen, G. (1992). Risk factor analysis for atrophic and exudative age-related macular degeneration. An epidemiological study of 1000 aged individuals. *Acta Ophthalmol (Copenh)*, 70(1): 66-72.

• Vingerling, J.R., Dielemans, I., Bots, M.L., Hofman, A., Grobbee, D.E., de Jong, P.T. (1995d). Age-related macular degeneration is associated with atherosclerosis. The Rotterdam Study. *Am J Epidemiol*, **142**(4): 404-409.

• Vingerling, J.R., Dielemans, I., Hofman, A., Grobbee, D.E., Hijmering, M., Kramer, C.F., de Jong, P.T. (1995a). The prevalence of age-related maculopathy in the Rotterdam Study. *Ophthalmology*, **102**(2): 205-210.

• Vingerling, J.R., Dielemans, I., Witteman, J.C., Hofman, A., Grobbee, D.E., de Jong, P.T. (1995b). Macular degeneration and early menopause: a case-control study. *Br Med J*, **310**(6994): 1570-1571.

• Vingerling, J.R., Hofman, A., Grobbee, D.E., de Jong, P.T. (1996). Age-related macular degeneration and smoking. The Rotterdam Study. *Arch Ophthalmol*, **114**(10): 1193-1196.

• Vingerling, J.R., Klaver, C.C., Hofman, A., de Jong, P.T. (1995c). Epidemiology of age-related maculopathy. *Epidemiol Rev*, **17**(2): 347-360.

• Vingrys, A.J. and Dwyer, P.S. (1990). Age related maculopathy with foveal sparing. *Clinical and Experimental Optometry*, **73**(5): 138-142.

• Vingrys, A.J. and King-Smith, P.E. (1988). A quantitative scoring technique for panel tests of color vision. *Invest Ophthalmol Vis Sci*, **29**(1): 50-63.

• Viswanathan, S., Frishman, L.J., Robson, J.G. (2000). The uniform field and pattern ERG in macaques with experimental glaucoma: removal of spiking activity. *Invest Ophthalmol Vis Sci*, **41**(9): 2797-2810.

• Viswanathan, S., Frishman, L.J., Robson, J.G., Harwerth, R.S., Smith, E.L., 3rd (1999). The photopic negative response of the macaque electroretinogram: reduction by experimental glaucoma. *Invest Ophthalmol Vis Sci*, **40**(6): 1124-1136.

• Viswanathan, S., Frishman, L.J., Robson, J.G., Walters, J.W. (2001). The photopic negative response of the flash electroretinogram in primary open angle glaucoma. *Invest Ophthalmol Vis Sci*, **42**(2): 514-522.

• Vuong, T.M. and Chabre, M. (1991). Deactivation kinetics of the transduction cascade of vision. *Proc Natl Acad Sci U S A*, **88**(21): 9813-9817.

• Wachtmeister, L. (1973a). On the oscillatory potentials of the human electroretinogram in light and dark adaptation. IV. Effect of adaptation to short flashes of light. Time interval and intensity of conditioning flashes. A Fourier analysis. *Acta Ophthalmol (Copenh)*, **51**(2): 250-269.

• Wachtmeister, L. (1974a). Luminosity functions of the oscillatory potentials of the human electroretinogram. *Acta Ophthalmol (Copenh)*, **52**(3): 353-366.

• Wachtmeister, L. (1980). Further studies of the chemical sensitivity of the oscillatory potentials of the electroretinogram (ERG) I. GABA- and glycine antagonists. *Acta Ophthalmol (Copenh)*, **58**(5): 712-725.

- Wachtmeister, L. (1981). Further studies of the chemical sensitivity of the oscillatory potentials of the electroretinogram (ERG). II. Glutamate-aspartate-and dopamine antagonists. *Acta Ophthalmol (Copenh)*, 59(2): 247-258.

- Wachtmeister, L. (1998). Oscillatory potentials in the retina: what do they reveal. *Prog Retin Eye Res*, 17(4): 485-521.

- Wachtmeister, L. and Dowling, J.E. (1978). The oscillatory potentials of the mudpuppy retina. *Invest Ophthalmol Vis Sci*, 17(12): 1176-1188.

- Wachtmeister, L. and el Azazi, M. (1985). Oscillatory potentials of the electroretinogram in patients with unilateral optic atrophy. *Ophthalmologica*, 191(1): 39-50.

- Wald, G. and Brown, P.K. (1965). Human colour vision and colour blindness. *Cold Spring Harb Symp Quant Biol*, 30: 345.

- Wali, N. and Leguire, L.E. (1992). Fundus pigmentation and the dark-adapted electroretinogram. *Doc Ophthalmol*, 80(1): 1-11.

- Walter, P., Widder, R.A., Luke, C., Konigsfeld, P., Brunner, R. (1999). Electrophysiological abnormalities in age-related macular degeneration. *Graefes Arch Clin Exp Ophthalmol*, 237(12): 962-968.

- Wang, G., Tanifuji, M., Tanaka, K. (1998). Funtional architecture in monkey inferotemporal cortex revealed by in vivo optical imaging. *Neurosci Res*, 32: 33-46.

- Wang, J.J., Mitchell, P., Smith, W. (1998). Refractive error and age-related maculopathy: the Blue Mountains Eye Study. *Invest Ophthalmol Vis Sci*, 39(11): 2167-2171.

- Wanger, P. and Persson, H.E. (1983). Pattern-reversal electroretinograms in unilateral glaucoma. *Invest Ophthalmol Vis Sci*, 24(6): 749-753.

- Warwick, R. (1976). Eugene Wolff's Anatomy of the Eye and Orbit. Philadelphia: Saunders.

- Wassell, J., Davies, S., Bardsley, W., Boulton, M. (1999). The photoreactivity of the retinal age pigment lipofuscin. *J Biol Chem*, 274 (34) 23828-23832.

- Wassle, H., Chun, M.H., Muller, F. (1987). Amacrine cells in the ganglion cell layer of the cat retina. *J Comp Neurol*, 265(3): 391-408.

- Webster, A.R., Heon, E., Lotery, A.J., Vandenburgh, K., Casavant, T.L., Oh, K.T., Beck, G., Fishman, G.A., Lam, B.L., Levin, A., Heckenlively, J.R., Jacobson, S.G., Weleber, R.G., Sheffield, V.C., Stone, E.M. (2001). An analysis of allelic variation in the ABCA4 gene. *Invest Ophthalmol Vis Sci*, 42(6): 1179-1189.

- Weiter, J.J., Delori, F., Dorey, C.K. (1988). Central sparing in annular macular degeneration. *Am J Ophthalmol*, 106(3): 286-292.

• West, S.K., Rosenthal, F.S., Bressler, N.M., Bressler, S.B., Munoz, B., Fine, S.L., Taylor, H.R. (1989). Exposure to sunlight and other risk factors for age-related macular degeneration. *Arch Ophthalmol*, 107(6): 875-879.

• West, S., Vitale, S., Hallfrisch, J., Munoz, B., Muller, D., Bressler, S., Bressler, N.M. (1994). Are antioxidants or supplements protective for age-related macular degeneration? *Arch Ophthalmol,* 112(2): 222-227.

• Wiegand, R.D., Giusto, N.M., Rapp, L.M., Anderson, R.E. (1983). Evidence for rod outer segment lipid peroxidation following constant illumination of the rat retina. *Invest Ophthalmol Vis Sci*, 24(10): 1433-1435.

• Wilden, U., Hall, S.W., Kuhn, H. (1986). Phosphodiesterase activation by photoexcited rhodopsin is quenched when rhodopsin is phosphorylated and binds the intrinsic 48-kDa protein of rod outer segments. *Proc Natl Acad Sci U S A*, 83(5): 1174-1178.

• Wilson, H.L., Schwartz D.M., Bhatt, H.R., McCulloch, C.E, Duncan, J.L. (2004). Statin and aspirin therapy are associated with decreased rates of choroidal neovascularization among patients with age-related macular degeneration. *Am J Ophthalmol,* 137(4): 615-24.

• Wing, G.L., Blanchard, G.C., Weiter, J.J. (1978). The topography and age relationship of lipofuscin concentration in the retinal pigment epithelium. *Invest Ophthalmol Vis Sci*, 17(7): 601-607.

• Wioland, N. and Bonaventure, N. (1984). Evidence for both photopic and scotopic characteristics in the c-wave of chicken and frog ERG. *Vision Res*, 24(2): 91-98.

• Witteman, J.C., Grobbee, D.E., Kok, F.J., Hofman, A., Valkenburg, H.A. (1989). Increased risk of atherosclerosis in women after the menopause. *Br Med J*, 298(6674): 642-644.

• Wood, C.C. (1982). Application of dipole localization methods to source identification of human evoked potentials. *Ann N Y Acad Sci*, 388: 139-155.

• Wu, G., Weiter, J.J., Santos, S., Ginsburg, L., Villalobos, R. (1990). The macular photostress test in diabetic retinopathy and age-related macular degeneration. *Arch Ophthalmol*, 108(11): 1556-1558.

• Wyszeki, G. and Stiles, W.S. (1982). Colour Science: Concepts and Methods, quantitative data and formulae. 2nd edition. New York: John Wiley.

• Xu, X. and Karwoski, C. (1995). Current source density analysis of the electroretinographic d wave of frog retina. *J Neurophysiol*, 73(6): 2459-2469.

• Yee, R. and Liebman, P.A. (1978). Light-activated phosphodiesterase of the rod outer segment. Kinetics and parameters of activation and deactivation. *J Biol Chem*, 253(24): 8902-8909.

• Yonemura, D., Kawasaki, K., Hasui, I. (1966). The early receptor potential in the human ERG. *Acta Soc Ophthalmol Jap*, 70: 766-768.

• Yonemura, D., Tsuzuki, K., Aoki, T. (1962). Clinical importance of the oscillatory potential in the human ERG. *Acta Ophthalmol (Copenh)*, **70**: S115-S123.

• Yoshikami, S. and Hagins, W.A. (1971). Light, calcium and the photocurrent of rods and cones. *Biophysiology Journal*, **11**: 47.

• Young, R.W. (1967). The renewal of photoreceptor cell outer segments. *J Cell Biol*, **33**(1): 61-72.

• Young, R.W. (1987). Pathophysiology of age-related macular degeneration. *Surv Ophthalmol*, **31**(5): 291-306.

• Young, R.W. (1988). Solar radiation and age-related macular degeneration. *Surv Ophthalmol*, **32**(4): 252-269.

• Young, R.W. and Bok, D. (1969). Participation of the retinal pigment epithelium in the rod outer segment renewal process. *J Cell Biol*, **42**(2): 392-403.

• Yu, M., Liang, X., Wen, F., Wu, D.Z., Luo, T. (1998). Analysis of oscillatory potentials of flash electroretinogram in frequency domain and time domain in retinal vein occlusion. *Yan Ke Xue Bao*, **14**(3): 176-181, 144.

• Zalutsky, R.A. and Miller, R.F. (1990). The physiology of somatostatin in the rabbit retina. *J Neurosci*, **10**(2): 383-393.

• Zeumer, C., Hanitzsch, R., Mattig, W.U. (1994). The c-wave of the electroretinogram possesses a third component from the proximal retina. *Vision Res*, **34**(20): 2673-2678.

• Zhang, H. (1994). Oscillatory potentials (OPs) in patients with age-related macular degeneration (AMD). *Invest Ophthalmol Vis Sci*, **35**(4): 1505.

• Zhao, J., Frambach, D.A., Lee, P.P., Lee, M., Lopez, P.F. (1995). Delayed macular choriocapillary circulation in age-related macular degeneration. *Int Ophthalmol*, **19**(1): 1-12.

• Zrenner, E., Baker, C.L., Hess, R.F., Olsen, B.T. (1987). Site of electroretinographic responses to pattern reversal and brightness stimuli in individual layers of the primate retina. *Fortschr Ophthalmol*, **84**(5): 491-495.

APPENDIX I

Subject Characteristics

Subject Initials	Age	Gender	VA /logMAR	Lens Grading			
				NO	NC	C	P
JB	57	F	0.0	2	2	0.5	0.5
GO	79	M	0.2	2	2	1	0.5
PG	66	F	0.2	2	2	1	1
CG	70	M	0.0	2.5	2.5	1	1
SM	68	F	0.0	2	3.5	0.5	2
CD	67	F	0.1	2	2	1	1
WD	75	M	0.2	3	3	2	2
RW	63	M	0.0	1.5	1.5	0.3	0.2
WF	69	M	0.1	2.5	2.5	1.5	1
MR	71	F	0.0	0.1	0.1	2.3	0.5
VE	80	F	0.1	4	4	3	2
MB	69	M	0.0	2.5	2.5	0.2	0.2
DJ	64	M	0.0	1	1	0.5	0.5
PA	76	M	0.0	1	1.7	0.1	0.1
GA	64	F	0.0	2.5	2.5	0.1	0.1
JJ	60	F	0.0	2	2	0.1	0.1
BB	64	F	0.0	1.5	1	0.5	0.5
KM	79	M	0.0	2	2	0.1	0.1
MA	72	F	0.0	0.1	0.1	0.1	0.1
AS	82	F	0.0	0.1	0.1	0.7	0.1
PS	71	M	0.0	2.5	2.5	2.5	1
DS	73	M	0.0	2	2.5	1	0.5
WT	76	M	0.0	0.1	0.1	0.1	0.1
GW	77	M	0.0	3	3	0.3	1
BC	76	M	0.0	1.5	1.5	0.1	0.1
RC	83	M	0.1	2	2	1.5	0.5
JC	84	F	0.1	0.1	0.1	0.5	0.1
VB	72	F	0.0	2	2	0.2	0.2

Table AI.1. Showing gender, age, VA, and lens opacity characteristics of 28 control subjects. Lens opacities are graded according to the LOCS III classification system (*Chylack et al, 1995*), in which NO refers to nuclear opacity, NC to nuclear colour, C to cortical opacities, and P to posterior subcapsular opacities.

Subject Initials	Age	Gender	VA /logMAR	ARM Group	Lens Grading			
					NO	NC	C	P
OG	80	F	0.3	1	3	3	1.5	1
JA	65	F	0.5	1	1.5	1.5	0.5	0.5
KS	82	F	0.3	1	3	3	2.5	2
WT	78	M	0.2	1	0.1	0.1	2.5	0.1
HG	73	M	0.2	1	4	3	2.8	2.5
JW	80	M	0.2	2	2	2	0.5	0.5
IJ	65	M	0.0	1	2	2	1	0.5
ER	72	F	0.2	2	2	2.5	1.7	0.2
DF	86	F	0.5	3	3	3.5	3	1
MP	66	F	0.5	2	2	2	3	1
Eree	86	F	0.3	1	2.5	2.5	1.5	1
AF	79	M	0.2	2	2	1.5	0.5	0.5
VW	60	F	0.0	2	1	1	0.5	0.5
DG	69	M	0.1	2	2	2	1.5	2.5
BJ	78	F	0.1	2	0.1	0.1	3	0.1
KG	79	M	0.3	1	2.5	2.5	1	0.7
JY	78	M	0.2	1	0.1	0.1	0.5	0.1
WD	65	M	0.1	2	0.7	0.7	0.1	0.1
LG	57	F	0.1	1	0.5	0.5	0.1	0.1
DC	65	M	0.2	3	2.3	2.3	0.5	0.1
JA	72	F	0.0	3	2	2	0.1	0.1
BF	72	F	0.3	2	2	2.5	0.5	0.1
PB	78	M	0.2	3	2.3	2.3	2	0.2
FB	82	M	0.1	3	3	3	0.1	0.1
BR	66	F	0.5	3	2	2	0.1	0.1
ME	73	F	0.1	3	2.5	2.5	0.1	0.1
MG	63	M	0.2	2	2	2	0.1	0.1
DB	76	F	0.0	1	3	3	0.7	0.5
JJ	66	F	0.0	2	2	2	0.5	0.1
RS	59	M	0.0	1	1.5	1.5	0.1	0.1
GP	75	M	0.2	3	3	2.5	0.5	0.5

Table AI.2. Table showing age, gender, VA, ARM grading, and lens opacity characteristics of 31 subjects with ARM. Lens opacities are graded according to the LOCS III classification system (Chylack et al, 1995), in which NO refers to nuclear opacity, NC to nuclear colour, C to cortical opacities, and P to posterior subcapsular opacities.

APPENDIX II

Fundus Grading

1. Grading of Drusen

1.1 Drusen morphology. Highest grade present within outer circle.
0) absent
1) questionable
2) hard drusen ($< C_1$, $125\mu m$)
3) intermediate, soft drusen ($> C_0 \leq C_1$; $>63\mu m \leq 125\mu m$)
4) large, soft distinct drusen ($> C_1$, $125\mu m$)
5) large, soft indistinct drusen ($> C_1$, $125\mu m$)
7) cannot grade, obscuring lesions
8) cannot grade, photo quality

1.2 Predominant drusen type within outer circle
0) absent
1) questionable
2) hard drusen ($< C_1$, $125\mu m$)
3) intermediate, soft drusen ($> C_0 \leq C_1$; $>63\mu m \leq 125\mu m$)
4) large, soft distinct drusen ($> C_1$, $125\mu m$)
5) large, soft indistinct drusen ($> C_1$, $125\mu m$)
7) cannot grade, obscuring lesions
8) cannot grade, photo quality

1.3 Number of drusen
0) absent
1) questionable
2) 1-9
3) 10-19
4) ≥ 20
7) cannot grade, obscuring lesions
8) cannot grade, photo quality

1.4 Drusen size
1) $<C_0$ ($<63\mu m$)
2) $\geq C_0 < C_1$ ($\geq 63\mu m$, $<125\mu m$)
3) $\geq C_1 < C_2$ ($\geq 125\mu m$, $<175\mu m$)
4) $\geq C_2 < C_3$ ($\geq 175\mu m$, $<250\mu m$)
5) $\geq C_3$ ($\geq 250\mu m$)
7) cannot grade, obscuring lesions
8) cannot grade, photo quality

1.5 Main location of drusen.
1) outside outer circle (mid-peripheral subfield)
2) in outer subfield
3) in middle subfield
4) in central subfield
7) cannot grade, obscuring lesions
9) cannot grade, photo quality

1.6 Area covered by drusen in subfield 1.5
1) <10%
2) <25%
3) <50%
4) $\geq 50\%$
7) cannot grade, obscuring lesion
8) cannot grade, photo quality

2. Grading of Hyperpigmentation and Hypopigmentation of the Retina

2.1 Hyperpigmentation
- 0) absent
- 1) questionable
- 2) present $<C_0$ ($<63\mu$m)
- 3) present $\geq C_0$ ($\geq63\mu$m)
- 7) cannot grade, obscuring lesions
- 8) cannot grade, photo quality

2.2 Hypopigmentation
- 0) absent
- 1) questionable
- 2) present $<C_0$ ($<63\mu$m)
- 3) present $\geq C_0$ ($\geq63\mu$m)
- 7) cannot grade, obscuring lesions
- 8) Cannot grade, photo quality

2.3 Main location hyper/Hypopigmentation.
- 1) outside outer circle (mid-peripheral subfield)
- 2) in outer subfield
- 3) in middle subfield
- 4) in central subfield
  - a. outside fovea (center point)
  - b. in fovea
- 7) cannot grade, obscuring lesions
- 8) cannot grade, photo quality

3. Grading of Geographic Atrophy

3.1 Presence
- 0) absent
- 1) questionable
- 2) present: $\geq C_2$
- 7) cannot grade, obscuring lesions
- 8) cannot grade, photo quality

3.2 Location
- 1) outside outer circle (mid-peripheral subfield)
- 2) in outer subfield
- 3) in middle subfield
- 4) in central subfield
  - a. not in fovea (center point)
  - b. in fovea
- 7) cannot grade, obscuring lesions
- 8) cannot grade, photo quality

3.3 Area covered
- 1) $\geq C_2 <C_3$ ($\geq175\mu$m $<250\mu$m)
- 2) $\geq C_3 <C_4$ ($\geq250\mu$m $<500\mu$m)
- 3) $\geq C_4$ and $<1000\mu$m (~central circle of grid)
- 4) $\geq1000\mu$m and $<3000\mu$m (~middle circle)
- 5) $\geq3000\mu$m and $<6000\mu$m (~outer circle)
- 6) $>6000\mu$m
- 7) cannot grade, obscuring lesions
- 8) cannot grade, photo quality

4. Grading of Neovascular AMD

4.1 Presence
  0) absent
  1) questionable
  2) present
  7) cannot grade, obscuring lesions
  8) cannot grade, photo quality

4.2 Typifying features
  1) hard exudates
  2) serous neuroretinal detachment
  3) serous RPE detachment
  4) haemorrhagic RPE detachment
  5) retinal haemorrhage
      a. subretinal
      b. in plane of retina
      c. subhyaloid
      d. intravitreal
  6) scar/glial/fibrous tissue
      a. subretinal
      b. preretinal
  7) cannot grade, obscuring lesions
  8) cannot grade, photo quality

4.3 Location
  1) outside outer circle (mid-peripheral subfield)
  2) in outer subfield
  3) in middle subfield
  4) in central subfield
      a. not underlying (in) fovea (center point)
      b. underlying (in) fovea
  7) cannot grade, obscuring lesions
  8) cannot grade, photo quality

4.4 Area covered
  1) $\geq C_2 < C_3$ ($\geq 175\mu m < 250\mu m$)
  2) $\geq C_3 < C_4$ ($\geq 250\mu m < 500\mu m$)
  3) $\geq C_4$ and $< 1000\mu m$ (~central circle of grid)
  4) $\geq 1000\mu m$ and $< 3000\mu m$ (~middle circle)
  5) $\geq 3000\mu m$ and $< 6000\mu m$ (~outer circle)
  6) $> 6000\mu m$
  7) cannot grade, obscuring lesions
  8) cannot grade, photo quality

Table AII.1. Grading table for classification of fundus appearance according to International classification and grading system for ARM and AMD (Bird et al, 1995).

Subject	Grading of Drusen						RPE pigment			G.A.			Neovascular AMD			
	1.1	1.2	1.3	1.4	1.5	1.6	2.1	2.2	2.3	3.1	3.2	3.3	4.1	4.2	4.3	4.4
JB	0	0	0	/	/	/	0	0	/	0	/	/	0	/	/	/
	0	0	0	/	/	/	0	0	/	0	/	/	0	/	/	/
GO	0	0	0	/	/	/	0	0	/	0	/	/	0	/	/	/
	0	0	0	/	/	/	0	0	/	0	/	/	0	/	/	/
PG	0	0	0	/	/	/	0	0	/	0	/	/	0	/	/	/
	0	0	0	/	/	/	0	0	/	0	/	/	0	/	/	/
CG	0	0	0	/	/	/	0	0	/	0	/	/	0	/	/	/
	0	0	0	/	/	/	0	0	/	0	/	/	0	/	/	/
SM	0	0	0	/	/	/	0	0	/	0	/	/	0	/	/	/
	0	0	0	/	/	/	0	0	/	0	/	/	0	/	/	/
CD	0	0	0	/	/	/	0	0	/	0	/	/	0	/	/	/
	2	2	2	1	2	1	0	0	/	0	/	/	0	/	/	/
WD	0	0	0	/	/	/	0	0	/	0	/	/	0	/	/	/
	0	0	0	/	/	/	0	0	/	0	/	/	0	/	/	/
RW	0	0	0	/	/	/	0	0	/	0	/	/	0	/	/	/
	0	0	0	/	/	/	0	0	/	0	/	/	0	/	/	/
WF	0	0	0	/	/	/	0	0	/	0	/	/	0	/	/	/
	0	0	0	/	/	/	0	0	/	0	/	/	0	/	/	/
MR	0	0	0	/	/	/	0	0	/	0	/	/	0	/	/	/
	0	0	0	/	/	/	0	0	/	0	/	/	0	/	/	/
VE	0	0	0	/	/	/	0	0	/	0	/	/	0	/	/	/
	0	0	0	/	/	/	0	0	/	0	/	/	0	/	/	/
MB	0	0	0	/	/	/	0	0	/	0	/	/	0	/	/	/
	0	0	0	/	/	/	0	0	/	0	/	/	0	/	/	/
DJ	0	0	0	/	/	/	0	0	/	0	/	/	0	/	/	/
	0	0	0	/	/	/	0	0	/	0	/	/	0	/	/	/
PA	0	0	0	/	/	/	0	0	/	0	/	/	0	/	/	/
	0	0	0	/	/	/	0	0	/	0	/	/	0	/	/	/
GA	0	0	0	/	/	/	0	0	/	0	/	/	0	/	/	/
	0	0	0	/	/	/	0	0	/	0	/	/	0	/	/	/
JJ	2	2	2	1	2	1	0	0	/	0	/	/	0	/	/	/
	0	0	0	/	/	/	0	0	/	0	/	/	0	/	/	/
BB	0	0	0	/	/	/	0	0	/	0	/	/	0	/	/	/
	0	0	0	/	/	/	0	0	/	0	/	/	0	/	/	/
KM	0	0	0	/	/	/	0	0	/	0	/	/	0	/	/	/
	0	0	0	/	/	/	0	0	/	0	/	/	0	/	/	/
MA	0	0	0	/	/	/	0	0	/	0	/	/	0	/	/	/
	0	0	0	/	/	/	0	0	/	0	/	/	0	/	/	/
AS	0	0	0	/	/	/	0	0	/	0	/	/	0	/	/	/
	0	0	0	/	/	/	0	0	/	0	/	/	0	/	/	/
PS	0	0	0	/	/	/	0	0	/	0	/	/	0	/	/	/
	0	0	0	/	/	/	0	0	/	0	/	/	0	/	/	/
DS	0	0	0	/	/	/	0	0	/	0	/	/	0	/	/	/
	0	0	0	/	/	/	0	0	/	0	/	/	0	/	/	/
WT	0	0	0	/	/	/	0	0	/	0	/	/	0	/	/	/
	0	0	0	/	/	/	0	0	/	0	/	/	0	/	/	/
GW	0	0	0	/	/	/	0	0	/	0	/	/	0	/	/	/
	0	0	0	/	/	/	0	0	/	0	/	/	0	/	/	/
BC	0	0	0	/	/	/	0	0	/	0	/	/	0	/	/	/
	0	0	0	/	/	/	0	0	/	0	/	/	0	/	/	/
RC	0	0	0	/	/	/	0	0	/	0	/	/	0	/	/	/
	0	0	0	/	/	/	0	0	/	0	/	/	0	/	/	/
JC	0	0	0	/	/	/	0	0	/	0	/	/	0	/	/	/
	0	0	0	/	/	/	0	0	/	0	/	/	0	/	/	/
VB	0	0	0	/	/	/	0	0	/	0	/	/	0	/	/	/
	0	0	0	/	/	/	0	0	/	0	/	/	0	/	/	/

Table AII.2. Table showing fundus grading characteristics of 29 control subjects, graded according to Bird et al, 1995.

Subject	Grading of Drusen						RPE pigment			G.A.			Neovascular AMD			
	1.1	1.2	1.3	1.4	1.5	1.6	2.1	2.2	2.3	3.1	3.2	3.3	4.1	4.2	4.3	4.4
JA	4	4	2	3	3	2	0	3	3	0	/	/	0	/	/	/
	3	3	2	3	2	1	0	3	3	0	/	/	0	/	/	/
OG	4	4	2	3	2	1	0	0	/	0	/	/	0	/	/	/
	4	4	3	4	2	1	0	0	/	0	/	/	0	/	/	/
KS	3	3	3	3	3	1	0	0	/	0	/	/	0	/	/	/
	3	3	2	2	4	1	0	0	/	0	/	/	0	/	/	/
WT	5	4	4	4	3	3	0	3	3	0	/	/	0	/	/	/
	5	4	3	4	3	2	0	3	3	0	/	/	0	/	/	/
HG	4	4	3	4	3	2	0	0	/	0	/	/	0	/	/	/
	0	0	0	/	/	/	0	2	3	0	/	/	0	/	/	/
JW	3	2	4	2	2	2	3	0	4	0	/	/	0	/	/	/
	0	0	0	/	/	/	0	0	/	0	/	/	2	8	4	8
IJ	4	4	4	4	3	2	0	0	/	0	/	/	0	/	/	/
	4	4	4	4	3	2	3	0	3	0	/	/	0	/	/	/
ER	4	3	3	3	2	1	0	0	/	0	/	/	0	/	/	/
	0	0	0	/	/	/	0	0	/	0	/	/	2	6	4	4
DF	4	4	2	4	4	2	0	0	/	0	/	/	0	/	/	/
	4	4	3	4	4	2	0	3	3	1	4	2	0	/	/	/
MP	0	0	0	/	/	/	0	0	/	0	/	/	0	/	/	/
	0	0	0	/	/	/	0	0	/	0	/	/	2	6	4	6
ERee	4	4	3	3	3	3	0	0	/	0	/	/	0	/	/	/
	4	4	4	3	3	4	0	0	/	0	/	/	0	/	/	/
AF	5	5	3	4	4	3	0	0	/	0	/	/	0	/	/	/
	0	0	0	/	/	/	0	0	/	0	/	/	2	5	4	5
VW	0	0	0	/	/	/	0	0	/	0	/	/	0	/	/	/
	0	0	0	/	/	/	3	0	3	0	/	/	2	6	2	3
DG	4	4	4	3	3	2	0	0	/	0	/	/	0	/	/	/
	4	4	3	3	3	1	0	0	/	0	/	/	2	5	3	3
BJ	4	4	4	3	3	2	0	3	3	0	/	/	0	/	/	/
	0	0	0	/	/	/	0	0	/	0	/	/	2	6	3	5
KG	5	5	2	3	3	1	3	3	3	0	/	/	0	/	/	/
	3	2	3	2	2	1	0	0	/	0	/	/	0	/	/	/
JY	3	2	4	2	2	3	0	0	/	0	/	/	0	/	/	/
	4	3	4	3	3	2	0	0	/	0	/	/	0	/	/	/
WD	3	2	3	2	3	3	0	0	/	0	/	/	0	/	/	/
	3	2	3	2	3	3	0	0	/	0	/	/	2	6	3	4
LG	2	2	2	2	2	1	0	0	/	0	/	/	0	/	/	/
	4	4	2	3	3	1	3	3	3	0	/	/	0	/	/	/
DC	5	4	3	4	3	3	3	0	3	0	/	/	0	/	/	/
	4	4	2	3	2	1	0	3	3	2	3	4	0	/	/	/
JA	3	2	2	3	3	2	0	0	/	0	/	/	0	/	/	/
	0	0	0	/	/	/	3	0	4	1	3	2	0	/	/	/
BF	4	4	4	4	3	4	0	0	/	0	/	/	0	/	/	/
	0	0	0	/	/	/	0	0	/	0	/	/	2	6	4	4
PB	4	4	4	4	3	4	0	0	/	0	/	/	0	/	/	/
	4	4	3	4	3	2	0	3	2	2	4	3	0	/	/	/
FB	4	4	4	3	3	3	0	3	4	1	3	2	0	/	/	/
	5	4	3	4	3	4	0	3	4	0	/	/	0	/	/	/
BR	4	4	2	4	2	1	0	0	/	2	4	4	0	/	/	/
	4	4	2	4	2	1	0	0	/	0	/	/	0	/	/	/
ME	5	4	4	4	4	4	0	0	/	0	/	/	0	/	/	/
	5	4	4	4	4	3	0	3	3	1	2	2	0	/	/	/
MG	5	5	3	4	3	3	0	3	4	0	/	/	0	/	/	/
	0	0	0	/	/	/	0	0	/	0	/	/	2	6	4	4
DB	4	4	3	3	2	2	0	0	/	0	/	/	0	/	/	/
	3	2	3	2	3	2	0	0	/	0	/	/	0	/	/	/
JJ	5	5	3	4	3	2	0	0	/	0	/	/	0	/	/	/
	0	0	0	/	/	/	0	0	/	0	/	/	2	6	4	4

317

RS	4	2	4	2	4	3	0	0	/	0	/	/	0	/	/	/
	4	2	4	2	4	3	0	0	/	0	/	/	0	/	/	/
GP	4	3	2	3	2	1	0	0	/	0	/	/	0	/	/	/
	0	0	0	/	/	/	0	3	2	1	4	2	0	/	/	/

Table AII.3. Table showing fundus grading characteristics of 31 subjects with ARM, graded according to Bird et al, 1995.

APPENDIX III

Electrophysiological Data
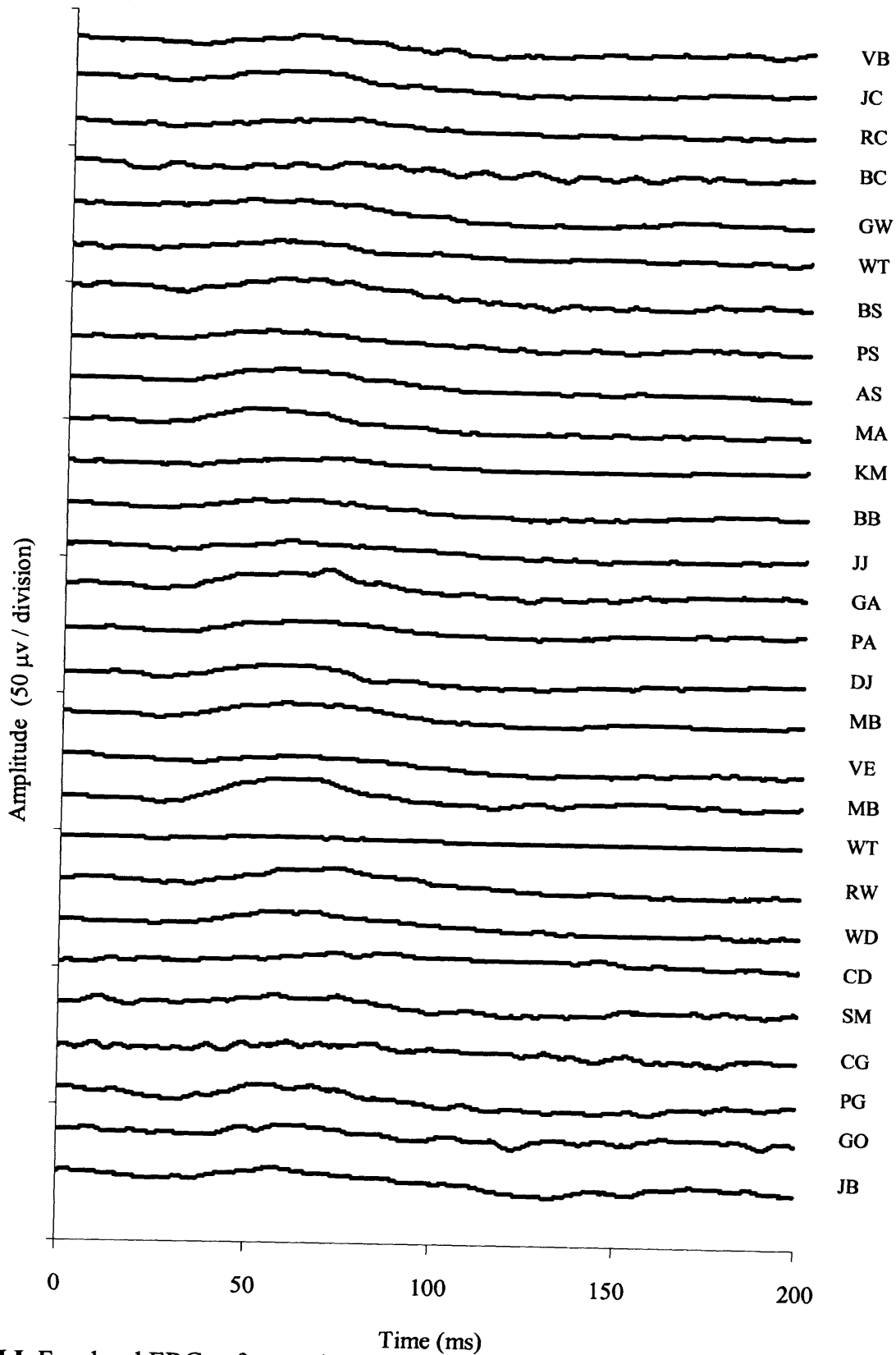
AIII.I. Focal rod ERGs of control subjects
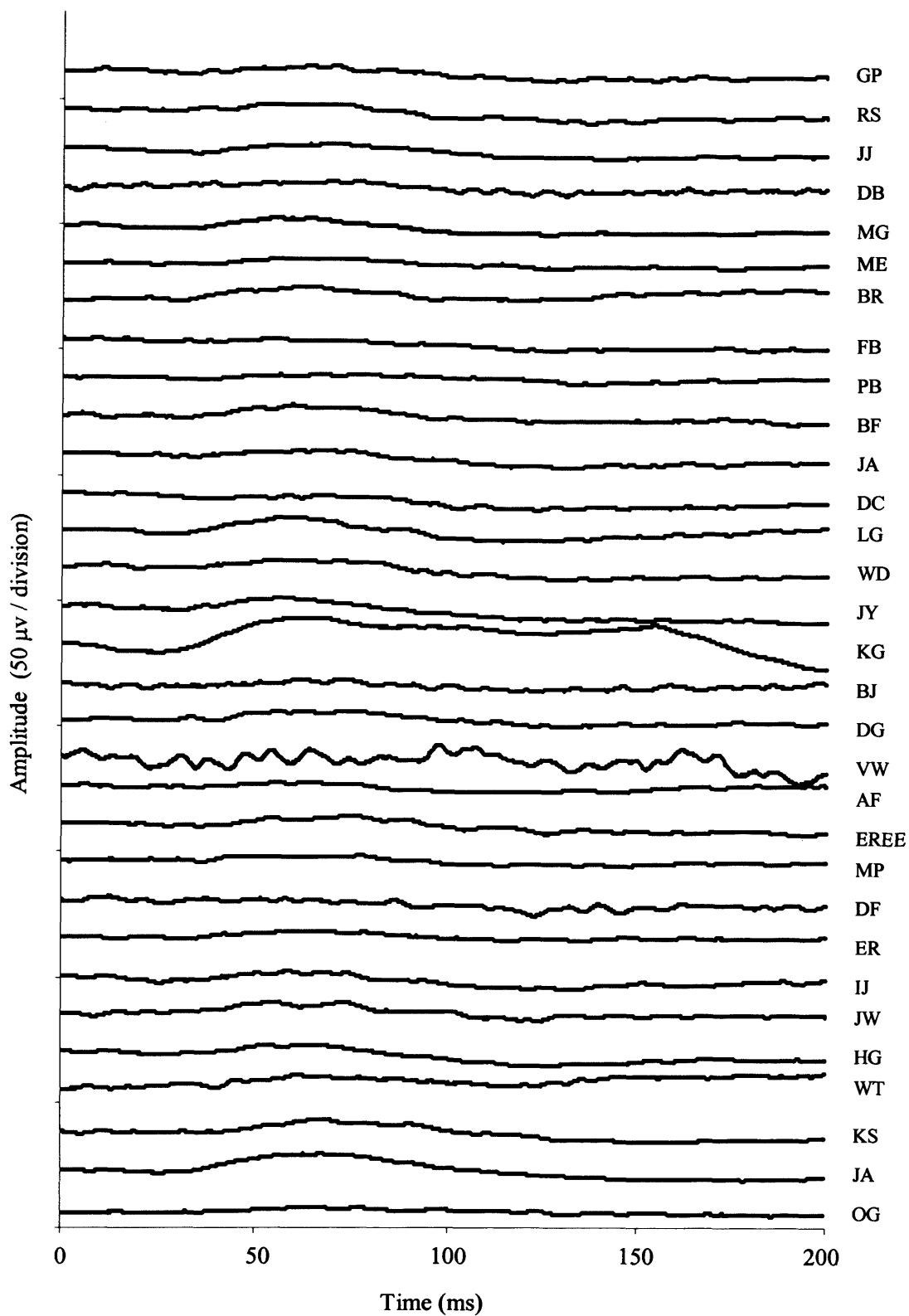
AIII.2. Focal Rod ERGs of subjects with ARM
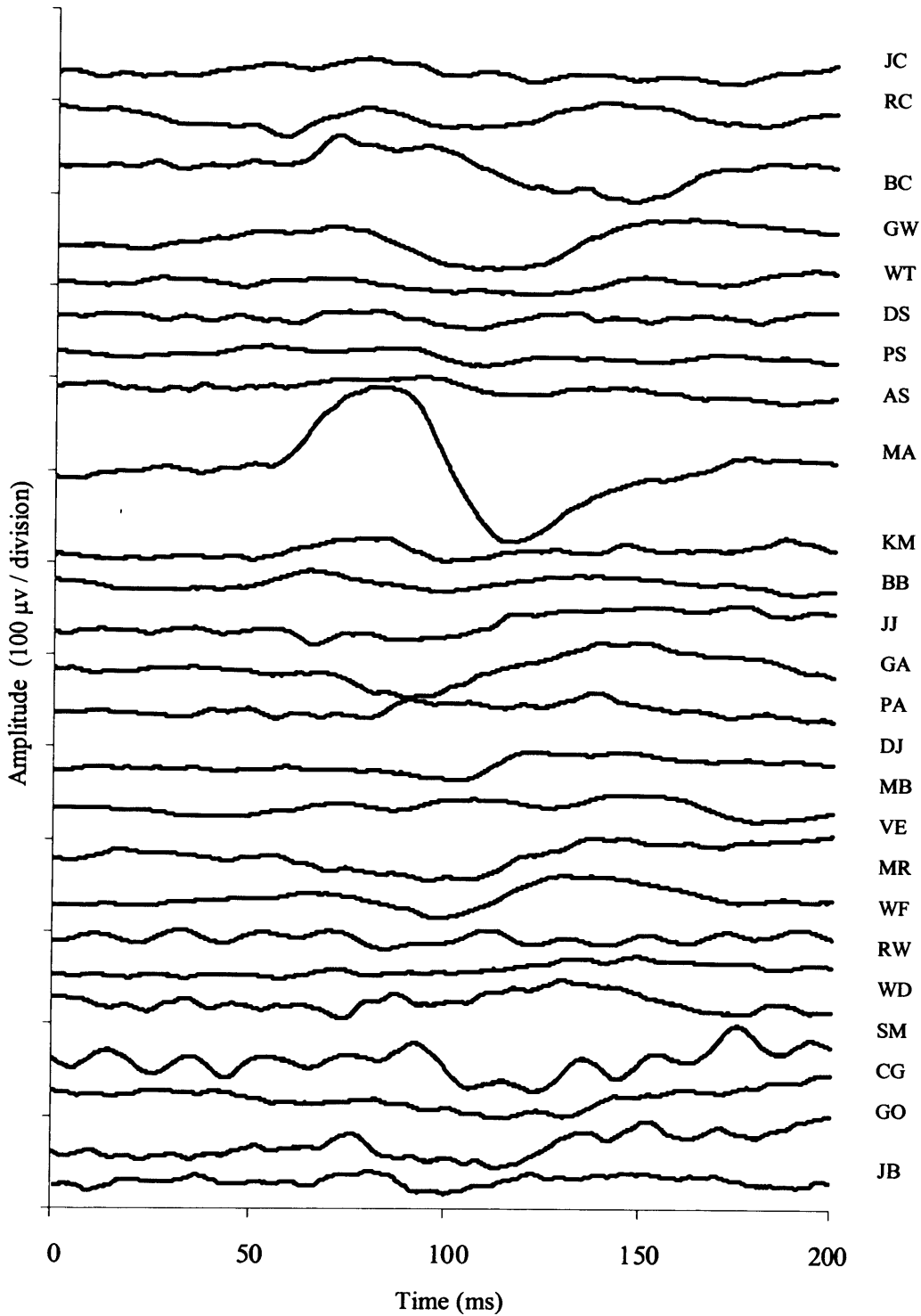
AIII.3. Rod VEPs of control subjects. Results were not obtained for subjects PG, CD, VB.
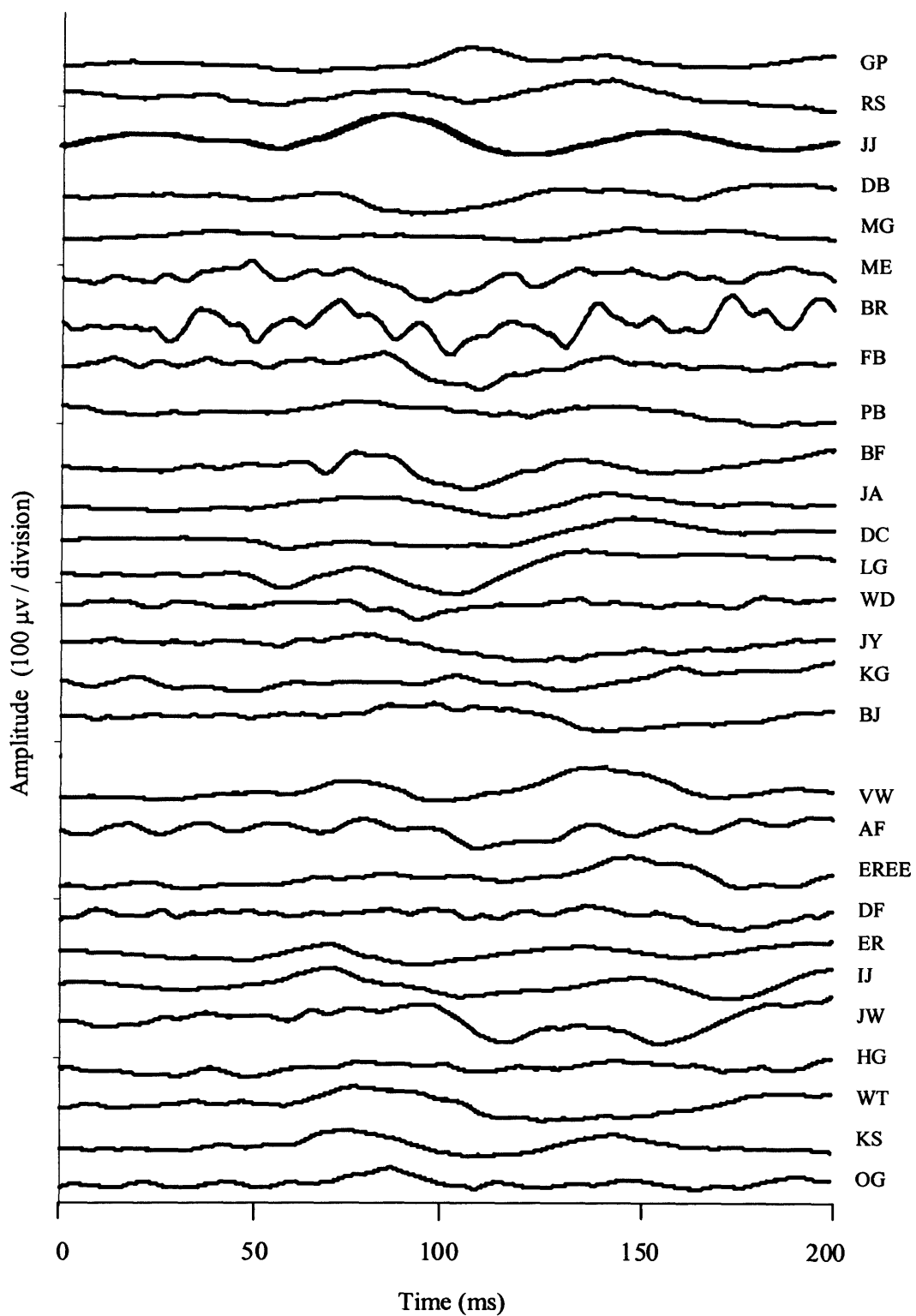
AIII.4. Rod VEPs of subjects with ARM. Results were not obtained for subjects JA, MP, DG.
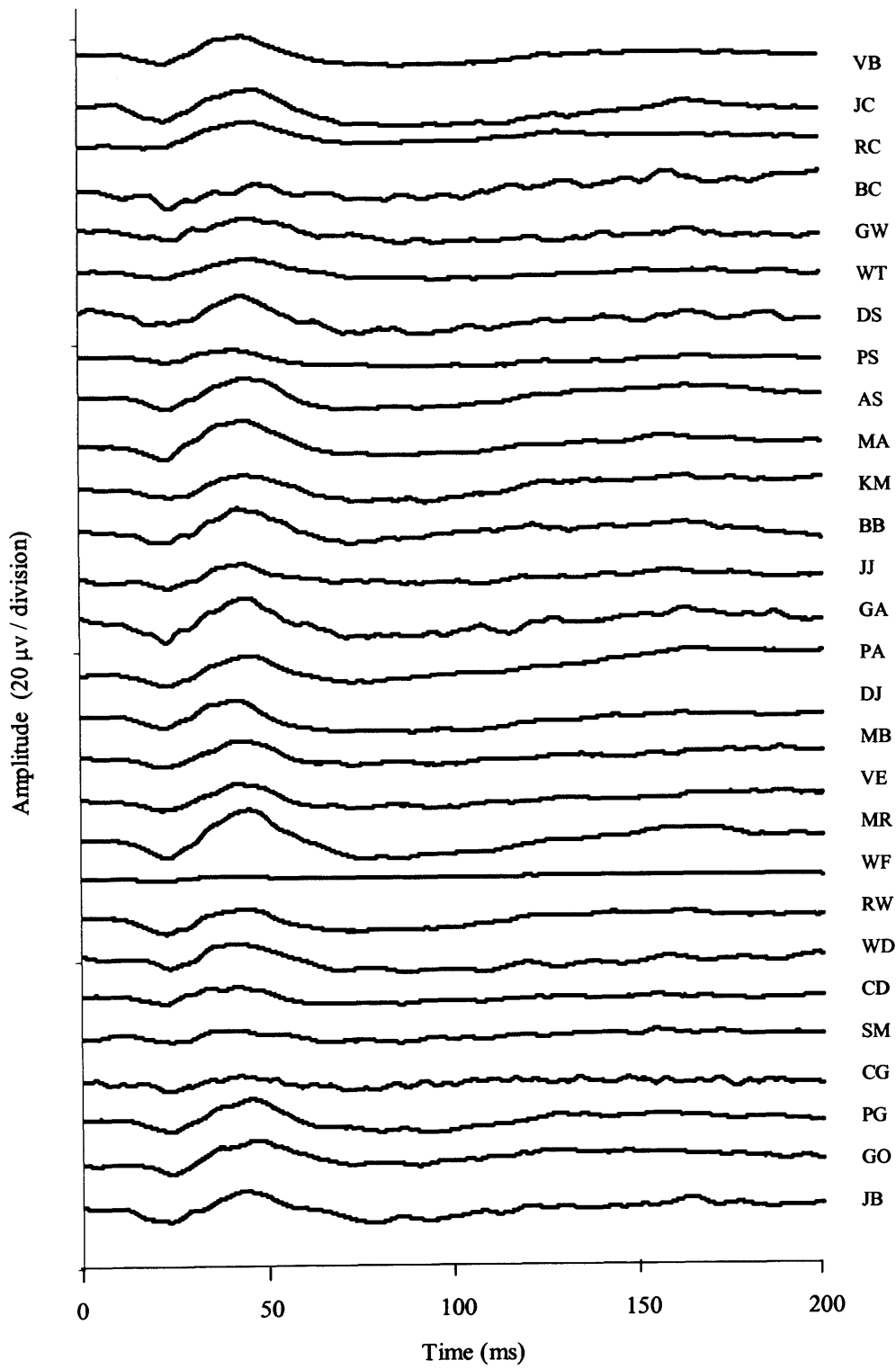
AIII.5. Focal 5 Hz cone ERGs of control subjects
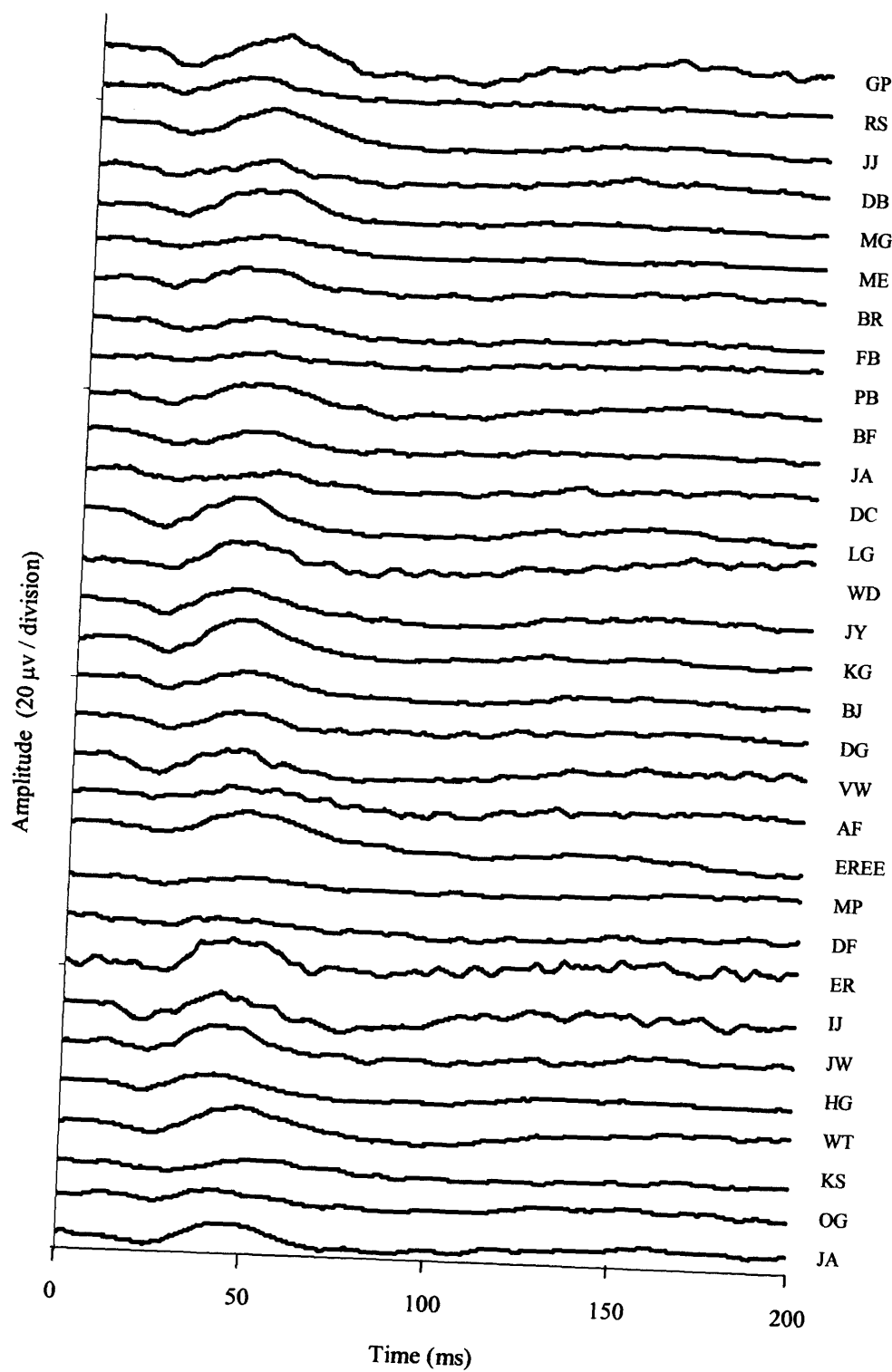
AIII.6. Focal 5 Hz cone ERGs of subjects with ARM
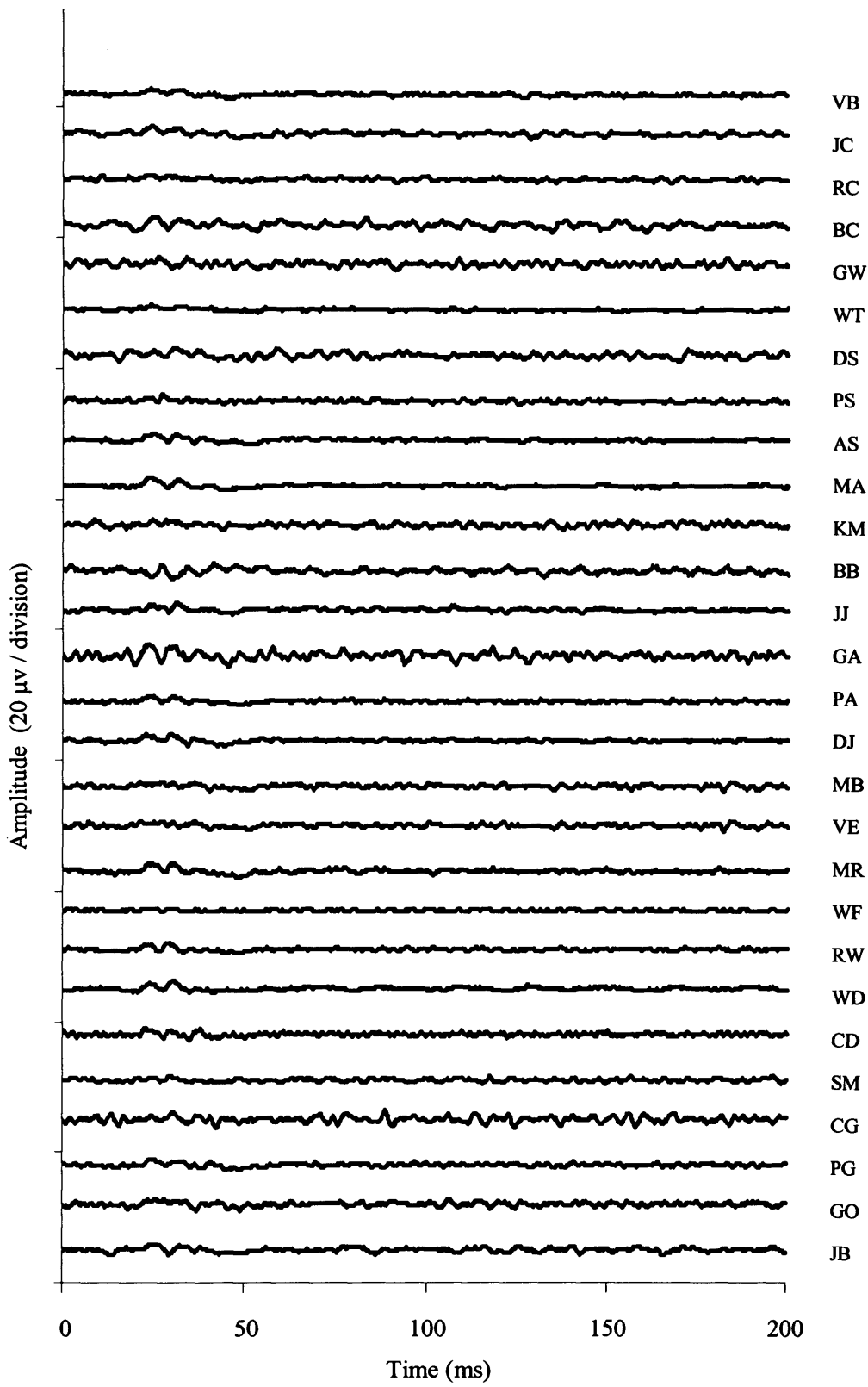
AIII.7. Focal OPs of control subjects
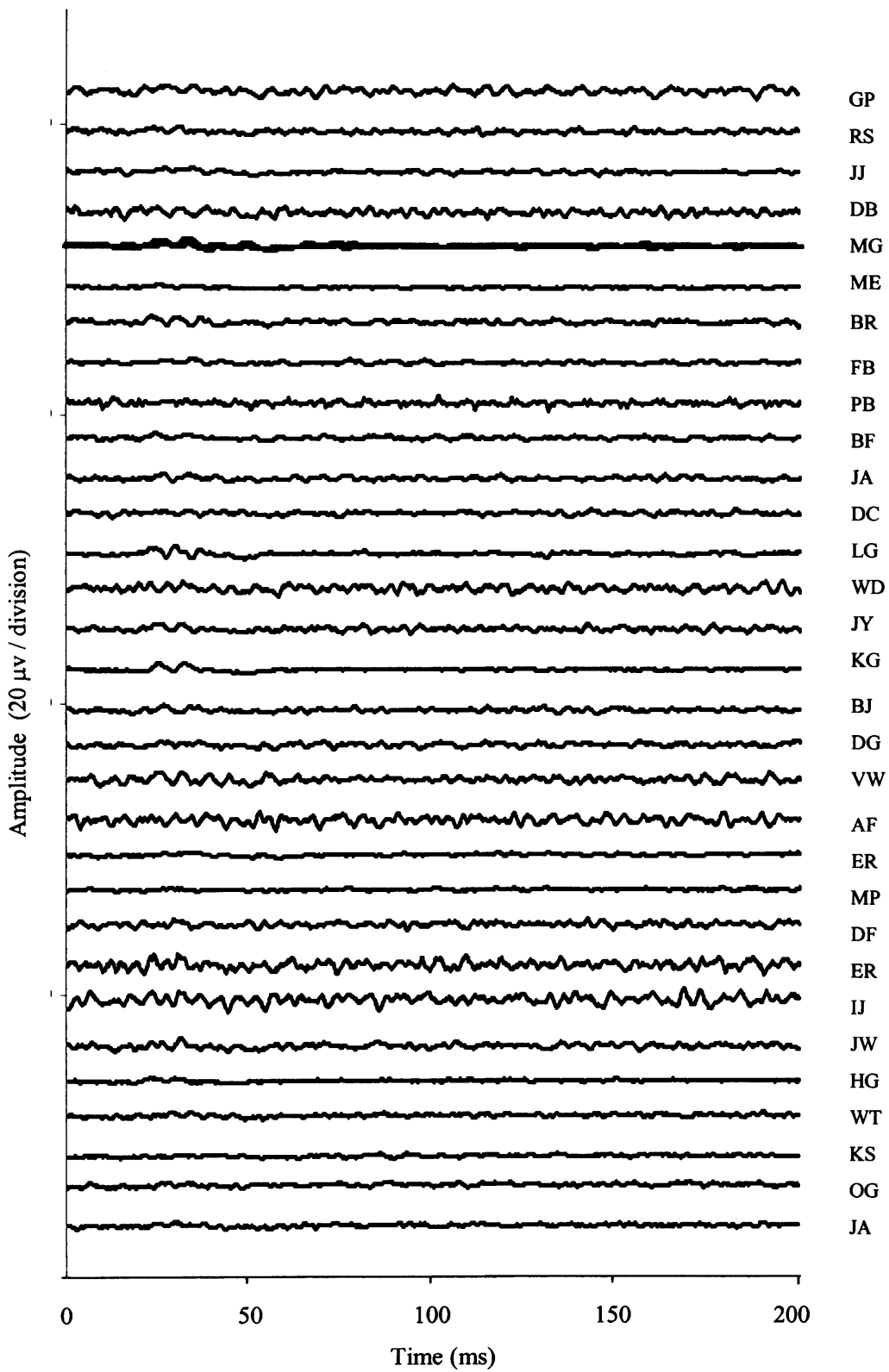
AIII.8. Focal OPs of subjects with ARM
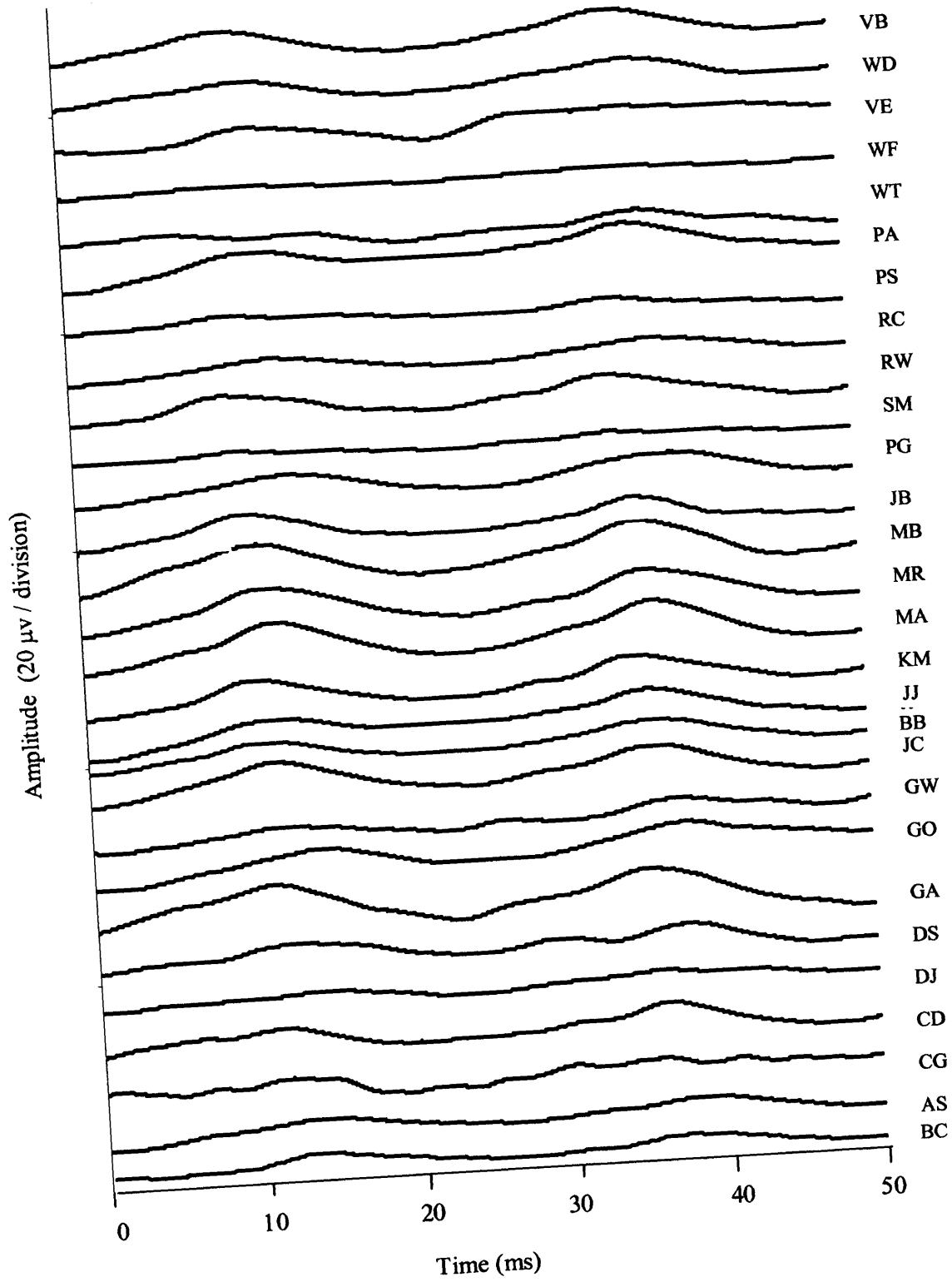
AIII.9. Focal 41 Hz cone ERGs of control subjects
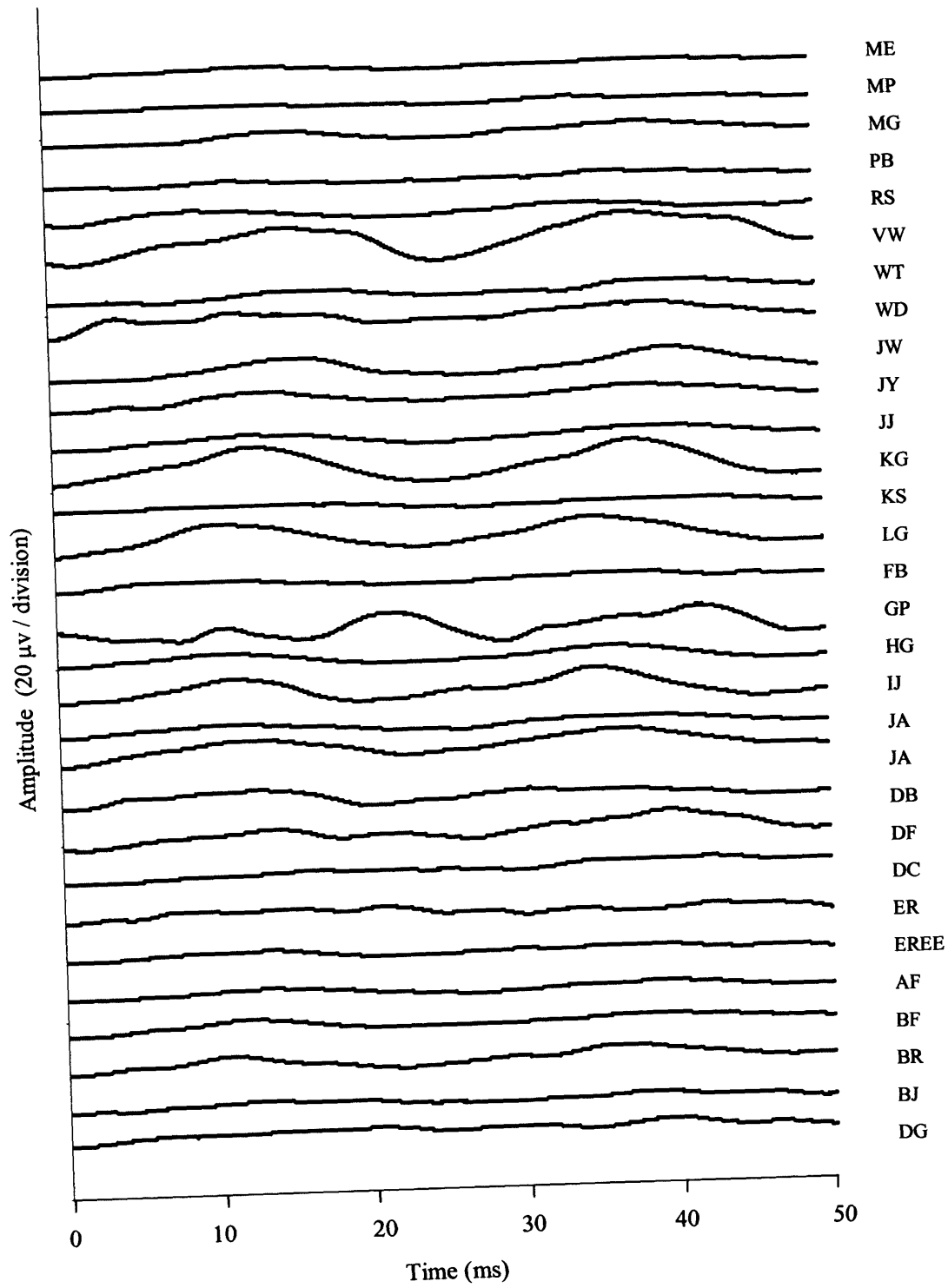
AIII.10. Focal 41 Hz cone ERGs of subjects with ARM
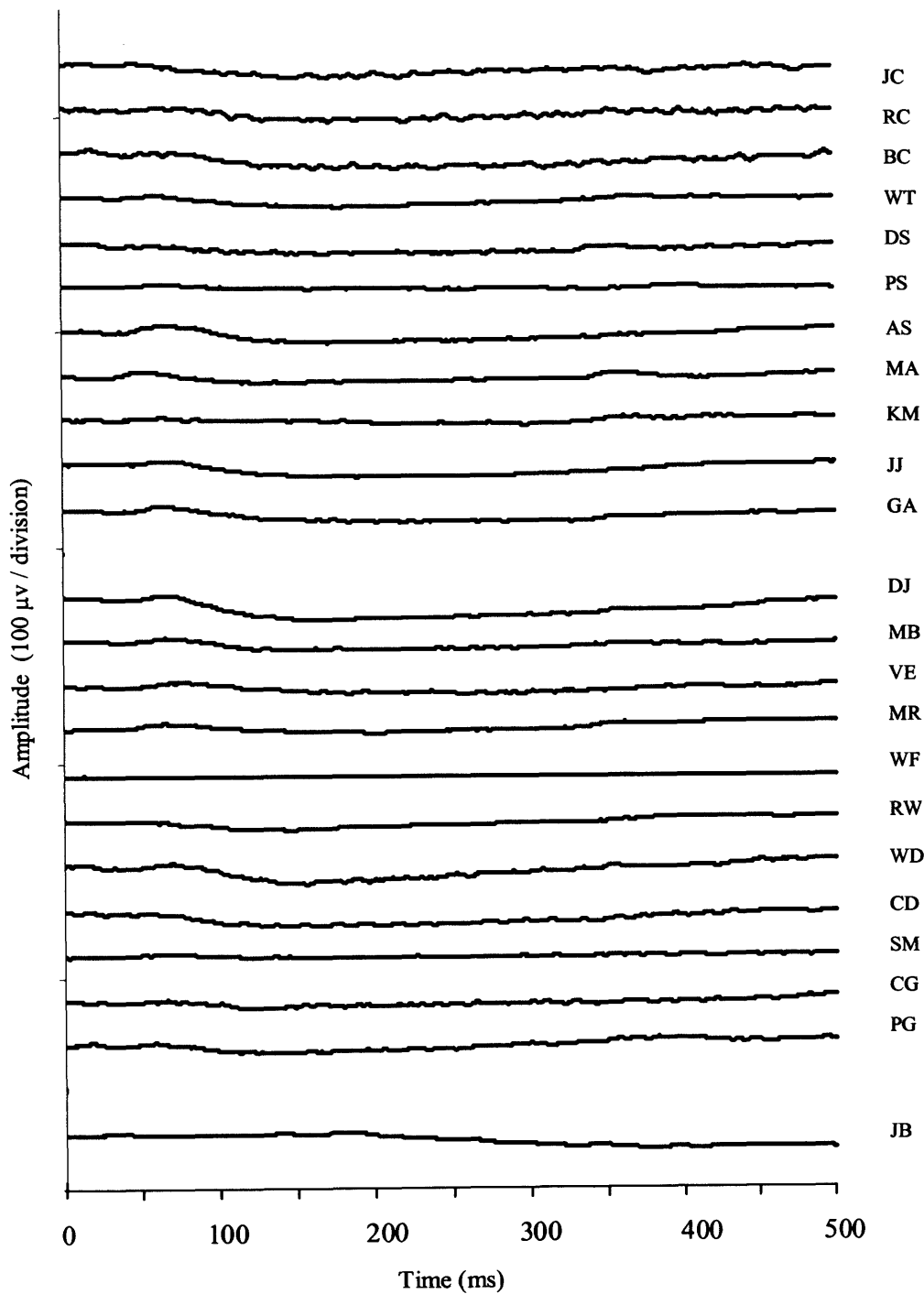
AIII.11. S-cone ERGs of control subjects. Results were not obtained for subjects GO, PA, GW, VB, BB.
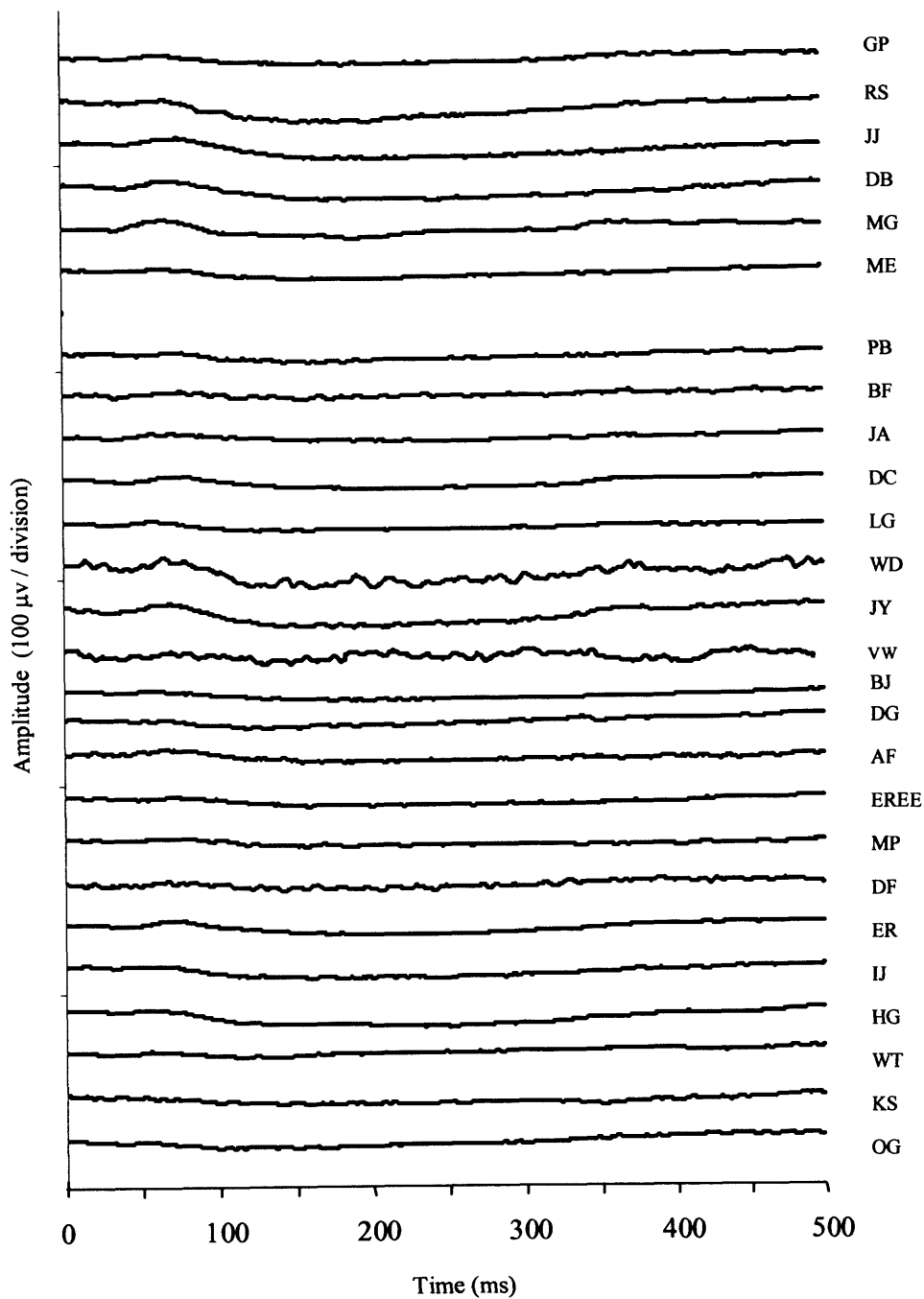
AIII.12. S-cone ERGs of subjects with ARM. Results were not obtained for subjects JA, JW, KG, FB, BR.
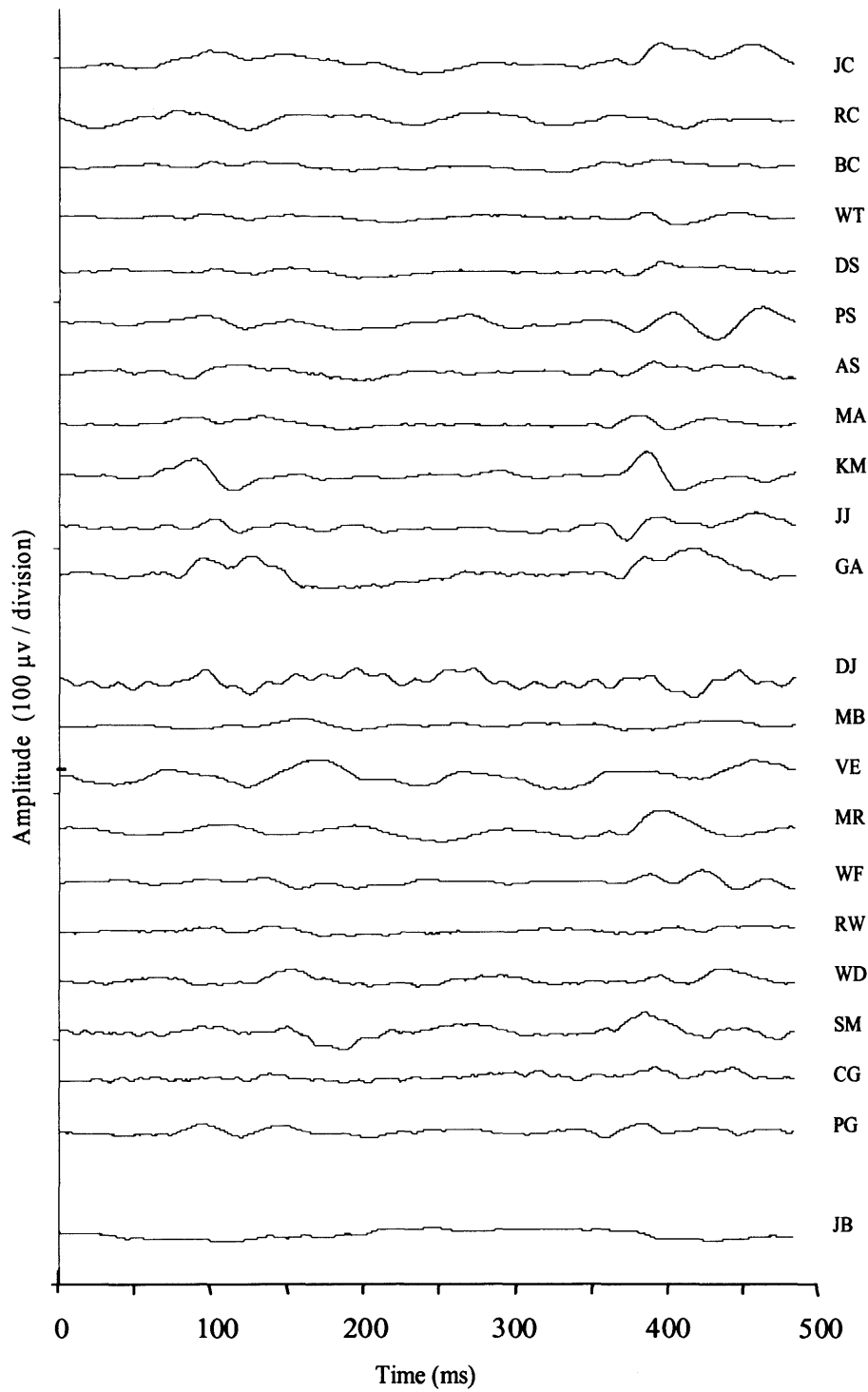
AIII.13. S-cone VEPs of control subjects. Results were not obtained for subjects GO, CD, PA, BB, VB
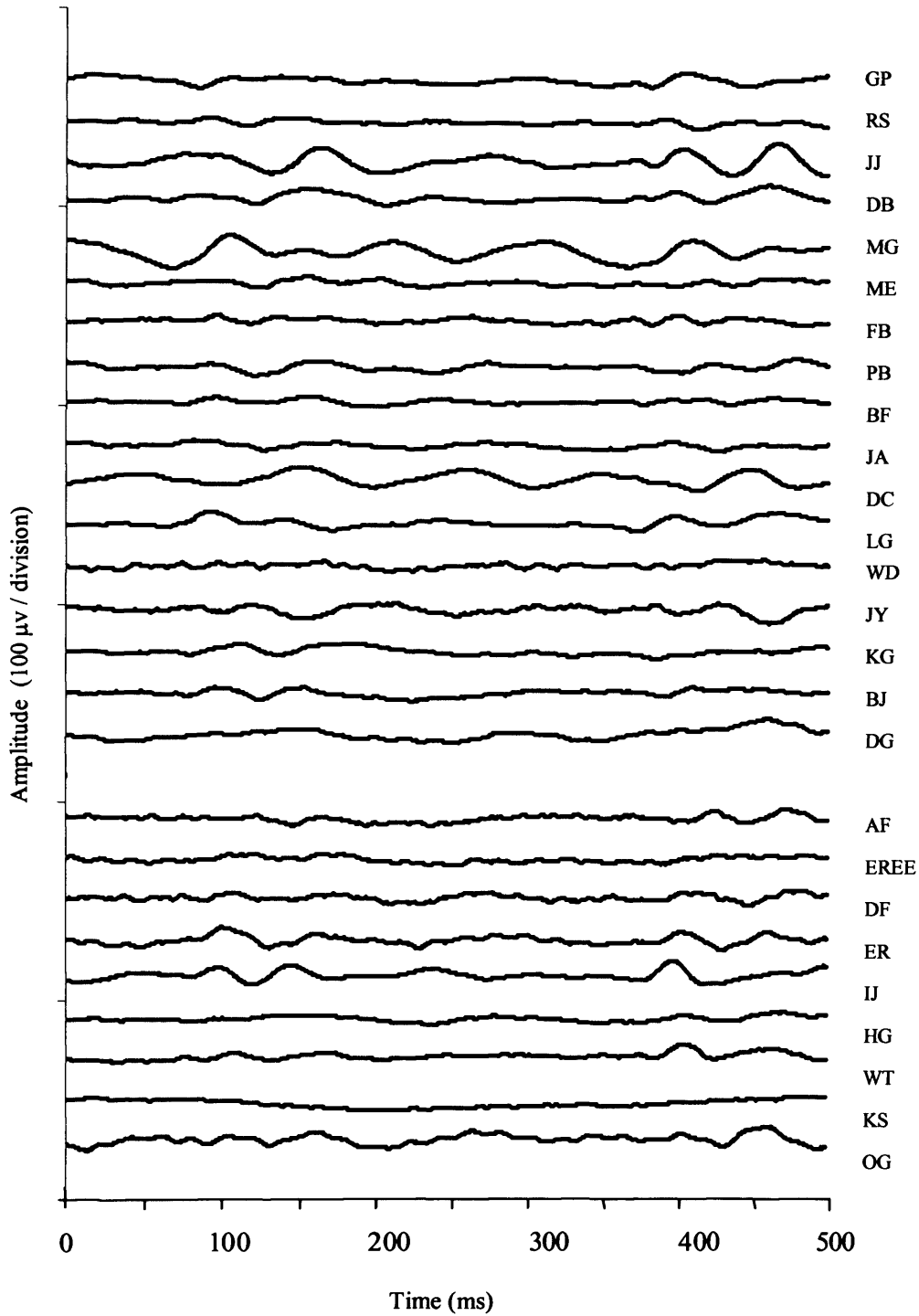
AIII.14. S-cone VEP of subjects with ARM. Results were not obtained for subjects JA, JW, MP, VW, BR.
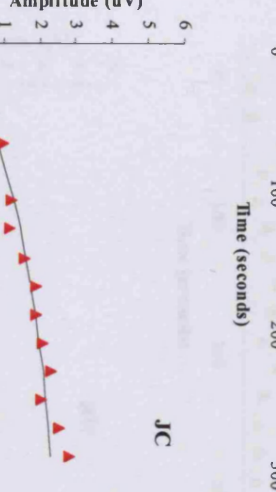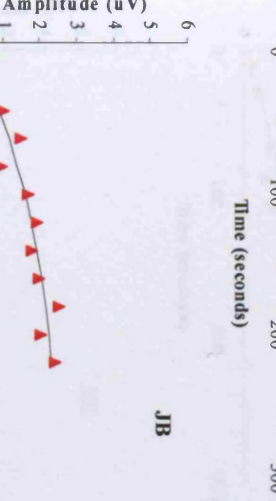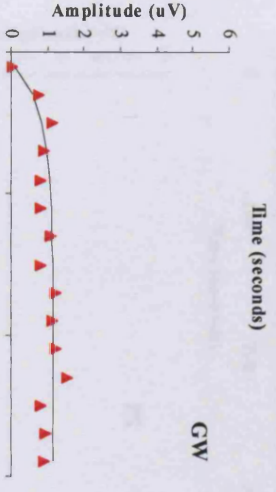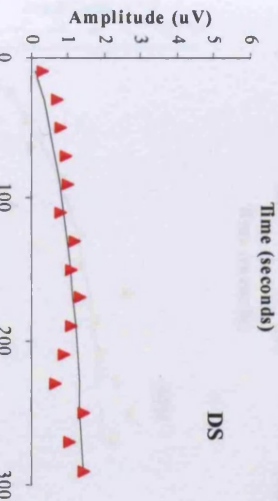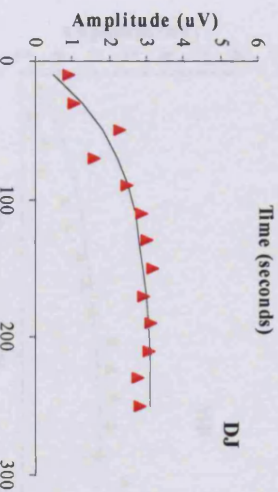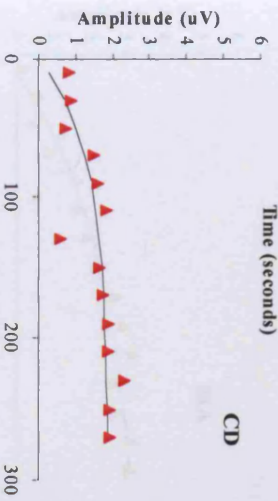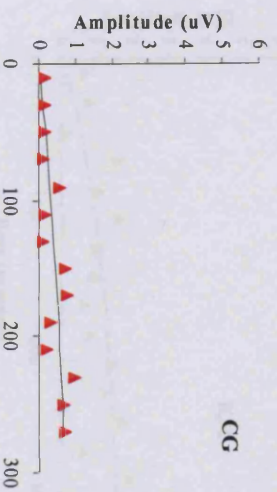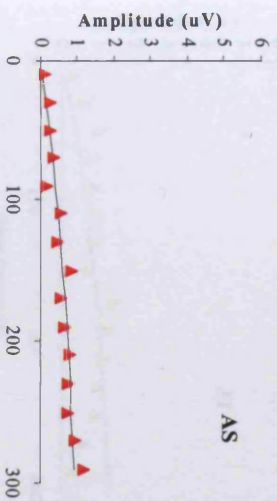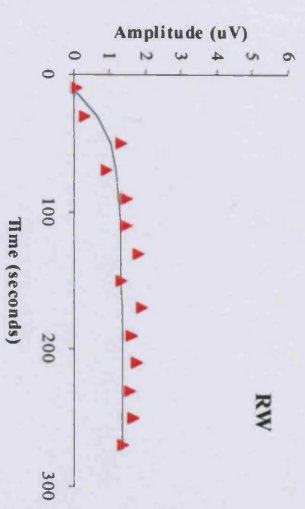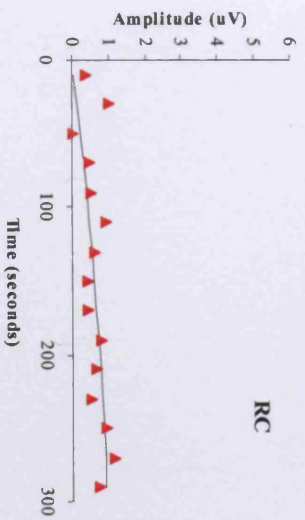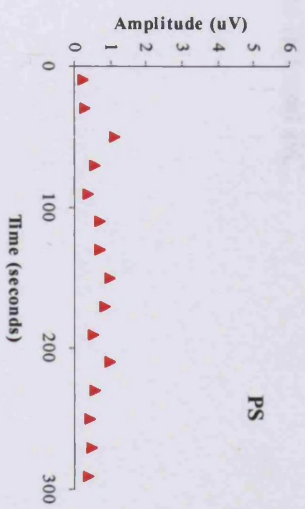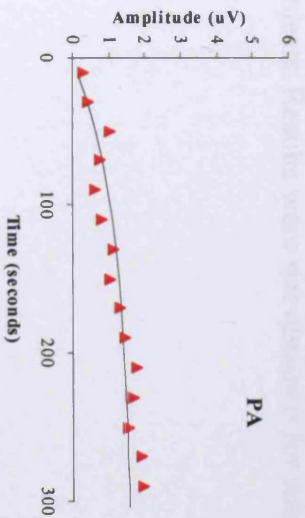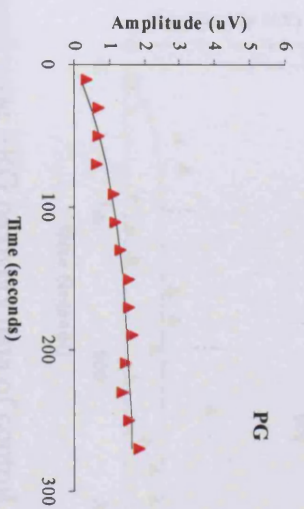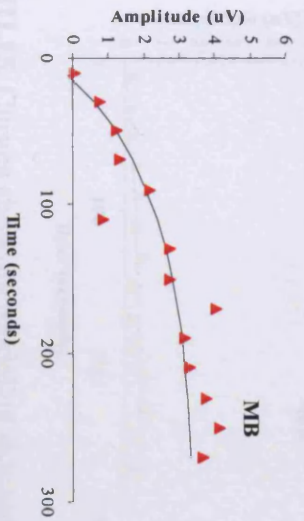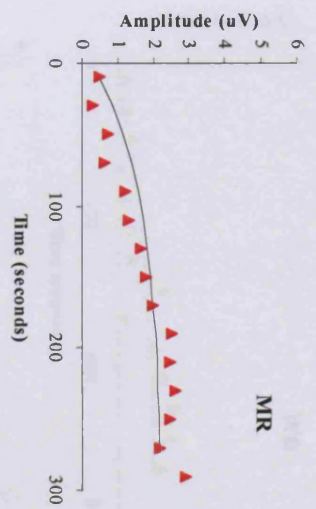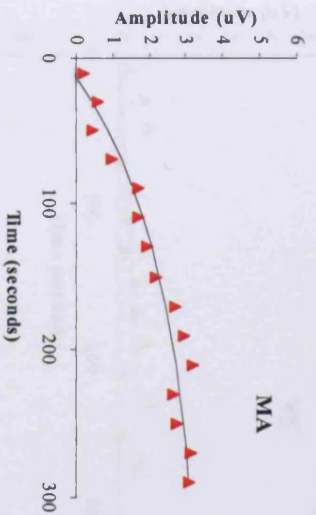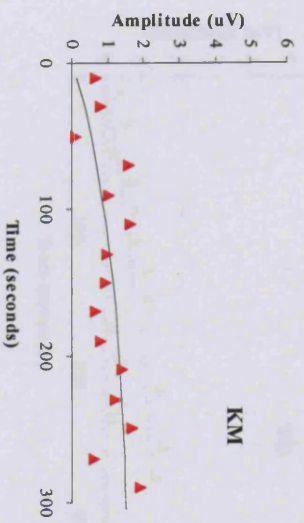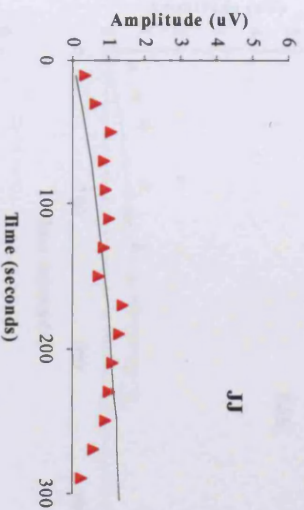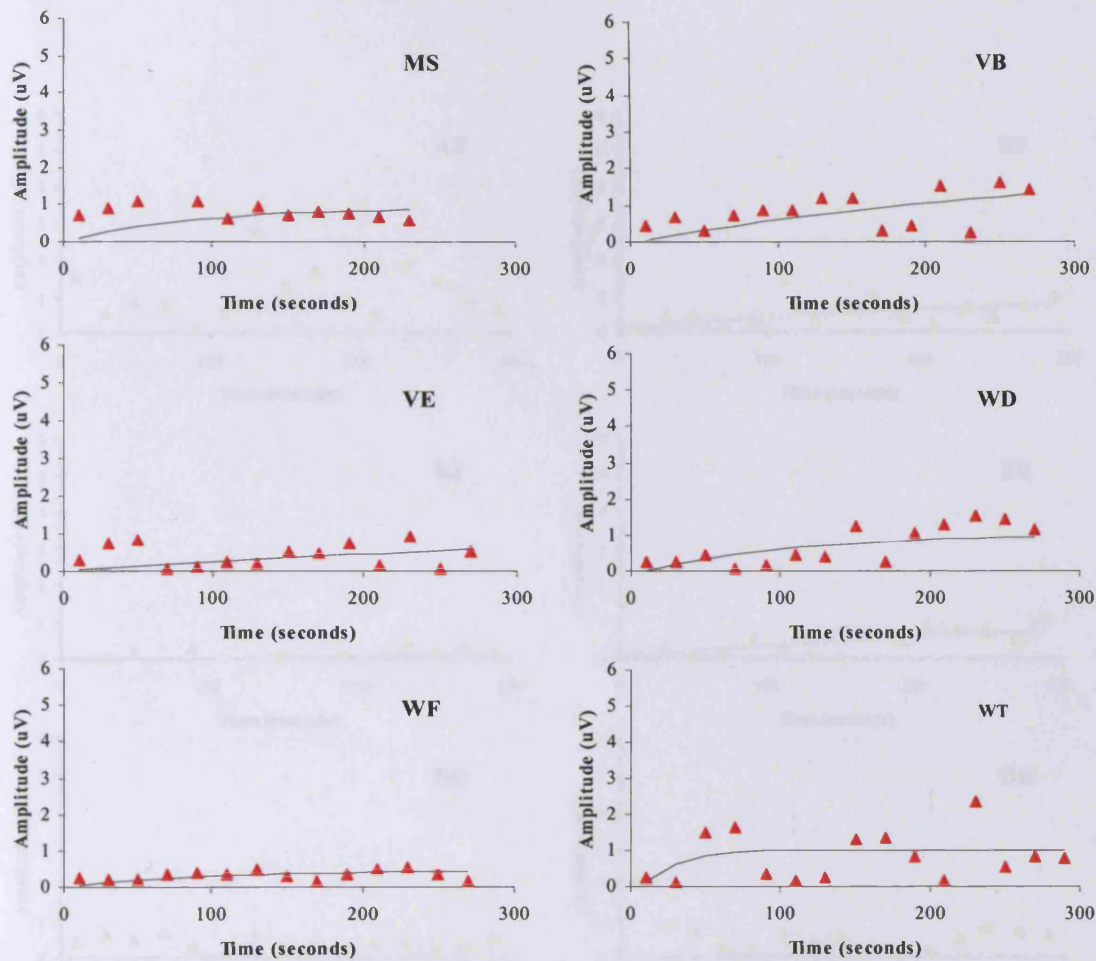
AIII.15. Curves showing modelled dynamic focal cone ERG recovery data of control subjects. Results were not obtained for subjects BB and BC.
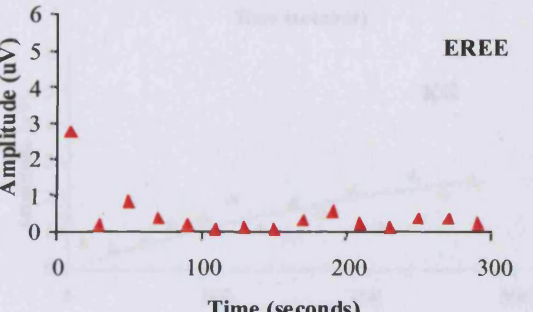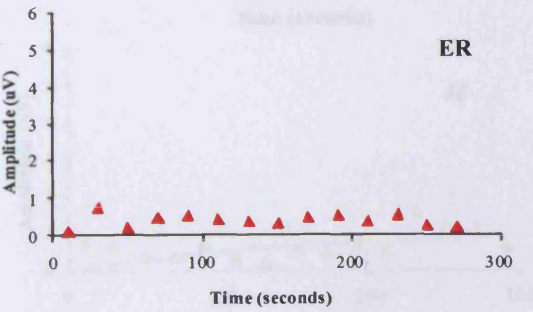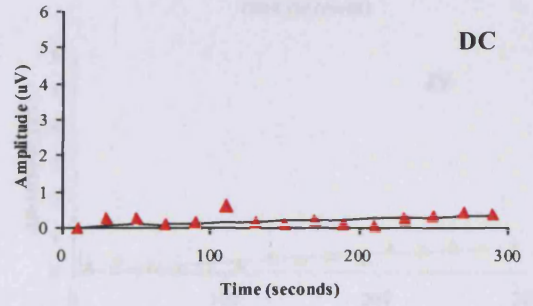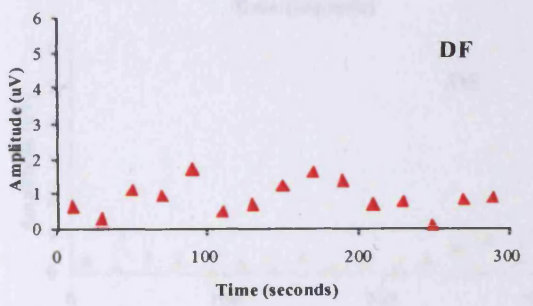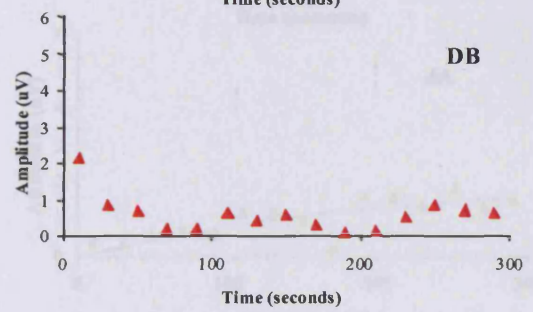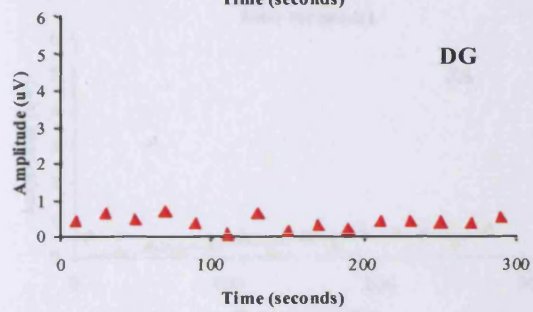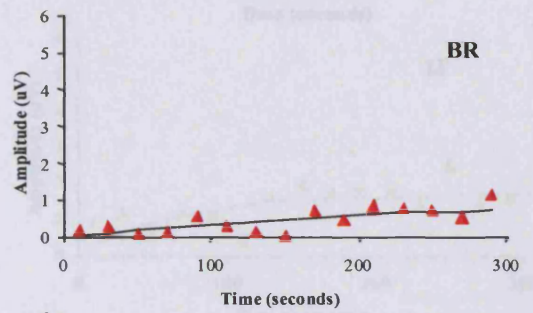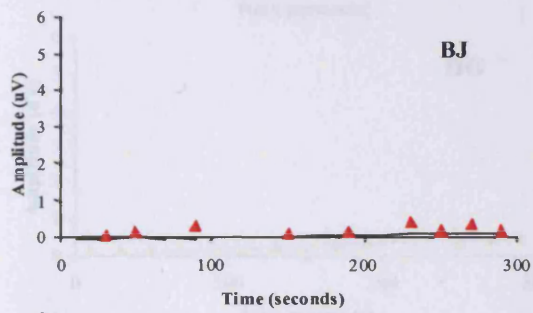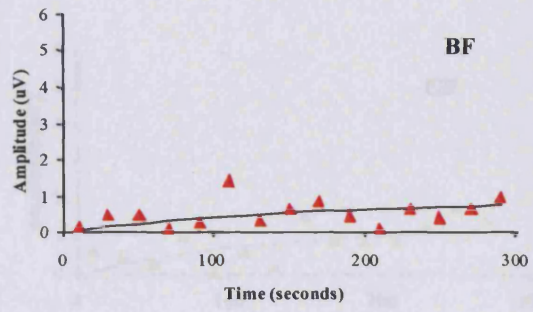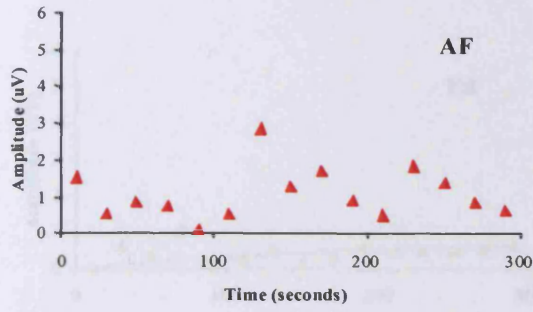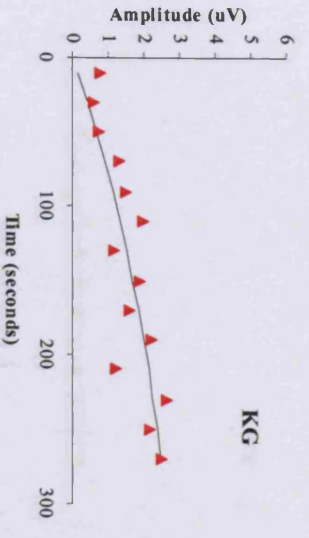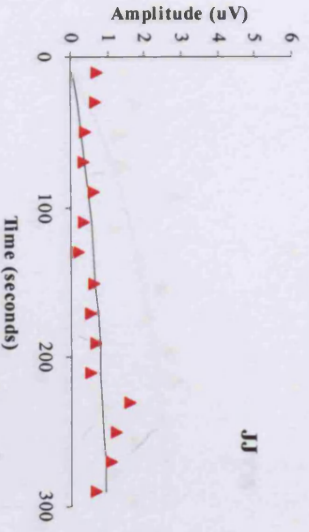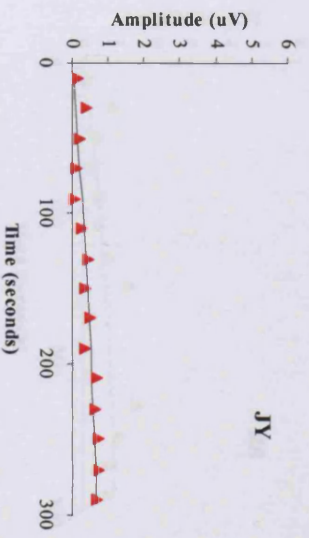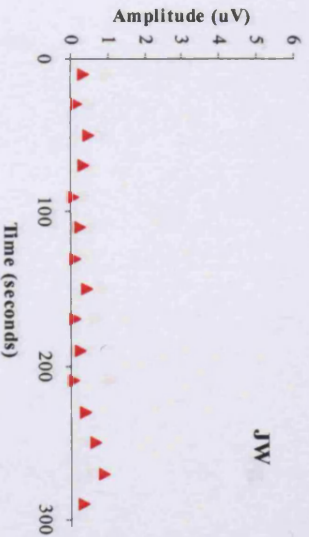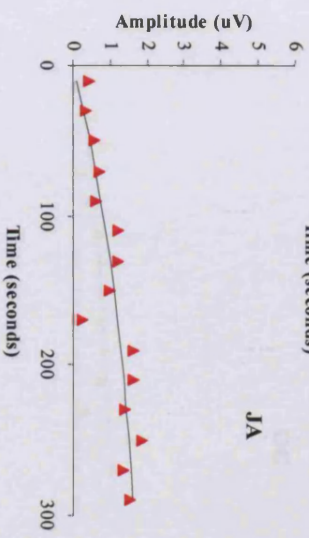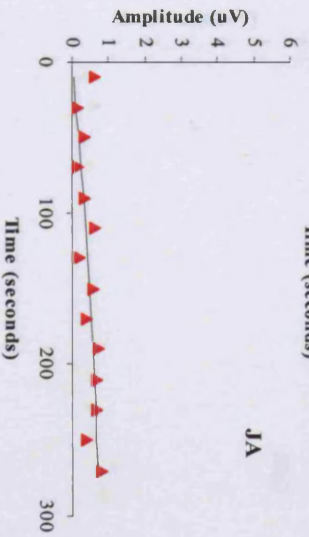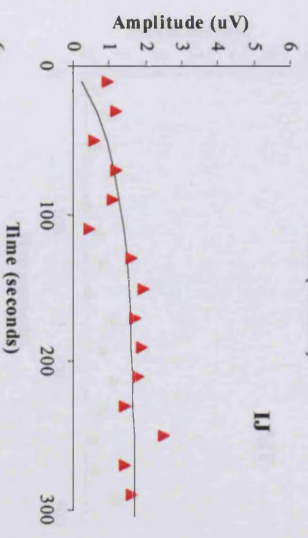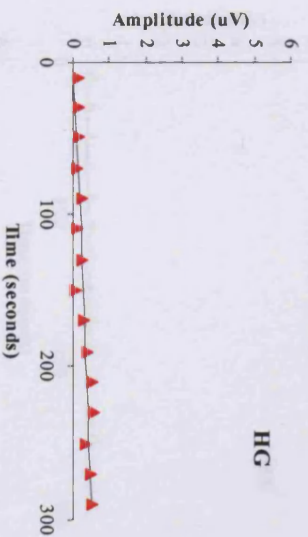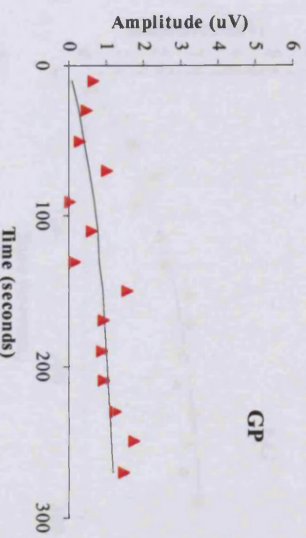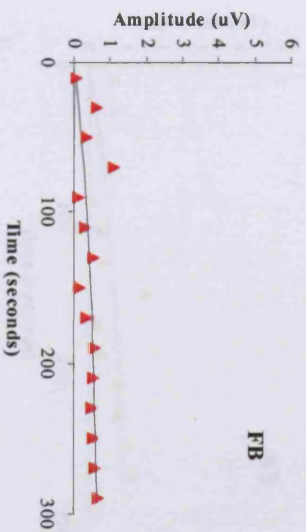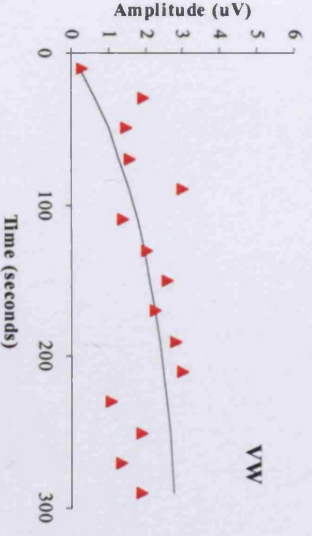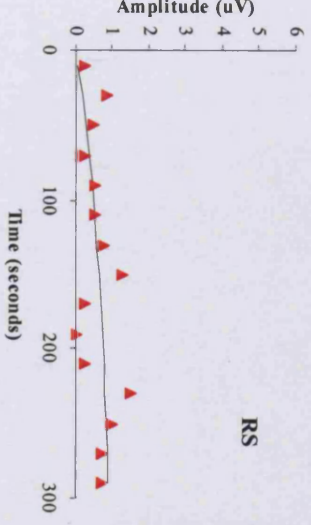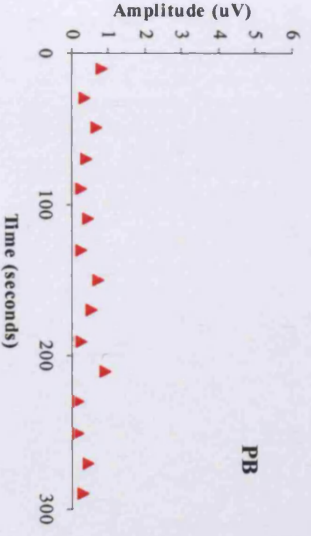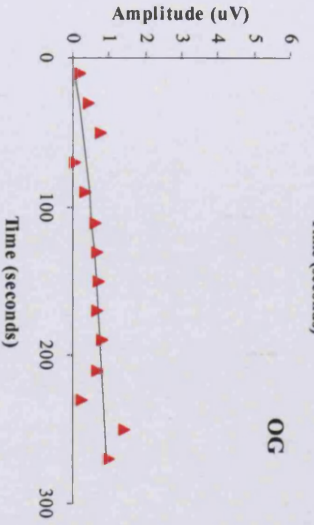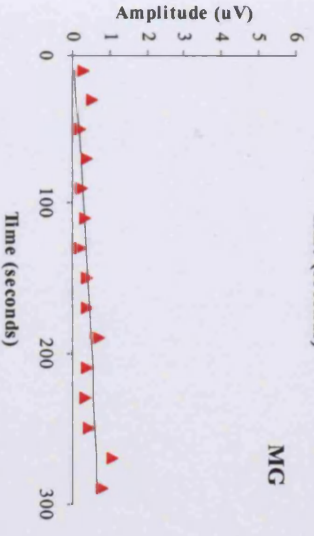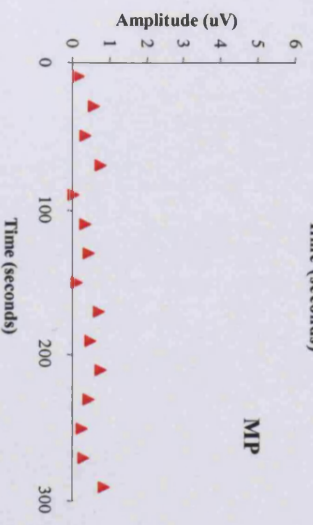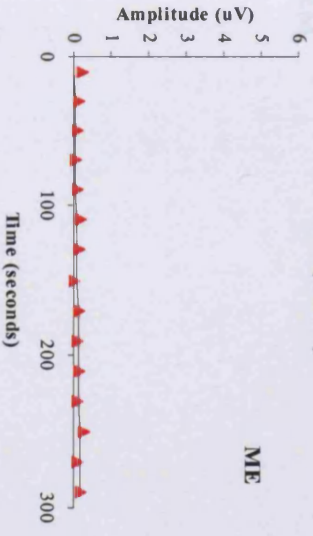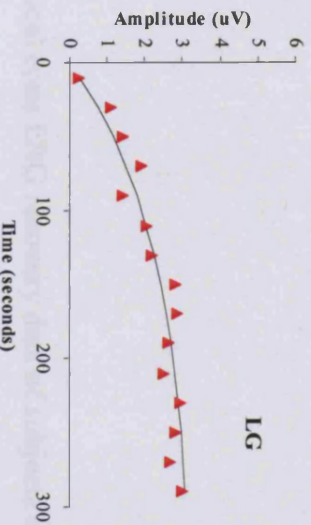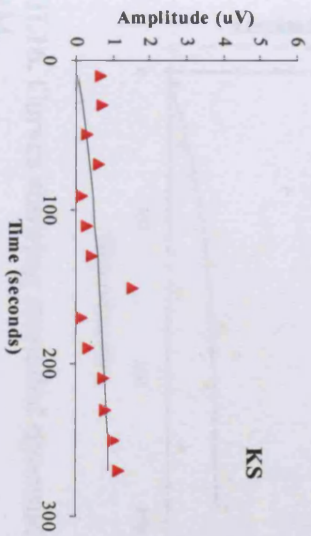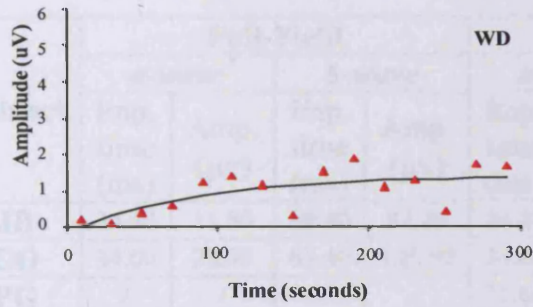
AIII.16. Curves showing modelled dynamic focal cone ERG recovery data of subjects with ARM.

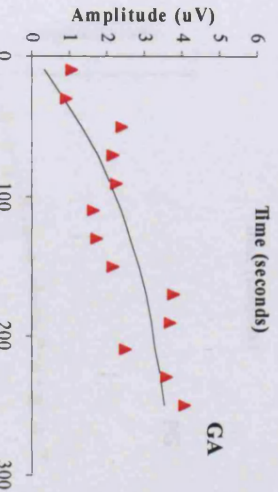| Subject	Full-Field a-wave Imp. time (ms)	Full-Field a-wave Amp. (μv)	Full-Field b-wave Imp. time (ms)	Full-Field b-wave Amp. (μv)	Focal a-wave Imp. time (ms)	Focal a-wave Amp. (μv)	Focal b-wave Imp. time (ms)	Focal b-wave Amp. (μv)	Ratio *Focal:full-field a-wave amp*	Ratio *Focal:full-field b-wave amp*
JB	34.40	11.80	69.40	97.20	36.20	2.40	57.20	4.00	0.20	0.04
GO	34.00	28.90	62.40	138.00	34.00	1.50	60.00	3.90	0.05	0.03
PG	/	/	/	/	31.60	4.20	56.00	5.60	/	/
CG	35.20	9.30	67.80	51.90	28.80	0.97	61.00	3.40	0.10	0.07
SM	31.20	8.40	59.60	84.60	/	0.00	58.40	4.10	0.00	0.05
CD	35.00	8.40	66.00	88.30	/	0.00	73.40	3.70	0.00	0.04
WD	34.00	6.30	73.20	100.10	34.00	1.10	57.20	4.70	0.17	0.05
RW	33.40	16.50	66.60	120.60	35.00	1.50	73.40	6.40	0.09	0.05
WF	35.80	3.00	70.00	12.50	26.20	0.39	60.20	1.10	0.13	0.09
MR	31.80	16.40	60.80	160.00	26.00	2.00	64.80	9.20	0.12	0.06
VE	33.40	3.60	66.80	129.60	37.20	0.57	64.40	2.80	0.16	0.02
MB	31.80	18.60	63.40	118.50	25.20	1.70	59.40	5.90	0.09	0.05
DJ	33.00	24.30	61.20	114.40	25.80	1.90	62.60	5.20	0.08	0.05
PA	31.60	19.80	62.80	167.80	28.00	0.67	60.40	4.40	0.03	0.03
GA	30.20	17.10	57.80	121.20	24.40	0.94	61.80	6.40	0.05	0.05
JJ	34.20	8.90	66.80	115.00	28.20	1.40	59.40	3.70	0.16	0.03
BB	31.00	26.00	59.00	128.70	21.00	1.30	62.40	3.70	0.05	0.03
KM	31.80	22.50	59.40	107.20	34.20	1.20	70.40	3.40	0.05	0.03
MA	25.80	5.60	81.40	97.30	23.40	0.83	55.60	5.80	0.15	0.06
AS	30.20	18.40	57.00	131.20	31.20	1.00	56.00	5.00	0.05	0.04
PS	35.80	5.20	93.20	50.20	25.20	0.22	54.20	3.40	0.04	0.07
DS	29.20	23.80	56.80	180.10	30.80	1.50	65.40	5.70	0.06	0.03
WT	33.20	25.60	63.60	92.40	22.80	0.89	58.20	3.70	0.03	0.04
GW	34.80	17.40	66.00	140.70	30.40	0.17	61.60	2.40	0.01	0.02
BC	33.20	16.20	65.60	140.30	/	0.00	74.00	0.97	0.00	0.01
RC	32.40	11.50	64.80	134.80	26.20	2.40	66.80	3.40	0.21	0.03
JC	31.00	18.00	60.60	114.00	27.40	1.60	60.40	4.40	0.09	0.04
VB	/	/	/	/	32.20	1.90	62.20	4.30	/	/

AIII.17. Table showing amplitude and implicit time data for control subjects for parameters of the rod ERG.

Subject	Full-Field				Focal				Ratio	
	a-wave		*b-wave*		*a-wave*		*b-wave*		*Focal:full-field a-wave amp.*	*Focal:full-field b-wave amp.*
	Imp. time (ms)	Amp. (μv)	Imp. time (ms)	Amp. (μv)	Imp. time (ms)	Amp. (μv)	Imp. time (ms)	Amp. (μv)		
JA	/	/	/	/	27.60	0.98	63.20	7.40	/	/
OG	35.00	5.10	65.00	39.50	/	0.00	63.80	2.70	0.00	0.07
KS	34.80	16.90	68.00	161.10	26.40	0.70	67.40	5.70	0.04	0.04
WT	33.00	32.20	58.20	170.50	39.60	0.01	61.20	5.30	0.00	0.03
HG	30.20	16.80	58.40	132.40	25.40	2.80	55.20	4.90	0.17	0.04
JW	33.40	12.90	65.80	128.40	/	0.00	54.60	4.30	0.00	0.03
IJ	32.00	19.20	63.80	106.60	25.60	3.00	59.20	4.80	0.16	0.05
ER	32.40	7.80	66.60	138.80	29.00	0.84	59.60	3.50	0.11	0.03
DF	32.80	26.30	61.80	72.60	/	0.00	/	0.00	0.00	0.00
MP	29.80	9.50	64.20	139.60	39.60	0.26	50.80	2.30	0.03	0.02
EREE	29.80	9.50	64.20	139.60	35.60	1.10	54.00	3.50	0.12	0.03
AF	29.60	12.40	62.20	122.40	35.60	0.31	62.80	2.00	0.03	0.02
VW	30.80	9.70	59.00	72.40	/	0.00	/	0.00	0.00	0.00
DG	34.60	4.90	68.20	101.50	39.60	0.37	63.40	3.80	0.08	0.04
BJ	33.60	17.30	68.40	100.40	/	0.00	63.40	2.90	0.00	0.03
KG	34.20	6.70	74.00	166.60	25.20	3.40	63.00	14.00	0.51	0.08
JY	29.60	12.40	62.40	122.40	35.60	0.31	62.40	2.00	0.03	0.02
WD	32.40	11.10	62.00	108.70	35.20	0.43	54.60	3.60	0.04	0.03
LG	31.00	22.40	55.80	152.10	29.80	1.80	61.00	7.20	0.08	0.05
DC	34.20	18.40	64.00	115.10	42.00	2.70	65.80	1.70	0.15	0.02
JA	32.60	31.50	61.20	144.00	33.40	1.40	66.80	2.90	0.04	0.02
BF	31.60	16.40	63.00	164.70	31.60	0.67	59.20	5.50	0.04	0.03
PB	33.40	11.80	66.00	83.30	29.00	0.65	66.00	1.90	0.06	0.02
FB	33.20	20.10	65.40	98.00	28.40	1.40	54.40	1.70	0.07	0.02
BR	32.40	18.10	62.60	188.30	28.80	0.13	61.00	6.20	0.01	0.03
ME	35.00	12.80	67.00	66.30	24.40	0.40	59.00	3.10	0.03	0.05
MG	/	/	/	/	22.00	1.00	55.00	4.50	/	/
DB	32.20	17.00	60.40	114.00	25.00	0.53	69.00	3.40	0.03	0.03
JJ	34.00	17.10	63.60	152.90	34.00	1.60	67.40	4.10	0.09	0.03
RS	31.80	20.80	61.20	123.30	28.60	0.55	67.60	3.40	0.03	0.03
GP	32.60	23.10	57.80	131.30	33.20	0.69	69.80	3.70	0.03	0.03

AIII.18. Table showing amplitude and implicit time data for subjects with ARM for parameters of the rod ERG.

Subject	Amplitude between 31-42 ms	Amplitude between 54-83 ms	Amplitude between 94-142 ms	Amplitude between 142-170 ms
JB	0.74	3.90	6.90	0.15
GO	0.16	2.20	8.70	5.20
CG	1.40	1.00	9.10	1.10
SM	4.90	1.50	13.00	12.90
WD	2.40	3.80	8.20	10.60
RW	1.00	0.96	5.40	0.33
WF	5.20	6.70	0.57	4.80
MR	1.10	1.60	16.30	9.40
VE	2.80	8.10	17.70	2.70
MB	0.63	1.90	4.70	7.00
DJ	0.67	0.39	10.90	3.40
PA	2.80	0.58	2.40	7.70
GA	0.60	7.50	22.80	5.10
JJ	1.70	3.40	13.20	0.94
BB	0.46	0.69	6.40	3.10
KM	0.15	34.60	31.50	11.20
MA	0.51	7.80	3.30	1.20
AS	0.17	2.90	4.10	4.20
PS	1.30	0.72	2.90	2.20
DS	0.49	4.10	2.10	0.69
WT	1.80	1.20	4.30	1.10
GW	2.10	3.00	13.10	3.70
BC	1.20	7.10	21.10	10.90
RC	0.54	10.00	9.70	8.30
JC	2.60	1.60	2.70	2.50

AIII.19. Table showing amplitude and implicit time data for control subjects for parameters of the rod VEP. Results were not obtained from subjects PG, CD, VB.

Subject	Amplitude between 31-42 ms	Amplitude between 54-83 ms	Amplitude between 94-142 ms	Amplitude between 142-170 ms
OG	3.80	11.30	2.30	1.90
KS	3.10	5.60	8.90	8.20
WT	1.70	1.10	4.10	1.10
HG	2.00	0.18	0.32	2.10
JW	0.62	1.80	2.20	0.38
IJ	0.77	2.10	1.10	1.30
ER	0.34	2.60	9.60	2.80
DF	3.00	2.30	0.02	10.60
EREE	2.40	7.80	12.60	14.00
AF	1.60	1.10	1.00	1.80
VW	3.30	4.30	19.40	17.30
BJ	1.40	6.50	16.10	4.80
KG	1.10	4.00	0.45	6.50
JY	1.20	4.30	3.40	2.20
WD	3.00	3.40	10.00	3.00
LG	1.40	7.10	23.40	0.59
DC	0.86	1.80	17.20	7.30
JA	1.80	6.20	6.70	7.20
BF	0.06	7.00	10.00	0.26
PB	1.50	5.50	0.87	7.70
FB	1.10	9.30	13.90	5.30
BR	4.80	3.10	9.60	9.00
ME	1.80	1.10	13.30	3.30
MG	1.20	0.24	4.90	0.87
DB	0.10	6.70	15.50	0.14
JJ	2.30	22.10	9.60	1.50
RS	2.00	9.10	10.10	13.70
GP	1.90	1.70	3.00	5.90

AIII.20. Table showing amplitude and implicit time data for subjects with ARM for parameters of the rod VEP. Results were not obtained from subjects JA, MP, DG.

Subject	Full-Field				Focal				Ratio	
	a-wave		b-wave		a-wave		b-wave		*Focal:full-field a-wave amp.*	*Focal:full-field b-wave amp.*
	Imp. time (ms)	Amp. (μv)	Imp. time (ms)	Amp. (μv)	Imp. time (ms)	Amp. (μv)	Imp. time (ms)	Amp. (μv)		
JB	26.00	13.60	47.40	28.10	23.40	2.30	43.20	4.90	0.17	0.17
GO	26.80	23.40	50.20	40.60	23.60	1.60	45.60	4.80	0.07	0.12
PG	26.20	23.30	48.40	49.10	23.60	2.00	45.00	5.30	0.09	0.11
CG	23.60	4.90	48.40	14.40	22.60	1.50	42.40	2.50	0.31	0.17
SM	24.40	7.70	46.00	16.70	23.80	0.55	42.60	1.80	0.07	0.11
CD	25.80	10.60	47.00	21.00	22.00	1.00	41.60	2.70	0.09	0.13
WD	26.00	11.80	47.40	26.10	23.40	2.00	42.00	4.00	0.17	0.15
RW	24.40	14.80	44.80	25.50	22.00	2.70	44.60	3.90	0.18	0.15
WF	26.60	3.20	46.40	3.80	22.40	0.17	34.20	0.62	0.05	0.16
MR	25.60	16.80	49.00	48.40	22.80	2.80	44.60	7.80	0.17	0.16
VE	28.40	8.00	51.40	17.10	21.60	1.70	41.60	4.20	0.21	0.25
MB	25.80	17.30	48.60	36.80	22.60	2.40	43.20	5.70	0.14	0.15
DJ	25.20	13.00	47.60	27.70	22.60	1.90	41.40	4.50	0.15	0.16
PA	25.80	21.00	48.80	52.70	23.40	1.70	45.00	4.80	0.08	0.09
GA	25.20	21.00	47.00	45.00	22.40	3.80	44.40	7.20	0.18	0.16
JJ	27.80	9.50	47.80	18.70	23.40	1.70	43.00	3.90	0.18	0.21
BB	23.40	13.90	44.00	41.90	22.40	2.10	41.60	5.60	0.15	0.13
KM	26.40	13.70	49.60	24.60	24.40	1.60	43.80	3.60	0.12	0.15
MA	25.00	18.10	45.80	44.70	23.00	2.20	43.80	6.40	0.12	0.14
AS	27.40	20.50	53.80	35.20	22.80	2.10	43.80	5.10	0.10	0.14
PS	25.00	16.00	48.80	28.90	22.60	0.89	41.00	2.10	0.06	0.07
DS	25.00	17.30	46.80	37.60	17.60	1.80	42.80	4.70	0.10	0.13
WT	26.60	13.90	48.80	21.40	22.60	0.89	44.00	3.20	0.06	0.15
GW	25.80	13.30	49.40	30.90	26.40	0.80	47.20	3.60	0.06	0.12
BC	25.00	10.60	49.20	30.60	24.40	2.80	47.40	4.10	0.26	0.13
RC	27.20	13.40	49.80	35.30	23.60	1.30	44.80	3.20	0.10	0.09
JC	25.80	25.90	47.60	25.10	23.60	2.50	47.20	5.30	0.10	0.21
VB	25.80	15.60	45.60	29.50	22.40	1.40	43.60	4.50	0.09	0.15

AIII.21. Table showing amplitude and implicit time data for control subjects for parameters of the 5 Hz cone ERG.

Subject	Full-Field a-wave Imp. time (ms)	Full-Field a-wave Amp. (μv)	Full-Field b-wave Imp. time (ms)	Full-Field b-wave Amp. (μv)	Focal a-wave Imp. time (ms)	Focal a-wave Amp. (μv)	Focal b-wave Imp. time (ms)	Focal b-wave Amp. (μv)	Ratio Focal:full-field a-wave amp.	Ratio Focal:full-field b-wave amp.
JA	25.40	12.00	48.00	26.00	23.80	1.70	42.80	3.90	0.14	0.15
OG	28.80	18.80	49.40	19.90	26.60	1.40	42.20	2.20	0.07	0.11
KS	33.20	8.50	58.60	16.80	30.00	1.20	52.20	2.30	0.14	0.14
WT	26.80	17.40	48.80	33.60	24.20	1.40	48.40	4.80	0.08	0.14
HG	23.40	13.00	42.40	24.90	21.80	1.20	41.20	3.20	0.09	0.13
JW	27.00	12.20	52.00	30.70	22.80	1.00	42.40	4.70	0.08	0.15
IJ	27.20	13.40	48.20	33.80	21.80	2.90	43.00	5.10	0.22	0.15
ER	25.80	23.00	47.80	45.50	26.60	1.40	45.00	5.90	0.06	0.13
DF	25.60	14.20	48.60	25.50	28.60	1.50	40.40	1.60	0.11	0.06
MP	24.00	10.60	48.00	24.10	25.80	1.20	48.80	1.50	0.11	0.06
EREE	26.20	12.50	48.60	19.50	25.60	1.10	46.80	3.90	0.09	0.20
AF	27.20	10.60	51.20	32.60	21.20	0.63	55.20	2.40	0.06	0.07
VW	26.20	16.50	49.40	23.50	22.80	3.00	46.60	4.40	0.18	0.19
DG	28.40	11.50	50.60	22.40	25.20	1.80	43.60	3.20	0.16	0.14
BJ	28.40	17.30	49.20	16.80	24.80	1.80	45.40	3.30	0.10	0.20
KG	26.80	15.90	53.00	34.40	24.20	1.60	45.60	6.20	0.10	0.18
JY	26.80	10.50	51.20	32.50	21.20	0.63	43.00	2.70	0.06	0.08
WD	25.60	12.30	48.00	47.00	25.60	1.40	41.00	5.00	0.11	0.11
LG	24.20	17.40	45.40	36.50	22.00	2.70	45.60	5.70	0.16	0.16
DC	27.60	13.90	51.20	36.60	25.40	1.40	52.00	2.00	0.10	0.05
JA	26.00	22.60	48.60	32.30	25.00	2.10	43.20	2.80	0.09	0.09
BF	26.00	17.10	50.40	50.90	22.80	1.50	46.40	4.10	0.09	0.08
PB	25.80	9.00	47.00	23.90	25.80	0.08	49.00	2.00	0.01	0.08
FB	27.00	13.40	49.40	25.70	25.60	1.70	45.80	2.60	0.13	0.10
BR	24.20	19.30	50.60	43.40	21.80	0.93	40.40	4.00	0.05	0.09
ME	26.60	8.10	47.00	10.90	22.60	0.83	46.60	2.30	0.10	0.21
MG	25.60	17.90	49.80	36.80	24.40	1.50	51.40	5.00	0.08	0.14
DB	25.00	14.30	45.40	22.40	18.40	1.30	47.00	3.50	0.09	0.16
JJ	25.80	12.90	47.80	34.60	24.20	1.90	47.80	4.90	0.15	0.14
RS	24.60	14.70	45.80	34.60	21.20	0.82	42.60	3.10	0.06	0.09
GP	24.80	21.60	47.20	45.10	24.80	3.20	50.40	6.00	0.15	0.13

AIII.22. Table showing amplitude and implicit time data for subjects with ARM for parameters of the 5 Hz cone ERG

Subject	Full-Field Implicit time				Full-Field Sum Amp. (μv)	Focal Implicit time				Focal Sum Amp. (μv)	Ratio Focal:full-field sum. Amp. ratio
	OP1	OP2	OP3	OP4		OP1	OP2	OP3	OP4		
JB	19.40	27.80	35.60	43.60	29.30	18.40	26.60	33.60	38.40	7.44	0.25
GO	13.80	20.40	27.20	35.80	23.80	19.80	26.00	33.60	/	3.48	0.15
PG	/	21.00	27.40	35.40	53.40	/	24.40	33.00	36.80	6.65	0.12
CG	/	27.40	33.80	43.20	21.70	/	25.00	30.80	38.00	6.90	0.32
SM	/	21.20	26.20	32.60	17.54	21.20	26.20	30.20	/	4.26	0.24
CD	/	27.00	33.40	44.00	23.00	/	23.40	29.80	37.80	8.55	0.37
WD	/	20.20	27.60	35.20	20.70	/	24.40	31.20	37.40	6.06	0.29
RW	19.60	25.80	32.60	40.80	26.94	/	23.80	29.00	36.00	6.16	0.23
WF	/	21.80	27.80	34.40	3.46	19.20	25.80	30.20	37.00	1.81	0.52
MR	/	27.00	33.80	41.00	30.17	/	24.80	30.80	37.80	7.54	0.25
VE	13.80	22.00	28.40	36.80	8.06	/	/	/	/	0.00	0.00
MB	19.40	26.60	35.00	44.80	26.91	18.80	23.80	32.20	39.00	7.64	0.28
DJ	21.00	26.80	34.40	43.60	33.31	/	23.60	30.40	36.40	6.95	0.21
PA	/	20.40	28.00	34.60	36.50	/	24.20	30.80	37.20	5.06	0.14
GA	/	20.20	26.80	33.60	34.84	18.20	23.60	31.20	37.40	16.70	0.48
JJ	/	22.00	28.60	35.80	8.55	/	25.00	32.00	38.80	5.34	0.62
BB	18.80	25.00	31.60	39.00	32.67	/	24.60	31.00	37.80	10.10	0.31
KM	/	21.00	27.60	35.00	13.46	/	25.20	29.00	/	3.83	0.28
MA	/	20.40	27.40	34.40	34.53	/	24.40	32.40	40.60	6.73	0.19
AS	/	22.20	29.60	36.80	17.93	/	25.20	31.80	38.40	7.17	0.40
PS	21.00	26.80	33.80	38.80	34.14	/	22.60	27.80	/	3.53	0.10
DS	18.60	26.80	33.60	41.60	26.67	18.20	25.40	30.80	37.60	6.97	0.26
WT	10.40	21.20	27.80	34.80	15.46	/	25.00	33.00	40.80	2.89	0.19
GW	/	27.20	34.20	41.60	30.36	/	27.00	34.40	/	4.90	0.16
BC	/	26.20	33.60	41.80	19.30	/	25.80	31.80	38.80	10.27	0.53
RC	23.40	29.20	34.40	39.00	21.39	.	24.00	31.00	/	2.06	0.10
JC	/	26.00	32.00	38.00	16.31	18.40	25.00	32.20	38.40	7.93	0.49
VB	20.20	27.60	35.40	42.80	23.09	/	24.60	30.20	40.00	3.83	0.17

AIII.23. Table showing amplitude and implicit time data for control subjects for parameters of the OPs

| Subject | Full-Field | | | | | Focal | | | | | Ratio |
| | Implicit time | | | | Sum Amp. (μv) | Implicit time | | | | Sum Amp. (μv) | Focal:full-field sum. amp. Ratio |
	OP1	OP2	OP3	OP4		OP1	OP2	OP3	OP4		
JA	18.60	26.60	/	/	12.44	/	/	/	/	0.00	0.00
OG	/	30.80	36.00	43.60	10.58	/	27.70	33.60	/	2.08	0.20
KS	/	23.00	37.20	/	6.50	/	/	/	/	0.00	0.00
WT	/	28.20	36.40	45.20	28.30	.	28.40	33.60	39.60	6.27	0.22
HG	18.40	24.60	31.40	38.80	28.14	/	22.80	29.20	/	2.95	0.10
JW	21.40	29.00	36.40	44.60	17.73	/	26.60	31.00	/	8.06	0.45
IJ	/	29.20	36.60	44.80	25.00	/	/	/	/	0.00	0.00
ER	20.20	26.80	34.00	43.00	44.66	/	24.20	27.80	30.20	13.20	0.30
DF	19.20	27.20	34.00	45.40	32.00	/	/	/	/	0.00	0.00
MP	/	25.80	33.20	44.00	24.70	/	26.20	/	/	1.26	0.05
EREE	/	27.40	34.20	44.60	15.10	/	26.40	35.60	42.40	3.56	0.24
AF	/	28.40	35.80	44.20	24.40	/	/	/	/	0.00	0.00
VW	/	27.00	34.60	46.40	22.90	/	25.40	31.40	38.40	10.60	0.46
DG	21.40	30.60	35.80	42.40	8.66	/	/	/	/	0.00	0.00
BJ	/	29.80	37.40	45.00	13.70	/	21.60	26.40	33.40	6.04	0.44
KG	21.20	28.00	35.80	42.80	26.18	/	25.40	32.00	38.60	6.40	0.24
JY	/	28.00	35.80	43.60	20.34	/	/	25.6	31.6	4.56	0.22
WD	8.00	20.60	26.80	35.40	44.13	/	/		/	0.00	0.00
LG	20.60	25.80	32.40	38.00	47.73	/	22.80	29.80	36.40	8.93	0.19
DC	22.00	29.20	37.40	45.60	17.18	/	/	/	/	0.00	0.00
JA	20.80	27.40	35.20	45.40	41.56	/	26.60	32.80	40.60	4.93	0.12
BF	22.40	28.00	35.00	44.00	31.66	/	24.40	/	/	2.30	0.07
PB	17.80	26.40	33.80	42.40	13.66	/	/	/	/	0.00	0.00
FB	21.20	28.20	35.00	43.80	20.60	/	26.00	33.80	41.80	3.74	0.18
BR	.	25.40	31.80	40.60	43.50	/	23.60	29.60	36.20	8.30	0.19
ME	20.20	30.60	35.20	/	6.06	/	25.00	34.40	42.00	1.89	0.31
MG	21.20	27.20	34.80	42.20	41.62	17.00	25.80	32.60	40.60	8.27	0.20
DB	19.00	26.40	32.80	41.40	27.86	/	/	/	/	0.00	0.00
JJ	13.80	20.00	26.60	34.60	18.35	13.80	26.00	33.40	41.00	5.74	0.31
RS	19.40	25.20	33.00	38.00	29.90	/	22.80	30.40	/	3.01	0.10
GP	20.20	26.20	33.80	43.80	44.10	21.00	27.40	/	/	3.82	0.09

AIII.24. Table showing amplitude and implicit time data for subjects with ARM for parameters of the OPs

347

Subject	Full-Field		Focal		Focal : full-field amplitude ratio
	Imp. time (ms)	Amp. (μv)	Imp. time (ms)	Amp. (μv)	
JB	15.00	18.60	13.85	3.10	0.17
GO	15.25	16.60	11.95	2.10	0.13
PG	12.65	19.80	10.55	2.30	0.12
CG	14.25	4.50	11.60	1.56	0.35
SM	11.55	7.40	12.00	0.80	0.11
CD	14.70	18.95	9.55	2.40	0.13
WD	13.90	10.10	10.35	2.00	0.20
RW	10.60	13.50	11.75	2.40	0.18
WF	13.65	2.70	11.80	0.48	0.18
MR	15.05	16.60	10.75	3.30	0.20
VE	14.25	3.35	9.95	1.95	0.58
MB	14.40	19.96	11.95	3.77	0.19
DJ	12.85	13.20	11.35	7.30	0.55
PA	13.25	19.95	11.40	1.70	0.09
GA	13.05	21.93	11.10	4.10	0.19
JJ	14.00	8.30	10.80	2.20	0.27
BB	11.75	23.20	12.20	2.20	0.09
KM	13.65	11.30	14.00	2.80	0.25
MA	13.85	25.97	10.30	3.83	0.15
AS	15.45	14.50	12.40	1.40	0.10
PS	13.25	14.80	8.55	0.98	0.07
DS	13.10	15.60	12.05	1.90	0.12
WT	13.25	6.40	13.05	0.76	0.12
GW	15.50	13.10	12.85	1.45	0.11
BC	13.20	12.30	11.60	1.45	0.12
RC	15.25	10.80	10.70	1.43	0.13
JC	13.65	19.60	13.85	2.90	0.15
VB	13.90	19.97	11.95	2.50	0.13

AIII.25. Table showing amplitude and implicit time data for control subjects for parameters of the 41 Hz cone ERG

Subject	Full-Field		Focal		Focal : full-field amplitude ratio
	Imp. time (ms)	Amp. (μv)	Imp. time (ms)	Amp. (μv)	
JA	12.20	11.20	11.10	1.10	0.10
OG	15.85	4.90	10.70	1.60	0.33
KS	17.70	4.55	8.50	0.50	0.11
WT	14.85	17.10	15.60	0.94	0.06
HG	11.15	13.60	10.60	1.60	0.12
JW	16.45	7.60	15.70	2.40	0.32
IJ	15.10	12.65	11.35	3.20	0.25
ER	13.85	14.40	11.80	1.80	0.13
DF	14.45	16.50	13.70	2.30	0.14
MP	13.55	11.70	11.15	0.57	0.05
EREE	13.15	6.45	13.40	0.70	0.11
AF	15.65	11.80	13.25	0.77	0.07
VW	16.30	22.50	15.05	4.30	0.19
DG	17.10	10.30	13.70	0.00	0.00
BJ	14.45	6.10	13.00	0.67	0.11
KG	15.30	18.50	12.85	4.10	0.22
JY	14.35	12.10	13.80	0.77	0.06
WD	14.50	14.30	11.60	1.50	0.11
LG	11.55	15.70	10.30	3.60	0.23
DC	14.05	7.85	16.15	0.71	0.09
JA	15.70	25.40	12.75	2.20	0.09
BF	14.25	14.70	11.75	0.95	0.07
PB	14.25	11.65	11.75	0.66	0.06
FB	12.60	9.50	10.10	0.87	0.09
BR	14.80	19.40	10.45	1.80	0.09
ME	14.85	3.13	13.25	0.51	0.16
MG	14.60	19.50	15.45	1.10	0.06
DB	14.60	12.30	12.65	1.60	0.13
JJ	16.40	8.30	12.55	1.27	0.15
RS	11.60	10.60	9.60	1.20	0.11
GP	14.20	35.70	12.05	2.07	0.06

AIII.26. Table showing amplitude and implicit time data for subjects with ARM for parameters of the 41 Hz cone ERG

Subject	a-wave Imp. time (ms)	a-wave Amp. (μv)	b-wave Imp. time (ms)	b-wave Amp. (μv)	PhNR	a-wave to b-wave amplitude ratio
JB	35.00	0.88	69.00	1.80	8.80	0.49
PG	32.00	1.30	58.00	1.70	5.10	0.76
CG	45.50	1.20	67.00	1.70	4.30	0.71
SM	/	0.00	70.50	1.30	2.00	0.00
CD	/	0.00	51.50	0.82	6.60	0.00
WD	26.00	1.20	70.00	2.20	9.90	0.55
RW	37.50	1.00	65.00	0.63	5.50	1.59
WF	38.50	0.18	58.50	0.16	0.38	1.13
MR	42.00	0.60	67.00	2.30	4.50	0.26
VE	47.00	0.91	77.50	2.80	5.90	0.33
MB	36.00	0.85	64.00	2.10	5.50	0.40
DJ	42.00	1.70	68.50	2.20	9.10	0.77
GA	32.50	1.50	67.00	3.10	7.60	0.48
JJ	45.00	0.38	64.50	1.30	7.30	0.29
KM	29.50	0.37	65.00	1.50	3.80	0.25
MA	24.50	0.98	56.00	3.00	5.20	0.33
AS	40.50	0.87	66.50	3.70	8.50	0.24
PS	40.00	0.28	68.50	1.20	2.40	0.23
DS	32.50	2.30	56.50	1.30	4.70	1.77
WT	34.50	0.91	62.50	1.60	5.70	0.57
BC	45.50	1.50	72.00	1.80	7.80	0.83
RC	44.50	1.50	79.00	2.00	6.70	0.75
JC	38.00	0.76	56.50	0.42	5.90	1.81

AIII.27. Table showing amplitude and implicit time data for control subjects for parameters of the S-cone ERG. Results were not obtained for subjects GO, PA, GW, VB, BB.

350

Subject	a-wave		b-wave		PhNR	a-wave to b-wave amplitude ratio
	Imp. time (ms)	Amp. (μv)	Imp. time (ms)	Amp. (μv)		
OG	37.50	2.10	53.50	1.20	3.60	1.75
KS	/	0.00	/	0.00	5.80	/
WT	34.00	0.92	56.00	1.50	3.20	0.61
HG	35.50	0.72	55.00	0.98	8.90	0.73
IJ	32.50	0.50	55.00	1.20	6.80	0.42
ER	38.00	0.81	72.00	3.00	7.50	0.27
DF	28.00	2.40	68.00	3.00	5.50	0.80
MP	34.50	1.20	59.50	1.60	4.40	0.75
EREE	48.50	0.30	71.50	1.40	4.70	0.21
AF	42.00	0.62	64.50	3.00	6.50	0.21
VW	/	0.00	68.00	1.00	1.90	0.00
DG	46.00	1.20	67.50	1.30	4.40	0.92
BJ	35.00	0.68	64.00	0.79	5.00	0.86
JY	42.00	1.50	64.50	3.00	6.50	0.50
WD	38.00	2.80	66.50	6.10	14.60	0.46
LG	32.00	1.30	58.50	1.90	4.80	0.68
DC	41.50	1.40	68.50	2.80	6.40	0.50
JA	28.50	0.70	60.00	2.20	3.70	0.32
BF	35.50	1.70	77.00	3.00	4.20	0.57
PB	50.00	1.30	69.50	1.70	5.80	0.76
ME	45.00	0.80	66.50	1.20	5.20	0.67
MG	36.00	0.90	67.00	4.80	9.40	0.19
DB	41.00	2.00	74.00	3.70	9.40	0.54
JJ	40.00	1.10	76.50	3.10	10.30	0.35
RS	39.00	1.80	67.50	2.00	11.30	0.90
GP	29.50	1.10	67.50	2.40	5.30	0.46

AIII.28. Table showing amplitude and implicit time data for subjects with ARM for parameters of the S-cone ERG. Results were not obtained for subjects JA, JW, KG, FB, BR.

Subject	Amplitude between 44.5-92.5 ms	Amplitude between 133-166.5 ms	Amplitude between 344-394.5 ms	Amplitude between 430-462.5 ms
JB	4.60	4.40	2.10	0.42
PG	4.40	0.34	2.80	2.00
CG	0.72	0.03	2.30	2.40
SM	2.10	1.50	8.80	2.40
WD	1.90	3.40	1.80	3.10
RW	.91	1.30	1.30	1.70
WF	.20	3.90	2.30	6.80
MR	1.80	1.00	7.30	4.90
VE	3.80	9.20	7.00	5.70
MB	2.00	3.30	1.70	0.39
DJ	3.60	5.80	2.50	10.90
GA	6.70	12.50	6.20	8.70
JJ	0.46	0.25	3.20	2.30
KM	7.60	2.20	8.90	4.10
MA	2.90	2.90	3.80	0.56
AS	3.00	1.90	3.20	2.20
PS	3.40	1.50	2.50	2.50
DS	1.10	2.40	1.20	0.19
WT	0.88	1.00	2.00	4.20
GW	2.10	1.10	2.30	6.30
BC	0.62	1.90	3.30	0.28
RC	3.40	5.50	3.20	2.70
JC	2.90	1.40	2.20	1.80

AIII.29. Table showing amplitude and implicit time data for control subjects for parameters of the S-cone VEP. Results were not obtained for subjects GO, CD, PA, BB, VB.

Subject	Amplitude between 44.5-92.5 ms	Amplitude between 133-166.5 ms	Amplitude between 344-394.5 ms	Amplitude between 430-462.5 ms
OG	3.20	5.80	1.80	9.80
KS	4.70	4.50	0.15	3.20
WT	0.69	3.60	3.10	4.20
HG	0.10	0.15	2.00	4.30
IJ	2.20	2.20	7.70	5.10
ER	8.40	2.40	5.50	6.10
DF	0.27	1.10	1.30	1.80
EREE	0.81	1.80	0.19	1.20
AF	0.88	1.40	2.30	0.62
DG	3.20	0.15	4.50	5.00
BJ	1.50	1.10	1.30	0.18
KG	1.50	4.90	0.70	0.14
JY	0.28	2.90	1.50	8.50
WD	0.08	1.20	1.00	1.20
LG	6.20	4.10	4.60	6.60
DC	4.40	1.90	5.30	0.18
JA	2.60	2.70	4.00	2.30
BF	2.30	2.10	1.20	3.10
PB	2.20	6.10	2.20	0.22
FB	2.00	0.19	3.20	0.42
ME	1.50	1.40	0.19	3.00
MG	4.30	0.67	5.20	3.80
DB	1.00	3.20	3.70	6.70
JJ	4.40	12.60	5.40	14.40
RS	1.00	1.60	1.40	0.07
GP	3.00	0.41	4.10	0.33

AIII.30. Table showing amplitude and implicit time data for control subjects for parameters of the S-cone VEP. Results were not obtained for subjects JA, JW, MP, VW, BR.

353

Subject	Time constant of Recovery
JB	127.19
GO	174.50
PG	98.06
CG	264.68
SM	91.58
CD	65.23
WD	103.17
RW	28.17
WF	80.58
MR	84.48
VE	454.99
MB	83.93
DJ	58.16
PA	102.94
GA	123.65
JJ	191.27
KM	128.08
MA	131.39
AS	264.00
PS	None measurable
DS	130.16
WT	24.78
GW	32.43
RC	271.89
JC	147.48
VB	343.10

AIII.31. Table showing time constant of recovery of dynamic focal cone ERG for control subjects. Results were not obtained for subjects BB and BC.

Subject	Time Constant of Recovery
JA	280.11
OG	204.42
KS	185.32
WT	93.73
HG	670.74
JW	None measurable
IJ	64.42
ER	None measurable
DF	None measurable
MP	None measurable
EREE	None measurable
AF	None measurable
VW	127.48
DG	None measurable
BJ	469.98
KG	258.24
JY	392.60
WD	81.14
LG	118.13
DC	270.76
JA	204.83
BF	176.18
PB	None measurable
FB	172.50
BR	393.67
ME	606.24
MG	253.67
DB	None measurable
JJ	173.91
RS	173.04
GP	134.02

AIII.32. Table showing time constant of recovery of dynamic focal cone ERG for subjects with ARM.

APPENDIX IV

Psychophysical Data

Subject	Final Sensitivity (Db)	Time to Rod-Cone Break (mins)	$\tau 1$	$\tau 2$
JB	50.63	12.82	0.11	0.27
PG	50.20	18.80	0.48	0.17
CG	50.10	14.20	0.45	0.12
SM	51.40	14.30	0.58	0.07
CD	50.00	13.30	0.11	2.20
WD	47.05	14.70	0.53	0.12
RW	50.00	14.15	0.09	0.34
WF	50.70	11.00	1.13	0.33
MR	49.80	15.90	0.99	0.27
VE	47.30	35.00	0.15	0.10
MB	53.00	17.50	0.45	0.07
DJ	55.00	9.50	0.40	0.18
PA	49.00	17.80	0.06	1.50
GA	53.60	12.60	0.85	0.13
JJ	51.90	11.00	0.84	0.08
KM	45.00	14.80	0.24	0.07
MA	53.40	20.10	0.35	0.16
AS	51.40	36.70	0.28	0.60
PS	51.10	11.70	3.26	0.17
DS	54.00	12.20	3.63	0.16
WT	45.00	25.30	0.18	0.09
GW	51.50	10.80	0.58	0.16
BC	55.60	12.08	0.64	0.12
RC	42.70	11.90	0.69	0.10
JC	47.60	47.90	0.04	1.55
VB	51.00	31.80	0.17	0.05

Table AIV.1. Dark adaptation parameters for control subjects. Results were not obtained for subjects GO and BB.

Subject	Final Sensitivity (Db)	Time to Rod-Cone Break (mins)	τ1	τ2
JA	43.40	16.00	0.26	1.38
OG	55.80	27.50	0.33	0.02
KS	21.13	>60.00	0.64	/
HG	46.00	17.00	0.20	0.06
JW	41.00	37.40	0.34	0.09
IJ	51.90	19.30	0.08	1.14
ER	27.00	>60.00	0.15	/
MP	35.00	36.20	0.08	0.09
EREE	48.00	30.60	0.15	0.04
AF	48.00	45.10	0.27	0.05
VW	51.00	12.90	0.90	0.18
DG	43.00	33.25	0.10	0.07
BJ	26.50	>60.00	0.07	/
KG	37.30	29.90	0.43	0.40
JY	48.00	31.30	0.23	0.06
WD	31.60	49.00	0.11	0.11
LG	47.20	25.00	0.17	0.11
DC	48.00	38.10	0.07	0.06
JA	51.20	28.30	0.33	0.11
BF	47.00	36.50	0.11	0.07
PB	51.00	13.80	2.10	0.08
FB	51.90	44.50	0.16	0.03
BR	35.00	32.20	0.32	0.40
ME	48.00	23.20	0.81	0.07
MG	37.70	33.60	0.17	0.20
DB	50.00	26.70	0.20	0.05
JJ	45.00	29.60	0.04	0.43
RS	45.40	12.70	1.50	0.25
GP	44.19	33.89	0.26	0.34

Table AIV.2. Dark adaptation parameters for subjects with ARM. Results were not obtained for subjects WT and DF.

357

Subject	Confusion Angle	S-index	C-Index
JB	61.98	1.38	1
GO	61.98	1.38	1
PG	61.98	1.38	1
CG	61.98	1.38	1
SM	61.98	1.38	1
CD	61.98	1.38	1
WD	61.98	1.38	1
RW	61.98	1.38	1
WF	20.02	1.62	1.85
MR	61.98	1.38	1
VE	61.98	1.38	1
MB	61.98	1.38	1
DJ	81.65	2.63	1.91
PA	61.98	1.38	1
CA	61.98	1.38	1
JJ	61.98	1.38	1
BB	61.98	1.38	1
KM	81.62	1.96	1.81
MA	71.92	2.60	1.75
AS	61.98	1.38	1
PS	61.98	1.38	1
DS	61.98	1.38	1
WT	75.75	1.57	1.20
GW	61.98	1.38	1
BC	53.0	1.53	1.13
RC	-84.75	1.45	1.72
JC	61.98	1.38	1
VP	61.98	1.38	1

Table AIV.3. Results of standard D15 test for control subjects

Subject	Confusion Angle	S-index	C-Index
JA	61.98	1.38	1
OG	61.98	1.38	1
KS	80.59	2.01	1.84
WT	-80.37	3.34	2.25
HG	61.98	1.38	1
JW	71.80	1.99	1.63
IJ	61.98	1.38	1
ER	61.98	1.38	1
DF	-83.96	2.80	2.37
MP	-56.66	2.35	3.08
EREE	61.98	1.38	1
AF	83.33	2.81	2.16
VW	61.98	1.38	1
DG	73.62	1.90	1.41
BJ	61.98	1.38	1
KG	62.98	3.03	2.49
JY	63.18	1.72	1.33
WD	71.62	1.5	1.13
LG	52.99	1.53	1.13
DC	78.82	1.70	1.31
JA	61.98	1.38	1
BF	61.98	1.38	1
PB	73.22	2.51	2.08
FB	75.61	2.10	1.78
BR	67.55	1.53	1.12
ME	87.49	2.30	2.08
MG	63.60	2.06	1.53
DB	61.98	1.38	1
JJ	61.98	1.38	1
RS	61.98	1.38	1
GP	82.07	2.53	1.83

Table AIV.4. Results of standard D15 test for subjects with ARM

Subject	Confusion Angle	S-index	C-Index
JB	61.4	1.42	1
GO	61.4	1.42	1
PG	61.4	1.42	1
CG	67.20	2.50	1.71
SM	61.4	1.42	1
CD	76.48	2.74	1.93
WD	61.4	1.42	1
RW	61.4	1.42	1
WF	22.49	1.78	1.92
MR	61.4	1.42	1
VE	61.4	1.42	1
MB	61.4	1.42	1
DJ	-86.2	2.97	2.12
PA	60.98	1.73	1.22
GA	67.44	1.23	1.07
JJ	61.4	1.42	1
BB	61.4	1.42	1
KM	-3.29	1.73	1.91
MA	79.76	2.47	2
AS	61.4	1.42	1
PS	-67.24	1.11	1.32
DS	61.4	1.42	1
WT	61.4	1.42	1
GW	61.4	1.42	1
BC	76.23	1.19	1.02
RC	79.99	2.79	2.11
JC	61.4	1.42	1
VP	76.23	1.19	1.02

AIV.5. Results of desaturated D15 test for control subjects

Subject	Confusion Angle	S-index	C-Index
JA	76.23	1.19	1.02
OG	73.75	2.01	1.84
KS	52.03	1.21	1.71
WT	85.99	2.42	1.91
HG	69.77	1.87	1.38
JW	-89.48	2.72	1.92
IJ	85.57	2.20	1.93
ER	-67.19	1.77	1.57
DF	84.11	2.30	1.99
MP	-83.73	2.91	3.53
EREE	61.4	1.42	1
AF	89.91	2.87	2.03
VW	61.4	1.42	1
DG	76.98	1.69	1.46
BJ	61.4	1.42	1
KG	61.61	1.73	1.52
JY	70.82	2.32	2.22
WD	87.55	1.60	1.40
LG	61.4	1.42	1
DC	-76.87	4.41	2.88
JA	61.4	1.42	1
BF	61.4	1.42	1
PB	85.53	2.99	2.87
FB	58.22	1.50	1.06
BR	61.4	1.42	1
ME	81.6	2.46	1.95
MG	65.11	2.03	1.61
DB	67.73	1.97	1.44
JJ	76.33	1.66	1.32
RS	66.8	1.67	1.18
GP	78.26	3.04	2.06

Table AIV.6. Results of desaturated D15 test for subjects with ARM.

APPENDIX V

Supporting Publications

Poster Presentation at the 40th Symposium of The International Society for Clinical Electrophysiology of Vision, Leuven, Belgium

Isolation of the Focal Rod ERG

Binns, A.M., Margrain, T.H.

Purpose: A simple, clinically applicable technique capable of isolating a focal rod ERG may be of value in the early detection and monitoring of age-related macular degeneration. This is because recent evidence has shown that parafoveal rods are lost early in the disease process. The response of the dark-adapted retina to a focal stimulus consists of two peaks, one from the central retina and a second, larger peak from the peripheral retina in response to scattered light. This second peak has previously been eliminated by subtracting a full-field response to a dimmer flash from the initial trace (*Sandberg, 1996*). In this study the ability of an adapting background to desensitise the peripheral retina and isolate the focal response was assessed.

Methods: Ten healthy young volunteers participated in the study. After 30 minutes dark adaptation an ERG was recorded (Medelec Synergy) in response to a 20 degree focal blue stimulus (5ms duration flash, 454nm, 0.5 Hz, 1.7 log scot tds.sec^{-1}) presented at the centre of a Ganzfeld bowl. The luminance of a diffuse green (525nm) background was altered systematically and its effects on the ERG waveform noted.

Results: The green background was able to suppress responses elicited from the peripheral retina, leaving an isolated focal rod response comparable to that obtained by Sandberg (*1996*). No response was obtained from a photopically matched red stimulus, indicating that there were no cone responses in these conditions.

Conclusions: This is a simple, clinically applicable technique that may be used to obtain a focal rod ERG. In the testing of older adults, allowances will be made for differing levels of scatter and absorption by ocular media.

<u>**Poster Presentation at ARVO Annual Meeting, Fort Lauderdale, Florida, May 2003**</u>

The ERG Photostress Test

Binns A.M., Margrain T.H.

Purpose: To develop an objective electroretinographic test capable of evaluating the recovery of macular function following exposure to bright light, and to assess the repeatability of the technique in healthy adults.

Method: Ten young adult volunteers participated in the study. Following pupil dilation, a steady state base-line electroretinogram (ERG) was elicited by exposing the eye to a circular amber (595nm) stimulus, with a time-averaged mean luminance of 30 $cd.m^{-2}.sec^{-1}$, flickering at 41 Hz. The stimulus, which subtended 20°, was surrounded by a luminance-matched annular white background designed to suppress responses from the peripheral retina. Responses from a DTL fibre electrode, and reference electrode placed ay the outer canthus were amplified, averaged and band-pass filtered using a Medelec Synergy System (filtered 1-100 Hz, 100 sweeps averaged). Subsequently the eye was light-adapted to a bright white background (5.6 log photopic trolands) for 2 minutes, and the recovery of the 41 Hz focal cone ERG was monitored for a period of 4 minutes. The resulting data was modelled using a single exponential function.

Results: In all cases there was no repeatable ERG immediately after the bleach. Baseline ERG amplitudes returned within 4 minutes. Determination of the coefficient of repeatability (of the recovery time constant) indicates that the ERG photostress test is unlikely to be a viable clinical tool.

Conclusion: The focal 41 Hz ERG is a quick and efficient method of obtaining objective information of the functional integrity of cone photoreceptors in the macular region. As such, it is an ideal technique for monitoring retinal recovery following a period of intense light adaptation. The ERG photostress test may be useful in the early detection of age-related macular degeneration, a disease that has previously been shown to affect the kinetics of the dark adaptation function. The long-wavelength stimulus should be relatively unaffected by age-related media changes, and thus suitable for use on older adults.

APPENDIX VI

The Conversion of Photopic to Scotopic Troland Values

λ(nm)	f (T→T')	λ(nm)	f (T→T')
400	58.39	550	1.20
410	71.67	560	0.822
420	60.11	570	0.543
430	42.87	580	0.347
440	35.51	590	0.215
450	29.80	600	0.131
460	23.52	610	0.0788
470	18.49	620	0.0481
480	14.20	630	0.0313
490	10.82	640	0.0213
500	7.57	650	0.0157
510	4.93	660	0.0128
520	3.28	670	0.0115
530	2.34	680	0.0105
540	1.70	690	0.0107

Table AVI.1. Conversion table of Photopic Troland Values (T) to Scotopic Troland Values (T') for monochromatic stimuli of different wavelengths (λ). T' = f (T→T') x T where f (T→T') = 2.489 V'(λ)/V(λ) (*After Wyszecki and Stiles, 1982, Table 2.4.4, p104*).

The above table pertains only to monochromatic light sources. Flash stimuli used in this report were provided by LEDs, which typically have a bandwidth of 20nm. An approximation of retinal illuminance was therefore made by using the wavelength of peak LED emission in all calculations. A further approximation was made in assuming an 8mm pupil diameter in all calculations.

The values for V(λ) used in this table are based on those defining the CIE 1931 chromaticity diagram. It should be noted that this is known to be inaccurate in the short wavelength region of the spectrum (*Wyszecki & Stiles, 1982, p258*). Wyszecki and Stiles also highlight the fact that inaccuracies in the short wavelength range of the spectrum may be exacerbated by the fact that the V(λ) and V'(λ) functions are based on subjects aged 30 years or less (*Wyszecki and Stiles, 1982, p258*).